Gene regulatory network downstream of MAPKs orchestrating embryogenesis and regeneration of the sea anemone Nematostella vectensis

Hereroa Johnston

UNIVERSITÉ CÔTE D'AZUR

ÉCOLE DOCTORALE
SCIENCES DE LA VIE ET DE LA SANTÉ

THÈSE DE DOCTORAT

Réseaux de régulation génétique en aval des MAPKs orchestrant l'embryogénèse et la régénération chez l'anémone de mer *Nematostella vectensis*

Hereroa JOHNSTON

Institute for Research on Cancer and Aging of Nice (IRCAN)

Présentée en vue de l'obtention du grade de docteur en Intéraction moléculaire et cellulaire **de l'**Université Côte d'Azur

Dirigée par : Eric RÖTTINGER

Soutenue le : 21/11/2018

Devant le jury, composé de :
Michel VERVOORT, PR1/HDR, Paris Diderot University
Stéphanie BERTRAND, MCU/HDR, Sorbonne Univerty
Stefano TIOZZO, CR, CNRS/HDR, Sorbonne University
Marina SHKRELI, CR, INSERM/HDR, Université Côte d'Azur
Aziz ABOOBAKER, Pr, Oxford University
Eric RÖTTINGER, DR2, CNRS/HDR, Université Côte d'Azur

"If everything regenerated there would be no death"

Richard J Goss, 1969

Acknowledgements

I would like to thank the entire Embryogenesis, Regeneration and Aging team, especially my thesis director Eric Röttinger. Eric, thank you for believing in me during my entire PhD and guiding me until the very end. I couldn't have wished for a better mentor. It would also not be possible without Aldine Amiel, who played an important part in my evolution process.

I wish to thank Jacob Warner and Karine Nedoncelle as well, besides being awesome lab mates and friends during these 4 years, they also provided me with great advices. Finally, I would like to mention Joao Carvallo, who came during the last phase of my PhD but nonetheless provided stimulating discussions and taught me a lot.

A big thank you goes to my dear PhD fellows and best friends, especially my dear Sanya Eduarda Kuzet, Tomas de Garay, Gaia Fabris, Paula Peressini, Torsten Felske and Racha Fayad with whom I shared tears and joys.

Last but not least, my family for their support all these years all the away from Tahiti and my Tahitian friends from the AEPF Nice for always making me feel at home.

Maururu outou paa toa

(Thanks to all of you)

Réseaux de regulation génétique en aval des MAPKs orchestrant l'embryogénèse et la regeneration chez l'anémone de mer *Nematostella vectensis*

(Gene regulatory network downstream of MAPKs orchestrating embyogenesis and regeneration of the sea anemone *Nematostella vectensis)*

Jury:

Président

Michel VERVOORT, PR1, Université Diderot Paris

Rapporteurs

Stéphanie BERTRAND, MCU/HDR, Sorbonne University

Stefano TIOZZO, CR, CNRS/HDR, Sorbonne University

Examinateurs

Marina SHKRELI, CR, INSERM/HDR, Université Côte d'Azur

Aziz ABOOBAKER, Pr, Oxford University

Titre : Réseaux de régulation génétique en aval des MAPKs orchestrant l'embryogénèse et la régénération chez l'anémone de mer, *Nematostella vectensis*

Résumé :

La régénération est un mode de développement qui, suite à un stress physique permet de reformer à l'identique des structures biologiques initialement développée au cours de l'embryogénèse. De plus, ce phénomène, plus ou moins développé en fonction des organismes, est néanmoins répandu chez les métazoaires, suggérant ainsi une origine monophylogénique. D'où l'hypothèse d'un lien étroit entre la régénération et l'embryogénèse. En me basant sur cette, pendant ma thèse hypothèse j'ai employé comme modèle, l'anémone de mer *Nematostella vectensis*. Ce modèle cnidaire offre l'opportunité unique de comparer la régénération d'un corps entier, dite extrême, à l'embryogénèse et ainsi étudier leurs liens au niveau moléculaire. Initialement établie en tant que modèle d'embryologie permettant d'étudier l'évolution des réseaux de régulation génétique (RRG) orchestrant les moments clé de l'embryogénèse. *Nematostella* se développe aujourd'hui en tant que modèle d'étude de la régénération extrême.

Au cours de ma thèse, j'ai tout d'abord participé à caractérisation tissulaire et cellulaire de la régénération de ce modèle afin d'établir un répertoire de référence des étapes clés. En employant ce répertoire et le criblage de 80 d'inhibiteurs de kinase, j'ai pu identifier plusieurs voies de signalisation régissant différentes étapes de la régénération, impliquant les MAPKs, JNK et ERK ainsi que plusieurs récepteurs de facteurs de croissances. Etant donné que ERK a également été décrit dans le processus de gastrulation chez *Nematostella*, j'ai contribué à l'établissement de son RRG associé. C'est donc en me basant sur ce RRG et une base de donnée transcriptomic complète de la régénération de ce modèle, que j'ai pu ainsi établir le RRG en aval de ERK associé à la régénération. Par cette approche j'ai pu démontrer la relation au niveau moléculaire entre ces processus développementaux et surtout identifier des aspects spécifiques à la régénération.

Mots clés: Régénération, Embryogénèse, RRG, *Nematostella vectensis*, MAPK

Title: Gene regulatory network downstream of MAPKS orchestrating embryogenesis and regeneration of the sea anemone, *Nematostella vectensis*

Abstract:

Regeneration is a developmental process that allows to regrow missing structures initially developed during embryogenesis, in response to injury. Although the ability to regenerate can be more or less dramatic depending on the organism, it is widely spread among metazoan, suggesting a monophyletic origin and a tight link with embryogenesis. Based on this hypothesis, I used during my thesis the sea anemone *Nematostella vectensis*, a cnidarian model offering the unique opportunity to compare whole body regeneration and embryogenesis in the same organisms and investigate the molecular relationship of these developmental trajectories. In fact, Nematostella was established as an embryonic model to study the evolution of gene regulatory network (GRN) underlying key developmental stages e.g. gastrulation. More recently it has also become an emerging model to study whole body regeneration.

I started my thesis by participating in a careful tissular and molecular characterization of the hallmarks of *Nematostella* regeneration in order to establish a comprehensive regeneration time line. By taking advantage of this information, I performed a kinase inhibitors screen of close to 80 compounds and identified several signaling pathways, including the MAPK ERK, JNK and growth factor receptor pathways, that regulate various steps of regeneration in *Nematostella*. As I was also involved in describing the ERG dependent gene regulatory network (GRN) underlying embryogenesis, I combined latter information with novel regeneration transcriptomic data to establish the ERK dependent GRN underlying regeneration. By this approach I was able to highlight the relationship between these developmental processes at the molecular level and especially identify regeneration-specific elements.

Key words: Regeneration, Embryogenesis, GRN, *Nematostella vectensis*, MAPK

Introduction overview

Regeneration is a fascinating process and through the introduction of my thesis I will provide you with a general overview of the current knowledge and questions in the filed. I will start from the history of regeneration and proceed to the cellular and molecular knowledge. In particular, I will emphasize on the kinase signaling pathways and their roles in orchestrating regeneration in the major regeneration models including vertebrates and invertebrates. Thereafter, I introduce the notion of gene regulatory networks, which I employed to understand the relation between two developmental trajectories of embryogenesis and regeneration. This is a century old question that is based on the observation that the end goal of these two trajectories is identical, *i.e.* a fully functional organism. As the final outcome is identical, it was hypothesized that the embryonic program is reused during regeneration. In order to address this historical question, I exclusively worked on the cnidarian model *Nematostella vectensis* that offers the unique opportunity to compare these two processes at the gene regulatory level within the same organism.

Introduction

1 The multiple aspects of regeneration

Regeneration is a developmental process allowing one organism to regrow a severed structure after injury. This ability has been observed in many different animals and contexts, naturally raising a certain amount of questions. In the following paragraph I will be describing the emergence of the regeneration field of study, the evolutionary aspects of regeneration, the knowledge acquired at the cellular levels and the animal models that have been developed to investigate this developmental trait.

1.1 The history of regeneration

The ability to regrow missing biological structures has fascinated mankind since ancient Greek mythology. For example, the second task of Heracles was to kill the nine-headed Learnean *Hydra*, but from every cut head, two others would regrow. Another myth about regeneration is the punishment of the titan Prometheus for stealing fire from the gods and give it to humanity. Zeus then condemned immortal Prometheus to have his eternally replenishing liver eaten every day by eagles. But these myths are not only legends. In fact, the cnidarian *Hydra* regenerates its head within a few days and human liver can indeed regenerate when injured. In addition, a large amount of other cases of regeneration can be observed in nature, such as the lizard's ability to regenerate its tail. Systematic research in the field of regenerative biology started almost three centuries ago. The first documented case of regeneration came from the naturalist Réaumur on crayfish (1712) followed by others such as Trembley on *Hydra* (1744), Bonnet on fresh water worms (1745) and

Spallanzani on Salamander and earthworm (1768). The early descriptive work of regeneration was based upon detailed morphological observation leading to setting up the first general principle of regeneration and biology in general. For instance, Bonnet, by studying worm regeneration, described that low temperature slows regeneration and he also tested the limits of head regeneration versus tail regeneration (Morgan 1901). Spallanzani, studied the life stage dependency of regeneration through regeneration experiments on tadpole tails, showing decreasing capacity as development proceeds. He also studied the effect of food on the regenerative ability of salamanders, and observed that starvation would induce a decrease in body size without affecting limb regenerating. These experiments set the course for the contemporary field of regeneration, trying to understand the "units" underlying the process of regeneration, from which arose fundamental questions such as: How is the injury signal integrated to trigger the regeneration response? How do "old" and "new" cells organize themself? (Brockes and Kumar 2008). In order to shed light on these questions, the fascination with regeneration pushed the field to explore this capacity in many different organisms. As Trembley wrote "I felt that nature is too vast, and too little known, for us to decide without temerity that this or that property is not found in one or another class of organized body" (Morgan 1901).

In the following section, I will present the distribution of the regenerative ability across the metazoan tree of live, keeping in mind the simple definition of regeneration I presented at the beginning of this section.

1.2 Phylogenetic distribution of regeneration

In order to understand the distribution of regeneration in the animal kingdom we must consider whether regeneration has evolved independently several times or

rather if regeneration is a monophyletic trait lost during the evolution of some species (Goss 1992). The french scientist Réaumur (1742) argued that the natural selection or regeneration could be explained by the “liability to injury”, meaning that the regeneration trait has emerged in organism resorting to autotomy *e.g* lezard tail, crayfish limbs, grasshoper legs... But there are other animals, which don’t employ autotomy and yet still possess extensive regeneration capacity such as the zebrafish for example (which I will present in section 1.4.1). However there is increasing evidence that regeneration was most probably lost over time and that this was shaped by a multiplicity of ecological factors (Bely and Nyberg 2010). Another argument to support this theory is the phylogenetic distribution of regeneration in the animal kingdom (Fig. 1). This developmental process has been extensively investigated in many different multicellular organisms, from basal metazoan lineages including Placozoa, Poriferan, Ctenophora, and Cnidaria, to chordates. In basal metazoan lineages regeneration is a common feature; in fact they can all perform whole body regeneration (Fig.1A). As organismal complexity increases, however, this capacity of reforming a whole organism through regeneration is less common. Instead, less extreme forms of regeneration that occur at different levels are observed (Fig.1B) (which I will describe in following section) and some organisms including birds cannot regenerate (Bely and Nyberg 2010). The fact that regeneration is present in a plethora of contexts *i.e.* various clade and different structures (*e.g.* limb or organ) (Fig. 2) implies that this feature is not a simple regrowth happening the same way in each context. Therefore, the attempt to find conserved traits to support the hypothesis of the monophyletic origin of regeneration requires identifying comparable points. For every regenerative event follows a conserved sequence of occurrences, wound healing, the mobilization of “building

units", and the re-organization of the regenerated structure or morphogenesis (Tiozzo and Copley 2015). In some case these "building units" have been identified as stem cells (Lai and Aboobaker 2018).

Figure 1:

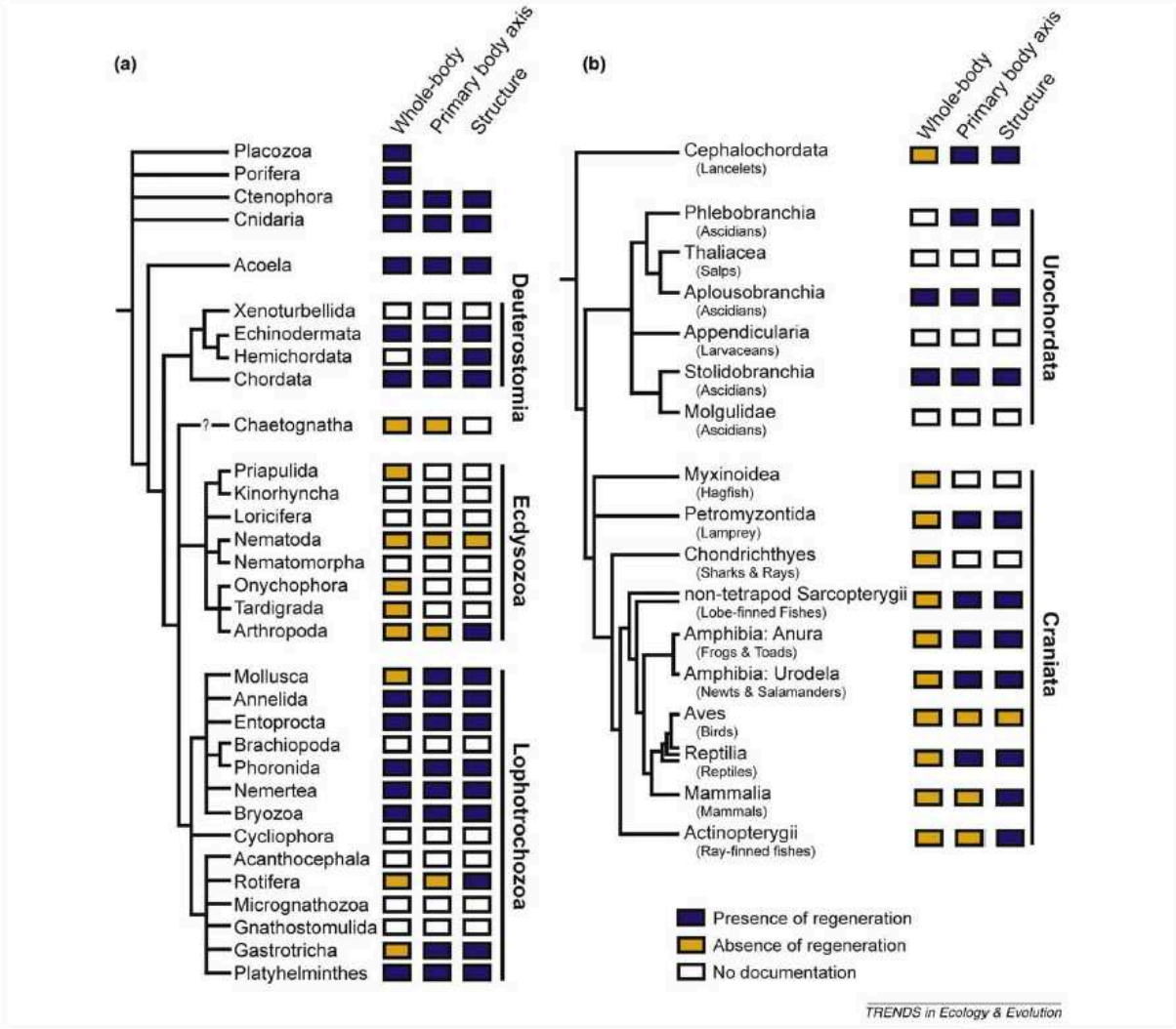

Phylogenetic distribution of regeneration across (a) the Metazoa and (b) the Chordata. 'Presence of regeneration' indicates that at least one well-substantiated report exists for regeneration in that taxon and does not imply that all species in that taxon can regenerate. 'Absence of regeneration' indicates that there is at least one well-substantiated report for the lack of regeneration in that taxon (and none indicating the presence of regeneration). We define 'whole-body regeneration' as the potential to regenerate every part of the body (although not necessarily simultaneously or from a tiny fragment). The ability to regenerate the primary body axis is scored independently for each taxon and does not assume homology of body axes across or within phyla. (Bely and Nyberg 2010)

1.3 Regeneration levels and cellular processes

As I mentioned in the previous section regeneration can be limited to certain extent depending on the organism (Bely and Nyberg 2010). Indeed, regeneration can be observed from simple cell regeneration to the reformation of a whole organism (Fig. 2). In every level, cells are the units of animal regeneration. But they can also regenerate their own structures as it is the case during axon regeneration (Huebner and Strittmatter 2009). On another level, an epithelium such as the epidermis can also regenerate (Yokoyama et al. 2011; Seifert et al. 2012). This is in opposition to scaring after which an epithelium is no longer organized in layers and cannot regenerate anymore (Wynn 2008). The following level of complexity in terms of organization is organ regeneration. The complexity is reflected by the need to rebuild multiple cell types with specific function and integrate a correct patterning for morphogenesis. For example, zebrafish heart regeneration requires new epicardial, endocardial and vascular cells that have to rearrange properly to recover the full functionality of the heart (Jopling et al. 2010; Kikuchi et al. 2011; Kikuchi et al. 2010; Itou et al. 2012; Zhao et al. 2014) . The next level is limb regeneration. In this context the complexity is apparent in that the replenishment of cells requires cell types from different embryonic layers and even from different types of tissue (soft and hard)(Currie et al. 2016; McCusker, Bryant, and Gardiner 2015). Additionally, the organization has to be tightly orchestrated to fully restore the entire panel of limb movements. Finally, some organisms are capable of extreme regeneration since they are endowed with the capacity of rebuilding a whole organism from pieces of tissue, thus encompassing all the previously cited levels of regeneration.

Figure 2:

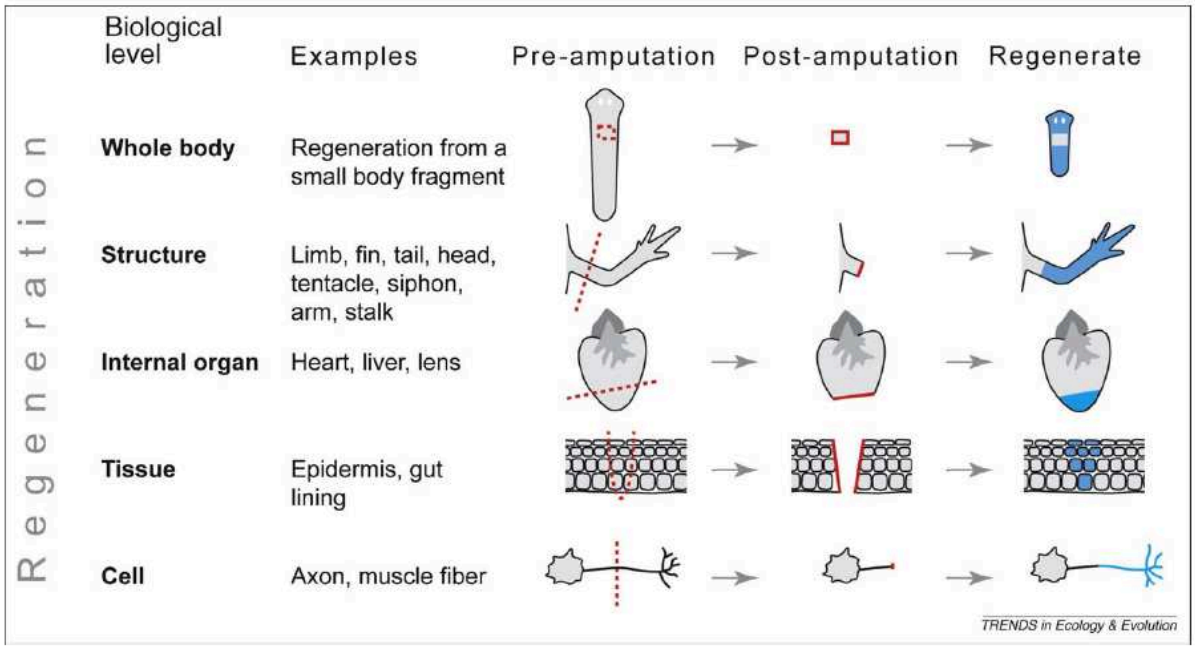

Regeneration at different levels of biological organization. A particular species might regenerate at all, none, or just a subset of these levels. Functional links between regenerative processes at successive levels are probable, but it remains unclear which aspects of regeneration are homologous across levels. Colony-level regeneration', as seen in colonial animals such as corals and ascidians, occurs through asexual reproduction rather than through regeneration of individuals and thus is not included here. Dashed red lines indicate amputation planes; solid red lines indicate wound surfaces; and blue fill indicates regenerated body parts (Bely and Nyberg 2010)

These different levels of regeneration will make use of various cellular processes carefully orchestrated for the sake of rebuilding parts and regaining functionality. Following injury, a stereotypic sequence of events takes place and initiates the proper cellular programs; wound sensing, wound healing and regrowth (Brockes and Kumar 2008). Injury sensing is the earliest step of regeneration and how the organism perceives it in order to trigger the regeneration program is still a pending questions. There are many potential signals to be investigated, chemical or physical. For instance bioelectricity has been investigated to ben an important signal in amphibians (D. S. Adams, Masi, and Levin 2007; Levin 2009; Levin 2007) and among the chemicals identified in wound sensing there are the reactive-oxygen

species (ROS) (Gauron et al. 2013), cytokines (Niethammer 2016) and also Mitogen-activated protein kinases (MAPK), which get phosphorylated in response to injury (Mori et al. 2002). Aside triggering regeneration, the detection of injury is in a more general manner a means to prevent vital body fluid (*e.g* blood) leakage. For instance, the first biological response to such insults is the formation of clots when the vascular system is damaged. This is the case in zebrafish heart regeneration (Jopling et al. 2010), newt limb regeneration (Repesh and Oberpriller 1980), or mouse liver regeneration (Kopec et al. 2017). The clots are composed of fibrin and platelets, which act as a plug at the injury sites (Xu et al. 2012). Interestingly, in the vicinity of clots in a regeneration permissive context, proliferation, one of the cellular hallmarks of regeneration, has been reported. This was discovered to be associated with the activation of thrombin, known to be involved in clots formation (Wolberg and Campbell 2008). Indeed, even in a clot-free context such as lens regeneration, it has been demonstrated that the transient activation of thrombin is leading to the proliferation of epithelial cells (Imokawa, Simon, and Brockes 2004; Imokawa and Brockes 2003). The same observation was also made during liver regeneration, where the critical signal for cell proliferation is released by activated platelet through a thrombin-dependent mechanism (Lesurtel et al. 2006). Beside the formation of clots, blood also transports the immune cells. Thus, the inflammatory response could be intuitively linked to wound sensing. In some cases however this can actually be a hindrance for regeneration if it promotes scaring (Mescher and Neff 2005a). By contrast, in a regenerative context the immune response has been described to be an important player. In fact, macrophages are important to modulate and initiate the regenerative response after injury (Godwin, Pinto, and Rosenthal 2013) and

inflammation is also important to promote cell proliferation(Kyritsis et al. 2012); (de Preux Charles et al. 2016)

The steps following wound sensing are wound healing and the regrowth of biological structures, both of which are closely overlapping. In order to re-develop missing structures, proliferation is a major hallmark yielding in new cells that originate from various sources depending on the regenerative context (Fig. 3). For instance, epithelial regeneration will rely on lineage-restricted progenitors (Fig 3A), which are stem cell capable to proliferate to renew their population and replenish the damaged tissue (Takeo, Lee, and Ito 2015). On the next level of regeneration in organ/limb reformation, new cells originate from multiple sources (Fig. 3B); adult stem cells *e.g.* the satellite cells in salamander muscle regeneration (Morrison et al. 2006), pre-existing cells that will de-differentiate to proliferate *e.g.* cardiomyocytes in zebrafish heart regeneration (Jopling et al. 2010) or transdifferentiate to recover another cell type *e.g.* frog lens regeneration (Henry et al. 2013). During whole body regeneration, such as the one observed in invertebrates, regeneration involves species specific multi-potent stem cells (Fig. 3C) such as the i-cells in *Hydra* (Bosch and David 1987) or the neoblasts in planarians (Wagner, Wang, and Reddien 2011).

This short overview of the different levels of regeneration and the multiple source of cells supporting the regeneration, stresses the necessity to develop a variety of model systems to study the diversity of regeneration, which I will review in the following section.

Figure 3:

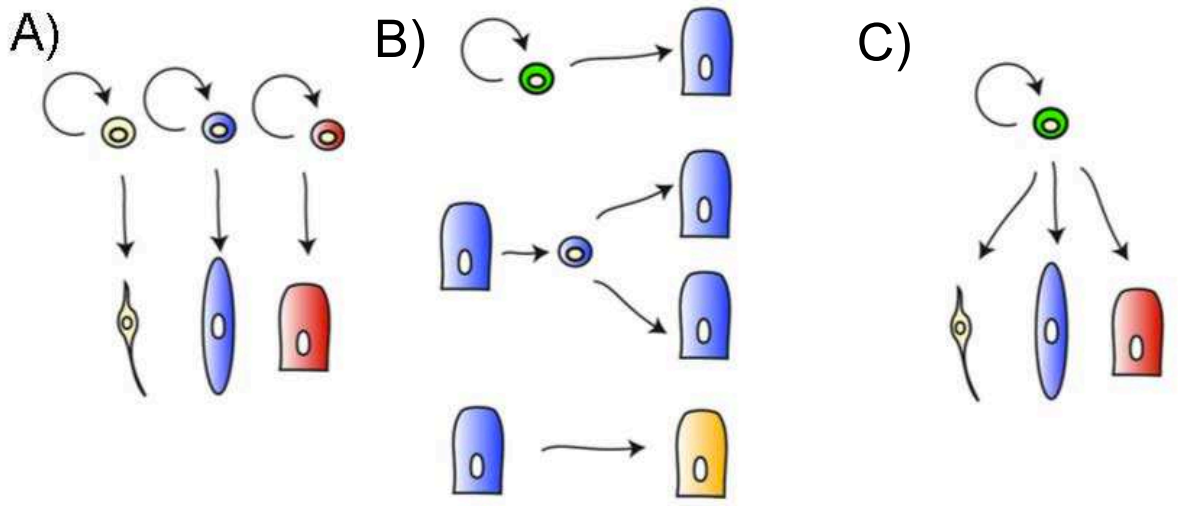

Sources for new cells in regeneration A. Different lineage-restricted progenitor cells (stem cell types are depicted) that each produce different differentiated cells. Each different tissue separately generates or harbors a restricted stem cell. These stem cells together can reconstitute the three different tissues, while any individual on its own is not sufficient to do so. B. Top) stem cells self-renew and produce one or more differentiated cells. Middle) dedifferentiation is the process by which a cell loses differentiated character to produce a progenitor cell that can divide to produce more differentiated cells. Bottom) transdifferentiation involves the change of one cell type into others. This could occur without division, or following de-differentiation of one cell type into a progenitor for additional cell types. C. A pluripotent progenitor cell (a stem cell is depicted) produces differentiated progenitor cells spanning multiple germ layers. There could exist multiple, and/or self-renewing intermediates along different lineage paths. (Derived from (Tanaka and Reddien 2011))

1.4 Notable regeneration model systems

Since the early days of regeneration research, many organisms across the entire metazoan tree of life, from sponges to vertebrates have been studied over the last century. Among them, several models stand out and have been established in the research community, the zebrafish *Danio rerio*, several urodele amphibian models such as the newt *Nophtalamus viridescens* or the axolotl *Abistoma mexicanum*. These models cover the structural levels of regeneration. Concerning whole body regeneration models, there are the historical models such as planarians and the fresh water polyp *Hydra*. Based on these extensively studied (in-)vertebrate models that I will recapitulate the major findings on regeneration in the upcoming section, starting by covering structural regeneration and finishing with whole-body regeneration.

1.4.1 Zebrafish

The zebrafish *Danio rerio* is found in rivers surrounding East India. It was developed as a research model in the 1970s in order to apply genetic analysis to vertebrate development (Streisinger et al. 1986). Indeed this model has an external development, transparent embryos, and a relatively short generation time (2-4month (Lawrence et al. 2012)). Over the last decade extensive resources, reported in the Zfin database (https://zfin.org (Howe et al. 2013)), have been developed to investigate the developmental processes of embryogenesis or regeneration. Indeed, aside its amenability as an embryonic model, the zebrafish can regenerate several structures such as its fins but also various organs like the heart, the central nervous system and the eye lens, which I will be covering in this section. Thus, the zebrafish is a valuable model to study vertebrate regeneration (Poss et al. 2000; Poss 2007; Gemberling et al. 2013).

Figure 4:

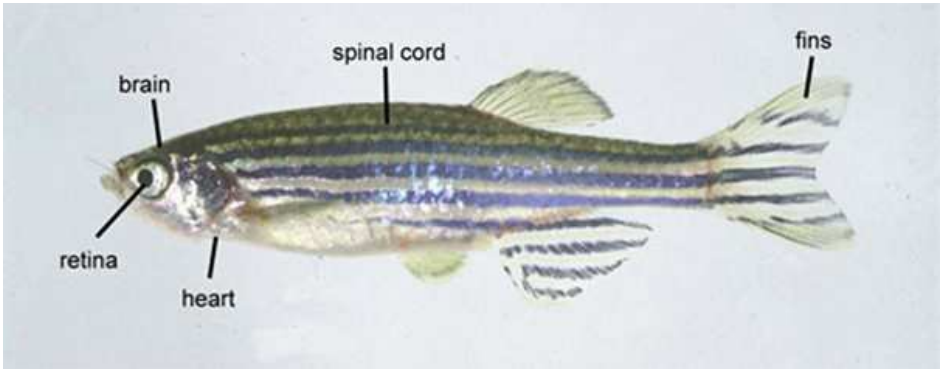

Photography of an adult zebrafish (*Danio rerio*) and the main structures studied during regeneration.

(https://www.uni-ulm.de/med/med-biomolbio/research-groups/weidinger/research-weidinger-lab/)

1.4.1.1 Zebrafish fin

The investigation of structural regeneration using this model has generally been focused on the regeneration of the caudal fin (Fig. 5A). The caudal fin has a symmetrical shape forming two lobes separated by a cleft. It is composed of segments of dermal bone rays and lined with specific cells called osteoblast(Tu and Johnson 2011). After amputation, each ray is capable of regenerating independently. However in the case of a transection spanning multiple rays their regeneration is synchronized to restore both size and shape of the caudal fin (Pfefferli and Jaźwińska 2015).

Figure 5:

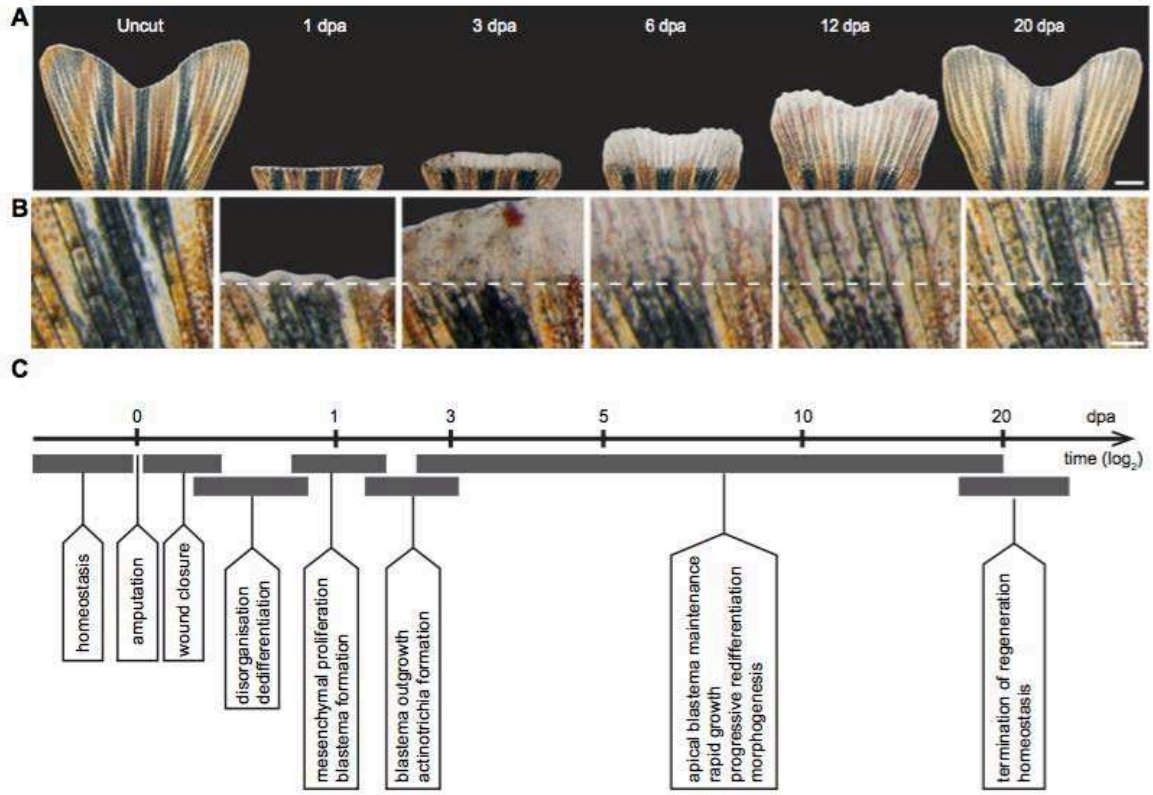

The regeneration process of the caudal fin in zebrafish (A) Time-lapse imaging of the same fin during the regeneration process at 27◦C. Uncut, the original fin prior to amputation presents a bi-lobed morphology. At 1 dpa, white tissue above the amputation consists of the wound epidermis and a few blastema cells. At 3 dpa, a white excrescence above the amputation plane contains the blastema, which, despite its uniform appearance, exhibits subdivisions at the cellular and molecular level. At 6 dpa, the outgrowth extends very rapidly; the white tissue is maintained at the fin margin, while the proximal outgrowth starts to display bone structures and pigmentation, which are the macroscopic markers of tissue redifferentiation. At 12 dpa, fin regeneration is at its advanced stage. At 20 dpa, the size of the fin nearly reaches its original size and pattern. The white margin of tissue remains at the tip for homeostatic growth/regeneration. (B) Higher magnifications of the fin surface at the position of amputation (white dashed line) at the respective time points are indicated in the upper panel (A). (C) The milestones of the fin regeneration process. Scale bars: (A) 1000 µm; (B) 200 µm (Pfefferli and Jaźwińska 2015)

Zebrafish fin regeneration comprises four stages (Fig. 5B). The first stage following amputation is wound healing where epidermal cells migrate to cover the stump (Poleo et al. 2001) (Fig. 5C 0dpa). During the second stage, there is a thickening of the covering epidermis (Fig. 5C, 1dpa), which is associated with the migration of fibroblasts and osteoblasts that originate from the bone ray segment proximal to the stump. Thirdly, mesenchymal cells proliferate below the epidermis covering the stump, giving rise to a blastema (Fig 5C, 1-3dpa). The profiles of the cells composing the blastema have been characterized with modern genetic fate mapping, highlighting a mosaic aspect of the blastema composed of unipotent stem cells (Tu and Johnson 2011). During zebrafish fin regeneration the osteoblasts will renew their population by de-differentiating for the sake of proliferation and later re-differentiate (Knopf et al. 2011). The same is valid for other cell type such as endothelium, epidermis and fibroblast, exhibiting a lineage restriction(Tu and Johnson 2011). Finally during the fourth and last stage, the blastema differentiates to reform the fin structure while the distal cells continue dividing to support the outgrowth (Poss et al. 2000) (Fig. 5C, 5-20dpa).

1.4.1.2 Zebrafish heart

The heart is composed of two types of chambers; the atrium where the blood flows into the heart and the ventricle responsible for expulsing the blood out of the heart. While mammalians posses two of each (left and right), the zebrafish heart is only made of one atrium and one ventricle (González-Rosa, Burns, and Burns 2017) (Fig. 6). A muscular wall supports the contractile function of the heart. The inside of the wall is known as the myocardium majorly composed of myocytes but also blood vessels and nerves. The inner part of the wall is covered by a layer of endothelial

cells, called the endocardium, while a layer of mesothelial cells, called the epicardium, covers the exterior part.

Figure 6:

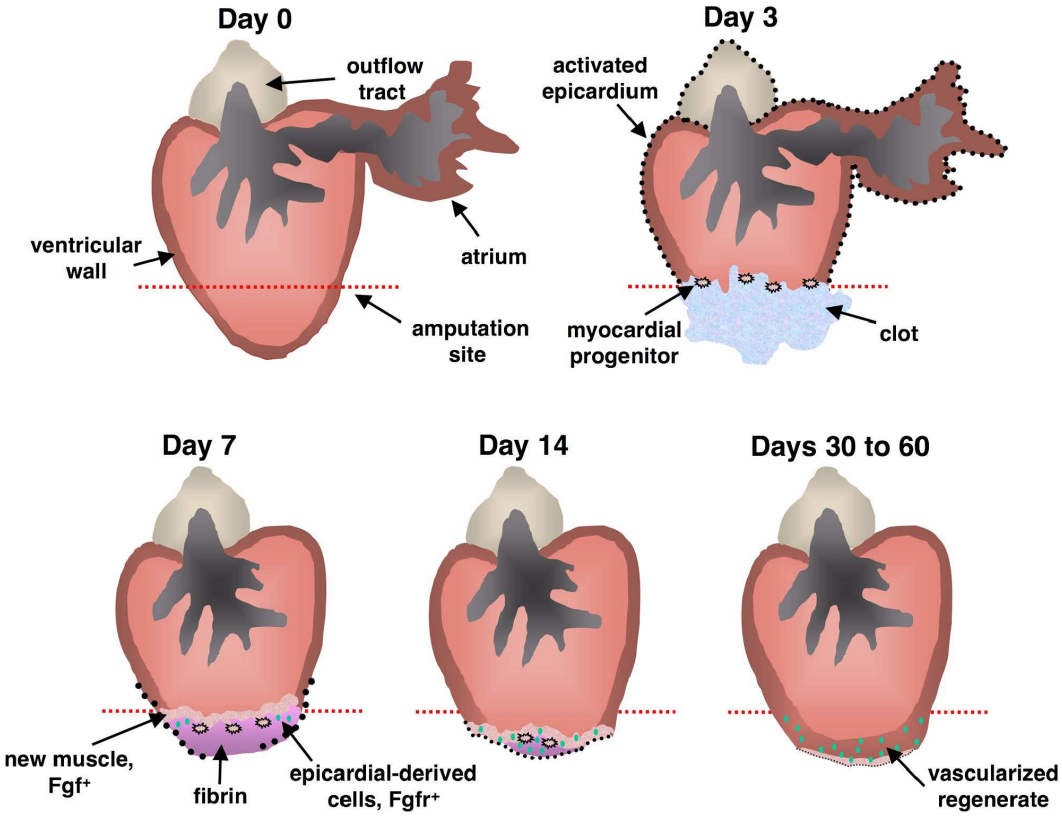

Diagram of zebrafish heart regeneration. Resection of the ventricular apex (0dpa). Clot formation, expansion of activated epicardium cells by 3 dpa (black dots). Fibrin deposit, activated epicardial cells begin to surround and invade the wound, proliferation of myocardial progenitor cells and first layers of new muscle a of By 7 dpa. To coordinate these epicardial and myocardial events, regenerating myocardium synthesizes Fgf17b and possibly other factors with the potential to recruit Fgfr2/Fgfr4-presenting epicardial cells. Epicardial-derived cells undergo EMT in response and vascularize the regenerate (green dots). Presence of new coronary vasculature by 14 dpa. Extends progenitor cell activity and facilitates restoration and expansion of the ventricular wall (stage 2) (Lepilina et al. 2006)

Multiple types of injury models have been developed for heart regeneration studies including surgical resection, cryo-injury, and genetic ablation. The surgical resection of the ventricular apex allows the investigation of the strict regeneration capacity of the heart, by monitoring the re-formation of heart morphology (Poss 2007). The cryoinjury is a way to mimic a myocardial infarction (González-Rosa et al. 2011; Chablais et al. 2011) and the inducible genetic ablation, which produces a massive injury by removing 60% of the cardiomyocytes, reproduces an end-stages heart failure (J. Wang et al. 2011). Even though there are multiple types of injury, the regeneration process still occurs in a similar fashion (Gemberling et al. 2013). Nevertheless, surgical resection represents the most complete case of regeneration. During surgical resection, the fist response to wounding is the formation of a clot (Fig. 6, Day3). This event is followed by the activation of the epicardium, which leads to the proliferation of de-differentiated cardiomyocytes that starts to cover the wound (Jopling et al. 2010; Kikuchi et al. 2010) (Fig. 6, Day3). In a similar manner, endocardium regeneration also recruits pre-existing endocardial cells (Zhao et al. 2014). Aside from the proliferation of de-differentiated cardiomyocyte, another critical step of regeneration is the migration of cardiomyocytes to the wound site (Itou et al. 2012) (Fig. 6, Day3). Then, epicardial cells start to proliferate, surround the regenerating wound and later act as a source of vascular support (Kikuchi et al. 2011) (Fig. 6, Day7). At this point the myocardium is already electrically coupled with the existing muscle and regeneration is achieved by the dissolution of the clot (Raya et al. 2003) (Fig. 6, Day30-60).

1.4.1.3 Zebrafish central nervous system

The zebrafish central nervous system (CNS) is composed of five distinct regions: i) olfactory bulb (OB), ii) dorsal telencephalon (DT), iii) optic tectum (OT), iv) cerebellum (CE) and v) spinal cord (SC) (Kroehne et al. 2011) (Fig. 7A). Beside the neurons, which are the functional unit of the CNS, there are also glial cells acting as a support for the neurons. There are four types of glial cells in the CNS, oligodendrocytes, astrocytes, ependymal cells, and the microglia. They are not only important for the maintenance of the neurons but they have also been described to be important for the regenerative process of the CNS, as reviewed in the following paragraph.

Figure 7:

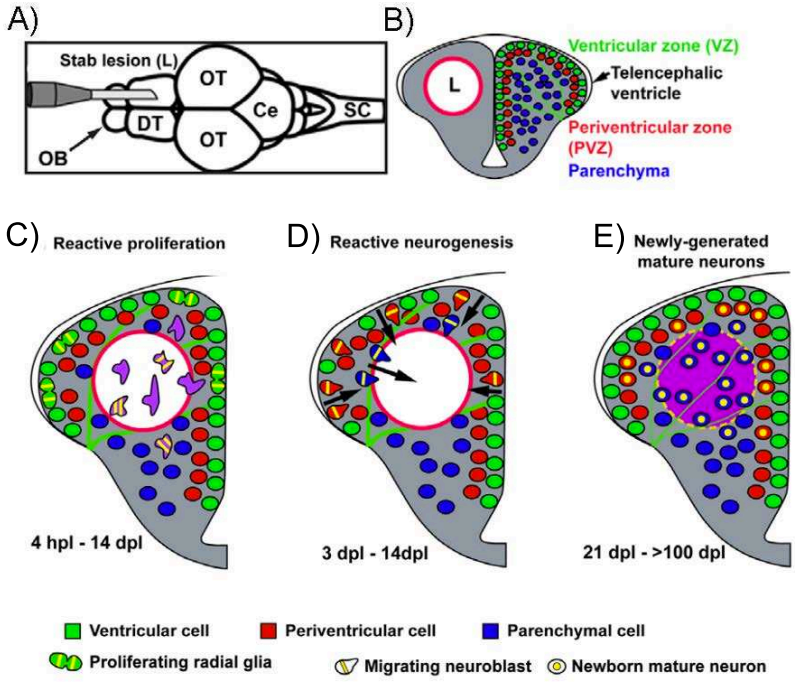

Zebrafish brain morphology and key events of regeneration in adult zebrafish telencephalon. A. Injury experiment, insertion of a canula into the telencephalon of an adult zebrafish causes a lesion canal (L) (dorsal view; OB, olfactory bulb; DT, dorsal telencephalon; OT, optic tectum: Ce, cerebellum; SC, spinal cord). B. Cross-sections in DT, neural progenitor containing ventricular zone (VZ, green). periventricular zone (PVZ, red, one or two cell diameters adjacent to the VZ). The uninjured central parenchyma (blue). (C) Resident microglia, invading leukocytes and ventricular radial glia enter a phase of reactive proliferation from 4 hpl to 14 dpl. (D) From 3 to 14 dpl, radial glia proliferation and neurogenesis (reactive neurogenesis). Migration of the newborn neuroblasts from the VZ towards the lesion. (E) From 21 to 100 dpl, newly generated mature and active neurons within the lesion site in the parenchyma and in the PVZ (Kroehne et al. 2011).

The zebrafish brain is composed of several progenitor cell niches, while adult mammals posses a restricted neurogenic area located in the ventricular zone of the telencephalon, (Kizil et al. 2012). Hence the zebrafish progenitor zones in the telencephalon, especially in the ventricular zone, are the most studied niches in the context of regeneration (Kizil et al. 2012) (Fig. 7B). In order to investigate regenerative capacity of the brain region a stab-lesion protocol has been developed (Kroehne et al. 2011; Schmidt et al. 2014) (Fig. 7A). The fist response after injury is an acute inflammatory reaction and an important proliferation of glial cells. Later during the regenerative process these glial cells function as a neuronal progenitor population (Kroehne et al. 2011) (Fig. 7C-D)

As part of the CNS the spinal cord regeneration was also investigated by using spinal section as an injury protocol. Like zebrafish brain regeneration, spinal cord regeneration is supported by the proliferation of glial cells (Goldshmit et al. 2012). The new glial cells will adopt a bipolar morphology to bridge the gap of the spinal cord section. The bridge formed is thereafter used for new axons to reach the opposite side and consolidate the glial bridge (Goldshmit et al. 2012). But in comparison to zebrafish brain regeneration where the proliferating glial cells also serve as progenitors, in the case of spinal regeneration these cells are participating to the replenishment of motor neurons (Becker et al. 1997; Reimer et al. 2008; Ohnmacht et al. 2016).

1.4.2 Urodele

Among the vertebrate models used to study regeneration, the class of amphibians contains highly regenerative species, such as the salamander (urodele) and *Xenopus* (anura). Between the two, urodeles are the champions of limb regeneration among vertebrates. More precisely, the axolotl, the newt and the salamander are the most extensively studied models.

Figure 8:

Ambystoma mexicanum *Pleurodeles waltii* *Nopthalamus viridescens*

Widely used urodele models in regeneration

https://fr.jarathana.nl/vissen/tropische-zoetwatervissen/krabben-kreeften-garnalen/pleurodeles-waltl-triton-de-waltl-m.html;http://www.wikiwand.com/fr/Salamandridae;
https://www.facebook.com/pg/%E9%A6%99%E6%B8%AF%E5%A2%A8%E8%A5%BF%E5%93%A5%E8%A0%91%E8%9E%88-%E5%85%AD%E8%A7%92%E6%81%90%E9%BE%8D-1467557290171064/posts/

1.4.2.1 Urodele limb

Typically, experiments on limb regeneration are carried out on the forelimb. The vertebrate forelimb is composed of three segments: the humerus, attached to the shoulders, the ulna and the radius that form the second segment and the carpal together with the digits that form the third segment. During regeneration experiments, amputation is executed at the end of the humerus, right before the elbow (Fig. 9). In the response to injury, the stump is covered by nearby keratinocytes that expand in volume to form the wound epidermis (Tanner et al. 2009), unlike zebrafish fin regeneration that relies on cell migration to cover the

stump (Poleo et al. 2001). Although limb regeneration also requires the formation of a blastema, the way for achieving proper reformation of the missing limb is different. It has been shown in axolotl that a nerve supply is needed for keratinocytes to undergo de-differentiation (Stocum 2011) and subsequently recruit dermal cells to initiate the formation of the blastema (Endo et al. 2007; Satoh et al. 2008; McCusker, Bryant, and Gardiner 2015). The formation of the blastema relies on a bulk of proliferating mesenchymal cells that originate partially from the de-differentiation of fibroblasts, but also from muscle cell progenitors that support the regeneration of different structures (Nacu et al. 2016; McCusker, Bryant, and Gardiner 2015) (Fig. 9).

Figure 9:

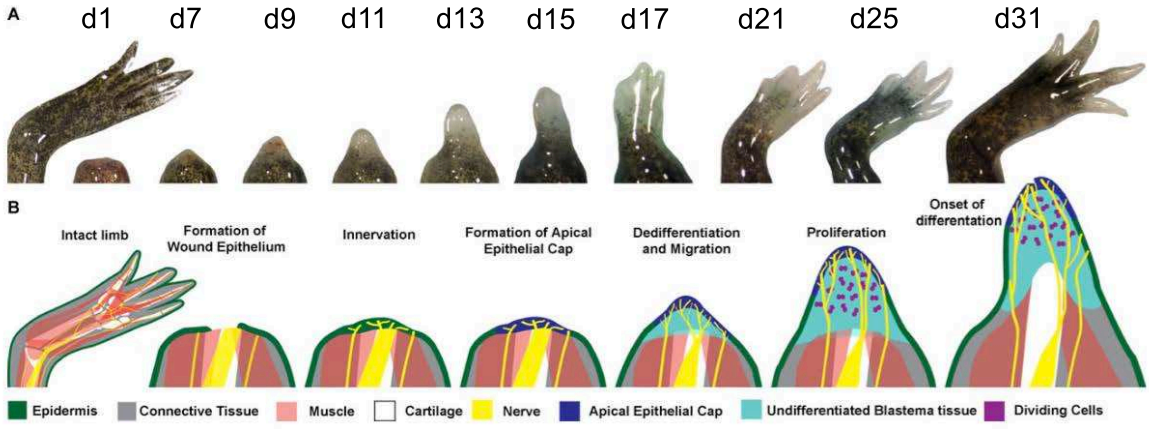

Urodele limb regeneration, e.g axolotl (A) Live images of the time course of limb blastema development showing an intact limb and 1 day, 7, 9, 11, 13, 15, 17, 21, 25, and 31 days post amputation. (B) The key steps in the regenerative process are highlighted during blastema development. Wound healing and formation of the wound epithelium. Innervation of the wound epithelium. Formation of the apical epithelial cap. Innitiation of blastema formation. Blstema growth by proliferation of undifferentiated cells and finaly the onset of differentiation. (McCusker, Bryant, and Gardiner 2015)

1.4.2.2 Urodele heart

The urodele heart is composed of an atrium and a ventricle much like the zebrafish heart (Cano-Martínez et al. 2010). Not only they are morphologically similar, but the urodele heart also possesses regenerative capacity (J. Oberpriller 1971; J. O. Oberpriller and Oberpriller 1974). Unfortunately the regenerative process of the axolotl heart has not been studied yet as thoroughly as is it was done for the zebrafish. Nevertheless, recent studies have confirmed the absence of scaring after injury and also the activation of cardiomyocyte proliferation (Cano-Martínez et al. 2010). Thus, this first study highlights, potential common strategies with the zebrafish model.

1.4.2.3 Urodele lens

Newt eyes have essentially the same structure as any vertebrates. The posterior end optic nerve connects the retina to the CNS. The retina tissue is what makes the majority of the eye structure and ends with the dorsal and ventral iris on the anterior end. Both, ventral and dorsal, parts are converging to the middle and connect with the lens. The lens it self is composed of multiple layers of lens fibers cells (Bassnett, Shi, and Vrensen 2011). Finally the eyes are separated from the outside by the cornea.

Figure 10:

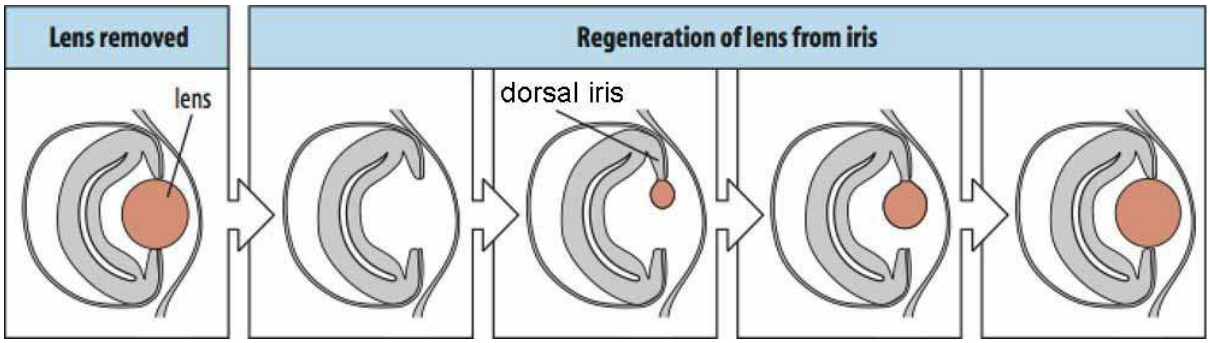

Diagram of len's Wolfian regeneration from the dorsal iris (gray), the regenerating lens is in red. (http://www.mun.ca/biology/desmid/brian/BIOL3530/DB_13/fig13_3.jpg)

Unlike other injuries there is no wound healing process reported for lens removal. There are two strategies adopted for lens regeneration, which differs between amphibians. The best described process, is the newt's Wolfian lens regeneration (Henry and Tsonis 2010) (Fig. 10). Upon removal of the lens, there is a dedifferentiation event from the pigment cells that are located on the dorsal iris. These undifferentiated cells loose their characteristic pigmentation and re-enter the cell cycle. Thereafter following proliferation, the cells undergo trans-differentitation into lens fiber cells to regenerate a new lens (Henry and Tsonis 2010). The way pigment epithelial cells regenerate the lens is one of the striking examples of trans-differentiation during regeneration.

1.4.2.4 Urodele CNS

The brain of salamander has restricted neurogenic niches that are located in the ventricular zone (Joven and Simon 2018; Parish et al. 2007). Although, neurogenic niches are also present in other vertebrate, only salamanders are able to regenerate after spinal transection at any axial level (Holtzer 1952; Holtzer 1951; Piatt 1955).

Injury experiments of spinal cord transection are performed on the tail of adult Salamander (Chernoff et al. 2002; Piatt 1955). There, the first step of regeneration is the activation of neighboring ependymal cells that will infiltrate that gap and form an ependymal bridge on which ependymal cells will proliferate (Butler and Ward 1967) This bridge will also act as a support for the axonal projections to reach the other edge (Butler and Ward 1967). In the context of tail amputation in larvae, the same process has also been reported.

Beside the spinal cord regeneration, CNS regeneration has also been explored in the axolotl brain regeneration, after the extirpation of the middle one-third of the telencephalon hemisphere (Kirsche 1983). Regeneration is accomplished by mitotic division of progenitors from the ventricular zone (Kirsche 1983) and results in reforming a similar morphology as the uninjured hemisphere (Kirsche 1983). Overall, although the salamander has a more restricted regenerative capacity of the CNS compared to zebrafish, the cellular strategies employed appear similar.

1.4.3 Planarian

Planarians are flatworms belonging to the Platyhelminthes phylum (Fig. 1) and include both, terrestrial or aquatic species (Campos et al. 1998). Many naturalists have reported their regenerative capacity during the eighteenth century and systematic studies have been performed since the nineteenth century (Elliott and Sánchez Alvarado 2013). As a triploblastic animal, planarians develop from three germ layers, ectoderm, endoderm, and mesoderm. At the anterior extremity they posses two sensory organs linked to the nervous system (Fig. 11B). Their diffuse nervous system is composed of two cephalic ganglia connected to two ventral longitudinal cords (Reddien and Sánchez Alvarado 2004). Their digestive system is quite rudimental and is made of an extensible pharynx, acting as a mouth and an anus at the same time. The pharynx is connected to three digestive branches (one anterior and two posterior) (Fig. 11B), the triclad, which is at the origin of their order name (Tricladita). They rely on three different types of muscles, longitudinal, diagonal and circular for mobility (Fig. 11C). Finally, the space between all these various structures is filled by mesenchyme, referred as parachyma (Reddien and Sánchez Alvarado 2004) (Fig. 11C). While planarians in general are capable of sexual reproduction as cross-fertilizing hermaphrodites, the main regeneration model

reproduce exclusively asexually *via* transverse fission and thus, is amenable for clonal culturing. The main species used for whole-body regeneration studies are *Schmidtea mediterranea* and *Dugesia japonica* (Rink 2013).

Figure 11:

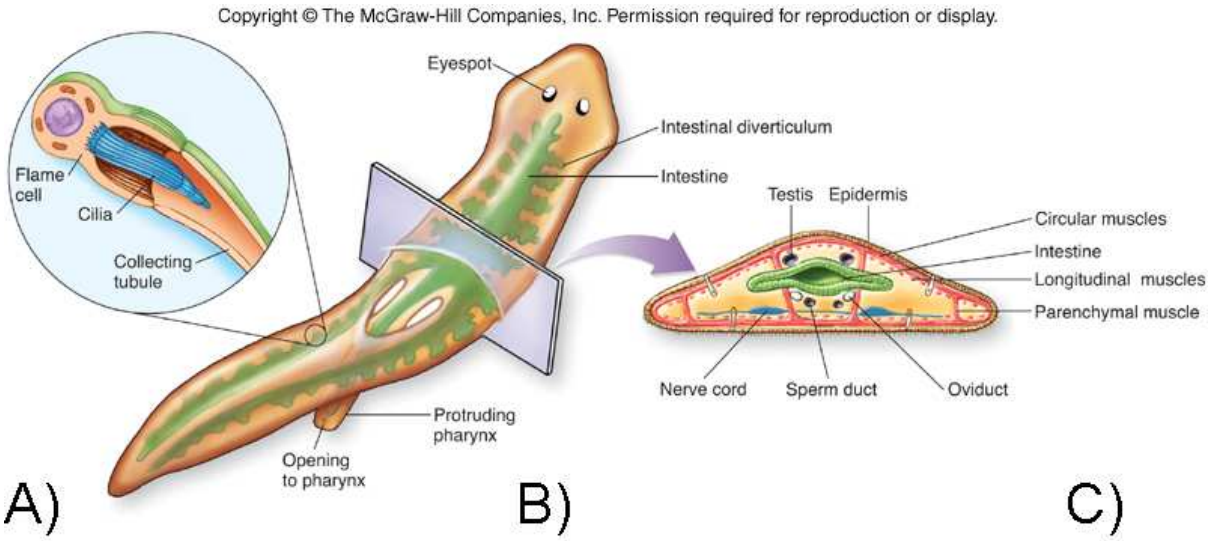

Planarian anatomy. A) focus on the kidney-like organ of planarian, B) general anatomy and C) transversal cut above the pharynx.

During regeneration experiments, the first response to injury reported was a strong muscular response at the amputation site to minimize the loss of cells (Newmark and Sánchez Alvarado 2002) (Fig. 12). Muscle contraction is followed by the production of mucus by specialized cells, called rhabdites, in order to cover the wound. Then a thin layer of epithelium spreads without proliferation, to covers the wound to achieve wound healing (Sánchez Alvarado and Newmark 1998) (Wagner, Wang, and Reddien 2011) (Fig. 12B). The regeneration process relies on a population of stem cells specific to planarians called neoblast, which are generally defined as dividing cells that participate in the homeostasis of the tissue in a non-regenerative context. Among these stem cells a sub-population of multipotent neoblast is capable of replacing any cell type called clonogenic neoblast (Wagner, Wang, and Reddien 2011) (Fig. 12B). During regeneration, neoblasts will migrate to the wound and abundantly proliferate (Salo and Baguna 1989; Wenemoser and Reddien 2010) (Fig. 12B). Subsequently, this burst of proliferation results in the formation of a mesenchymal bud called the blastema, the base of whole body regeneration of planarians (Sánchez Alvarado and Newmark 1998).

Figure 12**:**

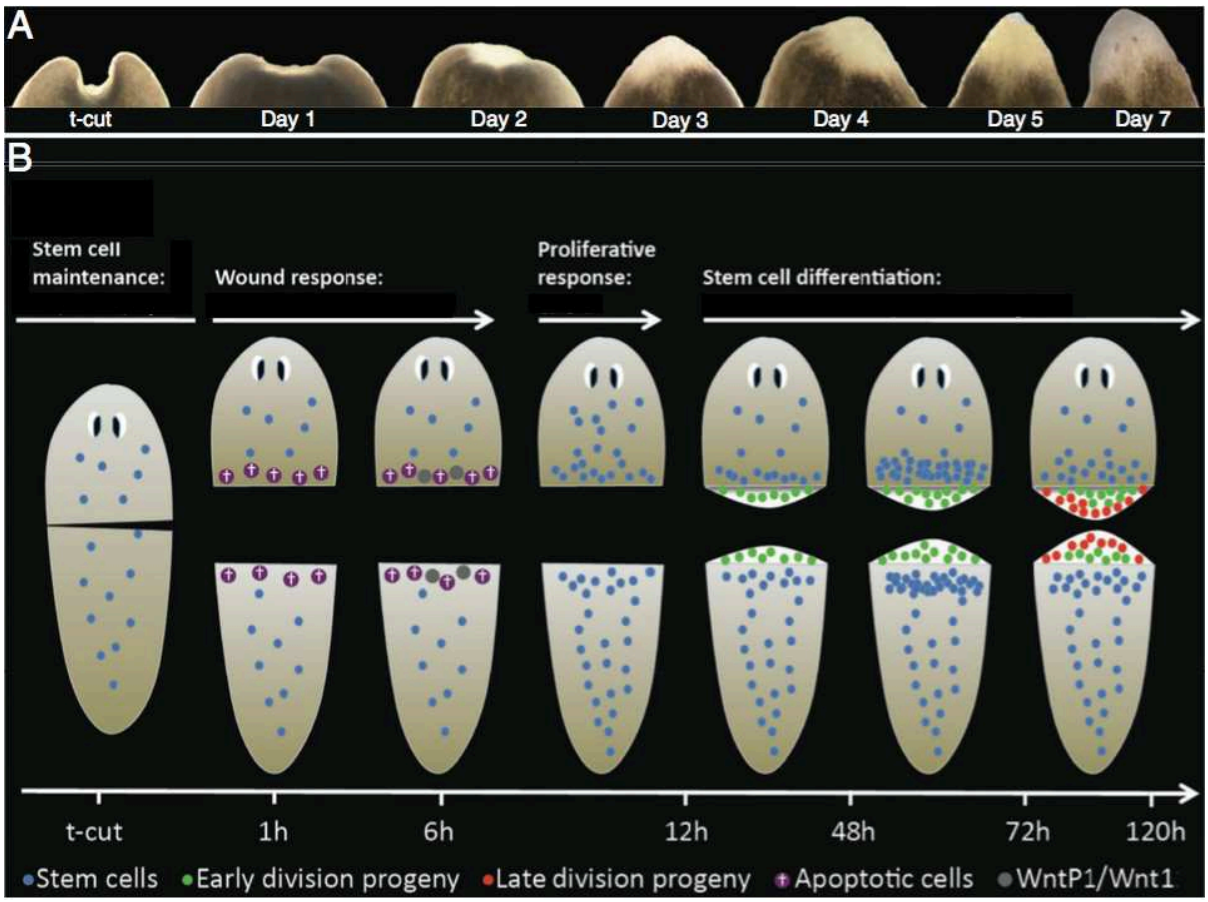

Regeneration phase in planarian. A. Head regeneration in S. mediterranea after transverse amputation (t-cut). B. After the wound response (1h-6h), Pre-patterning and noeblast recruitment (6h-12h). Neoblast proliferation and blastema formation (12h-48h). Blastema development (48h-72h). Neoblast differentiation (12h-120h) (adapted from (Gentile, Cebrià, and Bartscherer 2011)

1.4.4 Hydra

This hydrozoan fresh water polyp is part of the cnidarian phylum composed of diploblastic animals, which are the sister taxon of bilaterians. In terms of phylogeny it is closest to the model I worked on during my PhD, the anthozoan cnidarian *Nematostella vectensis* (Fig. 1). The *Hydra* polyp is composed of two epithelial cell layers, the endoderm lining the inside and the ectoderm facing the outside. An extracellular matrix and and the acellular mesoglea separate the two layers. The head is composed of a crown of tentacles surrounding the mouth. The opposite side of the head is called the food and allows the polyp to attach firmly on a substrate (Fig. 13A). The extreme regeneration capacity of *Hydra* was first discovered by the naturalist Abraham Trembley (1710 – 1784). He is the author of the first detailed scientific report on its regenerative capacity and his work has been followed-up centuries later with the re-emergence of the field of regeneration (Galliot and Schmid 2002). Basically if *Hydra* is cut in half the head will regrow a foot and *vice versa* in approximately in 4 to 5 days. But it is also the only organisms with sponges that is able to reform itself from cell aggregates after a complete dissociation(Custodio et al. 1998) (Technau et al. 2000). Unlike other regenerating organisms, *Hydra* can regenerate in the absence of proliferating cells utilizing only existing cells. From this particular regeneration strategy arose term “morphallaxis” (Bosch 2007). Together, these regenerative features make *Hydra* a unique model of regeneration. Although *Hydra* culture are mainly based on clonal populations (Bosch 2007), it is also amenable for transgenesis but with a limited access to embryonic material (Wittlieb et al. 2006).

Figure 13:

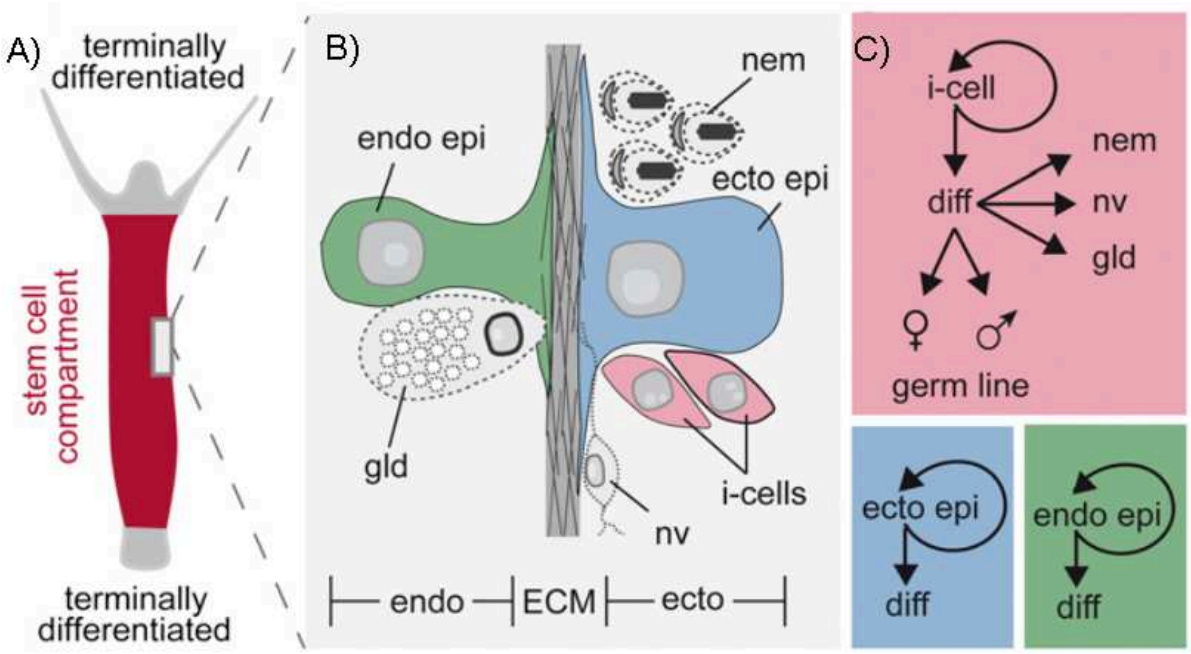

Stem cells in Hydra A) Scheme of the stem cell compartment in *Hydra*. B) The major cell types in *Hydra*. Stem cell lineages are colored, with derivatives of the interstitial cell lineage in gray. (C) The three independent stem cell systems in *Hydra*. Both epithelial cell lineages represent unipotent stem cells whereas interstitial stem cells exhibit multipotent features, as they are able to differentiate into various derivatives. diff, differen- tiation ecto, ectoderm; ECM, extracellular matrix; ecto epi, ectodermal epithelial cell; endo, endoderm; endo epi, endodermal epithelial cell; gld, gland cell; i-cell, interstitial stem cell; nv, nerve cell; nem, nematocyte.(adapted from (Boehm et al. 2012))

Regeneration of *Hydra* starts by a rapid wound healing characterized by a reorganization of the epithelium at the amputation site (Bibb and Campbell 1973), where the endodermal epithelial cells display unexpected mobility (Takaku, Hariyama, and Fujisawa 2005). Three stem cell populations support the reformation of head structures during *Hydra* regeneration (Fig. 13B): lineage restricted progenitors of ectoderm and endoderm (David and Plotnick 1980; Smid and Tardent 1986) and the specific *Hydra* stem cells, called interstitial stem cells (i-cells), capable of self-renewal that give rise to neurons, nematocytes, secretory cells and gametes (Bosch and David 1987) (Fig. 13C).

Overall, this review of the main regeneration models was aimed to cover a large spectrum of regeneration strategies. Nevertheless common cellular processes have also been teased out from these comparisons. These provide additional evidence of the conservation of regeneration mechanisms and support the monophyletic origin of this developmental phenomenon. Thus, investigating the signaling pathways orchestrating this diversity of regeneration strategies will potentially lead to a more insightful understanding of the molecular underpinnings driving regeneration and its evolution.

2 Orchestrating regeneration through phosphorylation

Kinases represent a family of phosphorylating enzymes that will activate or inhibit other proteins and are important for signal transduction. As such they are involved in the majority of signaling pathways (Bardwell and Shah 2006). These enzymes are found at every sub-cellular location including the cell membrane where they act as receptors. In the presence of their ligand they recruit cytoplasmic proteins to the cell membrane to transduce the external signal into the cell (Fig. 14). The external signal is either directed towards structural components of the cell for a direct physical response or directly to the nucleus where it activates a genetic program. In order to convey this information inside the cell, kinases are organized as a phosphorylation cascade, with an effector at the end of the pathway, *e.g.* a transcription factor for a genetic response.

Figure 14:

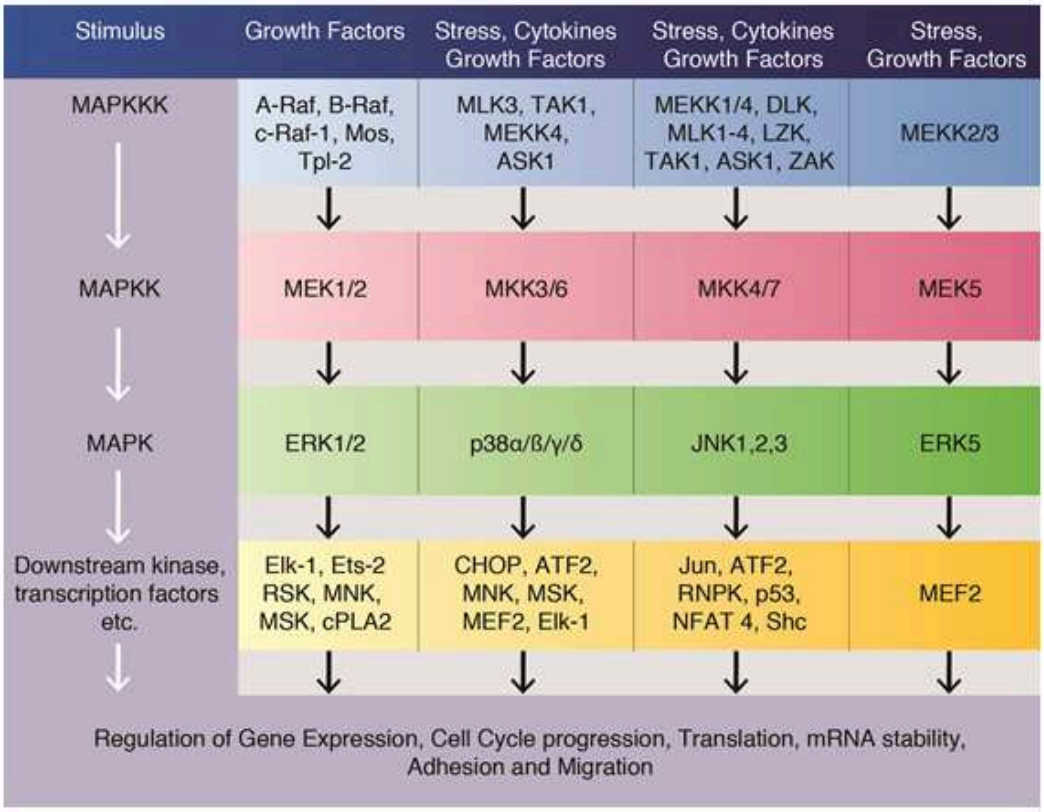

General overview of MAPK signaling (Roberts and Der 2007)

Among the large diversity of signaling pathways, the mitogen-activated kinases (MAPK) family has been described in all eukaryotic cells, ranging from yeast to animals (Gustin et al. 1998; M. Li, Liu, and Zhang 2011). In the animal kingdom this protein family is implicated in a plethora of cellular process (*e.g.* proliferation, differentiation, migration), hence their implication in development (F. Zhang et al. 2002). MAPK signaling forms a cascade of three kinases. The MAPKKK or MAP3 kinase is the first to be activated by small G protein responsible for sensing the activation of receptors such as receptors associated with kinase activity (RTK), G protein coupled receptors or directly by changes between the extracellular environment and the intracellular environment. The MAPKKK will in turn activates a

MAPKK or MAP2 kinase by phosphorylation, which will finally activate in the same manner the last member of the cascade, the MAPK. This kinase is responsible to transmit the external signal to an effector protein (Pearson et al. 2001) (Fig. 14).

The mammalian MAPK family contains 22 members, among which we can distinguish three evolutionary conserved cascades of MAPK: extracellular signal regulated kinase (ERK) pathways, p38 pathways, and c-jun NH2-terminal kinase (JNK) pathways (Fig. 14). Those MAPKs signaling have evolved to transmit different types of signals. The MAPKs ERK1 and ERK2 have been described to be downstream of MAPKK, MEK1, or MEK2, which in turn are known to be activated by the MAPKKKs Raf, Mps or TPL2 (REF). The p38 and JNK family of MAPK are also known as stress activated protein kinases and are involved in adaptation to stress. Both families share most of their upstream MAPKKK including MEKK, ASK, TAK, MLK and TPL2, but the MAPKK, MKK4 and MKK7 are specific to JNK activation while MKK3 and MKK6 are generally specific to P38 (REFs). Conversely, the activation of effector proteins is not strictly straightforward. In order to induce an adapted response from the cells, the MAPK modules signal to a combination of specific or common substrates to generate multiple outputs (Schaeffer and Weber 1999). Overall the MAPK pathways have been reported to be involved in a plethora of cellular processes *e.g.* migration, division, and differentiation which are early cellular responses involved in regeneration.

Many MAPKs have been shown to be important for various context of regeneration. For example ERK has been shown to direct blastema formation in vertebrates and invertebrates, such as zebrafish (Vargas et al. 2011), axolotl (Makanae et al. 2013) and planarian (Tasaki, Shibata, Nishimura, et al. 2011). I will discuss this more in detail below.

2.1 MAPK signaling during regeneration

2.1.1 ERK

The role of the vertebrate MAPK ERK during regeneration has been described in several contexts. For instance, it is active and required for zebrafish fin (Varga et al. 2014) and heart regeneration (P. Han et al. 2014; P. Liu and Zhong 2017). In fin regeneration the inhibition of ERK impairs blastema formation (Varga et al. 2014), while in heart regeneration, ERK has multiple roles. After injury pERK is localized at the injury site and its activation increases during the first days of regeneration (P. Liu and Zhong 2017). The knockdown of the MAPKK MEK (activator of ERK) results in a failure of regeneration and in fibrosis, implicating this pathway in the wound healing process (P. Liu and Zhong 2017). Besides wound healing, MEK/ERK also regulates the proliferation of cardiomyocytes essential for heart regeneration (P. Liu and Zhong 2017). This contrasts with regeneration of urodeles, where ERK has only been described during limb regeneration where it is involved with the blastema formation (Makanae et al. 2013).

In invertebrate whole body regeneration like the one observed in Planarian, ERK is rapidly activated after bisection (Tasaki, Shibata, Nishimura, et al. 2011) and forms a decreasing gradient from head to tail, promoting the orientation of head regeneration (Goodman et al. 2009; Umesono et al. 2013). In this context, the activation of ERK1/2 is required for specialized stem cells, termed neoblasts, to exit their proliferative state and differentiate into multiple cell lineage. There is a negative feedback loop between the MAPK phosphatase-related gene, mkpA and ERK1/2 necessary for proper neoblast differentiation. This is also true for tail and pharyngeal regeneration (Tasaki, Shibata, Nishimura, et al. 2011; Agata et al. 2014; Umesono et al. 2013). Inhibition of ERK1/2 does not only keep the neoblast from differentiating

but it also impairs blastema formation, which is suspected to be linked to a default of the neoblast migration program (Tasaki, Shibata, Nishimura, et al. 2011). These studies of the role of ERK during planarian head regeneration highlight a dual role of this MAPK during blastema formation and neoblast differentiation.

In the freshwater hydroid *Hydra,* ERK plays a central role during head development (Arvizu, Aguilera, and Salgado 2006). Interestingly, this kinase is also involved in head regeneration since the inhibition of ERK by pharmaceutical drugs completely blocks head reformation (Manuel et al. 2006). Similarly to planarian regeneration, the response to injury, is marked by a strong and rapid phosphorylation of ERK 1/2 which is correlated to an important upregulation of both mRNA and protein level (González-Rosa et al. 2011; Petersen et al. 2015). This rapid response has been shown to be mediated by several pathways such as PKC, STK and PI3K to coordinate head regeneration (Manuel et al. 2006). Moreover at the cellular level other studies have demonstrated that the early activation of ERK1/2 is required to trigger apoptosis, which in turn will induce compensatory proliferation necessary for head regeneration (Kaloulis et al. 2004; Chera et al. 2011).

Here I've discussed a variety of roles for ERK during both vertebrate and invertebrate regeneration. Strikingly, ERK is mainly involved in the injury response as a conserved signal in regenerative context (Owlarn et al. 2017) and in regulating cell proliferation in general.

2.1.2 JNK

The MAPK JNK is described as stress-associated kinase. In zebrafish fin regeneration, JNK is activated by reactive oxygen species, a by-product of the injury response, which in turn induces cell proliferation (Gauron et al. 2013). This MAPK is also is involved in blastema formation, where it is required specifically for

regeneration-dependent cell proliferation, in contrast to homeostatic proliferation that occurs in fin growth independently of JNK (Ishida et al. 2010). This regeneration-dependent cell proliferation is mediated by the phosphorylation of multiple Jun effectors, such as JunbI. JunbI has been shown to be important for the maintenance of blastema while the phosphorylation of Junb is required to regulate gene expression in epidermal cells (Ishida et al. 2010). Surprisingly, JNK hasn't been investigated yet in the context of urodele regeneration.

In invertebrates, like planarians, JNK is important for wound healing (Tasaki, Shibata, Sakurai, et al. 2011) and the regulation of injury response genes including *egrl1* and *runt1* (Almuedo-Castillo et al. 2014). Besides wound healing, JNK is also required for regeneration at the anterior (Tasaki, Shibata, Sakurai, et al. 2011; Almuedo-Castillo et al. 2014) and posterior poles (Almuedo-Castillo et al. 2014; Tejada-Romero et al. 2015). During anterior regeneration, JNK is activated during formation of the post-blastema zone regrouping the proliferating neoblast, thus supporting blastema growth (Tasaki, Shibata, Sakurai, et al. 2011). JNK also plays an essential role in regulating neoblast cell cycle by controlling the S-phase/M-phase transition (Tasaki, Shibata, Sakurai, et al. 2011), by modulation of the G2-phase (Almuedo-Castillo et al. 2014). During posterior regeneration it has been shown that the MAPK cascade composed of MAKK hem (MKK7), the MAPK JNK and the transcription factor Junl-1 is required for tail regeneration, through activation of the Wnt pathway (Tejada-Romero et al. 2015)

Despite an obvious candidate to investigate in the presence of an injury, JNK pathway was only briefly investigated during *Hydra* regeneration (Philipp et al. 2009). In homeostatic tissue, *NvJnk* is expressed in nematocytes (cnidarians-specific cells), where it is co-expressed with nematocyte-differentiation genes, including *HvZic* and

HvNowa. These observations suggest an involvement of JNK during nematocytes differentiation during homeostasis (Philipp, Holstein, and Hobmayer 2005). The expression of putative effectors of JNK, *HvFos-like* and *HvJun* are upregulated after head amputation, according to transcriptomic data (Petersen et al. 2015). Upon inhibition of JNK by SP600125, this treatment induces a delay of tentacles regeneration (Philipp et al. 2009), potentially mediated by cJun phosphorylation (Philipp et al. 2009).

While several studies in different organisms including zebrafish and planarian have indeed described a role for JNK during regeneration this has not been tested in other regeneration models including *Hydra*. This disparity thus warrants further study of this molecule in different contexts.

2.1.3 p38

The MAPK p38, like JNK, has been characterized in stress conditions (Obata, Brown, and Yaffe 2000). Unlike ERK and JNK, there are relatively few vertebrate studies on p38 and regeneration. During zebrafish heart regeneration, inhibition of p38 doesn't impair the regeneration process (Jopling et al. 2012). This is in contrast to the constitutive activation of p38 by MKK6, which inhibits proliferation of cardiomyocytes, thus impairing regeneration (Jopling et al. 2012). In a similar manner, p38 inhibition by SD203580 in urodele primary myocell cultures, induces cell proliferation by promoting de-differentiation (W.-H. Kim et al. 2012). Altogether these studies of p38 in zebrafish and urodele strongly suggest that p38 is a common negative regulator of cell proliferation. To support this, similar effects on cell proliferation have been reported in other non-regenerative contexts. For instance, during mouse heart development, while cardiomyocytes are actively proliferating, the inappropriate activation p38 prevents this process (Engel et al. 2005). Meanwhile in

post-embryonic development, when cardiomyocytes are no longer proliferating, p38 inhibition recapitulates their proliferating behavior (Engel et al. 2005).

In *Hydra* and planarian, few study have investigated this p38. In one planarian regeneration study, the authors used the p38 inhibitor, SB203580, which showed no effect on regeneration, thus concluding that p38 was not implicated in this process (Tasaki, Shibata, Nishimura, et al. 2011). In *Hydra*, p38 hasn't been investigated, and is absent from the transcriptomic and phosphoproteomic analysis of *Hydra* injury response and regeneration (Petersen et al. 2015).

Overall, in contrast to ERK and JNK, p38 is potentially a negative regulator of regeneration by blocking proliferation. The MAPK kinase family regulates various cellular processes in different regeneration contexts and has comparable roles even in distant model systems from vertebrates to invertebrates (Table 1). These implications of MAPK during regeneration are part of the reasons I focussed on this family of kinases, to investigate whole body regeneration in *Nematostella*.

Table 1: MAPK implication during regeneration

Kinase	Model	Level of regeneration	Role	References
ERK	Zebrafish	Fin regeneration	Blastema formation	Varga et al. 2014
		Heart regeneration	Wound healing	Liu et al. 2017
			Cardiomyocyte proliferation	Han et al.2014, Liu et al. 2017
	Axolotl	Lim regeneraiton	Blastema formation	Makanae et al. 2013
	Planarian	Whole body regeneration	response to injury	Tasaki et al. 2011
			oral/aboral axis	Goodman et al. 2009; Nishimura et al. 2012; Umesono et al. 2013
			neoblast differentitation	Tasaki et al. 2011; Umesono et al. 2013; Umesono et al. 2014
			Blastema formation	Tasaki et al. 2011
	Hydra	Whole body regeneration	response to injury	Manuel et al.2006; Petersen et al. 2015
			apoptosis-dependent proliferaiton	kaloulis et al. 2005; Chera et al. 2011
JNK	Zebrafish	Fin regeneration	Injury response	Gauron et al. 2013
			Regeneration-specific proliferation	Ishida et al.2010
			Bastema formation	Ishida et al.2010
	Axolotl	-	-	-
	Planarian	whole-body regeneration	Apoptosis-response to injury	Almuedo-castillo et al. 2014
			modeulate proliferation	Almuedo-castillo et al. 2014; Tasaki et al. 2011b
			Blastema formation	Tasaki et al. 2011b
			Posterior regeneration	Romero et al. 2015
	Hydra	-	-	-

2.2 Growth factor signaling

Intercellular signaling is fundamental to the coordination necessary for developmental processes including embryogenesis and regeneration. One notable receptor/ligand family involved in such cell-cell communication, are the Receptor Tyrosine Kinases (RTK) also known as growth factors receptors (GFR) (Marshall 1995; van der Geer, Hunter, and Lindberg 1994; Lemmon and Schlessinger 2010). There are six families of GFR, the fibroblast growth factors receptors (FGFR) (Bertrand, Iwema, and Escriva 2014), the epidermal growth factor receptors (EGFR) (Earp, Calvo, and Sartor 2003), the vascular endothelial growth factor receptors (VEGFR) (Clauss 2000) the platelet-derived growth factor receptors (PDGFR) (Fredriksson, Li, and Eriksson 2004), the insulin-like growth factor receptor (IGFR) (T. E. Adams et al. 2000) and NGFR (Trk) (Meakin and Shooter 1992; Wiesmann et al. 1999). GFR membrane receptors are composed of three parts: each subunit has a single hydrophobic transmembrane domain, an extracellular N-terminal region, and an intracellular C-terminal region (Hubbard 1999) (Fig. 15). The extracellular N-terminal region is characterized by conserved structures such as immunoglobulin-like or epidermal growth factor-like domains, fibronectin type III repeats, or cysteine-rich regions. The N-terminal region determines the specificity of each family of RTKs and confers to the receptor its ligand specificity (*e.g.* growth factors, cytokines, and hormones). The intracellular C-terminal region presents the highest level of conservation and includes the catalytic domain responsible for the kinase activity of these receptors, thus, GFR have been classified according to this domain (Hanks and Hunter 1995). Mechanistically, it is the binding of a ligand to the extracellular domain of the receptor that will induce the dimerization of the GFR, allowing their

activation by auto-phosphorylation. Upon activation, a substrate is phosphorylated to initiate the intracellular signaling cascade (Lemmon and Schlessinger 2010).

Figure 15**:**

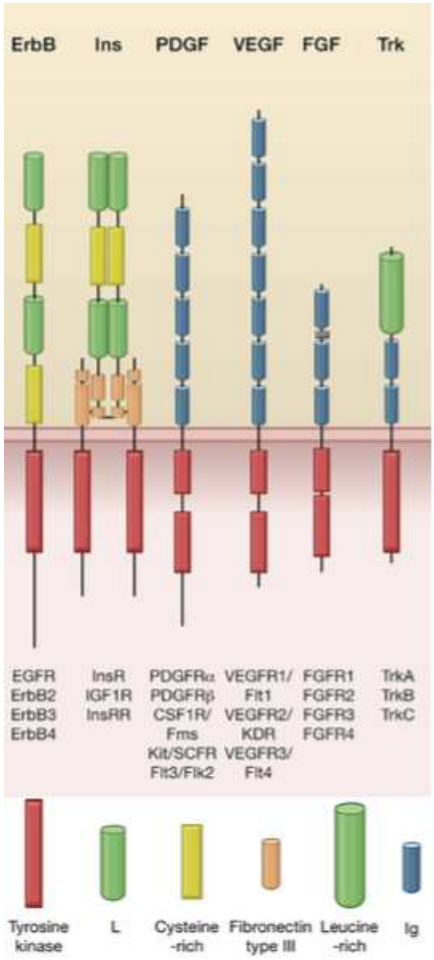

Human growth factor receptors structure

(from (Lemmon and Schlessinger 2010)**)**

2.2.1 Fibroblast growth factor pathway

The FGFR family appears early in animal evolution and were present in the common eumetazoan ancestor of Cnidaria and Bilateria (Bertrand, Iwema, and Escriva 2014; Rebscher et al. 2009). This GFR family of is well known to control key functions like cell and tissue movement, proliferation, differentiation, branching

morphogenesis and boundary formation (Affolter, Zeller, and Caussinus 2009; Kadam et al. 2009; Klingseisen et al. 2009)).

In zebrafish fin regeneration, the ligands Fgf24 and Fgf20a have been described to be involved in blastema formation and have been proposed to link the Fgfr1 receptor (Simões et al. 2014). Also the ligand Fgf20a and the receptor Fgfr1, were found expressed in the caudal fin blastema (Poss et al. 2000; Whitehead et al. 2005). Further studies have linked the Fgf pathway with blastema formation, since its inhibition lead to the failure of blastema formation (Poss et al. 2000). More precisely Fgfr1 was shown to be essential for cell proliferation during blastema formation (Y. Lee et al. 2005). During heart regeneration, Fgfr1 plays an important role as well. When Fgfr1 is knocked-down, heart regeneration fails and results in the formation of a scar (Lepilina et al. 2006). Other members of the Fgf pathway have also been described during heart regeneration, including the ligand Fgf17b which is expressed in the cardiomyocyte in response to injury, while the expression of the receptors Fgfr2 and Fgfr4 are only detected seven days later at the apical edge (Lepilina et al. 2006). During spinal cord regeneration, another set of Fgf pathway members have been implicated. In response to injury the expression of the ligand Fgf2, Fgf3 and Fgf8a is upregulated in association with the upregulation of Fgfr2 expression (Goldshmit et al. 2012). These data show that depending on the regeneration context, different sets of ligand and receptors of the Fgf pathway are expressed and associated to proliferation, migration different cellular behavior (Goldshmit et al. 2012).

Studies of urodele regeneration also display much evidence for the involvement of the Fgf pathway. It was known since the late 90's that this pathway controls the mitotic activity of salamander limb regeneration (Mescher and

Gospodarowicz 1979). Later it was reported that many Fgf ligand genes are expressed in this context *e.g fgf2*, *fgf4*, *fgf8* and *fgf10* (Christensen et al.2001; Christensen et al.2002; Han et al. 2001; Nacu et al. 2016; Makanae et al. 2014). Moreover, denervation experiments have shown that nerve cells serve as a source of Fgf ligands (Han et al. 2001; Mullen et al. 1996; Makanae et al. 2013; Makanae et al. 2014). However, the Fgf pathway is only able to initiate blastema formation through Fgf2 and Fgf8 and needs other factors to complete limb regeneration (Makanae et al. 2016). As for central nervous system (CNS) regeneration there is evidence of Fgf pathway involvement, given the upregulation of Fgf1 and Fgf4 expression in ependymal cells after spinal cord transection (Fahmy and Moftah 2010; F. Zhang et al. 2002; F Zhang et al. 2000). Similarly, in zebrafish, there is a differential expression of Fgf ligand according to the regenerative context, even though it is still lacking information about the implicated receptors.

In the planarian genome, two Fgf receptors, Fgfr1 and Fgfr2 have been identified (Cebrià et al. 2002). The receptor Fgfr1 has also been described to be expressed in the forming blastema, specifically accumulating in either brain or pharynx forming cells (Ogawa et al. 2002). There is a third Fgfr-like found in the planarian genome called Noudarake (Nkd). NKd lacks the kinase intracellular domain, thus potentially acting as a dominant-negative of Fgfr. When Ndk is knocked-down, the effect is ectopic brain formation in homeostatic tissue and regeneration alike (Cebrià et al. 2002). Similar to *Hydra* there is no evidence of a specific involvement of Fgf pathway in head regeneration (Agata and Umesono 2008).

In *Hydra*, despite being largely studied as a model of whole-body regeneration, the evidence of the involvement of the FGF pathway is scarce. The sole receptor described until now is the Fgfr-like receptor HvKringelchen, shown to be involved in the asexual reproduction process of *Hydra* (Sudhop 2004). Among the putative ligands of this Fgfr-like, there are only four of them (Krishnapati and Ghaskadbi 2013; Lange et al. 2014): HvFgfa, HvFgfc and HvFgfe that are expressed in the entire polyp, while HvFgff is expressed in all terminal region including the tip of the tentacles, foot and base of buds (Lange et al. 2014). Since the discovery of these ligands, there are no direct studies of this pathway during regeneration.

Despite many vertebrate regeneration studies highlighting the importance of Fgf pathways in the initiation of the blastema as well as being a conserved pathway in multicellular organisms, the role of the Fgf pathways during invertebrate whole-body regeneration is as yet largely unstudied.

2.2.2 Epidermal growth factor pathway

The Epidermal growth factor pathway (Egf) is also highly conserved during evolution. The Egf receptor (Egfr) is found in virtually all metazoa, from sponges to mammals, with the only exception being the cnidarians (D'Aniello et al. 2008). The vertebrates posses four class of receptors: Egfr (or ErbB1, HER1), ErbB2 (HER2, p185, neu) ErbB3 (or HER3, p160) and ErbB4 (or HER4), which function by dimerization (homo- or hetero-dimerization) upon ligand fixation. This family of receptors can bind multiple types of ligand besides the putative EGF, such as TGF-α, heparin-binding EGF-like growth factor (HB-EGF), amphiregulin (AR), betacelllulin (BTC), epiregulin (EPR), epigen and neuregulin (NRG) (Harris, Chung, and Coffey 2003; Laisney et al. 2010).

The EGFR pathway has been described to be important for regeneration of the zebrafish tail (Rojas-Muñoz et al. 2009), heart (Gemberling et al. 2015) and retina (Wan et al. 2012). During tail regeneration of Zebrafish embryos, *erb2* expression is activated at the injury site (Rojas-Muñoz et al. 2009). Furthermore, inhibition of EGFR by D168393 and AG1478 provokes a drop in cell proliferation and blocks regeneration. This finding was confirmed in Erb2 and Erb3 mutant knockouts (Rojas-Muñoz et al. 2009). In a similar manner, during heart regeneration, the inhibition of EGFR by AG1478 treatment reduces cardiomyocyte proliferation. Also, upon injury the expression of *nrg1* is upregulated in cardiomyocytes proliferating and its overexpression enhances cardiomyocyte mitotic activity (Gemberling et al. 2015). Moreover *ngr1* is also co-expressed with its putative receptors *erb2* and *erb3* (Gemberling et al. 2015), suggesting a control of proliferation by Erb2 and Erb3 receptors associated with Ngr1 ligand. In retina regeneration, EGFR pathway is also important for the control of proliferation and it is mediated by the ligand Hb-EGF and the MAPK ERK (Wan, Ramachandran, and Goldman 2012). Altogether these data highlight a common role of EGF pathway on activating proliferation in response to injury.

In urodele limb regeneration, inhibition of ErbB2 by Mutrinib resulted in an aberrant collagen deposit, suggesting impaired wound healing (Farkas et al. 2016). Interestingly, another study has shown the interaction between EGFRs and MAPK ERK pathway regulating the expression of matrix metalloproteinase 9, necessary for extracellular matrix remodeling during salamander limb regeneration(Vinarsky et al. 2005; Satoh et al. 2008). While, ErbB2 inhibition also decreased proliferation during the blastema formation, *nrg-1* was also described to be expressed in proliferating

cells in the blastema, thus suggesting that Nrg-1 is signaling through ErbB2 to activate cell proliferation in the blastema (Farkas et al. 2016).

The planarian genome encodes for six EGFRs and nine putative EGF ligands, eight EGF-like ligands and one NRG. In homeostatic tissue, the distribution of their expression profiles forms various pattern in the organism (Barberán et al. 2016). Overall ligands are mainly expressed in mature differentiated cells, while receptors are mostly expressed in sub-classes of neoblasts (Wagner, Wang, and Reddien 2011; Scimone et al. 2014). In regeneration, three EGFR have been well described. In 2011 Fraguas et al., described *smed-egfr-3* generally expressed in neoblasts and that RNAi mediated knock-down led to impaired regeneration. Although, blastema formation wasn't affected, regeneration couldn't proceed normally, implying the requirement of smed-egfr-3 for blastema cell differentiation (Fraguas, Barberán, and Cebrià 2011). Interestingly, a previous study has shown that ERK inhibition phenocopies the knockdown of *smed-egfr3* (Tasaki, Shibata, Nishimura, et al. 2011). Moreover, knockdown of *smed-egfr-3* also prevents phophorylation of ERK (Fraguas et al. 2017) suggesting that the control of differentiation by *smed-egfr-3* is mediated by ERK signaling. Similarly, the disruption of *smed-egfr-1* by RNAi, also leads to an abnormal regeneration of the digestive system, with an impaired differentiation step. In this context, the control of mitotic activity and proper differentiation of the gut was proposed to be mediated by the receptor smed-EGFR-1 and the lignad smed-NGR-1 (Barberán, Martín-Durán, and Cebrià 2016; Lei et al. 2016). As such, when both are disrupted, it leads to neoblasts hyper-proliferation causing an accumulation of progenitor cells in the mesenchyme (Barberán, Martín-Durán, and Cebrià 2016). The gene expression of *smed-egfr-5* and *smed-egf-6* is also described to be linked to the differentiation process of planarian specific cells, called flame cells (Fraguas,

Barberán, and Cebrià 2011; Barberán, Martín-Durán, and Cebrià 2016), which have kidney-like function. Overall, the EGFR pathway plays an important role in the differentiation of neoblasts during regeneration.

Curiously the Egf pathway appears to have different roles in vertebrates and invertebrates. During vertebrate regeneration Egf pathway is activating cell proliferation, contrasting with invertebrate regeneration, during which the Egf pathway is regulating cell differentiation.

2.2.3 Vascular endothelial growth factor and Plateled-derived growth factor pathways

In contrast to Fgf and Egf pathways the vascular endothelial growth factor (Vegf) and the platelet-derived growth factor (Pdgf) pathways are less conserved evolutionarily. These two pathways are mostly described in vertebrates, notably the Vegf pathway was named according to its effect on vascular endothelial cells during vasculogenesis (the formation of the circulatory system) and angiogenesis (the growth of blood vessels from pre-existing vasculature). Likewise, the name of PDGF was attributed to the induction of cell growth by factors released from activated-platelets. Even thought, the discovery of these pathways was tightly connected to blood vessel formation they have also been described to play important roles during regenerative processes as reviewed below.

In Zebrafish, Vegf pathways has been described during fin regeneration (Bayliss et al. 2006; Khatib et al. 2010) and heart regeneration (Marín-Juez et al. 2016), while the Pdgf pathway has been described during heart regeneration (Lien et al. 2006; J. Kim et al. 2010). In the case of fin regeneration, the gene ligands *vegf-a* and *vegf-c* are expressed in the regenerating tips (Bayliss et al. 2006; Khatib et al. 2010) co-localizing with expression of the blastema marker *msx* alongside the

expression of *vegfr-2* receptor (Bayliss et al. 2006). Curiously, the treatment with Vegfr inhibitor PTK787 doesn't block fin regeneration but only impair re-vascularization of the reforming fin, which matches the loss of *vegfr-2* expression (Bayliss et al. 2006). Therefore, suggesting that Vegf pathway is specifically required for regenerating the vascular system of the re-growing fin. In a similar manner, *vegf-c* is also expressed in response to injury during heart regeneration (Lien et al. 2006), alongside *vegf-aa* (Marín-Juez et al. 2016). Interestingly, Vegf-aa mutants are unable to regenerate properly after heart injury, which is linked to a reduced proliferation and a disorganized re-vascularization (Marín-Juez et al. 2016). Therefore, showing the involvement of Vegf pathway in regenerating the vascular system.

The Pdgf pathway is also implicated during heart regeneration of zebrafish, where the expression of the ligand *pdgf-a* and *pdgf-b* is upregulated in response to injury alongside the expression of the receptor *pdgfr-alpha*. In contrast to the Vegf pathway, inhibition of PDGFR by AG1296 does not affect re-vascularization but instead it decreases cardiomycytes proliferation (Lien et al. 2006).

In Urodeles, the Vegf pathway and the Pdgf pathways have been respectively investigated in tail and limb regeneration (Ritenour and Dickie 2017; Currie et al. 2016). In comparison to zebrafish, the Vegf pathway has surprisingly a similar role in Urodel tail regeneration. The treatment with the Vegfr inhibitor PTK787 doesn't prevent tail regeneration but only the re-vascularisation (Ritenour and Dickie 2017). While the Pdgf pathway, during limb regeneration controls the blastema formation by promoting fibroblast migration (Currie et al. 2016).

In invertebrates genome instead of PDGF receptor (PDGFR) or VEGF receptors (VEGFR) but a single family related to both have been characterized in

Caenorhabtidis elegans and *Drosophyla*, known as Pvr (D'Aniello et al. 2008). In the genome of the cnidarian *Nematostella* there is a variant of this family, which has been described as PDVEGFR-like (D'Aniello et al. 2008). Although, this family has been presented as a member of VEGFR in *Hydra* (Reddy, Bidaye, and Ghaskadbi 2011) and in the jellyfish species *Podocoryne carnea* (Seipel et al. 2004). Nevertheless, in *Hydra* this pathway is thought to be important for regeneration, since its inhibition impairs the regenerative ability (Krishnapati and Ghaskadbi 2013). Besides *Hydra*, the VEGF pathway has also been described in the regeneration process of peripheral circulatory system of the ascidian *Botryllus schlosseri* (Tiozzo et al. 2008). However, none of the PDGF or VEGF pathways have been described yet during the planarian regeneration process.

The genomic differences between vertebrates and invertebrates concerning the Vegf and Pdgf pathway make comparisons more difficult. Nevertheless, in vertebrates the Vegf pathway displays strong conservation of its role during regeneration.

2.2.4 Insulin-like growth factor receptor

The Insulin-like growth factor receptor (Igfr) is different than the Insulin receptor involved in glycemia regulation and binds to IGF-1 or IGF-2 (Boucher, Tseng, and Kahn 2010; T. E. Adams et al. 2000). This family is conserved among vertebrates (LeRoith et al. 1993; Hernández-Sánchez et al. 2008), while in invertebrate, only an Igfr-like has been described in Drosophila (LeRoith et al. 1993).

In zebrafish fin regeneration the Igf pathways is activated in response to injury (Chablais and Jaźwińska 2010). In fact, the ligand *igfb2* is upregulated in the forming blastema and the receptor IGFR is phosphorylated in the wound epidermis covering the forming bastema (Chablais and Jaźwińska 2010). Chablais et al., have shown

that the inhibition of Igfr with NVP-AEW541 or NVP-ADW742 blocked blastema formation and was linked to a decrease in cells proliferation and an increase of apoptosis in the wound epidermis. Knockdown of *igfb2* by small inhibitory molecules called morpholinos, phenocopies this effect. The authors have thus concluded that the ligand Igfb2 is required IGFR signaling activation in the wound epidermis to regulate the blastema formation. In heart regeneration, the Igf pathway also plays an important role. Huan et al. have shown that *igf2* expression is activated at the injury site and inhibition of IGFR with NVP-AEW541 blocked regeneration (Huang et al. 2013). The authors have confirmed this phenotype with the over-expression of a dominant-negative *Igf1ra,* in which case wound healing resulted in the formation of a scar and a decrease of cardiomyocytes proliferation. Therefore, these two studies suggest a conservation of Igf pathway role in controlling proliferation during zebrafish regeneration.

While in heart regeneration context of Urodele, aside from the upregulation of *igfr* expression at injury site, there are no further information about its role in the regeneration process (Godwin et al. 2017). As for invertebrate regeneration, Igfr have been described in *Nematostella* (D'Aniello et al. 2008; Steinmetz et al. 2017) but there still no evidence of its link with regeneration.

2.2.5 The nerve growth factor receptor

The nerve growth factor receptor (NGFR) (Meakin and Shooter 1992; Wiesmann et al. 1999) has been described in vertebrate nervous system development but hasn’t been yet identified among invertebrates (van Kesteren et al. 1998). While in a regenerative context, such as in the zebrafish heart regeneration, the only available data come from a heart failure model in which NGF restores heart failure by promoting cardiomyocytes proliferation (Lam et al. 2012). In Urodele, NGF

has been shown to promote axonal regeneration of the optic nerve (Turner and Glaze 1977; Glaze and Turner 1978). Although evidence of an Ngf pathway requirement for regeneration is scarce, it seems nevertheless to be important for vertebrate regeneration.

This overview of the implication of kinases in various regeneration contexts is the basis of my PhD work concerning the identification of signaling pathway orchestrating the regeneration of *Nematostella*. Indeed, here I have assembled a body of evidence that according to the specific regeneration context, either vertebrate or invertebrate, show there are many commonalities concerning the regulation of general cellular processes, such as wound healing, proliferation or differentiation (Table 1 & 2). But the identification of signaling pathway during the regeneration of *Nematostella* is only one part of my whole PhD, which is to compare embryogenesis to the regeneration at the gene regulatory network (GRN). Therefore, in the up-coming section I will introduce the problematic of my work and the basis of GRN investigation.

Table 2: Gowth factor receptors implication in regeneration

Kinase	Model	Type of regeneration	Role	References
FGFR	Zebrafish	Fin regeneration	Blastema formation	Simoes et al. 2014; Poss et al. 2000; Whitehead et al. 2005
			Proliferation in the blastema	Lee et al. 2005; Lepilina et al. 2006
		Heart regeneration	Injury response	Lepilina et al. 2006
			Wound healing	Lepilina et al. 2006
		Spinal cord regeneration	Injury response	Goldsmith et al. 2012
			Cell proliferation	Goldsmith et al. 2012
			Cell migration	Goldsmith et al. 2012
	Urodele	Limb regeneration	Cell proliferation	Mescher and Gospodarowicz 1979
			Blastema formation	Han et al. 2011; Nacu et al. 2016; Makanae et al. 2016
		Spinal cord regeneration	Injury response	Fahmy et al. 2010; Zhang et al.2002
	Planaria	Whole-body regeneration	Involved in CNS reformation	Cebria et al. 2002
	Hydra	-	-	-
	Zebrafish	Fin regeneration	Respose to injury	Rojas-munoz et al. 2009
			Cell proliferation	Rojas-munoz et al. 2009
		Heat regeneration	Cardyomyocyte proliferaiton	Gemberling et al. 2015
	Salamander	Limb regeneration	Nerve dependent-cell proliferation	Brockes and Kintner 1986
			ECM remodeling/wound healing	yang et al. 1999; Vinarsky et al. 2005; Satoh et al. 2008, Farkas et al. 2016
			Cell proliferation	Wang et al. 2000; Farkas et al., 2016
	Planaria	Whole-body regeneration	Neoblast differentiation	Fraguas et al. 2011; Barberan et al., 2016
			Neoblast proliferation	Lei et al. 2016

Table 2: Gowth factor receptors implication in regeneration

Kinase	Model	Type of regeneration	Role	References
Vegfr	zebrafish	fin regeneration	re-vascularisation	Bayliss et al. 2006
		heart regeneration	response to injury	Lien et al. 2006; Marin-juez et al. 2016
			re-vascularisation	Marin-juez et al. 2016
	urodele	tail regeneration	re-vascularisation	Ritenour et al. 2017
Pdgfr	zebrafish	heart regeneration	response to injury	Lien et al.2006
			cardiomyocytes proliferation	Lien et al.2006
	urodele	limb regeneration	fibroblast migration	Currie et al. 2016
Pdvegfr-like	*Hydra*	whole-body regeneration		Krishnapati et al. 2013
Igfr	zebrafish	fin regeneration	blastema formation	Chablais et al. 2010
			Cell proliferation	Chablais et al. 2010
			Inhibition of apoptosis	Chablais et al. 2010
		heart regeneration	response to injury	Huan et al. 2013
			wound healing	Huan et al. 2013
			cardiomyocyte proliferation	Huan et al. 2013
Ngfr	zebrafish	heart regeneration	cardiomyocytes proliferation	Lam et al. 2012

3 Embryogenesis and Regeneration

An historical question in regeneration biology is the relationship between embryonic development and regeneration (Morgan 1901). This question arose from the observation that the exact same structures initially developed during embryogenesis, are reformed during regeneration (would it make sense to cite the paper from Vervoort here?) .

Since the re-emergence of regeneration in life sciences, several studies have attempted to address this question using primarily the above-mentioned regeneration models. Early experiments in axolotl clearly demonstrated that developing limb bud and regenerating limb blastema reciprocally recapitulate each other patterning of limb development (Muneoka and Bryant 1982; Muneoka and Bryant 1984). As such, a majority of the studies support the idea of a shared activation of candidate gene expression between the two developmental trajectories. These comes from studies in newt, (Imokawa et al. 1997), axolotl (Gardiner and Bryant 1996; Carlson et al. 2001) and *Xenopus* limbs (Wang & Beck 2014), chicken elbow joint (Özpolat et al. 2012), *Xenopus* lens (Malloch et al. 2009) and organs such as the zebrafish liver (Sadler et al. 2007) and Mouse pancreas (Jensen et al. 2005). However, another study has identified genes that are specific to nerve development but not nerve regeneration in *Drosophila* (Binari, Lewis, and Kucenas 2013). And again other studies have identified genes that are specifically expressed during regeneration in axolotl (Gardiner et al. 1995) and zebrafish (Millimaki, Sweet, and Riley 2010).

From this overview of studies that primarily compares single candidate genes or genes sets, it becomes apparent that the general question about the relationship between embryogenesis and regeneration warrants further attention. These approaches have been proven limited, especially since embryonic development and

regeneration are triggered by different signals; fertilization of a totipotent egg or the injury that activates a coordinated stress response in a predefined cellular environment (i.e differentiated tissues) but essentially there is a temporal barrier for such comparative study.

In this regard, unbiased and/or large scale approaches such as intra-specific comparative transcriptomics or gene regulatory network studies are required to provide additional insight into this question and enable us to decipher the genetic logic that is activated specifically in response to injury.

4 Development from a gene regulatory network perspective

Development is a series of events, which continuously increases the complexity of organismal structures until a homeostatic state is achieved. Therefore, development is structured as a hierarchy, meaning that one domain will give rise to more specified domains and so on, thus increasing its spatial resolution and functionality. To illustrate this hierarchy, in tripoblastic organisms the three germ layers, ectoderm, endoderm and mesoderm are not segregated until the gastrulation after a long series of cell fate decisions (DAVIDSON 2006). Indeed during the blastula stages preceding gastrulation, these germ layers are specified long before they give rise to endodermal, ectodermal and mesodermal structures (Fig. 16A), indeed the endomesoderm GRN is uptstream the endormal and mesodermal GRN (Fig. 16B). The genetic program supporting this development is encoded in the genome, but the expression of genes in the right time and place implies a structured regulatory system responsible for tightly tuning their expression.

Figure 16:

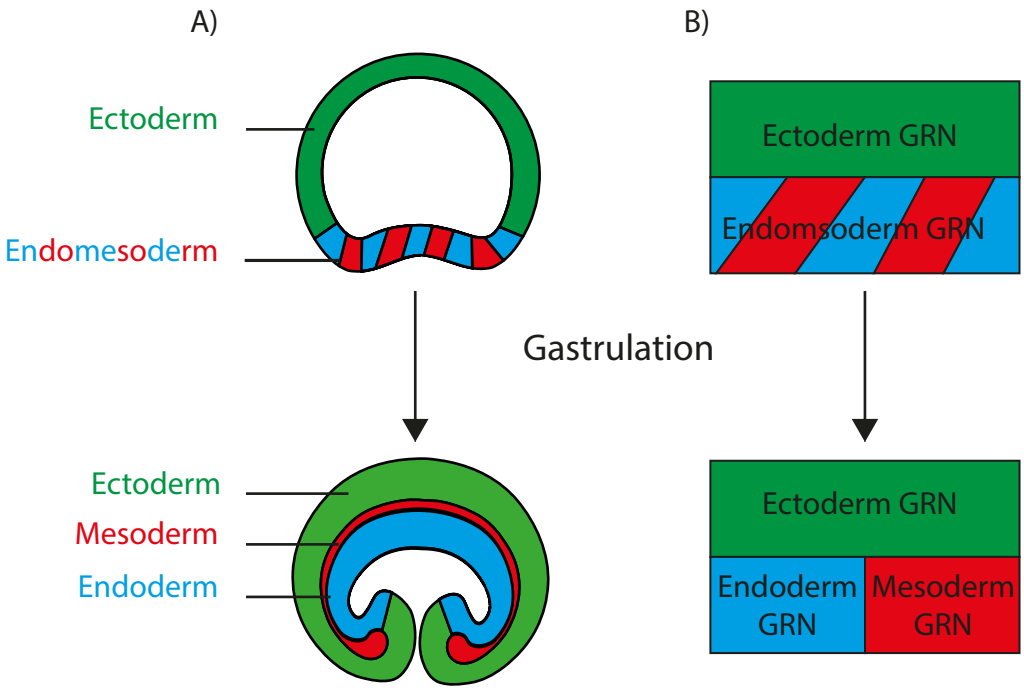

Germ layer specification diagram. A) Hypothetic example of a gastrulation event. B) Associated expression domain.

This regulatory system will also define the functionality and territorial specification, thus establishing the regulatory state represented by all genes expressed in a precise domain at a given time including transcription factors, signaling molecules and other effector genes (Peter 2017). The regulation of gene expression depends on two elements: a specific DNA sequence in the genome called a *cis*-element, participating to the regulation of promoter activity by recruiting *trans*-elements, which are genes that encode transcription factors or co-factors, that will bind to specific *cis*-elements. Depending on their combinations with other *trans*-elements and interactions with *cis*-elements, a gene promoter can be activated or silenced turning on or off gene expression. This association of *cis*- and *trans*-elements that modulate a gene's expression is called a *cis*-regulatory module (CRM) (DAVIDSON 2006). Therefore, the specific spatial and temporal expression of a

gene will depend on a combination of different CRMs. At a biological process level, several CRMs are associated to define a next regulatory-state, which is the fundamental driver of cell fate specifications and virtually all developmental processes. To illustrate this notion, in the example above concerning germ layer specification, the regulatory state of the endomesoderm, will proceed to define and give rise to the regulatory states of the segregated endoderm and mesoderm (Fig. 16B). Thus these regulatory states represent a causal link between the genome and gene expression which drive a biological processes, such as embryogenesis or regeneration and the summation of these states is what we term a gene regulatory network (GRN).

4.1 Topological model of GRN

The topological model of a GRN is a way to graphically represent the causal link between genomic information and spatially organized patterns. Each gene is represented by its CRM and the links forming the network are represented by the gene products interacting with another CRMs. For example the expression of a transcription factor, will bind to another CRM and subsequently activate the expression of that gene. Besides transcription factors, signaling molecules are also part of a GRN model, in order to visualize the communication between cells (Fig. 17. Overall the topological model contains all the possible interactions simplified as inputs and outputs (Fig. 17).

Figure 17:

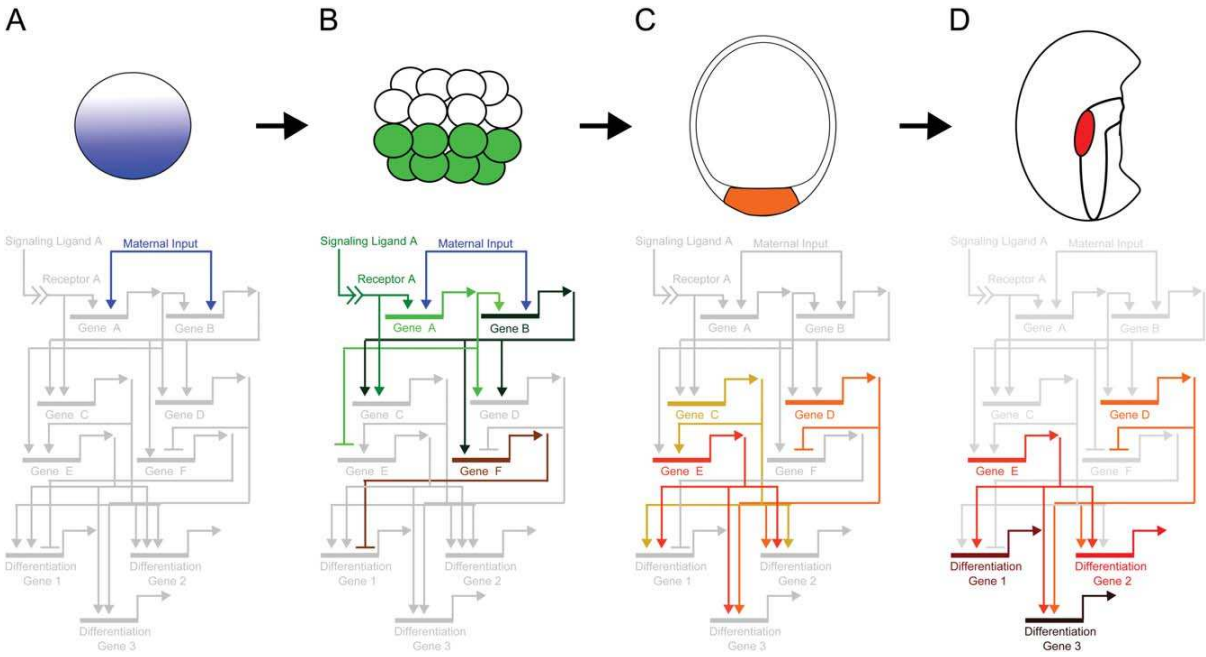

Gene regulatory networks explain developmental processes of cell specification over time. Top row is a schematic of embryonic development, bottom row is a schematic of a GRN that leads to specification of different territories. (**a**) A maternal input is localized asymmetrically in the egg and will activate a specific gene network in the only the cells that inherit this input. (**b**/**c**) Additional transcription factors are activated by the initial factors forming hierarchical networks. Signaling from adjacent cells can also affect the transcription of factors in "green" territory. (**d**) Differentiation genes are finally expressed only in the red territory because the temporal and spatial co-ordinates were appropriately coded by the upstream network (Hinman and Cheatle Jarvela 2014)

The linkages described in the model reveal different topologies in the network including auto regulatory loops where a gene can drive it's own expression; double negative gates where a repressor inhibits another repressor thus permitting a cell fate decision in a precise territory; and specification batteries that trigger cell fate commitment; just to name a few.

4.2 Experimental approach to establish a topological model

Establishing a GRN requires three fundamental steps: 1) Identification of the gene expression states; 2) Deriving genetic interactions, and 3) identifying the individual *cis*-regulatory modules (CRM)s in a gene.

The first step in establishing a GRN map is to define the regulatory state, which often means identifying genes expressed in the system of interest. This gene identification can be performed either by a candidate approach through qPCR or by using high-throughput technologies including, microarrays or RNA sequencing. This first step provides temporal expression information fundamental to a GRN. Thereafter, spatial expression can be surmised and this is traditionally performed by using *in situ* hybridization and now more commonly using single-cell RNA sequencing, in which gene expression can be directly linked to cell/tissue identity (Cao et al. 2017). This provides us with a map of gene expression from a spatio-temporal point of view.

Once expression states are known, the regulatory interactions must be defined. This can be achieved several ways including by a perturbation assay such as using a drug to disrupt a biological process and comparing the expression of genes in control and perturbed conditions to identify differentially expressed genes: those which are up-regulated or down-regulated. There are multiple perturbation strategies, including the knockout (KO) approach to generate a genetic null allele of a gene. Other methods include knockdown (KD) approaches, which disrupt mRNA translation or protein function. For instance, to interfere with mRNA translation, there are several tools available such as morpholino anti sense oligonucleotide (Draper, Morcos, and Kimmel 2001). This can be designed to interfere with RNA splicing by designing a morpholino complementary to a splicing site. Therefore, introducing

inappropriate, missed or cryptic splice patterns that inhibit protein function. A morpholino can also be designed to prevent the translation machinery by binding to the transcription initiation site. Other methods of gene expression perturbation depend on the organism and the presence of the RNA interference machinery (Hammond 2005): short hairpin RNA, small interfering RNA, micro RNA or Piwi interacting RNA approach can be use to direct the target gene mRNA toward the RNA interference machinery (Rao et al. 2009; Nandety et al. 2015). Interfering with RNA translation can also be complemented by perturbing the protein function through the introduction of a truncated form of a protein of interest *i.e* a dominant-negative form that will titrate the wild type function (Herskowitz 1987). The introduction of a dominant-negative form can be provided in various ways such as direct injection of the encoding mRNA, delivery of an expression plasmid, by transfection or soaking introducing recombinant plasmids via pre-soaked beads. In opposition to the KO approach, KD strategies induce only partial perturbations, thus combining them is essential to clarify the interpretation of the effects.

Overall, the choice of the strategy will be dictated by the model system and its amenability for functional studies but it also depends on the biological process investigated. For instance, all the strategies described in this section, are adaptable for embryology. In comparison, studying post-embryonic process such as regeneration, includes more intricate strategies, including inducible perturbation (KO or KD) requiring genome editing, which is more and more accessible with CRISPR/Cas9 technology (Doudna and Charpentier 2014).

After a perturbation strategy is optimized, we can perform a differential gene expression experiment. The gene of interest is inhibited and the potential downstream targets expression is measured by quantitative real time PCR (QPCR),

RNAseq. This will assess the type regulation exert by the gene of interest, including activator or inhibitor according to the downstream target. The level of expression measurement is integrated by a spatial analysis of the perturbation, to define a lost, restriction or expansion of expression domain. These quantitative and qualitative measurements will provide us with a map of the regulatory interaction between genes.

The final step of establishing a GRN to acquire the full depth of complexity of a genetic program is to identify the genomic sequence composing the CRM, which includes a *cis*-regulation assay. There are multiple approaches for resolving this part, which unfortunately still present many weak points. By its nature, identifying regulatory sequence is no easy task, since a regulatory sequence can be either upstream or downstream of a promoter and the genetic distances between them can be extremely variable. The fastest way to overcome this feature is to employ high throughput technology, such as Chip-seq (Park 2009), which can identify a panel of *cis*-elements bound by a transcription factor of interest. Nevertheless, such high throughput method still require experimental confirmation, such as reporter constructs where candidate CRMs are linked to a minimal promoter and fluorescent reporter, then serially mutated to identify the specific genetic sequences responsible for expression (Smith 2008).

Mapping the interactions between the genes during a biological process of interest and establishing a GRN, enables to understand the logic underlying the deployment of genome information. For instance, the comparative approach, between GRN across evolution has lead to the identification of a conserved circuit of genes called “kernel”, underpinning the endoderm specification across echinoderm and vertebrates (W.-F. Tseng et al. 2011; Davidson 2011). While, in my case I will

employ the GRN logic to investigate the relationship between two developmental processes in the same organism: embryogenesis and regeneration. And to do so, I took advantage of the biological features of the cnidarian *Nematostella vectensis*.

5 The cnidarian model system *Nematostella vectensis*

5.1 Cnidaria taxon in evo-devo

The Cnidaria taxon is well accepted as the sister taxon of bilaterians. They are characterized by the presence of stinging cells, nematocytes, which are found only in cnidarians. This taxon is divided into two clades, the Anthozoa and the Medusozoa. The former is composed of Scleractinians and Actinarians (broadly known as corals and sea anemones) while the latter contain the Hydrozoans, the Scyphozoans, and the Cubozoans (also known as jellyfish) (Fig. 18). Their body plan presents a radial symmetry and they develop from only two germ layers, the endomesoderm and the ectoderm, as opposed to the three germs layers of bilaterians (endoderm, mesoderm, and ectoderm). They are also devoid of any central nervous system and instead they exhibit a diffuse nervous system, called a nerve net (Arendt, Tosches, and Marlow 2016). These distinguishing features have attracted the attention of developmental biologist from the evo-devo field. Indeed the study of the cnidaria taxon offers the opportunity to investigate the emergence of the bilaterian developmental program and its underlying genetic toolkit (Technau and Steele 2011).

Figure 18:

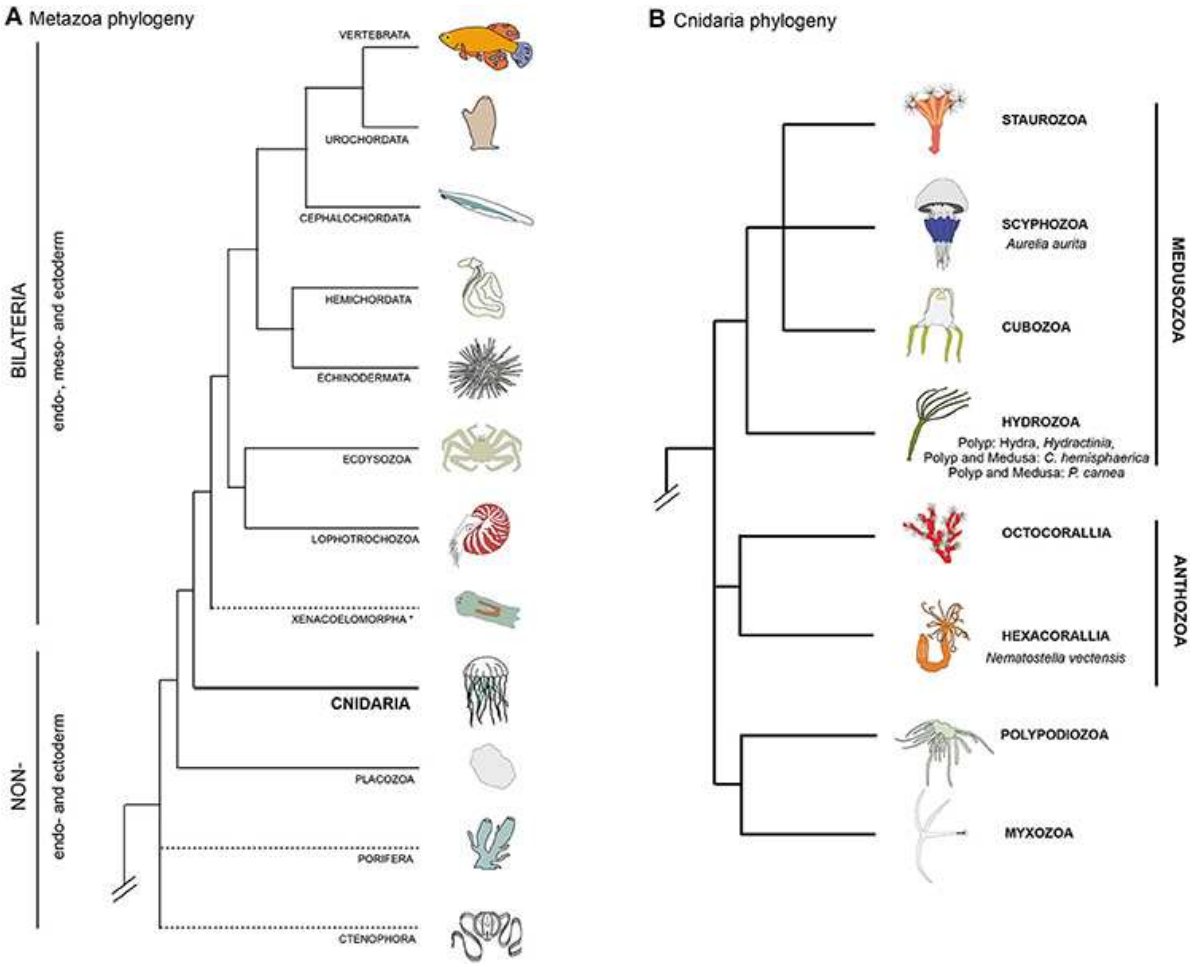

Bilaterian and cnidarian phyolgenies. (A) Metazoan phylogeny, highlighting the pivotal position of cnidarians as the sister group to extant bilaterian animals. The position of Ctenophora and Porifera (sponges) outside the Bilateria remains controversial (as indicated by dashed lines). **(B)** Cnidarian phylogeny showing the relationships between the main lineages based on recently published data (Leclère and Röttinger 2016)

While retaining a simple anatomy, advances in molecular biology, especially high-throughput technologies, have enabled the investigation of genetic programs underlying cnidarian development (Petersen et al. 2015; Stewart et al. 2017; Warner et al. 2018; Sebé-Pedrós et al. 2018),Warner et al, in submission). For instance the Wnt pathway is known to be involved in a plethora of developmental process among many taxa including animal vegetal axis formation in bilaterians. In cnidarians, the Wnt pathway is implicated in the initiation of the blastopore, thus highlighting the

homology between the oral-aboral axis of cnidarians to the animal-vegetal axis of bilaterians (P. N. Lee et al. 2006; Kusserow et al. 2005). Another example of a conserved axial patterning developmental pathway is the BMP signaling pathway, which is implicated in the dorso-ventral axis establishment in bilateria and has also been described during cnidarian embryonic development (Genikhovich et al. 2015). Despite the absence of dorso-ventral axis in cnidarians, this pathway is asymmetrically expressed similarly to bilaterians (Genikhovich et al. 2015). Additionally, as diploblastic organisms, cnidarians have also been used a model to investigated the evolution of segregation between endoderm and mesoderm (P. N. Lee et al. 2007; Wikramanayake et al. 2003; Röttinger, Dahlin, and Martindale 2012; Wijesena, Simmons, and Martindale 2017).

Altogether, these various field of study: nervous system development, axis patterning, and germ layer specification clearly demonstrate how the usefulness of cnidarians models for the investigation of evolution developmental processes in bilaterians.

5.2 The anthozoan Nematostella vectensis

Among cnidarians, the anthozoan *Nematostella vectensis* has been studied and cultured in laboratories since the early 90's (Hand and Uhlinger 1992). Indeed the ease of access to its embryonic material places *Nematostella* as an important embryonic model in comparison to hydrozoan and medusozoan models where the embryonic material was not always accessible for laboratory studies. Nevertheless, this has changed since the development of novel cnidarian models such as *Clytia* (Momose and Houliston 2007; Momose, Derelle, and Houliston 2008).

Figure 19:

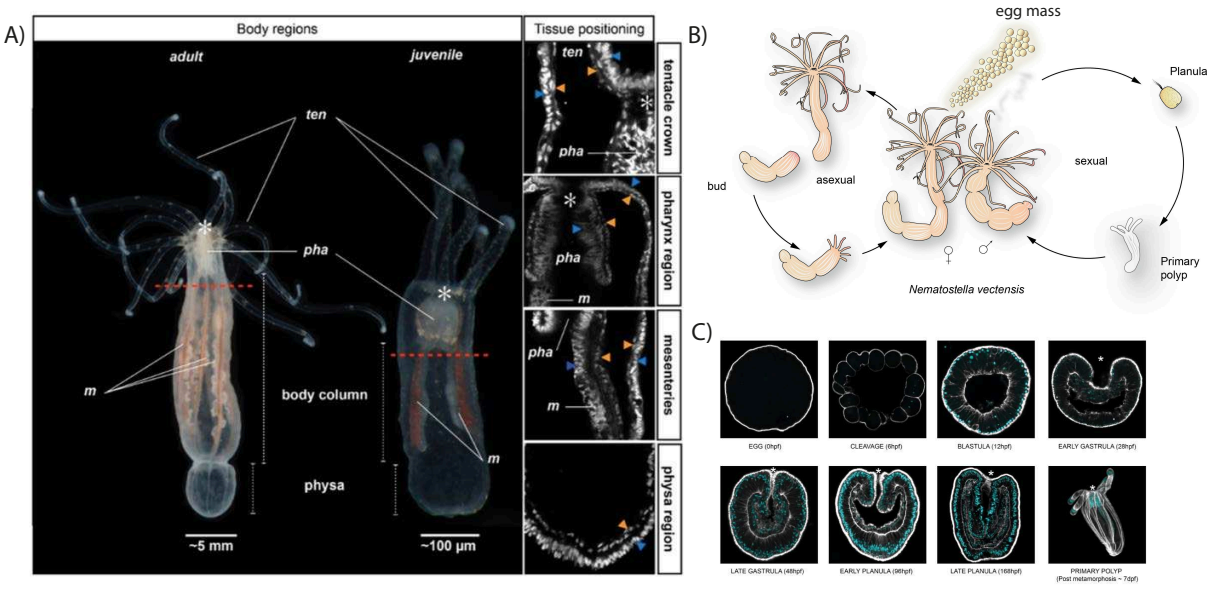

Cnidarian model system *Nematostella vectensis*. A. Photographs illustrating the general anatomy of adult (left) and juvenile (right) *Nematostella* oriented with the oral region to the top and aboral region to the bottom. Red dotted lines indicate the future amputation region to the top and aboral region to the bottom. Right panel is a close-up confocal stack images from nuclei DAPI staining. From top to bottom: tentacle; pharynx; mesenteries and physa regions. An asterisk (*) indicates the mouth opening. Orange and blue arrowheads indicate the gastrodermal and ectodermal epithelia, respectively. B) Life cycle of *Nematostella* representing asexual (left cycle) and sexual (right cycle) reproduction. C) Image of nuclei (DAPI - cyan) and actin (Phalloidin - white) staining representing *Nematostella* embryonic stages from the zygote stage to the primary polyp stage. * indicates the future oral opening. *ten, tentacles; ph, pharynx; m, mesenteries*. (Amiel et al. 2015);http://thenode.biologists.com/a-day-in-the-life-of-a-cnidarian-lab/lablife/;www.kahikai.org

The natural habitats of *Nematostella* are brackish estuaries and this sea anemone can be found on the coasts of the United Kingdom and north-eastern coasts of North American (Ref). The adult displays a simple morphology, composed of two tissue layers, the ectoderm and the gastroderm (also known as the endoderm or the endomesoderm) separated by an acellular matrix called the mesoglea. A crown of tentacles is located at the anterior pole of the body column where it surrounds the mouth, which itself is the most anterior part of the pharynx which forms the only opening between the external environment and the gastric cavity. Eight extensions of the pharynx termed mesenteries line the inside of the body

column and are responsible for digestion, in addition to carrying the gonads (Extavour et al. 2005; Steinmetz et al. 2017). This model is easily cultured in the laboratory, and can be maintained in non-circulating 1/3 seawater between 16°C to 22°C. Although *Nematostella* is capable of asexual reproduction through fission, they also reproduce sexually. Indeed when reaching sexual maturity, females will produce eggs that are embedded in a gelatinous mass. This is the only visible discrimination to males, which during spawning directly release sperm to the water (Darling et al. 2005). Under laboratory conditions spawning is induced by multiple stimuli, light, feeding, and temperature shock (Stefanik, Friedman, and Finnerty 2013).

Nematostella embryonic development is stereotypic, starting by symmetrical cell cleavages until a blastula develops (Fritzenwanker et al. 2007). From this stage the embryonic morphogenetic movements are initiated starting at gastrulation and proceed through invagination of the future endomesoderm, thus defining oral pole at the late blastula stage (Fig. 19C). Gastrulation (Fig. 19C), gives rise to the two germ layers: endomesoderm inside and ectorderm outside of the developing embryo (P. N. Lee et al. 2007; Röttinger, Dahlin, and Martindale 2012; Amiel et al. 2017). Thereafter, the pharynx will form from the blastopore, followed by the appearance of the first two mesenteries that are formed during the planula stage (Fig. 19C). After metamorphosis, the larva stops swimming, settles, and four tentacle buds develop at the oral pole during the primary polyp stage (Fig. 19C). From that point on, juveniles will slowly develop their tentacle crown and mesenteries until they reach the adult stage which exhibits eight mesenteries. In total the whole embryonic development occurs within a week at 22°C (Stefanik, Friedman, and Finnerty 2013). Since rearing *Nematostella* in artificial conditions is relatively simple, and one eggs mass contains

hundreds of eggs, it provides an easy access to biological material (Stefanik, Friedman, and Finnerty 2013).

5.3 *Nematostella vectensis* a perfect model to compare embryogenesis and whole body regeneration

As a model system in developmental biology, the genome of *Nematostella* has been sequenced and released in 2007 (Putnam 2007). With 450Mb it contains approximately 27,000 predicted genes with a surprisingly high degree of conservation to bilaterian gene sequences (Kusserow et al. 2005). Moreover the genome exhibits considerable stretch of sequences with conserved synteny and high conservation of intron-exon boundaries to vertebrate genomes (Putnam 2007).

Many molecular tools have been adapted to study *Nematostella* development. *Nematostella* is amenable for microscopy studies due to its size and semi-transparency of the embryos and juveniles. Thus, gene expression and protein localization studies are possible using *in situ* hybridization (Extavour et al. 2005; Genikhovich and Technau 2009) and immunohistochemistry (Extavour et al. 2005) respectively. Regarding functional studies, tools such morpholino based knockdowns (Magie, Pang, and Martindale 2005; Rentzsch et al. 2008; Layden, Boekhout, and Martindale 2012; Layden et al. 2013), mRNA mis-expression (Wikramanayake et al. 2003; Röttinger, Dahlin, and Martindale 2012; Layden et al. 2013), and transgenic reporter lines are also available (Renfer et al. 2010). Moreover with the development of CRISPR/Cas9 technology in *Nematostella*, allows for targeted knockout and is now routinely used in this system (Ikmi et al. 2014; Servetnick et al. 2017; Wijesena, Simmons, and Martindale 2017). Finally, high throughput technology such as ChIP-seq (Schwaiger et al. 2014), RNA-seq, (Tulin et al. 2013; Helm et al. 2013; Warner et al. 2018), and more recently single-cell RNA (Sebé-Pedrós et al. 2018) have been

adapted to *Nematostella*. This short listing of the toolkit for studying *Nematostella*, highlights the possibilities offered by this cnidarian model system to tackle a vast array of biological questions.

5.4 *Nematostella vectensis* as an embryonic model system

As previously discussed, *Nematostella* is a powerful model system for developmental biology studies, and it is used to investigate the evolutionary aspect of three major questions; axial patterning, mesoderm emergence and the development of the nervous system.

5.4.1 Early Oral-aboral axis patterning

Nematostella has been used to understand the relationship between the oral-aboral axis and the bilaterian anterior-posterior axis (AP axis). In bilaterians, the anterior pole is defined by the presence of a centralized nervous system and the site of future oral structures. Since cnidarians lack any centralized nervous structure, the oral pole has been defined according to the presence of the mouth and by default the opposite side was designated as the aboral pole.

The bilaterian hox genes have been used as markers of the AP axis in bilaterians but in *Nematostella*, despite having hox-like genes in its genome, there is no colinearity found with oral-aboral axis as opposed to the AP axis. Even though five anterior hox genes where found to be expressed in the pharynx during the planula stage (Finnerty et al. 2004) and two posterior hox genes where found to be expressed at the aboral pole (Finnerty et al. 2004). Yet the hox genes in *Nematostella* don't clearly specify the relationship between the oral-aboral axis and the AP axis. Instead, it has been demonstrated that *Nematostella* hox-like genes (Anthox6a, Anthox8, Anthox1a, Gbx), are required during radial segmentation,

suggesting an ancestral role of Hox genes in body patterning and axial segmentation before the evolution of the bilaterian AP axis (He et al. 2018).

Among other pathways investigated in Nematostella AP axis formation, the canonical Wnt / β-catenin (cWnt) pathway was an obvious candidate. Studies of cWnt pathway components during early embryonic development of *Nematostella* have shown the stabilization of β-catenin on one site of the 32-cell stage embryo (Wikramanayake et al. 2003; P. N. Lee et al. 2007). Subsequently, interference with this pathway, led to an abnormal endomesoderm specification and an abnormal pharynx (Wikramanayake et al. 2003; Röttinger, Dahlin, and Martindale 2012) therefore implicating the cWnt pathway in oral patterning. Indeed, investigation of downstream targets of the cWnt pathway, involving β-catenin and the transcription factor Tcf, showed that, they are expressed in staggered domains on the oral half of the blastula and Tcf is important for pharynx formation (Röttinger, Dahlin, and Martindale 2012). On the other hand the aboral pole of *Nematostella* has been shown to be under the control of the transcription factor Six3/6 as a key regulator (Sinigaglia et al. 2013). When knocked down the aboral pole is progressively re-specified into a more oral-like domain, indicated by the expansion of oral markers towards the aboral pole. Functional and expression data of oral patterning genes also suggest regulation from the oral pole (Sinigaglia et al. 2013). In summary, these data on *Nematostella* early oral-aboral patterning have highlighted conserved patterning genes and signaling pathways, playing similar role during bilaterians AP axis. Therefore the study of the GRN is necessary to reach a deeper understanding of this relationship.

5.4.2 The specification of germ layers in *Nematostella vectensis*

During bilaterian embryonic development, gastrulation gives rise to the ectoderm and the endoderm. Meanwhile the mesoderm is positioned between the endoderm and the ectoderm usually by means of an epithelial to mesenchymal transition (EMT). While the epidermis will arise from the ectoderm, internal organs are derived from the endoderm. Interstitial structures such as muscles are developed from the mesoderm. Non-bilaterians such as the cnidarian *Nematostella,* only develop from two germ layers. In this context the endomesoderm never segregates into the endoderm and mesoderm. Yet the gastrodermis derived from the endomesoderm has a bifunctionality; nutrient intake and contraction through myoepithelial cells (Jahnel, Walzl, and Technau 2014). Moreover, *Nematostella* endomesoderm will also exhibit endodermal and mesodermal markers such as Nvotx (Mazza et al. 2007; Röttinger, Dahlin, and Martindale 2012) and Nvgata respectively (Martindale, Pang, and Finnerty 2004). Taken altogether these observations suggest that the bilaterian endomesoderm genetic program shares some conserved features with that of cnidarians which potentially later evolved to segregate into endoderm and mesoderm. In order to gain novel insight into this hypothesis of segregation, researchers have investigated the GRN downstream of the cWnt pathway and the transcription factor Tcf according to its important role for patterning the presumptive endomesoderm of *Nematostella* (Röttinger, Dahlin, and Martindale 2012; Wikramanayake et al. 2003). By taking advantage of a microarray analysis, researchers have been able to identify 100 transcription factors and signaling molecules implicated in the specification of the endomesoderm. Moreover all the identified downstream targets of cWnt/Tcf are expressed at the oral pole, hence their link to the future internalized endomesoderm (Röttinger, Dahlin, and

Martindale 2012). Such an approach has enabled the establishment of the first GRN framework underlying endomesoderm specification in *Nematostella*. Furthermore, the genes NvfoxA, NvBra and NvOtx (A, B and C) have been identified in the presumptive endomesoderm of *Nematostella* (Röttinger, Dahlin, and Martindale 2012; Wijesena, Simmons, and Martindale 2017), which is comparable to the bilaterian endomesoderm specification sub network composed of Nvblimp1, Nvotx, Nvbra, NvfoxA and NvgataE (Hinman, Nguyen, and Davidson 2007) suggesting a potential conservation. Since the cWnt pathway is on of the earliest developmental signals to be activated during *Nematostella* embryogenesis, it is believed to be the most upstream input of endomesoderm specification. But interestingly members of the Fgf/Erk pathway are also part of the GRN, thus suggesting a possible involvement of this pathway during the specification of this germ layer (Röttinger, Dahlin, and Martindale 2012). Overall we can hypothesize that the bilaterian endomesodermal GRN derives from the cnidarians endomesoderm GRN.

5.4.3 Neurogenesis during Nematostella vectensis embryogenesis

The nervous system of *Nematostella* is comprised of a nerve net, spreading from both the ectoderm and the gastroderm, unlike bilaterian's highly structured nervous system (Marlow et al. 2009; Nakanishi et al. 2012). Expression of the earliest neuronal markers is reported to occur during the late blastula stage, before gastrulation, and exhibit a salt and pepper expression pattern (Marlow et al. 2009; Richards and Rentzsch 2015). The transcription factors NvSoxB2, NvAth-like and NvAshA (homologue of achaete-scute), known to be bilaterian proneuronal genes, are among the best candidate genes to drive *Nematostella* neurogenesis (Marlow et al. 2009; Nakanishi et al. 2012; Richards and Rentzsch 2015; Layden, Boekhout, and Martindale 2012). The genes NvanthoRFamide and Nvelav1 are used as

general markers of neuronal cell population (Layden, Boekhout, and Martindale 2012; Richards and Rentzsch 2014).

During Nematostella embryonic development, the first neuronal markers to be expressed are NvsoxB2 and Nvath-like expressed in proliferative cells (Richards and Rentzsch 2015; Richards and Rentzsch 2014), thus suspected to be makers of neuronal progenitors, in comparison NvashA and Nvelav1 are expressed in post-mitotic cells (Marlow et al. 2009; Nakanishi et al. 2012; Richards and Rentzsch 2015; Layden, Boekhout, and Martindale 2012). Indeed when NvsoxB2 or Nvath-like are knockeddown the expression of both NvashA and Nvelav1 are lost (Richards and Rentzsch 2015; Richards and Rentzsch 2014).

These findings thus give an overview of a neurogenic program during *Nematostella* embryogenesis and additional work has shown that the Notch signaling negatively regulate neurogenesis (Marlow et al. 2012; Layden and Martindale 2014). Yet the signaling pathway initiating the neurogenic program is still to be discovered. Overall, building a complete GRN underlying the neurogenesis of *Nematostella* will bring the opportunity to understand the relation with the bilaterian neurogenic program.

5.5 The extreme regeneration capacity of *Nematostella vectensis*

On top of being capable of sexual reproduction *Nematostella* can also reproduce asexually through a process of physal pinching (Reitzel et al. 2007) during which adults autonomously separate themselves from their most aboral structure termed the physa (Fig. 19A). Thereafter from the remaining piece of tissue a new individual arises, demonstrating a natural regenerative capacity. The mechanism behind the initiation of physal pinching remains unknown. Nevertheless the same regeneration events occur after the external stress of bisection, justifying the rise of

Nematostella in the field of regeneration, as a model of whole body regeneration (Darling et al. 2005).

Following bisection, *Nematostella* is capable of bidirectional regeneration, its physa will regenerate the oral half while the head will regenerate the aboral half (Darling et al. 2005; Reitzel et al. 2007; Schaffer et al. 2016). Therefore as a model system for developmental biology this sea anemone offers the unique opportunity to compare embryogenesis to whole body regeneration within the same animal. In opposition, well-established regeneration models, including *Hydra* and planarians, in which the access to embryonic material is less abundant (Martin et al. 1997; Wagner, Wang, and Reddien 2011). Conversely, traditional models in embryology such as drosophila, *Xenopus* or mouse display limited regenerative capacity. Zebrafish is a classical regeneration and embryonic model but is unable to perform whole body regeneration.

A first attempt of describing, the hallmarks of oral regeneration of isolated physa from adult *Nematostella* physal pinching has been published recently (Bossert, Dunn, and Thomsen 2013). The authors have reported five distinct morphological stages: stage 0, the open wound; stage 1, wound closed; stage 2, arching of the oral tissue; stage 3, appearance of tentacle buds; stage 4, mesenteries rearrangement; stage 5, complete reformation of the head (Bossert, Dunn, and Thomsen 2013). Despite being based solely on morphological observations, this staging system has illustrated a stereotypical progression of *Nematostella* oral regeneration.

Nematostella wound healing has been investigated after puncture of the body column (DuBuc, Traylor-Knowles, and Martindale 2014). In response to injury, the first cellular event reported was the presence of apoptotic cells followed by

actin enrichment around the puncture whole, two hours after injury. In terms of timing, wound closure was achieved in six hours, with almost no apoptotic cells left at the wound site (DuBuc, Traylor-Knowles, and Martindale 2014).

The vast majority of regeneration processes rely on cell proliferation to support replacement of lost structures (Tanaka and Reddien 2011), also witnessed during *Nematostella* regeneration following bisection (Passamaneck and Martindale 2012). As a matter of fact, in less than 24 hours, an accumulation of proliferative cells is observed at the amputation site, in the gastroderm, ectoderm and most oral side of the mesenteries (Passamaneck and Martindale 2012). This accumulation is then followed by a burst of proliferation, reasonably hypothesized to support the reformation of the head and tentacles (Passamaneck and Martindale 2012). Since the inhibition of proliferation blocks head regeneration, these results validate the importance of cell proliferation for the reconstruction of oral structures in *Nematostella* (Passamaneck and Martindale 2012).

At the molecular level very little is known about the genes and signaling pathways orchestrating *Nematostella* regeneration in comparison to embryogenesis. The first effort to identify genes involved in oral regeneration was focused on NvotxC, Nvfox and NvHox-*like* genes (Burton and Finnerty 2009), known to be expressed during embryogenesis (Martindale, Pang, and Finnerty 2004; Mazza et al. 2007; Finnerty et al. 2004)). Interestingly these embryonic genes seems to be re-expressed also during head regeneration even though the characterization of their expression profile by *in situ* hybridization have to be refined (Burton and Finnerty 2009). Nevertheless, these observations support a molecular relationship between *Nematostella* embryogenesis and regeneration. Moreover signaling pathways such as cWnt have also been implicated during regeneration (Trevino et al. 2011).

Following bisection and upon activation of this pathway using a pharmaceutical treatment, cWnt induces ectopic developmental axis leading to a multiple head phenotype. These studies confirm a deep relationship between the embryonic program and that of regeneration, given the fact that the cWnt pathway is also important for the specification of the oral domain during early steps of embryonic development (Röttinger, Dahlin, and Martindale 2012). Finally, during investigations of the wound healing process, the MAPK ERK has been shown to be implicated in the wound healing process and more generally for the whole regeneration process (DuBuc, Traylor-Knowles, and Martindale 2014). By using a microarray analysis after inhibition of MEK during the wound healing process this study has therefore provided for the first time a list of potential downstream targets of the MAPK ERK, and thus a starting point to build the GRN underlying wound healing.

6 Overview of my work

During my PhD I took advantage of the emerging regeneration model *Nematostella vectensis* to answer four main questions:

- What are the role and downstream GRN of MAPK ERK signaling during embryogenesis?
- What defines and characterizes the different steps of *Nematostella* regeneration?
- What are the signaling pathways orchestrating the different steps of regeneration?
- Is there a reuse of the embryonic program during whole body regeneration?

Nematostella has been used for over a decade to investigate the evolution of the genetic program underlying various aspects of embryonic and larval development. In particular, one study that studied in detail the role of cWNT signaling, has laid down the framework to decipher the GRN underlying endomesoderm specification prior to the onset of gastrulation (Röttinger, Dahlin, and Martindale 2012). As part of my PhD I worked on improving and extending this initial GRN and analyze the embryonic role and downstream targets of the MAPK MEK/ERK/Erg signaling pathway. This work yielded in the description of a global embryonic gene regulatory network highlighting the role MEK/ERK/Erg in axis patterning, germ layer specification and neurogenesis (Article 1, Article 2 - (Layden et al. 2016; Amiel et al. 2017)). Importantly, this study laid down the bases for the GRN level comparison of embryogenesis and regeneration that consisted in my overall aim of my PhD (see below).

Although the regenerative capacity of *Nematostella* was known since 1995 (Hand and Uhlinger 1992), only a few studies have characterized this feature. Unfortunately, these studies differed in their experimental approaches (age, dissection type, temperature) making it difficult to define particular hallmarks of regeneration. Thus, in another aspect of my PhD, I participated in a detailed morphological and basic cellular and molecular characterization of oral regeneration in *Nematostella*. This study enabled us to describe precise hallmarks of regeneration and develop tools to assess *in vivo* the morpholigical and cellular phenotypes of perturbation experiments (Article 3 - (Amiel et al. 2015)).

In addition, at the beginning of my PhD, very little information was available about the molecular mechanisms involved in the regenerative process in *Nematostella*. In order to gain molecular insight, I participated in a lab wide effort to establish a regeneration transcriptome covering the whole process of regeneration. These data, combined with existing and novel embryonic RNAseq data were implemented in a in-house developed public database that allows user to simultaneously visualize temporal embryonic and regeneration gene expression of their gene of interest (NvERTx.kahikai.org, Article 4 -(Warner et al. 2018)). Importantly, these transcriptomic resources played a major role in a global bio-informatics comparison of embryogenesis and regeneration that revealed that regeneration is only a partial re-activation of the embryonic program. In addition, this study revealed the existence of "regeneration-specific" genes and suggested that embryonic genes that are redeployed during regeneration are re-wired and interconnected with regeneration specific elements (Article 5 - Warner et al in submission).

While I was involved at various degrees in the above-mentioned studies (my contributions are addressed at the beginning of each result section), the main focus of my PhD was the comparison between embryogenesis and regeneration at the GRN level. I thus combined the findings and tools developed in the studies I was involved in, to focus on the role of MEK/ERK signaling during regeneration in *Nematostella* and decipher the underlying gene regulatory network. This work allowed me to i) identify a potential analogous role of MEK/ERK in launching morphogenesis during embryogenesis and regeneration and ii) functionally show that the embryonic program is partially redeployed, re-wired and connected to regeneration specific genes in order to reform lost body parts (Article 6 - Johnston et al. (a), in prep).

Finally, I initiated a kinase inhibitor screen in order to provide a global overview of potential signaling cascades involved in controlling the various phases of regeneration described in our first study on regeneration. This approach led me to identify several kinases that appear to be involved in orchestrating regeneration. In particular, I focused on investigating another MAPK, the stress-induced JNK and its role during the whole body regeneration process. This study enabled me to highlight a specific requirement of JNK that controls regeneration-specific proliferation at the onset of *Nematostella* regeneration (Article 7 – Johnston et al. (b), in prep).

Taken altogether, my PhD work has participated in establishing a novel whole body regeneration model, enabling me to address a historical question in the field and study the relationship between embryogenesis and regeneration at the gene regulatory network level.

Results

Chapter 1: The GRN underlying MEK/ERK signaling during *Nematostella* embryogenesis

This first chapter of the results section is constituted of two papers, concerning *Nematostella* embryogenesis. The overall aim of these related studies was to improve the resolution of the embryonic *Nematostella* GRN and in particular to decipher the roles and downstream targets of MEK/ERK signaling as well as its transcriptional effector, NvErg.

The downstream targets of MEK/ERK were identified using a genome wide microarray that served as a crucial support for both studies. The specific aim in(Layden et al. 2016) (2nd author, Article 1) was to decipher the neurogenic GRN downstream of MEK/ERK that gives rise to different neuronal cell types. As such I participated in the spatio-temporal characterization of the putative neuronal MEK/ERK targets that was used to establish the neurogenic GRN enabling us to identify specific neuronal population sub-networks.

In (Amiel et al. 2017) (co-first author, Article 2) the study was dedicated to decipher the specific roles of MEK/ERK signaling in germ layer specification and axial patterning prior to the onset of gastrulation. I participated in the spatio-temporal characterization of the MEK/ERK targets, performed a phylogenetic analysis of the Ets transcription factor family in *Nematostella* and participated in performing the experiments enabling us to determine that NvErg is one of the transcriptional effectors of a bipolar MEK/ERK GRN network signaling required germ layer specification and axial patterning.

Overall my input in these studies allowed us to laydown a global embryonic gene regulatory network that highlights the inputs of MEK/ERK signaling and that was crucial to compare embryogenesis and regeneration in *Nematostella* at the GRN level

Article 1: Layden, M. J., Johnston, H., Amiel, A. R., Havrilak, J., Steinworth, B., Chock, T., et al. (2016a). MAPK signaling is necessary for neurogenesis in Nematostella vectensis. BMC Biology, 1–19. doi:10.1186/s12915-016-0282-1

Article 2: Amiel, A. R. *, Johnston, H.*, Chock, T., Dahlin, P., Iglesias, M., Layden, M., et al. (2017). A bipolar role of the transcription factor ERG for cnidarian germ layer formation and apical domain patterning. *Developmental Biology*. doi:10.1016/j.ydbio.2017.08.015

(*) shared authorship

Article 1: MAPK signaling is necessary for neurogenesis in Nematostella vectensis.

Layden, M. J., Johnston, H., Amiel, A. R., Havrilak, J., Steinworth, B., Chock, T., et al. (2016).

BMC Biology, 1–19. doi:10.1186/s12915-016-0282-1

Layden et al. BMC Biology (2016) 14:61
DOI 10.1186/s12915-016-0282-1

BMC Biology

RESEARCH ARTICLE Open Access

MAPK signaling is necessary for neurogenesis in *Nematostella vectensis*

Michael J. Layden[1*], Hereroa Johnston[3], Aldine R. Amiel[3], Jamie Havrilak[1], Bailey Steinworth[2], Taylor Chock[2], Eric Röttinger[3] and Mark Q. Martindale[2*]

Abstract

Background: The nerve net of *Nematostella* is generated using a conserved cascade of neurogenic transcription factors. For example, *NvashA*, a homolog of the *achaete-scute* family of basic helix-loop-helix transcription factors, is necessary and sufficient to specify a subset of embryonic neurons. However, positive regulators required for the expression of neurogenic transcription factors remain poorly understood.

Results: We show that treatment with the MEK/MAPK inhibitor U0126 severely reduces the expression of known neurogenic genes, *Nvath-like*, *NvsoxB(2)*, and *NvashA*, and known markers of differentiated neurons, suggesting that MAPK signaling is necessary for neural development. Interestingly, ectopic *NvashA* fails to rescue the expression of neural markers in U0126-treated animals. Double fluorescence in situ hybridization and transgenic analysis confirmed that *NvashA* targets represent both unique and overlapping populations of neurons. Finally, we used a genome-wide microarray to identify additional patterning genes downstream of MAPK that might contribute to neurogenesis. We identified 18 likely neural transcription factors, and surprisingly identified ~40 signaling genes and transcription factors that are expressed in either the aboral domain or animal pole that gives rise to the endomesoderm at late blastula stages.

Conclusions: Together, our data suggest that MAPK is a key early regulator of neurogenesis, and that it is likely required at multiple steps. Initially, MAPK promotes neurogenesis by positively regulating expression of *NvsoxB(2)*, *Nvath-like*, and *NvashA*. However, we also found that MAPK is necessary for the activity of the neurogenic transcription factor *NvashA*. Our forward molecular approach provided insight about the mechanisms of embryonic neurogenesis. For instance, *NvashA* suppression of *Nvath-like* suggests that inhibition of progenitor identity is an active process in newly born neurons, and we show that downstream targets of *NvashA* reflect multiple neural subtypes rather than a uniform neural fate. Lastly, analysis of the MAPK targets in the early embryo suggests that MAPK signaling is critical not only to neurogenesis, but also endomesoderm formation and aboral patterning.

Background

Cnidarians (e.g., corals, sea anemones, and "jellyfish") are the closest group of animals to the Bilateria (all bilaterally symmetrical animals such as vertebrates, flies, and nematodes), and are thus an important taxon to understand the origin and evolution of complex traits such as nervous systems [1]. *Nematostella vectensis* is a proven cnidarian model because it is easy to maintain in laboratory culture, its genome is sequenced and annotated, and multiple tools exist for functional genetic approaches [1–6].

The *Nematostella* nervous system comprises endodermal and ectodermal nerve nets [7, 8]. Neuronal cell bodies are arranged in a "salt-and-pepper pattern" such that individual neurons are scattered amongst non-neural cell types. Differentiating neurons are first detected in the late blastula stage before invagination of the presumptive endodermal plate [7, 9]. Salt-and-pepper expression of both *NvsoxB(2)* and *Nvath-like* (also called *Nvarp3*) are the earliest known neurally expressed genes and they define proliferative neural progenitor cells [9, 10]. Shortly

* Correspondence: layden@lehigh.edu; mqmartin@whitney.ufl.edu
[1]Department of Biological Sciences, Lehigh University, Bethlehem, PA, USA
[2]The Whitney Marine Laboratory for Marine Science, University of Florida, St. Augustine, Florida, USA
Full list of author information is available at the end of the article

after *Nvath-like* and *NvsoxB(2)* are detected, expression of post mitotic neural markers such as *NvashA* and *Nvelav1* is detected [7–9, 11]. *Nvelav1* is broadly expressed in a large number of neurons, though it is still unclear if it is a pan-neuronal marker in *Nematostella* [8]. Morpholino (MO)-mediated knockdown of either *NvsoxB(2)* or *Nvath-like* results in a loss of expression of both *Nvelav1* and the neural subtype marker *NvashA* [9, 10]. *NvashA* is expressed in a smaller number of developing neurons at embryonic stages [11]. Functional characterization of *NvashA* clearly demonstrated that it is necessary and sufficient to promote expression of the neural marker *Nvelav1* and a number of putative neural subtype markers [11]. Based on previous work, a reasonable model for *Nematostella* neurogenesis is that Notch activity selects *Nvath-like* + *NvsoxB(2)* + neural progenitors from a pool of naïve cells; daughters of those progenitor cells express additional neurogenic genes such as *NvashA*, which in turn promote expression of post mitotic markers such as *Nvelav1* and neural subtype markers [1]. However, the upstream inductive mechanisms responsible for initiating neurogenic cascades in *Nematostella* remain elusive, as do the molecular programs that give rise to *NvashA*-independent neural subtypes during neurogenesis.

FGF, Wnt, BMP, and Mitogen-activated protein kinase (MAPK) signaling cascades regulate neural induction in multiple species [12–17]. FGF, Wnt, and MAPK all promote neural development in other species [12–14, 16], whereas BMP activity is best known for its role in suppressing neural induction of the forming central nervous systems of model systems [14, 15, 18]. In *Nematostella* the role of these signaling pathways during neural induction is unclear. Disruption of Wnt signaling does result in neural phenotypes. However, the phenotypes are attributable to disrupted axial patterning [19–21]. Neural phenotypes resulting from loss and gain of BMP activity are complicated in that either manipulation results in loss of neurons, and neural phenotypes are restricted to larval stages [22, 23]. FGF-mediated MAPK signaling is one of many ways to initiate a receptor tyrosine kinase (RTK) cascade. Investigation of FGF signaling in *Nematostella* has primarily focused on its role in apical organ formation, and no broad neural phenotypes are reported, with the caveat that the current array of neural markers did not exist at the time of the initial study [24]. To date, the impact of MAPK signaling on neurogenesis has not been reported in *Nematostella.*

RTK signaling cascades are characterized by a series of kinases that are activated by upstream kinase and in turn activate a downstream kinase. Near the end of the cascade, activated MEK kinase phosphorylates ERK, which can translocate to the nucleus to phosphorylate and activate a number of transcription factors. Multiple RTK signaling cascades converge on MEK. For example, in *Nematostella*, FGF signaling controls apical organ formation at larval stages, and pharmacological inhibition of MEK is able to phenocopy gene-specific MO-mediated knockdown of the FGF-receptor *NvfgfRa* [24]. The number of MAPK-like pathways that could be acting to regulate neural development in *Nematostella* is large. There are at least 12 FGF-like ligands and two FGF receptors in the *Nematostella* genome [2, 25]. Two ligands and one receptor (*Nvfgfa1*, *Nvfgfa2*, *NvfgfRa*) are expressed in the vegetal hemisphere/apical domain, the ligand *Nvfgf8* is expressed in the animal hemisphere and its descendants, and the receptor *NvfgfRb* in derivatives of both poles [24–26]. There are at least 25 additional receptors (Johnston & Röttinger, unpublished) that could activate MEK/ERK signaling in *Nematostella*. Because the number of possible RTKs is relatively high, one strategy to better understand how these genes might be acting to regulate neurogenesis is to inhibit MEK. Thus, a number of possible signaling pathways can be simultaneously disrupted to determine if MAPK signaling contributes to neural development.

Here we use U0126, a potent and specific inhibitor of MEK [27], to test if MAPK signaling plays a role in neurogenesis, and to determine if we can use this disruption to identify other putative neural genes in the early embryo. We show that treatment with U0126 reduces expression of *Nvath-like*, *NvsoxB(2)*, *NvashA*, and post-mitotic neural markers. Loss of embryonic neurogenesis following U0126 treatment cannot be rescued by *NvashA*, suggesting U0126 treatment desensitizes embryonic cells from responding to proneural cues. We performed a genome-wide expression array to identify new MEK downstream targets, enabling us to characterize 18 novel salt-and-pepper-expressed genes. We tested the role of the putative FGF receptor *NvfgfRa*, which was the most likely candidate pathway disrupted by U0126 in regards to neural marker expression. However, we found no evidence suggesting that *NvfgfRa* signaling regulates neurogenesis or any of the salt-and-pepper genes identified in the U0126 microarray. We also investigated the relationship of these novel salt-and-pepper genes with *NvashA*-dependent neurogenesis. We confirmed one positive and one negative target of *NvashA*, *Nvvsx-like* and *Nvath-like* respectively. Lastly, we expanded our study to gain insight into whether *NvashA* regulated one or multiple neuronal subtypes. Using transgenic animals and double fluorescent mRNA *in situ* hybridization, we confirmed that *NvashA* regulates at least two distinct neural subtypes; however, based on its expression pattern at later developmental stages [11], this number is likely much higher. Additionally, the identification of ~80 genes that are expressed in the presumptive endomesoderm and aboral pole suggests that MAPK signaling plays a key role in multiple aspects of *Nematostella* embryogenesis. Taken together, our data

and previously published results allow us to incorporate MEK, a key regulator, in a preliminary gene regulatory network describing embryonic *NvashA*-dependent neurogenesis, and provided us with a list of additional likely neurogenic genes, aboral genes, and endomesodermal genes for future studies.

Results

Determining ideal dose of U0126 to inhibit MEK inhibition

To determine the most effective concentration of U0126 to use for our analyses, we treated fertilized zygotes with increasing concentrations of U0126 and analyzed expression of the previously described U0126 target *Nvfgfa1* as well as two markers of the animal hemisphere, *Nvsprouty* and *Nvbra* [24, 25, 28, 29] (Fig. 1). *Nvsprouty* was expressed throughout a central domain at the animal pole in the presumptive endoderm (Fig. 1a, whereas *Nvbra* was expressed in a central ring surrounding the future endodermal tissue (Fig. 1h). These two additional markers were chosen because we observed gastrulation failures in preliminary tests of the U0126 compound on early embryos and, in bilaterians, expression of *sprouty* homologs is downstream of FGF signaling (Fig. 2) [30]. U0126 treatments of 1–10 μM reduced *Nvsprouty* expression, but had little to no impact on the expression of *Nvfgfa1* or *Nvbra* (Fig. 1a–d, g–j, m–p; Additional file 1: Table S1). However, at a concentration of 15 μM, both *Nvfgfa1* and *Nvsprouty* were undetectable in U0126-treated animals (Fig. 1e, q; Additional file 1: Table S1). Interestingly, treatment with 15 μM U0126 induced ectopic *Nvbra* expression within the endoderm-forming central domain (Fig. 1k, l), suggesting that MEK signaling actively represses *Nvbra* in the most central endoderm-forming domain. Based on the ectopic expression of *Nvbra* in the central domain as well as the complete inhibition of *Nvsprouty* and *Nvfgfa1* expression in 15 μM treatments (Fig. 1e, k, q; Additional file 1: Table S1), we concluded that 15 μM of U0126 is an effective dose, and it is unlikely phenotypes are due to toxicity.

Inhibition of MEK prevents ERK phosphorylation and gastrulation

To ensure U0126 treatment is inhibiting MEK, we screened embryos treated with either dimethyl sulfoxide (DMSO) as a control or U0126 for the presence of phosphorylated ERK (pERK) (Fig. 2) [31]. pERK staining in controls was detected at low levels in most cells of the blastula, but was enriched in the presumptive endoderm cells that undergo invagination (Fig. 2a). In U0126 treatments, a positive pERK signal above the general ectodermal staining was not detected (Fig. 2f). We further analyzed the morphological phenotypes induced by the

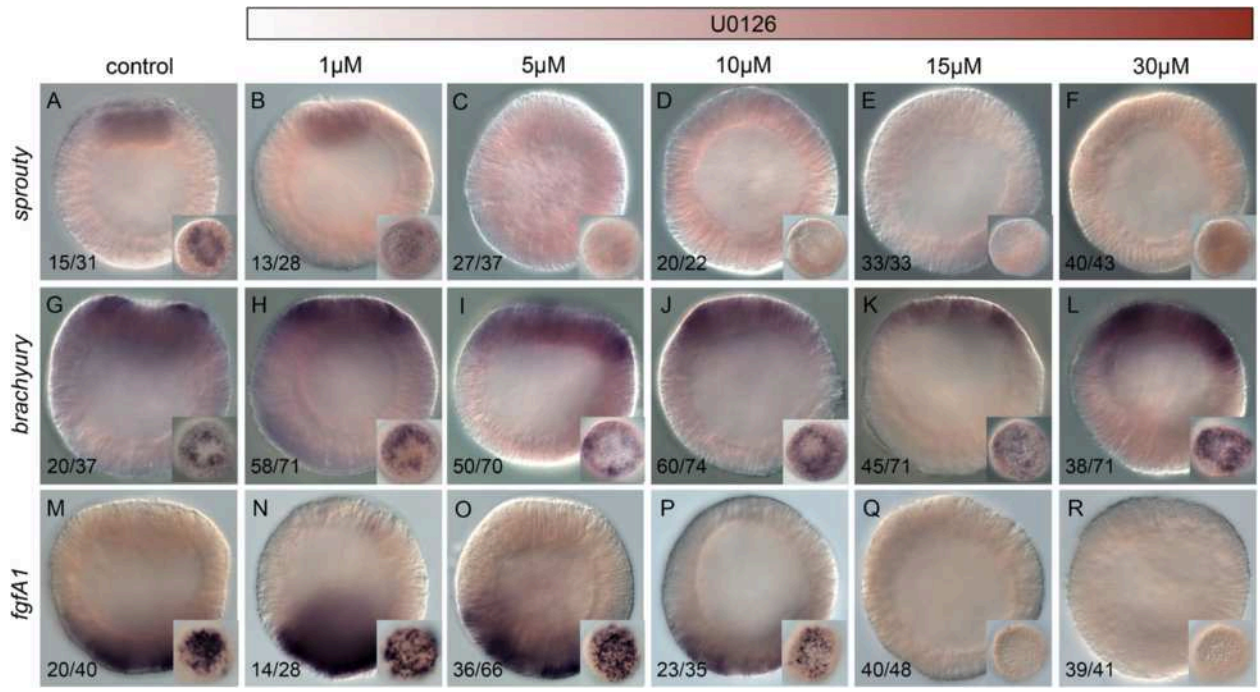

Fig. 1 Dose-dependent effects of the MEK inhibitor U0126 on embryonic gene expression. Control blastula stages at 24 hours post fertilization (**a, g, m**) and embryos treated with increasing concentrations of U0126 (**b**–**f**, **h**–**l**, **n**–**r**). In situ hybridization on blastula stages using *Nvsprouty* (**a**–**f**), *Nvbrachyury* (**g**–**l**), or *NvfgfA1* (**m**–**r**) antisense probes. All images are lateral views with the presumptive endomesoderm (animal pole, future oral pole) to the top. The insets correspond to animal pole views. Numbers in lower left corner correspond to the number of animals with phenotype pictured / total number of animals assayed

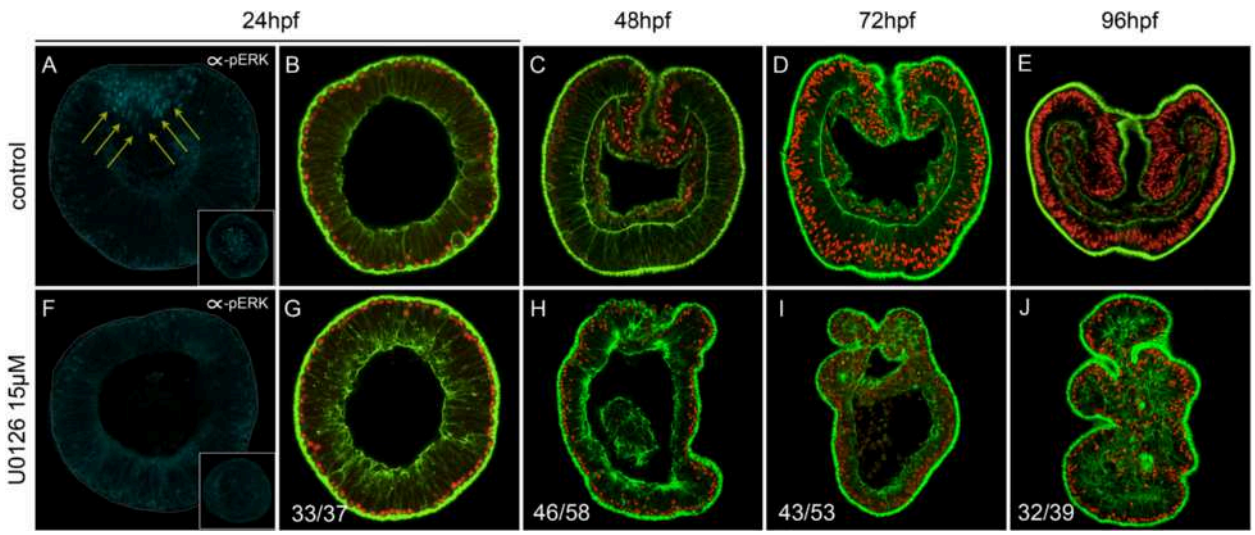

Fig. 2 U0126 blocks ERK activation, endomesoderm formation, and gastrulation. **a**–**e** Control embryos. **f**–**j** U0126-treated embryos. **a**, **f** Confocal z-sections using anti-phospho-ERK (*cyan*) to visualize activated ERK. The *gray* dotted lines indicate the outline of the embryo and *yellow arrows* the accumulation of phosphorylated ERK (*pERK*)-positive cells above background levels. **b**–**e**, **g**–**j** Confocal z-sections using phalloidin (*green*) to show f-actin filaments and propidium iodide (*red*) to visualize the nuclei. **a**, **b**, **f**, **g** Blastula stages [24 hours post fertilization (*hpf*)]. **c**, **h** Late gastrula stages (48 hpf). **d**, **i** Early planula (72 hpf). **e**, **j** Late planula (96 hpf). All images are lateral views with the animal/oral pole to the top. The insets in **a** and **f** correspond to animal pole views. Ratios in **g**–**j** indicate the number of embryos displaying the phenotype shown in the image to the total number of analyzed embryos

disruption of ERK signaling and observed that treated embryos dramatically failed to gastrulate and form a gut (Fig. 2g–j) compared to control embryos (Fig. 2b–e).

NvashA, *Nvath-like*, and *NvsoxB(2)* are globally downregulated in U0126-treated embryos

We next tested if U0126 treatment would disrupt expression of the known neural genes. We treated embryos with U0126 and scored for expression of known neural genes *NvashA*, *Nvath-like*, and *NvsoxB(2)* (Fig. 3). mRNA *in situ* hybridization on U0126-treated and control animals during early gastrula stages [24 hours post fertilization (hpf) at 17 °C] (Fig. 3) revealed that all three genes—*NvashA*, *NvsoxB(2)*, and *Nvath-like*—were globally reduced in U0126-treated animals (Fig. 3). However, they did not all display the same sensitivity to U0126. *Nvath*-like expression was undetectable in 82 % and *NvashA* expression was undetectable in 96 % of U0126-treated embryos (Fig. 3A, C). *NvsoxB2* expression was dramatically reduced, both in terms of the number of cells expressing it and in the level of expression (Fig. 3B), but expression was detectable in many more embryos than observed for either *NvashA* or *Nvath-like*. Interestingly, we identified *NvsoxB(2)* as being maternally expressed using the SeaBase database of transcriptomes (Additional file 2: Figure S1) [32–34]. To address whether or not U0126 might have a more severe impact on *NvsoxB(2)*, we treated animals at late gastrula stages for 24 hours with U0126 or DMSO control. We observed that *NvsoxB(2)* expression was not detectable in 87 % of U0126-treated cells (Additional file 3: Figure S2A). We also observed a strong reduction in *NvashA* expression in animals treated with U0126 for 24 hours after completion of gastrulation (Additional file 3: Figure S2B). These data suggest that the earliest known neurogenic transcription factors are globally reduced in U0126-treated animals, which indicates that neurogenesis is disrupted by U0126.

NvashA misexpression fails to rescue neurogenesis in U0126-treated animals

To test if U0126 treatment impacted neurogenesis, treated animals were allowed to develop until a time equivalent to the late gastrula stage and screened for expression of the broadly expressed neural marker *Nvelav1* and previously identified *NvashA* neural target genes by mRNA *in situ* hybridization. U0126 treatment dramatically reduced expression of neural markers, such that they were essentially undetectable (Fig. 4). Two exceptions were *NvLWamide-like* (PrtID# 242283, http://genome.jgi.doe.gov/Nemve1/Nemve1.home.html) and *NvanthoRFamide*, which showed staining in a few cells (Fig. 4A', 4H'), but both were reduced compared to control DMSO-treated animals. We conclude that treatment with U0126 results in a nearly complete loss of embryonic neural marker expression.

We next aimed to determine if loss of neural markers in U0126-treated animals could be rescued by misexpression of neurogenic transcription factors. *NvsoxB(2)* and *Nvath-*

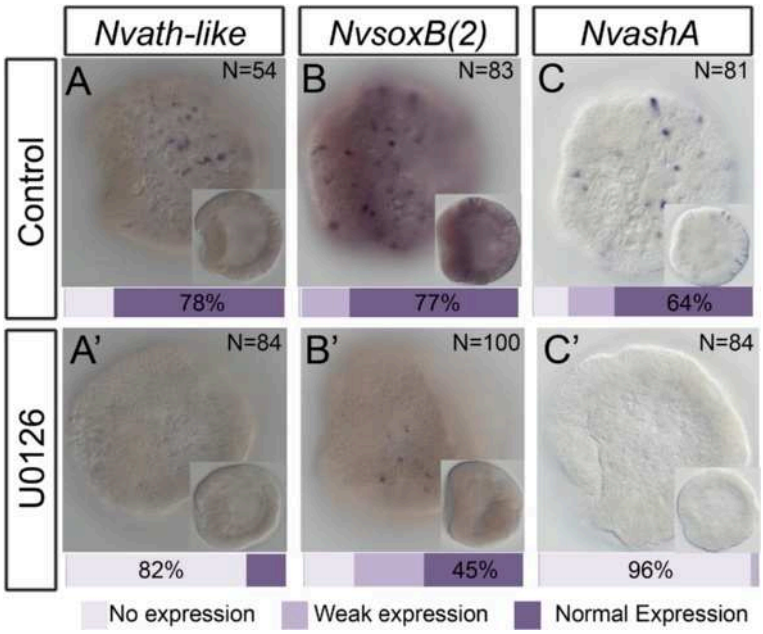

Fig. 3 U0126 treatment results in a global decrease in neurogenic transcription factors. mRNA *in situ* expression of *Nvath-like* (**A**), *NvsoxB(2)* (**B**), and *NvashA* (**C**) in control embryos treated with in 1/3× artificial seawater (ASW) with 0.1 % dimethyl sulfoxide (DMSO). Expression of *Nvath-like* (**A'**), *NvsoxB(2)* (**B'**), and *NvashA* (**C'**) in animals treated with 15 μm U0126 in 1/3× ASW with 0.1 % DMSO. Embryos were classified and quantified as the percent having normal expression, weak expression, or no expression. Refer to key in figure for classification of phenotypes. The phenotypic class with the highest percentage of embryos is indicated. All embryo images are of early gastrula stage. The main figure panels are ectodermal focal planes of lateral views with the presumptive oral side to the left. The insets show deeper focal planes used to confirm embryonic stage

like act upstream of *NvashA*, both have much broader roles than *NvashA* in neurogenesis, and both are expressed in neural progenitor cells [9, 10]. However, misexpression phenotypes are not reported for either of these genes. We were also concerned that over-activation of progenitor cell markers could result in a loss of neural markers due to an inability to transition from an undifferentiated to a differentiated state [35]. Thus, observing no rescue with misexpression of either *NvsoxB(2)* or *Nvath-like* could represent a false negative neural phenotype. *NvashA* is expressed in differentiated cells, and misexpression of *NvashA* has already been shown to be sufficient to induce ectopic neural marker expression [9, 11]. We injected in vitro transcribed *NvashA:venus* mRNA and treated animals with U0126. Surprisingly, we observed no rescue of the neural markers (Fig. 4A"–H"). To ensure that *NvashA:venus* behaves as previously reported [6, 11], we treated animals injected with *NvashA:venus* mRNA with U0126. High levels of NvAshA:Venus were still detectable and localized to the nucleus (Additional file 4: Figure S3). We conclude that *NvashA* is not sufficient to rescue neural marker expression in U0126-treated animals.

The failure of *NvashA* to rescue U0126-induced loss of neurogenesis might be a consequence of the reduced *NvsoxB(2)* and *Nvath-like* expression in U0126-treated animals. To address this hypotheses we took advantage of the previous observation that *NvashA* restores neural marker expression lost in animals with hyperactivated Notch signaling even though *NvsoxB(2)* and *Nvath-like* remain strongly downregulated [36]. To compare the downregulation of *NvsoxB(2)* and *Nvath-like* induced by hyperactivation of Notch to the downregulation observed in U0126-treated animals, we performed mRNA in situ hybridization experiments in *NvnotchICD:venus*-injected animals (Additional file 3: Figure S2). Injection of *NvnotchICD:venus* mRNA resulted in 83 % of animals showing no or weak *NvsoxB(2)* expression and 88 % of animals showing no *Nvath-like* expression (Additional file 3: Figure S2). Both genes were more severely reduced in *NvnotchICD:venus*-injected animals than they had been in U0126-treated animals (compare Fig. 3A, B to Additional file 3: Figure S2A, B). Taken together with previous reports that *NvashA* rescues neuronal loss induced by Notch hyperactivity without increasing *NvsoxB(2)* or *Nvath-like* expression, we argue that U0126 disrupts neurogenesis in two ways. It inhibits the expression of the neurogenic transcription factors *Nvath-like*, *NvsoxB(2)*, and *NvashA*, and it disrupts a yet unknown pathway that is also required for *NvashA* to promote neural fates.

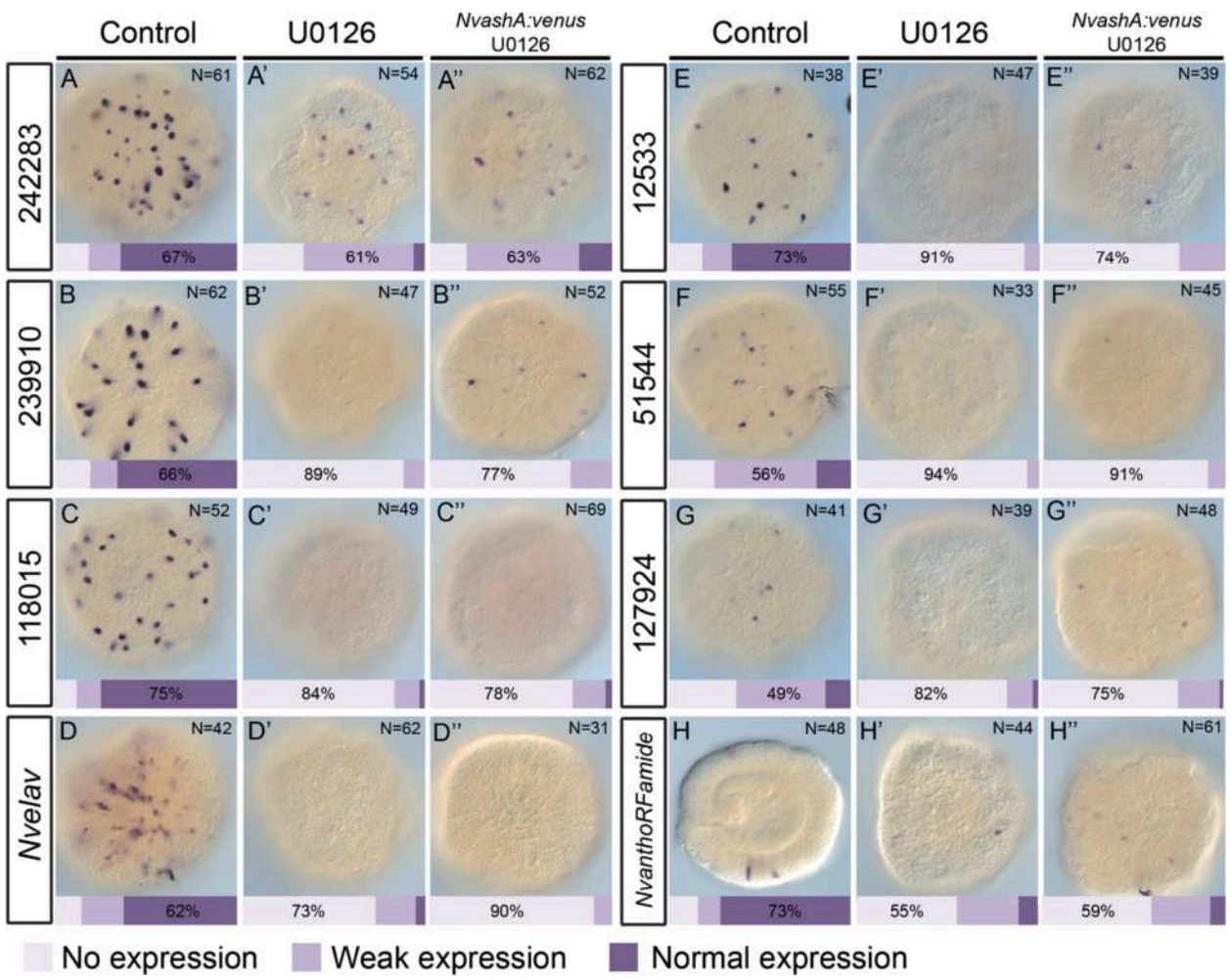

Fig. 4 *NvashA* is insufficient to rescue neuronal loss resulting from U0126 treatment. mRNA *in situ* expression of each gene is indicated in control embryos raised in 1/3× artificial seawater (ASW) with 0.1 % dimethyl sulfoxide (DMSO) (**A**–**H**), compared to embryos treated with 15 μm U0126 in 1/3× ASW with 0.1 % DMSO (**A′**–**H′**), and compared to embryos injected with *NvashA:venus* mRNA and treated with 15 μm U0126 in 1/3× ASW with 0.1 % DMSO (**A″**–**H″**). Genes are referred to by either name or protein ID number used in the *Nematostella genome* database v1.0 (http://genome.jgi.doe.gov/Nemve1/Nemve1.home.html). Embryos were classified and quantified as the percent having normal expression, weak expression, or no expression. The phenotypic class with the highest percentage of embryos is indicated. Treatment with U0126 strongly reduced all neural gene expression (compare **A′**–**H′** with **A**–**H**). Misexpression of *NvashA* in U0126-treated animals was not sufficient to rescue neuronal loss induced by U0126 treatment (compare **A″**–**H″** to both **A**–**H** and **A′**–**H′**). All animals in panels **A**–**G**, **A′**–**G′**, and **A**—**G″** are aboral ectodermal focal planes of 48 hours post fertilization embryos (late gastrula stage). Embryos in panels **H**, **H′**, and **H″** are a lateral view with oral side facing towards the left

NvashA target genes likely represent multiple distinct neuronal subtypes

We wanted to confirm that *NvashA* regulates multiple neuronal subtypes. Although *NvashA* is expressed in a subset of the nervous system, subtle differences in the expression domains of *NvashA* targets suggests that they describe distinct neural subtypes [11]. To test if *NvashA* regulates distinct neural subtypes we performed double fluorescent in situ hybridizations and created stable meganuclease-mediated transgenic reporters for two of the *NvashA* targets using an approximately 2000-base-pair genomic region immediately upstream of the start codon for both genes to drive expression of mCherry fluorescent protein (Fig. 5) [37]. We chose *NvLWamide-like* (PrtID# 242283) (Fig. 5a, b) and *Nvserum amyloid A-like* (PrtID# 239910) (Fig. 5a, c) because these genes represent *NvashA* targets with overlapping but slightly different expression patterns during development, and both genes were strongly downregulated in the U0126 microarray (see below; Additional file 5: Table S2, Additional file 6: Table S3). Both genes were expressed broadly throughout the aboral region of the embryo, but the *NvLWamide-like* expression domain extended more orally and encompassed a larger domain than that of

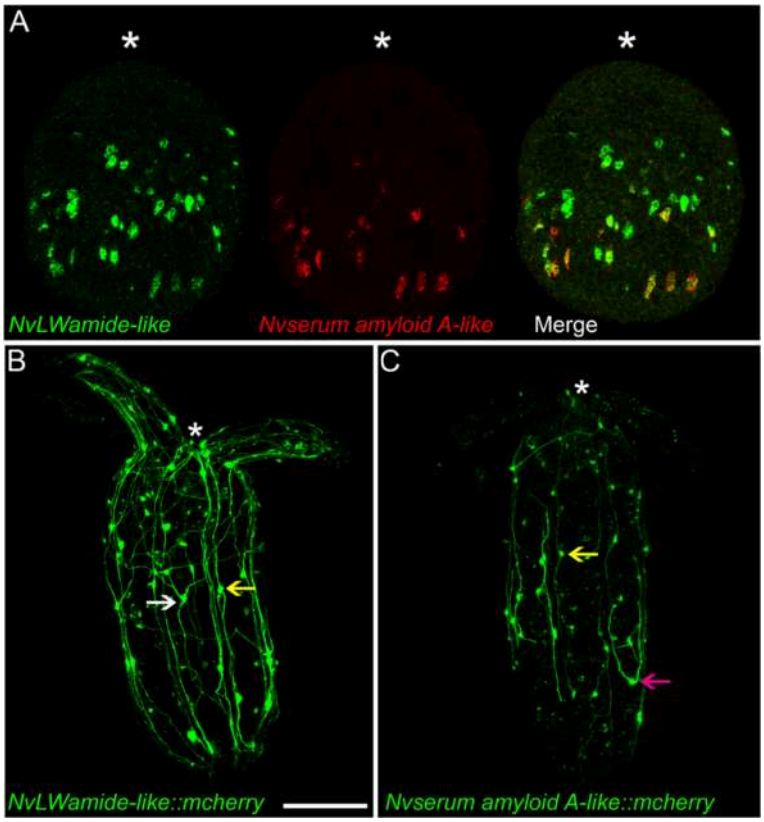

Fig. 5 *NvashA* regulates multiple neuronal subtypes. Shown are three-dimensional projections of two juvenile polyps shown with the oral side towards the top of the image. **a** Double fluorescent in situ hybridization of *NvLWamide-like* (*red*) and *Nvserum amyloid A-like* (*green*) in a late gastrula stage embryo. **b** The transgenic line for *NvLWamide::mcherry* expression is shown. Neural soma and neurites are observed throughout the body column and tentacles. Ectodermal neurons with three projections are observed in the body column (*white arrow*), which are not found in the other transgenic line. **c** The transgenic line for *Nvserum amyloid A-like::mcherry* is shown. There are many fewer neurons compared to *NvLWamide::mcherry*, but characteristic neurons are present. The U-shaped neuron that has two orally projecting neurites (*pink arrow*) is specific to this transgenic line. Both lines have neurons that are located just over the mesenteries and send projections orally and aborally in neural tracts overlaying the mesenteries (*yellow arrows*). In all images, asterisks indicate relative position of mouth

Nvserum amyloid A-like (Fig. 5a) [11]. *NvLWamide-like* was expressed in more cells than *Nvserum amyloid A-like* (Fig. 5a). Double fluorescent mRNA in situ hybridizations revealed that many of the *Nvserum amyloid A-like* expressing neurons (Fig. 5a, red) were also positive for *NvLWamide-like* (Fig. 5a, green). However, there were many examples of *NvLWamide-like*-only-positive cells and few examples of *Nvserum amyloid A-like*-only-positive cells (Fig. 5a). Thus, it is likely that there are at least three molecularly distinct neural subtypes that require *NvashA* for development.

We next compared the neurons labeled in each transgene to determine if the neurite projections from *Nvserum amyloid A-like* and *NvLWamide-like* neurons are similar or distinct. Although there were a number of neurons with similar neurites that projected along the oral–aboral axis in each transgene (Fig. 5b, c, yellow arrows), each transgene also labeled neurons with distinct morphologies (Fig. 5b, c, white and pink arrows, respectively). Consistent with the mRNA in situ hybridization results, the NvLWamide-like::mCherry labeled more cells than NvSerum Amyloid A-like::mCherry (compare Fig. 5b and c). Interestingly, there were distinct cell types present in each line [for example, NvLWamide-like::mCherry was expressed in ectodermal cells that had three neurites extending from the soma (Fig. 5b, white arrow), and NvSerum Amyloid A-like had unique neurons with neurites that extended out of either side of the soma and projected orally to form U-shaped neurons (Fig. 5c, pink arrow)] that could be reproducibly identified in individual transgenic animals. Although more extensive characterization is required for each of these transgenic lines, the fact that *NvashA* targets have distinct expression patterns and that neurons described by the transgenes of two *NvashA* targets display distinct morphologies support the conclusion that *NvashA* regulates multiple neuronal subtypes.

Identification of 100 genes downregulated and 22 genes upregulated by U0126 treatments

To determine if U0126 regulates other potential neurogenic genes and to identify novel targets of MEK signaling, we applied a forward molecular approach using a genome-wide expression microarray. Zygotes were treated with U0126 or DMSO until late blastula stage. At that point mRNA was extracted and used to generate labeled cDNA, which was hybridized to a custom expression microarray (Nimblegen, Inc.) that represents 24,021 predicted *N. vectensis* gene models [28]. The Pearson's correlation factor between biological replicates was mediocre (0.69), however, 926 genes were significantly ($P < 0.05$) upregulated and 1176 genes were significantly ($P < 0.05$) downregulated in U0126-treated embryos (Additional file 6: Table S3). Because our focus was to identify early embryonic patterning events, we screened the lists of genes to identify transcription factors, signaling molecules, and signaling modulators. This resulted in the identification of 100 genes that were downregulated and 22 genes that were upregulated by U0126 (Additional file 7: Table S4; Additional file 8: Table S5 [2, 7, 9, 11, 19, 24, 26, 28, 38–57]). Out of the 122 selected genes, the vast majority (86/122) possess strong orthology with members of various families of transcription factors (i.e., forkhead, pointed, homeodomain). Twenty-seven genes potentially encode ligands, modulators, or receptors of signaling pathways (i.e., Wnts), and nine genes show similarities with adhesion molecules, metalloproteases, or RNA binding proteins with described developmental functions in bilaterians (i.e., Ncam, Tolloid, Vasa) (Additional file 6: Table S3). To distinguish between previously published genes and newly identified ones, we used the best Blast Hit identification followed by "*-like*". Thus, with the exception of *Nvhes-like* and *Nvath-like* [9, 51], all gene names containing "*-like*" designate gene products described for the first time in this study.

Identification of putative neural genes

Neural genes are predicted to have a salt-and-pepper expression pattern, and thus determining the expression pattern of the 122 target genes would identify which genes exhibit salt-and-pepper expression associated with neural genes. We performed whole mount in situ hybridizations in the developing embryo at blastula stages (24 hpf) and at the end of gastrulation (48 hpf, Fig. 6). We excluded 16 genes because their expression patterns are already described at the blastula stage, but we did include genes whose early expression patterns had not yet been described (*Nvgata*, for example [23]). We were able to obtain clones for 98 of the remaining 106 genes and synthesized anti-sense probes. All original publications corresponding to a given gene (sequence identification and/or gene expression pattern) can be found in Additional file 7: Table S4 and Additional file 8: Table S5. Our in situ screen revealed reproducible patterns for 60 of the 98 genes we screened. Patterns could be grouped into one of three categories: (1) genes expressed in the animal hemisphere/presumptive endomesoderm of the blastula (24/98) (Additional file 9: Figure S4); (2) genes expressed in the vegetal hemisphere/aboral domain of the blastula (18/98) (Additional file 9: Figure S4); and (3) genes with the characteristic salt-and-pepper pattern consistent with being neural genes (18/98) (Fig. 6). We found no link between genes that are expressed broadly in the animal and vegetal hemispheres and neurogenesis, and thus will not discuss these genes further here.

Genes expressed in individual cells throughout the ectoderm

The 18 genes expressed in individual cells of the presumptive ectoderm at the blastula stage or in ectodermal body wall at the end of gastrulation were *Nvsox2*, *Nvpea-like3*, *Nvcoup-like1* (also called NR-like 12), *Nvcoup-like2* (also called NR-like 13) [55], *Nvelav-like*, *NvemxLX*, *Nvhd145*, *Nvtailless-like*, *Nvvsx-like*, *Nvgfi-like*, *Nvsox10-like*, *Nvhes-like3*, *Nvfoxq2-like3*, *NvfoxD3-like*, *Nvdkk-like3*, *Nvvegef-like1*, *Nvhox2*, and *Nvhd052* (Fig. 6). Eight genes (*Nvelav-like*, *NvemxLX*, *Nvtailless-like*, *Nvgfi-like*, *Nvdkk3-like3*, *Nvvegf-like1*, and *Nvhox2 and Nvhd052 we did not detect localized expression prior to the onset of gastrulation* (Fig. 6E,F,N,P,Za-Zd). Six genes (*Nvpea3-like*, *Nvcoup-like1*, *Nvvsx-like*, *Nvsox10-like*, *Nvhes-like3*, and *Nvfoxq2-like3*) were expressed in 5–15 cells (Fig. 6B, C, O, Q, R, Y). For four genes (*Nvsox2*, *Nvcoup-like2*, *Nvhd145*, and *NvfoxD3-like*), more than 15 cells were stained throughout the presumptive ectoderm at the blastula stage (Fig. 6A, D, M, Z).

At the end of gastrulation, we observed gene expression for all above-mentioned genes in individual cells (Fig. 6G–L, S–X, Ze–Zj, Zl). However, the localization and number of stained cells varied considerably. The only gene that appeared to be expressed in individual cells throughout the entire ectoderm (pharyngeal ectoderm, oral ectoderm, body wall ectoderm, sub-apical pole, and apical pole) was *Nvhes-like3* (Fig. 6X), which is reminiscent of a previously reported gene, *NvashA* [11, 51]. *Nvsox2* and *Nvcoup-like1* (Fig. 6G, I) were also expressed in a salt-and-pepper manner throughout all ectodermal domains, except the pharyngeal ectoderm. The largest group of genes (*Nvcoup-like2*, *Nvelav-like*, *NvemxLX*, *Nvhd145*, *Nvtailless-like*, and *Nvvsx-like*) was detected in the body wall ectodermal as well as the sub-apical and apical domains (Fig. 6J, K, L, S, T, U). Cells expressing *NvfoxD3-like* and *Nvdkk3-like3* (Fig. 6Zf, Zg) were detected in the oral and body wall ectoderm as well as the sub-apical pole domains; however, *Nvsox10-like*, *Nvfoxq2-like3*, and

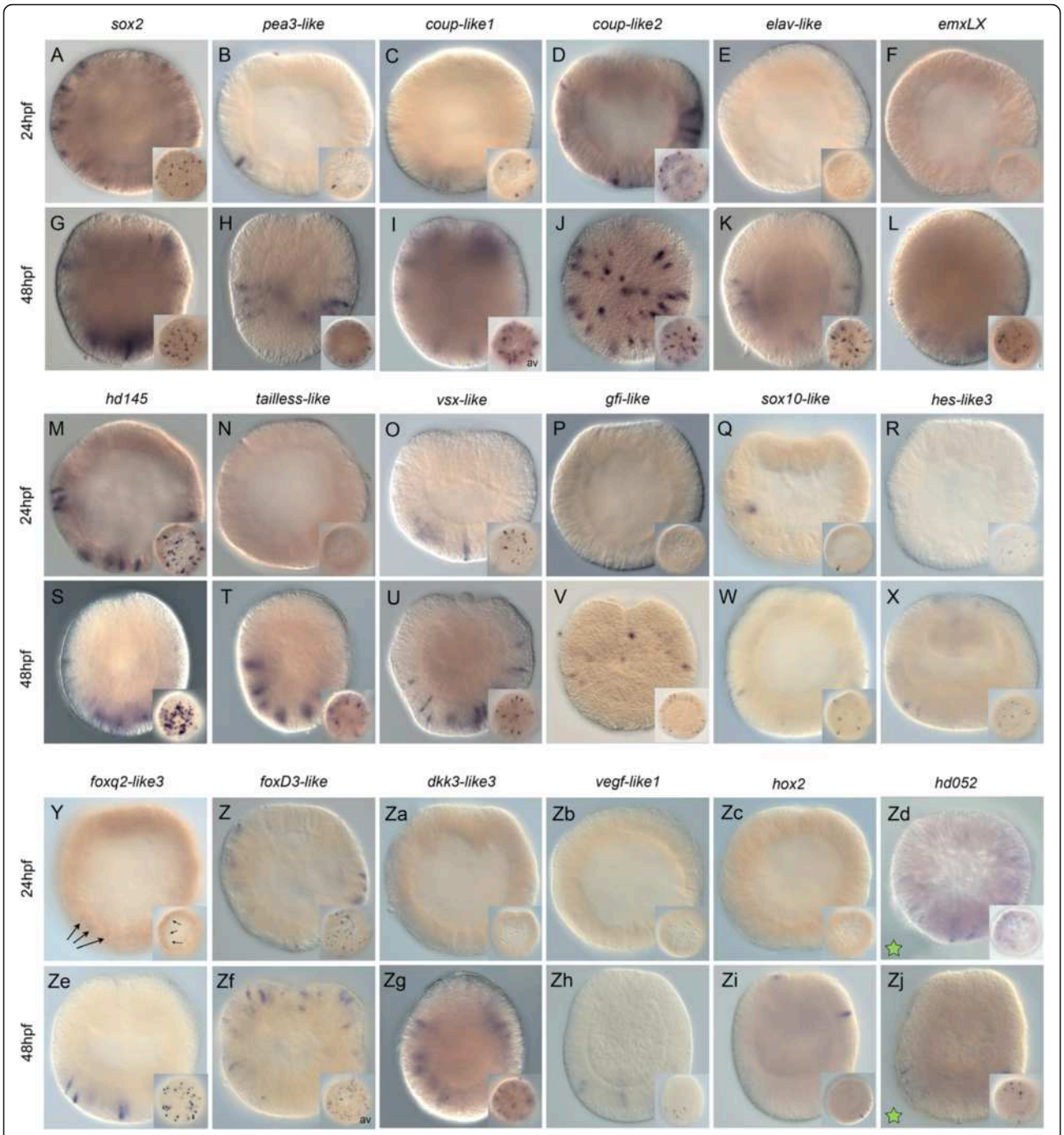

Fig. 6 U0126 targets expressed in individual cells throughout the ectoderm. Wild type salt-and-pepper gene expression analysis by in situ hybridization of genes differentially regulated by U0126 treatments. All animals are either blastula [24 hours post fertilization (*hpf*) – **A**–**F**, **M**–**R**, **Y**-**Zd**] or gastrula (48 hpf – **G**–**L**, **S**–**X**, **Ze**–**Zj**) stages. All images are lateral views with the animal pole to the top. The insets correspond to surface views. Antisense probes used as indicated. *Green stars* in Zd and Zj indicate that this gene was upregulated under U0126 conditions. All other genes were downregulated

Nvvegf-like were only detected in the body wall ectoderm and sup-apical domain (Fig. 6W, Ze, Zh). The genes with the most restricted expression domain were *Nvpea3-like*, *Nvgfi-like*, and *Nvhox2*, which were expressed in individual cells either within a circumferential territory (Fig. 6H, V) or in a patch within the body wall ectoderm (Fig. 6Zi), respectively. The variable expression patterns suggest that many of these genes are putatively expressed in distinct subsets of neurons, while a few broadly expressed genes might play larger roles during neural development.

Temporal gene expression analysis of salt-and-pepper genes

In situ hybridization provides crucial spatial information about gene expression but cannot be used quantitatively to determine the presence of maternal transcripts or zygotic upregulation of a given gene. However, this information is crucial for the design of functional studies, to predict potential genetic interactions, and to build gene regulatory networks [28]. In order to determine the temporal deployment of putative neural genes during early embryogenesis, we performed fine-scale quantitative reverse transcription PCR (RT-qPCR) on RNA/cDNA that was sampled from unfertilized eggs and every 2–4 h during embryogenesis up to the late gastrula stage (48 hpf) Additional file 10: Figure S5. We analyzed 21 salt-and-pepper genes identified both in this and in previous studies, including the known neural genes such as *Nvath-like* and *NvashA* [9, 11]. Five salt-and-pepper genes (*Nvfoxq2-like3*, *Nvcoup-like2*, *Nvelav-like*, *NvpaxA*, and *Nvvegf-like1*) were detectable in zygotes, indicating that they are maternal genes (Additional file 11: Figure S6). However, it is not yet clear what the significance of these genes is because none of these genes have broad expression patterns that might indicate a key early role for them in neurogenesis. The majority of salt-and-pepper genes, including the known neural regulators *Nvath-like* and *NvashA*, are not components of the maternally contributed mRNAs, which suggests that the earliest neural fates are induced in the embryo. As a group, the salt-and-pepper genes display a similar temporal deployment. The earliest zygotically regulated genes are *Nvath-like* (8–10 hpf), followed by *Nvhes3* (10–12 hpf), *NvfoxD3*, *Nvsox10-like* (12–14 hpf), *Nvfoxq2-like3*, and *Nvsox2* (16–18 hpf), and then the bulk of genes (12/21) are upregulated at either 18–20 hpf (*Nvcoup-like1*, *Nvcoup-like2*, *Nvgfi-like*, *Nvhd145*, *Nvtailless-like*, *Nvvsx-like*, and *Nvelav-like*) or 20–24 hpf (*Nvdkk-like3*, *Nvpea3-like*, *NvpaxA*, *Nvgcm*, and *NvashA*). Our temporal analysis demonstrated two key aspects. *Nvath-like*, which is the first neural gene to respond to treatment with DAPT and is thought to be the earliest acting neural gene [9], is in fact upregulated prior to other known neural genes. Second, the salt-and-pepper genes all showed strong upregulation between 10 and 24 hpf. The upregulation of genes is continuous in that different genes are upregulated at different times throughout the 10–24 hpf window. This argues that once salt-and-pepper gene expression is initiated there is a steady increase in the expression of distinct salt-and-pepper genes. Additionally, temporal differences in expression might reflect a hierarchal organization for their functions. The later concept is supported by the observation that *Nvath-like* (an upstream neural regulator) is detected much earlier than *NvashA*, which is expressed in differentiated neurons [9].

NvFGFRa does not regulate salt-and-pepper gene expression in the embryo

ERK-mediated FGF signaling can be inhibited by treatment with U0126 in *Nematostella* [24], and the *NvfgfRa* receptor is expressed broadly in the embryonic ectoderm, which makes it a likely candidate responsible for the U0126 neural phenotype and/or responsible for regulating some of the newly identified salt-and-pepper genes. We tested if *NvfgfRa* might have an early neural phenotype by injecting the previously described *NvfgfRa* MO into embryos [24] and scoring for changes in *Nvath-like*, *NvashA*, and the other 19 genes with salt-and-pepper gene expression identified in the U0126 microarray. qPCR analysis comparing control MO and *NvfgrRa* MO revealed that none of the salt-and-pepper genes responded to changes in *NvfgfRa* levels (Fig. 7). These data suggest NvFgfra signaling is not the U0126 target responsible for the loss of salt-and-pepper expressed genes in the early gastrula. However, there is a maternal contribution of *Nvfgfra* signaling genes [24]. To confirm that this FGF signaling was unlikely the source of the neural phenotype, we allowed morphant animals to grow to 48 hpf at 17 °C. In parallel, we allowed wild-type animals to grow until 24 hpf, when they are approximately at the late blastula/early gastrula stage. Animals were then treated with U0126 from 24 to 48 hpf. This treatment regimen allows for the maternal action of FGF components, thus mimicking a potential flaw in the *Nvfgfra* morphant approach. qPCR analysis of *NvashA* and *Nvfgfra* (a target of *Nvfgfra* MO [24]) demonstrated that *Nvfgfra* MO effectively inhibited known targets, but not *NvashA* (Additional file 12: Figure S7B). We saw similar results with SU5402 treatment (Additional file 12: Figure S7B). However, U0126 treatment resulted in a strong reduction in all genes assayed (Additional file 12: Figure S7). These data argue that FGF signaling is not the source of the neural phenotype. Thus, although the neural phenotype observed in U0126-treated animals is robust, it is still unclear what signaling pathway(s) targeted by U0126 regulates salt-and-pepper gene expression in the embryonic ectoderm.

NvashA regulates a small subset of the salt-and-pepper genes

We next wondered if *NvashA* acted to regulate any of the U0126 target genes. Based on the role of proneural genes in other animals we hypothesized that *NvashA* might act upstream of or suppress expression of subsets of the salt-and-pepper expressed U0126 targets. *NvashA* was knocked down or overexpressed using the previously described *NvashA* translation blocking MO and in vitro synthesized *NvashA:venus* mRNA [11]. We assayed U0126 salt-and-pepper target expression by qPCR after

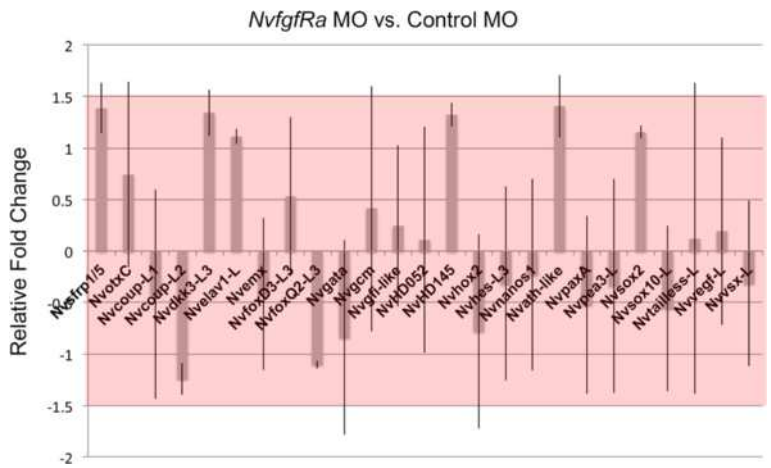

Fig. 7 *NvfgfRa* does not regulate U0126-dependent salt-and-pepper gene expression. Relative fold change calculated from quantitative polymerase chain reaction analysis of triplicate injections of the *NvfgfRa* morpholino (*MO*) or a control MO is graphed. Broadly expressed genes, *Nvsfrp1/5*, *NvotxC*, and *NvfgfRa*, are included as controls. The remaining genes are the salt-and-pepper expressed genes identified by the U0126 microarray. The *red box* indicates a region (1.5× to −1.5× fold change) that was defined as the cut off for a significant change in expression. Error bars represent standard error

disruption of *NvashA* and confirmed any genes that showed a response to *NvashA* disruption by mRNA in situ hybridization (Fig. 8). We included six control genes. Four negative controls (*Nvfgfra*, *Nvsfrp1/5-like*, *Nvsix3/6*, and *NvotxC*) represented broadly expressed regional patterning genes unlikely to respond to changes in *NvashA* function [19, 24, 54]. Two positive control genes, *NvLWamide-like* (PrtID# *242283*) and canalicular multispecific anion transporter (PrtID# 12533), are both confirmed positive targets of *NvashA* [11] and were both also downregulated in the U0126 array (Additional file 5: Table S2).

We first assayed for positive targets of *NvashA*. Overexpression of *NvashA* increased the expression of *Nvvsx-like*, *Nvgfi-like*, *Nvcoup-like1*, *Nvsox2*, and *Nvtailless-like* (Fig. 8a, light gray bars). However, *Nvvsx-like* expression was weakly upregulated following injection of *NvashA:venus* mRNA (Fig. 8a light grey bars; Fig. 8d), but *Nvvsx-like* was the only upregulated gene that decreased after *NvashA* knockdown by MO injection (Fig. 8a, dark gray bars; Fig. 8b). These data argue that *NvashA* is necessary and sufficient for the expression of *Nvvsx-like* (Fig. 8a–d). *NvashA* was sufficient but not necessary to regulate *Nvtailless-like* in the early gastrula. Overexpression of *NvashA* increased the expression of *Nvtailless-like* (Fig. 8a, light gray bars). However, *Nvtailless* expression was not dependent on *NvashA*, as its expression level was not decreased in *NvashA* morphants (Fig. 8a, dark gray bars). *Nvgfi-like*, *Nvcoup-like1*, and *Nvsox2* also all showed increases in expression following injection of *NvashA* mRNA (Fig. 8a, light gray bars). However, injection of *NvashA* MO also resulted in increased expression of all three genes (Fig. 8a, dark gray bars). Because reciprocal phenotypes are not observed between mRNA-injected and MO-injected animals, and both morphant and overexpression phenotypes were similar, it is unclear if changes in expression of *Nvcoup-like1*, *Nvsox2*, and *Nvgfi-like* reflect normal *NvashA* activity. Thus, we exclude these genes as targets of *NvashA* until *NvashA* mutant analysis can confirm that they are downstream of *NvashA* in the early gastrula. We conclude that *Nvvsx-like* is a positive target of *NvashA*.

We next investigated the 10 genes, *Nvath-like*, *NvemxLx*, *Nvhes-like3*, *Nvsox10-like*, *NvpaxA*, *Nvgcm*, *Nvgfi-like*, *Nvhd145*, *Nvcoup-like2*, and *Nvelav1*, that displayed changes in expression consistent with being putative negative targets of *NvashA*. *Nvhd145* and *Nvcoup-like2* expression was reduced in *NvashA*-overexpressing animals, but no change in either gene was observed in *NvashA* morphants (Fig. 8a; Additional file 4: Figure S3). These data suggest that although *NvashA* is sufficient to suppress *Nvhd145* and *Nvcoup-like2*, it does not likely regulate these genes during embryonic stages. *Nvath-like*, *NvemxLx*, *Nvhes-like3*, *Nvsox10-like*, *NvpaxA*, *Nvgcm*, *Nvgfi-like*, and *Nvelav1* showed increased expression at early gastrula stages in *NvashA* morphant animals (Fig. 8a, light gray bars), which suggests that they might be negative targets of *NvashA*. Only *Nvath-like* and *NvemxLx* showed reciprocal changes in expression in *NvashA* gain and loss of function (Fig. 8a, dark gray bars versus light gray bars). We were only able to confirm the changes in *Nvath-like* expression by mRNA in situ hybridization (Fig. 8e–g). In situ hybridizations with the *NvemxLx* probe on wild-type embryos often took >2 weeks to develop, and even then it was only detectable in very few cells and in only a few of the animals, arguing that it is expressed at low levels and that mRNA in situ hybridization is not sensitive enough to verify this gene. Relative expression strength can be

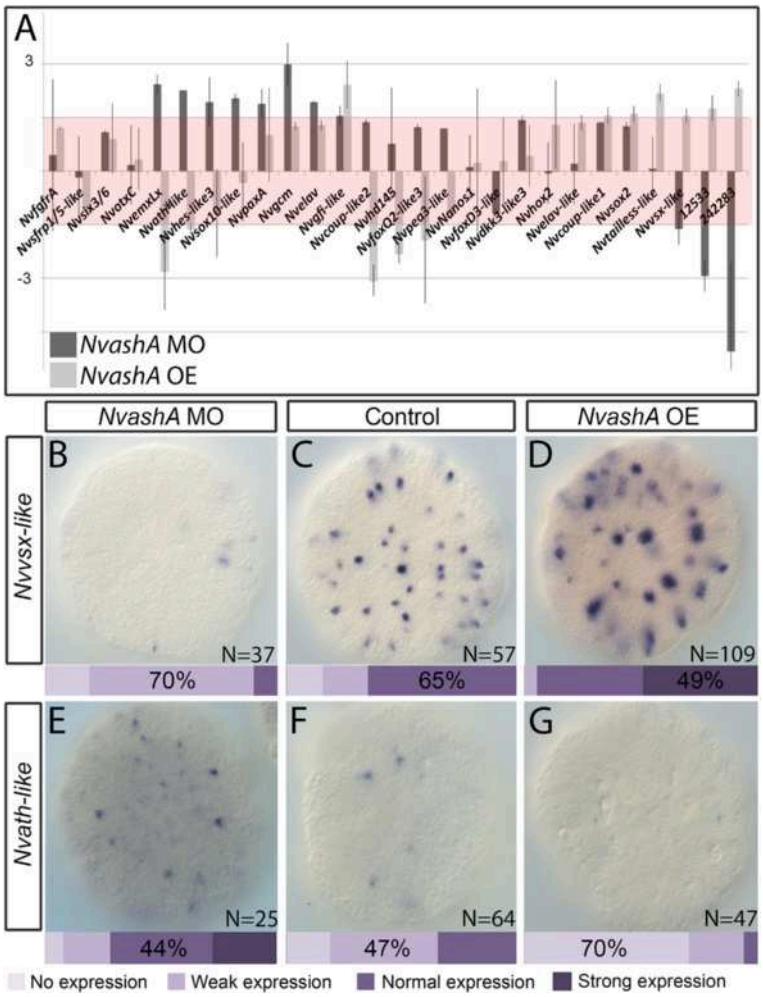

Fig. 8 *NvashA* regulates a subset of U0126-dependent salt-and-pepper expressed genes. **a** Relative fold change calculated from quantitative polymerase chain reaction analysis of triplicate injections of the *NvashA* morpholino (*MO*) versus a control MO (*dark gray bars*), or *NvashA:venus*-injected versus control *venus*-injected animals (*light gray bars*). Broadly expressed *NvfgfRa*, *Nvsfrp1/5*, *Nvsix3/6*, and *NvotxC* regional patterning genes were included as controls. Two positive control genes, 12533 and 242283, are included. The remaining genes are the salt-and-pepper expressed genes identified by the U0126 microarray. The *red box* indicates a region between 1.5× and −1.5× fold change that corresponds to an insignificant change in expression. The reciprocal phenotypes observed in *NvashA* MO and *NvashA:venus* mRNA-injected animals for *Nvvsx-like* (**b**–**d**) and *Nvath-like* (**e**–**g**) were confirmed by mRNA in situ hybridization. Embryos were classified and quantified as the percent having normal expression, weak expression, or no expression. The phenotypic class with the highest percentage of embryos is indicated. All embryo images are at the early gastrula stage. All images are ectodermal focal planes of aboral views. Error bars represent standard error

inferred by the qT value obtained for any given gene during qPCR analysis. Essentially, qT values above 35 are often associated with genes that are not expressed. We consistently obtained qT values of 32–33 for *NvemxLx*, arguing that it is in fact very weakly expressed. Although we could not confirm *NvemxLx* by mRNA in situ hybridization, it is likely a negative target of *NvashA* because it reproducibly showed reciprocal changes in expression in response to an increase or decrease in *NvashA* function (Fig. 8a). The remaining putative negative targets did not show reduced expression levels in *NvashA:venus* mRNA-injected animals, and with exception to *Nvsox10-like*, their increased expression in *NvashA* morphant animals could not be confirmed by mRNA in situ hybridization (Additional file 13: Figure S8; data not shown). The increased expression of *Nvelav1* in *NvashA* morphants was somewhat surprising, because it has already been shown to be a positive target of *NvashA* when assayed at later stages [11, 36]. However, *NvashA* only regulates a subset of *Nvelav1*-positive neurons [9–11], and thus we suspect that *NvashA* does not play a significant, if any, role in *Nvelav1* regulation at this early time point. We conclude that *Nvath-like*, *NvemxLX*, and *Nvsox10-like* are normally

suppressed by *NvashA* at embryonic stages, and that *NvashA* is sufficient to suppress expression of *Nvath-like* and *NvemxLX* but not *Nvsox10-like*.

Discussion

Preliminary gene regulatory network and model describing *NvashA*-dependent neurogenesis in the embryonic ectoderm

Based on previous observations and data presented here, we propose a model for and preliminary gene regulatory network describing *NvashA*-dependent neurogenesis in the early embryonic ectoderm of *Nematostella* (Fig. 9a, b). Based on U0126 phenotypes, we hypothesize that one or more not yet identified kinase signaling cascade(s) acting through MEK provides a global cue that is necessary for neural fates. It is not yet clear if all cells are competent to respond to this cue. However, it appears that the number of competent cells is greater than the number of cells that become neuralized, because evidence suggests that Notch signaling integrates the global cue to restrict a subset of cells to become *Nvath-like*- and *NvsoxB(2)*-positive neural progenitor cells (Fig. 9). Interestingly, we saw no evidence that either *Nvnotch* or *Nvdelta* were affected by U0126 treatment (Additional file 5: Table S2), which suggests that the refining activity of *Nvnotch* is independently controlled. It is not clear which, if either, transcription factor [*Nvath-like* or *NvsoxB(2)*] is nearer the top of the neural cascade. *NvsoxB(2)* is expressed maternally (Additional file 2: Figure S1), and both genes appear to be upregulated at approximately the same time in normal development (Additional file 2: Figure S1; Additional file 10: Figure S5). However, increased *Nvath-like* expression accumulates before *NvsoxB(2)* increases in animals with inhibited Notch activity [9]. Additionally, *NvsoxB(2)* and *NvashA* co-expression can be observed in post-mitotic cells, whereas *Nvath-like* and *NvashA* double-positive cells are never observed [9]. Post-mitotic neurons do not appear to express *Nvath-like* and they lose *NvsoxB2* expression. Lineage-specific pro-differentiation neural markers such as *NvashA* are not expressed until post-mitotic stages. The observation that *NvashA* suppresses *Nvath-like* expression suggests that one of its functions is to inhibit neural progenitor identity. This is contrary to reported interactions for *Nvath-like* and *NvashA* [9]. However, the previous study assessed phenotypes at later time points, and thus cannot account for potential phenotypes arising due to sustained loss of a key neurogenic gene causing system-wide defects. Here we look closer at the onset of neurogenesis, which provides less time for potential nonspecific phenotypes to arise. Certainly further efforts are needed to clarify this point. *NvashA* also promotes the expression of distinct individual neuronal subtype markers. The mechanism by which subtype markers are regulated is still unclear, but it is likely that regionally expressed oral–aboral patterning genes and the temporal window in which neural progenitors/neurons are born likely contribute to neural patterning [11, 19, 21].

It is not clear how only a subset of the *NvsoxB(2)* and *Nvath-like* double-positive cells give rise to *NvashA*-expressing cells. *NvsoxB(2)*, *Nvath-like*, and *NvashA* expression do not appear to be restricted to a distinct spatial domain [9, 11, 41]. One hypothesis is that progenitors give rise to different daughter cells with distinct identities, and that *NvashA* defines one such identity. This idea would be consistent with temporal patterning observed for neural progenitor lineages in *Drosophila* [58]. Alternatively, the time and position at which a progenitor is born might determine its identity and subsequently the identity of the neurons it generates [59, 60]. Regardless, functional studies support a much broader role for the progenitor marker *NvsoxB(2)*, and suggest that some additional mechanism is acting to restrict *NvashA* expression to a subset of the *NvsoxB(2)*-positive progenitors.

Additional putative neural genes identified here

We have identified 18 new genes expressed early (in late blastula/early gastrula) stages that are candidate neural regulators or neural subtype markers. The earliest expressed gene in our temporal analysis was *Nvath-like*, which had been previously identified as an early-acting neurogenic gene. Two genes turned on slightly after *Nvath-like* were *Nvhes3-like* and *NvfoxD3-like*. Previous studies suggest that *Nvhes3-like* is not sufficient to regulate neurogenesis at this stage, but it cannot yet be ruled out as a neural regulator because efficient *Nvhes3-like* knockdowns are not yet reported [36]. The next two genes to be expressed were *Nvsox2* and *Nvfoxq2-like*. Again, the broad expression of *Nvsox2* was similar to that of *NvfoxD3-like* and suggests that it may act broadly to regulate neurogenesis. *Nvfoxq2-like* genes displayed limited expression in the aboral region, suggesting their neurogenic potential is limited to neurons arising from that domain. The late-onset genes displayed both broad and restricted expression patterns, suggesting that at least some of these genes have roles regulating distinct neural subtypes. This is supported by the inclusion of *NvashA* as a late-onset gene. However, it must be noted that neurogenesis in *Nematostella* is a continuous process and late onset alone is not sufficient to suggest that a gene acts at the later steps in neurogenesis. Regardless, we have identified a number of putative neural genes, and future work will allow us to both determine which genes are definitively neural, and where each gene fits into the regulatory networks describing the earliest born neural subtypes in *Nematostella*.

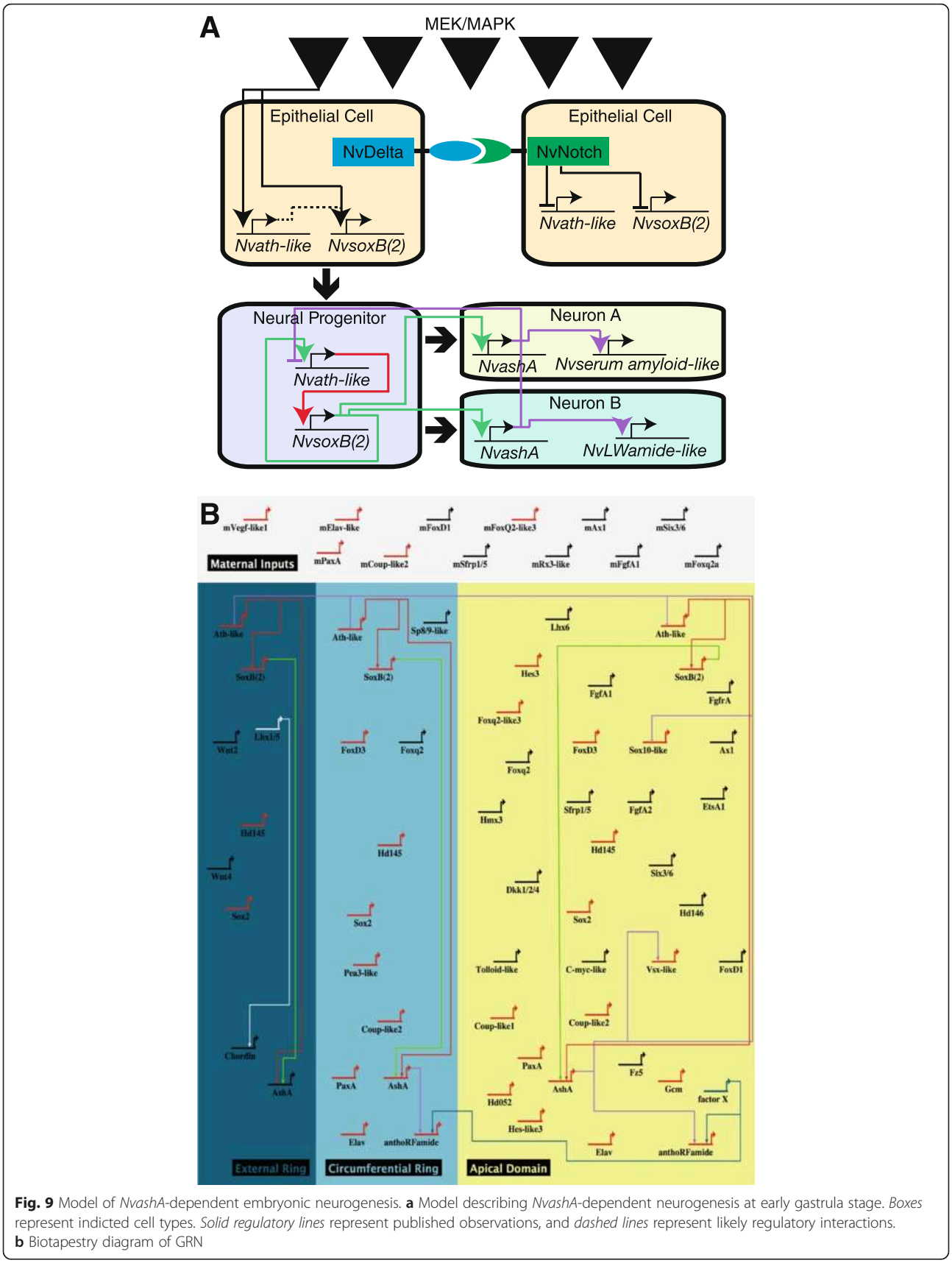

Fig. 9 Model of *NvashA*-dependent embryonic neurogenesis. **a** Model describing *NvashA*-dependent neurogenesis at early gastrula stage. *Boxes* represent indicted cell types. *Solid regulatory lines* represent published observations, and *dashed lines* represent likely regulatory interactions. **b** Biotapestry diagram of GRN

Neural induction in *Nematostella*

MAPK/MEK activity is required for the expression of key neural progenitor markers, suggesting that it might be a component of neural induction in *Nematostella*. Loss of neurogenesis following treatment with U0126 implies that a positive neurogenic cue is disrupted by U0126 treatment. It is tempting to speculate that FGF signaling may be responsible for neural induction, because FGF is a positive regulator of neural induction during vertebrate development [15] and MEK activity has been described to be downstream of FGF signaling in other systems. However, we report no phenotype when the broadly expressed *NvfgfRa* receptor was knocked down (Fig. 7). However, we still suspect that some MAPK signaling through MEK is necessary for neurogenesis. α–phospho-Erk staining was detected throughout the embryonic ectoderm, and this staining was reduced in U0126-treated animals (Fig. 2). Recently, MAPK signaling was shown to positively promote neurogenesis in salamander animal cap explants, in part by inhibiting BMP responsiveness due to decreased *smad1* expression [13]. However, expression of the putative neural marker *Nvgata* is not sensitive to the level of *Nvbmp2/4* in *Nematostella* gastrula [23]. Thus, the potential mechanism by which MAPK/MEK signaling promotes neural fates is not yet understood in *Nematostella*.

Possibly multiple neural inductive events during *Nematostella* neurogenesis

Multiple observations raise the hypothesis that distinct mechanisms may be necessary for neurogenesis in different spatiotemporal windows in *Nematostella*. First, *Nvbmp2/4* does not appear to impact neurogenesis at early embryonic stages, but expression of neural markers such as *Nvelav1* and *NvashA* are sensitive to the levels of *Nvbmp2/4* and *Nvbmp5/8* in planulae [22, 23]. Second, *NvashA* was not detected in U0126-treated embryos at early gastrula stages, but animals that were allowed to continue developing in the presence of U0126 begin to show *NvashA* expression, albeit in very few cells (Additional file 12: Figure S7). Third, very few *NvLWamide*-positive and *NvanthoRFamide*-positive cells were able to form in U0126-treated animals, which suggests that a subset of *NvLWamide* and *NvanthoRFamide* neurons may be U0126-independent. The potential for multiple neural programs acting in *Nematostella* suggest that efforts to isolate specific neurons born in unique spatiotemporal windows as well developing conditional alleles to investigate later time points in isolation will improve our understanding of neurogenesis in *Nematostella*.

Patterning genes identified in the UO126 microarray

In addition to the genes with a neural-like expression pattern, our forward molecular approach identified ~40 genes downstream of MEK that were expressed at the animal pole, including genes expressed in the presumptive endomesoderm and genes expressed at the aboral pole. These data suggest that MAPK acts broadly in the embryo to regulate germ layer specification as well as regional identities associated with axial patterning. UO126 treatment has been reported to suppress formation of the apical tuft at the aboral pole of the larva, likely via inhibition of NvFGFRa-mediated MAPK signaling [24, 26]. However, early embryonic patterning of the aboral domain has been largely understudied, and preliminary data suggest that distinct mechanisms act at early (embryonic) and late (larval) stages of aboral patterning [19]. Additional FGF receptors and ligands are detected in the oral domain of *Nematostella*, suggesting that FGF-mediated MAPK signaling normally regulates U0126 targets identified that display oral/animal pole expression [25]. However, targeted gene-specific knockdowns will be important to further determine exact mechanisms by which MEK activity impacts aboral and/or germ layer specification.

Conclusions

Our data indicate MAPK signaling is necessary for neurogenesis in the embryonic ectoderm of *Nematostella.* Our work also built upon previous observations to improve our understanding of the molecular mechanisms underlying cnidarian neurogenesis and described two transgenes that describe distinct neural subtypes in *Nematostella.* Lastly, we identified ~120 signaling molecules and transcription factors that act downstream of MEK in MAPK signaling. Future characterization of the genes will provide critical cues about the early patterning mechanisms acting during *Nematostella* development, which will be important to allow improved understanding about the origin and evolution of neurogenesis, axial patterning, and endomesoderm specification.

Methods

Culture and spawning of *Nematostella vectensis*

Adult *Nematostella* were cultivated either at the Kewalo Marine Laboratory/PBRC of the University of Hawaii (USA), the Whitney Laboratory for Marine Bioscience of the University of Florida (USA), the Institute for Research on Cancer and Aging of the University of Nice-Sophia-Antipolis (FRA), or Lehigh University (USA) according to the protocol described in [45]. Males and females were kept in separate glass bowls (250 ml) in 1/3× seawater (salinity: 12 pp) [5] at 17 °C in the dark and water was changed weekly. Animals were fed three/four times a week with pieces of oysters or brine shrimps. Manipulating the light cycle induced spawning and oocytes and sperm were collected separately [4].

The gelatinous mass around the eggs was removed with 4 % L-Cystein in 1/3× seawater before fertilization and then washed three times with 1/3× seawater. For the simultaneous development of the embryos, all oocytes were fertilized in glass dishes at the same time with 0.5 ml of diluted sperm. Fertilized eggs were kept in dark in filtered 1/3× seawater at 17 °C until the desired stage.

U0126 and SU5402 treatments

The MEK (U0126, Sigma, # U120) and FGF (SU5402, Sigma, # SML0443) antagonists were dissolved at a stock concentration of 10 mM in DMSO and added at to 1/3× filtered seawater to generate final concentrations as indicated. For SU5402, analysis was done at a final concentration of 20 μM, and for U0126 most experiments were conducted at a final concentration of 15 μM. Unless indicated, embryos were treated with the drug directly after fertilization and kept in the dark at 17 °C. If needed, U0126 was replaced every 24 h with fresh solutions to maintain activity. Treatments were compared to DMSO-treated control embryos. Embryos were fixed for in situ hybridization and morphological analysis at indicated stages. mRNA of embryos was extracted 24 hpf (late blastula stage) from two distinct biological replicates for microarray analysis.

RNA extraction, quantitative PCR, and microarray analysis

RNA extraction, qPCR, and microarray analysis were performed following protocols described in [46]. RNA for qPCR and microarray analysis was isolated with TriPure (Roche, #11667157001) or TRIzol (Invitrogen, #15596-026) according to the manufacturer's instructions, and genomic contamination removed using RNase-free DNase (Qiagen, #79254) for 15 min at 37 °C. The total amount of RNA was quantified with a NanoDrop 2000 spectrophotometer (Thermo Scientific) and the quality analyzed with a Bioanalyzer 2100 (Agilent Technologies Inc.). To generate cDNA, 1 μg of total RNA was used with the Advantage RT-PCR kit (Clontech, #639506) for qPCR analysis. For the fine-scale temporal analysis, total RNA was extracted from the following stages (in hpf): 0, 2, 4, 6, 8, 10, 12, 14, 16, 18, 20, 24, 28, 32, 40, and 48. qPCR analysis using a LightCycler 480 (Roche) utilizing LightCycler 480 SYBR Green 1 Master mix (Roche, #04887352001) was carried out as described previously [11]. Efficiencies for each gene-specific primer pair was determined using a fivefold serial dilution series and only primers with an efficiency ranging from 1.8 to 2.15 were used for further analysis (Additional file 14: Table S6). The housekeeping genes *Nvactin* and/or *Nvgadph* were used to normalize relative fold changes between control and manipulated embryos. Each qPCR analysis was repeated on at least three independent biological replicates and changes were analyzed using a Student's *t* test. Microarray analysis was conducted by sending 20 μg of total RNA (RIN value >8) to NimbleGen (Iceland) for further cDNA synthesis, labeling, and array hybridization. Two replicates were sent for each control and U0126-treated animals were sent. The 4-plex microarray (72,000 features) is an oligonucleotide-based chip version, custom designed and produced by NimbleGen Systems (Roche). Array data are available from http://www.ebi.ac.uk/arrayexpress/experiments/E-MTAB-4831/. Gene expression levels were normalized in the Nimblescan software according to [47, 48] and fold changes calculated by comparing expression values from control and treated embryos. Array results were screened based on the provided genome annotations assigned to each array spotID. If no clear blast hit or gene information was assigned to the prediction gene model from the Joint Genome Institute, we retrieved the genomic sequences from http://genome.jgi-psf.org/Nemve1/Nemve1.home.html for the given gene and performed manual BLAST (BLASTX) searches [49] against the NCBI database to determine the nature of the predicted gene product. All sequences from genes of interest have been used for BLAST analysis to confirm their nature and to determine previously published genes.

In situ hybridization, pERK, actin, and nuclear staining

Previously described gene sequences were used to subclone into pGemT (Promega, #A3600) from mixed stage cDNA. All other sequences used in this study were isolated in the course of a microarray analysis. Genome predictions as well as expressed sequence tag sequence information were combined to design primers (Additional file 15: Table S7) that allowed the amplification and cloning of genes between 0.5 kb and 2 kb as described above. Accession numbers for all analyzed genes in this study can be found in Additional file 6: Table S3 and Additional file 7: Table S4. Embryo fixation, probe synthesis, and in situ hybridization were performed as previously described [42]. The MegaScript Transcription Kit (Ambion) was used to synthesize 0.5–2 kb digoxigenin (DIG)-labeled (Roche, #11573152910) riboprobes. Hybridization of riboprobes (1 ng/μl) was carried out at 62 °C in 50 % formamide hybe buffer and visualization of the labeled probe was performed using NBT/BCIP as a substrate for the alkaline phosphatase-conjugated anti-DIG antibody (Roche, #11093274910). To analyze embryonic and larval morphology, we used Biodipy FL Phallacidin (Molecular Probes/Invitrogen, #B607) and propidium iodide (Sigma, #81845) to stain f-actin and the cell nuclei respectively as described previously [61]. To analyze embryonic localization of activated ERK, we used a monoclonal antibody that recognizes a phosphorylated epitope of the activated form of ERK [Phospho-p44/42 MAPK (Erk1/2) (Thr202/Tyr204);

Cell Signaling, # 4370)]. Antibodies were diluted at 1:200 in blocking solution (PBT (Phosphate Buffered Saline + 0.1 % Tween) + 10 % normal goat serum) overnight at 4 ° C. Following six washes in PBT, embryos were incubated with the secondary antibody (anti-rabbit Ig), and diluted at 1:250 for at least 4 h to overnight at 4 °C on a shaking rocker. Phosphate-buffered saline (PBS) was used for washes between antibodies. Specimens were mounted in 80 % glycerol.

Imaging

In situ hybridization images were taken on either a Zeiss AxioScop 2 mounted with an Axiocam camera triggered by Axiovision software (Carl Zeiss), a Zeiss Axio Imager A2 mounted with a Canon 6D triggered by Canon professional software, or a Nikon NTi using a Nikon DS-Ri2 color camera and the Elements software (Nikon). All expression patterns described here have been submitted to Kahi Kai, a comparative invertebrate gene expression database [62] hosted at http://www.kahikai.org/index.php?content=genes. Scoring of treatment phenotypes was performed on either a Zeiss Z-1 Axio imager or a Zeiss Axio Imager A2 microscope and confocal imaging was conducted on either a Zeiss LSM710 or Zeiss LSM Exciter microscope running the LSM ZEN software (Carl Zeiss). Fluorescent images were false-colored. The fluorescent channels were merged using ImageJ (http://rsbweb.nih.gov/ij/) and cropped to final size in Photoshop Cs6 (Adobe Inc.). Confocal images for Fig. 5 were processed using Imaris 8.1 (Bitplane).

Microinjection of mRNA and morpholinos

NvashA:venus or *venus* mRNA was injected into embryos at 150 ng/μl as previously described [6, 11, 36]. Antisense translation blocking MO against *Nvfgfra* [24] and *NvashA* [11] (GeneTools Inc.; Philomath, OR, USA) and a control MO (5′ AATAAAAAGAATGCCCCCT-CACCTCT 3′) with no known targets in the predicted *Nematostella* genome were injected at 1 mM concentrations.

Transgenic strain generation

To generate transgenic animals we amplified genomic DNA from position Scaffold21: 1349994-1347681 for *Nv239910* (serum amyloid A-like) and from Scaffold60: 1049346-1046951 for *Nv242283* (*NvLWamide-like).* Numbers correspond to genomic positions available in the *Nematostella* genome version 1.0 http://genome.jgi.-doe.gov/Nemve1/Nemve1.home.html. We cloned each fragment into the pNvT vector in front of the *mcherry* coding sequence as previously reported [37]. Animals were injected as previously reported [37], and stable F1 lines were identified by screening for fluorescence and outcrossing to wild-type animals.

Additional files

Additional file 1: Table S1. Dose-dependent effects of U0126 on *Nvsprouty*, *Nvbrachyury*, and *Nv-fgfA1* expression. Dose-dependent effects of U0126 analyzed by in situ hybridization. Analyzed U0126 concentration as indicated in Row 1 and number of embryos with phenotype scored based on expansion/reduction of the domain of expression as indicated in the column on the right. (XLS 33 kb)

Additional file 2: Figure S1. Summary of *NvsoxB(2)* RNA-seq data. Plot used data obtained from [33] from two duplicate RNA-seq data sets that generated transcriptomes over the first 19 hpf. Black trace shows average of two replicates. (JPG 471 kb)

Additional file 3: Figure S2. Changes in *NvashA*, *Nvath-like*, and *NvsoxB2* expression following drug treatments or in with increased Notch activity. mRNA in situ hybridization for *NvsoxB(2)* (**A**) and *NvashA* (**B**) in DMSO-treated control animals grown to early planula stages (48 hpf at 22 °C). *NvsoxB(2)* (**A′**) and *NvashA* (**B′**) expression in same stage animal treated with U0126 from 24 to 48 hpf or treated with SU5402 from 24 to 48 hpf (**B″**). mRNA in situ expression of *Nvath-like* (**C**) and *NvsoxB(2)* (**D**) in control embryos injected with the *venus* mRNA. Expression of *Nvath-like* (**C′**) and *NvsoxB(2)* (**D′**) in animals injected with *NvnotchICD:venus* (the intracellular domain of the Notch receptor), which has been previously shown to hyperactivate Notch signaling. Embryos were classified and quantified as the percent having normal expression, weak expression, or no expression. The phenotypic class with the highest percentage of embryos is indicated. In C and D, the main figure panels are ectodermal focal planes, and insets show deeper focal planes used to confirm embryonic stage. All images are of lateral views with the oral side to the left. (TIF 34682 kb)

Additional file 4: Figure S3. NvAshA:Venus localization in U0126-treated animals. NvAshA:Venus protein was detected at high levels and with strong nuclear localization in U0126-treated animals. (TIF 16187 kb)

Additional file 5: Table S2. Array data for *NvsoxB(2)*, *Nvnotch*, *Nvdelta*, and neural genes used for transgenes or controls in qPCR experiments. (XLSX 38 kb)

Additional file 6: Table S3. Genes with at least a 2-fold change after U0126 treatments based on our array analysis. (XLSX 3983 kb)

Additional file 7: Table S4. Selection of 22 genes upregulated after U0126 treatment. Selected genes that were significantly ($P < 0.05$) at least 2-fold upregulated by U0126 treatments. SpotID was the genome protein model ID (JGI) used for the array design. The gene name is based on the best BLAST hit and if available the previously published name(s) is used. Abbreviations are indicated in the table legend at the bottom. References are included in the main text. (XLSX 27 kb)

Additional file 8: Table S5. Selection of 100 genes downregulated after U0126 treatments. Selected genes that were significantly ($P < 0.05$) at least 2-fold downregulated by U0126 treatments. SpotID was the genome protein model ID (JGI) used for the array design. The gene name is based on the best BLAST hit and if available the previously published name(s) is used. Color code and abbreviations are indicated in the table legend at the bottom. References are included in the main text. (XLSX 37 kb)

Additional file 9: Figure S4. Summary of animal hemisphere and aboral expression genes identified by U0126 array. mRNA in situ patterns are included in a manuscript currently in preparation. (PDF 39 kb)

Additional file 10: Figure S5. Gene expression analyzed by quantitative polymerase chain reaction. Salt-and-pepper expressed genes as represented in Fig. 6. High-density gene expression profiles are represented by charts for all genes expressed at the blastula stage [24 hours post fertilization (*hpf*)] and/or gastrula stage (48 hpf) analyzed in this study. The y-axis indicates the relative fold change compared to unfertilized eggs. The *x*-axis indicates developmental time in hpf. Gene names as indicated in the top left corner and the Cp value in unfertilized eggs is indicated in the top right corner of each panel and was used to determine the presence of maternal transcripts in Fig. 6 (Cp > 34.00). *Cp* corresponds to the crossing point, also known as the cycle threshold (*Ct*) value. (PDF 599 kb)

Additional file 11: Figure S6. Summary temporal gene expression analysis. Summarized results of the temporal high density profiling (qPCR)

used to determine the presence of maternal transcripts and significant zygotic upregulation of a given gene expressed in individual cells of the ectoderm. *n.d.* Not determined. *Genes that have been identified and their spatial blastula and gastrula expression patterns characterized elsewhere (see Additional file 6: Table S3, Additional file 7: Table S4 and Additional file 8: Table S5). (PDF 62 kb)

Additional file 12: Figure S7. *NvashA* expression in animals with varied regiments of U0126 treatment. (**A**) *NvashA* expression in control animals, or in animals treated with U0126 continuously for 48 hours, or from 24 to 48 hpf. Unlike early stages when no *NvashA* expression could be detected (Fig. 3), *NvashA* expression was ultimately detected in U0126-treated animals by 48 hpf. Treatment with U0126 from 24 to 48 hpf reduced *NvashA* expression, but *NvashA* could be detected in many cells, albeit at reduced levels. (**B**) Levels of *NvashA* and *Nvfgfa1* as detected by qPCR at late gastrula stage (48 hpf at 17 °C) in animals injected with the *Nvfgfra* MO or treated with U0126 or SU5402 from 24 to 48 hpf. Relative expression levels are compared to control MO- or DMSO-treated animals respectively. The red box defines 1.5 to −1.5 fold change region. Error bars are standard error. (TIF 11166 kb)

Additional file 13: Figure S8. *NvashA* regulation of target genes in the embryonic ectoderm. Gene expression in *NvashA* morphants (**A–C**), control morpholino (**D–F**), and *NvashA* mRNA injected (**G**, **H**). Quantification below each image represents percent of embryos in each phenotypic class (see key in figure). All images except C and F are aboral views. C and F are oral views. Embryos were classified and quantified as the percent having normal expression, weak expression, or no expression.. The phenotypic class with the highest percentage of embryos is indicated. (TIF 21122 kb)

Additional file 14: Table S6. Primer pairs used in this study for qPCR analysis. (XLS 53 kb)

Additional file 15: Table S7. Primer pairs used in this study for gene cloning. (XLS 73 kb)

Acknowledgments
We would like to acknowledge Dr Uli Technau for providing reagents necessary to generate transgenic lines as well as the reviewers for providing helpful feedback.

Authors' contributions
MJL, ER, and MQM conceived of the study, performed experiments, analyzed data, and drafted the manuscript. ARA, BS, HJ, TC and JH generated, collected, and analyzed data. All authors read and approved the final manuscript.

Competing interests
The authors declare that they have no competing interests.

Author details
[1]Department of Biological Sciences, Lehigh University, Bethlehem, PA, USA. [2]The Whitney Marine Laboratory for Marine Science, University of Florida, St. Augustine, Florida, USA. [3]Université Nice Sophia Antipolis UMR 7284, CNRS UMR 7284, INSERM U1081, Institute for Research on Cancer and Aging, Nice, France.

Received: 20 March 2016 Accepted: 4 July 2016
Published online: 01 August 2016

References
1. Layden MJ, Rentzsch F, Röttinger E. The rise of the starlet sea anemone Nematostella vectensis as a model system to investigate development and regeneration. WIREs Dev Biol. 2016;1–21.
2. Putnam NH, Srivastava M, Hellsten U, Dirks B, Chapman J, Salamov A, et al. Sea anemone genome reveals ancestral Eumetazoan gene repertoire and genomic organization. Science. 2007;317:86–94.
3. Stefanik DJ, Friedman LE, Finnerty JR. Collecting, rearing, spawning and inducing regeneration of the starlet sea anemone, Nematostella vectensis. Nat Protoc. 2013;8:916–23.
4. Fritzenwanker JH, Technau U. Induction of gametogenesis in the basal cnidarian Nematostella vectensis (Anthozoa). Dev Genes Evol. 2002;212:99–103.
5. Hand C, Uhlinger KR. The Culture, sexual and asexual reproduction, and growth of the sea anemone *Nematostella vectensis*. Biol Bull. 1992;182:169–76.
6. Layden MJ, Röttinger E, Wolenski FS, Gilmore TD, Martindale MQ. Microinjection of mRNA or morpholinos for reverse genetic analysis in the starlet sea anemone, Nematostella vectensis. Nat Protoc. 2013;8:924–34.
7. Marlow HQ, Srivastava M, Matus DQ, Rokhsar D, Martindale MQ. Anatomy and development of the nervous system of Nematostella vectensis, an anthozoan cnidarian. Devel Neurobio. 2009;69:235–54.
8. Nakanishi N, Renfer E, Technau U, Rentzsch F. Nervous systems of the sea anemone Nematostella vectensis are generated by ectoderm and endoderm and shaped by distinct mechanisms. Development. 2012;139:347–57.
9. Richards GS, Rentzsch F. Regulation of Nematostella neural progenitors by SoxB, Notch and bHLH genes. Development. 2015;142:3332–42.
10. Richards GS, Rentzsch F. Transgenic analysis of a SoxB gene reveals neural progenitor cells in the cnidarian Nematostella vectensis. Development. 2014;141:4681–9.
11. Layden MJ, Boekhout M, Martindale MQ. Nematostella vectensis achaete-scute homolog NvashA regulates embryonic ectodermal neurogenesis and represents an ancient component of the metazoan neural specification pathway. Development. 2012;139:1013–22.
12. Wilson SI, Edlund T. Neural induction: toward a unifying mechanism. Nat Neurosci. 2001;4:1161–8.
13. Hurtado C, De Robertis EM. Neural induction in the absence of organizer in salamanders is mediated by MAPK. Dev Biol. 2007;307:282–9.
14. Gaulden J, Reiter JF. Neur-ons and neur-offs: regulators of neural induction in vertebrate embryos and embryonic stem cells. Hum Mol Genet. 2008;17:R60–6.
15. Stern CD. Neural induction: old problem, new findings, yet more questions. Development. 2005;132:2007–21.
16. Bertrand V, Hudson C, Caillol D, Povovici C, Lemair P. Neural tissue in Ascidian embryos is induced by FGF9/16/20, acting via a combination of maternal GATA and Ets transcription factors. Cell. 2003;115:615–27.
17. Nordström U, Jessell TM, Edlund T. Progressive induction of caudal neural character by graded Wnt signaling. Nat Neurosci. 2002;5:525–32.
18. Marchal L, Luxardi G, Thome V, Kodjabachian L. BMP inhibition initiates neural induction via FGF signaling and Zic genes. PNAS. 2009;106:17437–42.
19. Sinigaglia C, Busengdal H, Leclère L, Technau U, Rentzsch F. The bilaterian head patterning gene six3/6 controls aboral domain development in a cnidarian. PLoS Biol. 2013;11:e1001488.
20. Robinson R. Ciliate genome sequence reveals unique features of a model eukaryote. PLoS Biol. 2006;4:e304.
21. Marlow H, Matus DQ, Martindale MQ. Ectopic activation of the canonical wnt signaling pathway affects ectodermal patterning along the primary axis during larval development in the anthozoan Nematostella vectensis. Dev Biol. 2013;380:324–34.
22. Watanabe H, Kuhn A, Fushiki M, Agata K, Ozbek S, Fujisawa T, et al. Sequential actions of β-catenin and Bmp pattern the oral nerve net in Nematostella vectensis. Nat Commun. 2014;5:5536–14.
23. Saina M, Genikhovich G, Renfer E, Technau U. BMPs and chordin regulate patterning of the directive axis in a sea anemone. Proc Natl Acad Sci USA. 2009;106:18592–7.
24. Rentzsch F, Fritzenwanker JH, Scholz CB, Technau U. FGF signalling controls formation of the apical sensory organ in the cnidarian Nematostella vectensis. Development. 2008;135:1761–9.
25. Matus DQ, Thomsen GH, Martindale MQ. FGF signaling in gastrulation and neural development in Nematostella vectensis, an anthozoan cnidarian. Dev Genes Evol. 2007;217:137–48.
26. Sinigaglia C, Busengdal H, Lerner A, Oliveri P, Rentzsch F. Molecular characterization of the apical organ of the anthozoan Nematostella vectensis. Dev Biol. 2015;398:120–33.
27. Favata MF, Horiuchi KY, Manost EJ, Daulario AJ, Stradley DA, Fesser WS, et al. Identification of a novel inhibitor of mitogen-activated protein kinase kinase*. J Biol Chem. 1998;273:18623–32.
28. Röttinger E, Dahlin P, Martindale MQ. A framework for the establishment of a cnidarian gene regulatory network for "endomesoderm" specification: the inputs of ß-catenin/TCF signaling. PLoS Genet. 2012;8:e1003164.
29. Scholz CB, Technau U. The ancestral role of Brachyury: expression of NemBra1 in the basal cnidarian Nematostella vectensis (Anthozoa). Dev Genes Evol. 2003;212:563–70.

30. Hacohen N, Kramer S, Sutherland D, Hiromi Y, Krasnow MA. sprouty encodes a novel antagonist of FGF signaling that patterns apical branching of the Drosophila airways. Cell. 1998;92:253–63.
31. Yung Y, Dolginov Y, Zhong Y, Rubinfeld H, Michael D, Hanoch T, et al. Detection of ERK activation by a novel monoclonal antibody. FEBS Lett. 1997;408:292–6.
32. Fischer AHL, Mozzherin D, Eren AM, Lans KD, Wilson N, Cosentino C, et al. SeaBase: a multispecies transcriptomic resource and platform for gene network inference. Integr Comp Biol. 2014;54:250–63.
33. Tulin S, Aguiar D, Istrail S, Smith J. A quantitative reference transcriptome for Nematostella vectensis early embryonic development: a pipeline for de novo assembly in emerging model systems. Evodevo. 2013;4:16–1.
34. Helm RR, Siebert S, Tulin S, Smith J, Dunn CW. Characterization of differential transcript abundance through time during Nematostella vectensis development. BMC Genomics. 2013;14:266.
35. Shimojo H, Ohtsuka T, Kageyama R. Oscillations in notch signaling regulate maintenance of neural progenitors. Neuron. 2008;58:52–64.
36. Layden MJ, Martindale MQ. Non-canonical Notch signaling represents an ancestral mechanism to regulate neural differentiation. Evodevo. 2014;5:1–14.
37. Renfer E, Amon-Hassenzahl A, Steinmetz PRH, Technau U. A muscle-specific transgenic reporter line of the sea anemone, Nematostella vectensis. Proc Natl Acad Sci USA. 2010;107:104–8.
38. Srivastava M, Larroux C, Lu DR, Mohanty K, Chapman J, Degnan BM, et al. Early evolution of the LIM homeobox gene family. BMC Biol. 2010;8:4.
39. Ryan JF, Mazza ME, Pang K, Matus DQ, Baxevanis AD, Martindale MQ, et al. Pre-bilaterian origins of the hox cluster and the hox code: evidence from the sea anemone, Nematostella vectensis. PLoS One. 2007;2:e153–23.
40. Lee PN, Pang K, Matus DQ, Martindale MQ. A WNT of things to come: evolution of Wnt signaling and polarity in cnidarians. Semin Cell Dev Biol. 2006;17:157–67.
41. Magie CR, Pang K, Martindale MQ. Genomic inventory and expression of Sox and Fox genes in the cnidarian Nematostella vectensis. Dev Genes Evol. 2005;215:618–30.
42. Martindale MQ. Investigating the origins of triploblasty: 'mesodermal' gene expression in a diploblastic animal, the sea anemone Nematostella vectensis (phylum, Cnidaria; class, Anthozoa). Development. 2004;131:2463–74.
43. Fritzenwanker JH, Saina M, Technau U. Analysis of forkhead and snail expression reveals epithelial–mesenchymal transitions during embryonic and larval development of Nematostella vectensis. Dev Biol. 2004;275:389–402.
44. Matus DQ, Pang K, Daly M, Martindale MQ. Expression of Pax gene family members in the anthozoan cnidarian, Nematostella vectensis. Evol Dev. 2007;9:25–38.
45. Ryan JF, Burton PM, Mazza ME, Kwong GK, Mullikin JC, Finnerty JR. The cnidarian-bilaterian ancestor possessed at least 56 homeoboxes: evidence from the starlet sea anemone, Nematostella vectensis. Genome Biol. 2006;7:R64.
46. Kusserow A, Pang K, Sturm C, Hrouda M, Lentfer J, Schmidt HA, et al. Unexpected complexity of the Wnt gene family in a sea anemone. Nature. 2005;433:156–60.
47. Santagata S, Resh C, Hejnol A, Martindale MQ, Passamaneck YJ. Development of the larval anterior neurogenicdomains of Terebratalia transversa (Brachiopoda) provides insights into the diversification of larval apical organs and the spiralian nervous system. Evodevo. 2012;3:3.
48. Kumburegama S, Wijesena N, Xu R, Wikramanayake AH. Strabismus-mediated primary archenteron invagination is uncoupled from Wnt/β-catenin-dependent endoderm cell fate specification in Nematostella vectensis (Anthozoa, Cnidaria): implications for the evolution of gastrulation. Evodevo. 2011;2:2.
49. Matus DQ, Magie CR, Pang K, Martindale MQ, Thomsen GH. The Hedgehog gene family of the cnidarian, Nematostella vectensis, and implications for understanding metazoan Hedgehog pathway evolution. Dev Biol. 2008; 313:501–18.
50. Layden MJ, Meyer NP, Pang K, Seaver EC, Martindale MQ. Expression and phylogenetic analysis of the zic gene family in the evolution and development of metazoans. Evodevo. 2010;1:12.
51. Marlow H, Roettinger E, Boekhout M, Martindale MQ. Functional roles of Notch signaling in the cnidarian Nematostella vectensis. Dev Biol. 2012; 362:295–308.
52. Yasuoka Y, Kobayashi M, Kurokawa D, Akasaka K, Saiga H, Taira M. Evolutionary origins of blastoporal expression and organizer activity of the vertebrate gastrula organizer gene lhx1 and its ancient metazoan paralog lhx3. Development. 2009;136:2005–14.
53. Extavour CG, Pang K, Matus DQ, Martindale MQ. vasa and nanos expression patterns in a sea anemone and the evolution of bilaterian germ cell specification mechanisms. Evol Dev. 2005;7:201–15.
54. Mazza ME, Pang K, Martindale MQ, Finnerty JR. Genomic organization, gene structure, and developmental expression of three Clustered otx genes in the sea anemone Nematostella vectensis. J Exp Zool. 2007;308B:494–506.
55. Reitzel AM, Tarrant AM. Nuclear receptor complement of the cnidarian Nematostella vectensis: phylogenetic relationships and developmental expression patterns. BMC Evol Biol. 2009;9:230.
56. Sullivan JC, Sher D, Eisenstein M, Shigesada K, Reitzel AM, Marlow H, et al. The evolutionary origin of the Runx/CBFbeta transcription factors–studies of the most basal metazoans. BMC Evol Biol. 2008;8:228.
57. Chourrout D, Delsuc F, Chourrout P, Edvardsen RB, Rentzsch F, Renfer E, et al. Minimal ProtoHox cluster inferred from bilaterian and cnidarian Hox complements. Nature. 2006;442:684–7.
58. Isshiki T, Pearson B, Holbrook S, Doe CQ. Drosophila neuroblasts sequentially express transcription factors which specify the temporal identity of their neuronal progeny. Cell. 2001;106:511–21.
59. Jacob J, Maurange C, Gould AP. Temporal control of neuronal diversity: common regulatory principles in insects and vertebrates? Development. 2008;135:3481–9.
60. Skeath JB. At the nexus between pattern formation and cell-type specification: the generation of individual neuroblast fates in the Drosophila embryonic central nervous system. Bioessays. 1999;21:922–31.
61. Magie CR, Daly M, Martindale MQ. Gastrulation in the cnidarian Nematostella vectensis occurs via invagination not ingression. Dev Biol. 2007;305:483–97.
62. Ormestad M, Martindale MQ, Röttinger E. A comparative gene expression database for invertebrates. Evodevo. 2011;2:17.

Article 2: A bipolar role of the transcription factor ERG for cnidarian germ layer formation and apical domain patterning.

Amiel, A. R.*, Johnston, H.*, Chock, T., Dahlin, P., Iglesias, M., Layden, M., et al. (2017).

Developmental Biology. doi:10.1016/j.ydbio.2017.08.015

(*) shared authorship

Developmental Biology xxx (xxxx) xxx–xxx

Contents lists available at ScienceDirect

Developmental Biology

journal homepage: www.elsevier.com/locate/developmentalbiology

Evolution of developmental control mechanisms

A bipolar role of the transcription factor ERG for cnidarian germ layer formation and apical domain patterning

Aldine R. Amiel[a,1], Hereroa Johnston[a,1], Taylor Chock[b], Paul Dahlin[c], Marta Iglesias[d], Michael Layden[e], Eric Röttinger[a,*,2], Mark Q. Martindale[b,*,2]

[a] Université Côte d'Azur, CNRS, INSERM, Institute for Research on Cancer and Aging, Nice, France
[b] University of Florida, The Whitney Marine Laboratory for Marine Science, St. Augustine, FL, USA
[c] Stockholm University, Department of Ecology, Environment and Plant Sciences, Stockholm, Sweden
[d] University of Barcelona, Department of Genetics and Institute of Biomedicine, Barcelona, Spain
[e] Lehigh University, Department of Biological Sciences, Bethlehem, PA, USA

ARTICLE INFO

Keywords:
ERK signaling
Embryonic development
Gastrulation
Endomesoderm
Apical organ
ERG
ETS transcription factor
Gene regulatory network
Nematostella vectensis
Sea anemone
Cnidarian
Gene expression
Evolution

ABSTRACT

Germ layer formation and axial patterning are biological processes that are tightly *linked* during embryonic development of most metazoans. In addition to canonical WNT, it has been proposed that ERK-MAPK signaling is involved in specifying oral as well as aboral territories in cnidarians. However, the effector and the molecular mechanism underlying latter phenomenon is unknown. By screening for potential effectors of ERK-MAPK signaling in both domains, we identified a member of the ETS family of transcription factors, *Nverg* that is bipolarily expressed prior to gastrulation. We further describe the crucial role of NvERG for gastrulation, endomesoderm as well as apical domain formation. The molecular characterization of the obtained NvERG knock-down phenotype using previously described as well as novel potential downstream targets, provides evidence that a single transcription factor, NvERG, simultaneously controls expression of two different sets of downstream targets, leading to two different embryonic gene regulatory networks (GRNs) in opposite poles of the developing embryo. We also highlight the molecular interaction of cWNT and MEK/ERK/ERG signaling that provides novel insight into the embryonic axial organization of *Nematostella*, and show a cWNT repressive role of MEK/ERK/ERG signaling in *segregating* the endomesoderm *in two sub-domains*, while a common input of both pathways is required for proper apical domain formation. Taking together, we build the first blueprint for a global cnidarian embryonic GRN that is the foundation for additional gene specific studies addressing the evolution of embryonic and larval development.

1. Introduction

Fibroblast Growth Factor (FGF) induced ERK signaling plays a crucial role in various aspects of mesoderm formation and coordinating cell movements in bilaterian animals (Schulte-Merker and Smith, 1995; Burdine et al., 1997; Draper et al., 2003; Röttinger et al., 2004, 2008, 2015; Stathopoulos et al., 2004; Yasuo and Hudson, 2007; Ota et al., 2009; Bertrand et al., 2011; Green et al., 2013). FGFs bind to FGF Receptors (FGFRs) that are part of the RTK (Receptor Tyrosine Kinase) family, in order to activate an intracellular MAP Kinase (RAS/MEK/ERK) signaling cascade leading to the phosphorylation of transcription factors and thus the repression or activation of downstream targets (Bertrand et al., 2014). Well known transcriptional regulators whose activity can be controlled by MEK/ERK signaling, belong to the ETS domain containing family of transcription factors (Selvaraj et al., 2015).

Cnidarians are the extant sister group to all bilaterians and their phylogenetic position makes them very interesting for understanding the evolution of biological novelties (Martindale and Hejnol, 2009; Technau and Steele, 2011; Layden et al., 2016a). One intensely used cnidarian model is the anthozoan sea anemone *Nematostella vectensis* that can easily be cultured and manipulated under laboratory conditions and for which functional genomic tools are well established (Layden et al., 2016a, 2013; Hand and Uhlinger, 1992; Darling et al., 2005; Putnam et al., 2007; Ikmi et al., 2014). Based on the sequenced *Nematostella* genome (Putnam et al., 2007), 15 putative FGF ligands

* Corresponding authors.
E-mail addresses: eric.rottinger@unice.fr (E. Röttinger), mqmartin@whitney.ufl.edu (M.Q. Martindale).
[1] These authors contributed equally to the work.
[2] These authors also contributed equally to the work.

http://dx.doi.org/10.1016/j.ydbio.2017.08.015
Received 27 April 2017; Received in revised form 29 July 2017; Accepted 9 August 2017

and three potential receptors have been identified (Matus et al., 2007; Rentzsch et al., 2008) with the spatial expression patterns reported for three ligands and two receptors (Matus et al., 2007; Rentzsch et al., 2008; Röttinger et al., 2012). Two ligands and one receptor (*NvfgfA1, NvfgfA2, NvfgfrA*) are expressed in the vegetal hemisphere/apical domain, the ligand *Nvfgf8* is expressed in the animal hemisphere and its descendants, and the receptor *NvfgfrB* in derivatives of both poles. Interestingly, *Nvsprouty*, a well described downstream target and modulator of FGF signaling (Hacohen et al., 1998; Casci et al., 1999; Kramer et al., 1999), is also expressed in both extremities of the developing embryo/larvae (Matus et al., 2007). Only based on these expression patterns, FGF signaling has been suggested to play a role in gastrulation and neural development (Matus et al., 2007). However, the importance of the FGF pathway has so far only been analyzed at late stages of development and shown to be crucial for apical organ formation and metamorphosis (Rentzsch et al., 2008; Sinigaglia et al., 2013, 2014).

The vegetal pole of cnidarian embryos gives rise to the apical organ, characterized by an apical tuft, a group of long cilia, at the aboral most part of the planula larvae (Hand and Uhlinger, 1992; Rentzsch et al., 2008; Martindale et al., 2004). Recent studies have shown that a gene regulatory module involving the transcription factor Six3/6, FGF signaling as well as Frizzled 5/8, that potentially signals through ß-catenin, is required to specify and pattern the apical domain, form the apical tuft and subsequently allow the process of metamorphosis into a sessile juvenile (Rentzsch et al., 2008; Sinigaglia et al., 2013, 2014; Leclère et al., 2016). Unfortunately, little is known about the role of MEK/ERK signaling in the specification of the apical domain prior to the onset of gastrulation.

Cnidarians are so-called diploblastic animals that, although they possess the genetic toolkit involved in bilaterian mesoderm formation, lack a true mesodermal germ layer (Röttinger et al., 2012; Martindale et al., 2004; Technau and Scholz, 2003). A precise embryonic cell lineage analysis has yet to be performed in cnidarians due to the lack of a stereotyped cleavage program but existing labeling experiments clearly indicate that derivatives of cells from the animal hemisphere in *Nematostella* gives rise to the epitheliomuscular gut, the pharynx and the mouth of the planula larva (Lee et al., 2007; Fritzenwanker et al., 2007). In a previous study, we have defined three gene expression domains within the animal hemisphere of the blastula prior to the onset of gastrulation; the central domain, the central ring and the external ring that appears to give rise to the gut (bodywall endomesoderm), pharynx and mouth respectively (Röttinger et al., 2012). This work also showed that canonical WNT signaling (cWnt) is required for proper gene expression within all three domains, in particular for genes expressed within the central ring domain and normal pharynx formation (Röttinger et al., 2012). Interestingly, cWnt/TCF represses expression of the potential FGF ligand, *fgf8A,* in the central ring (animal hemisphere) restricting its expression to the central domain, suggesting a role of FGF induced ERK/MAPK signaling in endomesoderm formation (Röttinger et al., 2012). However, a recent study that focuses on the role of ERK/MAPK signaling in the initiation of the neurogenic program in *Nematostella* development, suggest that FGFR might not be the (sole) activator of this pathway in the presumptive endomesoderm (Layden et al., 2016b). The same authors have also shown that pharmacologically inhibition of ERK/MAPK signaling using U0126, a potent inhibitor of the ERK activating kinase MEK (Davies et al., 2000; DeSilva et al., 1998), after fertilization blocks gastrulation and endomesoderm formation (Layden et al., 2016b). As this treatment perturbs gene expression within the animal hemisphere as well as the apical domain, this further suggests a dual role of this pathway in germ layer formation and axial patterning (Layden et al., 2016b). In addition, by using a genome wide expression array approach, the authors have identified a large set of putative downstream targets of this pathway of which only the genes potentially involved in neurogenesis have been reported (Layden et al., 2016b).

In this study, we present the spatio-temporal expression of NvERG, a member of the ETS family of transcription factors that is expressed in both, the central domain of the animal hemisphere as well as in the apical domain of the vegetal hemisphere. Inhibition of NvERG phenocopies the effects of disrupting MEK/ERK signaling, causing the failure of gastrulation and endomesoderm formation as well as the perturbation of apical tuft development. Fine scale temporal and spatial gene expression analysis of genes identified in a differential genome wide expression array comparing DMSO (control) and U0126 treated embryos (Layden et al., 2016b) enabled us to describe 39 potential downstream targets of this pathway that are expressed in the presumptive endomesoderm as well as in the apical domain. Finally, molecular analysis of the resulting phenotype in NvERG morphants, highlights its crucial role for setting up the gene regulatory networks (GRNs) underlying endomesoderm forming within the central domain as well as apical domain patterning. Interestingly, we functionally confirmed a computational prediction (Abdol et al., 2017) that NvERG negatively regulates *Nvbra* expression in the central domain, in order to restrict its expression in the central ring. This work enables us today to draw a global blueprint of genetic interactions governing specification, patterning and morphogenic events underlying embryonic development of *Nematostella*.

2. Materials and methods

2.1. Culture and spawning of Nematostella vectensis

Adult *Nematostella* were cultivated either at the Kewalo Marine Laboratory/PBRC of the University of Hawaii (USA), the Whitney Laboratory for Marine Bioscience of the University of Florida (USA) or the Institute for Research on Cancer and Aging of the University of Nice-Sophia-Antipolis (FRA). Culture and spawning/fertilization was performed according to the protocol described in (Röttinger et al., 2012). Fertilized eggs were kept in dark in filtered 1/3 seawater at 16 °C until the desired stage.

2.2. RNA Extraction and quantitative PCR (qPCR)

RNA Extraction and quantitative PCR (qPCR) was performed following protocols described in (Röttinger et al., 2012): For the fine scale temporal analysis total RNA was extracted from the following stages (in hours post fertilization, hpf): 0, 2, 4, 6, 8, 10, 12, 14, 16, 18, 20, 24, 28, 32, 40, 48. *For the molecular phenotype analysis, total RNA was extracted 24hpf. Samples were obtained from three biological replicates and performed in three technical replicates*. qPCR analysis using a LightCycler 480 (Roche) utilizing LightCycler 480 SYBR Green 1 Master mix (Roche, #04887352001) was carried out as described previously (Layden et al., 2012). The full list of qPCR primer pairs and their efficiency used in this study can be found in Table S2 or (Layden et al., 2016b). The houskeeping genes *Nvactin* and/or *Nvgadph* were used to normalize relative fold changes between control and manipulated embryos and each qPCR analysis was repeated on independent biological replicates.

2.3. In situ hybridization, actin and nuclear staining

Previously described gene sequences were used to sub-clone into pGemT (Promega, #A3600) from mixed stage cDNA. All other sequences used in this study were isolated in the course of a microarray analysis (Layden et al., 2016b). Genome predictions as well as EST

sequence information were combined to design primer pairs (Table S3, (Layden et al., 2016b)) that allow the amplification and cloning of genes between 05.kb and 2 kb. PCR amplified cDNA fragments, corresponding to partial or full-length sequences of the gene of interest, have been cloned into pGEMT vectors (Promega, #1360). T7 and SP6 primers have been used to amplify the insert and subsequently used for anti-sense probe synthesis using either the T7 or SP6 promoters (Ambion, #AM1330, #AM1333). Probe integrity was validated by RNA electrophoresis and presented expression patterns observed in at least three independent experiments. Accession numbers for all analyzed genes in this study can be found in Layden et al. (2016b) *as well as* in Table S4, S5. Embryo fixation, probe synthesis and *in situ* hybridization were performed as previously described (Röttinger et al., 2012; Martindale et al., 2004). To analyze embryonic and larval morphology, we used Biodipy FL Phallacidin (Molecular Probes/Invitrogen, #B607), propidium iodide (Sigma, #81845) and an anti-acetylated tubulin antibody (Sigma, #T6793), to stain f-actin, the cell nuclei and the apical tuft respectively following the protocols described previously (Magie et al., 2007).

2.4. Nomenclature

Nomenclature of the newly identified genes follows the approach used in (Röttinger et al., 2012). To distinguish between previously published genes, and newly identified putative TFs and signaling molecules, we used the best Blast Hit identification, followed by "- like" to designate the newly identified gene sequences. While "Blast hit" approaches can be used to provide a general idea of the protein family, a detailed phylogenetic analysis is required to better resolve these gene orthologies, especially when paralogy issues or when multiple gene predictions are present for one gene family.

2.5. cDNA construction, MO-NvERG design and microinjection

cDNA constructs encoding the wild type ORF (NvERG) and a dominant negative form (NvERG-DB1) of NvERG, were generated by PCR using the following primers:

NvERG_FWD 5′ATGTATGGTTTAAGTTCAGAATC-3′
NvERG-DB1_FWD 5′-ATGTTCAATGCCAGCCCGATG-3′
NvERG_REV 5′GGCGTAGTAGGTCATACTGGC-3′

The reverse primer used in combination with both forward primers was lacking the stop codon for fusion with a C-terminal Venus fluorescent tag. All cDNA constructs were cloned, linearized and transcribed according to (Layden et al., 2013; Röttinger et al., 2012). mRNAs were injected in zygotes at final concentrations of 0.2–0.5 mg/ml. A splice blocking morpholino antisense oligonucleotide (Gene Tools) was designed (MO-NvERG 5′-CTTACTTTTTCTCAAGAC-GCACAGA-3′) to target the exon3-intron3 boundary of NvERG and used from 0.3 to 0.9 mM without noticeable toxicity. *A control MO* **(**MO-CTRL 5′- AGAGGAAGAATAACATACCCTGTCC-3′ (35)**)** *was also injected at a concentration of 0,9 mM. Animals were sorted after injection to eliminate the un-injected animals as indicated by the lack of fluorescence.* Microinjections were carried out as described in (Layden et al., 2013; Röttinger et al., 2012) and the following primers used to test the splice-blocking efficiency of the MO (Fig. 1):

NvERG_Mosplice_FWD 5′-ACCAAAGAACACGTTCGCCAGTGGA-3′,
NvEtsA_Mosplice_REV 5′ATCGCAAACCCCCAGGCTCTCC-3′

2.6. Imaging

in situ hybridization images were taken on either a Zeiss AxioScop 2 or a Zeiss Axio Imager A2 mounted with an Axiocam camera triggered by Axiovision software (Carl Zeiss). All expression patterns described here have been submitted to Kahi Kai, a comparative invertebrate gene expression database (Ormestad et al., 2011) hosted at http://www.kahikai.org/index.php?content=genes. Scoring of treatment phenotypes was performed on either a Zeiss Z-1 Axio imager or a Zeiss Axio Imager A2 microscope and confocal imaging was conducted on either a Zeiss LSM710 or Zeiss LSM Exciter microscope running the LSM ZEN software (Carl Zeiss). Fluorescent images were false-colored, the fluorescent channels merged using ImageJ (http://rsbweb.nih.gov/ij/) and cropped to final size in Photoshop Cs6 (Adobe Inc.).

3. Results

3.1. Nverg is expressed in the central and the apical domains

In recent reports from *Nematostella*, genes belonging to the family of ETS transcription factors have been identified and reported (Röttinger et al., 2012; Layden et al., 2016b). However, the entire complement of this transcription factor family in cnidarians is currently unknown. We have identified 12 genes that encode proteins predicted to contain an ETS DNA binding domain defining this family of transcription factors. A phylogenetic analysis of those factors has revealed that *Nematostella* possess members of 8 out of 11 ETS subfamiles (Fig. 1Aa, Fig. S1) (Laudet et al., 1993, 1999). We have further analyzed their spatio-temporal expression at late blastula stages and observed clear expression patterns for 3 genes (*Nvets-likeA (previously called NvelkA-like (*Röttinger et al., 2012*)), Nvpea3 (previously called Nvpea3-like (*Layden et al., 2016b*))* and *Nverg*. *Nvets-likeA* was identified to respond to over-activated canonical Wnt signaling (1-azakenpaullone treatments) and is expressed in the central domain (Röttinger et al., 2012). *Nvpea3*, identified to be downstream of ERK/MAPK signaling (U0126 treatments) is expressed in individual cells of a circumferential territory within the ectodermal body wall (Layden et al., 2016b). One gene that retained our particular attention was *Nverg*, whose transcripts were detected in a bi-polar manner within the central as well as the apical domains of the late blastula/very early gastrula (Fig. 1Ad,Ae). *While it is only detected in the central domain at blastula stages (Fig. 1Ad, inset), the apical expression appears progressively when the animal regions flattens prior to its invagination (Fig. 1Ad, Ae).* At later stages this gene was expressed within the forming mouth opening, the gastrodermis as well as the apical pole (Fig. 1Af). Interestingly, this gene has not been previously identified in any of the microarray studies analyzing the effects of blocking FGF signaling in the apical domain (Sinigaglia et al., 2014) or general ERK/MAPK inhibition (Layden et al., 2016b), suggesting that *it may have been missed or that its* activity might be regulated by post-transcriptional modifications. Fine-scale qPCR analysis of *Nverg* temporal gene expression revealed that it is maternally expressed and that the onset of zygotic expression occurs between 12 and 14 h post fertilization (hpf, at 17 C, Fig. 1Ab).

3.2. Inhibition of NvERG prevents formation of the gut and perturbs the genesis of the apical tuft

In order to block activity of NvERG during *Nematostella* development, we used a splice blocking morpholino (MO-NvERG) targeting exon three of this gene and thus creating a truncated version of the protein that is lacking the DNA binding domain (Fig. 1Ba). Microinjecting increasing concentrations of MO-NvERG into oocytes followed up by PCR revealed that MO-NvERG injection at 0.9 mM causes drastic splice defects (Fig. 1Bb). We further analyzed the morphological phenotypes induced by the disruption of NvERG function and observed that MO-NvERG morphants entirely failed to gastrulate and form a gut (Fig. 1Cf-h) compared to control embryos

(Fig. 1Cb-d). This resulting phenotype can be the direct consequence of the absence of morphogenetic movements required for gastrulation or indirectly, caused by the lack of bodywall endomesoderm that becomes the future gut. In addition, MO-NvERG also perturbs the formation of the apical tuft (Fig. 1Ch) as revealed by acetylated tubulin staining (Rentzsch et al., 2008). In order to confirm the specificity of MO-

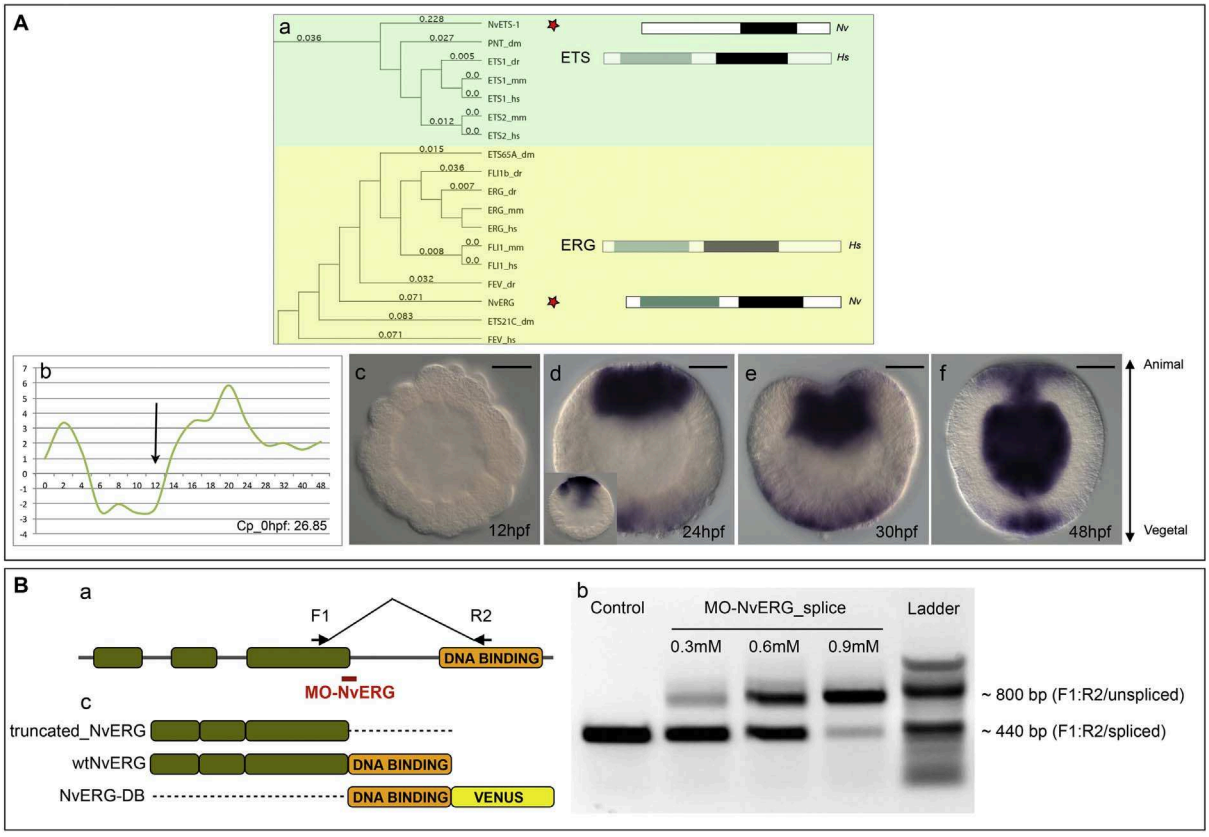

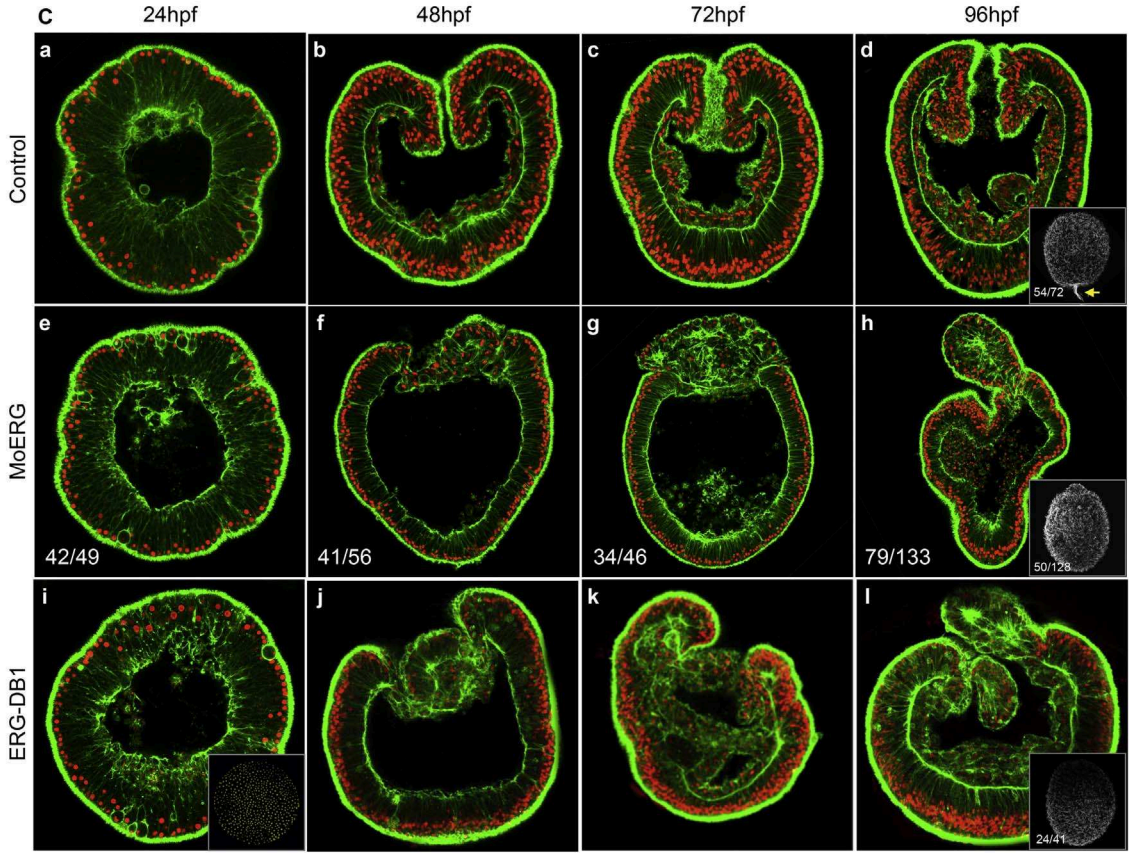

Fig. 1. NvErg is required for endomesoderm formation, gastrulation and participates in apical tuft development. (**A**) Identification of NvErg and analysis of its spatiotemporal expression. (**Aa**) Excerpt of the phylogenetic analysis of the ETS transcription factor complement in *Nematostella*, indicating the existence of NvERG and NvETS1 orthologs in cnidarians. The full analysis can be found in Fig. S1. To the right of the tree, the bars indicated the protein domain organization of either the human representative (*Hs*, greyed out rectangles) of the subfamily as well as the protein domain organization of the *Nematostella* ortholog (*Nv*). Green rectangles indicate the Pointed domain, black rectangles the ETS domain. (**Ab**) Temporal expression of *Nverg* analyzed by qPCR during embryonic development of the first 48 h post fertilization. The y-axis indicates relative fold changes compared to fertilized eggs. (**Ac-Af**) Spatial (*in situ* hybridization) expression of *Nverg* at early (Ac) and late (Ad) blastula, mid (Ae) and late (Af) gastrula stages. *Orientation of blastula stages was determined by the thickening of the animal pole prior to its invagination that was observable in certain embryos of a given batch at the analyzed time point.* Animal pole to the top and vegetal pole to the bottom. *The black bar in the upper right corner of Ac-Af indicates the scale bars: 50 μm* (**Ba**) Schematic representation of the genomic organization of NvERG, and the recognition site of MO-NvERG and the position of the PCR primers to verify the efficiency of the splice blocking morpholino. (**Bb**) Splice blocking efficiency of MO-NvERG analyzed by RT-PCR at increasing concentrations of MO-NvERG injected embryos. (**Bc**) Schematic representation of the protein structure of the various tools used in Fig. 1C and Fig. S2. (**C**) Morphological effects of inhibiting NvERG function during early *Nematostella* development. (Ca-Cd) Control embryos injected with MO-CTRL, **(Ce-Ch)** embryos injected with MO-NvERG or (Ci-Cl) mRNA encoding a dominant negative version of NvERG (NvERG-DB1) at 24 (Ca, Ce,Ci, late blastula), 48 (Cb, Cf,Cj, late gastrula), 72 (Cc, Cg,Ck, early planula) and 96 (Cd, Ch,Cl, late planula) hpf. All images are lateral views with the animal/oral pole to the top and confocal z-sections using phalloidin (green) to show f-actin filaments and propidium iodide (red) to visualize the nuclei. The insets in (Cd, Ch, Ci) correspond to lateral views of embryos stained with acetylated tubulin to visualize the presence or absence of the apical tuft (yellow arrow in Cd). The numbers in the insets indicate the number or embryos with the represented phenotype / total amount of analyzed animals.

NvERG, we performed a rescue experiment by overexpressing mRNA encoding a wild-type, Venus tagged version of NvERG after MO-NvERG injection, and observed that gastrulation movements are restored in the majority of analyzed embryos (Fig. S2A-G). A control rescue experiment using *TomatoNLS* mRNA instead of *NvERG: Venus*, failed to rescue the phenotype (Fig. S2D**,H)**, *showing that the rescued phenotype is NvERG specific*. We also microinjected a dominant negative form of NvERG (NvERG-DB) that is lacking the transactivation domain in the N-terminus of the protein (Pourtier-Manzanedo et al., 2003). While not as efficient as MO-NvERG, injection of NvERG-DB caused i) severe perturbations of gut formation and gastrulation movements (that appear to recover partially during later embryonic development) and ii) the perturbation of apical tuft development (Fig. 1i-l). All together these experiments show that NvERG is required for gut formation and participates in apical tuft genesis. Interestingly, this loss of NvERG function in *Nematostella* causes a phenotype that is strikingly similar to the one described from blocking ERK/MAPK signaling using U0126 (Layden et al., 2016b), supporting the idea that NvERG might be one of the effectors of ERK/MAPK signaling in the animal as well as the vegetal hemispheres.

3.3. Differential expression of ERK/MAPK targets along the animal-vegetal axis

A previous study has reported the differentially expressed genes identified in a genome-wide expression array comparing DMSO treated controls with U0126 treated blastula stages (Layden et al., 2016b). The spatial expression pattern presented in this study were focused on genes that were expressed in individual cells and that might be involved in early neurogenesis in *Nematostella* (Layden et al., 2016b). However, our *in situ* hybridization screen also revealed genes that were specifically expressed in the animal or vegetal hemispheres at blastula stages (24hpf) and at the end of gastrulation (48hpf) (Figs. 2 and 3). While we focused on newly identified genes, we included previously published genes in our analysis to either obtain additional spatial information (*e.g. Nvgata* (Martindale et al., 2004)) or because their expression domains had not been characterized during the initial period of our analysis (*e.g. Nvsix3/6, Nvfoxq2a* (Sinigaglia et al., 2013), *Nvsfrp1* (Sinigaglia et al., 2014) and *Nvfz5/8 (*Leclère et al., 2016*)*). All original publications corresponding to a given gene (sequence identification and/or gene expression pattern) can be found in (Layden et al., 2016b), Tables S4 and S5.

3.4. Genes expressed within the animal hemisphere (endomesoderm)

We observed 24 localized expression patterns within the animal hemisphere (*Nvmae-like, Nvbmp1-like, Nvmeis-like, Nvsix4/5, Nvrunt, Nvperlecan-like, Nvkielin-like, NvfosB-like, Nvtbx1, Nvfox1, NvpdgfR-like, Nvret-like2, Nvfgfr-like, Nvpou-like1, Nvpou-like2, Nvk50-5, Nvgata, NveHand-like, Nvfz1-like, Nvtbx20-like, Nvmusk-like, NvephrinB-like, Nvhd058, Nvhes-like2,* Fig. 2). While some genes were only faintly detected (*e.g. Nvtbx1, Nvfox1* (Fig. 2O,P)*),* only one gene, *Nvk50-5* was not detected at the blastula stage (but was by the gastrula stage)(Fig. 2Zb). However, among the 23 genes that displayed localized gene expression within the animal hemisphere at the blastula stage (24hpf @17 °C), only *Nvhes-like2* was detected in the central ring (Fig. 2Zp). All other analyzed genes were expressed in the central domain prior to the onset of gastrulation (*Nvmae-like, Nvbmp1-like, Nvmeis-like, Nvsix4/5, Nvrunt, Nvperlecan-like, Nvkielin-like, NvfosB-like, Nvtbx1, Nvfox1, Nvpdgfr-like, Nvret-like2, Nvfgfr-like, Nvpou-like1, Nvpou-like2, Nvgata, NveHand-like, Nvfz1-like, Nvtbx20-like2, Nvmusk-like, NvephrinB-like, Nvhd058,* Fig. 2A-F,M,O,Q,R,Y,Za,Zc,Zd,Zk-Zo).

However, at the end of gastrulation (48hpf at 17 °C), the expression domains of the same set of genes are not only restricted to a single domain as seen at the blastula stage, but are expressed in at least five distinct territories (Fig. 2G-L,S-X,Ze,Zj,Zq-Zv). Only *Nvgata* is expressed in individual cells within the ectoderm (Fig. 2Zi) confirming a previous description (Martindale et al., 2004). Six genes, *NvfosB-like, Nvhes-like2, Nvmae-like, runt, Nvk50-5* and *NvephrinB-like* are expressed only within the oral ectoderm (Fig. 2T,Zh,K,Zh,Zt). *Nvmeis* is expressed in the oral ectoderm, pharyngeal ectoderm, as well as pharyngeal and body wall endomesoderm (Fig. 2I). Transcripts of *Nvmusk-like* are only detected in the pharyngeal ectoderm (Fig. 2Zs) and expression of *Nvtbx20-like2* only in the pharyngeal endomesoderm (Fig. 2Zr). *Nvbmp1-like, Nvsix4/5, Nvperlecan-like, Nvkielin-like, Nvtbx1-like, Nvfox1, Nvpdgfr-like, Nvret-like2, Nvfgfr-like, Nvpou-like1, Nvpou-like2, NveHand-like, Nvfz1-like, Nvhd058*, transcripts are clearly detected in body wall endomesoderm and potentially also in the pharyngeal endomesoderm (Fig. 2H,J,L,Fig. 2H,J,L,S,U,V,W-,X,Ze,Zf,Zg,Zj,Zq,Zu,U,V,W,X,Ze,Zf,Zg,Zj,Zq,Zu).

3.5. Genes expressed within the ectoderm/apical domain

Our *in situ* hybridization screen also revealed expression patterns of 15 genes in continuous territories within the ectoderm/apical domain (*Nvdkk124, Nvsfrp1/5, Nvc-myc-like, Nvtolloid-like, Nvlhx6, Nvhd146, NvfoxD1, Nvsix3/6, Nvhmx3-like, Nvfoxq2a, Nvfz5/8, Nvax1, Nvrx3-like, Nvsp8/9-like, Nvwnt7B,* Fig. 3). At the blastula stage, we observed very restricted expression of *Nvdkk124, Nvc-myc-like* and *Nvlhx6* towards the vegetal most part of the embryo (Fig. 3A,C,E) and broader expression within the apical domain of *Nvsfrp1/5, Nvtolloid-like, Nvhd146. NvfoxD1, Nvsix3/6, Nvhmx3, Nvfoxq2, Nvfz5/8* and *Nvax1* (Fig. 3B,D,F,M-R). While we did not observe localized expression prior to gastrulation for *Nvrx3-like* (Fig. 3Y) transcripts of *Nvsp8/9-like* were detected in a circumferential ring (Fig. 3Z) and those of *NvWnt7B* faintly throughout the entire blastula but lacking a territory that appears to correspond to the central domain (Fig. 3Za).

Of the twelve genes that were exclusively expressed within the

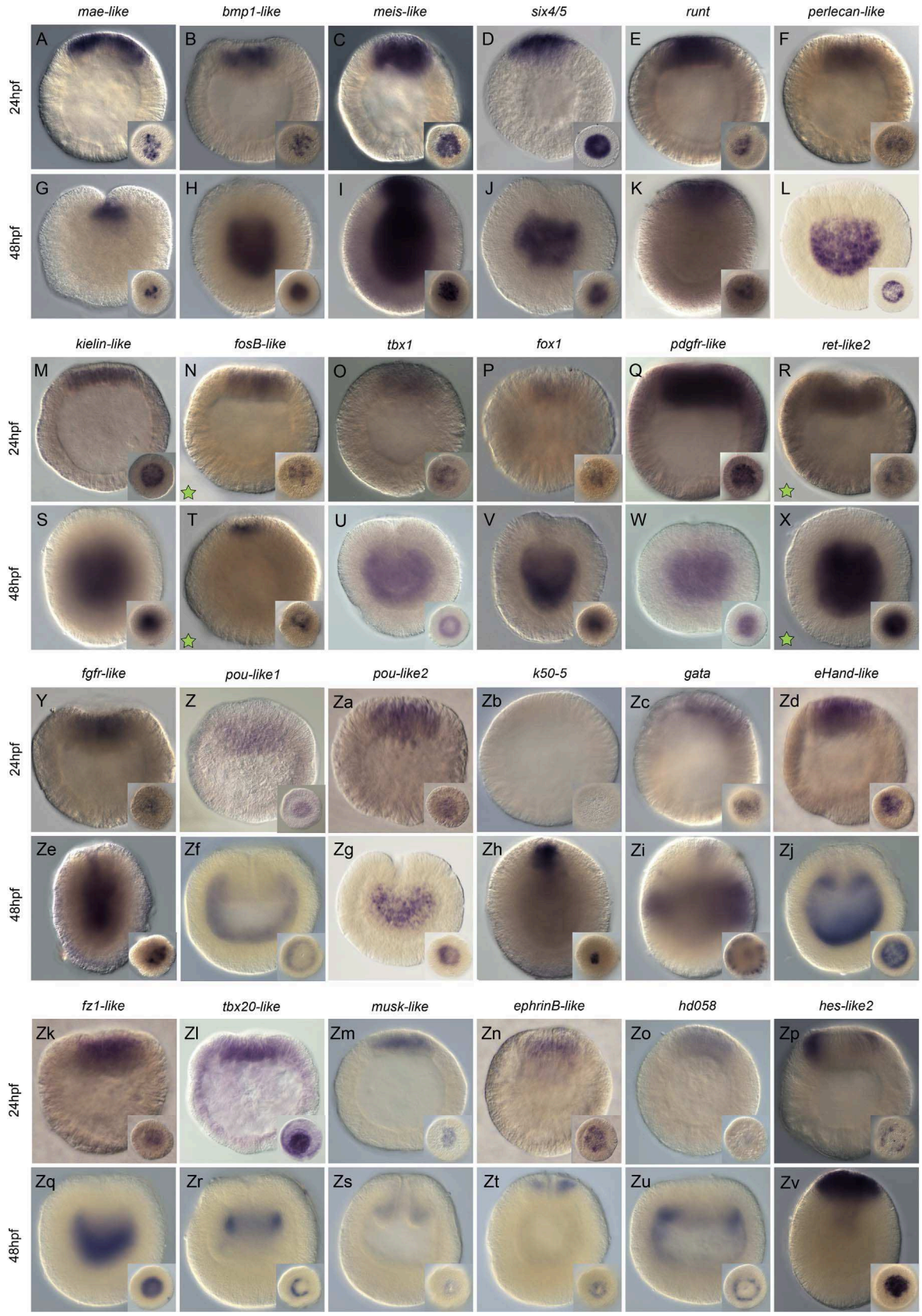

Fig. 2. MEK/ERK signaling targets expressed in the presumptive endomesoderm Wild-type endomesodermal gene expression analysis by *in situ* hybridization of genes differentially regulated by U0126 treatments. All animals are either blastula (24hpf - A-F, M-R, Y-Zd, Zk-Zp) or gastrula (48hpf – G-L, S-X, Ze-Zj, Zq-Zv) stages. All images are lateral views with the animal pole (presumptive endomesoderm) to the top. The insets correspond to animal pole views (A-G, I, K, M-R, T, Y-Zd, Zh, Zv, Zk-Zp) or optical cross-sections. Antisense probes used as indicated at the top of each pair of embryos. Green stars in N, T and R, X indicate that these genes were upregulated under U0126 conditions. All other genes were downregulated.

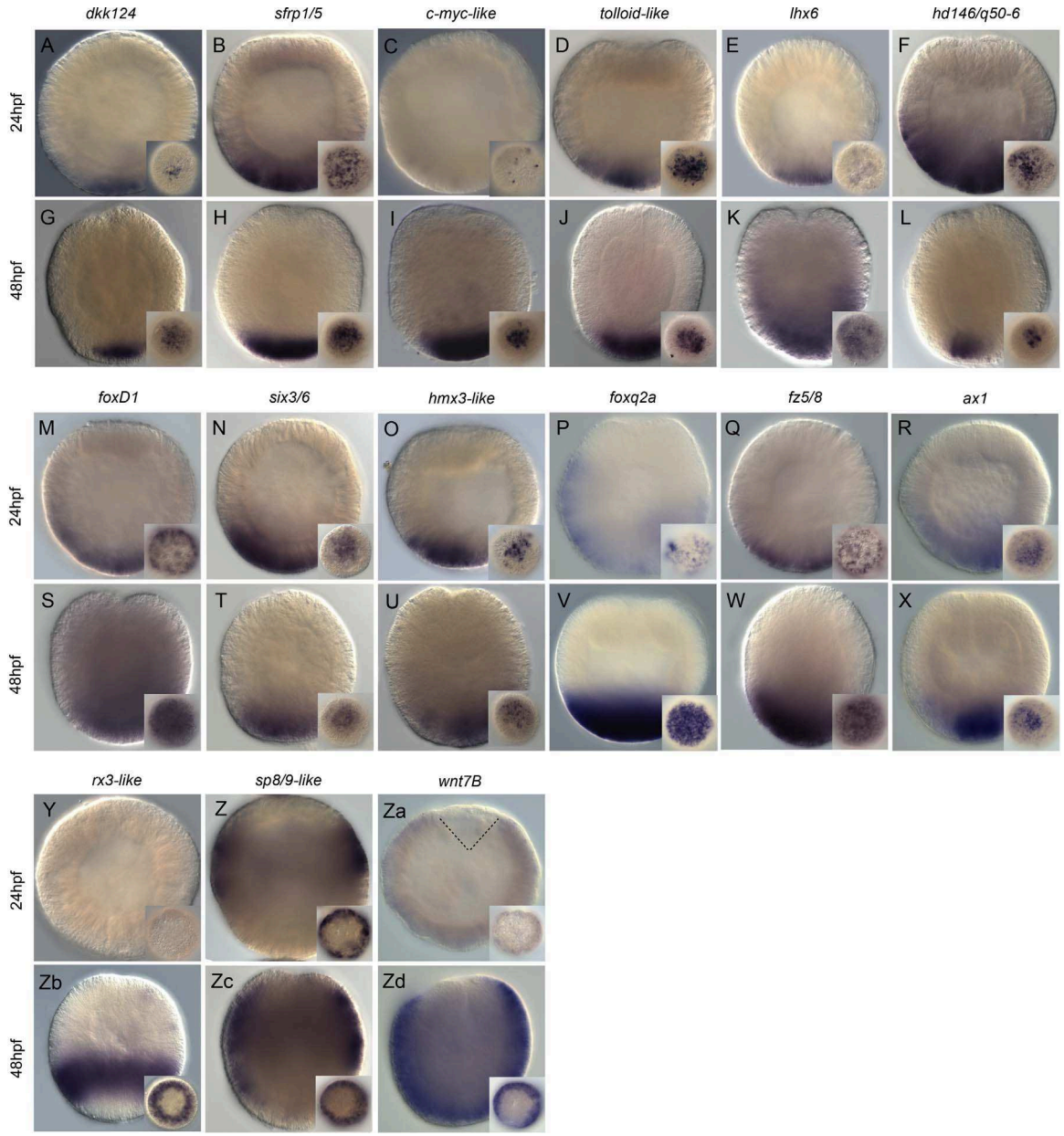

Fig. 3. MEK/ERK signaling targets expressed in broad ectodermal domains. Wild type ectoderm gene expression analysis by *in situ* hybridization of genes downregulated by U0126 treatments. All animals are either blastula (24hpf-A-F, M-R, Y-Za) or gastrula (48hpf – G-L, S-X, Zb-Zd) stages. All images are lateral views with the animal pole to the top. All insets correspond to vegetal pole / aboral views. Antisense probes used as indicated at the top of each pair of embryos.

apical domain of the blastula stage, one can distinguish two groups of genes based on their expression domains at the end of gastrulation (48hpf). While transcripts of *Nvlhx6, NvfoxD1, Nvfoxq2a* and *Nvfz5/8* are detected in a broader domain that appears to correspond to the sub-apical as well as the apical pole domains (Fig. 3K,Fig. 3K,S,V,W,V,W) expression of *Nvdkk124, Nvsfrp1/5, Nvc-myc-like, Nvtolloid-like, Nvhd146, Nvsix3/6, Nvhmx3-lik3* and *Nvax1* seem more restricted to only the apical pole (Fig. 3G,H,I,J,L,T,U,X). *Nvrx3-like* is restricted to a region of the gastrula stage that corresponds to the sub-apical pole domain (Fig. 3Zb), while *Nvsp8/9-like* expression is localized in a broader territory that spans the sub-apical pole and the body wall ectoderm (Fig. 3Zc) and *NvWnt7B* within the bodywall ectoderm, the sub- as well as the apical pole domains (Fig. 3Zd).

Of all gene expression patterns described here only *NvfosB-like* (Fig. 2N,T) and *Nvret-like2* (Fig. 2R,X) have been identified from the set of genes that were up regulated after U0126 treatments (Layden et al., 2016b). Thus, taken together these data strongly suggest that functional ERK/MAPK signaling is crucial for specification and patterning events throughout the entire embryo by the blastula stage. Additional double *in situ* hybridization experiments are required to fine-tune the precise boundaries of expression domains and the relationships that may exist with neighboring domains.

3.6. Temporal gene expression of endomesodermal and ectodermal genes

Spatial expression data, providing information about the presence of maternal transcripts or zygotic upregulation of a given gene, is crucial for the design of functional studies, to predict potential genetic interactions, and build gene regulatory networks (Oliveri and Davidson, 2004). We thus performed a fine scale RT-qPCR analysis (0-48hpf, every two hours) of 23 endomesodermal and 18 apical domain genes (Fig. 4C,D, Fig. S3). This set of analyzed genes contains most of the genes characterized above (Figs. 2

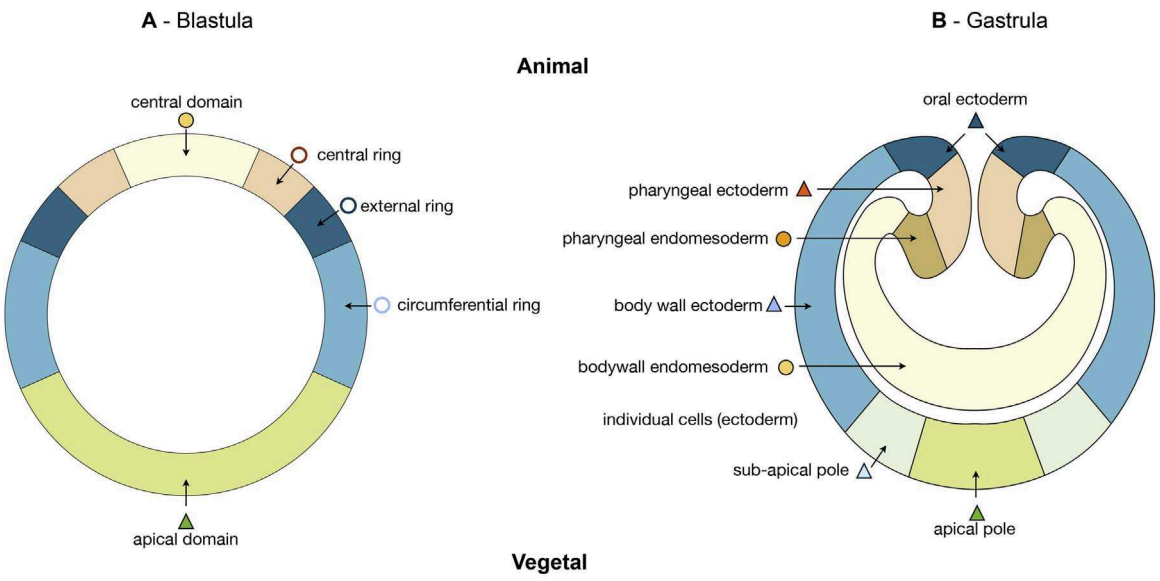

C Gene	Maternal (Cp)	Zygotic UP (hpf)	Expression @ 24hpf	Expression @ 48hpf
fosB-like ☆	**yes (33.01)**	8-10	●	▲
hes-like2	**yes (33.44)**	12-14	○	▲
musk-like	**yes (32.31)**	12-14	●	▲
six4/5	no (40.00)	12-14	●	●●
eHand-like	no (34.53)	16-18	●	●●
pdgfr-like	no (35.47)	16-18	●	●●
mae-like	no (34.56)	16-18	●	▲
fz1-like	no (37.41)	18-20	●	●●
gata	no (34.77)	18-20	●	★
kielin-like	no (39.14)	18-20	●	●●
meis	no (36.79)	18-20	●	▲▲●●
pou-like1	**yes (33.82)**	18-20	●	●●
pou-like2	no (35.07)	18-20	●	●●
runt	no (38.91)	18-20	●	▲
bmp1-like	no (35.18)	20-24	●	●●
fgfr-like	no (35.56)	20-24	●	●●
fox1	no (40.00)	20-24	●	●●
hd058	**yes (33.62)**	20-24	●	●●
k50-5	no (35.74)	20-24	n.d.	▲
perlecan-like	no (35.29)	20-24	●	●●
tbx1	no (40.00)	20-24	●	●●
ret-like2 ☆	**yes (24.51)**	n.d.	●	●●
ephrinB-like	-	-	●	▲

D Gene	Maternal (Cp)	Zygotic UP (hpf)	Expression @ 24hpf	Expression @ 48hpf
lhx6 *	no (37.87)	4-6	▲	△▲
sp8/9-like	no (36.96)	8-10	○	▲△
fgfA1 *, **	no (40.00)	8-10	▲	▲
fgfrA *	no (40.00)	8-10	▲	▲
ax1 *	**yes (31.67)**	10-12	▲	▲
fz5/8 *	no	10-12	▲	△▲
foxq2a *	**yes (30.07)**	12-14	▲	△▲
hmx3-like	no (40.00)	14-16	▲	▲
fgfA2 *	**yes (27.55)**	14-16	▲	▲
rx3-like	**yes (32.22)**	14-16	n.d.	△
sfrp1/5	**yes (27.51)**	14-16	▲	▲
dkk124 *	no (40.00)	16-18	▲	▲
hd146	no (37.67)	16-18	▲	▲
six3/6 *	**yes (33.64)**	16-18	▲	▲
c-myc-like	no (40.00)	18-20	▲	▲
tolloid-like	no (38.69)	18-20	▲	▲
foxD1	**yes (31.87)**	18-20	▲	△▲
wnt7b	no (40.00)	20-24	○○△	▲△▲

Fig. 4. High density gene expression profiling. (A, B) Schematic representation of stage-specific expression domains prior to, and after gastrulation movements. (C, D) Summarized results of the temporal high density profiling (qPCR) used to determine the presence of maternal transcripts and significant zygotic up-regulation of a given gene expressed in (C) endomesodermal, or (D) broad ectodermal domains (see Fig. S3 for details). The Cp value corresponds to the cycle number at detection threshold (crossing point). (hpf) hours post fertilization. Visual keys used to describe the spatial expression domain determined by *in situ* hybridization at 24hpf or 48hpf same as in A, B. (n.d.) Not determined. (*) Indicate genes that have been identified and their spatial blastula and gastrula expression patterns characterized elsewhere (see Tables S4 and S5 in Layden et al. (2016b) for references). However, to include them into our GRNs we performed qPCRs also for these genes (*i.e. fgfA1, fgfA2, ax1* etc...). (**) qPCR value from Röttinger et al. (2012).

and 3) but for the sake of enhancing the current view of the endomesodermal and ectodermal GRNs we also included genes whose ectodermal expression patterns were previously reported (see Fig. 4C,D and Tables S4 and S5 in Layden et al.(2016b) for references).

From the 41 analyzed genes, the vast majority (68%; n=28/41) were not expressed maternally (Cp value, corresponding to the cycle number at detection threshold > 34.00), only one gene did not show significant zygotic upregulation, while all remaining analyzed genes were zygotically expressed before the onset of gastrulation (20-24hpf, Fig. 4C,D). Within the endomesodermal genes (Fig. 4C), the first gene zygotically upregulated was *NvfosB-like* (8-10hpf), followed a few hours later first by *Nvhes-like2, Nvmusk-like, Nvsix4/5* (12-14hpf), then by *NveHand-like, Nvpdgfr-like, Nvmae-like* and *Nvtbx20-like2* (16-18hpf). The vast majority (14/23) within this group of genes, are zygotically upregulated either 18-20hpf (*Nvfz1-like, Nvgata, Nvkielin-like, Nvmeis, Nvpou-like1, Nvpou-like2, Nvrunt*) or 20-24hpf

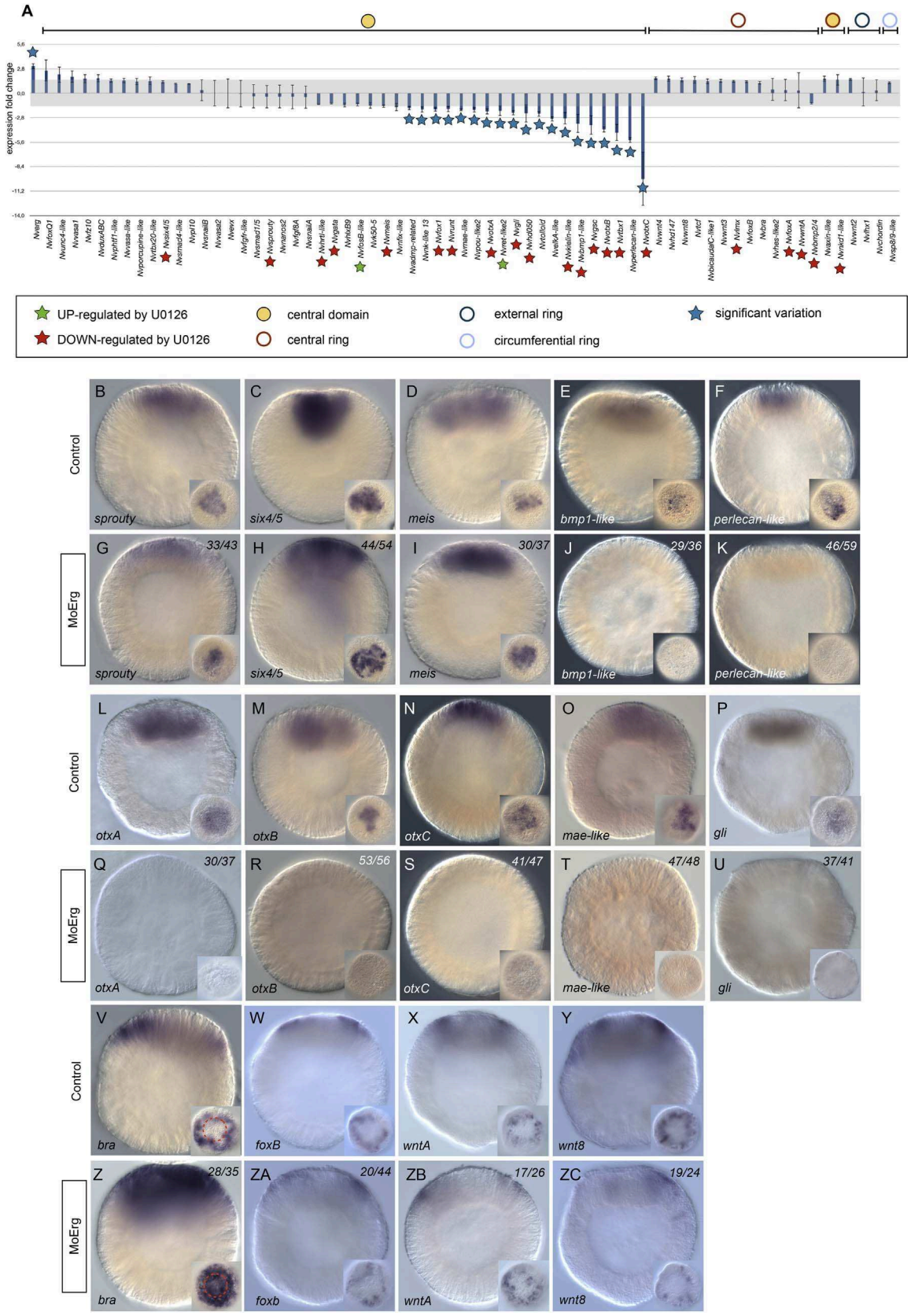

Fig. 5. Molecular phenotype analysis of Mo-NvERG injected embryos on genes expressed in the endomesoderm. (A) Changes in gene expression of 66 potential components of the cnidarian endomesoderm GRN within the animal hemisphere after NvERG knock-down compared to control embryos analyzed by qPCR. Changes in gene expression are indicated as relative fold changes compared to *MO-CTRL* injected embryos ($\bar{x} \pm$ sem, n = 3 per gene). The grey bar indicates no significant change in gene expression (−1.5,1.5). Information on the iconography (stars and circles) are indicated below the graph. Gene expression domains at the blastula stage are the same as Fig. 4A. (**B**) Analysis of the molecular effects of NvERG inhibition (G-K, Q-U, ZA-ZE) compared to control injections (B-F, L-P, V-Z) on endomesodermal gene expression analyzed by *in situ* hybridization. Antisense probes used as indicated in the bottom left corner of each image (also valid for the corresponding inset). The red dashed circle in (V, Z) indicates the central ring expression of *Nvbra* showing extension of its expression domain into the central domain. The numbers in the upper right corner indicates the ratio of embryos with perturbed gene expression to the total number of analyzed embryos. All images are lateral views with the presumptive endomesoderm (animal pole) to the top. Insets are animal pole views.

(*Nvbmp1-like, Nvfgfr-like, Nvfox1, Nvhd058, Nvk50-5, Nvperlecan-like, Nvtbx1-like*). Interestingly, the general zygotic activation pattern of the 18 *genes expressed in the ectoderm* (Fig. 4D) was earlier than the other group of genes. In fact, *Nvlhx6* was zygotically upregulated 4-6hpf, followed by *Nvsp8/9-like, NvfgfA1, NvfgfrA* (8-10hpf), *Nvax1*, *Nvfz5/8* (10-12hpf), *Nvfoxq2a* (12-14hpf), *Nvhmx3-like, NvfgfA2, Nvrx3-like* and *Nvsfrp1/5* (14-16hpf). While *Nvdkk124, Nvhd146* and *Nvsix3/6* are upregulated at 16-18hpf the last set of genes, *Nvc-myc-like, Nvtolloid-like*, *NvfoxD1* and *NvWnt7b* are zygotically regulated between 18-20hpf and 20-24hpf respectively.

3.7. NvErg is required to specify the central domain within the animal hemisphere

In order to identify downstream targets of NvERG required for gastrulation, endomesoderm as well as apical domain formation, we injected MO-NvERG into the fertilized egg and performed qPCR analysis on genes expressed in distinct domains along the animal-vegetal axis of the blastula stage (see Fig. 4A). Of the 47 genes expressed in the central domain, 18 genes (*Nvadmp-related, Nvfox1, Nvrunt, Nvmae-like, Nvpou-like2, NvotxA, Nvret-like2, Nvgli, Nvhd050, Nvtolloid, NvelkA-like, Nvkielin-like, Nvbmp1-like, Nvgsc, NvotxB, Nvtbx1, Nvperlecan-like* and *NvotxC*) were significantly down-regulated (Fig. 5A). The only gene that is up-regulated in this context is *Nverg* which might be caused by a stabilizing effect of the morpholino targeting *Nverg* (Sinigaglia et al., 2013). *In order to confirm that NvERG-DB causes a similar phenotype than Mo-NvERG even at the molecular levels, we performed qPCR analysis on NvERG-DB injected embryos at 24hpf. In line with the milder phenotype observed in latter animals at later developmental stages, the downregulation of gene expression shows a similar trend but not the same amplitude* (Fig. S4)**.** Genes that are expressed in both, the central domain as well as the central ring, or only restricted to the central, external or circumferential rings were not significantly affected by NvERG down-regulation (Fig. 5A).

We have further analyzed the molecular effect of perturbing NvERG function by *in situ* hybridization in order to confirm the qPCR data and to gain additional spatial insight. Analyzing the spatial expression patterns of central domain genes are in line with the qPCR data and showed that *nvsprouty*, *nvsix4/5* and *nvmeis* were unaffected in NvERG morphants (Fig. 5B-D,G-I). Further in agreement with the quantitative expression information, *Nvbmp1-like, Nvperlecan-like, NvotxA, NvotxB, NvotxC, Nvmae-like* and *Nvgli* are no longer/faintly detected in the majority of MO-NvERG injected embryos (Fig. 5E,F,J,K, L-P, Q-U). A report using computational approaches to predict gene interactions in *Nematostella* has suggested that NvERG in the central domain might repress *Nvbra* in order to restrict its expression to the central ring (Abdol et al., 2017). We therefore analyzed central ring gene expression (Fig. 5V-Y,Z-ZC) in MO-NvERG injected embryos, even though their expression levels didn't vary significantly in our qPCR assays. The *in situ* information obtained *for NvfoxB, NvwntA, Nvwnt8* (Fig. 5W-Y, ZA-ZC) were in line with the qPCR data and revealed no variations in response to NvERG inhibition. Interestingly though, *Nvbra* transcripts in NvERG morphants were now also detected in the central domain as well as the central ring (Fig. 5V,Z). The expanded expression domain of this gene highlights the importance of NvERG not only to induce expression of central domain genes, but also to repress specific gene expression in that domain. Thus, NvERG is crucial for the segregation of the central domain and central ring territories during early *Nematostella* development.

3.8. NvERG is a key player of the apical domain gene regulatory network

In addition to its expression in the central domain, *Nverg* transcripts are also detected in the apical domain (Fig. 1Ad-Af) raising the question about its role in patterning this territory. Quantitative molecular analysis of 15 genes expressed in the apical domain revealed that only five genes (*Nvsix3/6, Nvtolloid-like, Nvhd146* and *NvfoxD1*, *NvfgfA2*) are significantly downregulated after MO-NvERG injection *prior to the onset of gastrulation* (**24hpf,** Fig. 6A). Consistent with this result, spatial expression analysis revealed that no transcripts were detected in the apical domain for *Nvsix3/6, NvfoxD1*, *Nvhd146* and *NvfgfA2* for the majority of NvERG morphants (Fig. 6A, G-I,K). Surprisingly, we also observed a visible downregulation of *Nvsfrp1*/5 by *in situ* hybridization, although there was no striking effect observed by qPCR (Fig. 6A, J). These effects of NvERG down-regulation on genes expressed in the vegetal most domains are in line with the bipolar gene expression of this gene. In addition, these data *suggest that the phenotype of MO-NvERG on apical tuft formation* **(**Fig. 2**h)** *is a direct consequence of this knockdown, rather than an indirect effect caused by the failure of gastrulation.*

FGF/FGFR signaling and the transcription factor NvSix3/6 have been shown to play a crucial role for apical domain patterning at the end of gastrulation (Rentzsch et al., 2008; Sinigaglia et al., 2013). However, no information is available concerning the roles of those genes prior to the onset of gastrulation. In order to gain a better understanding about the relationship between NvFGFRA, NvSix3/6 and NvERG, we inhibited NvFGFRA and NvSix3/6 using previously described morpholinos (Rentzsch et al., 2008; Sinigaglia et al., 2013) and analyzed gene expression of the same set of apical domain genes (Fig. 6A, Q-U, Y-ZA) as for NvERG morphants. In NvSix3/6 morphant early gastrula, only *Nvlhx6* expression is affected (Fig. 6A, Y). However, inhibition of NvFGFRA shows that expression of *Nvlhx6, NvfgfA1, NvfgfA2, Nvsix3/6, Nvhd146* and Nvsfrp1/5 is downregulated (Fig. 6A). While *in situ* expression analysis clearly confirmed the loss of *NvfgfA2, Nvhd146, Nvlhx6* and Nvsfrp1/5 expression, the reduction of *Nvsix3/6* expression after blocking NvERG function seems subtle (Fig. 6Q-U). The clear overlap of NvFGFRA and NvERG downstream targets, strongly suggest that NvERG activity is partly mediated by NvFGFRA/MAPK signaling in the apical domain. *In addition, we have assessed whether apical domain expression of Nverg is NvSix3/6 or FgfrA dependent. While erg expression is not affected in Six3/6 morphants, the apical domain expression of erg is not detected anymore in MO-FgfrA injected embryos, suggesting that apical erg expression requires functional FgfrA signaling.*

4. Discussion

4.1. The ETS gene family in Nematostella

The ETS family of genes is evolutionarily conserved (Laudet et al., 1993, 1999; Degnan et al., 1993; Rizzo et al., 2006) and formed by transcriptional regulators involved in various aspects of development, differentiation, hormone responses and tumorgenesis (Röttinger et al., 2004; Kiyota et al., 2007; Kataoka et al., 2011; Kar and Gutierrez-Hartmann, 2013; Chen et al., 2013; Kawahara et al., 2015; Koh et al., 2016; Peng et al., 2016; Rizzo et al., 2016). Our genome wide survey of ETS transcription factors present in *Nematostella* revealed the presence of 12 members of this gene family (Fig S1). Nine of them belong to eight out of the eleven described subfamilies (SPI, ESE, TEL, TCF, ETS, ERG, ELG, PEA3). While we were not able to identify members of the PDEF, ELF and ERF subfamilies, we identified three additional genes (*Nvets-like-A*, *Nvets-like-B* and *Nvets-like-C*) that do not group in neither of the subfamilies but are predicted to contain an ETS domain (Fig S1). Expression information for *Nvpea3*, *Nvets-likeA* and *Nverg* have been reported ((Röttinger et al., 2012; Layden et al., 2016b), this study), however, additional work is needed to gain insight into the spatial and temporal expression dynamics of those transcription factors during cnidarian development.

The PDEF, ESE, TEL, ETS, ERG and ELG subfamilies in bilaterian animals are characterized, in addition to the ETS domain, by the

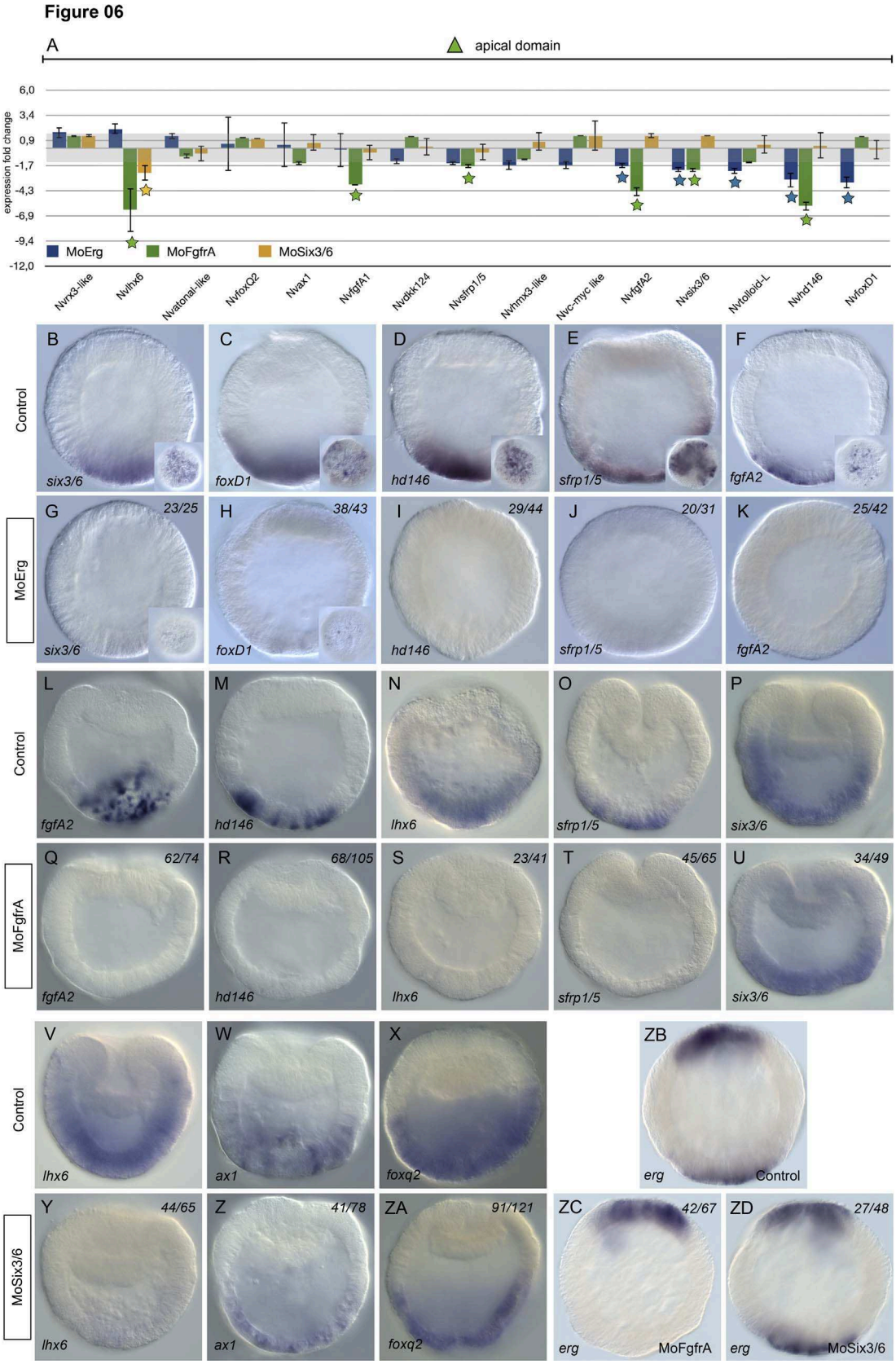

Fig. 6. Molecular phenotype analysis of MO-NvERG, MO-NvFGFRA and NvSix3/6 injected embryos on genes expressed in the apical domain. (A) Changes in gene expression of 15 potential components of the cnidarian apical domain GRN within the vegetal hemisphere after NvERG (blue), NvFGFRA (green) or NvSix3/6 (yellow) knock-downs compared to control embryos analyzed by qPCR. Changes in gene expression are indicated as relative fold changes compared to *MO-CTRL* injected control embryos ($\bar{x} \pm$ sem, n = 3 per gene). The grey bar indicates no significant change in gene expression (−1.5,1.5). Stars below the bars indicate significant variation. Analysis of the molecular effects of NvERG (G-K), NvFGFRA (Q-U) and NvSix3/6 (Y-ZA) inhibition compared to control injections (B-F, L-P, V-X) on apical domain gene expression analyzed by *in situ* hybridization. Antisense probes used as indicated in the bottom left corner of each image (also valid for the corresponding inset). The numbers in the upper right corner indicates the ratio of embryos with perturbed gene expression to the total number of analyzed embryos. All images are lateral views with the presumptive endomesoderm (animal pole) to the top.

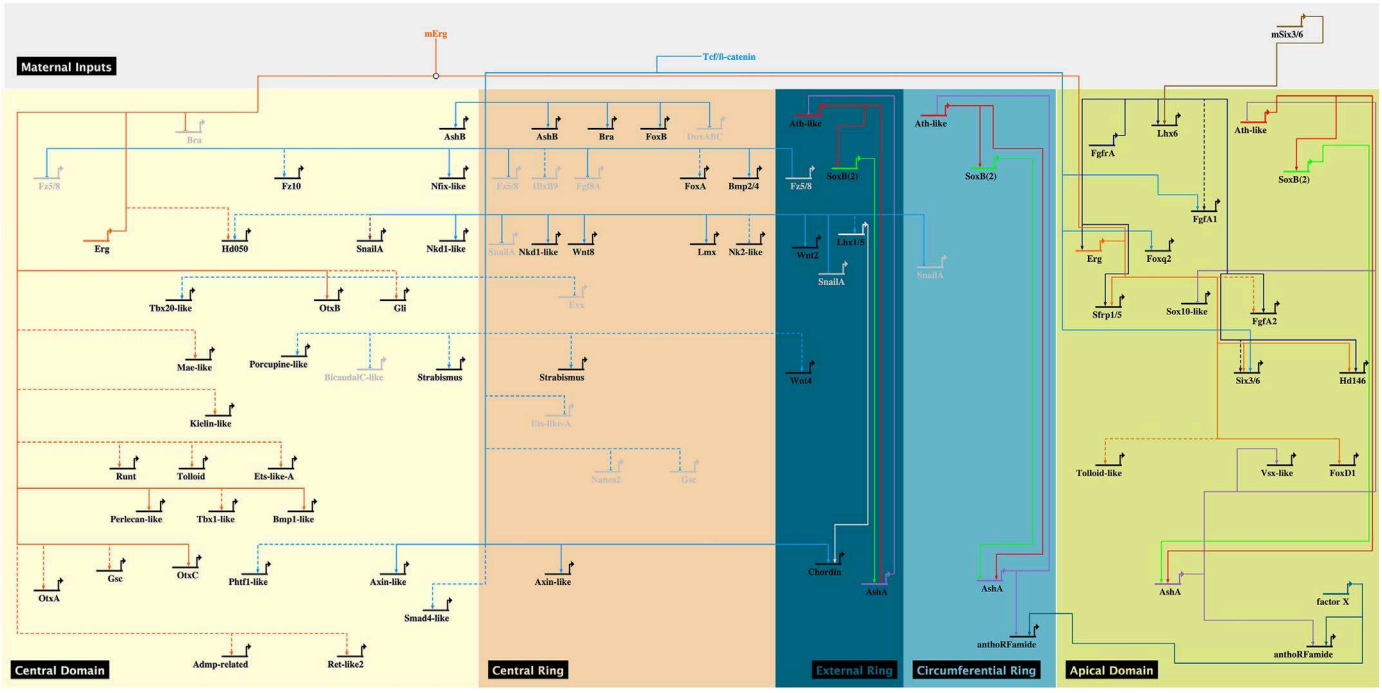

Fig. 7. Updated gene regulatory network orchestrating embryonic development in the cnidarian *N. vectensis*. Enhanced Biotapestry diagram (Longabaugh and Bolouri, 2006) of the gene regulatory network describing the gene deployment at 24hpf and regulatory interactions of endomesodermal, ectodermal and neuronal genes identified in previous studies (Röttinger et al., 2012; Leclère et al., 2016; Layden et al., 2016b, 2012; Yasuoka et al., 2009). No assumption on whether these interactions are direct or indirect is made. Solid lines indicate functional evidence obtained by qPCR as well as *in situ* hybridization, dashed lines indicate evidence obtained only by qPCR. The colored boxes represent the spatial domains as described in Fig. 4A. Genes inactivated by repression in a given territory are represented in light grey. Controversial results (Röttinger et al., 2012; Kumburegama et al., 2011b) about the role of cWnt/TCF signaling on *NvsnailA* expression is indicated by a red dashed arrow. The same GRN, including non-connected genes that are expressed within the specific territories is provided in Fig. S5. A first draft of the global GRN framework for body wall endomesoderm, pharynx (endomesoderm and ectoderm), mouth, body wall ectoderm, sub-apical and apical domain including components of the *Nematostella* nervous system at the end of gastrulation (48 hpf) is provided in Figure S6.

presence of a Pointed domain that is involved in a series of complex interactions with co-factors to modulate gene expression of downstream targets (Rizzo et al., 2006; Sharrocks, 2001; Gutierrez-Hartmann et al., 2007). To our surprise, the only ETS gene product in *Nematostella* predicted to possess a Pointed domain is NvERG (Fig S1), suggesting a potential modulation of its transcriptional activity by other Pointed domain containing proteins. Interestingly, one of the downstream targets of MEK/ERK signaling and NvERG we identified is NvMae-like, a Pointed domain containing protein described to regulate transcriptional activity of YAN (*Drosophila* ortholog of TEL) and Pointed (*Drosophila* ortholog of ETS-2) (Baker et al., 2001). *Nvmae-like* is zygotically expressed in the central domain under the control of NvERG suggesting that both proteins interact to potentiate transcriptional activity in this territory and further enhance segregation of specific domains within the animal domain.

4.2. *A global gene regulatory network orchestrating specification and patterning events of the early embryo*

Our data show that MEK/ERK signaling upstream of the transcription factor ERG is required during early embryogenesis in both hemispheres of the blastula: in the animal pole for specifying endomesoderm that probably lead indirectly to the observed failure of gastrulation and gut formation; in the vegetal pole, for specifying the apical domain and participating in apical tuft development. Thus, the present spatial and temporal expression data combined with the molecular characterization of NvERG specific knock-down experiments enabled us i) to add new genes to the existing endomesoderm GRN (Röttinger et al., 2012) in particular within the central domain of the blastula stage (Fig. 7), ii) extend this GRN to genes involved in early apical domain (ectoderm) specification at the same stage (Fig. 7), and iii) draft a global GRN framework for body wall endomesoderm, pharynx (endomesoderm and ectoderm), mouth, body wall ectoderm, sub-apical and apical domains, including components of the *Nematostella* nervous system (Fig. S5). In order to provide an up to date view of the genetic interactions during *Nematostella* development, the present networks (Fig. 7, Fig. S5) also include previously published functional data (Röttinger et al., 2012; Layden et al., 2012), (Rentzsch et al., 2008; Sinigaglia et al., 2013; Layden et al., 2016b, 2012; Kumburegama et al., 2011a). In the current version, no claim about direct genetic interactions is made, and additional experiments such as *cis*-regulatory or CHIP-seq analysis are required.

The present results clearly show that NvERG is one of the main transcription factors involved in this bi-polar activity and might be one of the effectors of MEK/ERK signaling. In fact, MEK/ERK signaling is known to control transcriptional activity (enhancer or repression) of ETS transcription factors by phosphorylating specific residues (Röttinger et al., 2004; Selvaraj et al., 2015; Hollenhorst, 2012; Huang et al., 2016). *Nverg* appears not to be transcriptionally controlled by MEK/ERK signaling as it was not identified as being one of the MEK/ERK downstream targets (Layden et al., 2016b). Nonetheless, we identified certain downstream targets of MEK/ERK (Layden et al., 2016b) that are also controlled by NvERG (*e.g. NvotxA,* Fig. 5), suggesting a functional control of NvERG by ERK/MEK signaling. Using a phosphorylation motif prediction software (PhosphoMotif Finder, www.hprd.org), we identified 196 potential Serine/Threonine Kinase/phosphatase motifs in NvERG, 15 of which might be more prone to be sensitive to regulation by ERK (Huang et al., 2016). However, a precise and systematic approach is required to identify the residue(s) responsible for the activation of ERG in *Nematostella*. Interestingly, we also observed that a few genes (*e.g. Nvsprouty*) downstream of MEK/ERK signaling (Layden et al., 2016b) are not sensitive to NvERG knock-down (Fig. 5), suggesting that other MEK/ERK transcriptional effectors are also involved in initiating the embryonic GRN in *Nematostella*.

4.3. Relation between cWnt and ERK pathway in endomesoderm specification

We have previously shown that cWNT controls expression of genes in different domains within the animal hemisphere, with a predominant role for proper gene expression within the central ring domain (Röttinger et al., 2012). In the present study, focusing only at the animal hemisphere, we have identified and characterized genes downstream of MEK/ERK signaling that are primarily expressed in the central domain at the blastula stage (Fig. 2). Among the genes down-regulated by U0126 treatments for which previous expression patterns have been reported, we can find genes expressed in the central domain (*Nvgli, Nvgsc, Nvhd50, Nvfix-like, NvotxA, NvotxB, NvotxC, Nvsprouty,* (Matus et al., 2007; Röttinger et al., 2012; Matus et al., 2008; Matus et al., 2006a; Ryan et al., 2006; Ryan et al., 2007; Chourrout et al., 2006; Mazza et al., 2007)), in the central ring (*Nvbmp2/4, NvfoxA, Nvlmx, NvwntA, Nvwnt3,* (Röttinger et al., 2012; Martindale et al., 2004; Chourrout et al., 2006; Matus et al., 2006b; Rentzsch et al., 2006; Fritzenwanker et al., 2004; Srivastava et al., 2010; Lee et al., 2006; Kusserow et al., 2005)), in both central ring and central domain (*Nvnkd1-like,* (Röttinger et al., 2012)) as well as those just in the external ring (*Nvlhx1*, (Röttinger et al., 2012; Yasuoka et al., 2009)). NvERG specific knockdown experiments show that a large part of MEK/ERK downstream targets within the central domain are also NvERG targets suggesting that within the central domain, MEK/ERK signaling might be mediated *via* NvERG at the transcriptional level. This in turn also suggests that in the other domains of the animal hemisphere, MEK/ERK signaling is mediated by other transcription factors that are yet to be identified.

Temporal qPCR data show that massive zygotic up-regulation of genes within the animal hemisphere identified from the UO126 array (Layden et al., 2016b) begins at about 16hpf (Fig. 4). Interestingly, a temporal qPCR analysis obtained from genes downstream of cWNT signaling show a similar massive zygotic up-regulation of genes but at an earlier stage of development (prior to 14hpf) (Röttinger et al., 2012). Thus, it appears that cWNT specifies a broad "endomesodermal" domain within the animal hemisphere early during embryonic development, and subsequently MEK/ERK signaling is activated to specify a sub-domain (the central domain) to restrict cWNT activity to the central ring domain. The fact that MEK/ERK and NvERG inhibition expand expression of the cWNT target and central ring gene *Nvbra* towards the central domain ((Layden et al., 2016b), Fig. 5) support the idea that MEK/ERK/ERG signaling has a major impact on specifying the central domain (the future gut) and preventing cWNT activity in this domain.

Within the animal hemisphere at blastula stages, perturbing cWNT signaling has a major impact on central ring gene expression (Röttinger et al., 2012), while inhibiting MEK/ERK/ERG activity blocks expression of mainly central domain genes (Fig. 5). The role of cWNT signaling on gastrulation movements has been addressed using different approaches obtaining various degrees of phenotypes (Röttinger et al., 2012; Leclère et al., 2016; Lee et al., 2007; Wikramanayake et al., 2003; Kumburegama et al., 2011b). Nonetheless, the latest study showed that by performing a morpholino-mediated inhibition of Nvßcatenin, gastrulation was blocked (Leclère et al., 2016). The present study shows that inhibition of ERG (Fig. 1) phenocopies inhibition of MEK/ERK signaling (Layden et al., 2016b) by also blocking (directly or indirectly) the invagination of the endomesoderm. It would be of importance to decipher the precise mechanisms and the molecular interplay between cWNT and MEK/ERK/ERG signaling in governing morphogenetic movements of gastrulation in *Nematostella*.

4.4. Endomesoderm GRN evolution

Comparative gene regulatory analyses in echinoderm embryos, has suggested the presence of an evolutionarily conserved network "kernel" required for endomesoderm formation (Hinman et al., 2007). This Kernel is composed of five transcription factors (*bra, foxA, otx, blimp1 and gataE*) that tightly interact *via* feedback loops and that severely affect endomesoderm formation when individually knocked-down (Hinman et al., 2007). Based on the observation that *Nvblimp* orthologs appear not to be expressed prior to the end of gastrulation (Martindale, unpublished) and that *Nvgata* transcripts were only described in individual cells of the ectoderm (Martindale et al., 2004), we have previously proposed that the cnidarians endomesodermal kernel is only composed of *NvfoxA*, *Nvbra* and *NvOtx* (*A*,*B* and *C*) (Röttinger et al., 2012). The present study, clearly shows that in addition to its ectodermal expression during gastrulation (Martindale et al., 2004) *Nvgata* transcripts are detected in the animal hemisphere at the blastula stage, strongly suggesting that this gene could be part of the cnidarian endomesoderm kernel. At the blastula stage *Nvbra* and *NvfoxA* (both downstream of cWNT signaling (Röttinger et al., 2012)) are expressed in the central ring while *Nvotx* (*A*,*B* and *C*) and *Nvgata* are expressed in the central domain. As NvERG is required to repress *Nvbra* expression in the central domain ((Abdol et al., 2017), this study), these observations foster the idea that rather than being a general endomesoderm kernel connected by feedback loops, those genes are required for the segregation of a central domain and a central ring prior to the onset of gastrulation. A careful analysis of their spatial expression during earlier developmental stages and importantly, functional studies to decipher the precise genetic interactions between those genes is required to better understand a evolutionary conservation of the endomesoderm kernel.

In sea urchins, MEK/ERK signaling, activated during later stages by FGF/FGFR and VEGF/VEGFR (Röttinger et al., 2004, 2008; Fernandez-Serra et al., 2004; Duloquin et al., 2007) is required for mesoderm formation. Interestingly, ETS1 is activated in the primary mesenchyme cells (PMC, mesoderm) by MEK/ERK and crucial for ERG expression (http://sugp.caltech.edu/endomes/#Veg-6–18-NetworkDiagram), PMC ingression and differentiation into the specific mesodermal lineage (Röttinger et al., 2004). On the other hand echinoderm cWNT signaling is required to initiate the general endomesoderm GRN and drive endoderm specification once the mesoderm specification program has been launched (Davidson et al., 2002a, 2002b). Our observations about i) cWNT initiating a broad endomesoderm GRN with a particular emphasis on central ring domain expression (Röttinger et al., 2012) and ii) MEK/ERK/ERG signaling being required to repress central ring fate (*Nvbra* expression) and specify the central domain illustrate the strong evolutionary conservation of this mechanism between cnidarians and echinoderms. Cnidarians are described not to form a true mesodermal germ layer. However, the expression of the classical mesodermal marker *brachyury* (Herrmann et al., 1990) in the central ring, as well as the activation of a MEK/ERK/ERG pathway (required for mesoderm formation in bilaterians (Dorey and Amaya, 2010)) in the central domain, provide additional compelling evidence that both domains together form subregionalized territories of the cnidarian endomesoderm. Tissue tracking experiments using photo-convertible fluorescent proteins (Amiel et al., 2015) are required to determine the fate of the central domain and ring. It might also be important to carry out a precise physiological analysis of the differentiated tissues that originated from the endomesodermal territory, to gain more insight in the evolutionary origin of mesoderm in bilaterians.

4.5. Relationship between cWnt and MEK/ERK/ERG signaling in patterning the apical domain

Several studies suggested a role of cWNT signaling in ectoderm patterning, as ectopically activating or inhibiting cWNT (Röttinger et al., 2012; Lee et al., 2007; Wikramanayake et al., 2003; Kumburegama et al., 2011b; Marlow et al., 2013), perturbs gene expression within the body wall ectoderm and apical domain. In particular, inhibiting ßcat

function causes the loss of *Nvfgfa1, NvfoxQ2* and *Nvsix3/6* expression in the apical domain (Leclère et al., 2016). In a previous study, we predominantly reported genes that were up-regulated following ectopic cWnt activation (Röttinger et al., 2012). However, about 30 genes were also downregulated under those conditions (Table S1). Interestingly, 14 out of the 30 identified genes are also down regulated after MEK/ERK inhibition (Layden et al., 2016b). Among these 14 genes downregulated following MEK/ERK inhibition, seven are expressed in the apical domain (*Nvtolloid-like, Nvsfrp1/5, Nvlhx6, Nvhmx3, Nvhd146, NvfoxD1, Nvax1* (Fig. 3)), four in individual cells throughout the ectoderm (*Nvhd145, Nvgfi-like, Nvgcm, Nvcoup-like2* (Layden et al., 2016b)) and two in derivatives of the animal pole (*Nvhes-like2, Nvgsc* (Fig. 2, (Röttinger et al., 2012)). Inhibition of NvERG has no detectable effect on genes expressed in the individual cells of the ectoderm (data not shown) or *Nvhes-like2* of the central ring (Fig. 5). However, perturbing NvERG function clearly blocks *Nvgsc* expression in the central domain (Fig. 5) and expression of *Nvtolloid-like, Nvsfrp1/5, Nvhmx3, Nvhd146* and *NvfoxD1* (Fig. 6) within the apical domain. These observations strongly support the idea of an antagonistic effect of cWnt and MEK/ERK/ERG signaling in a specific set of genes and that this signaling pathway interplay is crucial for patterning the apical domain. Importantly though, *Nvsix3/6* expression (a key regulator of apical domain formation (28)) requires the combined activity of cWnt (31) as well as MEK/ERK/ERG signaling further underlining the complex interplay of these two pathways to pattern the cnidarian embryonic body axis. Additional gene specific experiments as well as *cis*-regulatory analysis of the above mentioned genes would shed further light on the direct or indirect antagonistic effects of these two major developmental signaling pathways for cnidarian embryogenesis.

Funding

This project was funded by an NIH grant GM093116 to MQM, and supported by an ATIP-Avenir award (CNRS/INSERM – ITMO Plan Cancer **C13992AS**), a Marie-Curie Career Integration Grant (CIG – FP7 European Commission #631665) as well as by the Fondation pour la recherche sur le cancer (ARC **PJA2014120186**) to ER. Individual fellowships were provided by the FRM (Fondation pour la Recherche Médicale **SPF20130526781**) and the MESR (French Ministry of higher education and science) to ARA and HJ respectively.

Author contributions

ER, MJL and MQM – Conceived, designed and performed experiments. ARA, HJ, TC, PD, MI – generated, collected and analyzed data. ER, MQM - Contributed reagents/materials/analysis tools. ER, ARA, HJ, MQM - Drafted the manuscript. All authors read and approved the final manuscript

Competing interests

The author(s) declare(s) that they have no competing interests.

Acknowledgments

The authors thank individuals in the MQM, ER and ML labs and Dominic van Essen for discussions. The authors also acknowledge Valérie Carlin for animal care and the IRCAN's Molecular and Cellular Core Imaging (PICMI) Facility. PICMI was supported financially by Cancéropole PACA, Région Provence Alpes-Côte d'Azur, Conseil Départemental 06 and INSERM.

Appendix A. Supporting information

Supplementary data associated with this article can be found in the online version at doi:10.1016/j.ydbio.2017.08.015.

References

Amiel, A.R., Johnston, H.T., Nedoncelle, K., Warner, J.F., Ferreira, S., Röttinger, E., 2015. Characterization of morphological and cellular events underlying oral regeneration in the Sea Anemone, Nematostella vectensis. Int J. Mol. Sci. 16, 28449–28471. http://dx.doi.org/10.3390/ijms161226100.

Abdol, A.M., Röttinger, E., Jansson, F., Kaandorp, J.A., 2017. A novel technique to combine and analyse spatial and temporal expression datasets: A case study with the sea anemone Nematostella vectensis to identify potential gene interactions. Dev. Biol. 428 (1), 204–214.

Baker, D.A., Mille-Baker, B., Wainwright, S.M., Ish-Horowicz, D., Dibb, N.J., 2001. Mae mediates MAP kinase phosphorylation of Ets transcription factors in Drosophila. Nature 411, 330–334. http://dx.doi.org/10.1038/35077122.

Bertrand, S, Camasses, A, Somorjai, I, Belgacem, MR, Chabrol, O, Escande, M-L, et al., 2011. Amphioxus FGF signaling predicts the acquisition of vertebrate morphological traits. Proc. Natl. Acad. Sci. USA 108, 9160–9165. http://dx.doi.org/10.1073/pnas.1014235108.

Bertrand, S., Iwema, T., Escriva, H., 2014. FGF signaling emerged concomitantly with the origin of eumetazoans. Mol. Biol. Evol. 31, 310–318. http://dx.doi.org/10.1093/molbev/mst222.

Burdine, RD, Chen, EB, Kwok, SF, Stern, MJ, 1997. egl-17 encodes an invertebrate fibroblast growth factor family member required specifically for sex myoblast migration in Caenorhabditis elegans. Proc. Natl. Sci. USA 94, 2433–2437.

Casci, T., Vinós, J., Freeman, M., 1999. Sprouty, an intracellular inhibitor of Ras signaling. Cell 96, 655–665.

Chen, Y., Chi, P., Rockowitz, S., Iaquinta, P.J., Shamu, T., Shukla, S., et al., 2013. ETS factors reprogram the androgen receptor cistrome and prime prostate tumorigenesis in response to PTEN loss. Nat. Med. Nat. Res. 19, 1023–1029. http://dx.doi.org/10.1038/nm.3216.

Chourrout, D., Delsuc, F., Chourrout, P., Edvardsen, R.B., Rentzsch, F., Renfer, E., et al., 2006. Minimal ProtoHox cluster inferred from bilaterian and cnidarian Hox complements. Nature 442, 684–687. http://dx.doi.org/10.1038/nature04863.

Darling, J.A., Reitzel, A.R., Burton, P.M., Mazza, M.E., Ryan, J.F., Sullivan, J.C., et al., 2005. Rising starlet: the starlet sea anemone, Nematostella vectensis. Bioessays 27, 211–221. http://dx.doi.org/10.1002/bies.20181.

Davidson, E.H., Rast, J.P., Oliveri, P., Ransick, A., Calestani, C., Yuh, C.-H., et al., 2002a. A provisional regulatory gene network for specification of endomesoderm in the sea urchin embryo. Dev. Biol. 246, 162–190. http://dx.doi.org/10.1006/dbio.2002.0635.

Davidson, E.H., Rast, J.P., Oliveri, P., Ransick, A., Calestani, C., Yuh, C.-H., et al., 2002b. A genomic regulatory network for development. Science 295, 1669–1678. http://dx.doi.org/10.1126/science.1069883.

Davies, S.P., Reddy, H., Caivano, M., Cohen, P., 2000. Specificity and mechanism of action of some commonly used protein kinase inhibitors. Biochem J. 351, 95–105. http://dx.doi.org/10.1042/0264-6021:3510095.

Degnan, B.M., Degnan, S.M., Naganuma, T., Morse, D.E., 1993. The ets multigene family is conserved throughout the Metazoa. Nucleic Acids Res. 21, 3479–3484.

DeSilva, D.R., Jones, E.A., Favata, M.F., Jaffee, B.D., Magolda, R.L., Trzaskos, J.M., et al., 1998. Inhibition of mitogen-activated protein kinase kinase blocks T cell proliferation but does not induce or prevent anergy.. J. Immunol. Am. Assoc. Immnol 160, 4175–4181.

Dorey, K., Amaya, E., 2010. FGF signalling: diverse roles during early vertebrate embryogenesis. Development (Cambridge, England) 137, 3731–3742. http://dx.doi.org/10.1242/dev.037689.

Draper, B.W., Stock, D.W., Kimmel, C.B., 2003. Zebrafish fgf24 functions with fgf8 to promote posterior mesodermal development. Development 130 (4639–4654). http://dx.doi.org/10.1242/dev.00671.

Duloquin, L., Lhomond, G., Gache, C., 2007. Localized VEGF signaling from ectoderm to mesenchyme cells controls morphogenesis of the sea urchin embryo skeleton. Development (Cambridge, England) 134, 2293–2302. http://dx.doi.org/10.1242/dev.005108.

Fernandez-Serra, M., Consales, C., Livigni, A., Arnone, M.I., 2004. Role of the ERK-mediated signaling pathway in mesenchyme formation and differentiation in the sea urchin embryo. Dev. Biol. 268, 384–402. http://dx.doi.org/10.1016/j.ydbio.2003.12.029.

Fritzenwanker, J.H., Genikhovich, G., Kraus, Y., Technau, U., 2007. Early development and axis specification in the sea anemone Nematostella vectensis. Dev. Biol. 310, 264–279. http://dx.doi.org/10.1016/j.ydbio.2007.07.029.

Fritzenwanker, J.H.J., Saina, M.M., Technau, U.U., 2004. Analysis of forkhead and snail expression reveals epithelial-mesenchymal transitions during embryonic and larval development of Nematostella vectensis. Dev. Biol. 275, 389–402. http://dx.doi.org/10.1016/j.ydbio.2004.08.014.

Green S.A., Norris R.P., Terasaki M., Lowe C.J., 2013. FGF signaling induces mesoderm in the hemichordate Saccoglossus kowalevskii. Development (Cambridge, England). http://dx.doi.org/10.1242/dev.083790.

Gutierrez-Hartmann, A., Duval, D.L., Bradford, A.P., 2007. ETS transcription factors in endocrine systems. Trends Endocrinol. Metab. 18, 150–158. http://dx.doi.org/10.1016/j.tem.2007.03.002.

Hacohen, N.N., Kramer, S.S., Sutherland, D.D., Hiromi, Y.Y., Krasnow, M.A.M., 1998. sprouty encodes a novel antagonist of FGF signaling that patterns apical branching of the Drosophila airways. Cell 92, 253–263. http://dx.doi.org/10.1016/S0092-8674(00)80919-8.

Hand, C., Uhlinger, K.R., 1992. The culture, sexual and asexual reproduction, and growth of the sea anemone Nematostella vectensis. Biol. Bull. MBL 182, 169–176.

Herrmann, B.G., Labeit, S., Poustka, A., King, T.R., Lehrach, H., 1990. Cloning of the T gene required in mesoderm formation in the mouse. Nature 343, 617–622. http://

dx.doi.org/10.1038/343617a0.
Hinman, V.F., Nguyen, A., Davidson, E.H., 2007. Caught in the evolutionary act: precise cis-regulatory basis of difference in the organization of gene networks of sea stars and sea urchins. Dev. Biol. 312, 584–595. http://dx.doi.org/10.1016/j.ydbio.2007.09.006.
Hollenhorst, P., 2012. RAS/ERK pathway transcriptional regulation through ETS/AP-1 binding sites. Smallgtpases 3, 154–158. http://dx.doi.org/10.4161/sgtp.19630.
Huang, Y., Thoms, J.A.I., Tursky, M.L., Knezevic, K., Beck, D., Chandrakanthan, V., et al., 2016. MAPK/ERK2 phosphorylates ERG at serine 283 in leukemic cells and promotes stem cell signatures and cell proliferation. Leukemia 30, 1552–1561. http://dx.doi.org/10.1038/leu.2016.55.
Ikmi, A., McKinney, S.A., Delventhal, K.M., Gibson, M.C., 2014. TALEN and CRISPR/Cas9-mediated genome editing in the early-branching metazoan Nematostella vectensis. Nat. Commun. 5, 5486. http://dx.doi.org/10.1038/ncomms6486.
Kar, A., Gutierrez-Hartmann, A., 2013. Molecular mechanisms of ETS transcription factor-mediated tumorigenesis. Crit. Rev. Biochem. Mol. Biol. 48, 522–543. http://dx.doi.org/10.3109/10409238.2013.838202.
Kataoka, H., Hayashi, M., Nakagawa, R., Tanaka, Y., Izumi, N., Nishikawa, S., et al., 2011. Etv2/ER71 induces vascular mesoderm from Flk1+PDGFRα+ primitive mesoderm. Blood. Am. Soc. Hematol. 118, 6975–6986. http://dx.doi.org/10.1182/blood-2011-05-352658.
Kawahara, T., Shareef, H.K., Aljarah, A.K., Ide, H., Li, Y., Kashiwagi, E., et al., 2015. ELK1 is up-regulated by androgen in bladder cancer cells and promotes tumor progression. Oncotarget. Impact J. 6, 29860–29876. http://dx.doi.org/10.18632/oncotarget.5007.
Kiyota, T., Kato, A., Kato, Y., 2007. Ets-1 regulates radial glia formation during vertebrate embryogenesis. Organogenesis 3, 93–101.
Koh, B., Hufford, M.M., Pham, D., Olson, M.R., Wu, T., Jabeen, R., et al., 2016. The ETS family transcription factors Etv5 and PU.1 function in parallel to promote Th9 cell development. J. Immunol. Am. Assoc. Immunol. 197, 2465–2472. http://dx.doi.org/10.4049/jimmunol.1502383.
Kramer, S., Okabe, M., Hacohen, N., Krasnow, M.A., Hiromi, Y., 1999. Sprouty: a common antagonist of FGF and EGF signaling pathways in Drosophila. Development 126, 2515–2525.
Kumburegama, S., Wijesena, N., Xu, R., Wikramanayake, A.H., 2011a. Strabismus-mediated primary archenteron invagination is uncoupled from Wnt/β-catenin-dependent endoderm cell fate specification in Nematostella vectensis (Anthozoa, Cnidaria): implications for the evolution of gastrulation. EvoDevo 2, 2. http://dx.doi.org/10.1186/2041-9139-2-2.
Kumburegama, S., Wijesena, N., Xu, R., 2011b. Strabismus-mediated primary archenteron invagination is uncoupled from Wnt/β-catenin-dependent endoderm cell fate specification in Nematostella .... EvoDevo.
Kusserow, A., Pang, K., Sturm, C., Lentfer, J., Schmidt, H.A., Technau, U., et al., 2005. Unexpected complexity of the Wnt gene family in a sea anemone. Nature 433, 156–160. http://dx.doi.org/10.1038/nature03158.
Laudet, V., Niel, C., Duterque-Coquillaud, M., Leprince, D., Stéhelin, D., 1993. Evolution of the ETS gene family. Biochem. Biophys. Res. Commun. 190 (1), 8–14.
Laudet, V., Hänni, C., Stéhelin, D., Duterque-Coquillaud, M., 1999. Molecular phylogeny of the ETS gene family. Oncogene 18, 1351–1359. http://dx.doi.org/10.1038/sj.onc.1202444.
Layden, M.J., Boekhout, M., Martindale, M.Q., 2012. Nematostella vectensis achaete-scute homolog NvashA regulates embryonic ectodermal neurogenesis and represents an ancient component of the metazoan neural specification pathway. Development (Cambridge, England) 139, 1013–1022. http://dx.doi.org/10.1242/dev.073221.
Layden, M.J., Röttinger, E., Wolenski, F.S., Gilmore, T.D., Martindale, M.Q., 2013. Microinjection of mRNA or morpholinos for reverse genetic analysis in the starlet sea anemone, Nematostella vectensis. Nat. Protoc. 8, 924–934. http://dx.doi.org/10.1038/nprot.2013.009.
Layden, M.J., Rentzsch, F., Röttinger, E., 2016a. The rise of the starlet sea anemone Nematostella vectensis as a model system to investigate development and regeneration. Wiley Interdiscip Rev. Dev. Biol. 5 (4), 408–428. http://dx.doi.org/10.1002/wdev.222, WIREs Dev Biol. John Wiley & Sons, Inc.
Layden, M.J., Johnston, H., Amiel, A.R., Havrilak, J., Steinworth, B., Chock, T., et al., 2016b. MAPK signaling is necessary for neurogenesis in Nematostella vectensis. BMC Biol. 14, 61. http://dx.doi.org/10.1186/s12915-016-0282-1.
Leclère, L., Bause, M., Sinigaglia, C., Steger, J., Rentzsch, F., 2016. Development of the aboral domain in Nematostella requires β-catenin and the opposing activities of six3/6 and frizzled5/8. Development (Cambridge, England) 143, 1766–1777. http://dx.doi.org/10.1242/dev.120931.
Lee, P.N., Pang, K., Matus, D.Q., Martindale, M.Q.A., 2006. WNT of things to come: evolution of Wnt signaling and polarity in cnidarians. Semin Cell Dev. Biol. 17, 157–167. http://dx.doi.org/10.1016/j.semcdb.2006.05.002.
Lee, P.N., Kumburegama, S., Marlow, H.Q., Martindale, M.Q., Wikramanayake, A.H., 2007. Asymmetric developmental potential along the animal-vegetal axis in the anthozoan cnidarian, Nematostella vectensis, is mediated by Dishevelled. Dev. Biol. 310, 169–186. http://dx.doi.org/10.1016/j.ydbio.2007.05.040.
Longabaugh, W., Bolouri, H., 2006. Understanding the dynamic behavior of genetic regulatory networks by functional decomposition. Curr. Genom. 7, 333–341. http://dx.doi.org/10.2174/138920206778948718.
Magie, C.R., Daly, M., Martindale, M.Q., 2007. Gastrulation in the cnidarian Nematostella vectensis occurs via invagination not ingression. Dev. Biol. 305, 483–497. http://dx.doi.org/10.1016/j.ydbio.2007.02.044.
Marlow, H., Matus, D.Q., Martindale, M.Q., 2013. Ectopic activation of the canonical wnt signaling pathway affects ectodermal patterning along the primary axis during larval development in the anthozoan Nematostella vectensis. Dev. Biol. 380, 324–334. http://dx.doi.org/10.1016/j.ydbio.2013.05.022.
Martindale, M.Q., Hejnol, A., 2009. A developmental perspective: changes in the position of the blastopore during bilaterian evolution. Dev. Cell. 17, 162–174. http://dx.doi.org/10.1016/j.devcel.2009.07.024.
Martindale, M.Q., Pang, K., Finnerty, J.R., 2004. Investigating the origins of triploblasty: "mesodermal" gene expression in a diploblastic animal, the sea anemone Nematostella vectensis (phylum, Cnidaria; class, Anthozoa). Development (Cambridge, England) 131, 2463–2474. http://dx.doi.org/10.1242/dev.01119.
Matus, D.Q., Pang, K., Marlow, H., Dunn, C.W., Thomsen, G.H., Martindale, M.Q., 2006a. Molecular evidence for deep evolutionary roots of bilaterality in animal development. Proc. Natl. Acad. Sci. USA 103, 11195–11200. http://dx.doi.org/10.1073/pnas.0601257103.
Matus, D.Q., Thomsen, G.H., Martindale, M.Q., 2006b. Dorso/ventral genes are asymmetrically expressed and involved in germ-layer demarcation during cnidarian gastrulation. Curr. Biol. 16, 499–505. http://dx.doi.org/10.1016/j.cub.2006.01.052.
Matus, D.Q., Thomsen, G.H., Martindale, M.Q., 2007. FGF signaling in gastrulation and neural development in Nematostella vectensis, an anthozoan cnidarian. Dev. Genes Evol. 217, 137–148. http://dx.doi.org/10.1007/s00427-006-0122-3.
Matus, D.Q., Magie, C.R., Pang, K., Martindale, M.Q., Thomsen, G.H., 2008. The Hedgehog gene family of the cnidarian, Nematostella vectensis, and implications for understanding metazoan Hedgehog pathway evolution. Dev. Biol. 313, 501–518. http://dx.doi.org/10.1016/j.ydbio.2007.09.032.
Mazza, M.E., Pang, K., Martindale, M.Q., Finnerty, J.R., 2007. Genomic organization, gene structure, and developmental expression of three clustered otx genes in the sea anemone Nematostella vectensis. J. Exp. Zool. 308, 494–506. http://dx.doi.org/10.1002/jez.b.21158.
Oliveri, P., Davidson, E., 2004. Gene regulatory network controlling embryonic specification in the sea urchin. Curr. Opin. Genet. Dev..
Ormestad, M., Martindale, M., Rottinger, E., 2011. A comparative gene expression database for invertebrates. EvoDevo.
Ota, S., Tonou-Fujimori, N., Yamasu, K., 2009. The roles of the FGF signal in zebrafish embryos analyzed using constitutive activation and dominant-negative suppression of different FGF receptors. Mech. Dev. 126, 1–17. http://dx.doi.org/10.1016/j.mod.2008.10.008.
Peng, C., Zeng, W., Su, J., Kuang, Y., He, Y., Zhao, S., et al., 2016. Cyclin-dependent kinase 2 (CDK2) is a key mediator for EGF-induced cell transformation mediated through the ELK4/c-Fos signaling pathway. Oncogene 35, 1170–1179. http://dx.doi.org/10.1038/onc.2015.175.
Pourtier-Manzanedo, A., Vercamer, C., Van Belle, E., Mattot, V., Mouquet, F., Vandenbunder, B., 2003. Expression of an Ets-1 dominant-negative mutant perturbs normal and tumor angiogenesis in a mouse ear mode. Oncogene 22, 1795–1806. http://dx.doi.org/10.1038/sj.onc.1206215.
Putnam, N.H., Srivastava, M., Hellsten, U., Dirks, B., Chapman, J., Salamov, A., et al., 2007. Sea anemone genome reveals ancestral eumetazoan gene repertoire and genomic organization. Science 317, 86–94. http://dx.doi.org/10.1126/science.1139158.
Rentzsch, F., Anton, R., Saina, M., Hammerschmidt, M., Holstein, T.W., Technau, U., 2006. Asymmetric expression of the BMP antagonists chordin and gremlin in the sea anemone Nematostella vectensis: implications for the evolution of axial patterning. Dev. Biol. 296, 375–387. http://dx.doi.org/10.1016/j.ydbio.2006.06.003.
Rentzsch, F., Fritzenwanker, J.H., Scholz, C.B., Technau, U., 2008. FGF signalling controls formation of the apical sensory organ in the cnidarian Nematostella vectensis. Development 135, 1761–1769. http://dx.doi.org/10.1242/dev.020784.
Rizzo, F., Fernandez-Serra, M., Squarzoni, P., Archimandritis, A., Arnone, M.I., 2006. Identification and developmental expression of the ets gene family in the sea urchin (Strongylocentrotus purpuratus). Dev. Biol. 300, 35–48. http://dx.doi.org/10.1016/j.ydbio.2006.08.012.
Rizzo, F., Coffman, J.A., Arnone, M.I., 2016. An Elk transcription factor is required for Runx-dependent survival signaling in the sea urchin embryo. Dev. Biol. 416, 173–186. http://dx.doi.org/10.1016/j.ydbio.2016.05.026.
Röttinger, E., Besnardeau, L., Lepage, T., 2004. A Raf/MEK/ERK signaling pathway is required for development of the sea urchin embryo micromere lineage through phosphorylation of the transcription factor Ets. Developmet 131, 1075–1087. http://dx.doi.org/10.1242/dev.01000, The Company of Biologists Limited.
Röttinger, E., Saudemont, A., Duboc, V., Besnardeau, L., McClay, D., Lepage, T., 2008. FGF signals guide migration of mesenchymal cells, control skeletal morphogenesis [corrected] and regulate gastrulation during sea urchin development. Development 135, 353–365. http://dx.doi.org/10.1242/dev.014282.
Röttinger, E., Dahlin, P., Martindale, M.Q., 2012. A framework for the establishment of a cnidarian gene regulatory network for "endomesoderm" specification: the Inputs of ß-catenin/TCF signaling. PLoS Genet. 8, e1003164. http://dx.doi.org/10.1371/journal.pgen.1003164.t002.
Röttinger, E., DuBuc, T.Q., Amiel, A.R., Martindale, M.Q., 2015. Nodal signaling is required for mesodermal and ventral but not for dorsal fates in the indirect developing hemichordate, Ptychodera flava. Biol. Open. http://dx.doi.org/10.1242/bio.011809.
Ryan, J.F., Burton, P.M., Mazza, M.E., Kwong, G.K., Mullikin, J.C., Finnerty, J.R., 2006. The cnidarian-bilaterian ancestor possessed at least 56 homeoboxes: evidence from the starlet sea anemone, Nematostella vectensis. Genome Biol. 7, R64. http://dx.doi.org/10.1186/gb-2006-7-7-R64.
Ryan, J.F., Mazza, M.E., Pang, K., Matus, D.Q., Baxevanis, A.D., Martindale, M.Q., et al., 2007. Pre-bilaterian origins of the Hox cluster and the Hox code: evidence from the sea anemone, Nematostella vectensis. PLoS One 2, e153. http://dx.doi.org/10.1371/journal.pone.0000153.
Schulte-Merker, S., Smith, J.C., 1995. Mesoderm formation in response to Brachyury requires FGF signalling. Curr. Biol. 5, 62–67.
Selvaraj, N., Kedage, V., Hollenhorst, P.C., 2015. Comparison of MAPK specificity across

the ETS transcription factor family identifies a high-affinity ERK interaction required for ERG function in prostate cells. Cell Commun. Signal. BioMed. Cent. 13, 12. http://dx.doi.org/10.1186/s12964-015-0089-7.

Sharrocks, A.D., 2001. The ETS-domain transcription factor family. Nat. Rev. Mol. Cell Biol. 2, 827–837. http://dx.doi.org/10.1038/35099076.

Sinigaglia, C., Busengdal, H., Leclère, L., Technau, U., Rentzsch, F., 2013. The bilaterian head patterning gene six3/6 controls aboral domain development in a Cnidarian. PLoS Biol. 11, e1001488. http://dx.doi.org/10.1371/journal.pbio.1001488.s010, Levine M, editor.

Sinigaglia, C., Busengdal, H., Lerner, A., Oliveri, P., Rentzsch, F., 2014. Molecular characterization of the apical organ of the anthozoan Nematostella vectensis. Dev. Biol.. http://dx.doi.org/10.1016/j.ydbio.2014.11.019.

Srivastava, M., Larroux, C., Lu, D.R., Mohanty, K., Chapman, J., Degnan, B.M., et al., 2010. Early evolution of the LIM homeobox gene family. BMC Biol. 8, 4. http://dx.doi.org/10.1186/1741-7007-8-4.

Stathopoulos, A., Tam, B., Ronshaugen, M., Frasch, M., Levine, M., 2004. pyramus and thisbe: FGF genes that pattern the mesoderm of Drosophila embryos. Genes Dev. 18, 687–699. http://dx.doi.org/10.1101/gad.1166404.

Technau, U., Scholz, C.B., 2003. Origin and evolution of endoderm and mesoderm. Int. J. Dev. Biol. 47, 531–539.

Technau, U., Steele, R.E., 2011. Evolutionary crossroads in developmental biology: Cnidaria. Development 138, 1447–1458. http://dx.doi.org/10.1242/dev.048959.

Wikramanayake, A.H., Hong, M., Lee, P.N., Pang, K., Byrum, C.A., Bince, J.M., et al., 2003. An ancient role for nuclear beta-catenin in the evolution of axial polarity and germ layer segregation. Nature 426, 446–450. http://dx.doi.org/10.1038/nature02113.

Yasuo, H., Hudson, C., 2007. FGF8/17/18 functions together with FGF9/16/20 during formation of the notochord in Ciona embryos. Dev. Biol. 302, 92–103. http://dx.doi.org/10.1016/j.ydbio.2006.08.075.

Yasuoka, Y., Kobayashi, M., Kurokawa, D., Akasaka, K., Saiga, H., Taira, M., 2009. Evolutionary origins of blastoporal expression and organizer activity of the vertebrate gastrula organizer gene lhx1 and its ancient metazoan paralog lhx3. Development 136, 2005–2014. http://dx.doi.org/10.1242/dev.028530.

Chapter 2: Morphological, cellular and molecular characterization of *Nematostella* regeneration

This second chapter is describing our efforts to characterize in detail the entire *Nematostella* regeneration at the morphological, tissular, cellular and global molecular levels.

The first article (Amiel et al. 2015) (2nd author, Article 3) aimed at developing a detailed regeneration staging system and develop tools that serve as a common groundwork for future regeneration studies on this model. In this study, I developed the tool to characterize the global transcriptional activity (neo-, or hypertranscription) and participated in developing the bio-sorter as a mean to assess a specific metabolic state of the animals and the re-formation of the pharynx.

The second article (Warner et al. 2018) (contributing author, Article 4) was aimed at developing regeneration specific transcriptomic resources as well as an open-access online tool to mine the extensive amount of data. Personally, I was involved in the effort to provide sufficient material (> 21 000 dissected polyps) required to perform the RNAseq analysis for 16 time points of regeneration. Combined with existing and novel embryonic RNAseq data, this work finally resulted in a comprehensive comparative embryogenesis and regeneration transcriptomics database (nvertx.kahikai.org).

These resources were used in the third article (Warner et al in submission, contributing author, Article 5), to perform a unbiased large-scale comparative bio-informatics analysis that highlighted that regeneration is a partial redeployment of regeneration, enabled us to identify regeneration specific genes and gene modules and predict that re-expressed embryonic genes are re-wired and connected to regeneration specific genes to reform lost body parts. Personally, I was involved in validating the spatial expression of certain genes.

Taken together, in this chapter we developed the basic resources and tools to study the molecular mechanisms underlying whole body regeneration in *Nematostella* and laid down a hypothesis that I functionally validated in the last chapter.

Article 3: Amiel, A., Johnston, H., Nedoncelle, K., Warner, J., Ferreira, S., & Röttinger, E. (2015). Characterization of Morphological and Cellular Events Underlying Oral Regeneration in the Sea Anemone, Nematostella vectensis. International Journal of Molecular Sciences, 16(12), 28449–28471.

Article 4: Warner, J. F., Guerlais, V., Amiel, A. R., Johnston, H., Nedoncelle, K., & Röttinger, E. (2018). NvERTx: a gene expression database to compare embryogenesis and regeneration in the sea anemone Nematostella vectensis.*Development*, *145*(10), dev162867. doi:10.1242/dev.162867

Article 5: Jacob F. Warner, Aldine R. Amiel, Hereroa Johnston, and Eric Röttinger Regeneration is a partial redeployment of the embryonic gene network In submission

Article 3. Characterization of Morphological and Cellular Events Underlying Oral Regeneration in the Sea Anemone, Nematostella vectensis.

Amiel, A., Johnston, H., Nedoncelle, K., Warner, J., Ferreira, S., & Röttinger, E. (2015)

International Journal of Molecular Sciences, 16(12), 28449–28471.

International Journal of
Molecular Sciences

MDPI

Article

Characterization of Morphological and Cellular Events Underlying Oral Regeneration in the Sea Anemone, *Nematostella vectensis*

Aldine R. Amiel, Hereroa T. Johnston, Karine Nedoncelle, Jacob F. Warner, Solène Ferreira and Eric Röttinger *

Received: 8 September 2015; Accepted: 6 November 2015; Published: xx November 2015
Academic Editor: Francesc Cebrià

Institute for Research on Cancer and Aging, Université de Nice Sophia-Antipolis UMR 7284, INSERM U1081, CNRS UMR 7284, Nice 06107 Cedex 02, France; aldine.amiel@unice.fr (A.R.A.); j.hereroa@hotmail.fr (H.T.J.); Karine.Nedoncelle@unice.fr (K.N.); warner.jacob@gmail.com (J.F.W.); solene.ferreira.ca@gmail.com (S.F.)
* Correspondence: eric.rottinger@unice.fr; Tel.: +33-493-377-791

Abstract: Cnidarians, the extant sister group to bilateria, are well known for their impressive regenerative capacity. The sea anemone *Nematostella vectensis* is a well-established system for the study of development and evolution that is receiving increased attention for its regenerative capacity. *Nematostella* is able to regrow missing body parts within five to six days after its bisection, yet studies describing the morphological, cellular, and molecular events underlying this process are sparse and very heterogeneous in their experimental approaches. In this study, we lay down the basic framework to study oral regeneration in *Nematostella vectensis.* Using various imaging and staining techniques we characterize in detail the morphological, cellular, and global molecular events that define specific landmarks of this process. Furthermore, we describe *in vivo* assays to evaluate wound healing success and the initiation of pharynx reformation. Using our described landmarks for regeneration and *in vivo* assays, we analyze the effects of perturbing either transcription or cellular proliferation on the regenerative process. Interestingly, neither one of these experimental perturbations has major effects on wound closure, although they slightly delay or partially block it. We further show that while the inhibition of transcription blocks regeneration in a very early step, inhibiting cellular proliferation only affects later events such as pharynx reformation and tentacle elongation.

Keywords: regeneration; wound healing; tissue tracking; marine invertebrate; sea anemone; *Nematostella vectensis*

1. Introduction

Regeneration is the biological process that enables organisms to regrow missing body parts after amputation. This fascinating phenomenon has intrigued naturalists and scientists for more than 300 years. Among the first animals in which regeneration has been described was the freshwater polyp *Hydra*, a cnidarian that belongs to the group of hydrozoans. While regenerative potential has since then been described in other groups of cnidarians (Anthozoa [1,2], Cubozoa [3], and Scyphozoa [4]), the majority and most detailed cellular and molecular regeneration studies in this phylum have been carried out using Hydrozoa (reviewed in [5,6]). These studies highlight variations in the cellular mechanisms (e.g., cellular proliferation) underlying regeneration in different groups of cnidarians (the hydrozoan *Hydra vs.* the anthozoan *Nematostella* [7]). They also demonstrate variations within Hydrozoa (*Hydra vs. Hydractinia* [8]) and even within the same species; in *Hydra*, for example, the regenerative mechanism varies depending on the amputation site [9]. Therefore,

additional systems are required to determine whether common mechanisms govern regeneration throughout Cnidaria and to understand the evolution of this process within the animal kingdom.

The majority of cnidarian species belong to the Anthozoa class (sea anemones and corals) which diverges basally to their other cnidarian sister groups [10–12]. This places anthozoans at a key phylogenetic position to understand the evolution of the regeneration process among Cnidaria. Several anthozoans have been shown to display high regenerative capacities [1,2,13]. However, very little is known about the cellular/molecular mechanisms that underlie this process in these animals. The anthozoan sea anemone *Nematostella vectensis* (*Nv*) is a well-established system for the study of embryonic and larval development [13–18]. Interestingly, it is also able to regrow half of its oral or aboral body within five to seven days after bisection (Figure 1) [12,13].

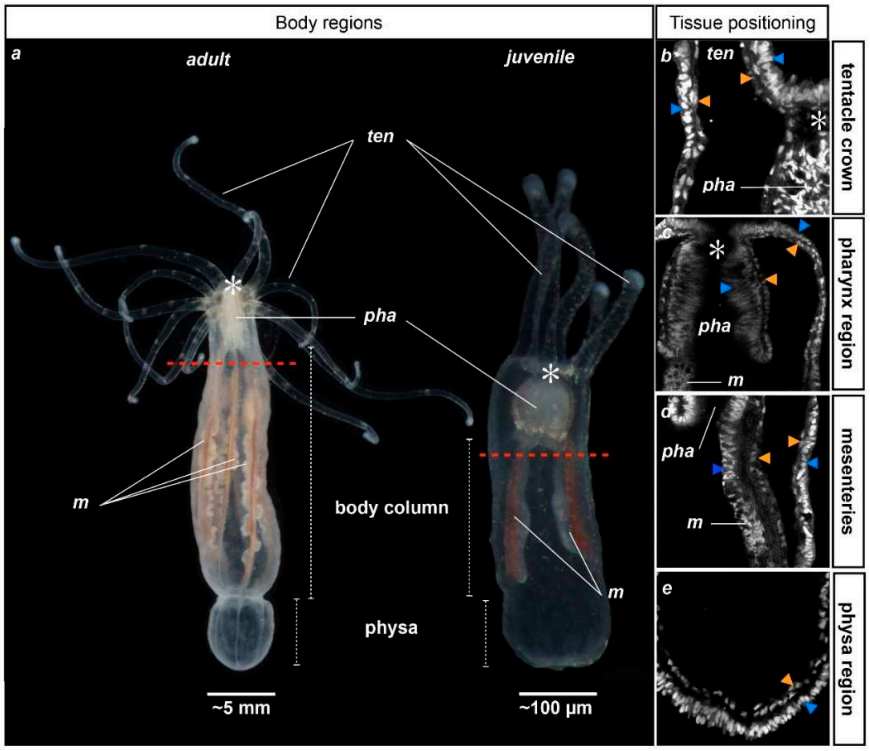

Figure 1. General anatomy of adult and juvenile *Nematostella vectensis*. Photographs illustrating the adult (**left**) and juvenile (**right**) morphology of *Nematostella*; (**a**) Polyps are oriented toward the oral region to the top and aboral region to the bottom. Red dotted lines indicate the future amputation site for the following experiments of this study. (**b**–**e**) Close-up confocal stack images of the tentacle (**b**); pharyngeal (**c**); mesenterial (along the body column) (**d**); or the physal (**e**) regions. Juvenile polyps were stained with DAPI to label the nuclei (white staining). An asterisk (*) indicates the position of the mouth. Orange and blue arrowheads indicate the gastrodermal and ectodermal epithelia, respectively. *ten*, tentacles; *pha*, pharynx; *m*, mesenteries.

Nematostella is a diploblastic animal comprised of an outer ectodermal epithelium and an inner gastrodermis that are separated by muscle fibers and the mesoglea (Supplementary Figure S1A,B). The oral region consists of a pharynx and tentacles that surround the mouth opening. Freshly metamorphosed juveniles possess four tentacles that are used to catch food that floats by, while adult polyps have up to 16 [19]. The body column (or scapus) ends in its aboral-most region in a structure that is called the physa (Figure 1; [20–22]). Inside the body cavity, internal structures termed mesenteries stretch from the pharynx to the physa and correspond to the digestive and reproductive organs of the animal (Figure 1). Two primary mesenteries are distinctly visible in juveniles, while eight mesenteries that produce the germ cells are found in adult *Nv* (Figure 1) [23].

Existing resources [24–27] as well as cellular and molecular tools developed by the *Nematostella* community (reviewed in [28], Layden *et al.*, submitted) have over the past few years increased the interest to study regeneration in this cnidarian. However, studies describing the morphological, cellular, and molecular events underlying this process are still sparse and very heterogeneous in their experimental approaches [7,12,13,29–35]. In particular, different studies used (i) animals of different ages (juveniles *vs.* adults); (ii) different amputation sites (sub-pharyngeal, supra-physa); and (iii) isolated body parts were left to regenerate at different temperatures (between 15 and 27 °C). The potential to regenerate into a functional organism appears to be similar between the different body parts of an adult *Nv* [12]. The temperature aspect has recently been addressed by Bossert and colleagues, who showed in a study describing a *Nematostella* staging system for the regenerating adult isolated physa (NRSS) that the regeneration speed is temperature-dependent [30]. However, no particular reason was mentioned for the choices of the above-mentioned criteria by the authors; importantly, there is nothing currently known about the influence of age on the regenerative capacity and/or cellular mechanism deployed by *Nematostella* to reform the missing body parts.

The majority of the studies on *Nematostella* regeneration have focused on oral regeneration following sub-pharyngeal amputation. In our present study, we show that there are no apparent differences in the cellular mechanisms underlying oral regeneration after sub-pharyngeal regeneration in juveniles compared to adults. We further lay down the basic framework to study oral regeneration in juvenile *Nematostella* by taking advantage of the ease of animal imaging at this stage. We carefully analyze and describe morphological and cellular events that define specific landmarks of regeneration. Additionally, we propose assays to assess wound healing success and pharynx re-formation. Finally, we show the usefulness of these assays and landmarks for phenotype characterization from perturbation experiments.

2. Results

2.1. Oral Regeneration Is Temperature—But Not Age-Dependent

While the age of adult *Nematostella* cannot yet be determined at a molecular or cellular level, one can distinguish juvenile and adult polyps from their anatomy (Figure 1). Previous studies describing regeneration in *Nematostella* have been carried out either in juveniles [7,34] or in adults [12,29–33,35]. However, it is not known if the regenerative capacities/mechanisms are conserved between the two. In order to determine if the timing of oral regeneration in *Nematostella* is age-dependent, we performed head amputation (bisection under the pharyngeal region; see red dotted line in Figure 1a) experiments in *Nematostella* juveniles and adults while following the timing of regeneration. This sub-pharyngeal amputation site was used in all of the following amputation experiments performed in this study. We analyzed the morphology of the regenerating animals at 22 °C (temperature used in [7]) each day for one week. We observed that both juveniles (20 out of 20 cases) as well as adults (10 out of 10 cases) regenerate with a similar timing (Figure 2).

We observed a specific sequence of events during the regeneration process (Figure 2). First, the mesenteries come into tight contact with the amputation site 24–48 h post-amputation (hpa, only observable in transparent juveniles). Next, at 72–96 hpa the tentacle bulbs become visible in juveniles and adults. Finally, there is a progressive elongation and formation of those structures up to 144 hpa (Figure 2). Interestingly, we also observed that the number of new regenerating tentacles corresponds to the number of tentacles present in the polyp before amputation. The four-tentacle juveniles regenerate four new tentacles and the 12+ tentacle adults regenerate 12+ new tentacles (Figure 2, 168 hpa).

In order to investigate if oral regeneration following sub-pharyngeal amputation is temperature-dependent as a function of age, we performed sub-pharyngeal bisections in *Nematostella* juveniles or adults and left them to regenerate at 16 °C (Supplementary Figure S2A,B). The timing of oral regeneration for both juveniles (20 out of 20 cases, Supplementary Figure S2A) and adults

(10 out of 10 cases, Figure S2B) is considerably slowed at 16 °C compared to 22 °C. In particular, the appearance of the tentacle bulbs is delayed by approximately 48–72 h in animals that regenerated at 16 °C. This observation is in line with a previous report that showed that the timing of regeneration for the isolated adult physa is temperature-dependent [30]. All following experiments were carried out at 22 °C for consistency and to be able to compare our findings to those reported by Passamaneck and Martindale and Bossert and colleagues [7,30].

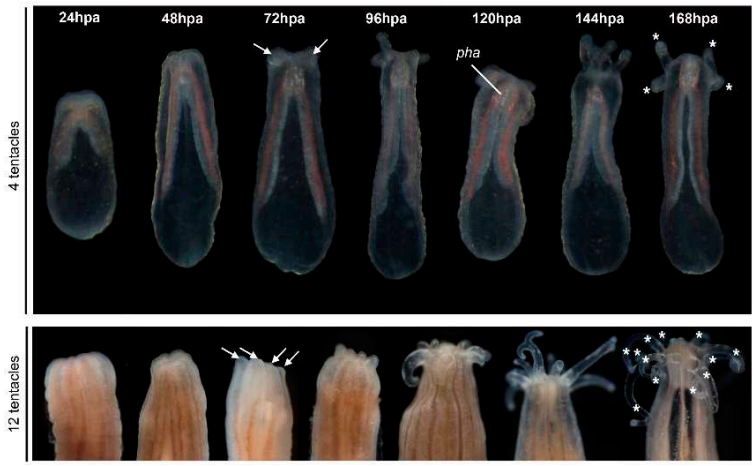

Figure 2. Timing of oral regeneration is similar in juveniles and adults. Comparison of the duration of oral regeneration between six-week-old juveniles (**upper** panel—four tentacles) and adults (**bottom** panel—12 tentacles). From left to right: regenerating polyps at 22 °C 24 h post-amputation (hpa), 48, 72, 96, 120, 144 and 168 hpa. At 72 hpa, in both juvenile and adult polyps, the tentacles bulbs are clearly visible (white arrows), and the pharynx starts to form in some individuals (only visible in transparent juveniles). Five days post-amputation (120 hpa), the juvenile and adult polyps are regenerated as indicated by the presence of the pharynx and elongated tentacles. The white asterisk at 168 hpa indicates the tentacles: four on the regenerating juvenile and 12 on the regenerating adult polyp.

2.2. Cell Proliferation Is Required during Head Regeneration in Adult Tissue

In *Nematostella*, cell proliferation is required for head regeneration in juveniles [7]. In order to determine the earliest time-point where this cellular proliferation is detectable, we performed EdU labeling at 1.30, 6, 12, 24, and 48 hpa. We found that while no staining is detectable at the two earliest time-points (data not shown), clear cellular proliferation is observed at 12 hpa at the amputation site (Figure 3Aa).

Cellular proliferation increases massively in this region between 24 hpa and 48 hpa, confirming a previous report (Figure 3Ab) [7]. Interestingly, and in contrast with previous observations, EdU-positive cells were not only detected in the ectodermal epithelium and the gastrodermis at the amputation site, but also in the oral-most regions of the mesenteries (Figure 3Ab).

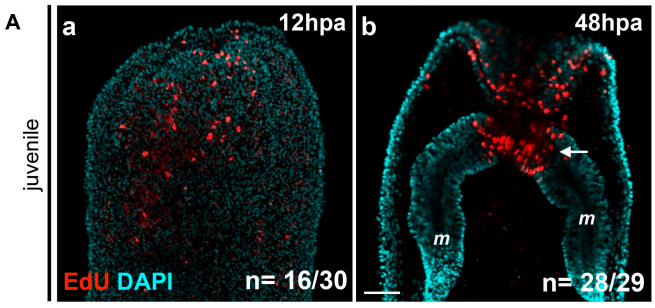

Figure 3. *Cont.*

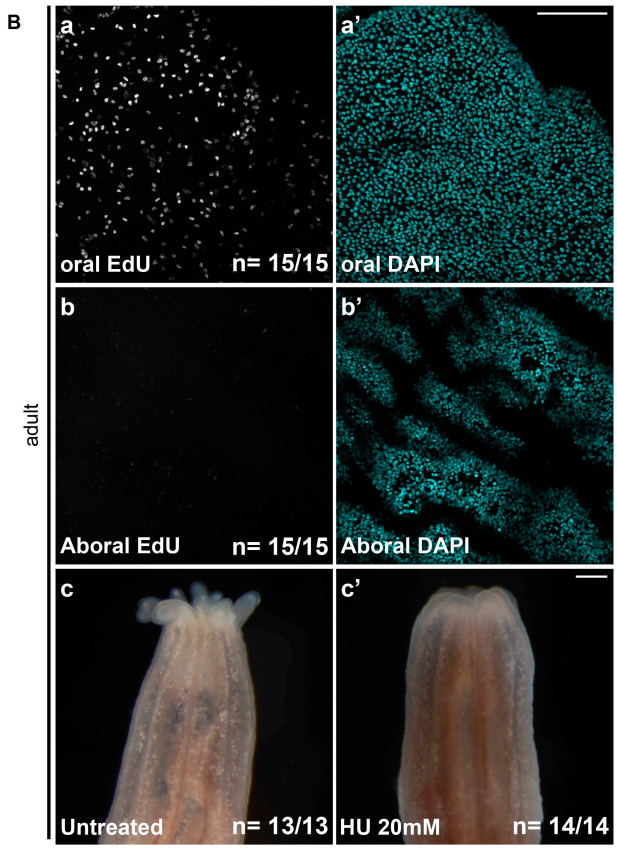

Figure 3. (**A**) Localized cellular proliferation in juveniles begins at 12 hpa at the amputation site. Overlapping confocal images in which the nuclei (DNA, cyan) were stained using DAPI and proliferating cells (red) were marked using an EdU labeling kit (**Aa**,**Ab**). Oral parts of the regenerating juveniles at 12 hpa (**Aa**) and 48 hpa (**Ab**). All animals are oriented with the amputation site to the top. The white arrow in (**b**) shows the presence of dividing cells in the most oral part of the mesentery tissues. Number of cases for the representative phenotype are in white at the bottom right of each image. *m*, mesentery; (**B**) Cell proliferation is necessary for adult tissue regeneration. Cell division is present during regeneration in adults after sub-pharyngeal amputation (**Ba**–**Bb'**). (**Ba**–**Bb'**) Confocal stack images in which the DNA (nucleus) is labeled with DAPI (cyan) and proliferating cells (white) were marked using an EdU labeling kit. (**Bc**,**Bc'**) Blocking cell proliferation using hydroxyurea (HU) blocks regeneration in the adult amputated polyps (**c'**) contrary to the regenerated untreated control (**c**). Number of cases for the representative phenotype are in white at the bottom right of each images (**Ba**,**Bb**,**Bc**,**Bc'**). Scale bar in (**Ab**) is 20 µm and applies to (**Aa**). Scale bar in (**Ba'**) is 50 µm and applies to (**Ba**,**Bb**,**Bb'**). Scale bar in (**Bc'**) is 1 mm and applies to (**Bc**).

In order to investigate if cell proliferation is also detectable during adult regeneration [7], we performed EdU staining on adult polyps 48 h after sub-pharyngeal amputation (Figure 3(Ba–Bb')). While no EdU-positive cells are detected in aboral tissues (Figure 3(Bb,Bb')), cellular proliferation is clearly visible at the amputation site in the adult tissue at 48 hpa (Figure 3(Ba,Ba')). We further tested if cellular proliferation, similarly to juveniles [7], is required for adult regeneration. To do this we used the pharmaceutical cellular proliferation inhibitor hydroxyurea (HU). Continuous treatment of HU for six days post-amputation blocks oral regeneration in the adult polyp (Figure 3(Bc,Bc')). Thus, cell division is also required for oral regeneration in adult *Nematostella.*

2.3. Wound Healing Occurs at 6 HPA

A recent report analyzed *Nematostella* wound healing after puncturing the body column with a glass needle [34]. The authors found that this process is visually completed after approximately 4 h (25 °C). In order to determine exactly when wound healing occurs in *Nematostella* juveniles, we performed DIC and confocal imaging on regenerating juveniles following sub-pharyngeal amputation at several time-points. While in some cases we were able to visualize a clear opening using DIC optics (Figure 4Aa), the three-dimensional folding and contraction of the tissues at the amputation site often made it hard to distinguish between a real wound or a depression that looked like an open wound (Figure 4(Ab–Ae)). Thus, determining the wound closure simply by imaging proves to be difficult. In addition, using classical staining/imaging approaches we are unable to distinguish between a closed wound or contraction of the surrounding myo-epithelia.

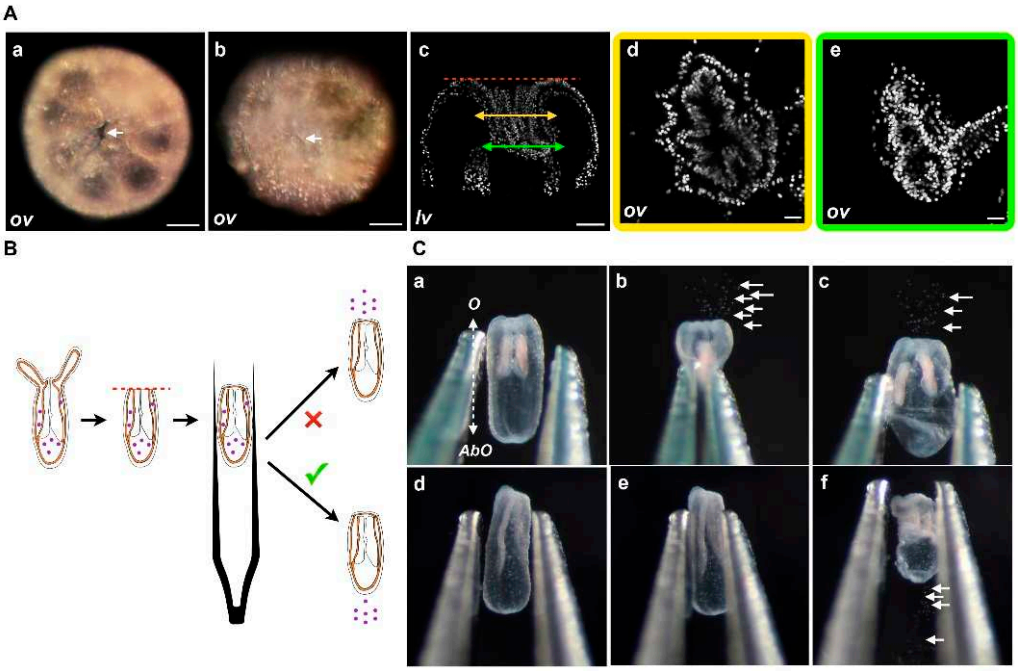

Figure 4. (**A**) Wound closure. Oral opening during *Nematostella* regeneration. Example of DIC images of the oral part, oral view (*ov*), at the amputation site of an example of the opening at 2 hpa (white arrows in (**Aa**)) or the closed wound at 6 hpa (white arrows in (**Ab**)); (**Ac**–**Ae**) are confocal images of the oral-most part of the same polyp in lateral view (*lv*) or details of the oral view (**Ad**,**Ae**); (**Ad**) (yellow frame) or (**Ae**) (green frame) correspond to the double yellow or green arrow slice, respectively, in (**c**); Because of the folding that occurs at the amputation site during the first hours of regeneration, the dynamics of the wound healing are hard to assess in DIC optic or confocal images. Scale bars are 20 μm in (**Aa**–**Ac**) and 10 μm in (**Ad**,**Ae**); (**B**) Diagram of the compression assay during regeneration. The purple dots represent the nematosomes. The red dotted line represents the amputation site. The forceps are laterally compressing the regenerating polyp body; (**C**) Time series of the compression assay in an opened (**Ca**–**Cc**) or a wound-closed (**Cd**–**Cf**) polyp. The dotted double arrow in (**Ca**) indicates the axial orientation of the animals shown in (**Ca**–**Cf**). *O*, Oral; *AbO*, Aboral.

In order to have a more robust way to address wound healing after sub-pharyngeal amputation, we developed a compression assay to assess the state of the opening at the amputation site. This assay uses nematosomes (Supplementary Figure S3) as a marker to follow the fluid dynamics present in the gastric cavity of *Nematostella* (Figure 4B,C).

Nematosomes are cellular aggregates formed by cnidocytes that are freely circulating within the *Nematostella* body [36]. When compressing a juvenile with an open wound, the nematosomes will be expelled at the amputation site. On the contrary, when the wound is closed, the nematosomes will either remain in the gastric cavity or leak out of the body cavity through the aboral pore. This pore is an opening with an unknown function located at the aboral-most region of the body (Supplementary Figure S4) [37]. We assume that nematosomes will exit the body cavity through the wound or the aboral pore depending on the wound healing status. To use this wound healing assay, we compressed the body column of sub-pharyngeal amputated juveniles at 0, 1, 2, 4, 6, 12 hpa and followed the behavior of the nematosomes (Figure 5).

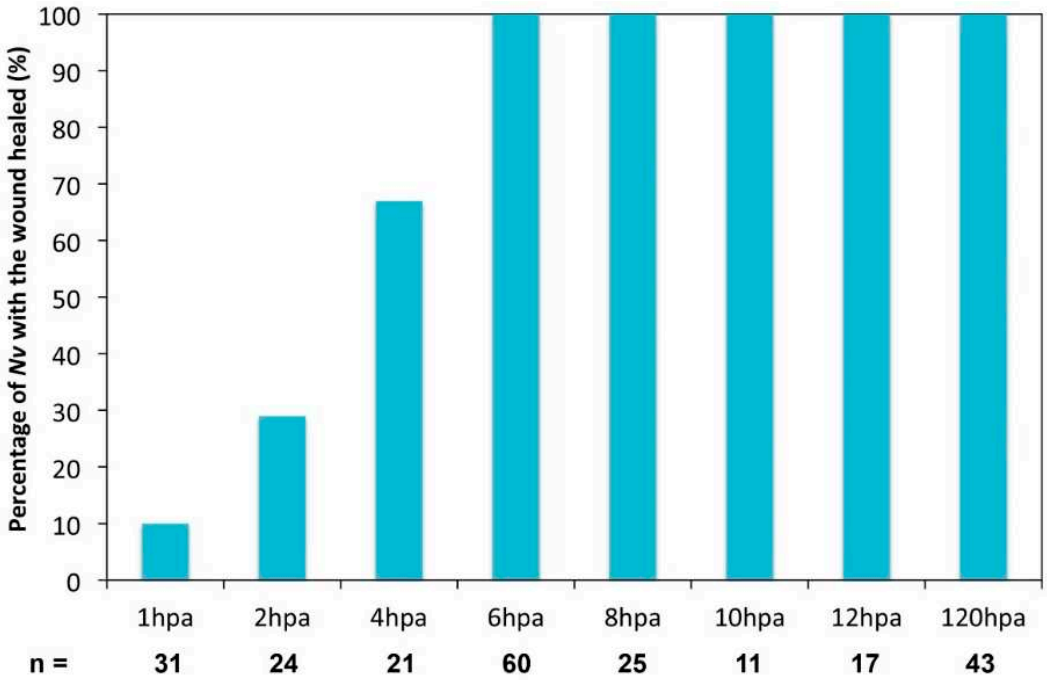

Figure 5. Wound healing assay.

Interestingly, at 1 and 2 hpa in the majority of cases (90% $n = 31$ and 71% $n = 24$, respectively), the nematosomes are forced to exit the body cavity through the amputation site (Figure 5), showing that the wound is not healed yet. However, at 4 hpa, the majority of the juveniles (67%, 14 out of 21 cases) exhibited nematosomes leaking through the aboral pore. This is the case for 100% of juveniles (22 out of 22 cases) at 6 hpa and later time-points (Figure 5). Thus, in *Nematostella*, the wound is closed between 4 and 6 hpa following a sub-pharyngeal amputation.

2.4. Mesentery Behavior and Pharynx Formation as Specific Landmarks for Oral Regeneration

The size and transparency of juvenile *Nematostella* make them more amenable for detailed imaging experiments than adults. We thus analyzed in detail the tissue behavior during oral regeneration of juveniles. We performed DNA labeling on regenerating juveniles following sub-pharyngeal amputation and observed the sequential events every 12 h from 0 to 144 hpa using confocal imaging (Figure 6).

Focusing on the behavior of the mesenteries and the pharynx reformation, we distinguish four main characteristic features: (Step 0) 0–12 hpa, no contact between the remaining mesenteries and the surrounding oral epithelia (Figure 6a); (Step 1) 12–48 hpa, contact of the remaining mesenteries between each other at their most oral site and with the surrounding epithelia at the amputation site (Figure 6b); (Step 2) 60–96 hpa, emergence of a space between the mesenteries and the epithelia at the amputation site (Figure 6c). The epithelia of the amputation site seems dragged down towards

the aboral region by the remaining mesenteries. This accentuates the protrusion of the developing tentacle bulbs; (Step 3) 72–120 hpa, the pharyngeal lip (basal part of the future pharynx) forms (Figure 6d). Interestingly, the pharyngeal lip appears to develop first from the oral-most part of the remaining mesenteries; (Step 4) 96–144 hpa, the pharynx is fully regenerated and the tentacles elongate (Figure 6e). Subsequently, the upper part of the pharynx forms (Step 4) progressively in the space that was previously created (Figure 6e) and corresponds to a highly proliferative region (Figure 3Ab).

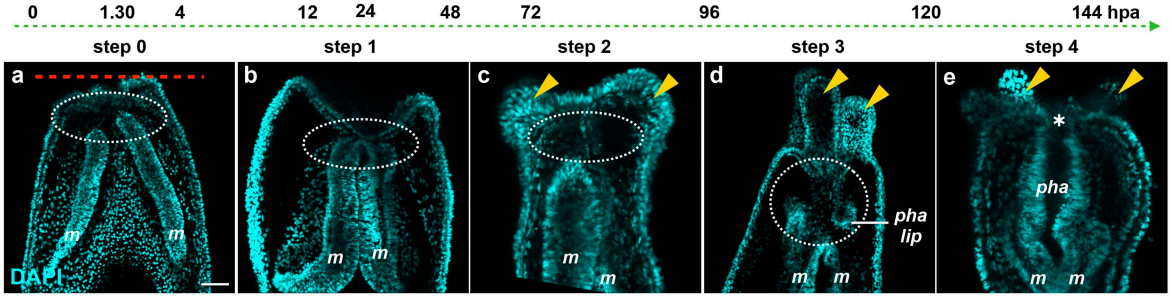

12 hpa	15/15 **100%**	0/15 **0%**	0/15 **0%**
24 hpa	21/21 **100%**	0/21 **0%**	0/21 **0%**
48 hpa	21/22 **95%**	1/22 **5%**	0/22 **0%**
72 hpa	9/23 **39%**	4/23 **17%**	10/23 **43%**
96 hpa	0/24 **0%**	13/24 **54%**	11/24 **46%**
120 hpa	0/24 **0%**	13/24 **54%**	11/24 **46%**
144 hpa	0/25 **0%**	0/25 **0%**	25/25 **100%**

Figure 6. Dynamics of the oral tissue during regeneration. The dynamic behavior of the oral tissue during regeneration was analyzed using confocal microscopy. (**a**–**e**) Confocal image stacks in which the DNA (nucleus) is labeled with DAPI (cyan). Five main phenotypes were observed between 0 and 144 hpa and are represented in this figure: (Step 0) the remaining parts of the mesenteries are separated together and from the epithelia at the amputation site (white dashed circle) (**a**); (Step 1) the remaining parts of the mesenteries are fused together and are in tight contact with the epithelia at the amputation site (white dashed circle) (**b**); (Step 2) an empty space forms between the remaining part of the mesenteries and the amputation site (white dashed circle) (**c**); (Step 3) the pharyngeal lip forms at the oral-most region of the remaining mesenteries, and the empty space becomes filled with nuclei (white dashed circle) (**d**); (Step 4) the pharynx is fully formed at the oral-most region of the remaining mesenteries (**e**). Numbers at the bottom of the image panel indicate the total number of analyzed specimens at 12, 24, 48, 72, 96, 120, 144 hpa and the number of cases representative of one of the described five steps in relation to the regeneration time in hours post-amputation (hpa). The amputation site is represented by a red dashed line in (**a**). Tentacle bulbs and elongated ones are shown by the yellow arrowhead (**c**–**e**). The white asterisk is the mouth opening (**e**). *m*, mesentery; *pha lip*, pharyngeal lip; *pha*, pharynx. Scale bar in (**a**) is 20 μm and applies to (**b**–**e**).

2.5. Fluorescence in the Pharyngeal Region as a Landmark for Pharynx Reformation

Nematostella, like other cnidarians, possesses endogenous fluorescence emitted by fluorescent proteins and/or fluorescence of the tissues. The six-week-old *Nematostella* juveniles display a green (excitation wave length at 488 nm) fluorescence (henceforth referred to as 488+) from a currently unknown origin (Figure 7A).

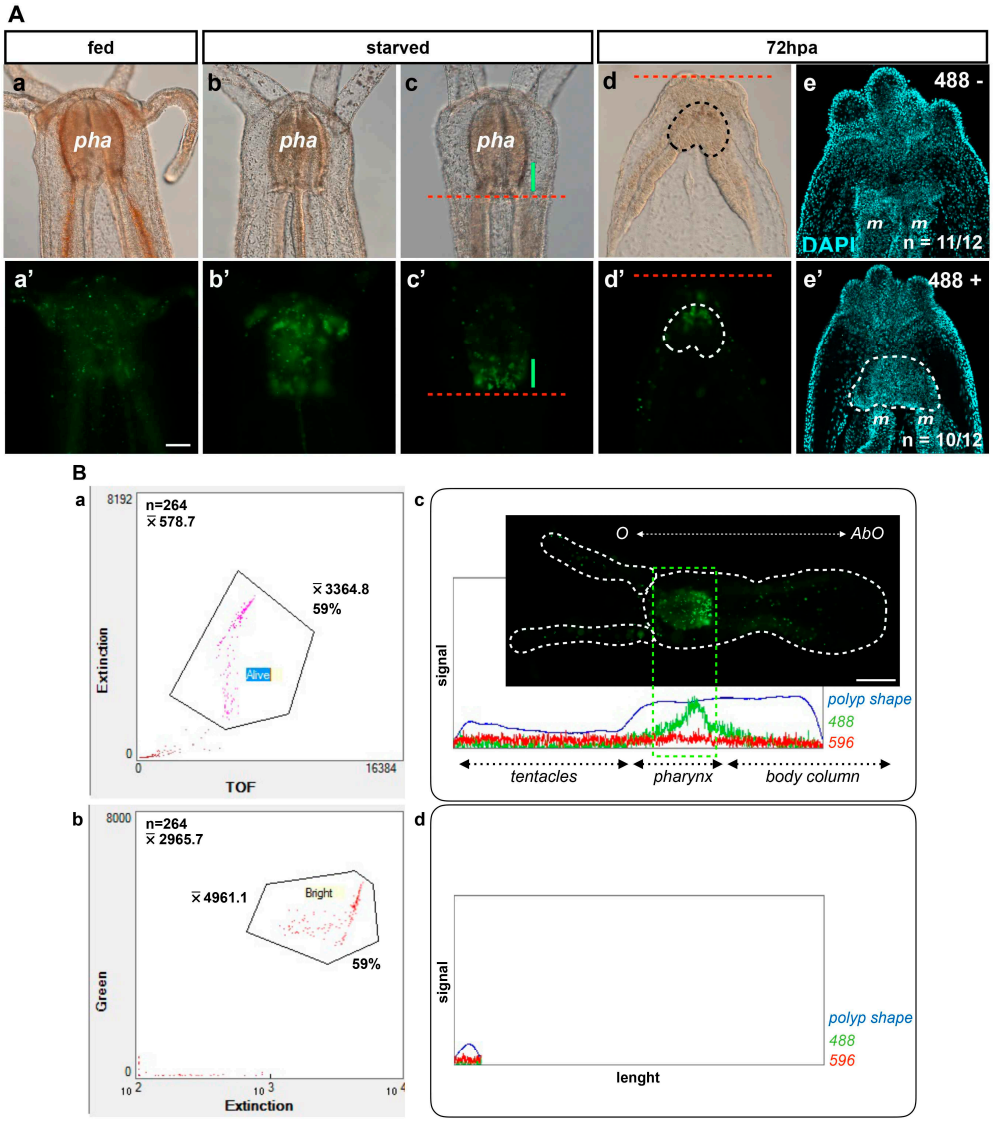

Figure 7. (**A**) Image of 488+ detection in the pharynx. Fed (**a**,**a'**), starved (**b**–**c'**), regenerating 72 hpa (**d**–**e'**) *Nematostella* polyp juveniles. DIC optic images (**a**–**d**). Epifluorescent images (**a'**–**d'**). The red dotted line labels the amputation site under the pharynx (**c**–**d'**). The green line in (**c**,**c'**) shows the 488+ fluorescence localized in the basal part of the pharynx. The area delimitated with the dotted line in **d** and **d'** is the region where the 488+ re-emerged in the polyp at 72 hpa. (**e**,**e'**) Confocal images at 72 hpa labeled for DNA (nuclei in cyan) on the 488-negative (**e**) and 488-positive (**e'**) polyp juvenile. The area delimitated with the white dotted line in (**e'**) (488+ regenerating polyps) shows the pharyngeal lip/pharynx in formation that is absent from the 488-negative regenerating polyps in which only the contact between the two mesenteries is visible. *pha*, pharynx; *m*, mesentery. Scale bar in (**Aa'**) is 20 µm and applies to (**Aa**–**Ae**,**Ab'**–**Ae'**); (**B**) Biosorter. The dot plot in (**a**,**b**) contains the sorting results of the animal by density (Extension) *vs.* mass (Time Of Flight—TOF) or by 488 fluorescence intensity (Green) *vs.* density (Extension), respectively, using a Biosorter system. (**c**,**d**) Examples of the Biosorter profiles (signal *vs.* length) of the bright fluorescent group (Bright in **b**, which corresponds to the Alive group in (**a**)) or the non-fluorescent group (unlabeled group localized at the bottom left of the two dot plots (**a**,**b**)). *O*, Oral; *AbO*, Aboral. Scale bar is 100 µm in (**Bc**).

The 488+ is randomly distributed throughout the entire body in freshly fed animals (Figure 7(Aa,Aa')). Interestingly, it became more and more localized to the pharynx when juvenile polyps were starved for one or two weeks (Figure 7(Ab,Ab',Ac,Ac')), suggesting a correlation of

this staining with a metabolic state of the animals. The varied metabolic states within one batch of animals could explain the asynchrony of regeneration. It may also contribute to differences in the cell proliferation rate observed between animals (see table below Figure 6; Röttinger, unpublished data). After sub-pharyngeal amputation, we observed that the 488+ re-emerges in the regenerating polyp in nearly half of the cases around 72 hpa (Table 1).

Table 1. The 488+ in hand-sorted regenerating polyps. Counting of the 488+ polyp juveniles at 24, 48, and 72 hpa. Two different experimenters performed blind counts. *Hand-sorter* 1 indicates the first experimenter and *Hand-sorter 2* the second.

–	*488*	**24 hpa**		**48 hpa**		**72 hpa**	
Hand-sorted	+	0/41	0%	4/66	6%	44/77	57%
	–	41/41	100%	62/66	94%	33/77	43%
Bio-sorted	+	3/41	7%	2/66	3%	31/77	40%
	–	38/41	93%	64/66	97%	46/77	60%

We thus used the localized green fluorescence in the pharynx of the uncut animal as a proxy to harmonize a batch of polyps before a series of cutting experiments. Sorting batches of uncut animals was performed using a large particle flow cytometer (Biosorter system, Union Biometrica) that enables the analysis of animals based on their length (time of flight, TOF), density (extinction), morphology (profiler), fluorescence, and the relative localization of the fluorescence along the animal body. In order to analyze the global amount of fluorescence intensity and its localization within the animals, we first defined debris (41% of the population; n = 264) based on morphology parameters (TOF and extinction parameters of each polyp; dot plot Figure 7Ba). We then measured the 488+ fluorescence intensity (the mean of fluorescence intensity is *mfi* = 4961.1) within the same batch (59% of the population; n = 264; dot plot Figure 7Bb). This 488+ can be localized within the profile of the animal using the Profiler software (Profile Figure 7Bc). Strikingly, the highest amount of 488+ fluorescence is localized in the region of the polyp where the pharynx is supposed to be.

In order to sort them in an automatic manner with the Biosorter, we identified a profile of interest (Figure 7Bc). We then bio-sorted 84 juveniles with this selected profile, performed sub-pharyngeal amputation, and followed their regeneration. In parallel, we hand-sorted 31 animals that size-matched and appeared in good condition without the use of the green auto-fluorescence proxy. All animals were cut below the pharynx, removing the 488+ at 0 hpa. Animals were then placed back into culturing conditions and the re-emergence of the 488+ was assessed in the regenerating polyps from hand-sorted *vs.* bio-sorted batches (Table 2).

Table 2. Emergence of the 488+ fluorescence during oral regeneration in the hand-sorted *versus* bio-sorted polyps at 72 and 120 hpa.

–	*488*	**72 hpa**		**120 hpa**	
Hand-sorted	+	14/33	42%	18/31	58%
	–	19/33	58%	13/31	42%
Bio-sorted	+	38/84	45%	51/84	61%
	–	46/84	55%	33/84	39%

Interestingly, both batches, hand-sorted *vs.* bio-sorted, displayed a similar heterogeneity in their individual advancement through the regeneration steps as reflected by the numbers of 488+ *vs.* 488− polyps in each batch of animals (Table 2). While the 488+-based selection did not yield a better or more synchronous regeneration, this experiment shows that the Biosorter system can be used as a tool to physically sort animals with precise criteria and/or analyze them for a specific phenotype in large-scale experiments in an unbiased manner. These data also show that the viability of the animals and their regeneration rate are not affected by the Biosorter system.

In order to determine if a correlation exists between the emergence of the 488+ and any previously described steps of regeneration, we sub-pharyngeally bisected juveniles and analyzed the phenotypes in detail of the 488+ and 488− polyps at 72 hpa. We observed that the 488+ starts to emerge in the oral-most part of the remaining mesenteries around 72 hpa (Figure 7(Ad,Ad')). Using confocal imaging on DAPI-stained (nucleus) animals we analyzed the detailed morphology of 488− and 488+ regenerating juveniles at 72 hpa. We observed that 488− are mainly at Step 2 (11 out of 12 cases) of the oral regeneration staging system described in Figures 6 and 7Ae. No pharynx in formation is visible. Interestingly, the 488+ are mainly at Step 3 or 4 (10 out of 12 cases), with a clear pharyngeal lip or pharynx in formation (Figure 7Ae'). These observations show a strong correlation between the initiation of pharynx formation (Steps 3 and 4) and the presence of 488+ in the regenerating juvenile after sub-pharyngeal amputation.

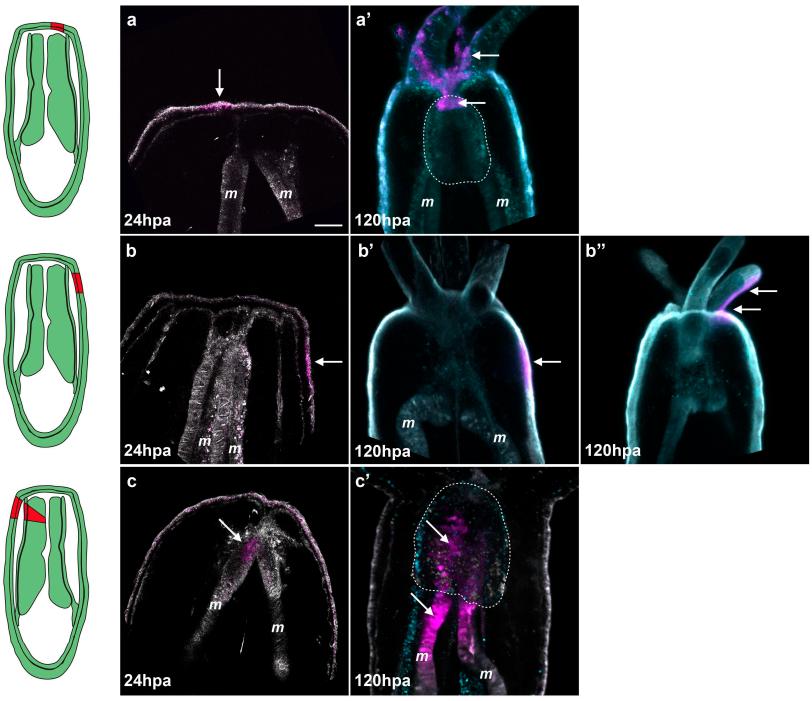

Figure 8. Tissue tracking experiment during regeneration. Spectral confocal images of *Nematostella* juveniles expressing Kaede photoconvertible fluorescent protein mRNA (**a**–**c'**). The Keade photoconverted region is represented in magenta and the non-photoconverted region in grey. Endogenous fluorescence is shown in turquoise to help visualize the morphology of the polyp (**a'**–**c'**); At 24 hpa, regions of interest (the epithelium central to the amputation site (**a**); the epithelium lateral to the amputation site (**b**), or the oral tip of the mesenteries (**c**)) were exposed to a UV laser resulting in permanent photo-conversion of the Kaede protein (magenta); The photoconversion at the central epithelium reveals integration of the converted patch (white arrows in (**a'**)) into the tentacles and most oral tip of the pharynx (white dotted line); Photoconversion of the lateral epithelium shows that this tissue remains in place during regeneration (white arrow in (**b'**)) or is incorporated into the adjacent tentacles (white arrows in (**b"**)); The photoconversion of the oral tip of the mesentery results in integration of the converted patch (white arrows in (**c'**)) into the pharynx (white dotted line). Scale bar is 20 μm in (**a**).

2.6. The Regenerating Pharynx Forms from the Oral Part of the Remaining Mesenteries

Taken together, our observations of the sequential events (Figure 6) and the 488+ emergence (Figure 7A) during regeneration led us to hypothesize that the regenerating pharynx after sub-pharyngeal amputation may come from the oral-most part of the remaining mesenteries. To test this hypothesis, we performed *in vivo* tissue tracking experiments in juveniles overexpressing *Kaede*

mRNA. KAEDE is a fluorescent protein that can be permanently photoconverted from green to red by exposing the expressing cells of interest to UV light [38]. For our tissue tracking experiments, we photoconverted three distinct regions of interest at 24 hpa: (1) the epithelia central to the amputation site (Figure 8a); (2) the epithelia lateral to the amputation site (Figure 8b); or (3) the oral tip of the mesenteries (Figure 8c).

It is important to note that when we convert the oral tip of the mesenteries, the laser must pass through the lateral epithelia and this region is also converted. After conversion we analyzed the location of the converted red fluorescence at eight days post-amputation (dpa) using spectral confocal imaging (see materials and methods). Spectral imaging measures the complete fluorescent spectrum of each pixel and matches these to pre-calibrated profiles. In our experiments we calibrated the profiles to detect converted Kaede, unconverted Kaede, and endogenous fluorescence. We found that the central epithelia of the amputation site gave rise to the tentacles in 19 out of 19 cases (Figure 8a,a′). Additionally, this region also gave rise to the mouth (oral-most part of the pharynx) in 15 out of 19 cases (four cases were undetermined) (Figure 8a,a′). The lateral epithelia remained in the lateral tissues after regeneration in four out of 11 cases and in the tentacles in seven out of 11 cases (Figure 8b,b′,b″). In neither central epithelia nor lateral epithelia conversions did we observe converted cells contributing to the pharynx. In the case of photoconverted mesenteries we observed converted KAEDE-expressing tissues in the newly formed pharynx in seven out of seven cases (Figure 8c,c′; Supplementary Figure S5). These animals also displayed converted tissues in their lateral epithelia and/or tentacles corresponding to the point of the laser entry during the conversion process. Since the lateral tissue remains in the lateral regions or ends up in the tentacles during regeneration but not the pharynx, we conclude that the converted tissue observed in the pharynx is indeed from the oral tip of the mesenteries, confirming our initial hypothesis (Figure 8c,c′; Supplementary Figure S5).

2.7. De Novo Transcription Is Induced First in the Gastrodermis at the Amputation Site

In order to reform missing body parts, an injured organism requires rapid activation of rRNA and tRNA transcription for proper protein biosynthesis of existing or new transcribed mRNA, as well as for cellular proliferation [39,40]. To characterize the transcription in *Nematostella*, we used EU-Click-it chemistry (Life Technologies, Carlsbad, CA, USA) to detect *de novo* transcription in *Nematostella* after amputation (Figure 9).

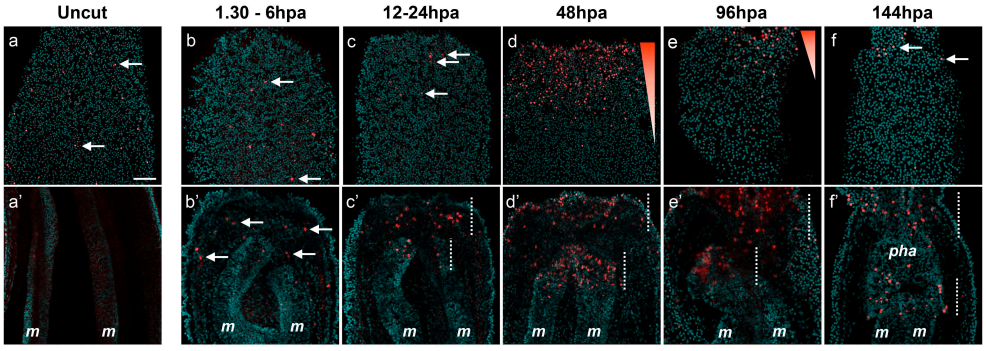

Figure 9. *De novo* transcription at the amputation site of the regenerating polyp. Overlap of confocal images showing *de novo* transcription (EU) in red and nucleus (DNA) staining in cyan in the oral epitheliums (**b**–**f**) and gastric cavity (**b′**–**f′**) of the amputated juvenile polyp. The uncut control is in (**a**–**a′**). The white arrows in **a**,**b**,**b′**,**c**,**f** show the cells that are undergoing *de novo* transcription. The white dotted lines in (**c′**–**f′**) show the regions in the body gastric cavity that are undergoing massive *de novo* transcription, the oral part of the mesenteries, and the epitheliums. All animals are oriented with the amputation site to the top. Scale bar in (**a**) is 20 µm and applies to all Figure 9 and Supplementary Figure S6.

This technology allows the visualization of EU (Ethynyl Uridine), a modified Uridine analog, incorporated into nascent RNA [41]. In uncut controls, *de novo* transcription is barely detectable and only a few cells were EU-positive (EU+) throughout the body epithelia (Figure 9a,a'). After sub-pharyngeal amputation, between 1.30 and 24 hpa, the *de novo* transcription pattern is similar to controls in regard to the epithelia (Figure 9b,c; Supplementary Figure S6(Aa,Aa')). However, in the same time frame, some EU+ cells start to emerge in increasing numbers in the internal oral tissues such as the mesenteries and gastrodermis (Figure 9b',c'). At 48 hpa, a strong EU+ signal is detected in the oral epithelia, both the ectodermis and gastrodermis, and the oral-most part of the remaining mesenteries (Figure 9d,d'; Supplementary Figure S6(Ac,Ac')). At 96 hpa, EU+ cells are present in the elongating tentacles with the exception of the tentacle tips (Supplementary Figure S6Ba). Staining progressively decreases in the oral epidermis but remains dense in the oral gastrodermis and in the oral-most part of the mesenteries where the new pharynx is developing (Figure 9e,e'). In the fully formed pharynx, at 144 hpa, only a few EU+ cells remain at the base of the tentacles and in the lower part of the pharynx (Figure 9f,f'; Supplementary Figure S6(Ae,Ae')).

2.8. Inhibition of Transcription or Proliferation has Different Effects on Regeneration

In order to determine the role of *de novo* transcription during regeneration in *Nematostella*, we treated amputated juveniles with the antibiotic Actinomycin D (AMD), an inhibitor of DNA-primed RNA synthesis [39]. In untreated controls, EU+ cells are massively detected at 48 hpa. As expected, at the same time-point no staining was observed in the regenerating juveniles that were treated with AMD from 36 to 48 hpa (Supplementary Figure S7a,b). Interestingly, we also observed that cell proliferation and regeneration were inhibited in AMD-treated animals (Supplementary Figure S7c,d).

A recent study has used hydroxyurea (HU) to efficiently block proliferation and regeneration in *Nematostella* [7]. However, nothing is known about the precise phenotype caused by the inhibition of cellular proliferation during regeneration. We thus amputated juveniles below the pharynx, treated them with either AMD or HU from 0 to 144 hpa, and scored wound healing success in addition to the exact stage at which regeneration was blocked using the above-described assays and morphological landmarks at 12, 72, and 144 hpa (Figure 10; Figure 11).

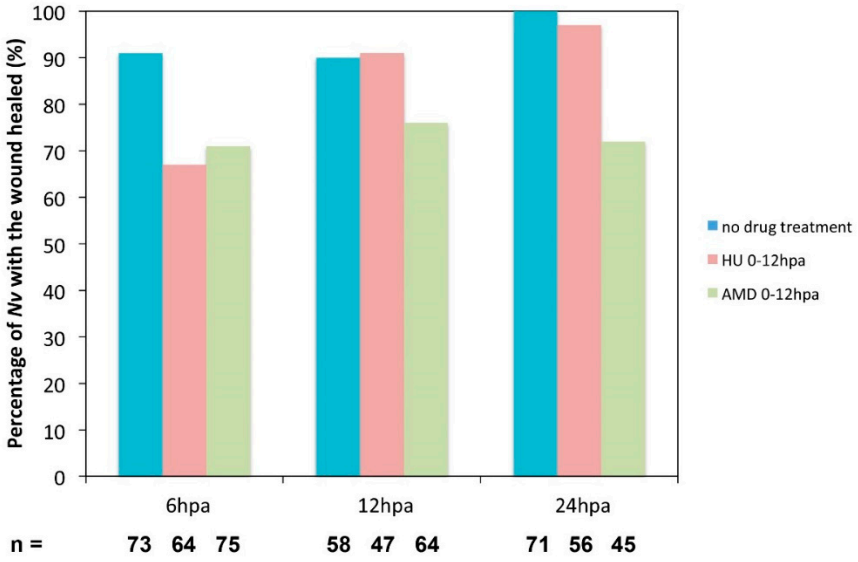

Figure 10. Effect of the inhibition of cell proliferation or transcription on the wound healing process. Hydroxyurea (HU; orange) was used at 20 mM to block cell proliferation, and Actinomycin D (AMD; green) was used at 10 ug/mL to block transcription. Both drugs were used in a time window from 0 to 12 hpa. The compression assay was performed at 6, 12, or 24 hpa.

We used the compression assay we described above (Figure 4) to assess wound healing under these experimental conditions. At 6 hpa, wound healing is delayed in a fraction of the HU-treated juveniles (33%, n = 58). At 12 hpa, almost all of the animals treated with HU are completely healed (91%, n = 47), although the process was delayed by approximately 6 h (Figure 10). However, in AMD-treated juveniles, 29% (n = 71) are not healed at 6 hpa, and a similar fraction remains open at 12 hpa (24%, n = 56) as well as 24 hpa (28%, n = 45) (Figure 10). This observation suggests that wound healing is not blocked but delayed when cell proliferation only is inhibited. However, when both *de novo* transcription and cell proliferation are blocked with the AMD treatment, wound healing does not occur in a subset of animals.

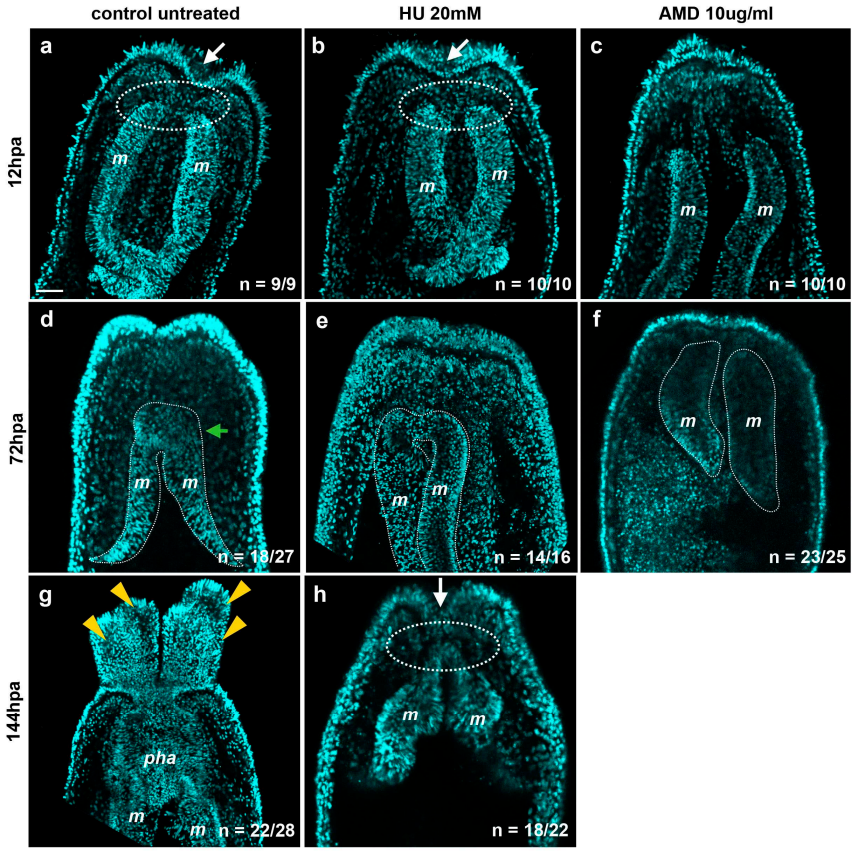

Figure 11. Inhibition of *de novo* transcription blocks regeneration at an earlier step than inhibition of cell proliferation. The experimental amputated polyps were treated with hydroxyurea (HU) to block cell proliferation or with Actinomycin D (AMD) to block *de novo* transcription from 0 to 144 hpa and analyzed at the indicated time-points. Confocal images showing the morphological phenotype using nuclear (DNA, cyan) staining in regenerating control (**a**,**d**,**g**) or experimental (**b**,**c**,**e**,**f**,**h**) polyps at 12 hpa (**a**–**c**); 72 hpa (**d**–**f**); or 144 hpa (**g**,**h**); The white arrows in (**a**,**b**,**h**) show the characteristic depression of the epithelium at the amputated site that correlates with the initiation of the contact between the remaining mesenteries and the surrounding epithelia (circle white dotted line in (**a**,**b**,**h**)); This depression and contact initiation are absent in the polyps treated with AMD (**c**). The green arrow in (**d**) indicates the forming pharyngeal lip. The white dotted lines in (**d**) to (**f**) indicate the mesenteries. The yellow arrowheads in (**g**) indicate the tentacles. *m*, mesenteries; *pha*, pharynx. All animals are oriented with the amputation site to the top. Number of cases for the representative phenotype are in white at the bottom right of each image. Scale bar in (**a**) is 20 µm and applies to all Figure 11.

Interestingly, we observed two strikingly different phenotypes at 12 hpa in the HU- *versus* AMD-treated juveniles. Similar to controls at 12 hpa, HU-treated polyps progress to Step 1 when the mesenteries are fused together and enter in contact with the surrounding epithelia at the amputation

site (Figure 11a,b). In addition, a characteristic depression is present in the epithelia at the amputation site in the control as well as in HU-treated polyps (Figure 11a,b). However, the AMD-treated regenerating juveniles appear to have been blocked in Step 0, right after the amputation, when the mesenteries are neither in contact with one another, nor with the epithelia of the amputation site (Figure 11c). The characteristic depression in the epithelia at the amputation site is absent as well.

To further characterize the phenotypes resulting from AMD or HU treatment, we assessed pharynx formation using the appearance of 488+ as a proxy at 72 hpa. In untreated regenerating juveniles, the 488+ fluorescence is observed in 62% (38 out of 61 cases). In AMD-treated juveniles, we never observed 488+ in 100% (52 out of 52 cases). We obtained similar results in HU-treated polyps in which 488+ never becomes detectable in 85% (53 out of 62 cases). In addition, no pharyngeal lip or tentacle bulbs were visible in either of the treatments (Figure 11e,f) as the polyps resulting from AMD or HU treatment remain blocked at Step 0 or Step 1, respectively. These data show that for both the inhibition of *de novo* transcription or cell proliferation, the pharynx never starts to form, suggesting that cell proliferation is required for pharynx formation.

At 144 hpa, HU-treated polyps still remain blocked at Step 1 (Figure 11h) compared to the controls in which a fully formed pharynx is present (Figure 11g). At 144 hpa, AMD-treated polyps were highly opaque and degraded (data not shown), suggesting a lethal effect of long-term inhibition of transcription. All together these results show that cell proliferation is required for both pharynx formation and tentacle elongation.

3. Discussion

3.1. Morphological and Cellular Landmarks for Oral Regeneration in Juveniles

In the present study, we describe in detail the morphological and cellular landmarks for regeneration (Figure 12). We also present *in vivo* tools that can be used to assess wound healing and pharynx formation in juveniles after sub-pharyngeal amputation.

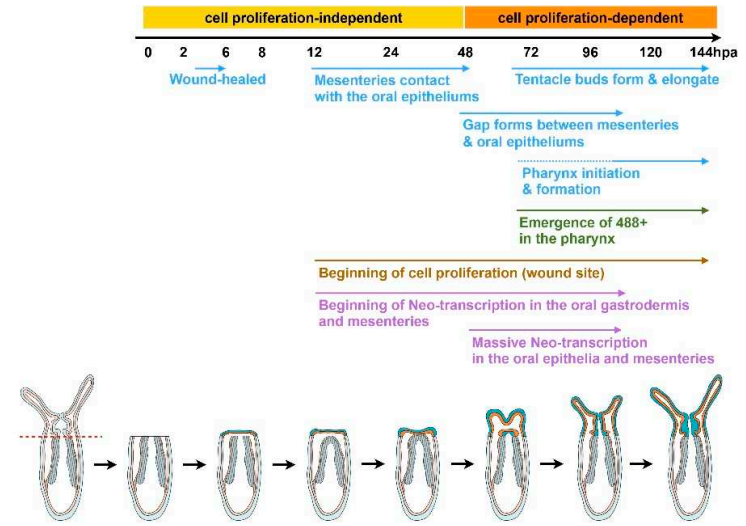

step 0	wound open, mesenteries neither in contact with one another, nor with the amputation site
step 0.5	wound healed, mesenteries neither in contact with one another, nor with the amputation site
step 1	mesenteries in contact with one another as well as with the amputation site
step 2	creation of a gap between mesenteries and oral epithelia, tentacle buds appear
step 3	appearance of 488+ autofluorescence, pharyngeal lip begins to form, tentacle buds elongate
step 4	fully formed pharynx, mouth opening, elongated tentacles, regenerated animal

Figure 12. Diagram summarizing the morphological and cellular events underlying oral regeneration in the sea anemone, *Nematostella vectensis*. The table below the illustration provides definitions for the various regeneration steps.

From a morphological point of view, we observe a stereotypic timeline of events: wound healing is completed after 4–6 hpa. Then, the mesenteries fuse together and contact the amputation site at about 12–24 hpa. This is followed by the emergence of a gap between the mesenteries and the wound site between 60 and 72 hpa. This space allows proper pharynx formation around 72–96 hpa by the means of rearrangement of pre-existing mesenteries and cell proliferation. This characteristic behavior of the mesenteries to form the pharynx is accompanied by tentacle bud formation and elongation to form a juvenile that is indistinguishable from its uncut siblings. Along with the morphological timeline, we further describe *de novo* transcription first in the gastrodermis and mesenteries at 12 hpa at the amputation site. Then, a massive wave of *de novo* transcription is activated at 48 hpa in the epidermis, gastrodermis, and in the mesenteries at the amputation site. Similarly, cellular proliferation is first detected at 12 hpa at the wound site and increases progressively over time. It is detected in the oral parts of the mesenteries at 24–48 hpa and remains at high levels until regeneration is achieved.

While these morphological landmarks can be used to define steps of regeneration, none of them can be associated with precise temporal information. This is because within a given batch of animals we observed that regeneration speed varies considerably and not all animals reach a given intermediate step (e.g., pharynx formation) at the same time (see table at the bottom of the Figure 6). However, the highest variation in timing seems to occur around 60–72 hpa. At earlier time points, the batch of regenerating juveniles seems more homogenous in their regeneration stages.

Our present study describes in detail the morphological and cellular events that are initiated either early (0–24 hpa) or late (60–96 hpa) during regeneration. In fact, we did not observe specific morphological or cellular events that are initiated in the period spanning this gap. However, it is known that cellular proliferation progressively increases [7] during this time frame. This suggests important cellular activity and possibly specification events that will subsequently give rise to the new body structures. One way to further characterize the regenerative timeline would be to use gene reporters. *Nematostella* is amenable for gene editing [42] and thus, to further develop this system for regenerative studies, an effort needs to be made in the development of transgenic lines that express genes during a given time span. These could not only highlight the beginning or the end of wound healing or the reformation of a given structure, but perhaps also indicate events that are currently not yet definable using morphology only (e.g., between 24 and 60 hpa). Initial efforts have been made to determine the genes involved in wound healing [34] that could be used for such approaches and this work should be expanded to other regenerative phases.

3.2. In Vivo Assays to Assess Wound Healing Success and Reformation of the Pharynx

We developed an *in vivo* assay to determine the success of wound healing after bisection of juveniles by taking advantage of the existence of nematosomes, free circulating aggregations of cells/cnidocytes. Upon compression of the animal with tweezers, the nematosomes exit the body cavity at the amputation site during the process of wound healing and exit through the aboral pore once wound healing is completed. However, we currently cannot exclude the fact that a reformed extracellular matrix or massive production of mucus may prevent the nematosomes from leaking through the wound site during the compression assay before the wound tissue is actually closed.

Unfortunately, the same assay cannot be used to determine the exact timing of mouth re-opening as in uncut juveniles the nematosomes are released through the aboral pore in all cases (100%, $n = 41$). This observation suggests that the fully developed mouth contracts strongly or that the connection between the body cavity and the tentacles disperses and decreases the mechanical forces that the forceps apply to the mouth region. We also tried to assess the timing of mouth opening by feeding the juveniles. However, the size of the animals (100–150 µm) requires that we feed them with smashed brine shrimp, which makes ingestion very heterogeneous within a batch and very difficult to assess. Therefore, detailed morphological and cellular analyses are required to determine the timing of mouth reopening in juveniles (Figure 6e).

In addition, we observe that an endogenous green fluorescence (488+) that is potentially associated with nascent nematosomes is detected ubiquitously in freshly fed animals but localized to the pharynx in juveniles that were starved for one or two weeks, reflecting potentially different metabolic states. We show that hand-sorting uncut animals by size (and health) or bio-sorting them by size and 488+ intensity/localization results in a similar proportion of 488+ and 488− at 72 and 120 hpa (Table 2). We conclude that the Biosorter system is a good way to select a homogenous batch of *Nematostella* polyps with high confidence from a batch of thousands of juveniles. These can be used for experimentation as has been done in other invertebrate and vertebrate models such as *C. elegans* or *D. rerio* [43,44]. In addition, we show that this 488+ correlates with the initiation of pharynx formation during regeneration (Figure 7(Ae–af')). As a consequence, we successfully used this endogenous fluorescent landmark to assess *in vivo* the reformation of the pharynx in regenerating juveniles after sub-pharyngeal amputation.

Both of the assays we present in this study, compression and emergence of 488+, enable us to determine precise events without having to fix and stain the animals. Thus, the same batch of animals can be followed over the course of the regeneration process. The perturbation experiments we carried out (AMD and HU), and for which we used the *in vivo* assays to determine the timing of the wound healing and the regenerative progression, further underline that these approaches are very useful in juveniles. Furthermore, adults also contain a large amount of free circulating nematosomes, display a strong and very characteristic red endogenous fluorescence in the pharynx caused by the expression of NvFP-7R (not detected in the four-tentacle juveniles), and exhibit green endogenous fluorescence throughout the body and the tentacles [45]. Thus, it would be interesting to use the nematosomes as well as the re-emergence of the pharyngeal NvFP-7R as unbiased assays to determine wound healing and pharynx formation during adult oral regeneration.

3.3. Sequence and Origin of the Regenerating Body Parts

We show that juvenile and adult *Nematostella* do not display any differences in the timing of regeneration or the requirement of cellular proliferation after sub-pharyngeal amputation. Thus, it would be crucial to extend this analysis and perform a systematic comparison of the isolated body parts in juveniles and adults. This could identify potential age-related differences or a complete conservation of the cellular (and potentially molecular) mechanisms underlying whole-body regeneration in *Nematostella* juveniles and adults. This is of particular importance since in *Hydra*, the mechanism involved in head regeneration differs depending on the region of amputation (sub-tentacle crown *vs.* mid-body) [9].

We chose to analyze regeneration in juveniles for the ease of imaging morphological details that are more difficult using adult tissues (due to their opacity, size, and fluorescence). However, the morphological characteristics and the staging system we describe for juvenile sub-pharyngeal regeneration cannot be simply extrapolated to adult regeneration and, in particular, it is not intended to replace or extend the existing staging system for regeneration from isolated adult physa in *Nematostella* [30].

In later study, Bossert and colleagues propose (based on macro photographs) that the regenerating adult mesenteries emanate from the most aboral region of the newly formed pharynx during oral regeneration from the isolated adult physa [30]. In contrast, using detailed confocal microscope data and *in vivo* fate-mapping experiments, our present study shows that, in the juveniles regenerating from sub-pharyngeal amputation, the most oral tissues of the mesenteries contribute to re-form a new pharynx.

The precise mechanisms by which mesenteries are formed during embryonic and larval development are poorly described. A first report proposes that these structures are formed by a combination of the pharyngeal ectoderm and body wall endoderm (Aman and Technau, unpublished in [46]). These observations suggest that in the regenerating polyp resulting from adult physa isolation, the mesenteries form in a similar way to those that form during embryonic development,

from the already formed pharynx (the origin of which is unclear) [30]. In the regenerating juvenile resulting from sub-pharyngeal amputation, the already present mesenteries are able to give rise to the lost pharynx (data observed in our present study). In order to gain greater insight into the plasticity of pharyngeal and mesenterial fates in all three contexts (embryogenesis, regeneration from isolated physa, or after sub-pharyngeal amputation), further studies focusing on the tissue/cellular molecular mechanisms underlying the origins of these tissues are crucial.

3.4. Importance of De Novo Transcription and Cell Proliferation during Regeneration

A previous study on the wound healing process in *Nematostella* showed that mRNA transcription for specific genes is upregulated as early as 1 h post-injury and that the wound signal seems to initiate from the gastrodermis [34]. Interestingly, we also observed a few dispersed EU+ cells, indicative of *de novo* transcription, in the gastrodermal tissues at the amputation site as early as 1.30–6 hpa. It is important to note that even if the size of the injury between these two studies ([34] *vs.* our present study) is different, the beginning of *de novo* transcription seems to correlate.

In the last part of our study, we used the described morphological landmarks as a regeneration staging system, in addition to our *in vivo* assays, to assess in detail the phenotypes obtained under experimental conditions. We showed that inhibition of *de novo* transcription or cell proliferation between 0 and 12 hpa delays or blocks wound healing, but only in the minority of cases. These data are consistent with the timing of *de novo* transcription and cell proliferation, which begin noticeably at 12 hpa, followed by massive waves at the amputation site between 24 and 48 hpa. However, we also showed that the phenotypes observed at 12, 72, and 144 hpa after AMD or HU treatments in regenerating juveniles are strikingly different. The HU treatment shows that the wound healing and early (Steps 0–1) of *Nematostella* regeneration are independent of cell proliferation. Contrary to this, the AMD treatment shows that the *de novo* transcription is required for those same early steps: fusion of the mesenteries to one another and to contact the epithelia at the amputation site (Steps 0–1). These treatments, HU or AMD, block all subsequent regeneration (Steps 2–4) as indicated by the absence of 488+ re-appearance, pharynx formation, and tentacle elongation. These observations strongly suggest that *de novo* transcription is required for the initial tissue dynamics of regeneration (from Steps 0–1), and that cell proliferation is required for later steps (Step 2–4) such as pharynx formation and tentacle elongation.

4. Materials and Methods

4.1. Animal Culture

Nematostella vectensis were cultured at the Institute for Research on Cancer and Aging, Nice (IRCAN) of the University of Nice. Adult and juvenile animals were cultured in 1/3X ASW (Artificial Sea Water; Tropic-Marin Bio-actif system sea salt (Tropic-Marin, Wartenberg, Germany) and maintained at 17 or 22 °C for adults and juveniles, respectively. Adults were fed five times a week with freshly hatched artemia. To obtain juveniles, spawning was carried out as described in [21]. Juveniles for cutting experiments were used six weeks after fertilization. Two-week-old juveniles were fed once a week for two weeks with 1 mL of smashed artemia and then starved for two weeks in order to minimize contamination/background caused by food particles.

4.2. Animal Bisection

Juveniles or adults were relaxed by adding 1 mL of 7.14% $MgCl_2$ in 5 mL 1/3 ASW and placed on a light table for 10 to 15 min. Six-week-old polyps were cut using a microsurgery scalpel n°15 (Swann-Morton, Sheffield, UK). Each cut was performed perpendicular to the oral–aboral axis of the body column.

4.3. Compression Assay

A circle was drawn on a slide with a hydrophobic pen (Dako Pen, Dako) and the relaxed regenerating polyps were placed on this circle in a droplet of 1/3 ASW + $MgCl_2$ 7.14%. The polyps were then compressed laterally with the tweezers 3C GRIP (Outils Rubis SA, Stabio, Switzerland). and the expulsion of the nematosomes was assayed. The wound was considered closed when, under pressure, the nematosomes did not leak through the amputated oral part. In this case, the nematosomes either leaked through the aboral opening or did not leak at all. The wound was considered as non-closed when nematosomes were expelled through the oral region. The compression rate is difficult to measure because of the variability among the polyps of the same batch (diverse sizes, metabolic rates, robustness of their tissues). However, to standardize the process, the compression was maintained and accentuated until the nematosomes leaked. In some cases, compression was increased to its maximum and the two tips of the tweezers met.

4.4. Staining

After relaxing adults or juvenile polyps in $MgCl_2$ for 10–15 min, animals were fixed in 4% paraformaldehyde (Electron Microscopy Sciences #15714, Hatfield, PA, USA) in 1/3 ASW for 1 h at 22 °C or overnight at 4 °C. Fixed animals were washed three times in PBT 0.2% (PBS1X + Triton 0.2%). To analyze the general morphology, Hoechst staining (Invitrogen #33342, Carlsbad, CA, USA) at 1/5000 was used to label the DNA/nucleus, and BODIPY® FL PhallAcidin 488 (Molecular Probes #B607, Eugene, OR, USA) staining was used at 1/200 to label actin microfilaments (cell membranes and muscle fibers).

4.5. Cell Proliferation (EdU) and De Novo Transcription (EU) Detection

To detect cellular proliferation Click-it EdU (5-ethynyl-2′-deoxyuridine) kits (Invitrogen #C10337 or #C10339, Carlsbad, CA, USA) were used following the protocol from [7]. The EdU was used at 300 uM following the protocol from [7]. To detect *de novo* transcription Click-it EU (5-ethynyl-2′-uridine) kit (Invitrogen #C10337, Carlsbad, CA, USA) was used following the manufacturer's protocol. EU was used at 1 mM.

4.6. Bio-Sorting

The Biosorter system (Union Biometrica, Holliston, MA, USA) equipped with the 2000 µm FOCA flow cell was calibrated with 500 µm beads. Using the Flowpilot software (Union Biometrica), polyps were analyzed for their morphology using the extinction coefficient, their length was analyzed using the Time Of Flight (TOF) between two sensors in the FOCA, and their green endogenous fluorescence intensity (488+) was emitted after a 488-laser excitation. For each animal, 488+ was characterized by measuring the intensity, the width, and the height of the peak in real time on live animals. The debris and small animals were excluded from the analysis based on the TOF and extinction parameters. The 488+ was localized in real time using the Profiler module that scans the profile of the object and integrates the measure of this endogenous fluorescence within this profile, allowing us to determine the relative localization of the 488+ in live polyps. For animal sorting, the optimal drop delay was determined using 500 µm beads and single-animal sorting was performed in 96-well plates filled with 100 µm 1/3 seawater.

4.7. Imaging

Live animals were imaged using a protocol described in [16]. The imaging setup was composed of either with a Zeiss Stereo Discovery V8 Discovery or a Zeiss Axio Imager A2 (both Carl Zeiss Microscopy GmbH, Jena, Germany) equipped with a Canon 6D digital camera, triggering two external Canon Speedlite 430 EX II Flashes and controlled by the Canon Digital Photo Professional software (Canon Inc., Tokyo, Japan). Images were edited using Adobe Lightroom 5 and/or Photoshop

CS6 software (Adobe Systems Inc., San Jose, CA, USA). Labeled animals were analyzed using a Zeiss LSM Exciter or Zeiss 710 confocal microscope running the ZEN 2009 software (Carl Zeiss Microscopy GmbH, Jena, Germany) from the IRCAN imaging platform (PICMI) or the iBV Platform of Resources in Imaging and Scientific Microscopy (PRISM), respectively. Each final image was reconstituted from a stack of confocal images using Z-projection (maximum intensity or standard deviation) of the ImageJ software (Rasband, W.S., ImageJ, U.S. National Institutes of Health, Bethesda, MD, USA).

4.8. Photoconversion Experiment

Fertilized *Nematostella* juveniles were injected with mRNA encoding the photoconvertable Kaede (green to red fluorescence) protein. At six weeks the juveniles were subject to sub-pharyngeal amputation. Then 24 h later, juveniles were relaxed for 10 min with 7.14% $MgCl_2$ in 1/3 ASW and mounted between slide and coverslip. The region of interest of the juvenile was photoconverted using a 405 nm wavelength laser on a Zeiss 510 confocal microscope. The specific region was photoconverted with the 405 nm laser at 100% power for 10 iterations (scans) and up to three repetitions at a scan speed less than 10 µs/pixel. When photoconverted, the juveniles were left to recover and regenerate for eight to nine days, then relaxed with 7.14% $MgCl_2$ in 1/3 ASW, mounted between slide and coverslip, and analyzed for the red patch of converted Kaede on a Zeiss 710 laser-scanning microscope. To separate photoconverted cells from endogenous fluorescence, using a lambda stack, spectral profiles of converted Kaede-expressing cells, unconverted Kaede-expressing cells, and endogenous red fluorescence were analyzed using a positive and negative control (converted Kaede- and unconverted Kaede-expressing juveniles, respectively). Several different red endogenous fluorescent cells were analyzed to account for variation. Finally, animals were imaged using the online fingerprinting mode and the 34-channel QUASAR detector (Zeiss LSM 710; Zeiss, Gottingen, Germany).

4.9. Drug Treatments Hydroxyurea (HU)—Actinomycin D (AMD)

Cellular proliferation was inhibited using HU (Sigma-Aldrich #H8627-5G, St. Louis, MO, USA) and transcription was blocked using the AMD (Enzo Life Sciences Inc. #ALX-260-020-M001, Farmingdale, NY, USA). HU was made up fresh at 20 mM in 1/3× ASW before each experiment. A stock solution of AMD prepared in DMSO and kept at −20 °C was diluted in 1/3X ASW to use at a final concentration of 10 µg/mL prior to each experiment. Each HU or AMD treatment was performed in a final volume of 500 µL 1/3× ASW in a 24-well plate using the adequate controls (1/3× ASW or DMSO). Pharmaceutical drugs were changed every 24 h to maintain their activity for the duration of the experiments.

5. Conclusions

In summary, our staging system for oral regeneration after sub-pharyngeal amputation, combined with our *in vivo* assays for wound healing and pharynx formation using naturally existing landmarks, is a precise way to assess the phenotypes resulting from experimental manipulation during regeneration in *Nematostella*. This study also begins to define the cellular and molecular mechanisms underlying the intriguing phenomenon of whole-body regeneration, providing a solid basis for further developing *Nematostella* as a new cnidarian regeneration system.

Supplementary Materials: Supplementary materials can be found at http://www.mdpi.com/1422-0067/16/12/26100/s1.

Acknowledgments: The authors thank the IRCAN for their support in setting up the laboratory and the Pasteur-IRCAN Molecular and Cellular Imaging Core Facility (PICMI) for providing access to the Zeiss LSM Exciter confocal microscope, the iBV Platform of Resources in Imaging and Scientific Microscopy (PRISM) for providing access to the Zeiss LSM 710 confocal microscope as well as the Cytometry Core Facility (CYTOMED) for providing access to the Union Biometrica BIOSORTER. In addition, we want to thank Julien Cherfils and Ludovic Cervera for their precious help on the Biosorter system. This project was funded by an ATIP-Avenir award (CNRS/INSERM/Plan Cancer), a Marie-Curie Career Integration Grant (CIG—FP7

European Commission) as well as grants from the "Association pour la Recherche sur le Cancer (ARC)" and the Région PACA to ER. Individual fellowships were provided by the FRM (Fondation pour la Recherche Médicale), the MESR (Ministry of higher education and science), the "Ligue contre le Cancer" as well as the ARC foundation to Aldine R. Amiel, Hereroa T. Johnston, Karine Nedoncelle, Jacob F. Warner, respectively.

Author Contributions: Aldine R. Amiel, Hereroa T. Johnston, Karine Nedoncelle, Jacob F. Warner and Eric Röttinger conceived and designed the experiments; Aldine R. Amiel, Hereroa T. Johnston, Karine Nedoncelle, Jacob F. Warner and Solène Ferreira performed the experiments; Aldine R. Amiel, Hereroa T. Johnston, Karine Nedoncelle, Jacob F. Warner, Solène Ferreira and Eric Röttinger analyzed the data; Eric Röttinger contributed reagents/materials/analysis tools; Aldine R. Amiel and Eric Röttinger wrote the paper.

Conflicts of Interest: The authors declare no conflict of interest.

References

1. Singer, I.I. Tentacular and oral-disc regeneration in the sea anemone, Aiptasia diaphana. 3. Autoradiographic analysis of patterns of tritiated thymidine uptake. *J. Embryol. Exp. Morphol.* **1971**, *26*, 253–270. [PubMed]
2. Sabine, A.M.; Smith, T.B.; Williams, D.E.; Brandt, M.E. Environmental conditions influence tissue regeneration rates in scleractinian corals. *Mar. Pollut. Bull.* **2015**, *95*, 253–264. [CrossRef] [PubMed]
3. Fischer, A.B.; Hofmann, D.K. Budding, bud morphogenesis, and regeneration in Carybdea marsupialis Linnaeus, 1758 (Cnidaria: Cubozoa). *Hydrobiologia* **2004**, *530*, 331–337.
4. Hargitt, C.W. Regeneration in Rhizostoma pulmo. *J. Exp. Zool.* **1904**, *1*, 73–94. [CrossRef]
5. Bode, H.R. Head regeneration in *Hydra*. *Dev. Dyn.* **2003**, *226*, 225–236. [CrossRef] [PubMed]
6. Galliot, B.; Ghila, L. Cell plasticity in homeostasis and regeneration. *Mol. Reprod. Dev.* **2010**, *77*, 837–855. [CrossRef] [PubMed]
7. Passamaneck, Y.J.; Martindale, M.Q. Cell proliferation is necessary for the regeneration of oral structures in the anthozoan cnidarian *Nematostella vectensis*. *BMC Dev. Biol.* **2012**, *12*, 34. [CrossRef] [PubMed]
8. Bradshaw, B.; Thompson, K.; Frank, U.; Alvarado, A.S. Distinct mechanisms underlie oral *vs.* aboral regeneration in the cnidarian *Hydractinia echinata*. *eLife* **2015**, *4*, e05506. [CrossRef] [PubMed]
9. Chera, S.; Ghila, L.; Dobretz, K.; Wenger, Y.; Bauer, C.; Buzgariu, W.; Martinou, J.-C.; Galliot, B. Apoptotic Cells Provide an Unexpected Source of Wnt3 Signaling to Drive *Hydra* Head Regeneration. *Dev. Cell* **2009**, *17*, 279–289. [CrossRef] [PubMed]
10. Zhang, Z.Q. Animal biodiversity: An introduction to higher-level classification and taxonomic richness. *Zootaxa* **2011**, *3148*, 7–12.
11. Daly, M.; Brugler, M.R.; Cartwright, P.; Collins, A.G. The phylum Cnidaria: A review of phylogenetic patterns and diversity 300 years after Linnaeus. Available online: https://kuscholarworks.ku.edu/handle/1808/13641 (accessed on 8 September 2015).
12. Darling, J.A.; Reitzel, A.R.; Burton, P.M.; Mazza, M.E.; Ryan, J.F.; Sullivan, J.C.; Finnerty, J.R. Rising starlet: The starlet sea anemone, *Nematostella vectensis*. *Bioessays* **2005**, *27*, 211–221. [CrossRef] [PubMed]
13. Reitzel, A.; Burton, P.; Krone, C.; Finnerty, J. Comparison of developmental trajectories in the starlet sea anemone *Nematostella vectensis*: Embryogenesis, regeneration, and two forms of asexual fission. *Invertebr. Biol.* **2007**, *126*, 99–112. [CrossRef]
14. Rentzsch, F.; Fritzenwanker, J.H.; Scholz, C.B.; Technau, U. FGF signalling controls formation of the apical sensory organ in the cnidarian *Nematostella vectensis*. *Development* **2008**, *135*, 1761–1769. [CrossRef] [PubMed]
15. Layden, M.J.; Boekhout, M.; Martindale, M.Q. *Nematostella vectensis* achaete-scute homolog NvashA regulates embryonic ectodermal neurogenesis and represents an ancient component of the metazoan neural specification pathway. *Development* **2012**, *139*, 1013–1022. [CrossRef] [PubMed]
16. Röttinger, E.; Dahlin, P.; Martindale, M.Q. A Framework for the establishment of a cnidarian gene regulatory network for "Endomesoderm" specification: The inputs of ß-catenin/TCF signaling. *PLoS Genet.* **2012**, *8*, e1003164. [CrossRef] [PubMed]
17. Leclère, L.; Rentzsch, F. RGM Regulates BMP-mediated secondary axis formation in the sea anemone *Nematostella vectensis*. *Cell Rep.* **2014**, *9*, 1921–1930. [CrossRef] [PubMed]

18. Genikhovich, G.; Fried, P.; Prünster, M.M.; Schinko, J.B.; Gilles, A.F.; Fredman, D.; Meier, K.; Iber, D.; Technau, U. Axis patterning by BMPs: Cnidarian network reveals evolutionary constraints. *Cell Rep.* **2015**, *10*, 1646–1654. [CrossRef] [PubMed]
19. Fritz, F.A.; Ikmi, A.; Seidel, C.; Ariel, P.; Gibson, C.M. Mechanisms of tentacle morphogenesis in the sea anemone *Nematostella vectensis*. *Development* **2013**, *140*, 2212–2223. [CrossRef] [PubMed]
20. Crowell, S. A new sea anemone from Woods Hole, Massachusetts. *Wash. Acad. Sci. Wash.* **1946**, *36*, 57–60.
21. Hand, C.; Uhlinger, K.R. The culture, sexual and asexual reproduction, and growth of the sea anemone *Nematostella vectensis*. *Biol. Bull.* **1992**, *182*, 169–176. [CrossRef]
22. Hand, C. Another sea anemone from California and the types of certain Californian anemones. *J. Wash. Acad. Sci.* **1956**, *47*, 411–414.
23. Extavour, C.G.; Pang, K.; Matus, D.Q.; Martindale, M.Q. vasa and nanos expression patterns in a sea anemone and the evolution of bilaterian germ cell specification mechanisms. *Evol. Dev.* **2005**, *7*, 201–215. [CrossRef] [PubMed]
24. Putnam, N.H.; Srivastava, M.; Hellsten, U.; Dirks, B.; Chapman, J.; Salamov, A.; Terry, A.; Shapiro, H.; Lindquist, E.; Kapitonov, V.V.; *et al*. Sea anemone genome reveals ancestral eumetazoan gene repertoire and genomic organization. *Science* **2007**, *317*, 86–94. [CrossRef] [PubMed]
25. Ormestad, M.; Martindale, M.; Rottinger, E. A comparative gene expression database for invertebrates. *EvoDevo* **2011**. [CrossRef] [PubMed]
26. Schwaiger, M.; Schonauer, A.; Rendeiro, A.F.; Pribitzer, C.; Schauer, A.; Gilles, A.F.; Schinko, J.B.; Renfer, E.; Fredman, D.; Technau, U. Evolutionary conservation of the eumetazoan gene regulatory landscape. *Genome Res.* **2014**. [CrossRef] [PubMed]
27. Fischer, A.H.L.; Mozzherin, D.; Eren, A.M.; Lans, K.D.; Wilson, N.; Cosentino, C.; Smith, J. SeaBase: A multispecies transcriptomic resource and platform for gene network inference. *Integr. Comp. Biol.* **2014**, *54*, 250–263. [CrossRef] [PubMed]
28. Technau, U.; Steele, R.E. Evolutionary crossroads in developmental biology: Cnidaria. *Development* **2011**, *138*, 1447–1458. [CrossRef] [PubMed]
29. Burton, P.M.; Finnerty, J.R. Conserved and novel gene expression between regeneration and asexual fission in *Nematostella vectensis*. *Dev. Genes Evol.* **2009**, *219*, 79–87. [CrossRef] [PubMed]
30. Bossert, P.E.; Dunn, M.P.; Thomsen, G.H. A staging system for the regeneration of a polyp from the aboral physa of the anthozoan cnidarian *Nematostella vectensis*. *Dev. Dyn.* **2013**, *242*, 1320–1331. [CrossRef] [PubMed]
31. Renfer, E.; Amon-Hassenzahl, A.; Steinmetz, P.R.H.; Technau, U. A muscle-specific transgenic reporter line of the sea anemone, *Nematostella vectensis*. *Proc. Natl. Acad. Sci. USA* **2010**, *107*, 104–108. [CrossRef] [PubMed]
32. Trevino, M.; Stefanik, D.J.; Rodriguez, R.; Harmon, S.; Burton, P.M. Induction of canonical Wnt signaling by alsterpaullone is sufficient for oral tissue fate during regeneration and embryogenesis in *Nematostella vectensis*. *Dev. Dyn.* **2011**, *240*, 2673–2679. [CrossRef] [PubMed]
33. Tucker, R.P.; Shibata, B.; Blankenship, T.N. Ultrastructure of the mesoglea of the sea anemone *Nematostella vectensis* (Edwardsiidae). *Invertebr. Biol.* **2011**, *130*, 11–24. [CrossRef]
34. DuBuc, T.Q.; Traylor-Knowles, N.; Martindale, M.Q. Initiating a regenerative response; cellular and molecular features of wound healing in the cnidarian *Nematostella vectensis*. *BMC Biol.* **2014**, *12*, 1–20. [CrossRef] [PubMed]
35. Tucker, R.P.; Hess, J.F.; Gong, Q.; Garvey, K.; Shibata, B.; Adams, J.C. A thrombospondin in the anthozoan *Nematostella vectensis* is associated with the nervous system and upregulated during regeneration. *Biol. Open* **2013**, *2*, 217–226. [CrossRef] [PubMed]
36. Williams, R.B. Studies on the nematosomes of *Nematostella vectensis* Stephenson (Coelenterata: Actiniaria). *J. Natl. Hist.* **1979**, *13*, 69–80. [CrossRef]
37. Shimizu, H.; Takaku, Y.; Zhang, X.; Fujisawa, T. The aboral pore of *Hydra*: Evidence that the digestive tract of *Hydra* is a tube not a sac. *Dev. Genes Evol.* **2007**, *217*, 563–568. [CrossRef] [PubMed]
38. Dittrich, P.S.; Schäfer, S.P.; Schwille, P. Characterization of the photoconversion on reaction of the fluorescent protein Kaede on the single-molecule level. *Biophys. J.* **2005**, *89*, 3446–3455. [CrossRef] [PubMed]
39. Sobell, H.M. Actinomycin and DNA transcription. *Proc. Natl. Acad. Sci. USA* **1985**, *82*, 5328–5331. [CrossRef] [PubMed]

40. Zhang, Q.; Shalaby, N.A.; Buszczak, M. Changes in rRNA transcription influence proliferation and cell fate within a stem cell lineage. *Science* **2014**, *343*, 298–301. [CrossRef] [PubMed]
41. Jao, C.Y.; Salic, A. Exploring RNA transcription and turnover *in vivo* by using click chemistry. *Proc. Natl. Acad. Sci. USA* **2008**, *105*, 15779–15784. [CrossRef] [PubMed]
42. Ikmi, A.; McKinney, S.A.; Delventhal, K.M.; Gibson, M.C. TALEN and CRISPR/Cas9-mediated genome editing in the early-branching metazoan *Nematostella vectensis*. *Nat. Commun.* **2014**, *5*, 5486. [CrossRef] [PubMed]
43. Rüegger, S.; Miki, T.S.; Hess, D.; Großhans, H. The ribonucleotidyl transferase USIP-1 acts with SART3 to promote U6 snRNA recycling. *Nucleic Acids Res.* **2015**, *43*, 3344–3357. [CrossRef] [PubMed]
44. Spaink, H.P.; Cui, C.; Wiweger, M.I.; Jansen, H.J.; Veneman, W.J.; Marín-Juez, R.; de Sonneville, J.; Ordas, A.; Torraca, V.; van der Ent, W.; *et al*. Robotic injection of zebrafish embryos for high-throughput screening in disease models. *Methods* **2013**, *62*, 246–254. [CrossRef] [PubMed]
45. Ikmi, A.; Gibson, M.C. Identification and In Vivo Characterization of NvFP-7R, a developmentally regulated red fluorescent protein of *Nematostella vectensis*. *PLoS ONE* **2010**, *5*, e11807. [CrossRef] [PubMed]
46. Tarrant, A.M.; Gilmore, T.D.; Reitzel, A.M.; Levy, O.; Technau, U.; Martindale, M.Q. Current directions and future perspectives from the third *Nematostella* research conference. *Zoology* **2015**, *118*, 135–140. [CrossRef] [PubMed]

Article 4: NvERTx: a gene expression database to compare embryogenesis and regeneration in the sea anemone Nematostella vectensis.

Warner, J. F., Guerlais, V., Amiel, A. R., Johnston, H., Nedoncelle, K., & Röttinger, E. (2018).

Development, *145*(10), dev162867. doi:10.1242/dev.162867

© 2018. Published by The Company of Biologists Ltd | Development (2018) 145, dev162867. doi:10.1242/dev.162867

TECHNIQUES AND RESOURCES

RESEARCH REPORT

NvERTx: a gene expression database to compare embryogenesis and regeneration in the sea anemone *Nematostella vectensis*

Jacob F. Warner, Vincent Guerlais, Aldine R. Amiel, Hereroa Johnston, Karine Nedoncelle and Eric Röttinger*

ABSTRACT

For over a century, researchers have been comparing embryogenesis and regeneration hoping that lessons learned from embryonic development will unlock hidden regenerative potential. This problem has historically been a difficult one to investigate because the best regenerative model systems are poor embryonic models and vice versa. Recently, however, there has been renewed interest in this question, as emerging models have allowed researchers to investigate these processes in the same organism. This interest has been further fueled by the advent of high-throughput transcriptomic analyses that provide virtual mountains of data. Here, we present *Nematostella vectensis* Embryogenesis and Regeneration Transcriptomics (NvERTx), a platform for comparing gene expression during embryogenesis and regeneration. NvERTx consists of close to 50 transcriptomic data sets spanning embryogenesis and regeneration in *Nematostella*. These data were used to perform a robust *de novo* transcriptome assembly, with which users can search, conduct BLAST analyses, and plot the expression of multiple genes during these two developmental processes. The site is also home to the results of gene clustering analyses, to further mine the data and identify groups of co-expressed genes. The site can be accessed at http://nvertx.kahikai.org.

KEY WORDS: Embryogenesis, Regeneration, Transcriptome, Database, Cnidarian, *Nematostella vectensis*

INTRODUCTION

A long-standing question in the field of regeneration is to what extent regenerative programs recapitulate development. Comparing gene expression during these two processes provides clues as to how genes activated during embryogenesis are re-deployed during regeneration. The majority of studies performing this comparison focus on the role of individual or small groups of genes (Binari et al., 2013; Carlson et al., 2001; Gardiner et al., 1995; Imokawa and Yoshizato, 1997; Kaloulis et al., 2004; Katz et al., 2015; Millimaki et al., 2010; Özpolat et al., 2012; Reitzel et al., 2007; Torok et al., 1998; Wang and Beck, 2014). Studies comparing transcriptomes of embryogenesis and limb regeneration in axolotls and zebrafish have been successful in identifying differentially expressed genes involved in these processes (Habermann et al., 2004; Mathew et al., 2009). A comparison of whole-body regeneration to embryogenesis has yet to be performed, and could help with further improving our understanding of how genes are used during embryogenesis and re-used during regeneration. One organism is especially amenable to this line of study: the sea anemone *Nematostella vectensis* (Fig. 1A) (Layden et al., 2016; Reitzel et al., 2007).

Nematostella has been used as a research model for embryonic development (Finnerty et al., 2004; Kusserow et al., 2005; Matus et al., 2006; Rentzsch et al., 2006; Wikramanayake et al., 2003). *Nematostella* reproduce sexually and, after fertilization, the zygote undergoes a series of cleavages to form a blastula. Gastrulation occurs at the animal pole and, shortly thereafter, the embryo enters a swimming planula stage during which the pharynx and internal structures, termed mesenteries, develop. After several days, this planula larva settles, develops tentacles, and enters a juvenile stage. *Nematostella* development research entered the age of genomics with the sequencing of its genome by Putnam and colleagues in 2007 (Putnam et al., 2007; Technau and Schwaiger, 2015). Since then, a large number of developmental genes have been identified in *Nematostella*, and many commonalities between *Nematostella* and bilatarian development have emerged (Amiel et al., 2017; Burton and Finnerty, 2009; Darling et al., 2005; Genikhovich et al., 2015; Layden and Martindale, 2014; Layden et al., 2012; Leclère et al., 2016; Matus et al., 2008; Meyer et al., 2011; Reitzel et al., 2007; Röttinger et al., 2012). With the advent of high-throughput transcriptomics, several studies have examined gene expression during embryogenesis at the whole-genome level (Helm et al., 2013; Fischer and Smith, 2013; Fischer et al., 2014; Tulin et al., 2013), firmly establishing *Nematostella* as an embryonic model.

More recently, *Nematostella* has shown to be a powerful model for regeneration. Upon bisection, *Nematostella* is capable of regenerating the missing body half after ∼6 days postamputation (Bossert et al., 2013). Following subpharyngeal amputation (head removal), regeneration occurs via a highly dynamic process: first, there is an initial wound healing phase of ∼6 h, then regeneration follows a stereotypic program in which the mesenteries fuse and, via subsequent cell proliferation, reform the missing pharynx and tentacles over the course of 6 days (Amiel et al., 2015). This process has been shown to be both cell proliferation dependent (Passamaneck and Martindale, 2012) and utilize dynamic tissue rearrangement, with large portions of unamputated tissue contributing to the reformed tissue (Amiel et al., 2015). The existence of adult stem cells and the role they might play in regeneration have yet to be uncovered. This process is known to use several developmental signaling pathways originally deployed during embryogenesis (DuBuc et al., 2014; Schaffer et al., 2016; Trevino et al., 2011). It remains unclear, however, if these pathways are deployed the same way, i.e. with similar or divergent regulatory logic. One way to address this question is to systematically compare gene expression profiles during embryonic development and regeneration, to identify groups of genes originally used during embryogenesis that are re-used during regeneration. To facilitate this line of study, we created *N.vectensis* Embryogenesis and

Université Côte d'Azur, CNRS, INSERM, Institute for Research on Cancer and Aging, Nice (IRCAN), 06107 Nice, France.

*Author for correspondence (eric.rottinger@unice.fr)

J.F.W., 0000-0002-9197-1587; A.R.A., 0000-0002-3049-2822; H.J., 0000-0001-8477-596X; K.N., 0000-0003-4096-4886; E.R., 0000-0002-2938-6774

Received 23 December 2017; Accepted 25 April 2018

Development (2018) 145, dev162867. doi:10.1242/dev.162867

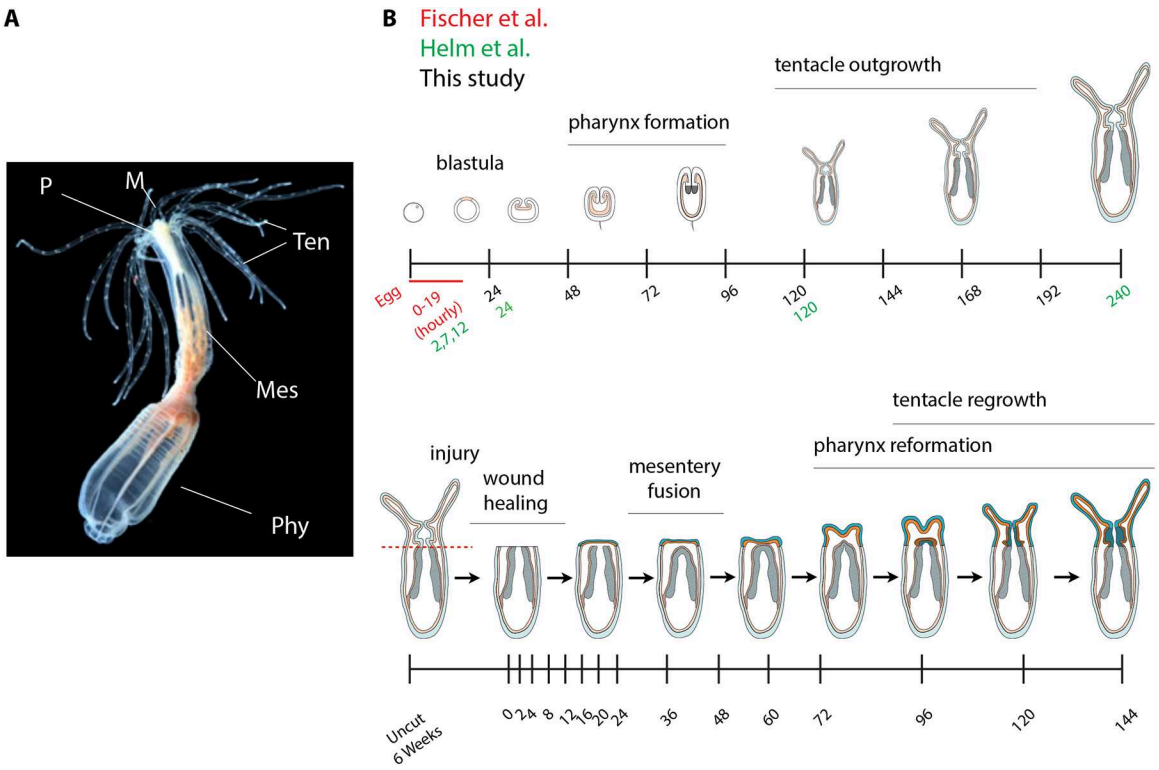

Fig. 1. Sampling strategy of data sets used in NvERTx. (A) *Nematostella* anatomy. *Nematostella* is a small sea anemone (~5 cm), with a mouth (M), pharynx (P) tentacles (Ten) and a body column with internal structures called mesenteries (Mes), the posterior section of which is termed the physa (Phy). (B) Schematic of RNAseq samples included in the NvERTx database. Three data sets spanning embryogenesis are included: one including data from Fischer and Smith (2013) and Fischer et al. (2014), sampled hourly from 0 hpf to 19 hpf; one including data from Helm et al. (2013), sampled at 2, 7, 12, 24, 120 and 240 hpf; and data from this study, sampled daily from 24 hpf to 192 hpf (250 embryos/time point, biological duplicates). Regeneration was sampled from 6-week-old animals at –1 (uncut), 0, 2, 4, 8, 12, 16, 20, 24, 36, 48, 60, 72, 96, 120 and 144 hpa (300 juveniles/time point, biological triplicates).

Regeneration Transcriptomics (NvERTx) – a quantitative gene expression database for comparing embryogenesis and regeneration in the sea anemone *N. vectensis*. NvERTx comprises several data sets spanning embryogenesis (Helm et al., 2013; Fischer and Smith, 2013; Fischer et al., 2014; Tulin et al., 2013; this study) and regeneration (this study). We used pooled RNA sequencing (RNAseq) data from *Nematostella* embryogenesis and regeneration to generate a *de novo* transcriptome assembly. Using this assembly, we then quantified each of the RNAseq data sets and clustered the transcripts to discover groups of genes that share similar expression. This tool can be used to find transcript sequences, identify co-expressed genes, and directly compare expression profiles during embryogenesis and regeneration. All of these data can be found in a searchable database that is accessible at www.nvertx.kahikai.org.

RESULTS AND DISCUSSION

NvERTx database: *de novo* assembly, annotation and data quantification

NvERTx is a quantitative gene expression database for embryogenesis and regeneration, consisting of several RNAseq data sets. It includes previously published data sets spanning very early embryogenesis to polyp from Helm et al. (2013) [sampled 2, 7, 12, 24, 120 and 240 h postfertilization (hpf)] and Fischer and Smith (2013) and Fischer et al. (2014) (sampled 0, 1, 2, 3, 4, 5, 6, 7, 8, 9, 10, 11, 12, 13, 14, 15, 16, 17, 18 and 19 hpf). To complement these and sample time points during tentacle genesis and pharynx formation, we generated an additional data set sampled at 24, 48, 72, 96, 120, 144, 168 and 192 hpf. Together, these data sets cover the major hallmarks of *Nematostella* development, including blastula (12-24 hpf), gastrula (24-48 hpf), planula (48-120 hpf) and juvenile (120-244 hpf) stages. The regeneration RNAseq data were sampled from 6-week-old juveniles after subpharyngeal amputation at –1 (uncut), 0, 2, 4, 8, 12, 16, 20, 24, 36, 48, 60, 72, 96, 120 and 144 h postamputation (hpa) (Fig. 1B). We chose these time points because they span the most important events of regeneration, including wound healing (0-6 hpa), pharynx reformation (24-72 hpa) and tentacle reformation (72-120 hpa) (Fig. 1A,B) (Amiel et al., 2015), all stages for which we have embryonic data spanning the initial development of these structures. For each of these data sets, we obtained the raw sequencing reads and used these as input for our quantitative workflow.

To quantify the RNAseq data, we performed a *de novo* transcriptome assembly, which we term NvERTx. We assembled this transcriptome using the short-read assembler Trinity (Haas et al., 2013), with combined paired-end reads from our regeneration data set and additional embryonic data from Tulin et al. (2013), sampled at 0, 6, 12, 18 and 24 hpf, as input (see Materials and Methods for complete workflow). The resulting assembly includes 234,381 transcripts with an N50 of 1678 and an average length of 837.30 bp (see Table S1 for assembly statistics). Each transcript is identified with a unique NvERTx.4 number. To annotate the transcriptome, we first identified the 231,294 transcripts with an open reading frame (ORF) and extracted the coding sequences using OrfPredictor (Min et al., 2005). We then compared the resultant protein sequences with NCBI's nonredundant protein database (NR) and the UniProt database using the Basic Local Alignment Search Tool (BLAST)-like tool PLAST (Nguyen and Lavenier, 2009). From these analyses we identified 85,475 transcripts with a significant hit to NR (e-value <5e-5), and 69,335 transcripts with a significant hit to the UniProt databases

Development (2018) 145, dev162867. doi:10.1242/dev.162867

(e-value <5e-5). Additionally, we compared each transcript with the current Nemve1 gene predictions (https://genome.jgi.doe.gov/Nemve1/Nemve1.home.html) using nucleotide BLAST (BLASTn), and identified 102,581 transcripts with a significant hit (e-value <5e-5) (Kent, 2002). Of these 102,581 Nemve1 hits, 19,565 represent unique Nemve1 'genes'. We found that 110,531 transcripts did not hit any of the three databases, a proportion typical of Trinity assemblies (Conesa et al., 2016), and could be noncoding sequences or other assembly artifacts (see Table S2 for full annotation statistics). For each of the 234,381 NvERTx transcripts, we provide all available annotations. We then used the transcriptome assembly to quantify each of the RNAseq data sets. We did this by aligning the reads using Bowtie2 (Langmead et al., 2009) and quantifying each transcript using RSEM and edgeR (Li and Dewey, 2011; Robinson et al., 2010). Transcripts with the same best Nemve1 hit were combined to obtain 'gene-level' quantification. To validate these data, we compared our RNAseq quantifications with results obtained by performing quantitative reverse transcription PCR (RT-qPCR) for several target genes using our in-house generated data sets, and observed a high level of concordance in their expression profiles (Figs S2 and S3; see Materials and Methods, 'RNAseq quality assurance' section). Finally, the three embryonic data sets were corrected for batch effects using the sva R package with time point as a categorical covariate (Leek et al., 2012) (see Materials and Methods for details). The quantified data sets are reported for each transcript in the database.

Retrieving expression plots, count tables and sequences

The NvERTx database can be accessed using multiple points of entry: by searching annotations (Fig. 2Ai), using BLAST (Fig. 2Aii) or exploring the co-expression clusters (Fig. 2Aiv) (see 'Exploring gene expression clusters' section). To demonstrate this, we use the *Nematostella* Brachyury protein (NvBra, NCBI GenBank ID AAO27886.2) as an example. To retrieve transcripts corresponding to *Nvbra*, we can use the search function to query the transcript annotations and enter the Nemve1 gene model ID from the current genome assembly (jgi|Nemve1|770), the NCBI GenPept accession number (gi|122058623), the NCBI GenBank accession number (AAO27886.2), or the gene name ('Brachyury') (Fig. 2Ai). Using any of these queries identifies several transcripts that correspond to *Nvbra* (Fig. 2B). Multiple matching transcripts reflect the different isoforms predicted by the transcriptome assembler. We can confirm which transcripts correspond to *Nvbra* by examining the annotations that are reported with the search results. It is normal for different isoforms to have slightly different annotations as each transcript was individually annotated. Clicking the NvERTx.4 numbers fills in the field on the left of the screen, enabling the user to directly compare their expression profiles by clicking 'Plot!' (Fig. 2Aiii).

Similarly, the BLAST tool can be used to retrieve NvERTx.4 transcripts using either a nucleotide (BLASTn) or protein (tBLASTn) query. The reported alignments can be then used to identify the correct transcripts. For example, using tBLASTn against the transcriptome with *Mus musculus* Brachyury (NCBI GenBank accession number AAI20808.1), we find several homologous transcripts, the first of which is *Nvbra* (Fig. 2C). Again, clicking the NvERTx.4 number fills in the field on the left of the screen, enabling the user to obtain the expression plots and annotations by clicking 'Plot!' (Fig. 2Aiii).

Once the NvERTx.4 IDs for *Nvbra*, NvERTx.4.100808 and NvERTx.4.100809, are selected we can query the database by clicking 'Plot!' on the left (Fig. 2Aiii). The first page that appears displays the transcripts' expression during regeneration and embryogenesis (Fig. 3A). We can see that the expression of *Nvbra* exhibits two peaks during regeneration, beginning at 8 hpa and 60 hpa, while during embryogenesis, *Nvbra* is expressed early, rapidly peaks at 20 hpf, then decreases throughout development. Note that the expression profiles for the two transcripts are perfectly superimposed and appear as one. This is because transcripts corresponding to the same Nemve1 best hit are quantified equivalently as they are from the same 'gene'. To distinguish transcript isoforms from separate genes we can compare the individual transcripts in the 'alignment' tab, where a MUSCLE sequence alignment is reported (Edgar, 2004) (Fig. 3F). In this case, we observe that NvERTx.4.100809 is a longer assembled isoform of *Nvbra*. The results tabset also includes the normalized count tables (Fig. 3B), transcript annotations (Fig. 3C), the sequences in FASTA format (Fig. 3D), and links to bibliographical resources including PubMed articles citing the protein and a PaperBlast query (Price and Arkin, 2017) (Fig. 3E). In the annotations tab, we can also see which co-expression cluster the transcript belongs to for embryogenesis and regeneration. Exploring these clusters is very useful for identifying co-expressed genes.

Exploring gene expression clusters

Co-expression analysis is particularly useful to identify genes that function in the same gene regulatory module. Co-expressed genes can also represent groups of genes that participate in a similar biological function. One method for identifying co-expressed genes is to cluster genes or transcripts by expression profile. For NvERTx, we performed fuzzy c-means clustering to regroup genes by expression profile, and provide those clusters in the 'Co-expression clusters' section of the site. These clusters can be used to identify transcripts that are co-expressed with a given gene of interest. Furthermore, comparing the membership of gene clusters during embryogenesis and regeneration can be used to identify groups of genes that function similarly during these processes.

The gene expression clusters can be browsed by either clicking a cluster in the 'Co-expression clusters' section (Fig. S1A) or by following a direct link from the annotation table of a transcript to its cluster (Fig. 3C). Using our previous example, *Nvbra*, from the annotations results, we can see that *Nvbra* participates in regeneration cluster two (R-2). When exploring R-2, we see all of the transcripts found in the cluster sorted by membership score. The score reflects how strongly a gene's expression matches the cluster core. By plotting several high-scoring transcripts, we can identify groups of co-expressed genes. For example, when we plot NvERTx.4.40781 (best NR hit: XP_015758878.1 forkhead box protein G1-like *Acropora digitifera*), NvERTx.4.57897 (best NR hit: AOP31964.1 dickkopf3-like 1 *N. vectensis*) and NvERTx.4.100808 (best NR hit: AAO27886.2 Brachyury protein *N. vectensis*), we see that they are indeed co-expressed with an initial expression peak between 4 hpa and 16 hpa, followed by a gradual rise from 36 hpa onward (Fig. S1Bii). By contrast, these genes are not co-expressed during embryogenesis and exhibit divergent expression patterns (Fig. S1Bi), raising the hypothesis that this particular grouping of genes is unique to regeneration. Using this method to find co-expressed genes is an effective way of identifying potential gene-regulatory modules and gene batteries. Importantly, assessing whether these genes are co-expressed during regeneration and embryogenesis can shed light on how these gene batteries are used or re-used during these two processes.

Differentially expressed genes

Comparing which genes are differentially expressed during embryogenesis and regeneration can provide important clues about

Development (2018) 145, dev162867. doi:10.1242/dev.162867

A

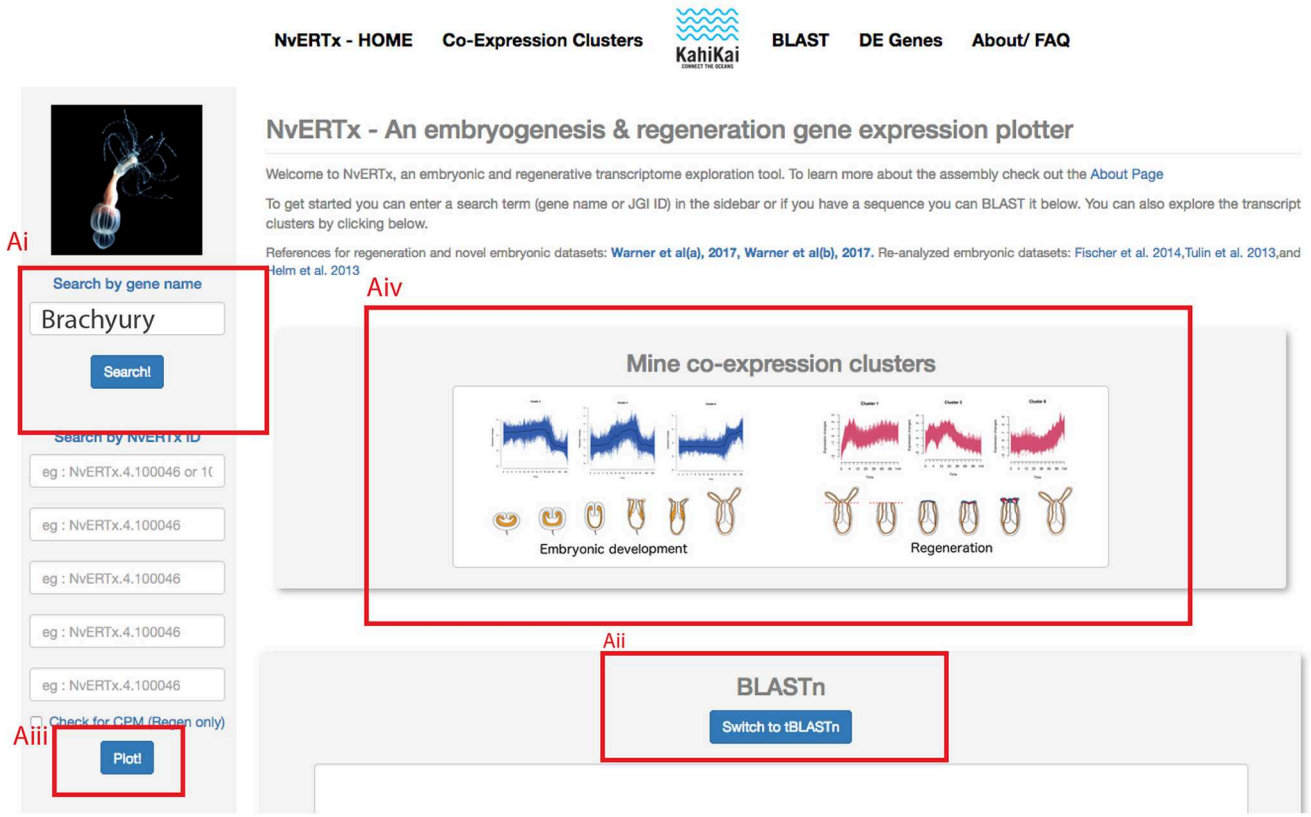

B

Search results

click on a row to view the other nr hits

Compare !

ID	Nemve1 hit	Nemve1 e-value	Uniprot id	Uniprot description	top nr_hit eval
NvERTx.4.100808	jgi|Nemve1|770|gw.137.1.1	0.0	Q17134	Brachyury protein homolog 1	gi|122058623|gb|AAO27886.2|Brachyury-like protein [Nematostella vectensis], 2e-119
NvERTx.4.100809	jgi|Nemve1|770|gw.137.1.1	0.0	A0A146ZVK6_FUNHE	Brachyury protein {ECO:0000313|EMBL:JAR70374.1}	None

C Blastplus results

TBLASTN 2.6.0+

Description

Compare !

contig	query	length	e-value	score	ident %
NvERTx.4.100809	AAI20808.1	3509	1.81112e-112	919.0	52.4
NvERTx.4.145171	AAI20808.1	985	2.94102e-57	490.0	47.5
NvERTx.4.145170	AAI20808.1	1116	1.15925e-56	490.0	48.7
NvERTx.4.73614	AAI20808.1	1420	7.95126e-55	484.0	45.8
NvERTx.4.73613	AAI20808.1	1624	8.87954e-55	488.0	45.8
NvERTx.4.145168	AAI20808.1	2491	1.86442e-54	497.0	51.9
NvERTx.4.159335	AAI20808.1	1335	2.02584e-53	473.0	48.9

Fig. 2. See next page for legend.

Development (2018) 145, dev162867. doi:10.1242/dev.162867

Fig. 2. NvERTx points of entry. (A) Screenshot of the NvERTx portal. (Ai) Users can search for genes using the gene name, Nemve1 accession number, or NCBI GenBank accession number. (Aii) The transcriptome can also be searched using BLASTn or tBLASTn. (Aiii) Multiple transcripts can be queried simultaneously. (Aiv) Users can also directly explore co-expression clusters from embryogenesis and regeneration to identify groups of co-expressed genes. (B) Screen shot of results from searching the annotations using the term 'Brachyury'. (C) tBLASTn results using *Mus musculus* Brachyury as a query (GenBank AAI20808.1) identify several homologous transcripts. The top scoring isoform is reported first.

how genes are initially deployed during embryonic development and if/how they are reused during regeneration. Systematically analyzing genes differentially expressed during regeneration has allowed for the discovery of 'regeneration-specific' genes in other models, including axolotl, zebrafish and newts (Bryant et al., 2017; Knapp et al., 2013; Looso et al., 2013; Mathew et al., 2009). To facilitate these lines of inquiry using NvERTx, we provide the results of intra-data-set pairwise differential gene-expression testing on the summarized Nemve1 genes. For each data set, we compare each time point to t_0, which is defined as 0 hpa for the regeneration data, 7 hpf (the estimated beginning of zygotic transcription) for the Fischer and Smith (2013), Fischer et al. (2014) and Helm et al. (2013) data, and 24 hpf (the first time point sampled) for the in-house embryonic data. The results of this testing can be queried on the DE Genes page, and an interactive volcano plot displaying the negative $\log_{10}$ false-discovery rate (FDR) as a function of fold change is generated (Fig. 4Ai,Bi). Each transcript is plotted as a single point, and multiple isoforms for a single gene are superimposed. Users can use the plot tools to click or drag-select the transcripts that are then displayed in the table below (Fig. 4Aii,Bii). These transcripts can then be compared by ticking the boxes in the table and querying the database as described above.

For example, when we select the three transcripts with the most dramatic fold change during embryogenesis from 7 hpf to 24 hpf (Fig. 4Ai, red dotted line box), we identify several transcripts corresponding to three predicted proteins (Fig. 4Aii). Querying the database shows that indeed these genes are highly expressed at 24 hpf (Fig. 4Aiii). Conversely, these genes show little variation during regeneration (Fig. 4Aiv). Likewise, when we examine differential expression during regeneration at 24 hpa, three genes show a large fold change (Fig. 4Bi, red dotted line box). Selecting these genes shows two predicted proteins and a T-box transcription factor (Fig. 4Bii). Comparing these genes, we see that all three are indeed upregulated at 24 hpa (Fig. 4Biv). Of these three, only the two predicted proteins show significant variation during embryogenesis (Fig. 4Biii, NvERTx.4.229217, NvERTx.4.119508), while no embryonic data are found for NvERTx.4.207772, meaning that this gene is not expressed at a detectable level in any of the embryonic data sets and could represent a 'regeneration-specific' gene.

Conclusion and future directions

NvERTx provides a platform to efficiently compare gene expression during embryogenesis and regeneration in *Nematostella*. Additionally, the comprehensive transcriptome provides high-quality transcript models that can be used to identify gene sequences. Using co-expression clusters, one can explore groups of genes that share similar expression patterns during embryogenesis and regeneration. Finally, mining the differentially expressed genes enables the identification of embryogenesis or 'regeneration-specific' genes. All of these tools are aimed at inspiring and building hypotheses concerning embryogenesis and regeneration for *Nematostella* and non-*Nematostella* researchers alike. Users can use their own groups of co-expressed genes to test for conservation of regeneration gene batteries, or to explore gene expression clusters to identify genes that share expression, and examine these in their own models.

As this web application is intended to complement and expand upon existing resources, we provided transcript models that have been annotated using a variety of gene/protein databases (NR, trEMBL, Nemve1). Sequencing technologies are evolving to achieve longer reads, and assemblers will soon provide more robust transcriptomes; in the future, we plan to take advantage of these technologies to improve our transcript models. We also plan to grow the database as future data sets examining embryogenesis and regeneration emerge. Finally, we foresee merging this resource with an existing spatial gene expression database found at http://www.kahikai.org/index.php?content=genes (Ormestad et al., 2011). This will enable the identification of syn-expression groups, genes that are co-expressed both spatially and temporally (Niehrs and Pollet, 1999), and further facilitate studies comparing differential gene usage during embryogenesis and regeneration.

MATERIALS AND METHODS

Animal culture, spawning and amputation

Adult *N. vectensis* were cultured at 16°C in the dark in 1/3 strength artificial sea water (ASW) as previously described (Amiel et al., 2017). Spawning was induced by feeding the animals with oysters the day before and transferring the animals to a light table for 12 h. Regeneration experiments were performed using 6-week-old juveniles as previously described (Amiel et al., 2017).

Transcriptomic data sets

The sequences that served as input into our *de novo* assembly consisted of two data sets: one spanning the first 24 h of embryogenesis originally reported by Tulin et al. (2013), and another spanning the first 144 h of regeneration generated in-house (see 'Library preparation and sequencing' section). The embryonic data set was downloaded from the Woods Hole Open Access Server (http://darchive.mblwhoilibrary.org/handle/1912/5613, last accessed 1 June, 2017) and includes Illumina HiSeq 100 bp paired-end sequencing prepared from *Nematostella* embryos at 0, 6, 12, 18 and 24 hpf. The regeneration data set includes Illumina NextSeq 75 bp paired-end sequencing from regenerating *Nematostella* at −1 (uncut), 0, 2, 4, 8, 12, 16, 20, 24, 36, 48, 60, 72, 96, 120 and 144 hpa (see 'Library preparation and sequencing' section for details). The sequence data that were used for transcript quantification are composed of four data sets. Three of the data sets spanned embryogenesis: one originally reported by Fischer and Smith (2013) and Fischer et al. (2014) (http://darchive.mblwhoilibrary.org/handle/1912/5981, last accessed 1 June, 2017) (Illumina HiSeq 100 bp paired-end replicates sampled hourly from 0 hpf to 19 hpf), a second embryonic data set originally reported in Helm et al. (2013) [NCBI Sequence Read Archive (SRA) project, PRJNA189768] (Illumina HiSeq 50 bp single-end replicates sampled from 2, 7, 12, 24, 120 and 240 hpf), and a third embryonic data set generated in house, sampled at 24, 48, 72, 96, 120, 144, 168 and 192 hpf (Illumina MiSeq 75Bp single-end replicates). The regenerative data used for quantification are the same as those used for the transcriptome assembly (Illumina NextSeq 75 bp single-end triplicates). Raw reads for the in-house generated data sets can be found in the NCBI SRA BioProject, under accession numbers PRJNA418421 and PRJNA419631.

Library preparation and sequencing

Two novel RNAseq data sets, one spanning embryonic, larval and postmetamorphic development and the other regeneration, were generated for this study. For the embryonic data set, ∼250 embryos per time point were cultured in 1/3 strength ASW at 18°C. At each time point, 24, 48, 72, 96, 120, 144, 168 and 192 hpf, the embryos were transferred to 500 ml Tri Reagent and homogenized for 15 s with a pestle. The resulting lysate was snap frozen in liquid nitrogen and stored at −80°C. This was repeated to obtain duplicates for each time point. After all the samples were collected,

Development (2018) 145, dev162867. doi:10.1242/dev.162867

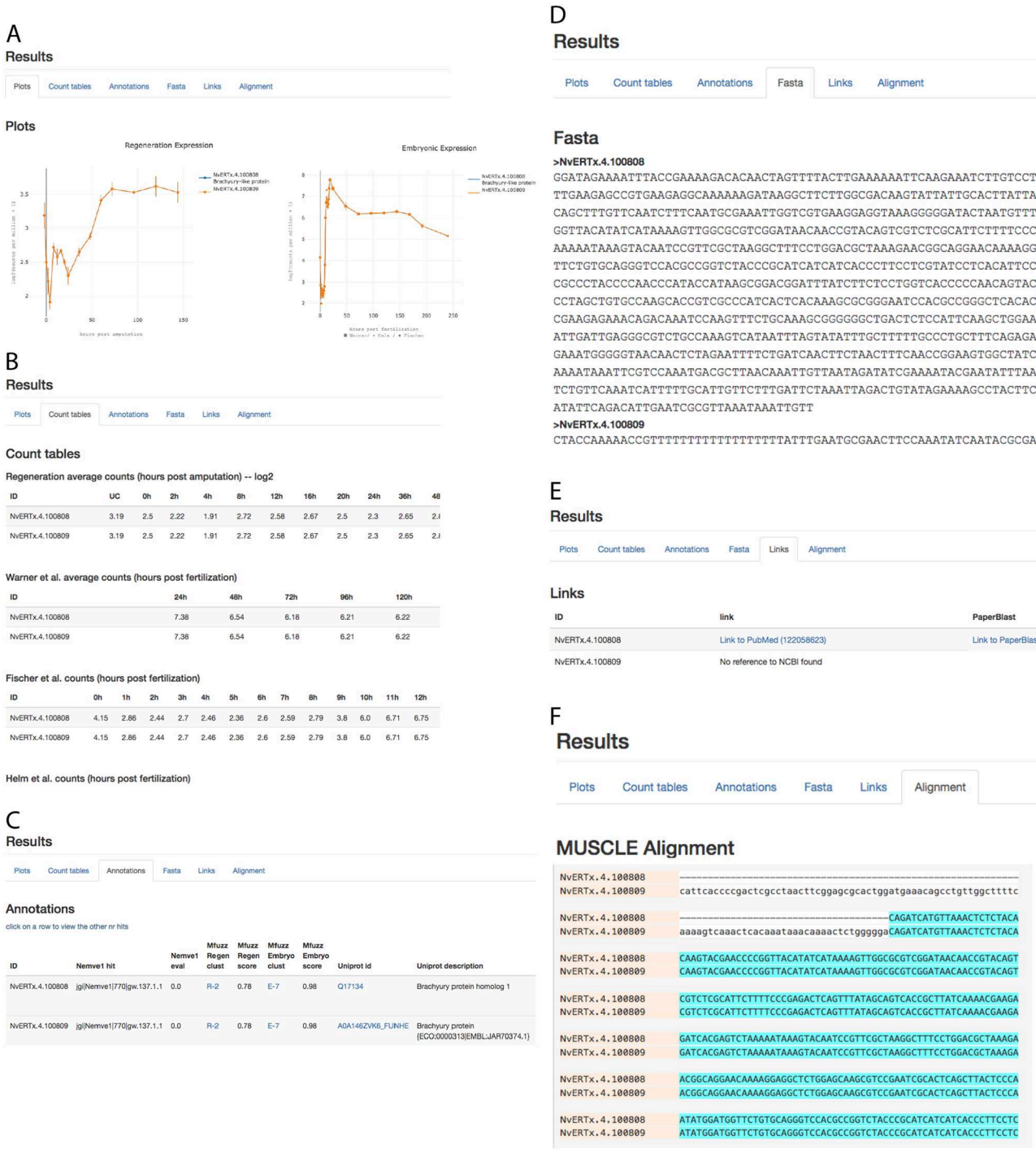

Fig. 3. Example results for the transcripts NvERTx.4.100808 and NvERTx.4.100809. (A) Expression plots for regeneration (left) and embryogenesis (right). The two transcripts are isoforms of the same genes so their expression profile plots and counts are equivalent. (B) Count data from each of the data sets. (C) Transcript annotations. (D) Sequences in FASTA format (the second sequence is shown cropped owing to space limitations). (E) Bibliographical resources including PubMed links and PaperBlast queries. (F) MUSCLE alignment to compare similar transcripts. The alignment shown is cropped to display the homologous region.

the RNA lysate was extracted using two phenol-chloroform extractions and precipitated with isopropanol. For the full extraction protocol, see Layden et al. (2013). The resulting nucleic acids were treated with the TURBO DNA-free kit from Invitrogen (AM1907) for 10 min at 37°C. The resulting RNA was quantified with a Qubit spectrometer, and RNA integrity was checked on an Agilent Bioanalyzer 2100. Then, 100 ng of RNA was used as input for an Illumina TruSeq Stranded mRNA Library Prep for NeoPrep Kit, and the libraries were prepared using an Illumina NeoPrep system. The 75 bp single-end sequencing was carried out on the NextSeq500 sequencer of the Institute for Research on Cancer and Aging, IRCAN Genomics Core Facility, Nice, France.

For the regenerative data set, ∼350 6-week-old *Nematostella* juveniles per time point were amputated below the pharynx. At each time point, –1, 0, 2, 4, 8, 12, 16, 20, 24, 36, 48, 60, 72, 96, 120 and 144 hpa, the juveniles were transferred to 500 ml Tri Reagent and homogenized for 15 s with a pestle. The resulting lysate was snap frozen in liquid nitrogen and stored at −80°C. This was repeated for each of the three replicates. After all samples were collected, the RNA was extracted as described above for the embryonic samples.

Development (2018) 145, dev162867. doi:10.1242/dev.162867

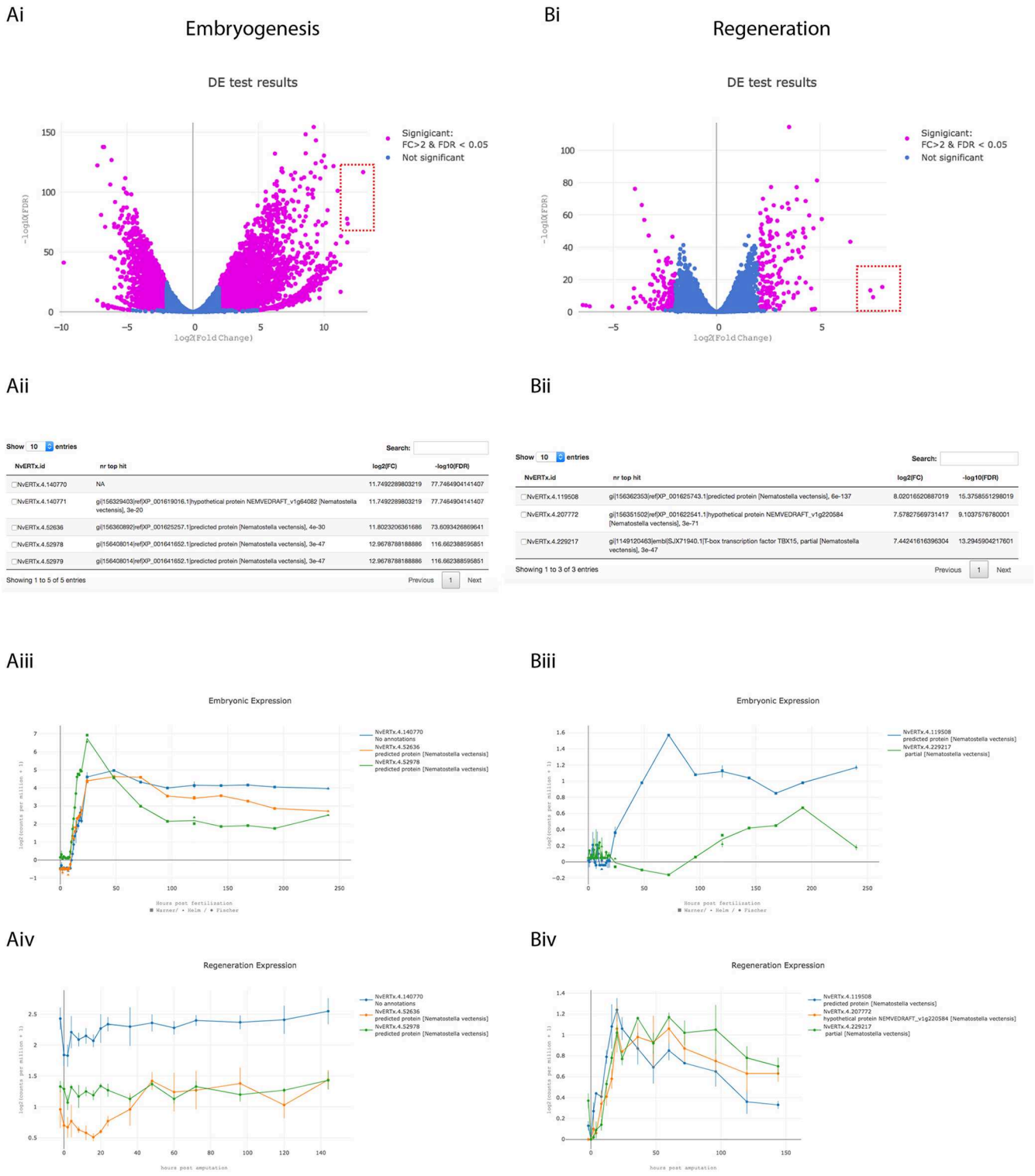

Fig. 4. Exploration of differentially expressed genes using the 'DE Genes' tool. Intra-data-set differential expression testing for summarized Nemve1 gene models. Each time point is compared with t_0, defined as 0 hpa for the regeneration data, 7 hpf (the estimated beginning of zygotic transcription) for the data from Fischer and Smith (2013), Fischer et al. (2014) and Helm et al. (2013), and 24 hpf (the first time point sampled) for the in-house embryonic data. (Ai,Bi) When a user selects a comparison, a volcano plot displaying the $-\log_{10}$(FDR) as a function of fold change is generated. Significant transcripts [FC>$\log_2$(2) and FDR <0.05] are colored magenta. Using the plot tools, multiple transcripts can be selected (red dotted line box, Ai,Bi) and a table is generated showing the corresponding transcripts (Aii,Bii). A user can compare these transcripts by ticking the corresponding box which fills the form on the left of the page. (Aiii,Aiv,Biii, Biv) The expression profiles shown here are then found on the results page.

Samples were stored in GenTegra-RNA stabilization reagent (GTR5100-S) and shipped to the NextGen Sequencing Core at the University of Southern California, CA, USA, for library preparation and sequencing. The samples were prepared with a KAPA Stranded RNA Kit (KR0960). Two replicates were sequenced as 75-bp single-end sequencing, and one replicate as 75-bp paired-end sequencing, on an Illumina NextSeq500 sequencer.

Development (2018) 145, dev162867. doi:10.1242/dev.162867

RNAseq quality control

All reads from each data set were processed equivalently. Reads were first quality filtered to remove low-quality reads and adapter trimmed using timmomatic (Bolger et al., 2014) and cutadapt (Martin, 2011), respectively.

Trinity *de novo* assembly

For the *de novo* assembly, paired-end reads from regeneration (–1, 2, 4, 8, 12, 16, 20, 24, 36, 48, 60, 72, 96, 120 and 144 hpa) and embryonic (0, 6, 12, 18 and 24 hpf) (Tulin et al., 2013) data sets were filtered of ribosomal sequences by aligning to *Nematostella* mitochondrial and ribosomal sequences using Bowtie2 (Langmead et al., 2009) and retaining the unmapped reads. These surviving reads were inputted into Trinity (v2.4.0) for assembly (Haas et al., 2013). To annotate the assembly, the ORFs were found using OrfPredictor (Min et al., 2005) and the resulting peptide sequences were compared with the NCBI NR database using the BLAST-like tool PLAST (Nguyen and Lavenier, 2009), with an e-value cutoff of 5e-5. The transcriptome was also compared with the UniProt databases, Swiss-Prot and trEMBL, using translated BLAST (BLASTx) and protein BLAST (BLASTp), respectively, with an e-value cutoff of 5e-5. The annotations were then compiled using the script totalannotation.py from the 'Simple Fool's Guide to Population Genomics via RNAseq' (De Wit et al., 2012).

Quantification

To quantify the RNAseq data, single-end reads for each data set, regeneration and the three embryonic data sets [from Fischer and Smith (2013), Fischer et al. (2014), Helm et al. (2013) and this study], were aligned to the Trinity assembly using Bowtie2 (Langmead et al., 2009). Read counts were quantified using RSEM (Li and Dewey, 2011). To account for the many isoforms per gene reported by Trinity, transcripts were compared with the Nemve1 filtered gene models using BLASTn, and counts for transcripts with the same Nemve1 hit were combined. Transcripts with low-read counts, those that did not have fewer than five counts in at least 25% of the samples, were excluded. Each data set was then normalized separately using the R package edgeR and the counts per million (cpm) mapped reads were calculated (Robinson et al., 2010). Intra-data-set differential expression testing for each Nemve1 gene model was carried out by comparing each time point to t_0 using edgeR [t_0=7 hpf for the Helm et al. (2013), Fischer and Smith (2013) and Fischer et al. (2014) data sets; t_0=24 hpf for the in-house embryonic data set; and t_0=0 hpa for the regeneration data set]. A significantly differentially expressed gene is defined as having an absolute fold change (FC) >2 and a false discovery rate (FDR) <0.05. To correct for batch effects of the embryonic data sets after normalization, the R function ComBat from the SVA packages was used on $\log_2$(cpm+1) transformed data using time point as a categorical covariate (Leek et al., 2012).

RNAseq quality assurance

To validate the accuracy of the in-house generated data sets (regeneration, embryonic) we performed RT-qPCR for several genes that exhibited variation across several time points. First, 500 ng of the same RNA used for library preparation for the regeneration and in-house embryonic data sets was used as input for a reverse transcription reaction using the Iscript Reverse Transcription Supermix Kit from Bio-Rad (1708840). The resultant cDNA was used as input for an RT-qPCR reaction using the FastStart Universal SYBR Green Master Mix from Sigma Aldrich (04913850001), and analyzed using an Applied Biosystems 7900HT 384-well plate qPCR machine, running 40 cycles with an annealing temperature of 60°C. Relative fold change (RFC) was calculated using the equation:

$$RFC = \frac{(E^{\Delta CtTarget})}{(E^{\Delta CtReference})}$$

ΔCt is the difference of the crossing threshold at the reference time point (defined as 24 hpf for the in-house embryonic data and 0 hpa for the regeneration data) and time point of interest, and E is the efficiency of the primer pair (Pfaffl et al., 2002). Actin was used as a reference gene (Forward: 5′-GGACAGGTCATCACCATTGGCAAC-3′; Reverse: 5′-CGGATTCCATACCCAGAAAGGAGG-3′; efficiency, 2.11). All other primer sequences, efficiencies and resultant traces are listed in Figs S2 and S3. Overall, the RT-qPCR expression profiles correlate with those of the RNAseq data sets (Figs S2 and S3).

Fuzzy c-means clustering and gene ontology term enrichment

The expression profiles for each Nemve1 gene model were clustered using the R package mFuzz (Kumar and Futschik, 2007) on the batch-corrected combined embryonic data set and the regeneration data set separately. The cluster number was set to 9 for the regeneration data and 8 for the embryonic data sets as these numbers represented the point at which the centroid distance between clusters did not significantly decrease when new clusters were added (inflection point). For each cluster, gene ontology (GO) term enrichment was calculated using a Fisher's exact test and the R package topGO on the GO terms identified from comparing the transcriptome with the UniProt database (all identified GO terms were used as a background model). The resulting GO term list was reduced and plotted using a modified R script based on REVIGO (Supek et al., 2011).

NvERTx website

The website was constructed using the Django python framework (https://www.djangoproject.com/). Plots are generated using the Plotly javascript library (https://plot.ly/javascript/). The source code for the website can be found at https://github.com/IRCAN/NvER_plotter_django. Data sets from the database can be found at http://ircan.unice.fr/ER/ER_plotter/about.

Acknowledgements

We thank Valerie Carlin for animal care; Christian Baudoin from the IRCAN Genomics Core Facility, and Charles Nicolet from the University of Southern California Sequencing Core Facility, for preparation and sequencing of the RNAseq libraries; and the IRCAN Genomics Core Facility for providing access to the NextSeq500 sequencer.

Competing interests

The authors declare no competing or financial interests.

Author contributions

Conceptualization: J.F.W., E.R.; Methodology: J.F.W., V.G., E.R.; Software: J.F.W., V.G.; Validation: J.F.W., E.R.; Formal analysis: J.F.W., V.G.; Investigation: J.F.W., A.R.A., H.J., K.N.; Resources: E.R.; Data curation: J.F.W., V.G.; Writing - original draft: J.F.W., E.R.; Writing - review & editing: J.F.W., A.R.A., E.R.; Visualization: J.F.W., V.G., E.R.; Supervision: E.R.; Project administration: J.F.W., E.R.; Funding acquisition: E.R.

Funding

This work was supported by ATIP-Avenir (Institut National de la Santé et de la Recherche Médicale and Centre National de la Recherche Scientifique) funded by the Plan Cancer (Institut National Du Cancer) [C13992AS], Seventh Framework Programme [631665], Association pour la Recherche sur le Cancer [PJA 2014120186 to E.R.; PDF20141202150 to J.F.W.], Fondation pour la Recherche Médicale [SPF20130526781 to A.R.A.], Ligue Contre le Cancer [to K.N.] and Ministère de l'Enseignement Supérieur et de la Recherche [to H.J.].

Data availability

In-house data sets generated for this study are available at the NCBI SRA BioProject, under accession numbers PRJNA418421 and PRJNA419631. The dataset originally reported by Helm et al. (2013) is available at the NCBI SRA BioProject, under accession number PRJNA189768. The dataset originally reported by Fischer and Smith (2013) is available in the Woods Hole Open Access Server (http://darchive.mblwhoilibrary.org/handle/1912/5981). The dataset originally reported by Tulin et al. (2013) is available in the Woods Hole Open Access Server (http://darchive.mblwhoilibrary.org/handle/1912/5613).

Supplementary information

Supplementary information available online at
http://dev.biologists.org/lookup/doi/10.1242/dev.162867.supplemental

References

Amiel, A. R., Johnston, H. T., Nedoncelle, K., Warner, J. F., Ferreira, S. and Röttinger, E. (2015). Characterization of morphological and cellular events underlying oral regeneration in the sea anemone, nematostella vectensis. *Int. J. Mol. Sci.* **16**, 28449-28471.

Amiel, A. R., Johnston, H., Chock, T., Dahlin, P., Iglesias, M., Layden, M., Röttinger, E. and Martindale, M. Q. (2017). A bipolar role of the transcription factor ERG for cnidarian germ layer formation and apical domain patterning. *Dev. Biol.* **430**, 346-361.

Binari, L. A., Lewis, G. M. and Kucenas, S. (2013). Perineurial glia require Notch signaling during motor nerve development but not regeneration. *J. Neurosci.* **33**, 4241-4252.

Bolger, A. M., Lohse, M. and Usadel, B. (2014). Trimmomatic: a flexible trimmer for Illumina sequence data. *Bioinformatics* **30**, 2114-2120.

Bossert, P. E., Dunn, M. P. and Thomsen, G. H. (2013). A staging system for the regeneration of a polyp from the aboral physa of the anthozoan Cnidarian Nematostella vectensis. *Dev. Dyn.* **242**, 1320-1331.

Bryant, D. M., Johnson, K., DiTommaso, T., Tickle, T., Couger, M. B., Payzin-Dogru, D., Lee, T. J., Leigh, N. D., Kuo, T.-H., Davis, F. G. et al. (2017). A tissue-mapped axolotl de novo transcriptome enables identification of limb regeneration factors. *Cell Rep.* **18**, 762-776.

Burton, P. M. and Finnerty, J. R. (2009). Conserved and novel gene expression between regeneration and asexual fission in Nematostella vectensis. *Dev. Genes Evol.* **219**, 79-87.

Carlson, M. R., Komine, Y., Bryant, S. V. and Gardiner, D. M. (2001). Expression of Hoxb13 and Hoxc10 in developing and regenerating Axolotl limbs and tails. *Dev. Biol.* **229**, 396-406.

Conesa, A., Madrigal, P., Tarazona, S., Gomez-Cabrero, D., Cervera, A., McPherson, A., Szcześniak, M. W., Gaffney, D. J., Elo, L. L., Zhang, X. et al. (2016). A survey of best practices for RNA-seq data analysis. *Genome Biol.* **17**, 13.

Darling, J. A., Reitzel, A. R., Burton, P. M., Mazza, M. E., Ryan, J. F., Sullivan, J. C. and Finnerty, J. R. (2005). Rising starlet: the starlet sea anemone, Nematostella vectensis. *BioEssays* **27**, 211-221.

De Wit, P., Pespeni, M. H., Ladner, J. T., Barshis, D. J., Seneca, F., Jaris, H., Therkildsen, N. O., Morikawa, M. and Palumbi, S. R. (2012). The simple fool's guide to population genomics via RNA-Seq: an introduction to high-throughput sequencing data analysis. *Mol. Ecol. Resour.* **12**, 1058-1067.

DuBuc, T. Q., Dubuc, T. Q., Traylor-Knowles, N., Traylor-Knowles, N. and Martindale, M. Q. (2014). Initiating a regenerative response; cellular and molecular features of wound healing in the cnidarian Nematostella vectensis. *BMC Biol.* **12**, 1.

Edgar, R. C. (2004). MUSCLE: multiple sequence alignment with high accuracy and high throughput. *Nucleic Acids Res.* **32**, 1792-1797.

Finnerty, J. R., Pang, K., Burton, P., Paulson, D. and Martindale, M. Q. (2004). Origins of bilateral symmetry: hox and dpp expression in a sea anemone. *Science* **304**, 1335-1337.

Fischer, A. H. L. and Smith, J. (2013). Nematostella High-density RNAseq time-course. *Woods Hole Open Access Server*. http://dx.doi.org/10.1575/1912/5981.

Fischer, A. H. L., Mozzherin, D., Eren, A. M., Lans, K. D., Wilson, N., Cosentino, C. and Smith, J. (2014). SeaBase: a multispecies transcriptomic resource and platform for gene network inference. *Integr. Comp. Biol.* **54**, 250-263.

Gardiner, D. M., Blumberg, B., Komine, Y. and Bryant, S. V. (1995). Regulation of HoxA expression in developing and regenerating axolotl limbs. *Development* **121**, 1731-1741.

Genikhovich, G., Fried, P., Prünster, M. M., Schinko, J. B., Gilles, A. F., Fredman, D., Meier, K., Iber, D. and Technau, U. (2015). Axis patterning by BMPs: cnidarian network reveals evolutionary constraints. *Cell Rep.* **10**, 1646-1654.

Haas, B. J., Papanicolaou, A., Yassour, M., Grabherr, M., Blood, P. D., Bowden, J., Couger, M. B., Eccles, D., Li, B., Lieber, M. et al. (2013). De novo transcript sequence reconstruction from RNA-seq using the Trinity platform for reference generation and analysis. *Nat. Protoc.* **8**, 1494-1512.

Habermann, B., Bebin, A.-G., Herklotz, S., Volkmer, M., Eckelt, K., Pehlke, K., Epperlein, H. H., Schackert, H. K., Wiebe, G. and Tanaka, E. M. (2004). An Ambystoma mexicanum EST sequencing project: analysis of 17,352 expressed sequence tags from embryonic and regenerating blastema cDNA libraries. *Genome Biol.* **5**, R67.

Helm, R., Siebert, S., Tulin, S., Smith, J. and Dunn, C. (2013). Characterization of differential transcript abundance through time during Nematostella vectensis development. *BMC Genomics* **14**, 266.

Imokawa, Y. and Yoshizato, K. (1997). Expression of Sonic hedgehog gene in regenerating newt limb blastemas recapitulates that in developing limb buds. *Proc. Natl. Acad. Sci. USA* **94**, 9159-9164.

Kaloulis, K., Chera, S., Hassel, M., Gauchat, D. and Galliot, B. (2004). Reactivation of developmental programs: the cAMP-response element-binding protein pathway is involved in hydra head regeneration. *Proc. Natl. Acad. Sci. USA* **101**, 2363-2368.

Katz, M. G., Fargnoli, A. S., Kendle, A. P., Hajjar, R. J. and Bridges, C. R. (2015). The role of microRNAs in cardiac development and regenerative capacity. *Am. J. Physiol. Heart Circ. Physiol.* **310**, H528-H541.

Kent, W. J. (2002). BLAT–the BLAST-like alignment tool. *Genome Res.* **12**, 656-664.

Knapp, D., Schulz, H., Rascon, C. A., Volkmer, M., Scholz, J., Nacu, E., Le, M., Novozhilov, S., Tazaki, A., Protze, S. et al. (2013). Comparative transcriptional profiling of the axolotl limb identifies a tripartite regeneration-specific gene program. *PLoS ONE* **8**, e61352.

Kumar, L. and Futschik, M. E. (2007). Mfuzz: a software package for soft clustering of microarray data. *Bioinformation* **2**, 5-7.

Kusserow, A., Pang, K., Sturm, C., Hrouda, M., Lentfer, J., Schmidt, H. A., Technau, U., von Haeseler, A., Hobmayer, B., Martindale, M. Q. et al. (2005). Unexpected complexity of the Wnt gene family in a sea anemone. *Nature* **433**, 156-160.

Langmead, B., Trapnell, C., Pop, M. and Salzberg, S. L. (2009). Ultrafast and memory-efficient alignment of short DNA sequences to the human genome. *Genome Biol.* **10**, R25.

Layden, M. J. and Martindale, M. Q. (2014). Non-canonical Notch signaling represents an ancestral mechanism to regulate neural differentiation. *EvoDevo* **5**, 30.

Layden, M. J., Boekhout, M. and Martindale, M. Q. (2012). Nematostella vectensis achaete-scute homolog NvashA regulates embryonic ectodermal neurogenesis and represents an ancient component of the metazoan neural specification pathway. *Development* **139**, 1013-1022.

Layden, M. J., Röttinger, E., Wolenski, F. S., Gilmore, T. D. and Martindale, M. Q. (2013). Microinjection of mRNA or morpholinos for reverse genetic analysis in the starlet sea anemone, Nematostella vectensis. *Nat. Protoc.* **8**, 924-934.

Layden, M. J., Rentzsch, F. and Röttinger, E. (2016). The rise of the starlet sea anemone Nematostella vectensis as a model system to investigate development and regeneration. *Wiley Interdiscip Rev. Dev. Biol.* **5**, 408-428.

Leclère, L., Bause, M., Sinigaglia, C., Steger, J. and Rentzsch, F. (2016). Development of the aboral domain in Nematostella requires β-catenin and the opposing activities of Six3/6 and Frizzled5/8. *Development* **143**, 1766-1777.

Leek, J. T., Johnson, W. E., Parker, H. S., Jaffe, A. E. and Storey, J. D. (2012). The sva package for removing batch effects and other unwanted variation in high-throughput experiments. *Bioinformatics* **28**, 882-883.

Li, B. and Dewey, C. N. (2011). RSEM: accurate transcript quantification from RNA-Seq data with or without a reference genome. *BMC Bioinformatics* **12**, 323.

Looso, M., Preussner, J., Sousounis, K., Bruckskotten, M., Michel, C. S., Lignelli, E., Reinhardt, R., Höffner, S., Krüger, M., Tsonis, P. A. et al. (2013). A de novo assembly of the newt transcriptome combined with proteomic validation identifies new protein families expressed during tissue regeneration. *Genome Biol.* **14**, R16.

Martin, M. (2011). Cutadapt removes adapter sequences from high-throughput sequencing reads. *EMBnet. J.* **17**, 10-12.

Mathew, L. K., Sengupta, S., Franzosa, J. A., Perry, J., La Du, J., Andreasen, E. A. and Tanguay, R. L. (2009). Comparative expression profiling reveals an essential role for raldh2 in epimorphic regeneration. *J. Biol. Chem.* **284**, 33642-33653.

Matus, D. Q., Pang, K., Marlow, H., Dunn, C. W., Thomsen, G. H. and Martindale, M. Q. (2006). Molecular evidence for deep evolutionary roots of bilaterality in animal development. *Proc. Natl. Acad. Sci. USA* **103**, 11195-11200.

Matus, D. Q., Magie, C. R., Pang, K., Martindale, M. Q. and Thomsen, G. H. (2008). The Hedgehog gene family of the cnidarian, Nematostella vectensis, and implications for understanding metazoan Hedgehog pathway evolution. *Dev. Biol.* **313**, 501-518.

Meyer, E. J., Ikmi, A. and Gibson, M. C. (2011). Interkinetic nuclear migration is a broadly conserved feature of cell division in pseudostratified epithelia. *Curr. Biol.* **21**, 485-491.

Millimaki, B. B., Sweet, E. M. and Riley, B. B. (2010). Sox2 is required for maintenance and regeneration, but not initial development, of hair cells in the zebrafish inner ear. *Dev. Biol.* **338**, 262-269.

Min, X. J., Butler, G., Storms, R. and Tsang, A. (2005). OrfPredictor: predicting protein-coding regions in EST-derived sequences. *Nucleic Acids Res.* **33**, W677-W680.

Nguyen, V. H. and Lavenier, D. (2009). PLAST: parallel local alignment search tool for database comparison. *BMC Bioinformatics* **10**, 329.

Niehrs, C. and Pollet, N. (1999). Synexpression groups in eukaryotes. *Nature* **402**, 483-487.

Ormestad, M., Martindale, M. Q. and Röttinger, E. (2011). A comparative gene expression database for invertebrates. *EvoDevo* **2**, 17.

Özpolat, B. D., Zapata, M., Daniel Frugé, J., Coote, J., Lee, J., Muneoka, K. and Anderson, R. (2012). Regeneration of the elbow joint in the developing chick embryo recapitulates development. *Dev. Biol.* **372**, 229-238.

Passamaneck, Y. J. and Martindale, M. Q. (2012). Cell proliferation is necessary for the regeneration of oral structures in the anthozoan cnidarian Nematostella vectensis. *BMC Dev. Biol.* **12**, 34.

Pfaffl, M. W., Horgan, G. W. and Dempfle, L. (2002). Relative expression software tool (REST) for group-wise comparison and statistical analysis of relative expression results in real-time PCR. *Nucleic Acids Res.* **30**, e36.

Price, M. N. and Arkin, A. P. (2017). PaperBLAST: text mining papers for information about homologs. *mSystems* **2**, e00039-e00017.

Putnam, N. H., Srivastava, M., Hellsten, U., Dirks, B., Chapman, J., Salamov, A., Terry, A., Shapiro, H., Lindquist, E., Kapitonov, V. V. et al. (2007). Sea anemone genome reveals ancestral eumetazoan gene repertoire and genomic organization. *Science* **317**, 86-94.

Development (2018) 145, dev162867. doi:10.1242/dev.162867

Reitzel, A. M., Burton, P. M., Krone, C. and Finnerty, J. R. (2007). Comparison of developmental trajectories in the starlet sea anemone Nematostella vectensis: embryogenesis, regeneration, and two forms of asexual fission. *Invertebr. Biol.* **126**, 99-112.

Rentzsch, F., Anton, R., Saina, M., Hammerschmidt, M., Holstein, T. W. and Technau, U. (2006). Asymmetric expression of the BMP antagonists chordin and gremlin in the sea anemone Nematostella vectensis: implications for the evolution of axial patterning. *Dev. Biol.* **296**, 375-387.

Robinson, M. D., McCarthy, D. J. and Smyth, G. K. (2010). edgeR: a Bioconductor package for differential expression analysis of digital gene expression data. *Bioinformatics* **26**, 139-140.

Röttinger, E., Dahlin, P. and Martindale, M. Q. (2012). A framework for the establishment of a cnidarian gene regulatory network for "endomesoderm" specification: the inputs of ß-catenin/TCF signaling. *PLoS Genet.* **8**, e1003164.

Schaffer, A. A., Bazarsky, M., Levy, K., Chalifa-Caspi, V. and Gat, U. (2016). A transcriptional time-course analysis of oral vs. aboral whole-body regeneration in the Sea anemone Nematostella vectensis. *BMC Genomics* **17**, 718.

Supek, F., Bošnjak, M., Škunca, N. and Šmuc, T. (2011). REVIGO summarizes and visualizes long lists of gene ontology terms. *PLoS ONE* **6**, e21800.

Technau, U. and Schwaiger, M. (2015). Recent advances in genomics and transcriptomics of cnidarians. *Mar Genomics* **24**, 131-138.

Torok, M. A., Gardiner, D. M., Shubin, N. H. and Bryant, S. V. (1998). Expression of HoxD genes in developing and regenerating axolotl limbs. *Dev. Biol.* **200**, 225-233.

Trevino, M., Stefanik, D. J., Rodriguez, R., Harmon, S. and Burton, P. M. (2011). Induction of canonical Wnt signaling by alsterpaullone is sufficient for oral tissue fate during regeneration and embryogenesis in Nematostella vectensis. *Dev. Dyn.* **240**, 2673-2679.

Tulin, S., Aguiar, D., Istrail, S. and Smith, J. (2013). A quantitative reference transcriptome for Nematostella vectensis early embryonic development: a pipeline for de novo assembly in emerging model systems. *EvoDevo* **4**, 16.

Wang, Y.-H. and Beck, C. W. (2014). Distal expression of sprouty (spry) genes during Xenopus laevis limb development and regeneration. *Gene Expr. Patterns* **15**, 61-66.

Wikramanayake, A. H., Hong, M., Lee, P. N., Pang, K., Byrum, C. A., Bince, J. M., Xu, R. and Martindale, M. Q. (2003). An ancient role for nuclear beta-catenin in the evolution of axial polarity and germ layer segregation. *Nature* **426**, 446-450.

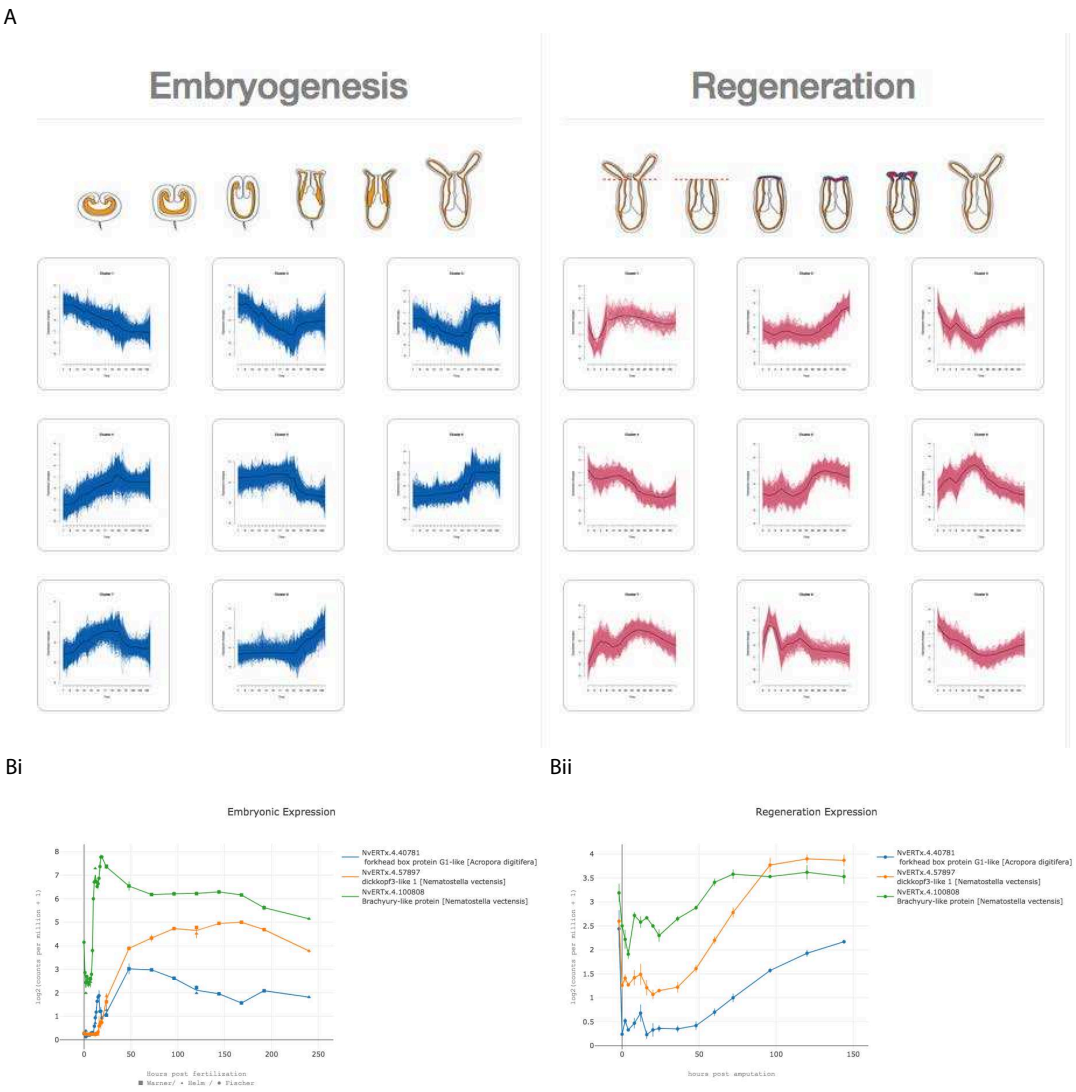

Figure S1: The NvERTx Co-Expression Clusters Page. A) Screen shot of the Co-expression Clusters page. Users can directly explore co-expression clusters to identify groups of genes that share expression patterns during embryogenesis (blue) or regeneration (red). B) Example output plots from NvERTx comparing multiple gene expression patterns. Three genes from regeneration cluster 2, *Nvbra* (NvERTx.4.100808, yellow), *Nvdickkopf3* (NvERTx.4.57897, red), and a FoxG1-like protein (NvERTx.4.40781, blue) are co-expressed during regeneration (i) but not embryogenesis (ii).

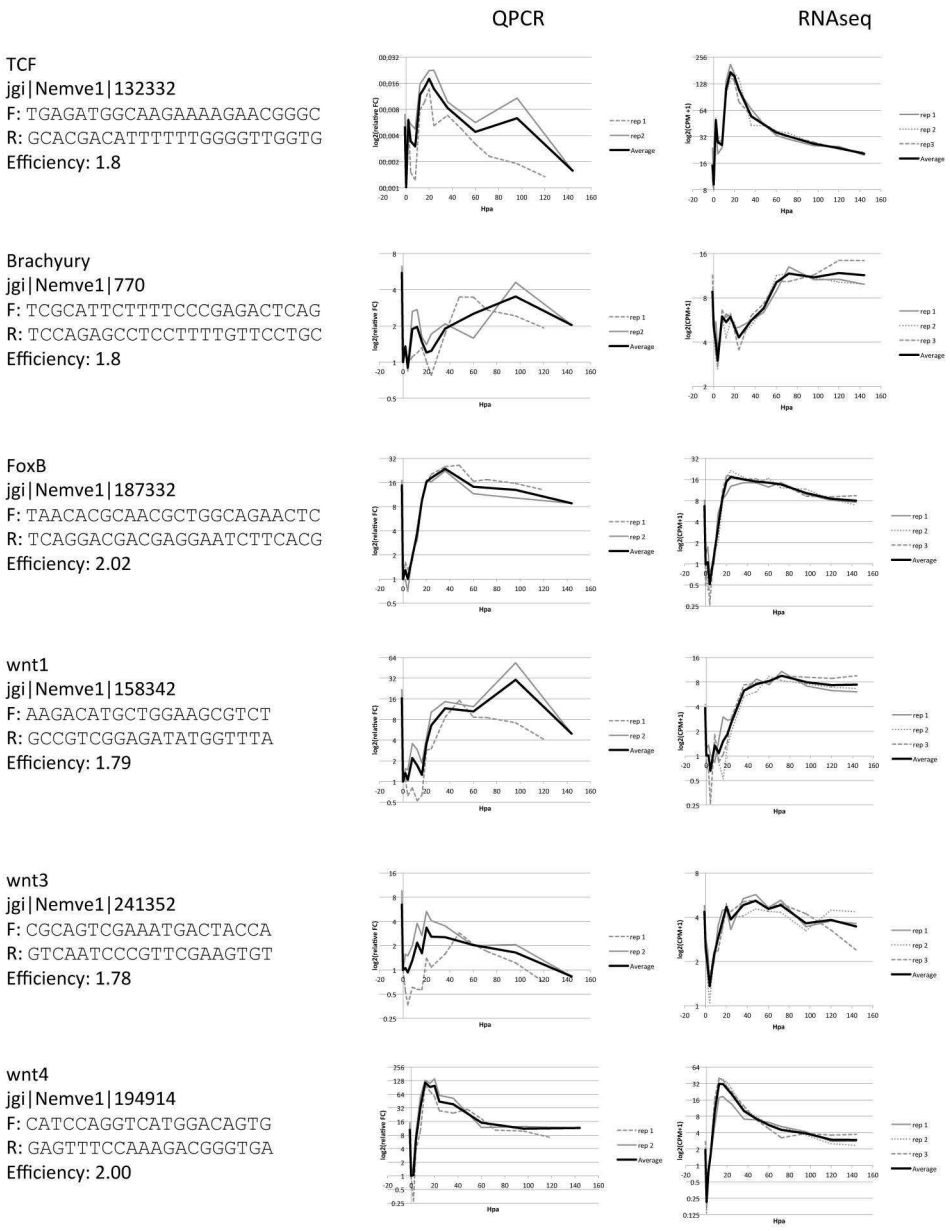

Figure S2: RT-QPCR of selected genes compared to regeneration RNAseq data. RT-QPCR traces (replicates grey, average black) are shown in terms of log2(relative fold change) versus hours post regeneration (Hpa). RNAseq traces (replicates grey, average black) are shown in terms of log2(counts per million +1) versus Hpa.

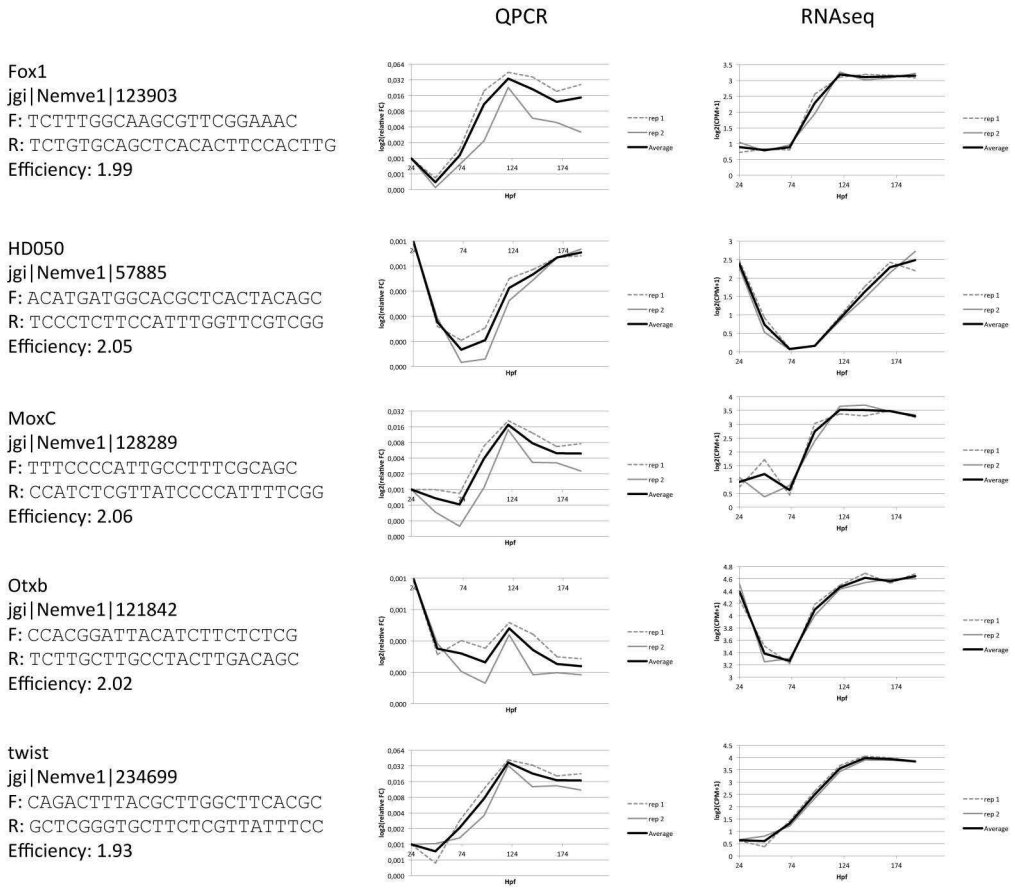

Figure S3: RT-QPCR of selected genes compared to embryogenesis RNAseq data (Warner dataset). RT-QPCR traces (replicates grey, average black) are shown in terms of log2(relative fold change) versus hours post fertilization (Hpf). RNAseq traces (replicates grey, average black) are shown in terms of log2(counts per million +1) versus Hpf.

Table S1: Assembly statistics from Trinity assembly.

N50	1678
Median contig length	384
Average contig length	837.30
Total assembled bases	196247212

Table S2: NvERTx.4 annotation statistics. 234,381 transcripts map to 19,565 unique Nemve1 genes.

Total assembled transcripts	234381
Transcripts with ORF	231294
Transcripts without ORF	3087
Transcripts with hit to nr	85475
Transcripts with hit to uniprot	69335
Transcripts with hit to Nemve1	102581
Unique Nemve1 'genes'	19565
Transcripts without annotation	110531

Article 5: Regeneration is a partial redeployment of the embryonic gene network

Jacob F. Warner, Aldine R. Amiel, Hereroa Johnston and Eric Röttinger

In submission

Regeneration is a partial redeployment of the embryonic gene network

Jacob F. Warner, Aldine R. Amiel, Hereroa Johnston, and Eric Röttinger*

Université Côte d'Azur, CNRS, INSERM, Institute for Research on Cancer and Aging, Nice (IRCAN), Nice, France

*Please direct correspondence to:

Eric Röttinger

T: +33 (0)6 63 97 01 78

E: eric.rottinger@unice.fr

Abstract

For more than a century, researchers have been trying to understand the relationship between embryogenesis and regeneration (Morgan, 1901). A long-standing hypothesis is that biological processes originally used during embryogenesis are re-deployed during regeneration. In the past decade, we have begun to understand the relationships of genes and their organization into regulatory networks responsible for driving embryogenesis (Davidson et al., 2002; Röttinger et al., 2012) and regeneration (Lobo and Levin, 2015; Rodius et al., 2016; Srivastava et al., 2014) in diverse taxa. Here, we compare these networks in the same species, the sea anemone *Nematostella vectensis*, a uniquely suited embryonic and whole-body regeneration model to investigate how regeneration re-uses genetic interactions originally set aside for embryonic development (Layden et al, 2017). We show that at the transcriptomic level the regenerative program partially re-uses elements of the embryonic gene network that are interconnected with many genes which are only activated during regeneration. We further identified co-expression modules that are either i) highly conserved between these two developmental trajectories and involved in core biological processes or ii) regeneration specific modules that drive cellular events unique to regeneration. Finally, our functional validation reveals that apoptosis is a regeneration-specific process in *Nematostella* and is required for the initial steps of the regeneration program. These results indicate that regeneration reactivates gene modules to accomplish basic cellular functions but deploys novel network logic to activate the regenerative process. Our unique comparative transcriptomics approach thus highlights regeneration specific gene module arrangements necessary for activation of the regenerative program and demonstrates how certain organisms are capable of re-deploying novel arrangements of gene modules to regenerate.

Regeneration of cells, tissues, organs, appendages or even entire body parts is a widespread, however, still rather poorly understood phenomenon in the animal kingdom. A long-standing question in the field of regeneration is whether and to what extent embryonic gene programs that are initially used to build and organism are re-used during regeneration (Morgan, 1901). Several transcriptomic studies of regeneration have highlighted the importance of re-deployed developmental pathways (Bryant et al., 2017) (Habermann et al., 2004) (Hutchins et al., 2014) (Mathew et al., 2009) (Rodius et al., 2016) (Schaffer et al., 2016). Other studies have directly compared embryonic and regenerative gene expression of single or groups of genes. Among these studies, some have identified genes that are specific to embryonic development (Binari et al., 2013), while other studies identified genes which are specifically expressed during regeneration (Gardiner et al., 1995; Millimaki et al., 2010). Again others have found embryonic genes that are re-used during regeneration to some extent (Imokawa and Yoshizato, 1997) (Carlson et al., 2001) (Torok et al., 1998) (Özpolat et al., 2012) (Wang and Beck, 2014). It is clear that this question warrants further study comparing the global transcriptomic landscape of embryogenesis and regeneration. The sea anemone *Nematostella vectensis* (Cnidaria, Anthozoa) is a uniquely suited embryonic and novel whole body regeneration model and is ideal for this line of inquiry (Fig. 1A, Layden et al. 2017, Burton et al, 2009). *Nematostella* has long been used as a model system for embryonic development, the evolution of body patterning, and gene regulatory networks (Hand and Uhlinger, 1992; Wikramanayake et al., 2003, Röttinger et al, 2012). More recently, *Nematostella* has emerged as a powerful whole-body regeneration model as it capable of re-growing missing body parts in less than a week (Amiel et al., 2015; Bossert et al., 2013; Burton and Finnerty, 2009; Dubuc et al., 2014; Passamaneck and Martindale, 2012; Schaffer et al., 2016; Trevino et al., 2011) Regeneration in *Nematostella* follows a dynamic but highly stereotypical morphological and cellular program involving tissue re-arrangement and the *de novo* formation of body structures (Amiel et al., 2015). Initiation of this process requires a crosstalk between tissues and two

populations of fast and slow cycling stem cells (Amiel et al, in revision). Many developmental signaling pathways are deployed during regeneration (Trevino et al., 2011) (Dubuc et al., 2014) (Schaffer et al., 2016) however their function and regulatory logic remains unknown. Here, we take advantage of this model to definitively address the historical hypothesis that regeneration re-uses embryonic gene network logic and decipher genetic signatures unique to regeneration. We performed a genome wide embryogenesis *vs* regeneration transcriptomic comparison using deeply sampled transcriptomic datasets in order to identify gene modules specific to regeneration.

Regeneration is a partial re-deployment of embryonic development

To compare embryogenesis and regeneration on a global genome-wide scale we employed four RNAseq datasets, one spanning 16 time points of regeneration (Warner et al., 2018) and three spanning a total of 34 embryonic time points (Fischer and Smith, 2014; Helm et al., 2013; Warner et al., 2018). In order to directly compare the data, raw sequencing reads were processed, mapped and quantified using the same workflow for all datasets (see materials and methods for quantification details). As the embryonic data were the result of several previous studies including this one, we applied a batch correction using developmental time-point as a categorical covariate (Fig. S2) (Leek et al., 2012). To assess the transcriptomic states underlying embryogenesis we performed principal component analysis (PCA) on batch corrected embryonic data (Fig. 1B). We found that the majority of gene expression changes occur during the first day of embryonic development from cleavage to blastula stage (Fig. 1B, 7 hours post fertilization (hpf) – 24hpf, PC1 proportion of variance 61%; PC2 proportion of variance 19%) indicating large transcriptomic differences in early embryogenesis. From 96hpf onwards the samples exhibited modest changes in transcriptional variation indicating that the major events of embryogenesis are completed by this stage (96hpf-240hpf). When we examined the regenerative program using PCA (Fig. 1C), we observe three distinct transcriptional programs: a wound-healing phase (0-8hpa) is followed by the activation of the early regenerative program (8-

20 hours post amputation (hpa)) in which the samples are distributed along the second principal component (PC2 proportion of variance = 24%, Fig. 1C). From 20hpa onwards, the majority of variation in gene expression is explained by the first principal component during the late regenerative phase (PC2 proportion of variance = 48%, 20hpa-144hpa, Fig.1C). Towards the end of regeneration, we observe the transcriptomics profile approaching the uncut samples indicating a return to steady state. These profiles correlate with the major events of sub-pharyngeally induced oral regeneration in *Nematostella* and indicate that our sampling strategy effectively covers the major transcriptional hallmarks of regeneration (Amiel et al., 2015).

We then directly compared the transcriptomic variation of regeneration and embryogenesis using the same PCA approach and found that the transcriptional changes during regeneration were relatively modest to those observed during embryogenesis with the vast majority of variation in the first two principal components being driven by the embryonic data (PC1 proportion of variance = 67%, PC2 proportion of variance = 16%, Fig 1D). This indicates that the transcriptional dynamics of embryogenesis is more profound than those of regeneration. This finding was buttressed by comparing the number of 'dynamically expressed genes', those which are significantly differentially expressed (fold change > $\log_2(2)$ and false discovery rate < 0.05) at any time point compared to t_0, 0hpa for regeneration and 7hpf (onset of zygotic transcription) for embryogenesis. Embryogenesis exhibited more than ten times the number of dynamically expressed genes compared to regeneration (15610 and 1255 genes respectively, Fig. 1E). These results show that regeneration employs far fewer genes to accomplish the same task of constructing a functional animal.

Identification of "regeneration-specific" genes

Among those genes dynamically expressed during regeneration, a small fraction, 124 genes, exhibit differential expression (fold change > $\log_2(2)$ and false

discovery rate < 0.05) only during regeneration which we term ‘regeneration specific’ (supplemental table 1). Indeed 48 of these genes are only detectable during regeneration indicating they are transcriptionally silent until regeneration activation (Fig. 1F). Interestingly, several of the 124 regeneration specific genes, for example Wntless (jgi|Nemve1|100430) and Agrin (jgi|Nemve1|196727), have previously been reported to be important regulators of regeneration in bilaterians (Adell et al., 2009; Bassat et al., 2017). Furthermore among these 124 regeneration specific genes, 45 have no known homology in the Uniprot database (plastp, e-value cutoff <0.05, see methods for annotation details). These results indicate not only a possible evolutionary conservation of gene use in regeneration, but also identify additional genes that may play important roles in regeneration. When we performed a gene ontology (GO) term enrichment analysis on these regeneration specific genes, we found a suite of biological process GO terms relating to Wnt protein secretion (e.g. Wntless), metabolic processes and apoptotic cell death, indicating an essential role for these processes in regeneration (Fig. 1G).

Embryonic gene modules are partially re-deployed during regeneration

As regeneration uses less than one tenth the number of genes compared to embryogenesis we were next interested in how these genes were deployed and arranged into expression networks to determine if embryonic network modules themselves are reused in a reduced capacity or if regeneration deploys novel module arrangements. To investigate this we first used fuzzy c-means clustering to group the genes by expression profile (Kumar and E Futschik, 2007). We regrouped the gene expression profiles into eight embryonic clusters (Fig. 2A) and nine regeneration clusters (Fig. 2D). From this we identified gene modules that were activated early in both processes (cluster 4-embryogenesis, cluster 6-regeneration, Fig. 2A,D) and that contained many canonical developmental genes: wntA (jgi|Nemve1|91822|e_gw.28.3.1), lhx1 (jgi|Nemve1|95727|e_gw.40.28.1) and foxA (jgi|Nemve1|165261|estExt_gwp.C_580130) in embryonic cluster 4 (Fig. 2B) and

tcf (jgi|Nemve1|132332|e_gw.308.28.1), spr (jgi|Nemve1|29671|gw.51.137.1), and runX (jgi|Nemve1|129231|e_gw.262.50.1) in regeneration cluster 6 (Fig. 2B). The early activation of these genes was confirmed by *in situ* hybridization at 24hpf (embryogenesis, Fig. 2C) and 20hpa (regeneration) and (Fig. 2F). From this analysis we conclude that classical developmental genes are involved in the early phases of both embryogenesis and regeneration. It remained unclear, however, if these developmental genes were arranged in the same co-expression modules.

We next analyzed whether the same groups of genes were co-regulated during embryogenesis and regeneration, by testing if gene expression observed during both processes were arranged in similar co-expression modules. We compared on a gene-cluster membership basis between regeneration and embryonic clusters to identify significant overlaps. Regeneration modules with high overlap of a specific embryonic module indicate a shared or re-used network logic since the same suite of genes are deployed as a bloc in both processes. Regeneration modules with low overlap to any single embryonic modules on the other hand are likely to be *de novo* genetic arrangements specific to regeneration. We found that the majority of the regeneration modules exhibited significant overlap with one or more embryonic modules (Fig. 3A, B). These 'conserved' modules also exhibited high preservation permutation co-clustering zStatistics (>2, conserved, >10 highly conserved; permutations = 1000) (Langfelder et al., 2011). Importantly, we also identified two modules, R-1 and R-6, which exhibited relatively low significant overlap with embryonic modules, indicating that these are 'regeneration specific' module arrangements. To further investigate these regeneration specific modules, in addition to the conserved and re-used embryonic modules, we calculated GO-term enrichment for each. We found that in general, highly conserved modules were enriched in GO-terms corresponding to homeostatic cell processes while lowly, conserved regeneration specific modules were enriched in GO-terms describing developmental signaling pathways (Fig. SX). This suggests that modules containing genes responsible for

basic cellular functions are largely re-used and co-expressed between embryogenesis and regeneration, while those including genes that are important for the activation of developmental processes are regeneration specific arrangements. Two clusters that exemplify these findings are R-5 and R-6. R-5, a conserved cluster (zStatistic 6.94) showed strong enrichment of cell-proliferation related GO-terms (Fig. 3C). When we examined exemplar genes (with intra module membership scores >0.95) *ercc6-like* (jgi|Nemve1|110916|e_gw.103.120.1), *rad54B* (jgi|Nemve1|209299|fgenesh1_pg.scaffold_103000074), *mcm10* (jgi|Nemve1|131857|e_gw.301.8.1), *cyclin-B3* (jgi|Nemve1|208415|fgenesh1_pg.scaffold_92000031), we observed co-expression patterns that correlate well to the timing of proliferation activation during *Nematostella* regeneration with an activation at 24hpa, a peak at 48hpa, and a taper off thereafter (Amiel et al., 2015; Passamaneck and Martindale, 2012)(Fig. 3C). These exemplar genes are also co-expressed during embryogenesis (cluster E-1), further demonstrating module conservation. In contrast to this conserved module is the regeneration specific module R-6. This module showed strong enrichment of GO-terms relating to apoptosis and developmental signaling pathways. When we examined 4 exemplar genes tcf (jgi|Nemve1|132332|e_gw.308.28.1), bax (jgi|Nemve1|100129|e_gw.55.77.1), runX (jgi|Nemve1|129231|e_gw.262.50.1), bcl2 (jgi|Nemve1|215615|fgenesh1_pg.scaffold_232000029), we observed co-expression during regeneration but divergent profiles during embryogenesis indicating that this grouping of genes is indeed 'regeneration specific' (Fig 3D).

Apoptosis is specifically required for *Nematostella* regeneration

Having observed a strong enrichment for apoptosis related GO-terms in the list of 124 regeneration-specific genes (Fig. 1F,G) and in the regeneration specific module R-6 (Fig. 3Di-Diii), we investigated the role of apoptosis during the regenerative process. Several genes relating to apoptosis, including bax (jgi|Nemve1|100129|e_gw.55.77.1), caspase-3

(jgi|Nemve1|100451|e_gw.57.87.1), bcl2 (jgi|Nemve1|215615|fgenesh1_pg.scaffold_232000029), and an additional bcl2 (which we term bcl2-B, jgi|Nemve1|128814|e_gw.255.21.1), belong to module R-6, with bax additionally being a 'regeneration specific gene, and are activated shortly after amputation (Fig .4A). We performed a time series of TUNEL staining to examine the dynamics of apoptosis during embryogenesis and regeneration and only observed a burst of apoptotic activity after amputation at the cut site as early as 1.5 hpa which perdured through 60hpa (Fig. 4B, Fig. SX). To test whether or not apoptosis was indeed a regeneration specific process we used the apoptosis inhibitor ZVAD to block apoptosis during embryogenesis and regeneration. *Nematostella* treated with ZVAD from 0hpf developed normally, showed no developmental defect (Fig. 4C) and metamorphosed timely (not shown). In contrast, regenerating *Nematostella* treated with ZVAD from 0hpa were blocked in a very early regenerative stage preventing the physical interaction between the fused oral tip of the mesenteries and the epithelia of the wound site (Fig. 4C). Furthermore, regenerating animals treated with ZVAD exhibited little to no cell proliferation indicating that a constructive function of apoptosis is necessary for the induction of cell proliferation and the ensuing regenerative program (Fig. 4C). While the importance of apoptosis in regeneration has been previously proposed in *Hydra* (Chera et al., 2009), we conclude from our work that apoptosis is a regeneration-specific process in *Nematostella*.

In this work we used whole genome transcriptomic profiling and identified regeneration specific gene signatures. By comparing the embryonic and regenerative gene expression modules, we identified a gene module deployed early in regeneration that involves apoptosis, a developmental process we then show to be specific to regeneration. Furthermore, we show that embryonic gene modules, including those coding for cell proliferation and homeostatic processes, are to a significant extent re-activated during the regenerative process. Thus regeneration is a partial re-use of the embryonic genetic programs but with

important differences in its activation, which in the case of *Nematostella*, depends on apoptotic signals. The approach used to identify these genetic programs, comparative transcriptional profiling, highlights the utility in considering not just individual gene use but how those genes are arranged into co-expression modules. Here we investigated one module and the role apoptosis plays in regeneration but we anticipate further studies on gene module use during embryogenesis and regeneration as the community continues to investigate expression dynamics during these two processes thanks in part to a database (nvertx.kahikai.org) containing all of the data from this study (Warner et al., 2018). Further studies, especially those comparing regeneration activation across species, will provide novel insight into our understanding of why certain organisms can regenerate while others can't and could unlock hidden regenerative potential in poorly regenerating organisms.

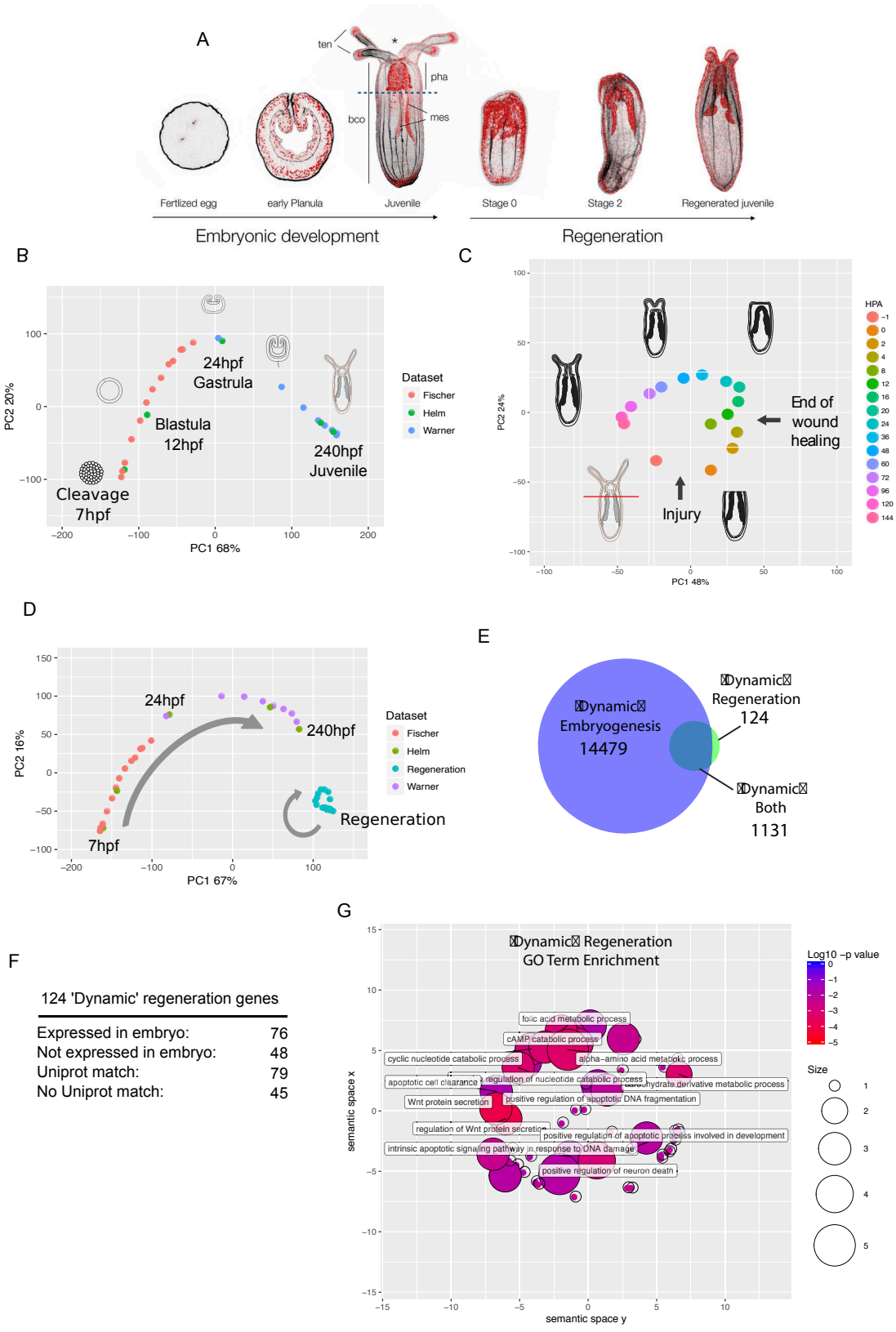
A
ten
*
pha
bco
mes
Fertlized egg
early Planula
Juvenile
Stage 0
Stage 2
Regenerated juvenile
Embryonic development
Regeneration
B
24hpf
Gastrula
Blastula
12hpf
240hpf
Juvenile
Cleavage
7hpf
PC1 68%
PC2 20%
Dataset
Fischer
Helm
Warner
C
End of
wound
healing
Injury
PC1 48%
PC2 24%
HPA
D
24hpf
240hpf
7hpf
Regeneration
PC1 67%
PC2 16%
Dataset
Fischer
Helm
Regeneration
Warner
E
'Dynamic'
Embryogenesis
14479
'Dynamic'
Regeneration
124
'Dynamic'
Both
1131
F
124 'Dynamic' regeneration genes
Expressed in embryo: 76
Not expressed in embryo: 48
Uniprot match: 79
No Uniprot match: 45
G
'Dynamic' Regeneration
GO Term Enrichment
folic acid metabolic process
cAMP catabolic process
cyclic nucleotide catabolic process
alpha-amino acid metabolic process
apoptotic cell clearance
regulation of nucleotide catabolic process
positive regulation of apoptotic DNA fragmentation
Wnt protein secretion
regulation of Wnt protein secretion
positive regulation of apoptotic process involved in development
intrinsic apoptotic signaling pathway in response to DNA damage
positive regulation of neuron death
semantic space x
semantic space y
Log10 −p value
Size

286

Figure 1: Comparison of embryonic and regenerative transcritpomes. (**A**) General morphology of *Nematostella during* embryonic development and regeneration (black: actin/phalloidin, red: nuclei/DAPI). **(B)** Principal component analysis (PCA) of three embryonic datasets: Fischer et al. (red), sampled at 7, 8, 9, 10, 11, 12, 13, 14, 15, 16, 17, 18, 19 hpf; Helm et al. (green), sampled at 7, 12, 24, 120, 240 hpf and Warner et al. (blue) sampled at 24, 48, 72, 96, 120, 144. 168, 192 hpf. The majority of variation is observed in the first 24 hours of development. (**C**) PCA of regeneration dataset sampled at Uncut, 0, 2, 4, 8, 12, 16, 20, 24, 36, 48, 60, 72, 96, 120, 144 hpa. Regeneration proceeds through a wound healing phase (0-8 hpa) followed by the early regenerative program (12-36 hpa) and ending with a late regenerative program which approaches the uncut condition (48-144 hpa). (**D**) PCA of embryonic versus regeneration samples. Embryogenesis (red, green, purple) exhibits far greater transcriptomic variation than regeneration (blue). (**E**) Comparison of differentially expressed ($|FC| > \log_2(2)$ & FDR < 0.05 for any timepoint comparison against t_0 where t_0 = 7hpf for embryogenesis and 0hpa for regeneration) 'dynamic' genes during embryogenesis (blue) and regeneration (green). Embryogenesis deploys more than 10 times the number of genes. 124 genes are only dynamically expressed during regeneration. (**F**) Details of the regeneration specific genes expression and classification. (**G**) GO term enrichment for regeneration specific genes.

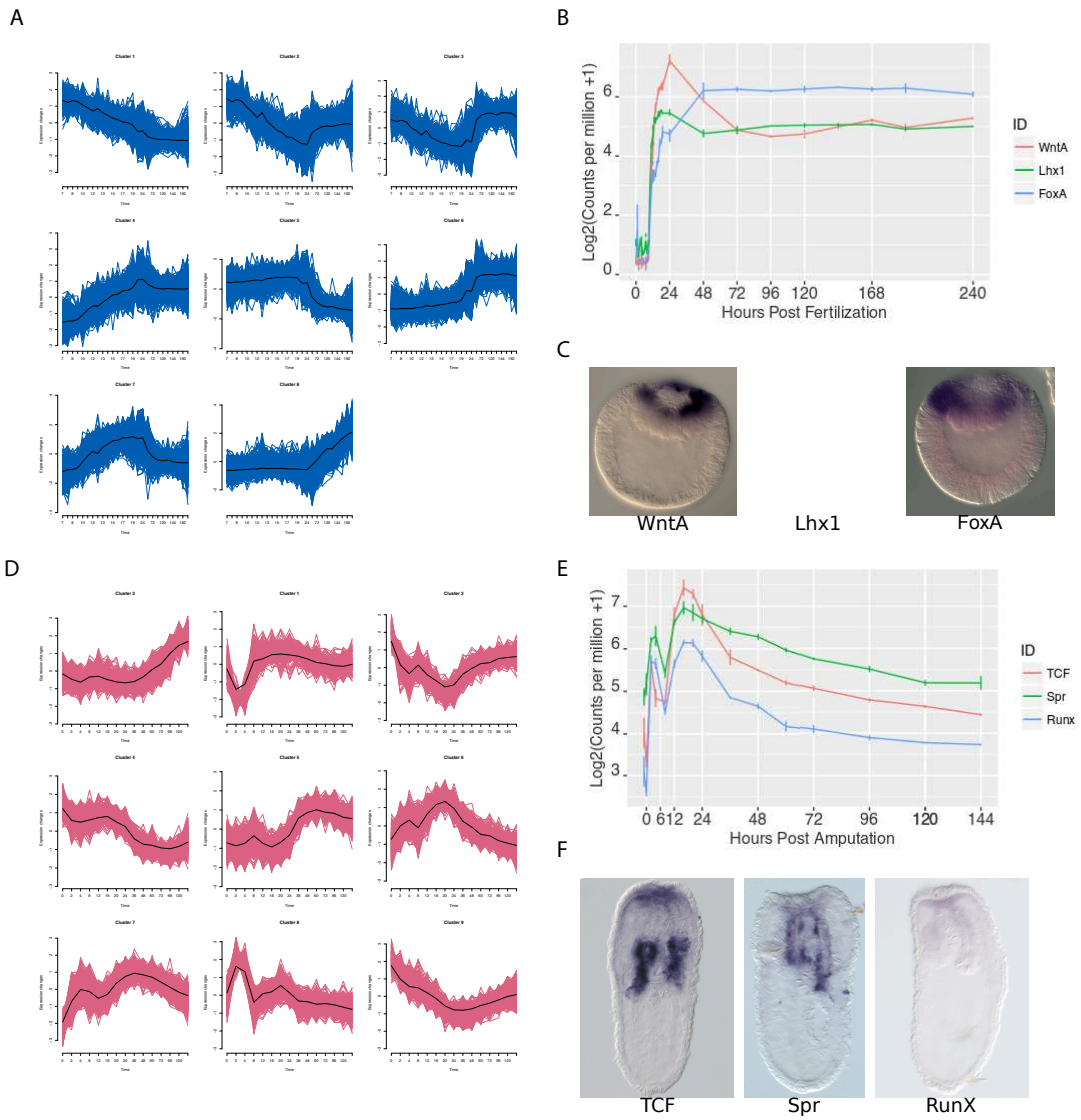

Figure 2: Embryonic and Regenerative gene expression forms discrete clusters. (**A**) Fuzzy c-means clustering of embryonic gene expression. Each cluster is plotted with standardized expression along the y-axis and developmental time along the x-axis. Black trace denotes the cluster core (centroid). (**B**) Exemplar gene expression from a cluster activated early during embryogensis (E-4; WntA, Lhx1, FoxA). (**C**) *In situ* hybridization at 24hpf confirms early activation of this gene cluster. (**D**) Fuzzy c-means clustering of regeneration gene expression. (**E**) Exemplar gene expression from a cluster activated in the early regenerative program (R-6; TCF, Spr, Runx). (**E**) *In situ* hybridization confirms early activation of these genes.

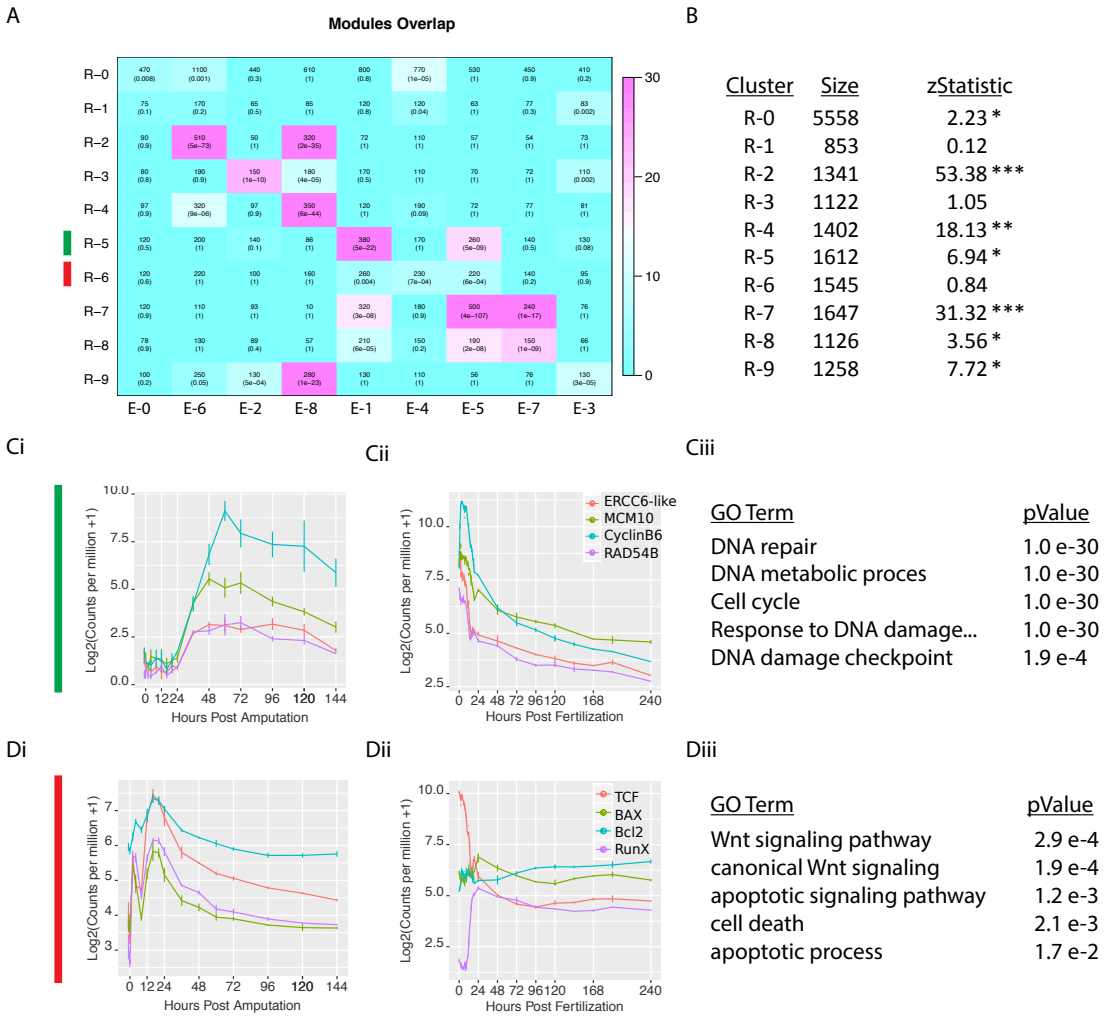

Figure 3: Embryonic gene modules are partially redeployed during regeneration. (**A**) Overlap table of regeneration versus embryonic modules. In each cell, the overlap itself is quantified along with the pvalue (fischers exact test). Color indicates $-\log_{10}$(pvalue), with a brighter magenta indicating a more significant overlap. R-0 and E-0 contain genes that are not assigned to any module. (**B**) Table indicating the size, and the co-clustering zStatistic. A zStatistic >2 (*) indicates moderate module conservation, >10 (**) high sconervation > 30 (***)very high conservation). (**C**) The conserved module R-5 with exemplar genes (ERCC6-like, RAD54B, MCM10, CyclinB6) showing coexpression during regeneration (**Ci**) and embryogenesis (**Cii**). GO-term enrichment identifies terms

associated with cell proliferation (**Ciii**). (**D**) The regeneration specific module R-6 with exemplar genes (TCF, BAX, RunX, and Bcl2) showing co-expression during regeneration (**Di**) but divergent expression during embryogenesis (**Dii**). GO-term enrichment identifies terms associated with apoptosis and wnt signaling (**Diii**).

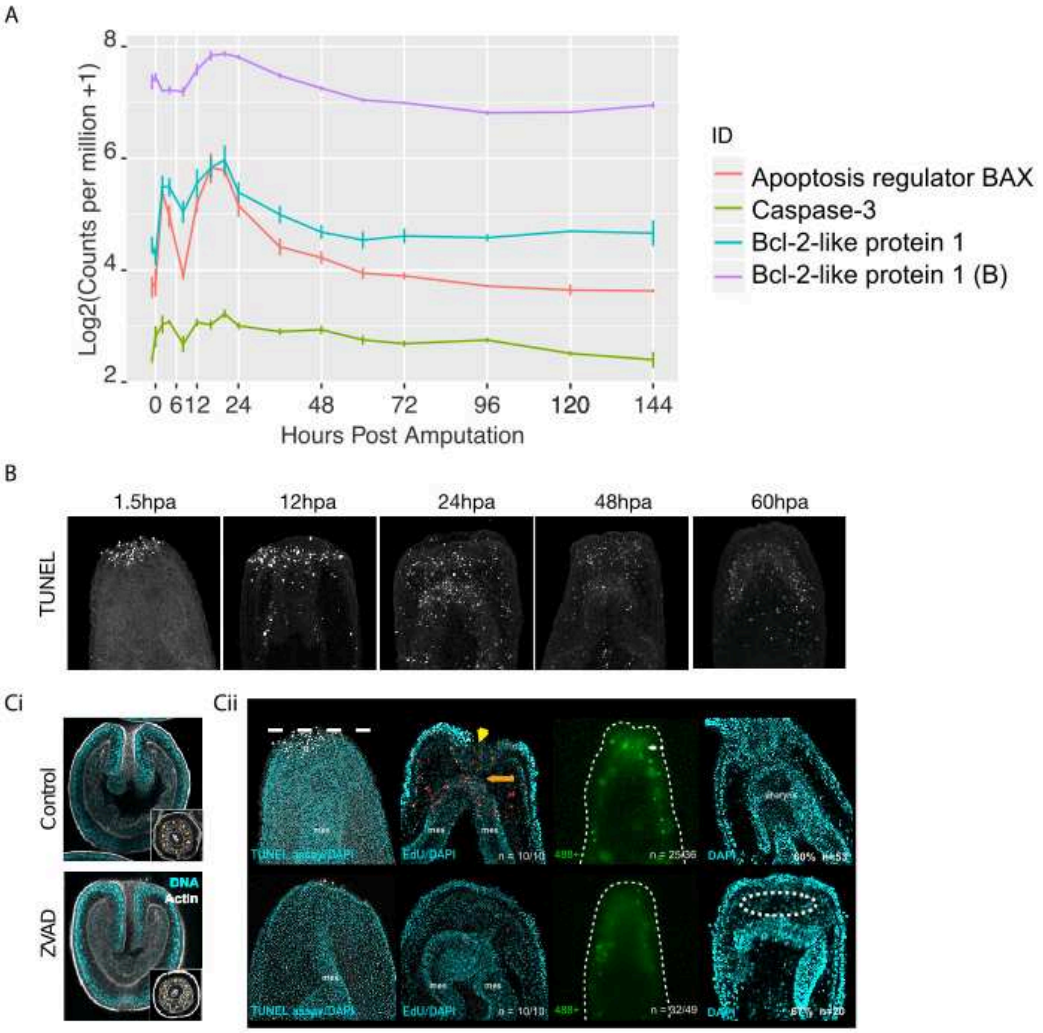

Figure 4: Apoptosis is required for regeneration, not embryogenesis. (**A**) Apoptosis genes (BAX, Caspase-3,Bcl2-like protein 1) found in the regeneration specific module R-6 are activated early in response to injury. (**B**) After

amputation, apoptosis marked by TUNEL staining is localized early to the wound site at 1.5hpa. This staining continues through 60hpa. (**Ci**) Treatment with the apoptosis inhibitor zVAD does not affect embryonic development (48hpf). (**Cii**) Conversely zVAD treatment blocks regeneration at an early stage. TUNEL staining of zVAD treated regenerates confirms apoptosis inhibition. Cell proliferation (Edu, red) is also strongly reduced. Autofluorescence of the pharynx does not reappear (488, green) indicating a failure of regeneration. Morphology at 144hpa also shows a clear lack of pharynx (dashed circle) and tentacles in zVAD treatment.

Supplementary figures:

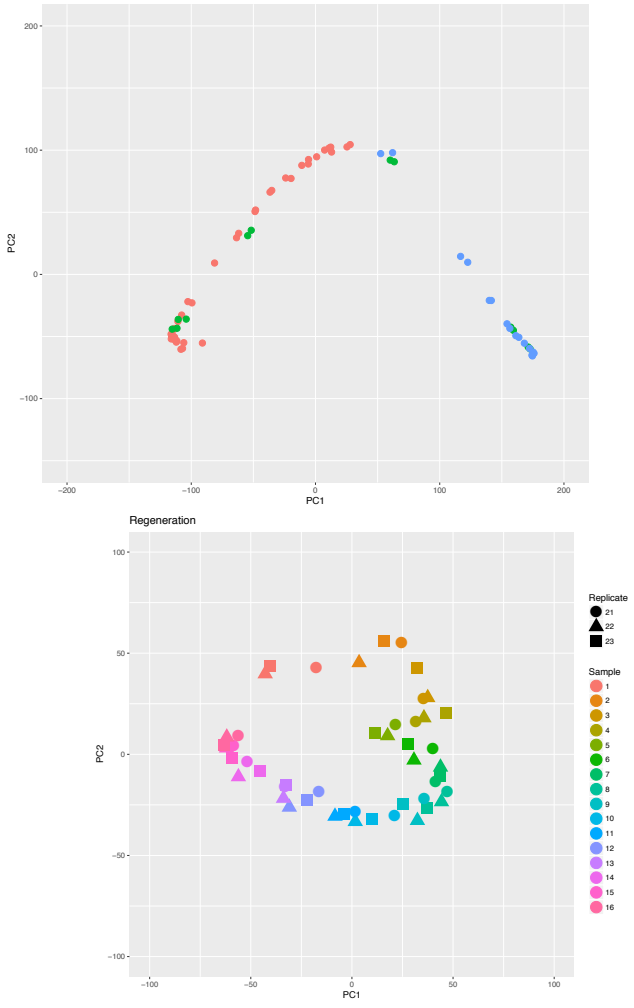

S1: PCA of individual replicates for embryo and regeneration

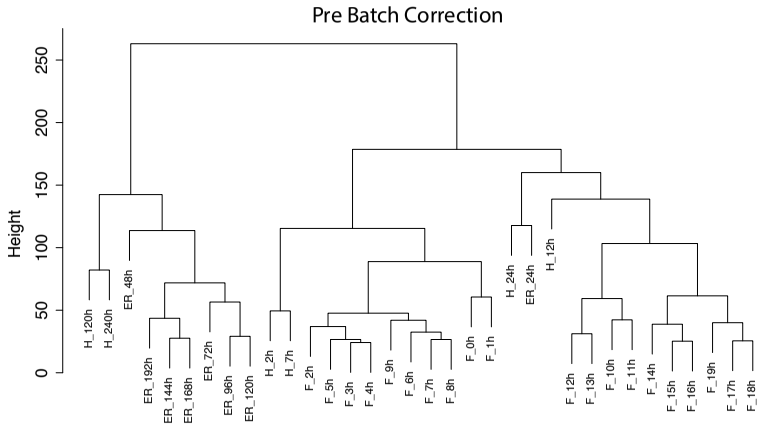

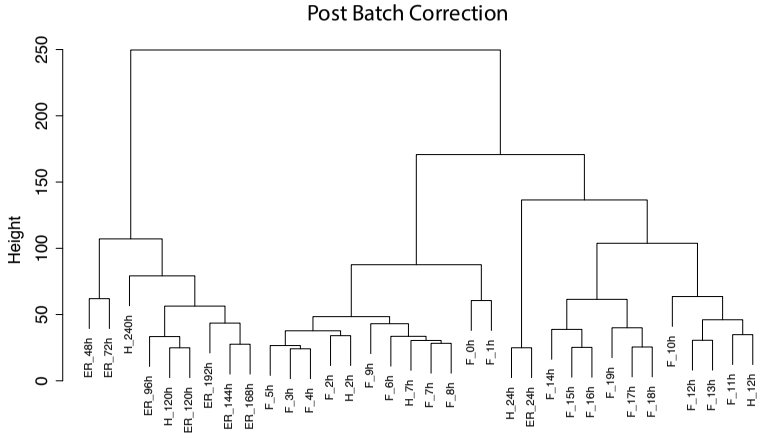

S2: Sample tree pre, post batch correction.

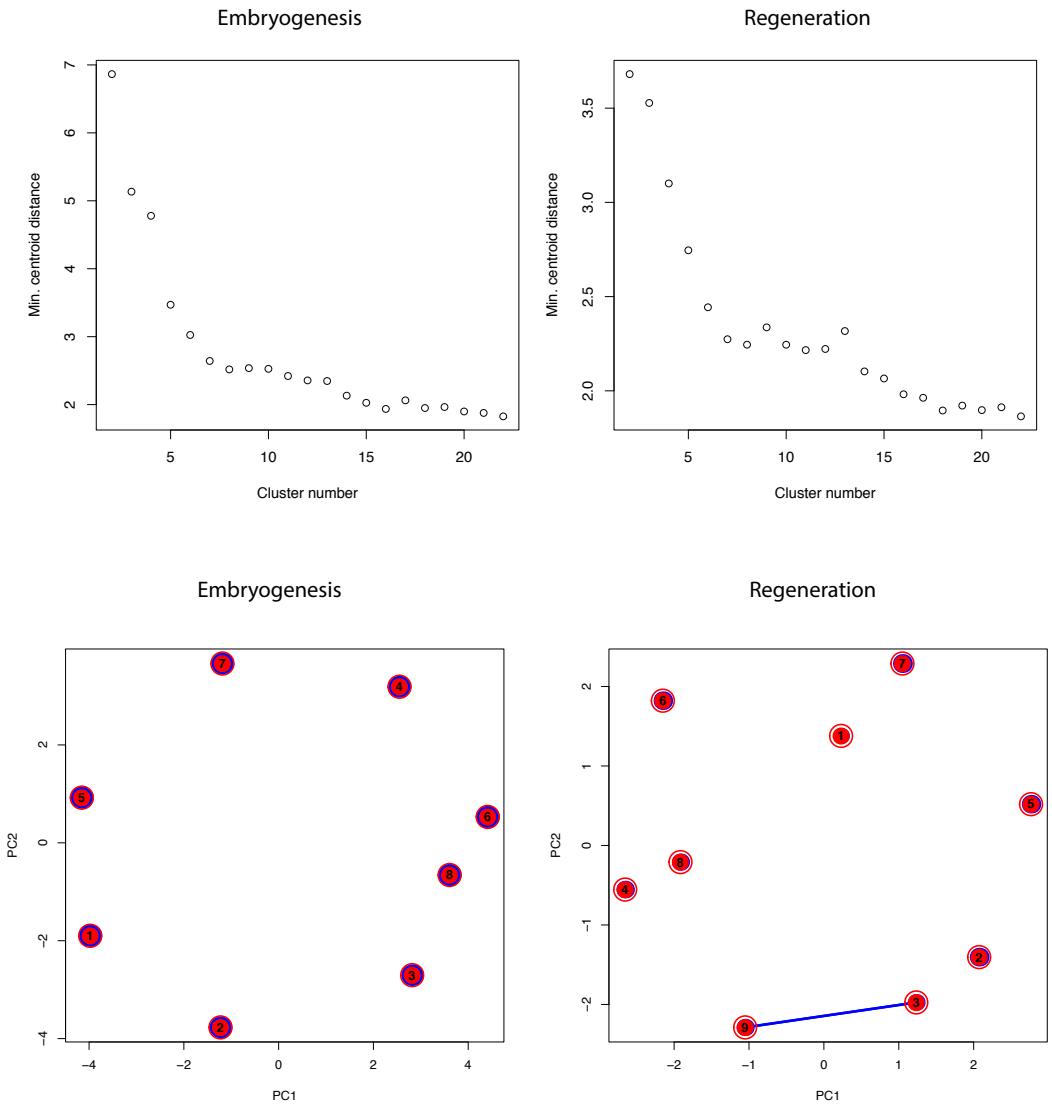

S3: mFuzz overlap PCA plots.

(Too big for this manuscript.)

S4: Bubble plots for embryo and regen clusters.

References

Adell, T., Salò, E., Boutros, M. and Bartscherer, K. (2009). Smed-Evi/Wntless is required for beta-catenin-dependent and -independent processes during planarian regeneration. *Development* **136**, 905–910.

Amiel, A. R., Johnston, H. T., Nedoncelle, K., Warner, J. F., Ferreira, S. and Röttinger, E. (2015). Characterization of Morphological and Cellular Events Underlying Oral Regeneration in the Sea Anemone, Nematostella vectensis. *Int J Mol Sci* **16**, 28449–28471.

Bassat, E., Mutlak, Y. E., Genzelinakh, A., Shadrin, I. Y., Baruch Umansky, K., Yifa, O., Kain, D., Rajchman, D., Leach, J., Riabov Bassat, D., et al. (2017). The extracellular matrix protein agrin promotes heart regeneration in mice. *Nature* **547**, 179–184.

Bossert, P. E., Dunn, M. P. and Thomsen, G. H. (2013). A staging system for the regeneration of a polyp from the aboral physa of the anthozoan Cnidarian Nematostella vectensis. *Dev. Dyn.* **242**, 1320–1331.

Bryant, D. M., Johnson, K., DiTommaso, T., Tickle, T., Couger, M. B., Payzin-Dogru, D., Lee, T. J., Leigh, N. D., Kuo, T.-H., Davis, F. G., et al. (2017). A Tissue-Mapped Axolotl De Novo Transcriptome Enables Identification of Limb Regeneration Factors. *Cell Rep* **18**, 762–776.

Burton, P. M. and Finnerty, J. R. (2009). Conserved and novel gene expression between regeneration and asexual fission in Nematostella vectensis. *Dev. Genes Evol.* **219**, 79–87.

Carlson, M. R., Komine, Y., Bryant, S. V. and Gardiner, D. M. (2001). Expression of Hoxb13 and Hoxc10 in developing and regenerating Axolotl limbs and tails. *Developmental Biology* **229**, 396–406.

Chera, S., Ghila, L., Dobretz, K., Wenger, Y., Bauer, C., Buzgariu, W., Martinou, J.-C. and Galliot, B. (2009). Apoptotic cells provide an unexpected source of Wnt3 signaling to drive hydra head regeneration. *Developmental Cell* **17**, 279–289.

Davidson, E. H., Rast, J. P., Oliveri, P., Ransick, A., Calestani, C., Yuh, C.-H., Minokawa, T., Amore, G., Hinman, V., Arenas-Mena, C., et al. (2002). A genomic regulatory network for development. *Science* **295**, 1669–1678.

Dubuc, T. Q., Traylor-Knowles, N. and Martindale, M. Q. (2014). Initiating a regenerative response, cellular and molecular features of wound healing in the cnidarian Nematostella vectensis. *BMC Biol.* **12**, 24.

Fischer, A. H. L. and Smith, J. (2014). Nematostella High-density RNAseq time-

course.

Habermann, B., Bebin, A.-G., Herklotz, S., Volkmer, M., Eckelt, K., Pehlke, K., Epperlein, H. H., Schackert, H. K., Wiebe, G. and Tanaka, E. M. (2004). An Ambystoma mexicanum EST sequencing project: analysis of 17,352 expressed sequence tags from embryonic and regenerating blastema cDNA libraries. *Genome Biol.* **5**, R67.

Hand, C. and Uhlinger, K. R. (1992). The culture, sexual and asexual reproduction, and growth of the sea anemone Nematostella vectensis.

Helm, R., Siebert, S., Tulin, S., Smith, J. and Dunn, C. (2013). Characterization of differential transcript abundance through time during Nematostella vectensis development. *BMC Genomics* **14**, 266.

Hutchins, E. D., Markov, G. J., Eckalbar, W. L., George, R. M., King, J. M., Tokuyama, M. A., Geiger, L. A., Emmert, N., Ammar, M. J., Allen, A. N., et al. (2014). Transcriptomic Analysis of Tail Regeneration in the Lizard Anolis carolinensis Reveals Activation of Conserved Vertebrate Developmental and Repair Mechanisms. *PLoS ONE* **9**, e105004.

Imokawa, Y. and Yoshizato, K. (1997). Expression of Sonic hedgehog gene in regenerating newt limb blastemas recapitulates that in developing limb buds. *Proc. Natl. Acad. Sci. U.S.A.* **94**, 9159–9164.

Kumar, L. and E Futschik, M. (2007). Mfuzz: a software package for soft clustering of microarray data. *Bioinformation* **2**, 5–7.

Langfelder, P., Luo, R., Oldham, M. C. and Horvath, S. (2011). Is my network module preserved and reproducible? *PLoS Comput. Biol.* **7**, e1001057.

Leek, J. T., Johnson, W. E., Parker, H. S., Jaffe, A. E. and Storey, J. D. (2012). The sva package for removing batch effects and other unwanted variation in high-throughput experiments. *Bioinformatics* **28**, 882–883.

Lobo, D. and Levin, M. (2015). Inferring regulatory networks from experimental morphological phenotypes: a computational method reverse-engineers planarian regeneration. *PLoS Comput. Biol.* **11**, e1004295.

Mathew, L. K., Sengupta, S., Franzosa, J. A., Perry, J., La Du, J., Andreasen, E. A. and Tanguay, R. L. (2009). Comparative expression profiling reveals an essential role for raldh2 in epimorphic regeneration. *J. Biol. Chem.* **284**, 33642–33653.

Morgan, T. H. (1901). *Regeneration*.

Özpolat, B. D., Zapata, M., Daniel Frugé, J., Coote, J., Lee, J., Muneoka, K. and Anderson, R. (2012). Regeneration of the elbow joint in the developing

chick embryo recapitulates development. *Developmental Biology* **372**, 229–238.

Passamaneck, Y. J. and Martindale, M. Q. (2012). Cell proliferation is necessary for the regeneration of oral structures in the anthozoan cnidarian Nematostella vectensis. *BMC Developmental Biology* **12**, 34.

Rodius, S., Androsova, G., Götz, L., Liechti, R., Crespo, I., Merz, S., Nazarov, P. V., de Klein, N., Jeanty, C., González-Rosa, J. M., et al. (2016). Analysis of the dynamic co-expression network of heart regeneration in the zebrafish. *Sci Rep* **6**, 26822.

Röttinger, E., Dahlin, P. and Martindale, M. Q. (2012). A framework for the establishment of a cnidarian gene regulatory network for “endomesoderm” specification: the inputs of ß-catenin/TCF signaling. *PLoS Genet* **8**, e1003164.

Schaffer, A. A., Bazarsky, M., Levy, K., Chalifa-Caspi, V. and Gat, U. (2016). A transcriptional time-course analysis of oral vs. aboral whole-body regeneration in the Sea anemone Nematostella vectensis. *BMC Genomics* **17**, 718.

Srivastava, M., Mazza-Curll, K. L., van Wolfswinkel, J. C. and Reddien, P. W. (2014). Whole-body acoel regeneration is controlled by Wnt and Bmp-Admp signaling. *Curr. Biol.* **24**, 1107–1113.

Torok, M. A., Gardiner, D. M., Shubin, N. H. and Bryant, S. V. (1998). Expression of HoxD genes in developing and regenerating axolotl limbs. *Developmental Biology* **200**, 225–233.

Trevino, M., Stefanik, D. J., Rodriguez, R., Harmon, S. and Burton, P. M. (2011). Induction of canonical Wnt signaling by alsterpaullone is sufficient for oral tissue fate during regeneration and embryogenesis in Nematostella vectensis. *Dev. Dyn.* **240**, 2673–2679.

Wang, Y.-H. and Beck, C. W. (2014). Distal expression of sprouty (spry) genes during Xenopus laevis limb development and regeneration. *Gene Expr. Patterns* **15**, 61–66.

Warner, J. F., Guerlais, V., Amiel, A. R., Johnston, H., Nedoncelle, K. and Röttinger, E. (2018). NvERTx: a gene expression database to compare embryogenesis and regeneration in the sea anemone Nematostella vectensis. *Development* **145**, dev162867.

Wikramanayake, A. H., Hong, M., Lee, P. N., Pang, K., Byrum, C. A., Bince, J. M., Xu, R. and Martindale, M. Q. (2003). An ancient role for nuclear beta-catenin in the evolution of axial polarity and germ layer segregation. *Nature* **426**, 446–450.

Chapter 3: Investigation of the gene regulatory network underlying regeneration

This last chapter takes benefit from all the studies I described in the previous chapters and focuses on gaining insight into the molecular mechanisms underlying regeneration in *Nematostella* to establish a framework for the first regeneration GRN in this model in order to compare it to the *Nematostostella* embryogenesis GRN.

The sixth article (Johnston et al, in prep, first author, Article 6) focuses on the role of MEK/ERK signaling during regeneration, its downstream GRN logics and the comparison between embryogenesis and regeneration at the GRN level. In this study, I designed and carried out almost all experiments/analysis and took as much benefit as possible from all the previous studies I was involved in. In a first step, we confirmed and refined the importance of MEK/ERK signaling during regeneration in *Nematostella*. Most importantly, I then determined that this morphogenetic role might be analogous to the one described during embryogenesis (see chapter 1) and I used that information to identify that a partial and rewired embryonic program is embedded in the regeneration GRN. I thus functionally validate the hypothesis emitted by our previous study (Article 5).

Finally, the last article (Johnston et al, in prep, first author Article 7) summarizes preliminary data from a study for which I designed and performed a kinase inhibitor screen to identify additional kinases inputs required for the various steps of *Nematostella* regeneration. Among the several candidate kinases that I identified during this screen, I focused in particular on the MAPK JNK and show its specific role in the control of the injury induced and regeneration-specific cell proliferation.

Overall, this last chapter takes together all previous studies I was involved in during my PhD, unravels particular molecular mechanisms involved in whole body regeneration in *Nematostella* and enables me to compare the relationship between embryogenesis and regeneration at the GRN level.

Article 6: Johnston. H., Nedoncelle. K., Röttinger. E. Whole body regeneration requires a rewired embryonic gene regulatory network logic.
In preparation

Article 7: Johnston. H., Gaggioli. C., Röttinger. E. (in prep). A kinase inhibitor screen reveals that JNK MAPK regulates regeneration-specific cell proliferation in the sea anemone *Nematostella vectensis.*
In preparation

Article 6: Whole body regeneration requires a rewired embryonic gene regulatory network logic

Johnston. H., Nedoncelle. K. and Röttinger. E.

In preparation and should be submitted for publication before the end of the year

Whole body regeneration requires a rewired embryonic gene regulatory network logic

Hereroa Johnston[1], Karine Nedoncelle[1], and Eric Röttinger[1]*

[1] Université Côte d'Azur, CNRS, INSERM, Institute for Research on Cancer and Aging, Nice (IRCAN), Nice, France

§

*Please direct correspondence to:

Eric Röttinger

T: +33 (0)6 63 97 01 78

E: eric.rottinger@unice.fr

Introduction

Regeneration is a developmental process, that after autotomy or injury enables the organism to regrow structures that are functionally identical to the lost ones (Sánchez Alvarado 2000). To illustrate the variability of this process, regeneration can be categorized into two broad levels; structural regeneration and whole body regeneration. The first one, mainly described in vertebrates, includes regrowth at the cellular (*e.g* axonal regeneration(Goldshmit et al. 2012; Kroehne et al. 2011)) or tissue/organ levels (*e.g* liver regeneration (Michalopoulos 1997; Sadler et al. 2007) as well as the reformation of whole appendages (*e.g* salamander limbs (McCusker, Bryant, and Gardiner 2015)). Whereas whole body regeneration, exclusively described in invertebrates (Galliot and Schmid 2002; Rink 2013; Gazave et al. 2013; Czarkwiani et al. 2016), encompasses all types of structural regeneration to reform substantial body parts, or reform entire organisms from small body fragments. Like structural regeneration, whole body regeneration must integrate polarity and positional identity cues with pre-existing body structures to re-establish the body dimensions and the major developmental axes; anterio-posterior, dorso-ventral and left-right(Gurley et al. 2010; Carlson et al. 2001; Makanae, Mitogawa, and Satoh 2014)).

All of the developmental axes cited above are known to arise during embryogenesis, the developmental process from which multicellular organisms arises. Even though embryogenesis and regeneration differ in their initial context (i.e. one fertilized egg, *vs* numerous differentiated/undifferentiated cells), both developmental trajectories grow/re-grow the same structures that are able to carry out the same functions. This

observation was at the origin of a historical question in regeneration biology concerning the relationship between embryogenesis and regeneration (Morgan, 1901). More recently, researchers wondered to what extend regeneration reuses the molecular mechanisms originally deployed during embryonic development. By comparing individual gene expression/function during embryonic development and structural regeneration several studies in vertebrates have shown that i) notch signalling was not re-activated during motor neuron regeneration(Binari, Lewis, and Kucenas 2013) or on the opposite ii) regeneration-specific *hox* expression or Sox2 function during axolotl limb and zebrafish inner ear hair cell regeneration, respectively (Gardiner et al. 1995; Millimaki, Sweet, and Riley 2010). However, additional studies indicate a conserved and/or modified re-expression of *hox* genes during axolotl limb regeneration (Gardiner and Bryant 1996; Carlson et al. 2001). The same observation has been reported during different organ regeneration, *e.g* liver, pancreas, lens where genes involved in embryonic development of the cited organs, are re-expressed during their regeneration (Jensen et al. 2005; Sadler et al. 2007). While, these studies suggest at least a partial re-use of the structure/appendage developmental program during their regeneration, very little is known about the relationship between embryonic development and whole body regeneration. The reason for this is that such comparison is difficult to perform in the classical and well-known whole body regeneration models. Planarians and *Hydra* are unquestionably powerful whole body regeneration models that have increased our understanding of this intriguing phenomenon(Petersen et al. 2015; Galliot 2004; Umesono et al. 2013; Wenemoser et al. 2012). However, they are

78 unfortunately rather difficult models to study their embryonic development
79 because of a more restricted access to embryonic material (Genikhovich et al.
80 2006; Davies et al. 2017) compared to classical developmental models (i.e
81 drosophila, *c. elegans* etc...).

82 One emerging whole body regeneration model that is perfectly suited to
83 compare embryogenesis and whole body regeneration at the gene regulatory
84 network level is the sea anemone *Nematostella vectensis* (Cnidaria,
85 Anthozoa,(Burton and Finnerty 2009; Finnerty and Martindale 1999; Warner
86 et al. 2018) Fig 1A). A body of studies on the embryonic development of
87 *Nematostella* has begun to establish the gene regulatory networks (GRNs)
88 underlying axial patterning and germ layer specification, in order to
89 understand its development and build a solid groundwork for evolutionary
90 comparative studies (Röttinger, Dahlin, and Martindale 2012; Genikhovich et
91 al. 2015; Layden et al. 2016; Leclère et al. 2016; Amiel et al. 2017; Botman et
92 al. 2015; Abdol et al. 2017). Emerging from this consensus work, a
93 comprehensive GRN of germ layer specification preceding the onset of
94 morphogenetic movements of gastrulation has been proposed (Amiel et al.
95 2017). More recently, several studies have focused on the whole body
96 regenerative capacity of *Nematostella* that is able to regrow missing body
97 parts within five days after bisection (Darling et al. 2005; Burton and Finnerty
98 2009; Trevino et al. 2011; Passamaneck and Martindale 2012; Bossert, Dunn,
99 and Thomsen 2013; Amiel et al. 2015; Schaffer et al. 2016; Warner et al.
100 2018; DuBuc, Traylor-Knowles, and Martindale 2014) Fig 1K). Oral
101 regeneration after sub-pharyngeal amputation in *Nematostella* is occurring in
102 a stereotypical manner, following five well-defined steps that lead to the

reformation of the oral structures (Amiel et al. 2017). The initial proliferation independent step (Amiel et al. 2017) leads to a tissue crosstalk between the mesenteries (digestive and reproductive tissue) and the bodywall epithelia at the amputation site in order to launch a proliferation and stem cell dependent regenerative response (Amiel et al, BioRxv). While our understanding of the molecular mechanisms underlying regeneration in *Nematostella* remains sparse(Burton and Finnerty 2009; Trevino et al. 2011; DuBuc, Traylor-Knowles, and Martindale 2014), recent studies have developed transcriptomic resources describing various time points during regeneration (Schaffer et al. 2016; Warner et al. 2018). In addition, we have created a unique and freely accessible online database to simultaneously compare gene expression during embryogenesis and whole body regeneration in this research model (Warner et al. 2018). A thorough bio-informatics analysis of these embryonic and regeneration datasets has interestingly revealed that regeneration is a partial redeployment of embryonic development and suggested an important rearrangement of the embryonic GRN during regeneration (Warner et al, in submission).

Previous work has described the MEK/ERK dependent gene regulatory network underlying embryonic development (Layden et al. 2016; Amiel et al. 2017) and suggested a role of this pathway in wound healing and regeneration (DuBuc, Traylor-Knowles, and Martindale 2014). Thus, in order to functionally verify the observation of a rewiring of embryonic network elements during regeneration, we have investigated in detail the role of MEK/ERK signaling during regeneration and described its underlying gene regulatory network at the onset of regeneration. While we show that

MEK/ERK signaling is not required for wound healing or the initiation of proliferation, we highlight its crucial role in the maintenance of proliferation and the onset of the regeneration program. By crosschecking embryonic GRN information (Röttinger, Dahlin, and Martindale 2012; Layden et al. 2016; Amiel et al. 2017), with novel information about the molecular dynamics during regeneration (Warner et al. 2018); Warner et al, BioRxv) and combining them with a systematic functional analysis, we not only confirm at the GRN level that regeneration is a partial redeployment of the embryonic GRN, but that its components are rewired during regeneration and interconnected to novel downstream targets, including regeneration specific genes. Overall, this study provides a functional answer to a long-lasting and historical question in regenerative biology, establishes a first comprehensive framework for the GRN describing whole body regeneration and defines the bases for further comparative molecular work to gain insight into the evolution of regeneration and attempt to understand why certain animals possess whole body regenerative capacities, while others don’t.

Results:

1. ERK signalling is activated in immediate response to injury.

In order to characterise the activity of ERK in response to the amputation stress in *Nematostella*, we used a monoclonal antibody directed against the activated phosphorylated form of ERK (pERK) at various time points during regeneration. As control, we also detected the total amount of ERK protein using a monoclonal antibody directed against (tERK). On western blot (Fig. 1a), tERK as well as pERK, are detected during the whole time course of regeneration, including in the uncut animal. Upon inhibition of MEK by U0126, a potent antagonist of ERK(Davies et al. 2017; DeSilva et al. 1998), only pERK is abolished (Fig 1a). A direct comparison of pERK levels between the uncut and the first 20hpa, is surprisingly showing a rapid decrease of the activation signal by 6hpa, while tERK level is unaffected (Fig 1i). These results indicate that the activity of ERK is post-translationally controlled rapidly in response to the amputation stress. Importantly, pERK level is still detected at 6, 12 and 24hpa and is completely down regulated when MEK is blocked (Fig. 1a).

When performing whole mount immuno-staining using the same pERK antibody to analyse the spatio-temporal activation of this kinase (Fig. 1b-l), we observed a ubiquitous staining along the body column in the uncut polyp and at 0hpa (Fig 1b). In contrast, as early as 1hpa, pERK is activated in the ectodermal and gastrodermal epithelia at the amputation site and in the most oral tips of the endodermal epithelia of the mesenteries (Fig 1c). When the wound is closed (6hpa) and at 10-12hpa, pERK remains detected at the amputation site in the body wall epithelia and the tips of the mesenteries (fig

1c-e). As regeneration proceeds and reaches step 1 at 24hpa (mesenteries fused together and in tight contact with the epithelia at the amputation site, (Amiel et al. 2015), pERK staining becomes a merged continuum between the mesenteries and the amputation epithelia (Fig 1f). Consistent with our western blot analysis (Fig.1a), pERK staining is completely lost in juveniles that were treated with U0126 (Fig 1l).

Taken together our spatio-temporal analysis of ERK activation in *Nematostella* in control uncut animal and during regeneration, indicates that ERK is ubiquitously active throughout the tissues of the body and that upon amputation the overall activity of ERK is only restricted at a precise location of the amputation site and maintained during the whole head regeneration process (Fig 1c – 1k) indicating a potential role of this pkinase in the process of head regeneration in *Nematostella*.

2. Inhibition of MEK/ERK delays wound healing and is crucial for the onset of regeneration.

According to a previous study (DuBuc, Traylor-Knowles, and Martindale 2014) and our observations of an injury-induced localization of ERK activity at the amputation site, one initial role of pERK in *Nematostella* could be the coordination of tissue dynamic during the wound healing process. To test this hypothesis, we used the *in vivo* compression assay developed in (Amiel et al. 2015), to address the opening status of the wound – open or closed - in controls and U0126 treated animals between 0 and 8hpa. Compared to DMSO treated controls, the percentage of closed wound is lower in U0126 treated animals as soon as 4hpa. At this time, 20% (4 out of 20 cases) of the controls and only 6% (2 out of 32 cases) of the U0126 treated juveniles exhibit

195 a clear healed wound (Fig. 2A). At 6hpa, 82% (19 out of 23 cases) of the
196 controls closed their wounds, while only 65 % (15 out of 23 cases) do in
197 UO126 treated conditions. Comparably to the control and previous study
198 (Amiel et al. 2015), wound healing is nearly terminated at 6hpa and the
199 control reach the 100% (25/25) at 8hpa). However, only 85% (13/15) of the
200 treated animals were successful in healing their wounds (Fig. 2A). In order to
201 test whether wound healing was completely blocked or only delayed after
202 MEK/ERK inhibition, we continued our wound healng assay after 8hpa and
203 observed that at 10hpa, UO126 treated animals closed their wound in 94%
204 (17 out of 18 cases). In conclusion, MEK/ERK inhibition does not block but
205 significantly delays wound healing.
206 In order to get insight into a more precise implication of ERK during the
207 various phases of the stress induced regenerative response, we have treated
208 sub-pharyngeally amputated juveniles with U0126 during various time course
209 of regeneration and assessed phenotype at 144hpa using the staging system
210 of *Nematostella* regeneration develop in Amiel et al., 2015. Continuous
211 treatment using U0126, beginning right after amputation up to 144hpa,
212 resulted in a very reproducible arrest of the regeneration process in step 0.5
213 (after wound healing) (Fig 2c), indicating a complete arrest of regeneration
214 and a crucial role of MEK/ERK for transitioning from step 0 to step 1. When
215 treatment was started at 24 or 48hpa up to 144hpa, regeneration was blocked
216 at step 2 (Fig 2c), and steps 2 or 3 (Fig 2c), respectively. Taken into account
217 that at 24 and 48hpa the vast majority of animals are in step 1 (Amiel et al.
218 2015), the present results suggest that MEK/ERK is not involved in the
219 transition between step 1 and 2, but for the subsequent and proliferation-

dependent phases of regeneration. Finally treatments between 72 and 144hpa did not affect regeneration, as the amputated animals reached step 3 and 4 (Fig 2c) in the same proportions as controls (Fig 2c). Hence, our results indicate that MEK/ERK is crucially required for initiating a regenerative response (steps 0.5-1) as well as enabling proper re-formation of the lost body parts (steps 2-3).

As described above, inhibition of MEK/ERK signalling causes a delayed of wound healing (Fig. 2a) and a arrest of the regeneration process in step 0.5 (Fig. 2c). To distinguish a potential link between the roles of this signalling pathway during wound healing and the initiation of regeneration after the wound is healed, we compared the effects of U0126 treatments starting at 0hpa or at 8hpa (Fig 2d) (when wound healing is completed in control animals Fig. 2a, (Amiel et al. 2015) or reaching step 1 (Fig. 2c). While 75% (15/24) of control DMSO treated animals reached step 1, in both U0126 conditions (treatment start at 0hpa or 8hpa) all animals are blocked at step 0.5 (Fig. 2e) with the mesenteries separated from the epithelium (Fig. 3c, 3e). Thus, these results indicate that although MEK/ERK signalling plays a critical role in reaching step 1, the observed delay in wound healing (Fig. 2a) appears not involved in this transition.

3. MEK/ERK signalling is required for maintaining cell proliferation during regeneration

As in most metazoan regeneration research models, cellular proliferation is activated upon amputation and required for reforming missing body structures in *Nematostella* (Passamaneck and Martindale 2012; Amiel et al. 2015). In order to investigate whether MEK/ERK signalling is required for

245 the initiating or maintenance of cellular proliferation during regeneration, we
246 have carried out U0126 treatments at various timeframes during regeneration
247 and assessed the amount of cells in S-phase (named EdU+ cells) at the end
248 of the treatment.

249 The potential effects of U0126 on the initiation of cell proliferation was
250 assessed by performing treatments between 0-20hpa and 8-20hpa (Fig 3a),
251 followed by EdU staining at 20hpa that corresponds to a time point preceding
252 the burst of cell proliferation observed at 24hpa (Passamaneck et al. 2012,
253 Amiel et al. 2015). To our surprise, we did not observe a significant variation
254 of cellular proliferation neither in the localisation (Fig. 3b'-e'), nor in the total
255 amount of EdU+ cells (Fig. 3f) between U0126 treated animals and untreated
256 controls for both treatment starting points (0hpa or 8hpa). These results
257 indicate that the ERK signalling pathway did not affect the initiation of cell
258 proliferation. These data suggest that the block of the regeneration process in
259 step 0.5 resulting from the treatment with UO126 between 0 and 144hpa,
260 seems to come form a role of ERK in the morphogenetic movement occurring
261 in the early step of regeneration.

262 Because we previously describe a second role of MEK/ERK in
263 transitioning from step 2 to 3 (Fig.2c) and that we know from a previous study
264 that it is a transition cell proliferation-dependent (Amiel et al. 2015), we
265 access the effects of U0126 treatment in the maintenance of cell proliferation
266 in these later steps. To do so, we applied U0126 for 24h starting at various
267 time points during regeneration (0-24hpa, 24-48hpa, 48-73hpa and 72-96hpa)
268 (Fig 3g), and we counted EdU+ cells in the body wall epithelia (Fig. 3h) as
269 well as in the epithelia of the mesenteries (Fig. 3i). Confirming our results (Fig.

2c), For a treatment between 0-24hpa, we observed that the levels of cell proliferation at 24hpa is similar to the controls untreated animals (Fig. 3h,i). However, for a treatment between 24-48hpa, the burst of cell proliferation detected in controls is drastically reduced in both, body wall and mesenteries (Fig. 3h,i). This is also observed in animals treated with the MEK inhibitor when animal are treated between 48-72hpa and 72-96hpa (Fig. 3h,i). However, the decrease in proliferation is not as drastic compared to the 24-48hpa condition (Fig. 3h,i), suggesting that additional compensatory mechanisms may be involved in cell proliferation maintenance at later time points during *Nematostella* regeneration. Overall, these observations indicate that MEK/ERK is not required for initiating but rather for maintaining cell proliferation that is crucial for the step 2 to 3 transition. Taken together all our results show that the kinase MEK/ERK plays two distinct roles during regeneration: i) the first one during proliferation-independent steps, in the initiation of regeneration from step 0.5 to 1, potentially thought the control of morphogenetic movement; ii) the second role during proliferation-dependent steps, for the maintenance of cell proliferation required for the transition between steps 2 and 3.

4. Identification of potential MEK/ERK downstream targets at 20hpa

A detailed GRN involving the MEK/ERK signalling pathway and its role during embryogenesis has been recently published (Amiel, Jonsthon et al., 2016). In addition, an extensive unbiased bio-informatics analysis comparing RNAseq datasets spanning embryogenesis and regeneration in *Nematostella* has suggested that regulatory elements that are shared between these two developmental trajectories are rewired to create a regeneration-specific

network (Warner et al, in submission). In order to functionally confirme/validate this hypothesis, we first generate a framework of the GRN involving MEK/ERK signalling during regeneration, then performed a comparison between the published GRNs of embryogenesis and the one we generated for regeneration. To do so, we established a framework for the MEK/ERK dependent network module of the regeneration process at 20hpa and compare it to the embryonic GRN that was established for the 24 hours post fertilization (hpf) time point (Röttinger, Dahlin, and Martindale 2012; Layden et al. 2016; Amiel et al. 2017). Latter also contains the MEK/ERK dependent network module involved in tissue specification and the onset of gastrulation (Layden et al. 2016; Amiel et al. 2017). Two main reasons justify the comparison between these two GRNs at these time points: i) they both are at the onset of morphogenetic movements (i.e. gastrulation (Amiel et al. 2017) and invagination/tissue reorganization of the amputation site (Amiel et al. 2015), and ii) inhibiting MEK/ERK signalling perturbs both of these tissular rearrangements (embryogenesis: (Layden et al. 2016), regeneration: this study).

We have shown that MEK/ERK signalling is required following wound healing for the transition from Step 0 to 1. In order to identify potential MEK/ERK downstream targets responsible for launching a regenerative response during this transition, we took advantage of available *Nematostella* transcriptomic regeneration data and recently developed data mining tool (nvertx.kahikai.org, (Warner et al. 2018); Warner et al, in submission). Using the differential gene expression feature, we identified 2,263 transcripts that were differentially expressed with at least a 2-fold change between 0 and

20hpa (Fig.4a). We then compared the associated genes with all genes identified to be either WNT or MEK/ERK downstream targets during embryogenesis (Röttinger, Dahlin, and Martindale 2012; Layden et al. 2016; Amiel et al. 2017). From the embryonic MEK/ERK downstream targets (Layden et al. 2016; Amiel et al. 2017) we identified 19 out of 88 upregulated and 6 out of 88 downregulated genes at 20hpa (Table 1). From the embryonic WNT downstream targets (Röttinger, Dahlin, and Martindale 2012), we also identified 10 out of 33 genes that were upregulated and 4 out of 33 genes that were downregulated at the same time point (Table 2). In order to include potential regeneration specific inputs into the MEK/ERK regeneration GRN, we took advantage of the identification of 124 genes that possess a regeneration specific expression dynamics (Warner et al, in submission). Interestingly, 84 of those genes display a differential gene expression at 20hpa compared to 0hpa; 40 of them are upregulated and 44 downregulated (Table 3). When analysing the global temporal expression patterns of the genes belonging to the three above-mentioned dynamically expressed set of genes, we observed that four regeneration clusters are recurrent, namely the cluster R-1, R-5, R-6 and R-7 (Fig 4b – 4e). Among which the most represented cluster being the cluster R-6 (Fig 4d), which share little conservation with any other embryonic cluster (Warner et al, in submission).

5. At the onset of regeneration MEK/ERK signalling activates regeneration-specific, reuses embryonic MEK/ERK and co-opts embryonic WNT genes.

To assess whether the above-identified genes are downstream targets of MEK/ERK, we treated sub-pharyngeally amputated animals with U0126

345 and analyzed their expression levels at 20hpa by qPCR (Fig 5a). Strikingly, 18
346 out of 19 embryonic MEK/ERK downstream targets that are upregulated at
347 20hpa (Table 1) were all downregulated by U0126 treatments (Fig. 5b). The
348 only exception is *Nvbmp1-like.* None of the six embryonic MEK/ERK
349 downstream targets that are downregulated at 20hpa, are affected when
350 MEK/ERK is inhibited (Fig. 5b). When we analysed the embryonic WNT
351 downstream targets we obtained similar effects: i.e. 10 out of 11 embryonic
352 WNT downstream targets that are upregulated at 20hpa (Table 2) were all
353 downregulated by U0126 treatments (Fig. 5c). Only *Nvsmad4-like* as well as
354 none of the four embryonic WNT downstream that are downregulated at
355 20hpa are not affected by U0126 (Fig. 5c). Finally, for the regeneration
356 specific pool of genes, we assessed only 26 out of the 40 genes that are
357 upregulated at 20hpa. Among those 26 genes only 19 were downregulated by
358 U0126 (Fig. 5d). We then sought to uncouple the MEK/ERK downstream
359 targets i) activated in direct response to the immediate activation of pERK
360 after amputation and potentially involved in the wound healing process, and ii)
361 the ones that are involved initiating the regenerative response after the wound
362 is healed. In order to do so, we treated sub-pharyngeally amputated animals
363 with U0126 after wound healing from 8-20hpa and performed qPCR analysis
364 (Fig 5a) with all MEK/ERK downstream targets determined above (Fig. 5b –
365 5c). Interestingly, our results indicated that all the previously identified
366 downstream targets of MEK/ERK are also downregulated by the inhibition of
367 MEK after wound healing, thus, directly linked to the initiation of regeneration.
368 To have a better understanding of MEK/ERK downstream targets correlated
369 with regeneration, we characterized their expression domains by whole mount

370 *in situ* hybridization at 20hpa (FIG 6Aa). This analysis revealed that in addition
371 to a distinct expression domain in the aboral part of the physa (P, e.g.
372 *Nvfgf8A*, Fig 6z), MEK/ERK downstream targets are expressed in four distinct
373 domains of the amputation site and in the mesenteries. In particular, we
374 distinguish expression within the ectodermal epithelium at the amputation site
375 (AE, Fig 6a, 6b, Fig 6Aa), the gastrodermal epithelium at the amputation site
376 (AG Fig 6d – 6g, Fig 6Aa), the oral tip of the mesenteries close to the
377 amputation site (AMT Fig 6h – 6l, Fig 6Aa) as well as the entire mesenteries
378 (M, (Fig 6q – 6y, Fig 6Aa). Even though there are five distinct expression
379 domains, most of the genes are expressed in multiple domains (Fig 66m – 6p,
380 Fig 6Aa) that is expressed in AG/AMT and M. Interestingly three of the
381 identified domains (AE, AG and AMT, P) are overlapping with the localization
382 of pERK (Fig 1f, 1l). This observation is in line with MEK/ERK downstream
383 targets that are expressed in those domains, and suggest a systemic and
384 indirect activation (e.g. secreted ligands) of gene expression in the
385 mesenteries activated by MEK/ERK signalling in response to the amputation
386 stress.

Finally, and in order to confirm our qPCR results, we have performed *in situ* hybridization experiments after amputation and inhibition of MEK/ERK for the following genes: *NvfoxB, Nvrunt, Nvaxin-like, Nvtwist, NvHd050, Nvsprouty, Nvmae-like and NvfgfA2* (Fig 7). For these genes we also verified their expression profile in the uncut animals before inhibiting MEK. In the uncut animals (Fig 7ai – hi), four different profile have been drawn out, i) a ubiquitous expression in the entire body column (*Nvfoxb and Nvrunt*) (Fig 7ai, 7bi), ii) in the vicinity of the mouth (*Nvaxin-like,Nvsprouty, Nvtwist*) (Fig7ci , 7di, 7ei), iii) in the pharynx (*NvHd050, Nvmae-like*) (Fig 7fi, 7gi) and iv) physa (*NvfgfA2*) (Fig 7hi). Interestingly the genes already expressed ubiquitinously and near the mouth have their expression restricted to body wall epithelium at the amputation site at 20hpa (Fig 7aii – 7ei) (e.i nom des genes), while the genes already expressed at the pharynx have their expression domain relocate to the mesenteries during regeneration (Fig 7fii, 7gii) (e.i nom des genes) and the expression in the physa remain unchanged (Fig 7hii) (e.i nom des genes). But after a continuous treatment with U0126 from 0 to 20hpa, except for *NvHd050* still present in the mesenteries (Fig 7fiii), all the studied genes in this experiment are no longer expressed regardless of the expression domain at 20hpa (Fig 7aiii – 7hiii).

This comparison of the expression domain between the uncut animal and the 20hpa polyps, with or without treatment with U0126, suggests that the oral/aboral axis seems to be maintained during regeneration and that MEK/ERK inhibition by U0126 affects all the domains. Taken together, we have identified 39 downstream targets of MEK/ERK and identified four distinct expression domains in regenerating *Nematostella* enabling us to draw a first framework of the gene regulatory network specifically launched at the onset of whole body regeneration in *Nematostella* (Fig. 8). Importantly, our comparison between the embryonic and the regeneration GRNs driven by the MEK/ERK signalling pathway, highlights a regeneration specific network logic that in addition to re-deploying embryonic MEK/ERK downstream targets, co-opts embryonic WNT targets and importantly governs the expression of regeneration specific genes.

Discussion

The main objective of this study was to functionally investigate the historical question about the relationship between embryogenesis and regeneration at a molecular GRN level. To do so, we took advantage of the emergence of a novel complementary whole body regeneration model *Nematostella vectensis* that is particularly well suited to address this line of inquiry at the molecular and functional levels (Layden, Rentzsch, and Röttinger 2016). *Nematostella* has originally been used as a model to study the evolution of developmental process (Layden, Rentzsch, and Röttinger 2016). Thus, a wealth of functional data have been obtained enabling us to establish a comprehensive GRN underlying germ layer specification, neurogenesis and axial patterning at the onset of the morphogenetic movements of gastrulation in *Nematostella* (Röttinger, Dahlin, and Martindale 2012; Layden et al. 2016; Amiel et al. 2017). One of the key signalling pathways involved in the coordination of the above mentioned developmental processes in *Nematostella* is the MEK/ERK pathway (Layden et al. 2016; Amiel et al. 2017). A recent unbiased large-scale bio-informatics analysis comparing embryonic development and regeneration of *Nematostella* has suggested that the regeneration GRN reuses embryonic components but in a dramatically rewired manner (Warner et al. 2018), (Warner et al, in submission). Our current data focus on the GRN driven by MEK/ERK signalling pathway during regeneration and its comparison with the one that have been established during embryogenesis. A recent unbiased large-scale bio-informatics analysis comparing embryonic development and regeneration of *Nematostella* has suggested that the regeneration GRN reuses embryonic

445 components but in a dramatically rewired manner (Warner et al. 2018),
446 Warner et al, BioRXiv). Our current data not only verify and validate this
447 hypothesis. We therefore i) deciphered the role of MEK/ERK signalling in
448 response to the amputation stress in *Nematostella*, ii) determined a relevant
449 comparison point between regeneration and embryogenesis, iii) identified
450 downstream targets of MEK/ERK signalling at the onset of regeneration
451 enabling us to draft a first whole body regeneration GRN and iv) compare it to
452 the MEK/ERK GRN module underlying *Nematostella* embryogenesis. Using
453 this approach, our data functionally show that core elements of the embryonic
454 gene regulatory network are partially re-deployed and connected to
455 regeneration specific elements in order to reform a functional organism.
456

457 **Distinct implications of the MEK/ERK signalling in various steps of**
458 **regeneration.**

459 The present work has revealed that MEK/ERK signalling in *Nematostella* is
460 activated in immediate response to amputation and its inhibition has only
461 limited impact on wound healing as wound closure is delayed for few hours. In
462 a similar manner, Dubuc and colleagues have reported a rapid activation of
463 MEK/ERK after puncture of the body wall epithelia of *Nematostella* (DuBuc,
464 Traylor-Knowles, and Martindale 2014). In contrast however, it appears that
465 blocking MEK/ERK signalling in those conditions prevents wound closure
466 (DuBuc, Traylor-Knowles, and Martindale 2014). This divergent observation
467 might either be linked to the different injury context (puncture - (DuBuc,
468 Traylor-Knowles, and Martindale 2014) *vs* amputation - this study) or the
469 timing of assessing wound healing success (6hpi - (DuBuc, Traylor-Knowles,

and Martindale 2014) *vs* 10hpa - this study). Nonetheless, those results clearly show that pERK activation is a conserved injury response feature among metazoans. In fact, pERK is activated immediately after amputation at the injury site in *Hydra* (Manuel et al. 2006; Petersen et al. 2015), planarian (Tasaki et al. 2011; Agata et al. 2014; Owlarn et al. 2017) as well as in vertebrates models regeneration (zebrafish heart regeneration (liu2017), axolotl spinal cord regeneration (Sabin2016). It is interesting to note that in planarians, a recent study has shown that inhibition of MEK/ERK does not block wound-healing neither (Owlarn et al. 2017). This observation suggests that the involvement of this signalling pathway in a generic wound response (Owlarn et al. 2017) is conserved among whole body regeneration models, without being essential for wound closure.

While not being essential for wound healing in *Nematostella*, we have nonetheless revealed that the MEK/ERK pathway is crucial for tissue remodelling, launching the genetic network and maintaining proliferative activity in order to reform tissues and body parts. More precisely, we showed that during regeneration *per se*, this pathway has two distinct roles; in a cell proliferation-independent manner during the transition from step 0.5 to step 1 and in a cell proliferation-dependent manner during the transitions of later steps (Fig 2c). Importantly, these results are in line with previous observations describing proliferation-independent (wound healing and initiation of regeneration up to stage 1) one proliferation-dependent phases (reformation or lost body parts) of the wound healing/regeneration process in *Nematostella* (Amiel et al. 2015). Further analysis of the upstream activator of MEK/ERK

494 and the downstream effectors in each context will contribute to have a better
495 understanding of how this single pathway is reused in multiple contexts.
496 MEK/ERK signalling has been shown to activate programmed cell death
497 (apoptosis) in the well known cnidarian whole body regeneration model
498 *Hydra*, causing the release of Wnt3 and the induction of cellular proliferation
499 at the amputation site (Chera et al. 2009; Kaloulis et al. 2004). In
500 *Nematostella*, puncture or sub-pharyngeal amputation induces apoptosis
501 shortly after injury at the wound site (DuBuc, Traylor-Knowles, and Martindale
502 2014) Warner et al, in submission). In contrast to *Hydra* though, in none of the
503 two wounding conditions U0126 treatment has a visible effect on the
504 activation of apoptosis after injury (DuBuc, Traylor-Knowles, and Martindale
505 2014). These results are in line with our results showing that inhibition of
506 apoptosis using Z-VAD blocks the onset of proliferation (Amiel et al. BioRXiv),
507 while inhibition of MEK/ERK using U0126 does not affect the onset but the
508 maintenance of the stress induced mitotic activity (this study). This scenario is
509 compellingly similar to what has been observed in planarians. In fact, in this
510 whole body regeneration model amputation-induced pERK activation is
511 required for tissue remodelling and regeneration-associated proliferation,
512 however, not for wound healing, the induction of apoptosis or the onset of
513 wound-induced proliferation (Owlarn et al. 2017). Overall these results
514 suggest a conserved early apoptosis-independent role of MEK/ERK signalling
515 in *Nematostella* and planarians for creating the proper conditions to initiate
516 and maintain the regeneration program after wound healing. This appears
517 different to the apoptosis-dependent role in *Hydra*. Thus, further studies using
518 additional whole body regeneration models are required to gain additional

519 insight into the evolution of the role(s) of MEK/ERK signalling in launching the
520 reformation of lost body parts.

521 **Potential activators of MEK/ERK signalling during regeneration**

522 The analysis of the role of MEK/ERK during regeneration has highlighted
523 several events regulated by this pathway. Notably it is implicated in the
524 response to injury by controlling gene expression (DuBuc, Traylor-Knowles,
525 and Martindale 2014), participating in timely wound healing (Fig 2a), the
526 transition to step 1 (Fig 2c, 2e) and also for maintaining of cell proliferation in
527 later steps (Fig 3h, 3i). This naturally questions the upstream signals of
528 MEK/ERK during these different events.

529 Receptor Tyrosine Kinases are largely associated with the activation of
530 MEK/ERK signalling in a large variety of physiological and pathological
531 contexts (Lemmon and Schlessinger 2010). We thus investigated the RTKs
532 present in the genome of *Nematostella* and analysed their expression
533 patterns during regeneration. A previous study has described a total of 19
534 metazoan RTK families, of which 10 contain cnidarian orthologs (D'Aniello et
535 al. 2008). In order to gain insight into the entire RTK complement of
536 *Nematostella,* we screened the genomic (Putnam 2007) as well as
537 transcriptomic resources (Warner et al. 2018) and identified genes encoding
538 for 26 putative RTKs (Supp Table 1). We further performed a phylogenetic
539 tree analysis using the predicted kinase domains (Supp Fig 1) and confirmed
540 the existence of 9/10 cnidarian RTK families. Interestingly, among the growth
541 factor receptors of *Nematostella*, we noticed the absence of members of the
542 Pdgfr or Vegfr families. Instead, we confirmed the presence of four genes
543 related to both families, previously described *as pdvegfr-like* genes (D'Aniello

et al. 2008). While most *Nematostella* genes clustered to one or the other RTK family, three genes were not directly linked to any of the distinct families; two of them that are closely related to the DDR subclass, named ddr-likeA and ddr-likeB and one, named rtk8, that does not cluster with any family and thus, possibly representing a cnidarian or *Nematostella* specific RTK.

By taking advantage of a recently developed *Nematostella* embryogenesis and regeneration transcriptomic database (nvertx.kahikai.org, (Warner et al. 2018) we extracted the temporal expression profiles for each identified RTK (Table S1). Out of the nine defined co-expression clusters (Warner et al. 2018), Warner et al. in submission), the identified RTKs are distributed in six of them; R1 (1 out of 26, upregulation between 4-8hpa), R3 (5 out of 26, upregulation between 24-120hpa), R4 (3 out of 26, progressive downregulation between 16-96hpa), R6 (12 out of 26, two peaks of upregulation at 4 and 20hpa), R8 (3 out of 26, one peak of upregulation at 4hpa) and R9 (2 out of 26, progressive downregulation between 0-24hpa followed by a progressive upregulation). A part from the whole Fgfr family (*NvfgfrA*, *NvfgfrB* and *Nvfgfr-like*) found in the regeneration cluster R6, we did not observe any expression cluster preference associated to the RTK family; 3 out 5 Eph in R6, 3 out 5 Tie in R3 and 2 out of 4 Pdvegfr-like in R8 (Fig.S2). Nevertheless, those temporal expression patterns indicate that the identified RTKs are expressed at every stage of regeneration, from early injury-response (R1, R6, R8) to early (R6) and late (R3, R9) regeneration steps. This in turn suggests a possible and complex activation cascade of MEK/ERK during *Nematostella* wound healing and regeneration that is orchestrated by the various identified RTKs.

To pursue this line of inquiry, we performed a more detailed expression analysis of the growth factor receptor families Fgfr and Pdvegfr-like as well as their potential ligands by whole mount *in situ* hybridization. Both of the expression profile of Nvpdvegfr-like A and NvpdvegfrlikeD display a pic at 2hpa (Fig.S1b) and their expression domain is restricted to the AE (Fig. S1c, S1d). While *Nvvegf-like* and *Nvvegf-like2* also present an expression pic at 2hpa (Fig.S1e) but the localization is on the gastrodermis side (Fig.S1f, S1g). These expression profiles are suggesting a crosstalk between the two epithelium at the amputation site, potentially involved in the wound healing response or an early regeneration response starting at 2hpa. But more precise gene specific perturbation experiments are needed in the future to understand the precise activation/crosstalk of RTKs and pERK.

Rewired re-deployment of the embryonic GRN during whole body regeneration

Recent studies on the role of MEK/ERK/Erg signalling during embryonic development in *Nematostella* has highlighted the crucial implication of this pathway in specifying and invaginating the endomesoderm, specifying the nervous system and axial patterning prior to the onset of gastrulation (Layden et al. 2016; Amiel et al. 2017). In the following section we will discuss to what extend these roles have been maintained during the regenerative process.

Tissue re-specification and morphogenetic movements

Comparing two developmental trajectories such as embryonic development and regeneration naturally raises the questions about the

potential comparable analogies of these processes. Besides terminal differentiation that must lead to the identical cellular and physiological functions, the early phases of wound-response and regeneration initiation are particularly difficult to analogize {Vervoort:2011ch}. Indeed, embryonic development begins with the fertilization of a totipotent cell (the oocyte), while wound healing/regeneration is initiated by the physical stress of amputation in a tissue that is defined by its positional information and that is composed of terminally differentiated and in most cases lineage specific progenitor and/or multi-potent stem cells. Nonetheless, in our study we were able to define roles of MEK/ERK signalling during embryogenesis and regeneration that may represent analogous features in both trajectories.

By focusing on the role of MEK/ERK in the launch of the regenerative program we observed that this pathway is crucial for the tissue rearrangement leading to the contact of the mesenteries with the amputation epithelia (step 1, Fig. 3b, (Amiel et al. 2015). This might be comparable to the morphogenetic movements of gastrulation that is blocked when embryos are treated with U0126 (Layden et al. 2016). During embryonic *Nematostella* development, MEK/ERK/Erg signalling is required for specifying endomesoderm and it has been proposed that the role of this pathway in the onset of gastrulation is indirectly caused by the missing germ layer (Amiel et al. 2017). The same logic can also be applied for the mesenterial movement towards the amputation epithelia as the lost *NvfoxB* (Fig 7aiii)*, Nvrunt* (Fig 7biii)*, Nvaxin-like* (Fig 7ciii) and *Nvtwist* (Fig 7eiii) gene expression at the amputation site gastrodermis may indicate the loss of tissue re-specification that in turn is required for triggering these tissular rearrangements. Interestingly, the

phenotypes of U0126 in both developmental trajectories affect morphogenetic movements (direct or indirect) without impairing cellular proliferation ((Layden et al. 2016), this study). Further investigating this relationship between tissue specification and morphogenetic movement will help strengthening the analogy of the implication of MEK/ERK signalling during both developmental during both developmental trajectories.

Following this analogy, we performed qPCRs at 20hpa during the transition towards step 1. Interestingly, all downstream targets of MEK/ERK normally expressed in the forming and invaginating endomesoderm during embryonic development (Amiel et al. 2017)that are also highly expressed at 20hpa, are with only one exception all down regulated by U0126 during regeneration (Fig. 5b, 5e). When we reused the same workflow at 48hpa, as we did at 20hpa, with the 88 embryonic MEK/ERK downstream targets, when MEK/ERK is required for regeneration maintaining cell proliferation, not all genes are downregulated following U0126 treatments (Fig.S2). These result suggest a different rewiring, compare to 20hpa, of these embryonic genes at 48hpa (Table S2). Taken together this further supports the analogous role of MEK/ERK between the onset of gastrulation and the onset of regeneration and that the underlying network at 20hpa is more related to the embryonic network than the network downstream of MEK/ERK at 48hpa.

In addition to embryonic MEK/ERK downstream targets, we also identified embryonic cWNT downstream targets (Röttinger, Dahlin, and Martindale 2012) as well as regeneration specific genes (Warner et al. in submission) that are highly upregulated at 20hpa (Table 2 and Table 3). Their characterization at 20hpa, as well as their response to inhibition of MEK/ERK signalling during

643 regeneration led to the assembly of the first GRN framework underlying the
644 initiation of whole body regeneration (Fig 8). Surprisingly, but in line with the
645 potential analogy described above, more than half (14/25) of the genes
646 expressed in the amputation gastrodermis (AG) and/or the mesenteries (M)
647 such as *runt, axin-like, musk-like, porcupine-like, smad4-like, sprouty, fz10,*
648 *nkd1-like, mae-like, bicaudalC-like, hd050, phtf1-like, pdvegfr-like* and *fox1*,
649 have previously been described to be part of the central domain at the onset
650 of gastrulation (Röttinger, Dahlin, and Martindale 2012; Amiel et al. 2017).
651 However, while all of them are MEK/ERK downstream targets during
652 regeneration (Fig. 5), it is important to note that not all of them are embryonic
653 MEK/ERK downstream targets. Indeed, 12 out of 28 are embryonic cWNT
654 downstream targets that have been integrated into the MEK/ERK GRN
655 module during regeneration. This observation further supports the rewiring of
656 the embryonic GRN during regeneration.

657 **Axial patterning along the oral-aboral axis during regeneration**

658 During embryonic development MEK/ERK/Erg signalling controls 23
659 genes, such as *Nvfgfa, Nvsix3/6, Nvfz5/8,* that are involved in axial patterning
660 of the embryo/larva (Amiel et al. 2017; Rentzsch et al. 2008; Sinigaglia et al.
661 2013; Leclère et al. 2016). While during the onset of oral regeneration these
662 aboral genes are not upregulated at 20hpa and not downstream of MEK/ERK
663 either such is the case of Nvsix3/6 (Fig. 5b). Therefore suggesting that the
664 program underlying embryonic aboral patterning is not required during oral
665 regeneration.

666 Among those 23 genes, only fgfA2 which was expressed in the aboral
667 domain during embryogenesis (Amiel et al. 2017; Rentzsch et al. 2008;

668 Sinigaglia et al. 2013) is still expressed in the most aboral end of the polyps
669 (Fig. 7hi) and it appears to be upregulated at 20hpa at the tip of the physa
670 (Fig.6z, 7hii). While U0126 treatments block *NvfgfA2* expression in the physa
671 (Fig 7hiii). Hence, suggesting that the oral/aboral axis is maintained during
672 regeneration and an indirect control of MEK/ERK over the aboral domain
673 during regeneration at least. Also it appears that during the homeostasis of
674 the tissue some downstream targets of MEK/ERK are already expressed
675 nearby the mouth ephitelia, such as *Nvaxin-like* (Fig. 7ci), *Nvsprouty* (Fig. 7di)
676 and *Nvtwist* (Fig. 7ei) or in the pharynx *e.i Nvhd050* (Fig. 7fi) and *Nvmae-like*
677 (Fig. 7gi), furthermore supporting the conservation of the oral/aboral axis. In a
678 different manner some downstream targets of MEK/ERK, previously
679 described in the endomesodermal domain at 24hpf (Amiel et al. 2017), seems
680 to be ubiquitiously expressed in the body column *e.i NvfoxB* and *Nvrunt* (Fig.
681 7ai, 7bi). While upon sub-pharyngeal amputation, their expression domain is
682 relocated to the amputation site at 20hpa (Fig. 7aii, bii) suggesting a reuse of
683 the embryonic expression domain.

684 **Neural re-genesis**

685 The MAPK ERK has been described to be also upstream of the
686 neurogenic program occuring before gastrulation (Layden et al. 2016). In this
687 study a precise circuit have been described upstream of *NvashA*-dependent
688 neurogenesis, in which *Nvath-like* and *NvsoxB(2)* are the most upstream
689 genes of the circuit, and 15 additional genes (table S3) with a salt and pepper
690 expression profile. Among these additional genes only *Nvhes1/3* is
691 upregulated at 20hpa and is at the same time downstream of MEK/ERK at
692 20hpa (Fig. 5b, 5e) and at 48hpa (Fig. S2). While *Nvath-like* is upregulated at

48hpa (table S3) without being downstream of MEK/ERK (Fig. S2). Moreover the embryonic cluster of these salt and pepper genes (table S3) have no correlation with their regeneration clusters. Beside all these genes are highly expressed at 24hpf before gastrulation in contrast to regeneration where the regeneration clusters have various activation time points *e.i,* R6, R5, R3, R2 (nvertx.kahikai.org, (Warner et al. 2018)). Overall these data are supporting the idea of a different network underlying the neural re-genesis during regeneration in comparison to the embryonic neurogenic program.

Interestingly during regeneration the genes are clustered between the regeneration clusters R6 (*Nvpea3-like, NvsoxB(2*)), R5 (*Nvcouplike1, Nvath-like, Nvhes3*), R3 (*Nvcouplike2, Nvgcm, Nvhd145*) and R2 (*Nvsox10-like, NvpaxA, NvashA, Nvhes-like3, nvfoxD3-like, Nvsox2*) (Table S3). Which all have an activation phase after different time point *e.i,* 8hpa, 16hpa, 24hpa and 36hpa respectively, thus suggesting that the neurogenic program occurring before gastrulation seems to be stretched during regeneration. Even though the most upstream genes of the *NvashA*-dependent neurogenesis circuit, *NvsoxB*(2) and *Nvath-like* still belongs to the earliest activated regeneration cluster.Altogether these preliminary data on putative neurogenic program during regeneration are suggesting a different wiring in comparison to embryogenesis but a more precise characterization their spatial and temporal expression profile is still required.

Regeneration specific re-wiring of the embryonic GRN

Using an unbiased large-scale bioinformatics approach to compare embryonic and regeneration gene expression at a global scale, a recent study has shown that regeneration is a partial redeployment of regeneration, has

identified a list of genes with a regeneration specific expression dynamics and importantly, has suggested that regeneration follows a regeneration specific network logic (Warner et al. 2018). The present work functionally tested and validated this hypothesis by dissecting the role of the MEK/ERK signalling pathway during embryonic development and regeneration in the same organisms, the sea anemone *Nematostella*. We have characterised the role of MEK/ERK during regeneration and identified a potential analogous implication in germ layer/tissue specification and the coordination of morphogenetic movements, the absence of an axial patterning program (not needed) and a disconnected neural program. We have further shown at a signalling pathway scale, that indeed regeneration is a partial re-activation of the embryonic program. Importantly, our data functionally validate the re-wiring of the embryonic network as MEK/ERK signalling during regeneration integrates embryonic cWNT genes. During embryogenesis, MEK/ERK and cWnt signalling have both been described to be involved in endomesoderm formation and patterning the primary axis (Wikramanayake et al. 2003; Lee et al. 2007; Röttinger, Dahlin, and Martindale 2012; Leclère et al. 2016; Layden et al. 2016; Amiel et al. 2017). While both pathways are important for those developmental processes, their downstream targets display no overlap with the exception of 14 genes antagonistically regulated by both pathways (Röttinger, Dahlin, and Martindale 2012; Layden et al. 2016; Amiel et al. 2017). Moreover, during embryogenesis cWnt signalling appears to be active prior to MEK/ERK signalling (Röttinger, Dahlin, and Martindale 2012; Leclère et al. 2016; Layden et al. 2016; Amiel et al. 2017). Thus it is intriguing to see that during regeneration their respective downstream targets are redeployed at the

743 same time (20hpa) and that now MEK/ERK signalling controls members of
744 both embryonic pathways. To get a better idea of the extend of rewiring,
745 additional experiments are required to decipher the role of cWnt signalling
746 during regeneration, to understand the cWNT network module and to see if
747 the chronological order of cWnt and MEK/ERK pathway activation is
748 conserved, synchronized or inverted.

749 The ultimate evidence of a regeneration specific network logic comes
750 from our results showing that genes with regeneration specific expression
751 dynamics (Warner et al. in submission) are expressed at 20hpa and part of
752 the MEK/ERK downstream gene network. Among those genes one, Nvbax,
753 has been associated to apoptosis ((Moya et al. 2016). Functional studies
754 blocking apoptosis during embryogenesis and regeneration has revealed that
755 programmed cell death is specifically required for very early phases of
756 regeneration and not for embryonic development (Warner et al. in
757 submission). This observation suggests that additional members of the
758 MEK/ERK regeneration GRN may have specific roles in initiating the whole
759 body regenerative response in *Nematostella*. Thus, additional functional and
760 *cis*-regulatory studies are required to properly understand this regeneration
761 specific network logic and enable us to discover regeneration specific
762 regulatory elements that could be use to control pro-regenerative factors, as it
763 has recently been done to modulate the regenerative potential of vertebrate
764 organs (Kang et al. 2016).

Figures

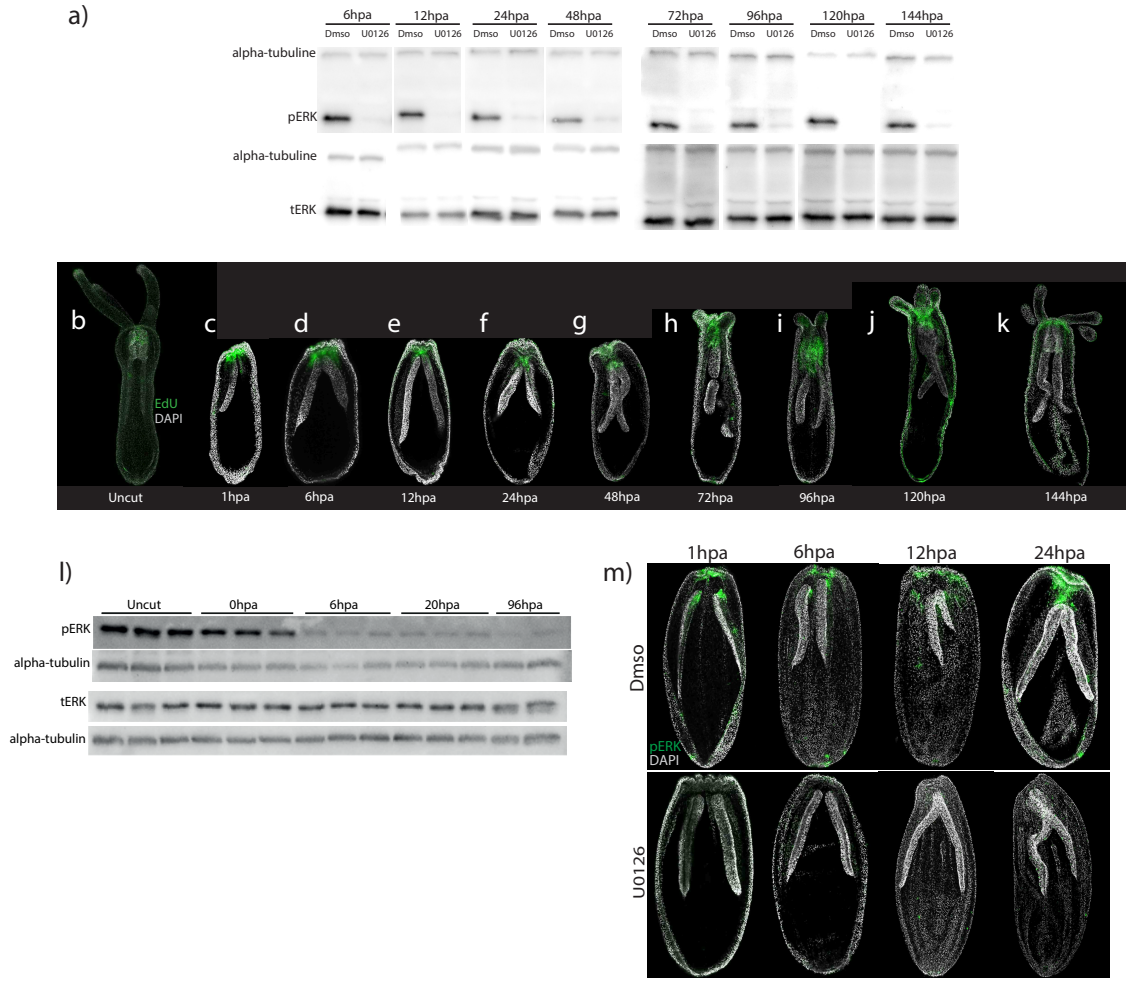

Figure 1: pERK expression profile during regeneration and after inhibition with U0126. a) Western blots against the phosphorylated form of ERK (pERK) and total ERK (tERK). Alpa-tubulin is used as a loading control in both pERK and tERK. The protein were extracted from control treated polyps (0.1%Dmso) or treated animals with 10µM U0126 (U0126), at 6hpa, 12hpa, 24hpa,48hpa, 72hpa, 96hpa, 120hpa and 144hpa. b – k) Immuno-staining against pERK (green) and counter staining with DAPI (grey). The polyps were fixed whole (b) or after amputation at 1 (c), 6 (d), 12 (e), 24 (f), 48 (g), 72h (h), 96 (i), 120 (j) and 144h (k). l) Immuno-staining against pERK and DAPI counter staining of the nuclei at 1, 6, 12, and 24hpa comparing the control treated (0.1%Dmso) to polyps treated with 10µM of U0126 after sub-pharyngeal bisection.

a)

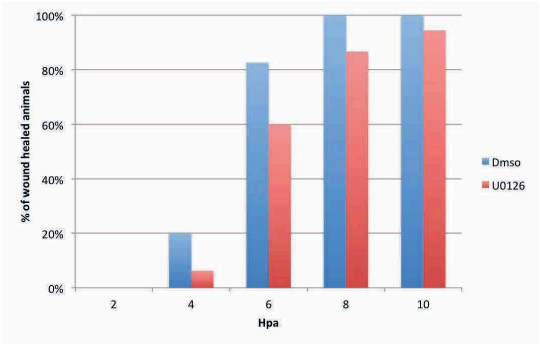

Dmso	0/25	4/20	19/23	25/25	23/23
U0126	0/31	2/32	15/25	13/15	17/18

b)

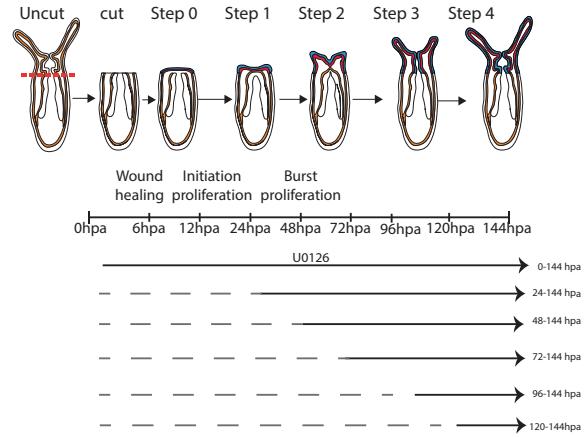

c)

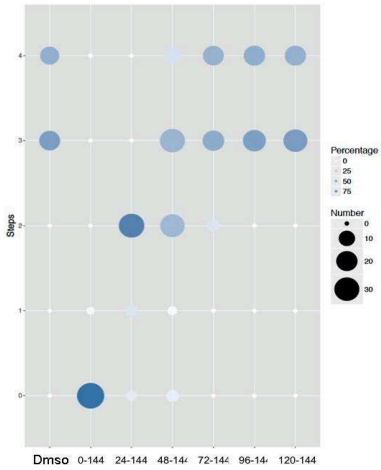

d)

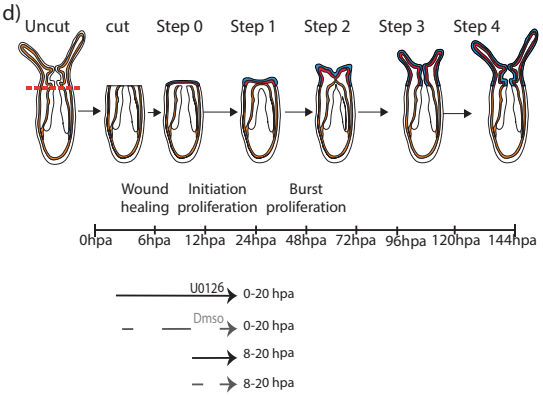

e)

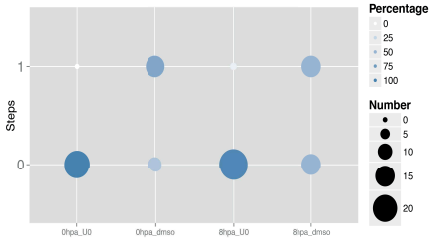

Figure 2: Effect of MEK inhibition by U0126 at the tissuelar level and on the wound healing.

a) Regeneration diagram of the tissular and cellular hallmarks of N.vectensis regeneration; step 0: the mesenteries and the body wall epithelium of the amputation site a separated, step 1: connection between the mesenteries tips and the body epithelium at the amputation site which display a characteristic depression, step 2: appearance of the tentacles buds, step 3: elongation of the tentacles buds and formation of the pharyngeal lip and step 4 elongation of the tentacles and formation of the pharynx with a mouth opening. Underneath the regeneration diagram is represented the associated workflow of MEK's inhibition after various time of regeneration e.i 24hpa, 48hpa, 72hpa, 96hpa and 120hpa. b) Dot plot displaying the distribution of the five regeneration steps at 144hpa, within each treatment with 10µM of U0126 compared to control condition with Dmso (0.1%Dmso). The five steps are placed on the y-axis and the different treatment are displayed on the x-axis. The size of the dots represent the number of polyps per steps per treatment and the bleu shade defines the percentage each of polyps per steps per treatment. c) Diagrams of the compression assay results after U0126 treatments (10µM) (in red) compared to control treated Dmso (0.1%Dmso) (in blue) at 2hpa, 4hpa, 6hpa, 8hpa and 10hpa. The exact numbers are reported in the table underneath the graph. d) Regeneration diagram with the performed treatment with U0126 (10µM) between 0hpa and 20hpa or 8hpa and 20hpa (grey solid lines), compared to Dmso control conditions (0.1%Dmso) (grey dash lines). e) Dot plot displaying the repartition of polyps between step 0 and step 1 for the different treatment and associated controls.

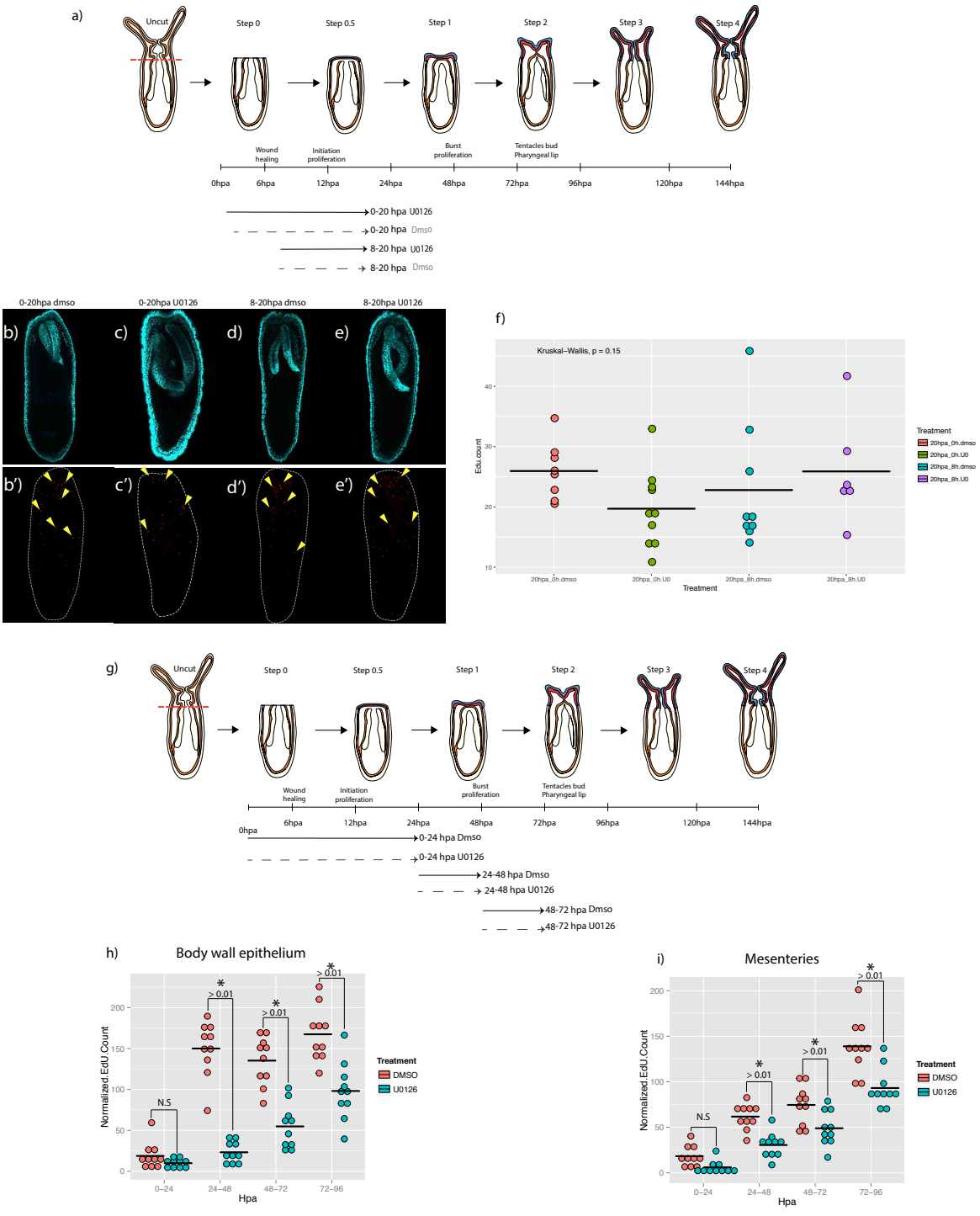

804

805 **Figure 3: EdU staining of proliferation and counting of EdU+ cells after**

806 **inhibition of MEK.**

a) Regeneration diagram with the performed U0126 treatment (10µM) between 0hpa and 20hpa or 8hpa and 20hpa (grey solid lines), compared to the control treatment with 0.1%Dmso (grey dash lines). b-f) DAPI staining of the nuclei (cyan) to visualize the polyp's morphology after treatment with either U0126 (10µM) or 0.1%Dmso. b'-f') EdU staining of proliferating cells (EdU+ in red) in the whole animal delimited by dashed lines. g) Graph of the EdU+ cells counting in the whole polyp after treatments performed in a). The y-axis represent the number of EdU+ cells per 100µM and on the x-axis are all the different treatments while each dot represent a single animal. A Kruskall-Wallis test was performed to assess if there are significant differences between each condition. h) Regeneration diagram with the performed U0126 treatment (10µM) of 24 hours (grey solid lines), compared to the control treatment with 0.1%Dmso (grey dash lines). The polyps were fixed at the end of every treatment. i-j) Graph of the EdU+ cells counting in the whole body wall epithelium (i) and in the whole mesenteries (j) after the treatments performed in h). The y-axis represent the number of EdU+ cells per 100µM and on the x-axis are all the different treatments while each dot represent a single animal. A Student t-test was performed between treatment control of each (* p-value < 0,01, N.S p-value >0.01).

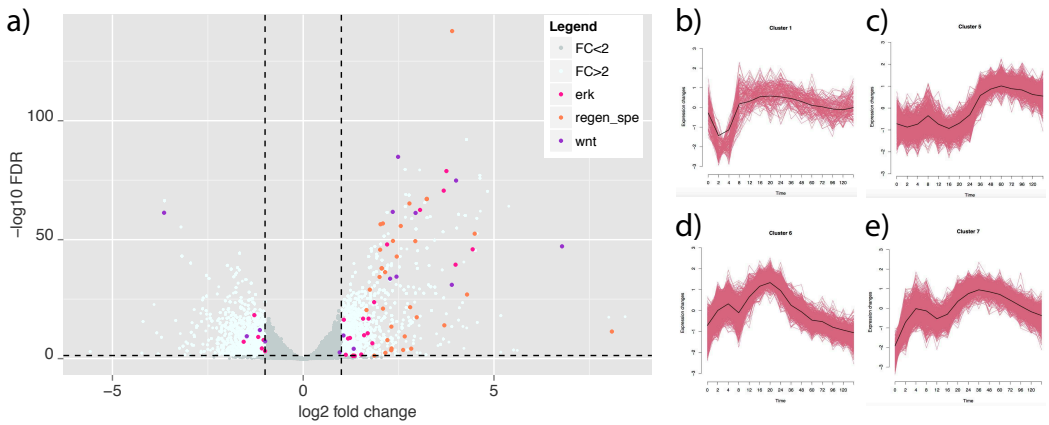

Figure 4: Volcano plot comparing time regeneration time point 0hpa and 20hpa from the regeneration transcriptomic data base NvERTx. a) The transcriptomic data have been extracted from the NvERTx database of *N.vectensis* regeneration (Warner et al., 2018). All the genes with a log2 fold change superior to 1 (vertical dash line) and a –log10 FDR superior to 1 (horizontal dash line) are significantly up regulated or down regulated at 20 hpa compared to 0 hpa (light grey dots) conversely they are not significantly different from 0hpa (dark grey dots). The embryonic downstream targets of erk with an expression level significantly different between 0hpa and 20hpa are in pink, the embryonic downstream targets of wnt with an expression level significantly different between 0hpa and 20hpa are in purple and the regeneration specific genes (regen_spe) with an expression level significantly different between 0hpa and 20hpa are in orange. b-e) Regeneration clusters represented among the all the genes with an upregulation of their expression at 20hpa compared to 0hpa, b) R-cluster 1, c) R-cluster 5, d) R-cluster 6 and e) R-cluster 7.

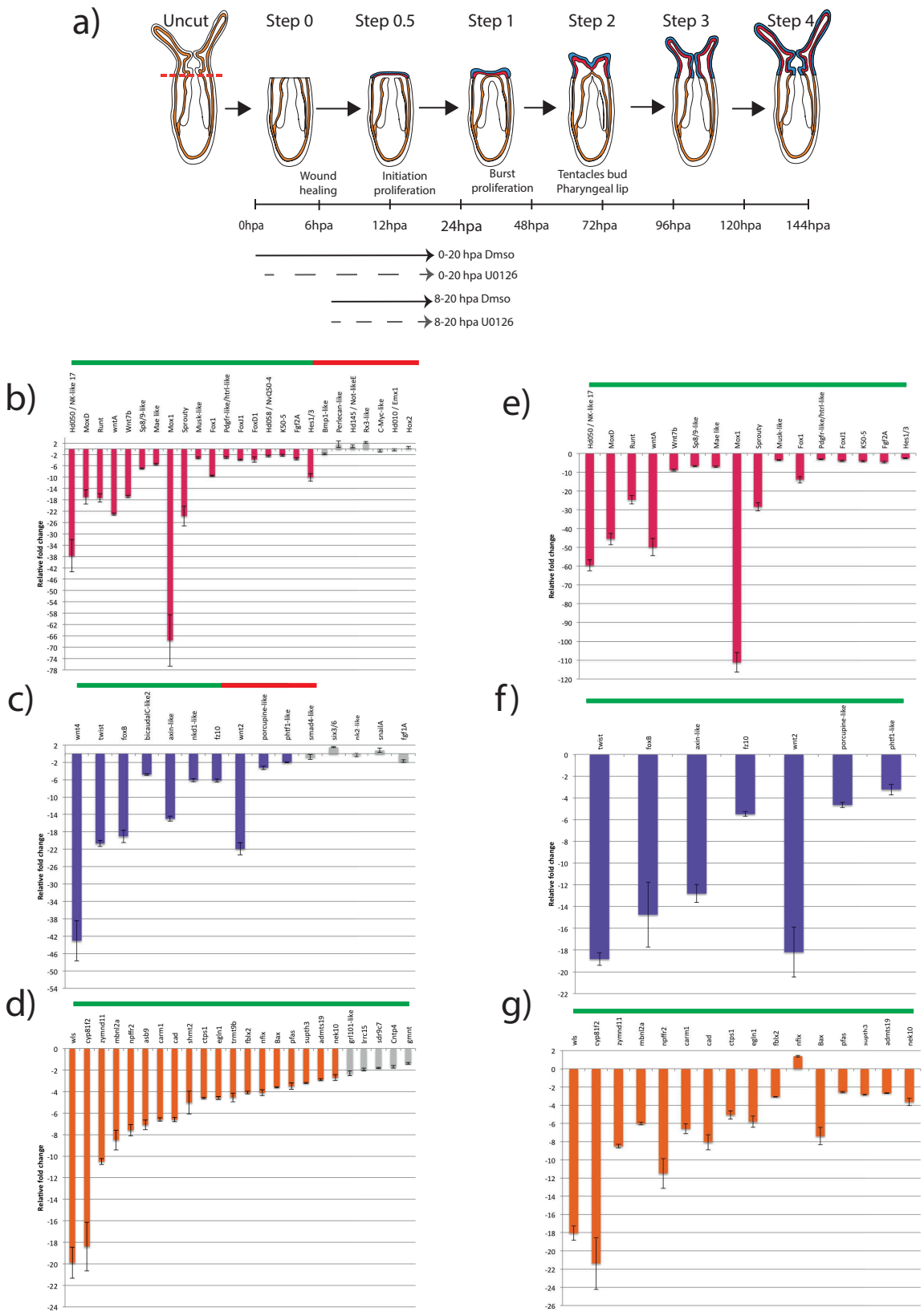

844

845 **Figure 5: qPCR data of the selected candidate genes after inhibition of**

846 **MEK by U0126 before and after wound healing**

847 a) Regeneration diagram and the inhibition experiment of MEK by U0126
848 starting before wound healing (0-20hpa) and after wound healing (8-20hpa). b-
849 d) qPCR performed with the cDNA extracted from the polyps treated with U0126
850 between 0-20hpa. e-g) qPCR performed with the cDNA extracted from the
851 polyps treated with U0126 between 8-20hpa. In b) and e) represent the set of
852 genes from the embryonic downstream target of Erk, c) and f) the set of genes
853 from the embryonic downstream target of wnt and in d) and g) a set of genes
854 from the regeneration specific pool. Each set of genes are composed of genes
855 upregulated between 0-20hpa from the volcano plot (green bar) or
856 downregulated between 0-20hpa from the volcano plot (red bar). The y-axis
857 represent the expression fold change difference between U0126 treated versus
858 the control 0.1% Dmso and the fold change superior to -2 are in grey. e-g) are
859 all the genes from each set with a fold change expression inferior to -2 in the
860 experiement in a).

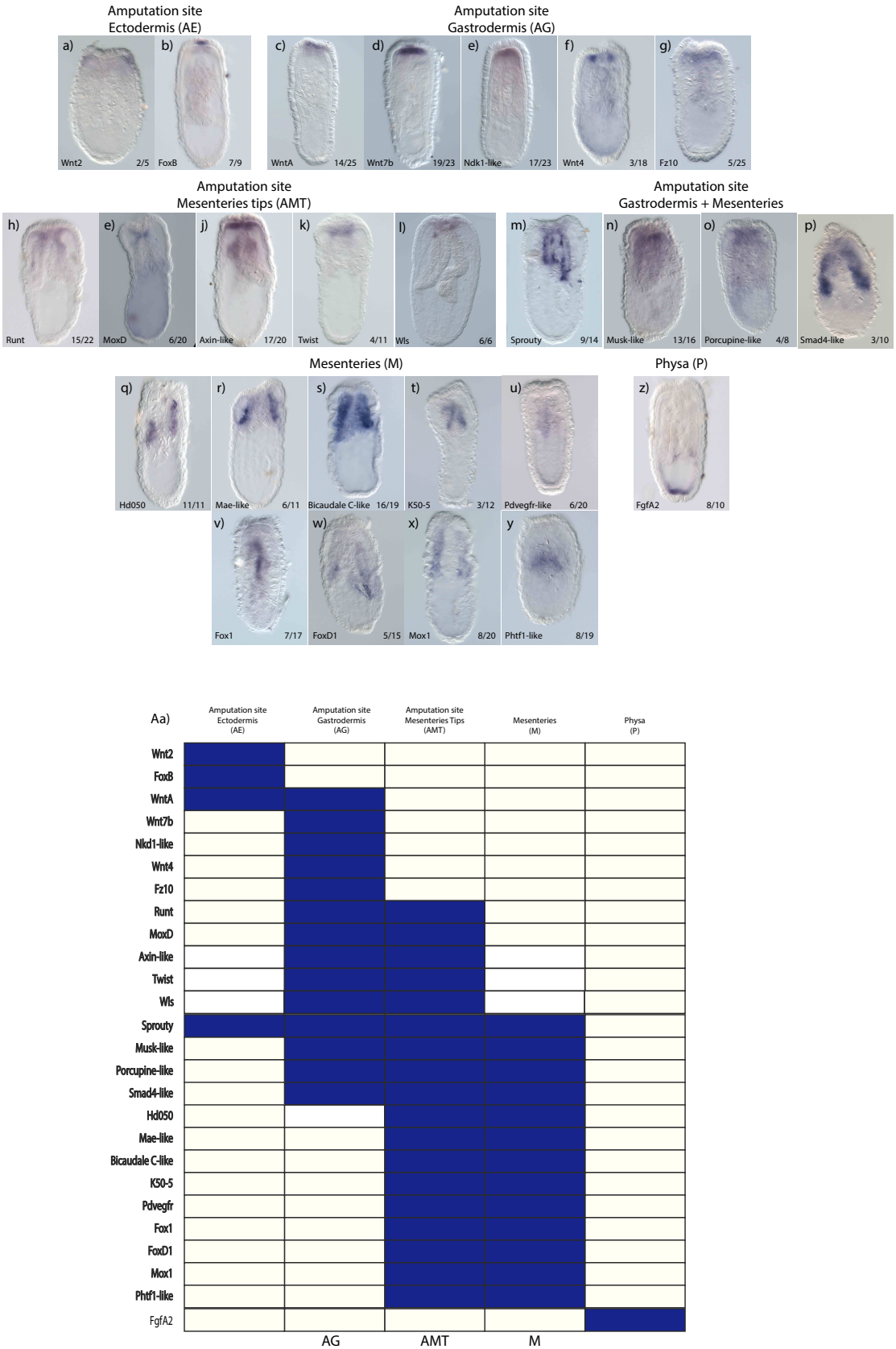

Figure 6: Whole mount *in situ* hybridization of the genes affected by U0126 at 20hpa.

a-b) Genes expressed in the ectodermis of the amputation site (AE). **c-g)** genes expressed in the gastrodermis of the amputation site (AG). **h-l)** genes expressed in the tips of the mesenteries at the amputation site (AMT). **m-p)** genes expressed in the whole mesenteries (M) and the AMT and also the AG. **q-y)** genes expressed only in the mesenteries. **z)** genes expressed at the opposite site of the amputation site in the physa. **Aa)** Matrix of all the expression profile presented in **a-z)**.

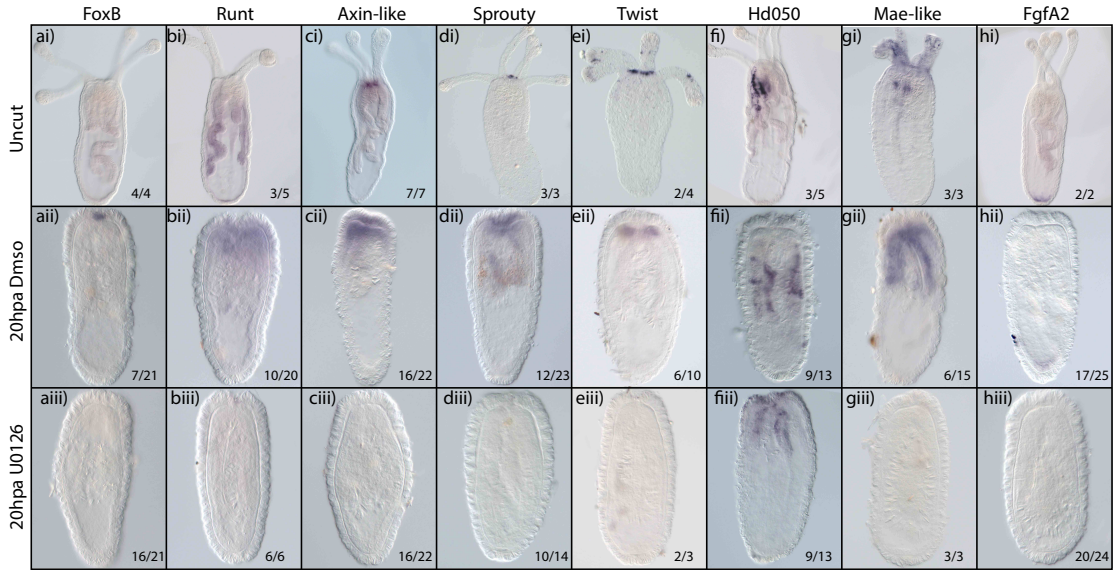

Figure 7: Whole mount *in situ* hybridization after inhibition of MEK by U0126 ai-hi) Genes expression profile in uncut polyps. aii-hii) genes expression profile at 20hpa after control treatment with 0.1%Dmso. aiii-hiii) genes expression profile at 20hpa after a continuous treatment with 10µM U0126.

a)

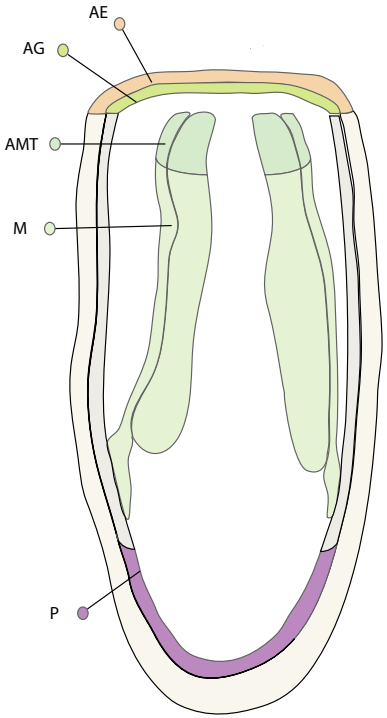

Step 0
20 hpa

b)

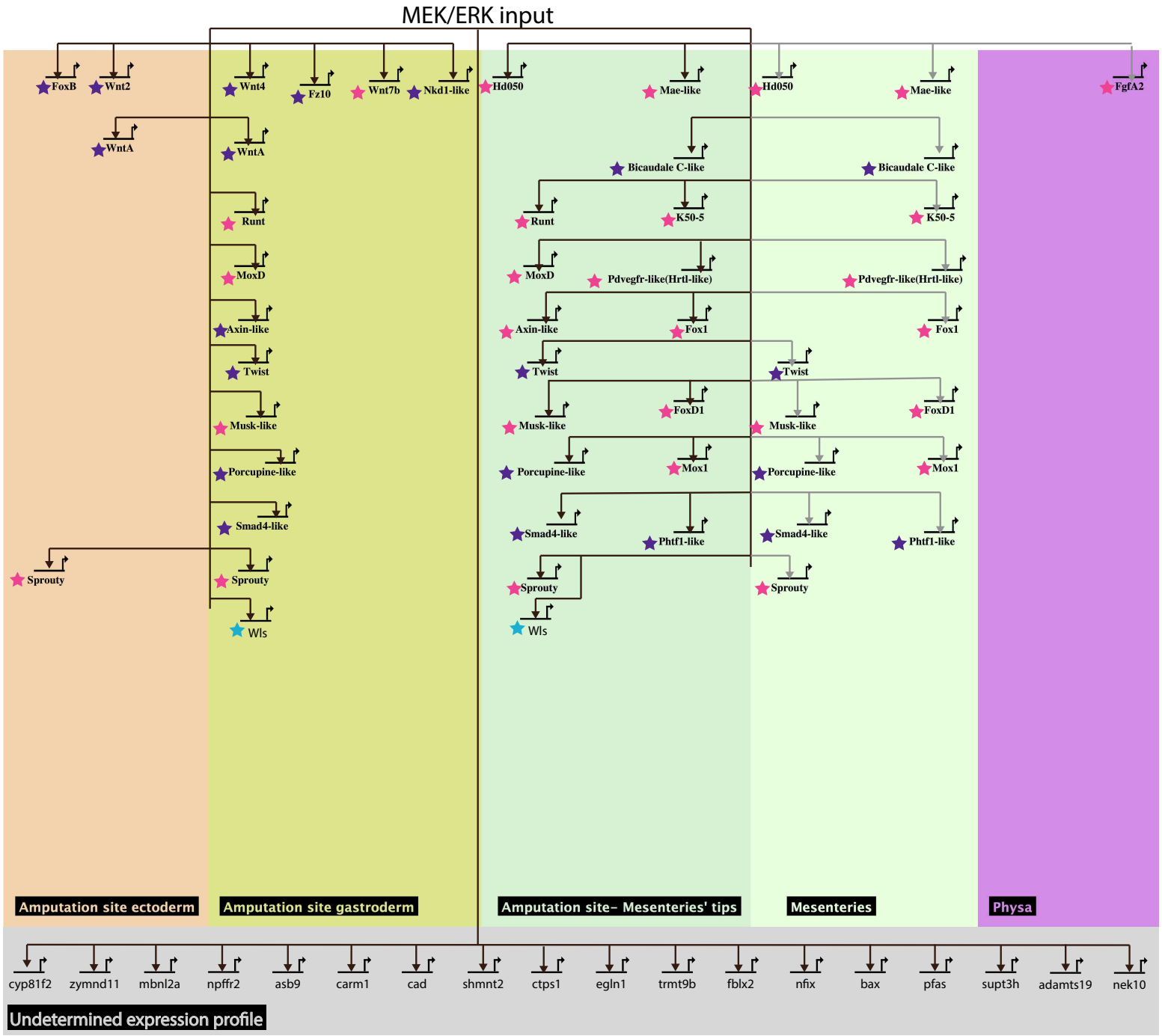

Figure 8: Framework work of the GRN downstream of MEK/ERK inputs during regeneration at 20hpa. **a)** Diagram of a polyp's morphology after a sub-pharyngeal bisection at 20hpa depicting the various expression domains identified by whole mount *in situ* hybridization, AE (orange), AG (green), AMT (pale green), M (light pale green) and P (purple). **b)** Framework work of the GRN downstream of MEK/ERK inputs (brown arrows) during regeneration at 20hpa containing all the genes downregulated by U0126 at 20hpa and from which the expression domain have been identified among which there is the set of genes from the embryonic downstream targets of Erk (pink star), the set of embryonic downstream target of Wnt (purple stars) and the set of regeneration specific genes (blue stars). All the other genes without an identified expression domain are place under GRN framework in the undertermined expression profile (grey zone).

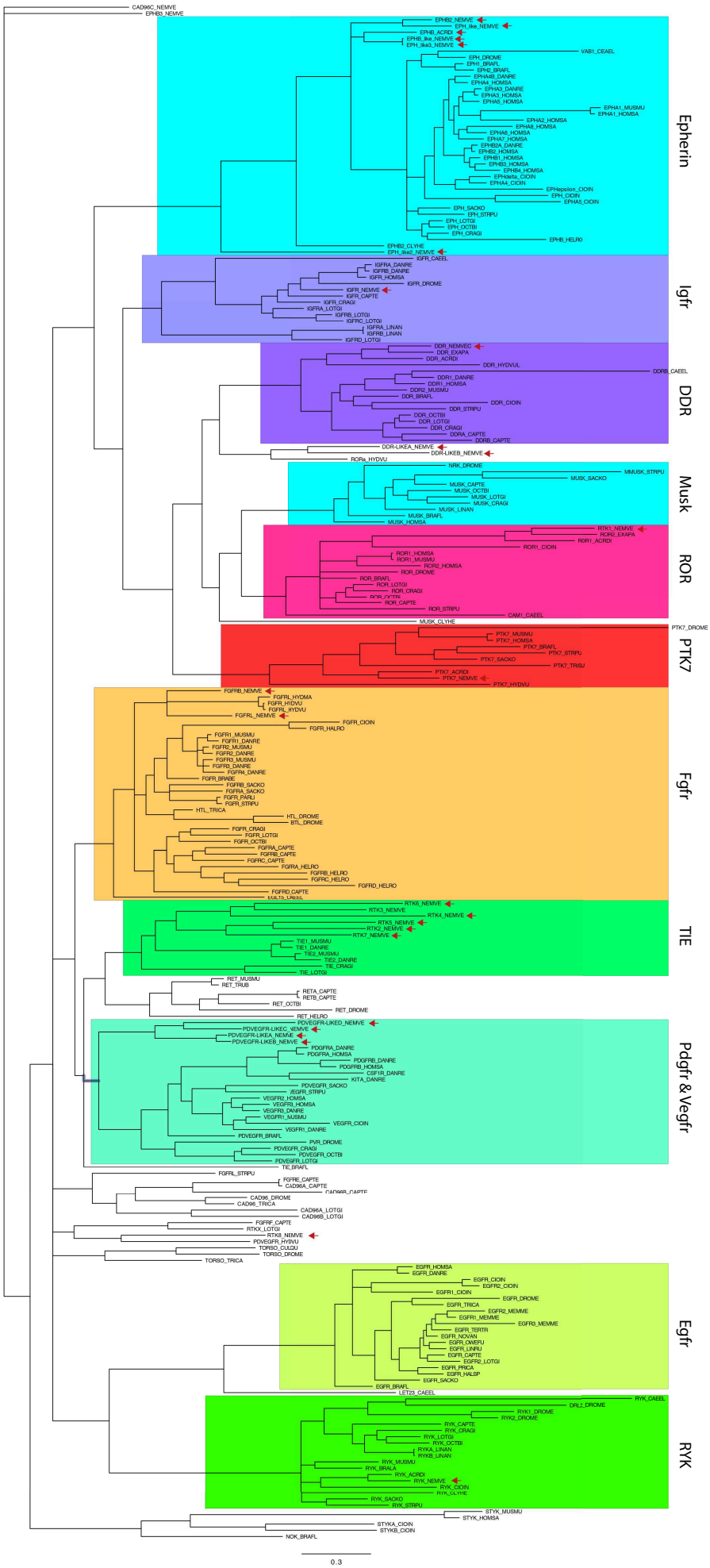
Epherin
Igfr
DDR
Musk
ROR
PTK7
Fgfr
TIE
Pdgfr & Vegfr
Egfr
RYK
0.3

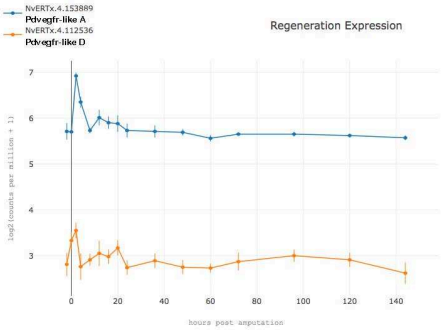
NvERTx.4.153889
Pdvegfr-like A
NvERTx.4.112536
Pdvegfr-like D
Regeneration Expression
log2(counts per million + 1)
hours post amputation

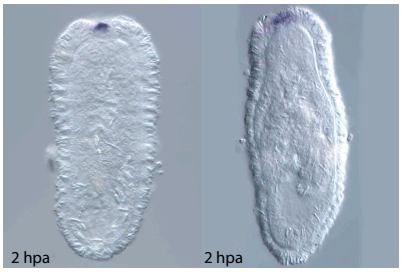
Pdvegfr-like A
Pdvegfr-like D
2 hpa
2 hpa

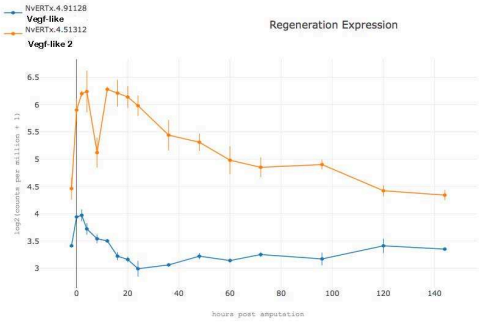
NvERTx.4.91128
Vegf-like
NvERTx.4.51312
Vegf-like 2
Regeneration Expression
log2(counts per million + 1)
hours post amputation

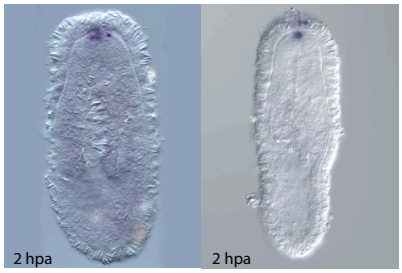
Vegf-like
Vegf-like2
2 hpa
2 hpa

Figure S1: Phylogeny of Nematostella RTK members A) Phylogenetic analysis based on the kinase of domain of 11 RTK familly : Epherin, Igfr, DDR, Musk, ROR, PTK7, Fgfr, TIE, Pdgfr, Vegfr, Egfr and RYK. SYK members has been used as outgroup. The 26 RTK of Nematostella are indicated with an red arrow. B) Transcripts expression profile of 2 members of Nematostella Pdvegfr-like family, Pdvegfr-like A (bleu) and Pdvegfr-likeD (orange) with their spatial expression profile at 2hpa. C) Transcripts expression profile of 2 putative ligand of Nematostella Pdvegfr-like family, Vegfr-like (bleu) and Vegfr-like2 (orange) with their spatial expression profile at 2hpa.

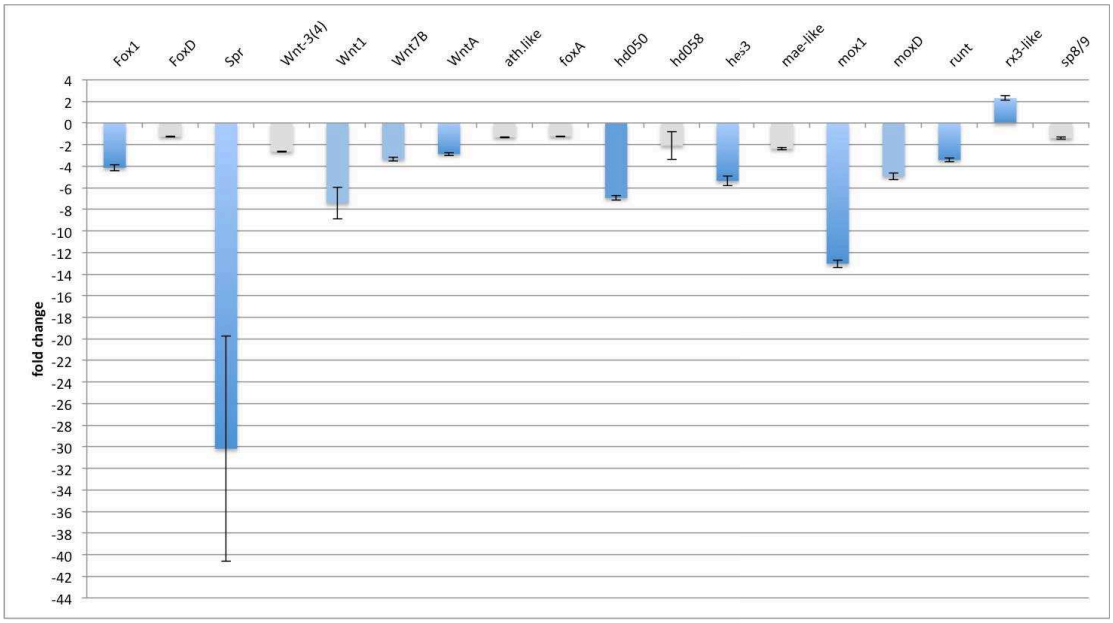

Figure S2: qPCR at 48hpa on juveniles treate with U0 between 24-48hpa. Embryonic downstream targets of MEK/ERK upregulated at 48hpa (Table S2). The genes significantly affected by U0126 are in blue while the non-affected are in grey.

905 Table 1: Embryonic downstream targets of MEK/ERK significantly regulated at
906 20hpa. The genes from the list of downstream targets of MEK/ERK from
907 (Layden et al. 2016) was queried against the regeneration transcriptomic
908 data. All the genes with a significant fold change superior to 2 (up- and down-
909 regulate) between the time point 0hpa and 20hpa are listed.
910
911 Table 2: Embryonic downstream targets of cWnt significantly regulated at
912 20hpa. The genes from the list of downstream targets of cWnt from (Röttinger,
913 Dahlin, and Martindale 2012) was queried against the regeneration
914 transcriptomic data. All the genes with a significant fold change superior to 2
915 (up- and down- regulate) between the time point 0hpa and 20hpa are listed.
916 Table 3: Regeneration specific genes significantly regulated at 20hpa. The
917 genes from the list of regeneration specific genes from Warner et al. in
918 submission was queried against the regeneration transcriptomic data. All the
919 genes with a significant fold change superior to 2 (up- and down- regulate)
920 between the time point 0hpa and 20hpa are listed.
921
922 Table S1: Identified RTK in *Nematostella* genome. List of RTK from the
923 Nematostella genome analysed in the phylogenetic analysis of RTK families.
924
925 Table S2: Embryonic downstream targets of MEK/ERK significantly regulated
926 at 48hpa. The genes from the list of downstream targets of MEK/ERK from
927 (Layden et al. 2016) was queried against the regeneration transcriptomic
928 data. All the genes with a significant fold change superior to 2 (up- and down-
929 regulate) between the time point 0hpa and 48hpa are listed.

Table 1: Embryonic downstream targets of MEK/ERK significantly regulated at 20hpa

NvERTx.4	Gene name	R_Clust	Foldchange20hpa	Nemve1_tophit
NvERTx.4.120132	FoxJ1	6	up-regulated	jgi|Nemve1|65438|gw.34.211.1
NvERTx.4.130710	Bmp 1 like	1	up-regulated	jgi|Nemve1|94984|e_gw.38.33.1
NvERTx.4.132141	WntA	1	up-regulated	jgi|Nemve1|91822|e_gw.28.3.1
NvERTx.4.136435	K50-5	1	up-regulated	jgi|Nemve1|113102|e_gw.116.148.1
NvERTx.4.202662	Pdgfr-like/htrl-like	6	up-regulated	jgi|Nemve1|158493|estExt_gwp.C_40076
NvERTx.4.220026	Hd050 / NK-like 17	1	up-regulated	jgi|Nemve1|57885|gw.15.184.1
NvERTx.4.51828	Hes3	5	up-regulated	jgi|Nemve1|204200|fgenesh1_pg.scaffold_49000009
NvERTx.4.52739	FoxD1	5	up-regulated	jgi|Nemve1|165603|estExt_gwp.C_620176
NvERTx.4.54137	Musk-like	6	up-regulated	jgi|Nemve1|125819|e_gw.223.23.1
NvERTx.4.57017	Hd058 / Q50-4	6	up-regulated	jgi|Nemve1|69041|gw.55.217.1
NvERTx.4.64399	Sprouty	6	up-regulated	jgi|Nemve1|29671|gw.51.137.1
NvERTx.4.65412	Fgf2A	6	up-regulated	jgi|Nemve1|196402|fgenesh1_pg.scaffold_2000024
NvERTx.4.6665	Fox1	1	up-regulated	jgi|Nemve1|123903|e_gw.205.1.1
NvERTx.4.75546	Wnt7b	1	up-regulated	jgi|Nemve1|210076|fgenesh1_pg.scaffold_116000032
NvERTx.4.77035	MoxD	1	up-regulated	jgi|Nemve1|128296|e_gw.248.4.1
NvERTx.4.77043	Mox1	5	up-regulated	jgi|Nemve1|128275|e_gw.248.7.1
NvERTx.4.77307	Sp8/9-like	1	up-regulated	jgi|Nemve1|99612|e_gw.53.52.1
NvERTx.4.82946	Mae like	6	up-regulated	jgi|Nemve1|39874|gw.31.152.1
NvERTx.4.92297	Runt	6	up-regulated	jgi|Nemve1|129231|e_gw.262.50.1
NvERTx.4.127819	Perlecan-like	3	down-regulated	jgi|Nemve1|213715|fgenesh1_pg.scaffold_183000001
NvERTx.4.35183	Hd010 / Emx1	3	down-regulated	jgi|Nemve1|117718|e_gw.148.118.1
NvERTx.4.52057	Hox2	2	down-regulated	jgi|Nemve1|91593|e_gw.27.3.1
NvERTx.4.59503	Hd145 / Not-likeE	3	down-regulated	jgi|Nemve1|239167|estExt_fgenesh1_pg.C_120143
NvERTx.4.60787	C-Myc-like	5	down-regulated	jgi|Nemve1|82891|e_gw.6.263.1
NvERTx.4.63085	Rx3-like	4	down-regulated	jgi|Nemve1|184843|estExt_GenewiseH_1.C_620202

Table 2: Embryonic cWnt significantly regulate at 20hpa

NvERTx.4	Gene name	R_Clust	Fold.change.20.h	Nemve1_tophit
NvERTx.4.114443	wnt2	6	up-regulated	jgi|Nemve1|242584|estExt_fgenesh1_pg.C_670032
NvERTx.4.116641	axin-like	1	up-regulated	jgi|Nemve1|182113|estExt_GenewiseH_1.C_340142
NvERTx.4.121117	porcupine-like	6	up-regulated	jgi|Nemve1|51461|gw.85.146.1
NvERTx.4.127048	smad4-like	6	up-regulated	jgi|Nemve1|18576|gw.137.32.1
NvERTx.4.161677	nkd1-like	6	up-regulated	jgi|Nemve1|245445|estExt_fgenesh1_pg.C_1600029
NvERTx.4.166798	phtf1-like	7	up-regulated	jgi|Nemve1|239957|estExt_fgenesh1_pg.C_220086
NvERTx.4.183809	bicaudalC-like2	6	up-regulated	jgi|Nemve1|135116|e_gw.351.22.1
NvERTx.4.35039	foxB	7	up-regulated	jgi|Nemve1|187332|estExt_GenewiseH_1.C_990063
NvERTx.4.48250	wnt4	1	up-regulated	jgi|Nemve1|194914|estExt_GenewiseH_1.C_4440001
NvERTx.4.59627	twist	1	up-regulated	jgi|Nemve1|234699|estExt_fgenesh1_pm.C_530001
NvERTx.4.80873	fz10	1	up-regulated	jgi|Nemve1|168924|estExt_gwp.C_1170009
NvERTx.4.142825	snailA	3	down-regulated	jgi|Nemve1|236363|estExt_fgenesh1_kg.C_50021
NvERTx.4.185247	nk2-like	4	down-regulated	jgi|Nemve1|68616|gw.26.321.1
NvERTx.4.68610	fgf1A	3	down-regulated	jgi|Nemve1|247007|estExt_fgenesh1_pg.C_2620002
NvERTx.4.97389	six3/6	4	down-regulated	jgi|Nemve1|130873|e_gw.286.29.1

Table S3: Salt and pepper embryonic MEK/ERK downstream target at 20hpa and 48hpa

NvERTx_ID	Gene_name	Mfuzz_R_Clust	Fold 0_20	Fold 0_48	Uniprot_ID	Nemve1_tophit
NvERTx.4.14710	Sox2	2	n.s	up	Q6RVD7	jgi|Nemve1|239130|estExt_fgenesh1_pg.C_120063
NvERTx.4.95111	FoxD3-like	2	n.s	n.s	Q9DEN3	jgi|Nemve1|39632|gw.32.224.1
NvERTx.4.59801	Hes-like3 (Hl3)	2	n.s	n.s	Q01071	jgi|Nemve1|242118|estExt_fgenesh1_pg.C_570049
NvERTx.4.69501	AshA	2	n.s	n.s	Q6XD76	jgi|Nemve1|136184|e_gw.370.17.1
NvERTx.4.59856	PaxA	2	n.s	up	Q90268	jgi|Nemve1|243681|estExt_fgenesh1_pg.C_950002
NvERTx.4.47955	Sox10-like	2	n.s	n.s	Q6RVD7	jgi|Nemve1|120772|e_gw.173.50.1
NvERTx.4.82519	Coup-like2 / NR13	3	n.s	n.s	Q60632	jgi|Nemve1|189134|estExt_GenewiseH_1.C_1360001
NvERTx.4.230051	Gcm	3	n.s	n.s	Q27403	jgi|Nemve1|130307|e_gw.278.27.1
NvERTx.4.59502	Hd145 / Not-likeE	3	n.s	n.s	Q91770	jgi|Nemve1|239167|estExt_fgenesh1_pg.C_120143
NvERTx.4.44368	Vsx-like	5	n.s	n.s	Q61412	jgi|Nemve1|244054|estExt_fgenesh1_pg.C_1060041
NvERTx.4.139645	Coup-like1 / NR12	5	n.s	n.s	P43135	jgi|Nemve1|165424|estExt_gwp.C_600191
NvERTx.4.35293	NvAth-like	5	n.s	up	O42202	jgi|Nemve1|19204|gw.168.50.1
NvERTx.4.51828	Hes3	5	up	up	O57337	jgi|Nemve1|204200|fgenesh1_pg.scaffold_49000009
NvERTx.4.102249	Elav-like	6	n.s	n.s	B5DF91	jgi|Nemve1|214798|fgenesh1_pg.scaffold_210000018
vERTx.4.102227	SoxB(2)	6	up	n.s	Q21305	jgi|Nemve1|207820|fgenesh1_pg.scaffold_84000076
NvERTx.4.141644	Pea3-like	6	n.s	n.s	Q9CXC9	jgi|Nemve1|16815|gw.138.35.1
NvERTx.4.122746	FoxQ2-like3	9	n.s	n.s	Q6P2Z3	jgi|Nemve1|96685|e_gw.43.186.1

Table S2: Embryonic MEK/ERK downstream targets upregulated at 48hpa

NvERTx_ID	Gene_name	Mfuzz_R_Clust	old change 0_48hp	Uniprot_ID	Nemve1_tophit.x
NvERTx.4.220026	Hd050 / NK-like 17	1	up-regulated	P53547	jgi|Nemve1|57885|gw.15.184.1
NvERTx.4.132141	wntA	1	up-regulated	P28047	jgi|Nemve1|91822|e_gw.28.3.1
NvERTx.4.77035	MoxD	1	up-regulated	F1Q4R9	jgi|Nemve1|128296|e_gw.248.4.1
NvERTx.4.77307	Sp8/9-like	1	up-regulated	Q0VA40	jgi|Nemve1|99612|e_gw.53.52.1
NvERTx.4.107815	Wnt3	1	up-regulated	Q2LMP1	jgi|Nemve1|241352|estExt_fgenesh1_pg.C_440031
NvERTx.4.75546	NvWnt7b	1	up-regulated	Q3L254	jgi|Nemve1|210076|fgenesh1_pg.scaffold_116000032
NvERTx.4.6665	Fox1	1	up-regulated	Q64731	jgi|Nemve1|123903|e_gw.205.1.1
NvERTx.4.14710	NvSox2	2	up-regulated	Q6RVD7	jgi|Nemve1|239130|estExt_fgenesh1_pg.C_120063
NvERTx.4.59856	NvPaxA	2	up-regulated	Q90268	jgi|Nemve1|243681|estExt_fgenesh1_pg.C_950002
NvERTx.4.74420	NvDkk3-like3	2	up-regulated	Q90839	jgi|Nemve1|247589|estExt_fgenesh1_pg.C_3190005
NvERTx.4.73097	FoxA	5	up-regulated	Q7T1R4	jgi|Nemve1|165261|estExt_gwp.C_580130
NvERTx.4.52739	NvFoxD1	5	up-regulated	Q61850	jgi|Nemve1|165603|estExt_gwp.C_620176
NvERTx.4.56073	NvWnt1	5	up-regulated	P24257	jgi|Nemve1|158342|estExt_gwp.C_30479
NvERTx.4.36348	NvRx1 / NvQ50-1	5	up-regulated	Q9I9A2	jgi|Nemve1|39668|gw.15.164.1
NvERTx.4.63365	NvHd037 / NvQ50-	5	up-regulated	Q06453	jgi|Nemve1|99140|e_gw.52.186.1
NvERTx.4.77043	Mox1	5	up-regulated	F1Q4R9	jgi|Nemve1|128275|e_gw.248.7.1
NvERTx.4.51828	Hes1/3	5	up-regulated	O57337	jgi|Nemve1|204200|fgenesh1_pg.scaffold_49000009
NvERTx.4.35293	NvAth-like	5	up-regulated	O42202	jgi|Nemve1|19204|gw.168.50.1
NvERTx.4.145168	NvTbx4/5-like	5	up-regulated	Q9IAK8	jgi|Nemve1|242507|estExt_fgenesh1_pg.C_650052
NvERTx.4.92297	Runt	6	up-regulated	Q01196	jgi|Nemve1|129231|e_gw.262.50.1
NvERTx.4.82946	Mae like	6	up-regulated	Q9Y603	jgi|Nemve1|39874|gw.31.152.1
NvERTx.4.57017	NVHd058 / NvQ50-	6	up-regulated	A1A546	jgi|Nemve1|69041|gw.55.217.1
NvERTx.4.64399	Sprouty	6	up-regulated	O43597	jgi|Nemve1|29671|gw.51.137.1

Table S1: Identified RTK in *Nematostella vectensis* genome

NvERTx_ID	R_Clust	Uniprot_ID	RTK.family	Tree.name	Nemve1_tophit
NvERTx.4.114279	1	Q01973	Ror	ror	jgi|Nemve1|21450|gw.43.17.1
NvERTx.4.176916	3	Q07497	Eph	eph-like2	jgi|Nemve1|116411|e_gw.138.27.1
NvERTx.4.148161	3	Q62838	Ddr-like	ddr-likeB	jgi|Nemve1|92237|e_gw.29.11.1
NvERTx.4.60705	3	P16092	Tie	rtk2	jgi|Nemve1|122799|e_gw.193.14.1
NvERTx.4.106986	3	Q06807	Tie	rtk4	jgi|Nemve1|132322|e_gw.308.1.1
NvERTx.4.62705	3	Q90Z00	Tie	rtk5	jgi|Nemve1|87477|e_gw.16.150.1
NvERTx.4.72887	4	Q62838	Ddr-like	ddr-likeA	jgi|Nemve1|109636|e_gw.95.30.1
NvERTx.4.183666	4	Q8AXC7	NA	rtk8	jgi|Nemve1|119330|e_gw.161.36.1
NvERTx.4.158465	4	Q02763	Tie	rtk6	jgi|Nemve1|120496|e_gw.171.13.1
NvERTx.4.65599	6	Q16832	Ddr	ddr	jgi|Nemve1|163453|estExt_gwp.C_400097
NvERTx.4.136364	6	O13146	Eph	eph-like	jgi|Nemve1|10376|gw.212.5.1
NvERTx.4.130817	6	P09759	Eph	eph-like3	jgi|Nemve1|234961|estExt_fgenesh1_pm.C_770008
NvERTx.4.215906	6	P29323	Eph	ephB-like	jgi|Nemve1|207152|fgenesh1_pg.scaffold_77000049
NvERTx.4.161255	6	O42127	Fgfr	fgfr-like	jgi|Nemve1|81258|e_gw.4.95.1
NvERTx.4.175940	6	P18460	Fgfr	fgfrA	jgi|Nemve1|98570|e_gw.50.142.1
NvERTx.4.142367	6	P18460	Fgfr	fgfrB	jgi|Nemve1|31143|gw.4.71.1
NvERTx.4.153884	6	P22607	Pvr-like	pdvegfr-likeB	jgi|Nemve1|94997|e_gw.38.20.1
NvERTx.4.192904	6	Q8BKG3	Ptk7	ptk7	jgi|Nemve1|229403|fgenesh1_pm.scaffold_74000014
NvERTx.4.71788	6	Q02858	Tie	rtk3	jgi|Nemve1|1620|gw.470.9.1
NvERTx.4.202662	6	Q95YM9	Tie	rtk7	jgi|Nemve1|158493|estExt_gwp.C_40076
NvERTx.4.153210	6	Q01887	Ryk	ryk	jgi|Nemve1|1139|gw.239.8.1
NvERTx.4.92528	8	Q25197	Igfr	igfr	jgi|Nemve1|198971|fgenesh1_pg.scaffold_12000194
NvERTx.4.153889	8	P18460	Pvr-like	pdvegfr-likeA	jgi|Nemve1|94990|e_gw.38.17.1
NvERTx.4.78874	8	P18461	Pvr-like	pdvegfr-likeC	jgi|Nemve1|87445|e_gw.16.43.1
NvERTx.4.205755	9	Q07496	Eph	ephB2	jgi|Nemve1|173481|estExt_gwp.C_2540048
NvERTx.4.112536	9	P11362	Pvr-like	pdvegfr-likeD	jgi|Nemve1|199615|fgenesh1_pg.scaffold_16000065

930 Table S3: Salt and pepper embryonic MEK/ERK downstream targets. The
931 genes from the list of salt and pepper downstream targets of MEK/ERK from
932 (Layden et al. 2016) was queried against the regeneration transcriptomic
933 data. All the genes are listed with their regulation between the time point 0hpa
934 and 20hpa and also between 0hpa and 48hpa.

935 ## Material and methods

936 ### Animal care and handling

937 The sea anemones are cultured in 1/3 ASW (Artificial Sea Water;
938 Tropic-Marin Bio-actif system sea salt (Tropic-Marin, Wartenberg, Germany))
939 at the Institute of Research on Cancer and Aging of Nice of the University of
940 Nice. The Adults are reared at 16°C and fed three times a week with freshly
941 hatched artemia. The spawning cycle is kept monthly between four colonies
942 and it is carried out as described in (Hand and Uhlinger 1992). The juveniles
943 are reared differently at 22°C and feeding starts from week two with smashed
944 artemia until week 8 once a week, thereafter lived artemia are used.

945 ### Animal bisection, wound healing and regeneration experiment

946 Regeneration experiments were all performed on six weeks old
947 juveniles starved for two weeks for proliferation experiment and less than one
948 week for whole-mount *in situ* hybridization.. Prior the cutting animals are
949 relaxed for 5 min in 5ml of 1/3ASW on a light table then 1ml of 7.13% of
950 MgCl2 in ASW is added to keep the animals paralyzed. The bisection under
951 the pharynx is done using a microsurgery scalpel n°15 (Swann-Morton,
952 Sheffield, UK). At the end of cutting the animals are washed three times with

1/3 ASW and incubated at 22°C in darkness for regeneration. Whereas for the wound healing experiment were performed following the protocoled from (Amiel et al. 2015).

The MEK inhibitor, U0126 was purchased from Sigma (ref: U120-1MG) and resuspended in Dmso for a stock solution of 10 mM. Each treatment with U0126 where performed with a final concentration of 10 µM in 1/3 ASW while incubated in darkness.

Fixation and animal staining

Before the fixation, the juveniles are relaxed for 5 to 10 min on light before adding 7.13% MgCl2 for another 5 to 10 min. Then the animals are gently transferred to eppendorff tubes, coated with PBw 0.1% (1X PBS + 0.1% Tween-20), for fixation. The fixation is carried out by incubating the samples with 4% paraformaldehyde (Electron Microscopy Sciences #15714, Hatfield, PA, USA) in 1/3 ASW for one hour at room temperature or overnight at 4°C. Thereafter the samples are washed five times with PBw 0.1%.

To analyze the general morphology, Hoechst staining (Invitrogen #33342, Carlsbad, CA, USA) at 1/5000 was used to label the nucleus, and BODIPY® FL PhallAcidin 488 (Molecular Probes #B607, Eugene, OR, USA) staining was used at 1/200 to label actin microfilaments (cell membranes and muscle fibers). Additionally, for cell proliferation analysis was carried out using the Click-it EdU kit (Invitrogen #C10337 or #C10339, Carlsbad, CA, USA) following the protocol from (Passamaneck and Martindale 2012). To visualize the activity of MEK/ERK we used an antibody directed against its active form, p-ERK (Cat.#4377; Cell Signaling Technology) and the protocol was used as described in (DuBuc, Traylor-Knowles, and Martindale 2014).

Whole-mount *in situ* hybridization

The whole-mount *in situ* hybridization (WISH) was performed as described in (Genikhovich and Technau 2009). The juveniles were relaxed and were fix as described in (Genikhovich and Technau 2009) then stored in 100% Methanol (MeOH) at -20°C. Upon analysis the samples where rehydrated before being transferred into 24-wells plate (Falcon® 24-well multiwall plate with low evaporation lid) for the rest of the protocol. The pre-treatment was performed with 0.01mg/ml of Proteinase K for precisely 20 min at 22°C and stopped with two washes of 5 min with PBw 0.1% + 2 mg/ml of Glycine. Thereafter the samples were treated with three different baths of 5 min with triethanolamine. The first one composed 1% of triethanolamine in PBw 0.1%, the same second one was supplemented with 3 µl of acetic anhydride per 500 µl and the third one with 6 µl of acetic anhydride per 500 µl. The pre-treatment ended with two washes with PBw 0.1%.

After the pre-treatment the samples were refix with 4% paraformaldehyde in PBw 0.1% for one hour at room temperature and washed with five bath of PBw 0.1%.

Thereafter the samples were pre-conditioned in hybridization solution (Formamide 50%, SSC 5X pH 4.5, heparin 50µg/ml, Tween-20 0,1%, SDS 1%, Salmon sperm DNA 100µg/ml) for 10 min at room temperature before being pre-hybridized in fresh hybridization solution overnight at 62°C in a humid chamber. The probes used in this study were synthetized according to the protocol described in (Amiel et al. 2017), and were diluted to 0.1 ng/µl in fresh hybridization solution. Before use the probes are denatured at 85°C for 10 min then added to the samples overnight at 62°C in a humid chamber.

The probes were washed out with three bath of decreasing percentage of hybridization solution and increasing solution of SSC 2X pH 7 (25%, 50% and 75%) at 62°C. Followed by three washes in solutions of decreasing percentage of SSC 0.2% and increasing percentage of PBw 0.1% (25%, 50% and 75%) at room temperature before the blocking solution of Maleic acid buffer pH7.5 with 1% Boehringer-Mannheim blocking reagent in for two hours at room temperature.

The revelation relied on the detection of the antibody anti-Dig/AP used at 1:5000 in blocking solution and incubated at 4°C overnight. The excess of antibody was removed with ten washes of PBw 0.1%. Finally the sample were conditioned for the revelation with bath of alkaline phosphatase buffers (NaCl 100nm, MgCl2 50mM, Tris pH9.5 100mM, Tween-20 0.5%). The first wash is without MgCl2 and two following are with MgCl2. At last the revelation is carried out with 3.3µl NBT (100mg/ml) and 3.3µl of BCIP (50mg/ml) per ml of alkaline phosphatase buffer on ice.

Protein extraction and Western blot

The proteins were extracted from 15 adults per replicate and each experiment was performed in triplicate. The animals where placed in 1.5 ml eppendorff tubes and spin on bench centrifuge to pellet the animals and remove as much 1/3 ASW as possible. Immediately after, 300µl of lysis buffer (HEPES 50mM, NaCl 150mM, NaF 100mM, EDTA 10mM, NA4P207 10mM) was added for five round of 10 sec sonication with incubation on ice between each round. Thereafter 200µl of Lysis buffer with 1% Triton X-100 and the protease inhibitor cocktail (Apoprotine 20µg/ml, Vanadate 1mM, AEBSF 250µg/ml, Leupeptine 5µg/ml) is mixed to the sonicated samples. Finally the

samples are centrifuged at 12,000 rpm for 20 min at 4°C, to pellet the remaining tissue and transfer the supernatant into a new tube that will be store at -80°C. The protein concentration of the samples was assessed using the BC assay protein quantification kit (Interchim Upima, 40840A) and each sample was subsequently aliquot by mixing 75µl of protein extract with 25µl of Laemmli buffer 4x (Bio-Rad #1610747) and stored at -20°C. Before loading the aliquoted samples onto the 7.5% SDS polyacrylamide gel, they were denaturated with an incubation at 85°C for 5 min.

The electrophoresis was performed with 30µg of protein following the protocol described in (Gilmore, Wolenski, and Finnerty 2012) in migration buffer (Tris 3g/L, Glycine 14.2g/L, SDS 1%), while the transfer was performed in transfer buffer (Tris 3g/L, Glycine 14,4g/L, 20% Ethanol). Afterward the nitrocellulose membrane was saturated with salin buffer (Tris 0,24g/L, NaCl 1,63g/L, 5% BSA, 0.5% Tween-20), the membrane was incubated 1 hour at room temperature with the primary antibody anti-pERK (Cat.#4377; Cell Signaling Technology) diluted 1/2500 into the salin buffer. Revelation was carried out by chimioluminescence (EMD Millipore™ Substrats de chimioluminescence HRP Western Luminata™) on a chemioluminescence Imaging –Fusion SL (Vilber).

RNA extraction and quantitative PCR (qPCR)

RNA Extraction and quantitative PCR (qPCR) were performed following protocol described in (Röttinger, Dahlin, and Martindale 2012). In order to obtain enough material approximately 160 juveniles were pooled per replicate and each experiment was performed in three biological replicate. qPCR analysis using a 7900HT Fast Real-Time PCR System with 384-Well Block Module (Applied Biosystem) utilizing Faststart universal SYBR Green

Master (FSUSGMMRO Roche) was carried out as described previously (Layden, Boekhout, and Martindale 2012). The full list of qPCR primer pairs and their efficiency used in this study can be found in Table S2 or (Layden et al. 2016). The houskeeping genes Nvactin and/or Nvgadph were used to normalize relative fold changes between control and treated juvenile and each qPCR analysis was repeated on independent biological replicates.

Phylogenetic tree reconstruction

Amino acid sequences of Pkinase_Tyr domain (Pfam:PF07714) (Sonnhammer et al. 1998) from RTKs of *N. vectensis* and of other selected metazoan species were retrieved. Sequences were aligned using Clustal Omega (Sievers et al. 2011) using the HMM profile of the Pkinase_Tyr (PF07714) domain. Sequences for which the domain sequence was too short were deteled from the alignment. Bayesian inference (BI) tree was inferred using MrBayes 3.2.6 (Ronquist et al. 2012), with the model recommended by ProtTest 1.4 (Darriba et al. 2011) under the Akaike information criterion (JTT+I+Γ), at the CIPRES Science Gateway portal (Miller et al. 2015). Two independent runs were performed, each with 4 chains and one million generations. A burn-in of 25% was used and a fifty majority-rule consensus tree was calculated for the remaining trees. The obtained tree was customized using FigTree v.1.4.0. (http://tree.bio.ed.ac.uk/software/figtree/).

Imaging

in situ hybridization images were taken on either a Zeiss Axio Imager A2 mounted with an Axiocam camera triggered by Axiovision software (Carl Zeiss). Scoring of treatment phenotypes was performed on either a Zeiss Axio

Imager A2 microscope or a Zeiss LSM710 for confocal imaging running the LSM ZEN software (Carl Zeiss). Fluorescent images were false-colored, the fluorescent channels merged using ImageJ (http://rsbweb.nih.gov/ij/) and cropped to final size in Photoshop Cs6 (Adobe Inc.).

Acknowledgements

The authors also acknowledge Aldine Amiel for the discussion, Jacob Warner for the bioinformatics guidance, Stéphanie Bertrand for the phylogenetic analysis, Valérie Carlin for animal care and the IRCAN's, the trainee Arthur Gilson, Lou Petard, Marie Morrain, Claire Dalmasso for their contribution in the experiments. The Van Obberghen lab and in particular Gaia Fabris and Nadine Gautier for the western blot reagent and apparatus. Molecular and Cellular Core Imaging (PICMI) Facility. PICMI was supported financially by Cancéropole PACA, Région Provence Alpes-Côte d′Azur, Conseil Départemental 06 and INSERM.

Competing interests

The authors declare no competing or financial interests

Author contributions

HJ, KN and ER – Conceived, designed and performed experi- ments. HJ, KN – generated, collected and analyzed data. ER, - Contributed reagents/materials/analysis tools. HJ, ER - Drafted the manuscript. All authors read and approved the final manuscript

Funding

This work was supported by ATIP-Avenir (Institut National de la Santé et de la Recherche Médicale and Centre National de la Recherche Scientifique) funded by the Plan Cancer (Institut National Du Cancer, C13992AS), Seventh Framework Programme (631665), Association pour la Recherche sur le Cancer (PJA 2014120186) to ER, la Ligue Nationale Contre le Cancer to KN the Ministère de l'Enseignement Supérieur et de la Recherche as well as the Fondation pour la recherche médicale (FDT 20170437124) to HJ.

Reference

Abdol, Amir M, Eric Röttinger, Fredrik Jansson, and Jaap A Kaandorp. 2017. "A Novel Technique to Combine and Analyse Spatial and Temporal Expression Datasets: a Case Study with the Sea Anemone Nematostella Vectensis to Identify Potential Gene Interactions.." *Developmental Biology* 428 (1): 204–14. doi:10.1016/j.ydbio.2017.06.004.

Agata, Kiyokazu, Junichi Tasaki, Elizabeth Nakajima, and Yoshihiko Umesono. 2014. "Recent Identification of an ERK Signal Gradient Governing Planarian Regeneration.." *Zoology (Jena, Germany)* 117 (3): 161–62. doi:10.1016/j.zool.2014.04.001.

Amiel, Aldine R, Hereroa Johnston, Taylor Chock, Paul Dahlin, Marta Iglesias, Michael Layden, Eric Röttinger, and Mark Q Martindale. 2017. "A Bipolar Role of the Transcription Factor ERG for Cnidarian Germ Layer Formation and Apical Domain Patterning.." *Developmental Biology*, August. doi:10.1016/j.ydbio.2017.08.015.

Amiel, Aldine, Hereroa Johnston, Karine Nedoncelle, Jacob Warner, Solène Ferreira, and Eric Röttinger. 2015. "Characterization of Morphological and Cellular Events Underlying Oral Regeneration in the Sea Anemone, Nematostella Vectensis." *International Journal of Molecular Sciences* 16 (12): 28449–71. doi:10.3390/ijms161226100.

Binari, L A, G M Lewis, and S Kucenas. 2013. "Perineurial Glia Require Notch Signaling During Motor Nerve Development but Not Regeneration." *Journal of Neuroscience* 33 (10): 4241–52. doi:10.1523/JNEUROSCI.4893-12.2013.

Bossert, Patricia E, Matthew P Dunn, and Gerald H Thomsen. 2013. "A Staging System for the Regeneration of a Polyp From the Aboral Physa of the Anthozoan Cnidarian Nematostella Vectensis." *Developmental Dynamics : an Official Publication of the American Association of Anatomists* 242 (11): 1320–31. doi:10.1002/dvdy.24021.

Botman, Daniel, Fredrik Jansson, Eric Röttinger, Mark Q Martindale, Johann de Jong, and Jaap A Kaandorp. 2015. "Analysis of a Spatial Gene Expression Database for Sea Anemone Nematostella Vectensis During Early Development.." *BMC Systems Biology* 9 (1): 63. doi:10.1186/s12918-015-0209-4.

Burton, Patrick M, and John R Finnerty. 2009. "Conserved and Novel Gene Expression Between Regeneration and Asexual Fission in Nematostella Vectensis." *Development Genes and Evolution* 219 (2): 79–87. doi:10.1007/s00427-009-0271-2.

Carlson, M R, Y Komine, S V Bryant, and D M Gardiner. 2001. "Expression of Hoxb13 and Hoxc10 in Developing and Regenerating Axolotl Limbs and Tails.." *Developmental Biology* 229 (2): 396–406. doi:10.1006/dbio.2000.0104.

Chera, Simona, Luiza Ghila, Kevin Dobretz, Yvan Wenger, Christoph Bauer, Wanda Buzgariu, Jean-Claude Martinou, and Brigitte Galliot. 2009. "Apoptotic Cells Provide an Unexpected Source of Wnt3 Signaling to Drive Hydra Head Regeneration.." *Developmental Cell* 17 (2): 279–89. doi:10.1016/j.devcel.2009.07.014.

Czarkwiani, Anna, Cinzia Ferrario, David Viktor Dylus, Michela Sugni, and Paola Oliveri. 2016. "Skeletal Regeneration in the Brittle Star Amphiura Filiformis."

Frontiers in Zoology, April. Frontiers in Zoology, 1–17. doi:10.1186/s12983-016-0149-x.

D'Aniello, S, M Irimia, I Maeso, J Pascual-Anaya, S Jimenez-Delgado, S Bertrand, and J Garcia-Fernandez. 2008. "Gene Expansion and Retention Leads to a Diverse Tyrosine Kinase Superfamily in Amphioxus." *Molecular Biology and Evolution* 25 (9): 1841–54. doi:10.1093/molbev/msn132.

Darling, John A, Adam R Reitzel, Patrick M Burton, Maureen E Mazza, Joseph F Ryan, James C Sullivan, and John R Finnerty. 2005. "Rising Starlet: the Starlet Sea Anemone, Nematostella Vectensis.." *BioEssays : News and Reviews in Molecular, Cellular and Developmental Biology* 27 (2): 211–21. doi:10.1002/bies.20181.

Darriba, Diego, Guillermo L Taboada, Ramón Doallo, and David Posada. 2011. "ProtTest 3: Fast Selection of Best-Fit Models of Protein Evolution." *Bioinformatics (Oxford, England)* 27 (8): 1164–65. doi:10.1093/bioinformatics/btr088.

Davies, Erin L, Kai Lei, Christopher W Seidel, Amanda E Kroesen, Sean A McKinney, Longhua Guo, Sofia Mc Robb, Eric J Ross, Kirsten Gotting, and Alejandro Sánchez Alvarado. 2017. "Embryonic Origin of Adult Stem Cells Required for Tissue Homeostasis and Regeneration.." *eLife* 6 (January). doi:10.7554/eLife.21052.

DeSilva, D R, E A Jones, M F Favata, B D Jaffee, R L Magolda, J M Trzaskos, and P A Scherle. 1998. "Inhibition of Mitogen-Activated Protein Kinase Kinase Blocks T Cell Proliferation but Does Not Induce or Prevent Anergy.." *Journal of Immunology (Baltimore, Md. : 1950)* 160 (9): 4175–81.

DuBuc, Timothy Q, Nikki Traylor-Knowles, and Mark Q Martindale. 2014. "Initiating a Regenerative Response; Cellular and Molecular Features of Wound Healing in the Cnidarian Nematostella Vectensis.." *BMC Biology* 12 (1). BioMed Central Ltd: 24. doi:10.1186/1741-7007-12-24.

Finnerty, J R, and M Q Martindale. 1999. "Ancient Origins of Axial Patterning Genes: Hox Genes and ParaHox Genes in the Cnidaria.." *Evolution & Development* 1 (1): 16–23.

Galliot, Brigitte. 2004. "Signaling Molecules in Regenerating Hydra," October, 1–10.

Galliot, Brigitte, and Volker Schmid. 2002. "Cnidarians as a Model System for Understanding Evolution and Regeneration.." *The International Journal of Developmental Biology* 46 (1): 39–48.

Gardiner, D M, and S V Bryant. 1996. "Molecular Mechanisms in the Control of Limb Regeneration: the Role of Homeobox Genes.." *The International Journal of Developmental Biology* 40 (4): 797–805.

Gardiner, D M, B Blumberg, Y Komine, and S V Bryant. 1995. "Regulation of HoxA Expression in Developing and Regenerating Axolotl Limbs.." *Development* 121 (6): 1731–41.

Gazave, Eve, Julien Béhague, Lucie Laplane, Aurélien Guillou, Laetitia Préau, Adrien Demilly, Guillaume Balavoine, and Michel Vervoort. 2013. "Posterior Elongation in the Annelid Platynereis Dumerilii Involves Stem Cells Molecularly Related to Primordial Germ Cells." *Developmental Biology* 382 (1). Elsevier: 246–67. doi:10.1016/j.ydbio.2013.07.013.

Genikhovich, Grigory, and Ulrich Technau. 2009. "In Situ Hybridization of Starlet Sea Anemone (Nematostella Vectensis) Embryos, Larvae, and Polyps.." *Cold*

Spring Harbor Protocols 2009 (9). Cold Spring Harbor Laboratory Press: pdb.prot5282. doi:10.1101/pdb.prot5282.

Genikhovich, Grigory, Patrick Fried, M Mandela Prünster, Johannes B Schinko, Anna F Gilles, David Fredman, Karin Meier, Dagmar Iber, and Ulrich Technau. 2015. "Axis Patterning by BMPs: Cnidarian Network Reveals Evolutionary Constraints." *CellReports* 10 (10). The Authors: 1646–54. doi:10.1016/j.celrep.2015.02.035.

Genikhovich, Grigory, Ulrich Kürn, Georg Hemmrich, and Thomas C G Bosch. 2006. "Discovery of Genes Expressed in Hydra Embryogenesis.." *Developmental Biology* 289 (2): 466–81. doi:10.1016/j.ydbio.2005.10.028.

Gilmore, Thomas, Francis Wolenski, and John Finnerty. 2012. "Preparation of Antiserum and Detection of Proteins by Western Blotting Using the Starlet Sea Anemone, Nematostella Vectensis." *Protocol Exchange*, December. doi:10.1038/protex.2012.057.

Goldshmit, Yona, Tamar E Sztal, Patricia R Jusuf, Thomas E Hall, Mai Nguyen-Chi, and Peter D Currie. 2012. "Fgf-Dependent Glial Cell Bridges Facilitate Spinal Cord Regeneration in Zebrafish.." *The Journal of Neuroscience : the Official Journal of the Society for Neuroscience* 32 (22). Society for Neuroscience: 7477–92. doi:10.1523/JNEUROSCI.0758-12.2012.

Gurley, Kyle A, Sarah A Elliott, Oleg Simakov, Heiko A Schmidt, Thomas W Holstein, and Alejandro Sánchez Alvarado. 2010. "Expression of Secreted Wnt Pathway Components Reveals Unexpected Complexity of the Planarian Amputation Response." *Developmental Biology* 347 (1): 24–39. doi:10.1016/j.ydbio.2010.08.007.

Hand, C, and K R Uhlinger. 1992. "The Culture, Sexual and Asexual Reproduction, and Growth of the Sea Anemone Nematostella Vectensis.." *The Biological Bulletin* 182 (2): 169–76. doi:10.2307/1542110.

Jensen, Jan Nygaard, Erin Cameron, Maria Veronica R Garay, Thomas W Starkey, Roberto Gianani, and Jan Jensen. 2005. "Recapitulation of Elements of Embryonic Development in Adult Mouse Pancreatic Regeneration.." *Gastroenterology* 128 (3): 728–41.

Kaloulis, Kostas, Simona Chera, Monika Hassel, Dominique Gauchat, and Brigitte Galliot. 2004. "Reactivation of Developmental Programs: the cAMP-Response Element-Binding Protein Pathway Is Involved in Hydra Head Regeneration.." *Proceedings of the National Academy of Sciences* 101 (8): 2363–68.

Kang, Junsu, Jianxin Hu, Ravi Karra, Amy L Dickson, Valerie A Tornini, Gregory Nachtrab, Matthew Gemberling, Joseph A Goldman, Brian L Black, and Kenneth D Poss. 2016. "Modulation of Tissue Repair by Regeneration Enhancer Elements." *Nature* 532 (7598): 201–6. doi:10.1038/nature17644.

Kroehne, Volker, Dorian Freudenreich, Stefan Hans, Jan Kaslin, and Michael Brand. 2011. "Regeneration of the Adult Zebrafish Brain From Neurogenic Radial Glia-Type Progenitors.." *Development* 138 (22). Oxford University Press for The Company of Biologists Limited: 4831–41. doi:10.1242/dev.072587.

Layden, Michael J, Fabian Rentzsch, and Eric Röttinger. 2016. "The Rise of the Starlet Sea Anemone Nematostella Vectensis as a Model System to Investigate Development and Regeneration.." *Wiley Interdisciplinary Reviews. Developmental Biology* 5 (4). John Wiley & Sons, Inc.: 408–28. doi:10.1002/wdev.222.

Layden, Michael J, Hereroa Johnston, Aldine R Amiel, Jamie Havrilak, Bailey Steinworth, Taylor Chock, Eric Röttinger, and Mark Q Martindale. 2016. "MAPK Signaling Is Necessary for Neurogenesis in Nematostella Vectensis." *BMC Biology*, July. BMC Biology, 1–19. doi:10.1186/s12915-016-0282-1.

Layden, Michael J, Michiel Boekhout, and Mark Q Martindale. 2012. "Nematostella Vectensis Achaete-Scute Homolog NvashA Regulates Embryonic Ectodermal Neurogenesis and Represents an Ancient Component of the Metazoan Neural Specification Pathway.." *Development* 139 (5). Oxford University Press for The Company of Biologists Limited: 1013–22. doi:10.1242/dev.073221.

Leclère, Lucas, Markus Bause, Chiara Sinigaglia, Julia Steger, and Fabian Rentzsch. 2016. "Development of the Aboral Domain in Nematostella Requires B-Catenin and the Opposing Activities of Six3/6 and Frizzled5/8.." *Development* 143 (10). Oxford University Press for The Company of Biologists Limited: 1766–77. doi:10.1242/dev.120931.

Lee, Patricia N, Shalika Kumburegama, Heather Q Marlow, Mark Q Martindale, and Athula H Wikramanayake. 2007. "Asymmetric Developmental Potential Along the Animal-Vegetal Axis in the Anthozoan Cnidarian, Nematostella Vectensis, Is Mediated by Dishevelled.." *Developmental Biology* 310 (1): 169–86. doi:10.1016/j.ydbio.2007.05.040.

Lemmon, Mark A, and Joseph Schlessinger. 2010. "Cell Signaling by Receptor Tyrosine Kinases.." *Cell* 141 (7): 1117–34. doi:10.1016/j.cell.2010.06.011.

Makanae, Aki, Kazumasa Mitogawa, and Akira Satoh. 2014. "Co-Operative Bmp- and Fgf-Signaling Inputs Convert Skin Wound Healing to Limb Formation in Urodele Amphibians.." *Developmental Biology* 396 (1): 57–66. doi:10.1016/j.ydbio.2014.09.021.

Manuel, Gema C, Rosalia Reynoso, Lydia Gee, Luis M Salgado, and Hans R Bode. 2006. "PI3K and ERK 1-2 Regulate Early Stages During Head Regeneration in Hydra.." *Development, Growth & Differentiation* 48 (2). Blackwell Publishing Asia: 129–38. doi:10.1111/j.1440-169X.2006.00847.x.

McCusker, Catherine, Susan V Bryant, and David M Gardiner. 2015. "The Axolotl Limb Blastema: Cellular and Molecular Mechanisms Driving Blastema Formation and Limb Regeneration in Tetrapods.." *Regeneration (Oxford, England)* 2 (2): 54–71. doi:10.1002/reg2.32.

Michalopoulos, G K. 1997. "Liver Regeneration." *Science* 276 (5309): 60–66. doi:10.1126/science.276.5309.60.

Miller, Mark A, Terri Schwartz, Brett E Pickett, Sherry He, Edward B Klem, Richard H Scheuermann, Maria Passarotti, Seth Kaufman, and Maureen A O'Leary. 2015. "A RESTful API for Access to Phylogenetic Tools via the CIPRES Science Gateway." *Evolutionary Bioinformatics* 11 (April): EBO.S21501. doi:10.4137/EBO.S21501.

Millimaki, Bonny B, Elly M Sweet, and Bruce B Riley. 2010. "Sox2 Is Required for Maintenance and Regeneration, but Not Initial Development, of Hair Cells in the Zebrafish Inner Ear.." *Developmental Biology* 338 (2): 262–69. doi:10.1016/j.ydbio.2009.12.011.

Moya, Aurelie, Kazuhiro Sakamaki, Benjamin M Mason, Lotte Huisman, Sylvain Forêt, Yvonne Weiss, Tara E Bull, et al. 2016. "Functional Conservation of the Apoptotic Machinery From Coral to Man: the Diverse and Complex Bcl-2 and Caspase Repertoires of Acropora Millepora." *BMC Genomics*, January. BMC

Genomics, 1–20. doi:10.1186/s12864-015-2355-x.
Owlarn, Suthira, Felix Klenner, David Schmidt, Franziska Rabert, Antonio Tomasso, Hanna Reuter, Medhanie A Mulaw, et al. 2017. "Generic Wound Signals Initiate Regeneration in Missing-Tissue Contexts.." *Nature Communications* 8 (1). Nature Publishing Group: 2282. doi:10.1038/s41467-017-02338-x.
Passamaneck, Yale J, and Mark Q Martindale. 2012. "Cell Proliferation Is Necessary for the Regeneration of Oral Structures in the Anthozoan Cnidarian Nematostella Vectensis.." *BMC Developmental Biology* 12 (1). BioMed Central Ltd: 34. doi:10.1186/1471-213X-12-34.
Petersen, Hendrik O, Stefanie K Höger, Mario Looso, Tobias Lengfeld, Anne Kuhn, Uwe Warnken, Chiemi Nishimiya-Fujisawa, et al. 2015. "A Comprehensive Transcriptomic and Proteomic Analysis of Hydra Head Regeneration.." *Molecular Biology and Evolution* 32 (8): 1928–47. doi:10.1093/molbev/msv079.
Putnam, Nicolas H. 2007. "Sea Anemone Genome Reveals Ancestral Eumetaozoan Gene Repertoire and Genomic Organization." *Science* 317 (5834): 83–86. doi:10.1126/science.1143254.
Rentzsch, Fabian, Jens H Fritzenwanker, Corinna B Scholz, and Ulrich Technau. 2008. "FGF Signalling Controls Formation of the Apical Sensory Organ in the Cnidarian Nematostella Vectensis.." *Development* 135 (10). The Company of Biologists Ltd: 1761–69. doi:10.1242/dev.020784.
Rink, Jochen C. 2013. "Stem Cell Systems and Regeneration in Planaria.." *Development Genes and Evolution* 223 (1-2): 67–84. doi:10.1007/s00427-012-0426-4.
Ronquist, Fredrik, Maxim Teslenko, Paul van der Mark, Daniel L Ayres, Aaron Darling, Sebastian Höhna, Bret Larget, Liang Liu, Marc A Suchard, and John P Huelsenbeck. 2012. "MrBayes 3.2: Efficient Bayesian Phylogenetic Inference and Model Choice Across a Large Model Space." *Systematic Biology* 61 (3): 539–42. doi:10.1093/sysbio/sys029.
Röttinger, Eric, Paul Dahlin, and Mark Q Martindale. 2012. "A Framework for the Establishment of a Cnidarian Gene Regulatory Network for 'Endomesoderm' Specification: the Inputs of SS-Catenin/TCF Signaling.." Edited by Mary C Mullins. *PLoS Genetics* 8 (12). Public Library of Science: e1003164. doi:10.1371/journal.pgen.1003164.
Sadler, Kirsten C, Katherine N Krahn, Naseem A Gaur, and Chinweike Ukomadu. 2007. "Liver Growth in the Embryo and During Liver Regeneration in Zebrafish Requires the Cell Cycle Regulator, Uhrf1.." *Proceedings of the National Academy of Sciences* 104 (5). National Academy of Sciences: 1570–75. doi:10.1073/pnas.0610774104.
Sánchez Alvarado, A. 2000. "Regeneration in the Metazoans: Why Does It Happen?." *BioEssays : News and Reviews in Molecular, Cellular and Developmental Biology* 22 (6): 578–90. doi:10.1002/(SICI)1521-1878(200006)22:6<578::AID-BIES11>3.0.CO;2-#.
Schaffer, Amos A, Michael Bazarsky, Karine Levy, Vered Chalifa-Caspi, and Uri Gat. 2016. "A Transcriptional Time-Course Analysis of Oral vs. Aboral Whole-Body Regeneration in the Sea Anemone Nematostella Vectensis.." *BMC Genomics* 17 (September): 718. doi:10.1186/s12864-016-3027-1.
Sievers, Fabian, Andreas Wilm, David Dineen, Toby J Gibson, Kevin Karplus,

Weizhong Li, Rodrigo Lopez, et al. 2011. “Fast, Scalable Generation of High-Quality Protein Multiple Sequence Alignments Using Clustal Omega.” *Molecular Systems Biology* 7 (October). Nature Publishing Group: 1–6. doi:10.1038/msb.2011.75.

Sinigaglia, Chiara, Henriette Busengdal, Lucas Leclère, Ulrich Technau, and Fabian Rentzsch. 2013. “The Bilaterian Head Patterning Gene Six3/6 Controls Aboral Domain Development in a Cnidarian..” *PLoS Biology* 11 (2). Public Library of Science: e1001488. doi:10.1371/journal.pbio.1001488.

Sonnhammer, Erik L L, Sean R Eddy, Ewan Birney, Alex Bateman, and Richard Durbin. 1998. “Pfam - Multiple Sequence Alignments and HMM-Profiles of Protein Domains..” *Nucleic Acids Research* 26 (1): 320–22.

Tasaki, Junichi, Norito Shibata, Osamu Nishimura, Kazu Itomi, Yoshimichi Tabata, Fuyan Son, Nobuko Suzuki, et al. 2011. “ERK Signaling Controls Blastema Cell Differentiation During Planarian Regeneration..” *Development* 138 (12). Oxford University Press for The Company of Biologists Limited: 2417–27. doi:10.1242/dev.060764.

Trevino, Michael, Derek J Stefanik, Richard Rodriguez, Shane Harmon, and Patrick M Burton. 2011. “Induction of Canonical Wnt Signaling by Alsterpaullone Is Sufficient for Oral Tissue Fate During Regeneration and Embryogenesis in Nematostella Vectensis.” *Developmental Dynamics : an Official Publication of the American Association of Anatomists* 240 (12): 2673–79. doi:10.1002/dvdy.22774.

Umesono, Yoshihiko, Junichi Tasaki, Yui Nishimura, Martina Hrouda, Eri Kawaguchi, Shigenobu Yazawa, Osamu Nishimura, Kazutaka Hosoda, Takeshi Inoue, and Kiyokazu Agata. 2013. “The Molecular Logic for Planarian Regeneration Along the Anterior-Posterior Axis..” *Nature* 500 (7460): 73–76. doi:10.1038/nature12359.

Vervoort, Michel. 2011. “Regeneration and Development in Animals.” *Biological Theory* 6 (1): 25–35. doi:10.1007/s13752-011-0005-3.

Warner, Jacob F, Vincent Guerlais, Aldine R Amiel, Hereroa Johnston, Karine Nedoncelle, and Eric Röttinger. 2018. “NvERTx: a Gene Expression Database to Compare Embryogenesis and Regeneration in the Sea Anemone Nematostella Vectensis..” *Development* 145 (10). Oxford University Press for The Company of Biologists Limited: dev162867. doi:10.1242/dev.162867.

Wenemoser, Danielle, Sylvain W Lapan, Alex W Wilkinson, George W Bell, and Peter W Reddien. 2012. “A Molecular Wound Response Program Associated with Regeneration Initiation in Planarians..” *Genes & Development* 26 (9). Cold Spring Harbor Lab: 988–1002. doi:10.1101/gad.187377.112.

Wikramanayake, Athula H, Melanie Hong, Patricia N Lee, Kevin Pang, Christine A Byrum, Joanna M Bince, Ronghui Xu, and Mark Q Martindale. 2003. “An Ancient Role for Nuclear Beta-Catenin in the Evolution of Axial Polarity and Germ Layer Segregation..” *Nature* 426 (6965): 446–50. doi:10.1038/nature02113.

Article 7: A kinase inhibitor screen reveals that JNK MAPK regulates regeneration-specific cell proliferation in the sea anemone *Nematostella vectensis*

Johnston. H., Gaggioli. C. and Röttinger. E.

In preparation

A kinase inhibitor screen reveals that JNK MAPK regulates regeneration-specific cell proliferation in the sea anemone *Nematostella vectensis*

Hereroa Johnston[1], Cedric Gaggioli[1] and Eric Röttinger[1]*

[1] Université Côte d'Azur, CNRS, INSERM, Institute for Research on Cancer and Aging, Nice (IRCAN), Nice, France

*Please direct correspondence to:

Eric Röttinger

T: +33 (0)6 63 97 01 78

E: eric.rottinger@unice.fr

Abstract

Regeneration is the developmental trajectory during which organisms restore cell structures, organs, appendages or even entire bodies after injury. During this process, injured tissues have to integrate the cellular states and positional cues in order to rebuild the lost structures. Signaling pathways play important roles in this sensing as well in the immediate stress response initiating wound healing and regeneration. The sea anemone *Nematostella vectensis* is an emerging whole body regeneration models that has biological features that are complementary to historical models such as *Hydra* and planarians. However, little is known about the signaling pathways driving its regenerative process. Given the pivotal role of kinases in most of the signaling pathways, we thus performed a medium-sized kinase inhibitor screen to uncover those implicated in *Nematostella* regeneration. Doing so, we uncovered 14 kinases that seem to be involved in coordinating various steps of whole body regeneration, among which we focused on the role of JNK MAPK. Interestingly, JNK appears to be constitutively active in the homeostatic tissue and only slightly up-regulated upon injury. Nonetheless, this MAPK plays a critical role in launching the regenerative program specifically via the injury induced cell proliferation leading to the reformation of all lost body parts.

Introduction

Regeneration is considered as an alternative developmental trajectory that leads to the reformation of a fully functional organism after injury or the loss of body parts. Although this regenerative ability is widely spread among metazoans, it doesn't necessarily occur at the same levels in all animals (Bely and Nyberg 2010). In particular, one can distinguish regeneration at i) the cellular level (*e.g* axonal regeneration) or tissue/organ levels (*e.g* liver regeneration (Michalopoulos 1997; Sadler et al. 2007) as well as the reformation of whole appendages (*e.g* salamander limbs (McCusker, Bryant, and Gardiner 2015)). Whereas whole body regeneration, exclusively described in invertebrates However, the most extreme level of regeneration, is iv) the so-called whole body regeneration during which isolated body parts can reform entire animals within a few days. This whole body regeneration is observed exclusively in invertebrates such as the historical regeneration models planarians and *Hydra* (Elliott and Sánchez Alvarado 2013; Bosch 2007). Disregarding the regeneration level or the used research model, regeneration involves common cellular processes such as the activation of stem cells, potential de-, or trans-differentiation, cell migration and proliferation (Jopling et al. 2012; Tanaka and Reddien 2011). The observation of shared cellular processes between some or all regeneration models, suggests potential common molecular mechanisms that govern these different regenerative contexts. Accordingly, some signaling pathways (e.g. ERK signaling) have been associated to specific injury-induced cellular behaviors such cell proliferation or migration in a variety of research models (Varga et al. 2014; P. Liu and Zhong 2017; Makanae et al. 2013; Tasaki, Shibata, Nishimura, et al. 2011; Manuel et al. 2006). In this regards kinases play a particular interesting role, as they

have been associated to a large variety of cellular processes during regeneration. Kinases are phosphorylating enzymes recruited for transducing extracellular signals to the nuclei, by activating effectors such as transcription (Seger and Krebs 1995). For instance the MAPK ERK is involved in the blastema formation in Zebrafish fin regeneration (Varga et al. 2014), Axolotl limb regeneration (Makanae et al. 2013) and planarian (Tasaki, Shibata, Nishimura, et al. 2011) or the EGFR receptor kinase regulating cell proliferation in Zebrafish fin regeneration (Rojas-Muñoz et al. 2009) heart regeneration (Gemberling et al. 2015) and Axolotl limb regeneration (Farkas et al. 2016).

In addition, in a recent study we studied the role of MEK/ERK signaling during regeneration of the sea anemone *Nematostella vectensis* (Johnston et al, in prep) and our results suggest a very conserved role of this pathway in response to injury as it was reported during regeneration of the planarian *Schmidtea mediterranea* (Tasaki, Shibata, Nishimura, et al. 2011). In fact, in both models, MEK/ERK is rapidly activated at the amputation site after injury.

The anthozoan cnidarian *Nematostella vectensis* is an emerging whole body regeneration model with unique features to study embryonic development and regeneration in the same organisms (Layden et al. 2016). Cnidarian are the extant sister group to bilaterian animals, and *Nematostella* has been developed since more than two decades primarily (but not exclusively) for investigating the evolution of axial pattering and germ layer formation (Wikramanayake et al. 2003; Darling et al. 2005). More recently, *Nematostella* is getting increasing attraction (Passamaneck and Martindale 2012; Schaffer et al. 2016; Amiel et al. 2015; Warner et al. 2018), Johnston et al, in prep,) in regard to its extreme regenerative capacity and complementarity with existing cnidarian regeneration models (e.g. *Hydra, Hydactinia*). Regeneration in *Nematostella* undergoes well-defined stereotypical morphological changes and after wound healing depends on cellular proliferation (Amiel et al. 2015). In addition, regeneration requires a tissue crosstalk between the mesenteries and the epithelia of the amputation site that is involved in activating two potential stem cell populations. Those in turn migrate towards the amputation site and actively participate in the reformation of lost body parts (Amiel et al, in revision). Although extensive transcriptomic data for regeneration are available (Schaffer et al. 2016; Warner et al. 2018), information about the molecular underpinning remains sparse. In fact, so far only cWnt and MEK/ERK signaling have been associated to regeneration (Burton and Finnerty 2009; DuBuc, Traylor-Knowles, and Martindale 2014), Johnston in prep). Latter pathway was used to functionally test an hypothesis resulting from a global transcriptomic comparison between embryonic development and regeneration (Warner et al, in submission).

111 Importantly, this functional study enabled us to show that the embryonic MEK/ERK
112 gene regulatory network is partially redeployed, rewired and interconnected with
113 regeneration specific elements to allow the reformation of lost body parts (Johnston
114 et al, in prep). Unfortunately, this works covers only a small portion of Nemastostella
115 regeneration.

116 *Nematostella* is a research model with easy access to large quantities of
117 biological material and for which the entire life cycle can be covered in the
118 laboratory (Hand and Uhlinger 1992). While *Nematostella* would be suitable for
119 genetic, mutagenic or small molecule screens, so far no such projects have been
120 reported. Therefore, and in order to identify elements/signaling pathways that are
121 involved in coordinating the various process of *Nematostella* regeneration program,
122 we performed a kinase inhibitor screen and assessed their effects on the
123 reformation of oral body parts. In total, we screen 78 compounds described to block
124 activities of a large range of kinases. Following the primary screen that revealed 28
125 compounds affecting regeneration in *Nematostella*, we pursued our study with a
126 detailed characterization of one of them, the MAPK JNK. Building on our current
127 knowledge and tools available to study oral regeneration in *Nematostella*, we have
128 been able to show that JNK activity is crucial for the onset of regeneration through
129 the regulation of regeneration-specific cell proliferation.
130

Results

1. *Nematostella vectensis* is amenable for screening pharmacological compounds affecting whole body regeneration

In order to gain insight into the roles that kinases play in the whole body regeneration process of *Nematostella*, we used a library of commercially available kinase inhibitors. This library is composed of 80 pharmaceutical inhibitors of described activity, targeting a total 30 different membrane-associated or cytoplasmic kinases (ENZO BML-2831 SCREEN-WELL® Kinase Inhibitor library). The overall screening strategy is illustrated in Figure 1A and described in detail in material & methods. Basically, the screen was performed in 24-well plates and each drug was tested at 10µM on 40 sub-pharyngeally amputated juveniles (Amiel et al. 2015). The tested kinase inhibitors were added right after amputation (0hpa), renewed every 48 hours post amputation (hpa) to maintain activity and screened for the final phenotype 144hpa. During the entire period, animals and inhibitors were kept protected from light to avoid any potential photosensitive inactivation of the drugs. After 144hpa, the effects of the treatments on the regeneration process were assessed under a binocular and scored for the presence (Fig. 1B) or absence (Fig. 1C) of a reformed head (indicated by the presence of a new pharynx and a tentacle crown), as well as for any toxic effect (Fig. 1D). We further took into account whether the added compound precipitated at 10µM in 1/3X ASW (Fig. 1E).

A summary of the obtained results from this screen is shown in Figure 1F. 28 out of the 78 tested kinase inhibitors had no visible effect on oral regeneration and resembled control animals (Fig. 1B, Table 2), while 22 were toxic or precipitate at 10µM (Fig. 1D,E Table 3). However, for 28 kinase inhibitors we determined clear perturbations in the reformation of the lost oral body parts (Fig. 1C, Table 1). Importantly, the screened compound included U0126, a potent MEK inhibitor that was previously shown to be crucial for oral regeneration in *Nematostella* (DuBuc, Traylor-Knowles, and Martindale 2014), Johnston et al. in prep) that served us an internal positive control for the efficacy of the screen. The identified candidate kinases can be assembled into seven signaling pathways which have all been investigated during various regeneration context *i.e* MAPK (ERK and JNK) signaling is crucial for early steps of planarian regeneration(Tasaki, Shibata, Nishimura, et al. 2011; Agata et al. 2014), PI-3k/akt antler regeneration (Z. Liu et al. 2018), PI3-K/BTK, pancreas regeneration (Lee et al. 2018), PI3K/ERK for Hydra regeneration(Manuel et al. 2006), the cAMP/PKA for rat liver regeneration (Cheng et al. 2012), Src signaling for zebrafish fin regeneration (Yoo et al. 2012), and mTOR pathway in mice liver regeneration planarian (Fouraschen et al. 2013; González-Estévez et al. 2012)..

2. **JNK kinase plays a crucial role in *Nematostella* regeneration**

In total 14 different kinases are targeted by the 28 pharmacological drugs that inhibit regeneration in *Nematostella*. Namely, the EGFR, VEGFR, PDGFR, Mek, Btk, JNK, Src, CamkII, PKA, PKC, PKG, MLCK, CDK and mTOR kinases appear to be crucially required for the reformation of lost body parts (Table 1). It is important to

note that among those compounds, not all inhibitors potentially affecting the same kinase have redundant loss of regeneration phenotypes in *Nematostella*. For example, U0126 inhibits MEK's activation level (Davies et al. 2000) and blocks regeneration, while PD-98059 that also blocks MEK's activation (Davies et al. 2000) has no visible effects (Table 1 & 2). As the kinase inhibitors used in the present screen have been validated for mammalian cells, this observation indicates potential differences in the protein sequences and domain organization of the targeted kinases that make the tested compounds no equally potent. The roles of Mek and its potential activators, the Receptor Tyrosine Kinases PD/VEGFR and FGFR have been studied in detail in a previous study (Johnston et al. in prep). Among the other kinases that appear to affect regeneration in *Nematostella* when their function is perturbed (Fig. 1F, Table 1), we focused in the present study on the stress-associated MAPK JNK (c-Jun N-terminal kinase). In fact, JNK has been shown to be involved in the immediate stress response following injury in distant models such as planarians and zebrafish (Almuedo-Castillo et al. 2014; Gauron et al. 2013). Here we investigate the precise role of JNK during early stress response, wound healing and the onset of regeneration in *Nematostella*.

The pharmacological JNK inhibitor SP600125 is among the compounds that blocked oral regeneration in *Nematostella* in 100% of the cases at 10µM (Fig. 1C,F, Table 1). Using a previously published staging system (Amiel et al. 2015), we characterized the inhibitor phenotype more detailed at the morphological levels and determined that inhibiting JNK blocks regeneration at step 1, right after wound healing and the moment when the oral tips of the mesenteries enter in contact with the amputation site (Fig. 2A,E,E'). In contrast, control DMSO treated juveniles

reached steps 3 (reforming tentacles and pharyngeal lips, 33% - 4/12) and 4 (reformed tentacles, pharynx and opened mouth, 66% - 8/12) after 144hpa (Fig. 2A,B,B'. In order to define a lower optimal concentration for the following experiments and thus limiting the potential off-targeting effect, we repeated the experiment but with slightly lower concentrations of SP600125, namely 7,5µM and 5µM (Fig. 2). Amputated and SP600125 treated juveniles at 7,5µM were blocked in 100% of the cases (23/23) in step 1 (Fig. 2A,D,D'). This is identical to the numbers obtained for 10µM treatments (Fig. 2A, E,E'). However, when the treatment was performed at 5µM only 75% (18/24) of the animals were blocked in step 1, while the remaining 25% (6/24) were blocked in step 3 (Fig. 2A,C,C'). We thus decided to proceed with SP600125 treatments at 7,5µM for the subsequent experiments.

3. Slight up-regulation of Nve-jnk expression and Nve-JNK activation upon injury

Using the mammalian (MmMAPK8 (JNK), UniProtID: Q91Y86) we searched an extensive *Nematostella* transcriptomic database (Warner et al. 2018), nvertx.kahikai.org) and identified one gene (jgi|Nemve1|92175|e_gw.29.1.1) that has 72,5% identity with its murine counterpart and for which the best NrHit corresponds to an *Acropora digitifera* (coral) JNK prediction (data not shown). The identification of only one *jnk* gene in *Nematostella* is in line with the presence of only one JNK in *Hydra* (Philipp, Holstein, and Hobmayer 2005) as well as the recent identification and characterization of a single JNK in the coral *S. pistillata* (Courtial et al. 2017) and suggests that cnidarians possess only one copy of this MAPK. Further taking advantage of the *Nematostella* temporal gene expression database (Warner

et al. 2018) we analyzed expression of the *Nve-jnk* transcript (NvERTx.4.177983) during the process of regeneration (Fig. 3A). Interestingly, *Nve-jnk* appears to be homeostasically expressed in uncut juveniles and only slightly (less than 2-fold variation) up-regulated upon injury (Fig. 3A). Nonetheless, a first up-regulation is observed between 2-4hpa and a second one after wound healing between 8-36hpa (Fig. 3A) suggesting an active role in the immediate stress response and the onset of regeneration after 8hpa.

However, MAP Kinases such as JNK, require the phosphorylation of specific residues for their functional activation (Davis 2000). Thus, in order to gain insight into the JNK activation pattern following injury, we used a polyclonal antibody that is specifically directed against the dually phosphorylated and active form of JNK (pJNK, Promega # V7931) during 24 hours following amputation (Fig. 3B). **The following results are preliminary results that need to be confirmed by additional experiments**. In line with our observation of homeostatic *Nve-jnk* expression (Fig. 3A), but in contrast to what is observed in human fibroblasts and coral extracts under physiological conditions (Courtial et al. 2017), we clearly detected pJNK in uncut juveniles (Fig. 3B). As only one JNK has been identified in *Nematostella,* we were puzzled to observed two bands in our western blot analysis: one major band at about 40kDa that is close to the predicted size of 39,6kDa (https://www.bioinformatics.org/sms/prot_mw.html) and one very minor band that is close to 50kDa. Anisomycin, a known agonist of JNK is frequently used to test the specificity of the antibody (Rosser et al. 2004; Courtial et al. 2017). In *Nematostella*, anisomycin treatments at 1µg/ml, only slightly increases the 40kDa band, but very strongly increased the detected amount of the 50kDa band (Fig. 3B). Interestingly,

after amputation the 50kDa band does not vary during the first 24 hours. However, the 40kDa band intensity seems to increase slightly after injury up to 4hpa (Fig. 3B) compared to uncut controls, suggesting that pJNK is activated upon injury. In the following hours, the pERK levels remain at this slightly increased, but stable level (Fig. 3B). **While this observation appears to be in line with what we observed at the *Nve-jnk* gene expression levels (Fig. 3A), the loading control required to perform a quantitative analysis of the western blot results, was not useable and thus, needs to be redone.** Unfortunately the antibody against pJNK couldn't be use to assay the effectiveness of the inhibition of JNK by SP600125 because this drug doesn't prevent the phosphorylation of JNK but rather the phosphorylating activity of this kinase (Bennett et al. 2001).

Taken together, these observation suggest that a) the homeostatic and basal 40kDa activity observed in uncut animals can only slightly increased after stimulation with either anisomycin or after injury and b) that either a bigger splice variant of JNK or another JNK-like MAPK that we missed, is also recognized by the polyclonal AB and sensitive to anisomycin. Additional studies to understand the entire phylogeny of the MAPK complement in *Nematostella* is required to shed further light on this question.

4. JNK is important for the onset of regeneration

Our experiments during which we continuously treated amputated animals with SP600125 have shown that JNK in *Nematostella* is blocking regeneration after reaching the first step (Fig. 2E,E'). In order to obtain a better resolution of the window of action of JNK in response to amputation, SP600125 treatments were

started at different moment after bisection; 24, 48 and 96 hpa and were maintained up to 144hpa (Fig. 3C). Regenerating animals were fixed at every beginning of treatment (DMSO 0-24hpa, DMSO 0-48hpa and DMSO 0-96hpa) as well as at the end of regeneration at 144hpa (DMSO 0-144hpa, SP 24-144hpa, SP 48-144hpa and SP96-144hpa). A schematic representation of the experimental design is shown in Figure 3C. Figure 3D is the statistical analysis of the obtained phenotypes and the majority phenotype for each condition is shown in the panels of Figure 3E. In agreement with a previous study (Amiel et al. 2015), DMSO treated controls are in step 1, steps 1 and 2, steps 3 and 4, and step 4 at 24, 48, 96 and 144hpa respectively (Fig. 3D-H). When amputated animals were treated with SP600125 from 24-144hpa, the final phenotype is identical to a continuous 0-144hpa treatment that blocks regeneration in step 1 (Fig. 2E,E', 3D,I). Moreover the step 1 phenotype observed after the inhibition of JNK from 24-144hpa, exhibits an apparent thickening of the tissue at the tips of the mesenteries in 100% of the cases (Fig. 3F) compared to control step 1 after 0-24hpa DMSO treatments (Fig. 3E). Interestingly, animals treated with SP600125 from 48-144hpa or 96-144hpa, reached systematically the final steps of regeneration 3 and 4 (Fig. 3D,H,J) with the same proportions that DMSO treated animals from 0-96hpa (Fig. 3D,J). Taken into account that not all animals reached step 4 like 0-144hpa DMSO treated controls (Fig. 3D,K), this observation suggests a slight delay in the late regenerative processes caused by the inhibition of JNK.

All together these results indicate that JNK in *Nematostella* plays an important role in pushing the stress response phase to an advanced step 1 and thus preparing the tissue at the amputation site to the transition towards step 2 and all subsequent steps of regeneration. In fact, when JNK is inhibited at 24hpa when all

animals reached step 1, regeneration is blocked at this stage. However, when the process proceeds and the animals are in an advanced step 1 / early step 2 phase, inhibition has no/only minor effects on the final success of regeneration. This clearly shows the importance of JNK signaling in early phases of regeneration.

5. Regeneration-specific cell proliferation regulated by JNK

Cell proliferation is witnessed in *Nematostella* as part of the tissue homeostasis (Fig. 4A') (Passamaneck and Martindale 2012). It is also known that sub-pharyngeal amputation *Nematostella* induces cell proliferation at the amputation site and that it is strictly required for reforming lost body parts (Passamaneck and Martindale 2012; Amiel et al. 2015). In addition, the transition between steps 1 and 2 is proliferation dependent as inhibition of this cellular process blocks all animals in step 1 (Amiel et al. 2015). Interestingly, the results described above strongly suggest a crucial role of JNK signaling for the transition between steps 1 and step 2. Thus, we investigated the relation between JNK and cell proliferation under homeostatic and regenerative conditions (Fig. 4). As *Nve-jnk* expression and JNK activity are present homeostatically in uncut animals, we first wondered whether JNK signaling is involved in homeostatic cell proliferation in *Nematostella*. In order to test that, we treated uncut animals with DMSO or SP600125 for 24 hours and analyzed cell proliferation via the presence of EdU+ cells (cells in S-phase) (Fig. 4A,A',E,E'). Interestingly, we did not observe a significant difference between these two conditions where Edu+ cells are observed throughout the body column in the body wall epithelia, the pharynx as well as the mesenteries (Fig. 4A,A',E,E',I,J).

We then wondered whether JNK signaling was involved regeneration-induced cell proliferation that participates in the reformation of the oral structures in *Nematostella* (Passamaneck and Martindale 2012; Amiel et al. 2015). To address this question, we performed three different 24 hours SP600125 treatments, between 24-48hpa (Fig. 4F,F'), 36-60hpa (Fig. 4G,G') and 48-72hpa (Fig. 4H,H'). At the end of every window of treatment, EdU was incorporated for 30 minutes prior to fixing the regeneration animals. As it was previously reported from DMSO treated *Nematostella* (Passamaneck and Martindale 2012; Amiel et al. 2015), proliferation is increasing progressively at the amputation site in both the body wall epithelia and the oral tips of the mesenteries (Fig. 4B',C',D'). However, when bisected animals were treated with SP600125 between 24-48hpa, cell proliferation is significantly reduced in all tissue types (Fig. 4F',I,J). To our surprise, we observed that inhibiting JNK signaling in amputated *Nematostella* between 36-60hpa or 48-72hpa drastically and significantly inhibits cell proliferation within the body wall epithelia (Fig. 4G',H',I), while cell proliferation in the mesenteries is barely and not significantly affected (Fig. 4J) compared to controls. **While, experiments are missing to test the role of JNK signaling on the onset of regeneration-induced cell proliferation**, our data suggest an important role of JNK signaling in the early phases of the proliferative burst at the amputation site during the transition from step 1 to step 2. In later phases of regeneration, JNK appears to be differentially required for maintaining cellular proliferation of particular cell populations within the body wall epithelia at the amputation site, but not the mesenteries.

Conclusion

In this study we have shown that *Nematostella* is amenable for screening approaches of pharmacological inhibitors in a regenerative context. As a consequence we have screened 78 pharmacological kinase inhibitors and identified 28 compounds targeting 14 different kinases that inhibit regeneration. Among these hits, this study has focused on the implication of the JNK MAPK pathway during whole body regeneration in *Nematostella*. Intriguingly, this stress-associated kinase appears constitutively expressed and active during homeostasis of the animals and only slightly up-regulated upon injury and during regeneration. A precise morphological and cellular characterization of the JNK inhibition phenotype further highlights the importance of this kinase for the initiation of the regeneration process (transition step 1 to step 2) and by regulating regeneration-specific cell proliferation. Interestingly, inhibiting JNK in uncut controls does not affect cell proliferation in homeostatic conditions, thus opening the path to investigate the genetic program underlying the control of regeneration specific cell proliferation. Taken together, our results suggest that the slight increase in JNK activity upon injury is sufficient for launching the stress response and induce regeneration-specific cell proliferation required for reforming lost body parts.

Discussion

Nematostella regeneration is amenable for screening compound libraries

Based on the biological features of *Nematostella*, such as a controlled a fairly short life cycle (~2 months, Röttinger unpublished), the access to large amounts of biological material, the small size of juveniles and that maintaining laboratory cultures is cheap and straight forward (Hand and Uhlinger 1992), this cnidarian offers the great opportunity for mutagenesis, genetic or compound screens. However, no such experimental approaches have been reported so far in *Nematostella*. In the present study, we performed a semi-large screening of pharmacological compounds by using regeneration as a proxy and identified kinases involved during whole body regeneration in this sea anemone. While we observed loss of regeneration phenotypes, we did not identify any compound that accelerates the regeneration process or led to ectopic oral structures.

As seen above, we were able to successfully carry out this compound screen, however, we nevertheless observed certain caveats that need to be taken into account in future compound screening efforts. The fix concentration of 10µM we used for the screen was the same for all compounds. This concentration was determined according to the range of concentrations used in *Nematostella* to perturb specific pathways during embryonic development or adults (Rentzsch et al. 2008; Trevino et al. 2011; Röttinger, Dahlin, and Martindale 2012; Marlow et al. 2012; DuBuc, Traylor-Knowles, and Martindale 2014). As a drawback, setting a unique concentration may lead to false negative results could explain the

ineffectiveness of some drugs at 10µM. For instance the kinases CDK, EGFR, PDGFR, Mek, PKA, PKG and PKC had many inhibitors blocking regeneration at 10µM, while other inhibitors targeting the same kinases didn't affect regeneration at the same concentration (Table 2). Another example for which the 10µM concentration might be to low, is the inhibitors for PI3K. In fact, in our screen none of the two PI3K inhibitors were visibly affecting regeneration in *Nematostella* (Table 2). As Pi3K plays a crucial role during *Hydra* regeneration (Manuel et al. 2006), we performed preliminary test on the effects of LY297002 at 15µM and observed the loss of tentacle regeneration after 144hpa (data not shown). On the other hand, a similar logic is also applicable to compounds that are toxic for a given concentration. For example, H9HCL that targets PKC (as well as PKA and PKG) will block regeneration. However, Hypermicin a specific inhibitor of PKC will show no phenotype, while palmitoyl-D-carnitin another specific inhibitor of PKC will be toxic at 10µM. In sum, this clearly indicates that by performing medium or large size screens at fixed concentration we can support that compounds that cause a phenotype are indicative of a role of the targeted pathway in the regeneration process. On the other hand, the absence of a phenotype, or toxicity is clearly not indicative of the dispensable role of pathways in this process. More concentration depended assays and more importantly, gene specific approaches are required to fully address this question.

Another aspect to take into account is that the kinase inhibitor library we used in our study contains compounds for which the kinase specific effects have been validated in mammalian cells. This does not necessarily mean that the targeted sites are conserved throughout evolution and cause the same effects in cnidarians. In this study, we identified 28 inhibitors that in theory target 14 different kinases and

block regeneration in *Nematostella*. For most of the kinases targeted by these inhibitors, homologs are found in the sea anemone genome (Putnam 2007). Intriguingly, 9 inhibitors that appear to affect specifically EGFR in mammalians, this growth factor receptor has not been identified in the *Nematostella* genome (D'Aniello et al. 2008), (Johnston et al, in prep). This naturally raises the question about the specificity of the compound in *Nematostella*, i.e. targeting other growth factor receptors. Thus, additional experiments are required to precisely address the mode of function of these EGFR inhibitors in *Nematostella* and gene specific approaches needed to confirm the preliminary results issued by the compound screen.

Conservation of JNK signaling during regeneration

The MAPK JNK has been described in multiple regeneration contexts, including vertebrate and invertebrates (Ishida et al. 2010; Tasaki, Shibata, Sakurai, et al. 2011; Philipp, Holstein, and Hobmayer 2005). The activation of this kinase by the ROS has been link to two roles during fin regeneration of the Zebrafish (Ishida et al. 2010). One role of JNK is to regulate the expression of genes in the blastema epidermis, which is mediate by the transcription factor Junb, while the other role is mediated by the transcription factor Junl1 (Ishida et al. 2010). The latter signaling pathway is up-stream of the regeneration-specific proliferation necessary for the blastema formation (Ishida et al. 2010).

In invertebrates, such as Planarian, JNK is also controlling various aspect of regeneration (Tasaki, Shibata, Sakurai, et al. 2011; Almuedo-Castillo et al. 2014; Tejada-Romero et al. 2015). At the anterior pole, its first role is related to wound

426 healing, during which it is responsible for the activation of the wound healing genes
427 *runt* and *egrl1* (Tasaki, Shibata, Sakurai, et al. 2011). While in the next step of
428 regeneration, JNK is responsible for promoting the neoblast proliferation during the
429 formation of the blastema by modulating the cell cycle (Tasaki, Shibata, Sakurai, et
430 al. 2011). In comparison, at the posterior pole, JNK signaling pathway has been
431 dissected and the MKK7 (hem) have been describe to pJNK, which in turn
432 phosphorylate the transcription factor Junl-1 (Tejada-Romero et al. 2015).

433 In another cnidarian, JNK pathway has also been implicated with
434 regeneration (Philipp, Holstein, and Hobmayer 2005). In Hydra, HyJnk and its
435 putative effectors Hvfos and hvJun are upregulated in response to the amputation
436 (Petersen et al. 2015). Moreover, it has been demonstrate that JNK pathway is also
437 signaling through *HvJun* (Philipp, Holstein, and Hobmayer 2005).

438 The role of JNK in these various regeneration contexts is supporting the role
439 of NvJnk in promoting the regeneration-specific proliferation we reported in this
440 study. Moreover, it also reveals an important conservation of JNK role in
441 regeneration between vertebrates and invertebrates. Additionally, there is
442 apparently also an apparent conservation of JNK signaling through its putative
443 effectors Jun (Davis 2000). Therefore investigating this link between JNK and Jun in
444 *Nematostella* would bring more evidence of this conservation but furthermore if
445 true, it would be a valuable proxy to validate the specificity of JNK inhibitor
446 SP600125.

Next step of the study

The present study lays the foundation for further investigations concerning the molecular implication of JNK signaling. Although the upregulation/activation of expression is only limited, it nonetheless appears to be involved in initiating the regeneration-specific phase of the stress response program. It would be therefore interesting to figure out what signal(s) are activating JNK at the gene expression and activity levels. In Hydra, ROS appears to be involved in this process and it would therefore be interesting to investigate if this role of ROS signaling is conserved also in *Nematostella*. Another important aspect is to identify the genetic program downstream of JNK signaling. Using a comprehensive transcriptomic database (Warner et al. 2018), we have access to all genes expression profiles during the regeneration process and in particular the expression profiles of putative effector of the JNK pathways such as *atf, elk* or *c-jun*, genes encoding for transcription factors (Davis 2000). Interestingly, six putative effector genes of JNK are present in *Nematostella* genome: *Nvjun1* (NvERTx.4.74934) *Nvjun2* (NvERTx.4.59115), *Nvatf2* (NvERTx.4.99632), *Nvelk* (NvERTx.4.4.92233), *Nvelk-1* (NvERTx.4.17448) and *Nvelk-4* (NvERTx.4.70389). These putative effector can be regroup according to their expression profile, a first group with an early activation of their expression after 12hpa (*Nvatf2*, *NvElk* and *NvElk-1*) and another group expressed later after 36hpa (*Nvjun1*, *Nvjun2* and *Nvelk-4*). Therefore, suggesting two different role of JNK mediated by different effectors.

468 Based on their expression profiles we could subsequently identify candidate
469 downstream targets with similar expression patterns. Refining the JNK activation
470 pattern *in situ*, combined with the spatial expression pattern of the effectors and
471 potential downstream targets will further enable us define syn-expression groups,
472 potentially involved in the same signaling pathway. Ultimately, the true downstream
473 targets need to be validated by gene specific KO or KD experiments followed by gene
474 expression assays
475

Figures

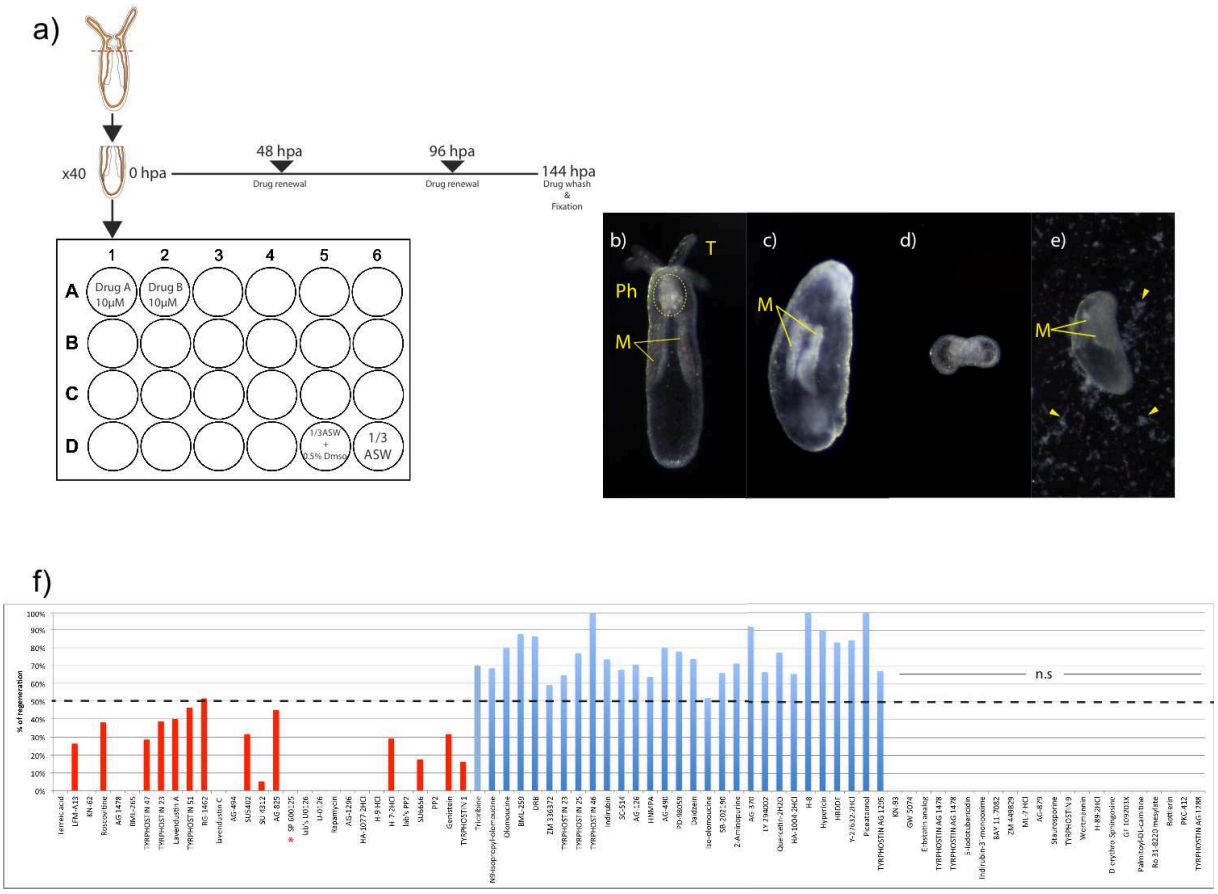

Figure 1: Screening of the kinase inhibitors library during *N.vectensis* regeneration. In **a)** is presented the workflow of the screening. In a 24-well plate 40 cut juveniles were placed per well and treated with 10µM of drug in 1/3 ASW. Two wells were kept as control: one was dedicated for 1/3 ASW+0.5% Dmso and the other one only contained 1/3 ASW as a control for regeneration. Over the 144 hours of treatment each drug was renewed every 48 hpa. In total 22 drugs where tested per 24-well plate. In **b-e)** are image of the phenotypes used to assess the effect of the drugs on regeneration, **b)** fully regenerated polyp, **c)** inhibited regeneration, **d)** complete degradation of the polyp and **e)** when drugs precipitate (yellow arrows). In **f)** the overall results from the screening of 78 kinase inhibitors. A drug was retained as affecting regeneration if there where less than 50% of the juveniles that have regenerate (red bars). Inversely, over 50% of regeneration in the well, the drugs where classified as

none affecting regeneration at 10µM (blue bars). Lastly some drugs couldn't be tested at 10µM because either they precipitate or were toxic (n.s). *Hpa, hours post-amputation; ASW, artificial seawater; n.s, not significant*; T*, tentacles; Ph, pharynx; M, mesenteries*.

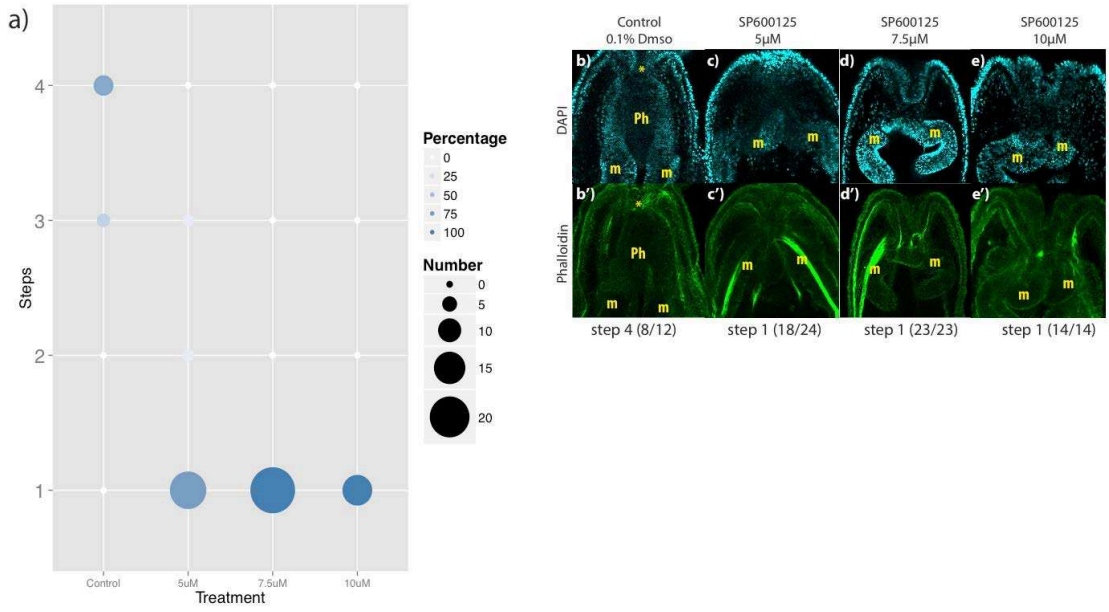

Figure 2: Dose-dependent regeneration assay of the JNK's inhibitor SP600125.

In **a)** is a Dot plot of the different steps after 144 hpa of continuous treatment with SP600125 at different concentrations . The size of the dots represent the number of animals per steps while the color intensity represent the percentage of animals. In **b-c)** and **b'-c')** the morphology of each major phenotype with a dual straining of DAPI (cyan) and phalloidin (green) staining to visualize the nuclei and the actin respectivel. In **b)** and **b')** a fully regenerated head, in **c-e)** and **c'-e')** a step 1 phenotype.**, the mouth opening; Ph, pharynx; m, mesenteries.*

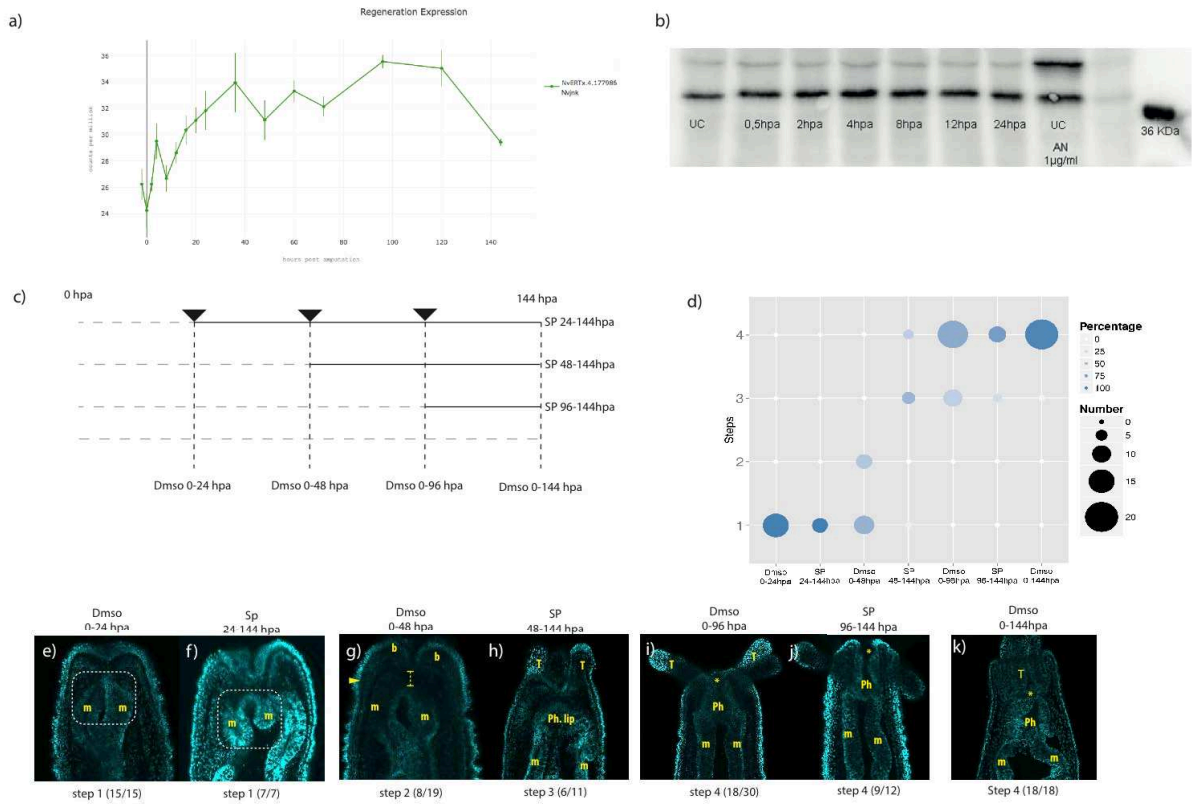

Figure 3: JNK expression profile and its window of action

In **a)** the transcript expression profile of *Nvjnk* from the transcriptomic data base NvERTx and its associate NvERTx identification code. In **b)** Westernblot of pJNK with protein extracted from uncut polyps (*UC*) and polyps at 0.5hpa, 2hpa, 4hpa, 8hpa, 12hpa and 24hpa with a positive control for the antibody pJNK with protein extracted from uncut polyps treated for 30 minutes with 1µg anysomycine (*An*). In **c)** work flow of the time window experiment performed with 7.5µM SP600125 (JNK inhibitor) starting at different time post-amputation, 24hpa, 48hpa and 96hpa and fiwed at 144hpa, with the associate control 0.75% Dmso started at 0hpa and fixed at the beginning of each treatment, 24hpa, 48hpa, 96hpa. In **d)** Dot plot of the time window experiment. In **e-k)** DAPI staining of the most represented steps in Dmso controls (**e**, **g**, **I**, **k**) and treated with SP600125 (**f**, **h, j**) animals. The dashed box (**e** and **f**) highlight the different morphology of the mesenteries of Dmso controls step 1 at 24hpa and treated animals from 24-144hpa (*m, mesenteries; b, buds; Ph, pharynx; T, tentacles; *, mouth opening;, Ph. Lip, pharyngeal lip).*

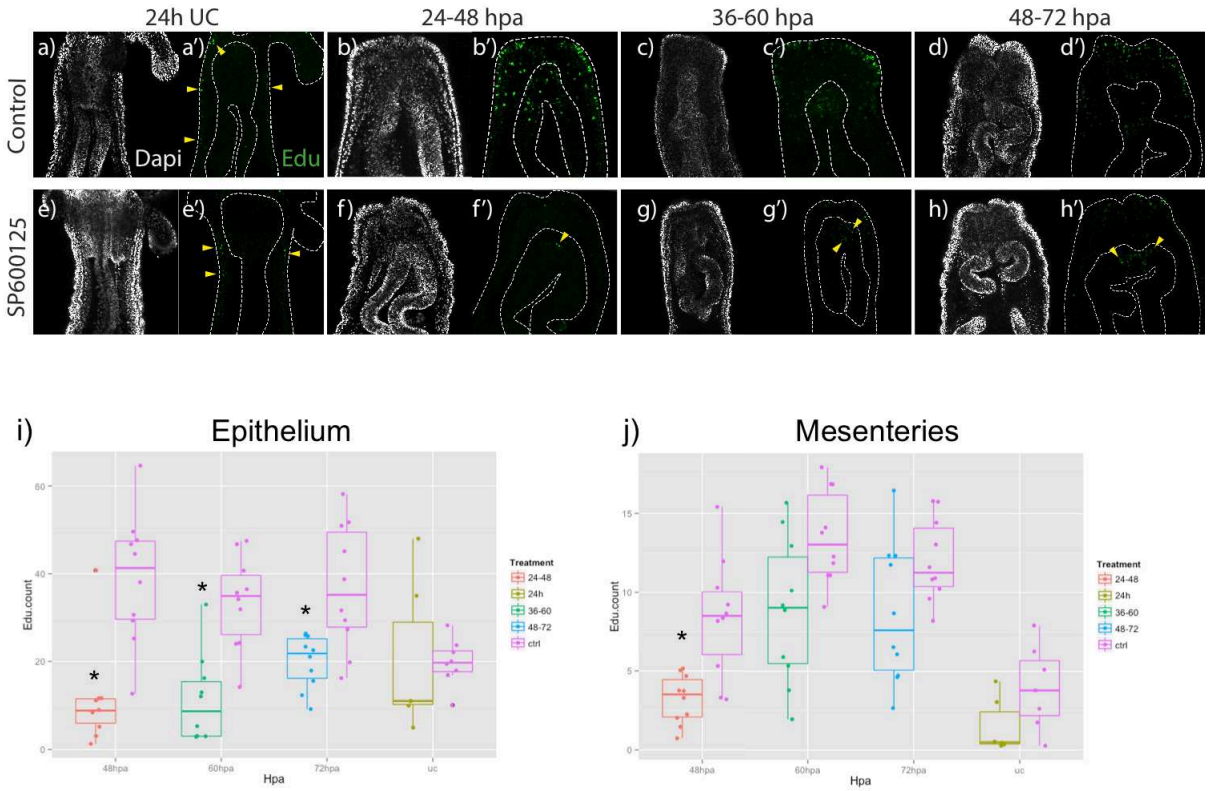

525

526 **Figure 4: The effect of inhibiting JNK on cell proliferation by EdU staining**

527 In **a** – **h** and **a**' – **h'**) proliferating cells stained with EdU click-it technology with
528 the EdU+ cells are in green aditioned with counter staining of the nuclei with
529 DAPI in grey. The animal where treated for 24 hours, with 0.075% Dmso
530 (Control) (**a - d** and **a' - d'**) or 7.5µM SP600125 (**e** – **h** and **e'** - **h'**), before 30
531 minutes of EdU incorporation and fixation at 48 hpa (**b** and **b'**), 60 hpa (**c** and
532 **c'**), 72 hpa (**d** and **d'**) and in the uncut animals (uc) (**a** and **a'**). Box plot of
533 separated EdU+ cells counting (cells per 100µM) between the body wall
534 epithelium (**i**) and the mesenteries (**j**) for each window of 24 hours treatment.

535

Table 1: List of kinase inhibitors affecting regeneration at 10µM

Kinase Inhibitor	Target(s)	% of regeneration
Terreic acid	BTK	0%
LFM-A13	BTK	26%
KN-62	CaMK II	0%
Roscovitine	CDK	38%
AG 1478	EGFRK	0%
BML-265	EGFRK	0%
TYRPHOSTIN 47	EGFRK	29%
TYRPHOSTIN 23	EGFRK	39%
Lavendustin A	EGFRK	40%
TYRPHOSTIN 51	EGFRK	46%
RG-1462	EGFRK	52%
AG-825	EGFRK (HER1-2)	45%
lavendustin C	EGFRK, CaMK II	0%
AG-494	EGFRK, PDGFRK	0%
SU5402	FGFR	32%
SU 4312	Flk1 (VEGFR 2)	5%
SP 600125	JNK	0%
lab's U0126	Mek	0%
U-0126	Mek	0%
Rapamycin	mTOR	0%
AG-1296	PDGFRK	0%
HA-1077·2HCl	PKA, PKG	0%
H-9·HCl	PKA, PKG, MLCK, and PKC.	0%
H-7·2HCl	PKA, PKG, MLCK, and PKC.	29%
lab's PP2	Src	0%
SU6656	Src	18%
PP2	Src	0%
Genistein	Tyrosine Kinases	32%
TYRPHOSTIN 1	Tyrosine kinases	16%

Table 2: List of kinase inhibitors not affecting regeneration at 10µM

Kinase Inhibitor	Target(s)	of regeneratiect on regenerat	
Triciribine	Akt signaling pathway	70%	no
N9-isopropyl-olomoucine	CDK	68%	no
Olomoucine	CDK	80%	no
BML-259	Cdk5/p25	88%	no
DRB	CK II	86%	no
ZM 336372	cRAF	59%	no
TYRPHOSTIN 23	EGFRK	65%	no
TYRPHOSTIN 25	EGFRK	77%	no
TYRPHOSTIN 46	EGFRK, PDGFRK	100%	no
Indirubin	GSK-3beta, CDK5	73%	no
SC-514	IKK2	68%	no
AG-126	IRAK	70%	no
HNMPA	IRK	64%	no
AG-490	JAK-2	80%	no
PD-98059	Mek	78%	no
Daidzein	Negative control for Genistein.	74%	no
Iso-olomoucine	Negative control for olomoucine.	52%	no
SB-202190	p38 MAPK	66%	no
2-Aminopurine	p58 PITSLRE beta1	71%	no
AG-370	PDGFRK	92%	no
LY 294002	PI 3-K	67%	no
Quercetin·2H2O	PI 3-K	78%	no
HA-1004·2HCl	PKA, PKG	66%	no
H-8	PKA, PKG	100%	no
Hypericin	PKC	90%	no
HBDDE	PKC alpha, PKC gamma	83%	no
Y-27632·2HCl	ROCK	85%	no
Piceatannol	Syk	100%	no
TYRPHOSTIN AG 1295	Tyrosine kinases	67%	no

Table 3: List of kinase inhibitors toxic or precipitating at 10µM

Kinase Inhibitor	Target(s)	% of regeneration	Effect on regeneration
KN-93	CaMK II	n.s	toxic
GW 5074	cRAF	n.s	toxic
Erbstatin analog	EGFRK	n.s	toxic
TYRPHOSTIN AG 1478	EGFRK	n.s	toxic
TYRPHOSTIN AG 1478	EGFRK	n.s	toxic
5-Iodotubericidin	ERK2, adenosine kinase, CK1, CK2,	n.s	toxic
Indirubin-3'-monooxime	GSK-3beta	n.s	toxic
BAY 11-7082	IKK pathway	n.s	toxic
ZM 449829	JAK-3	n.s	toxic
ML-7·HCl	MLCK	n.s	toxic
AG-879	NGFRK	n.s	toxic
Staurosporine	Pan-specific	n.s	toxic
TYRPHOSTIN 9	PDGFRK	n.s	toxic
Wortmannin	PI 3-K	n.s	toxic
H-89·2HCl	PKA	n.s	toxic
D-erythro-Sphingosine	PKC	n.s	toxic
GF 109203X	PKC	n.s	toxic
Palmitoyl-DL-carnitine	PKC	n.s	toxic
Ro 31-8220 mesylate	PKC	n.s	toxic
Rottlerin	PKC delta	n.s	toxic
PKC-412	PKC inhibitor	n.s	toxic
TYRPHOSTIN AG 1288	Tyrosine kinases	n.s	toxic

Material and methods

Animal care and handling

Sea anemones are cultured in 1/3 ASW (Artificial Sea Water; Tropic-Marin Bio-actif system sea salt, Wartenberg, Germany)) at the Institute of Research on Cancer and Aging of Nice of the University of Nice. Adults are reared at 16°C and fed three times a week with freshly hatched *Artemia*. The spawning cycle is kept monthly between four colonies and it is carried out as described in (Hand and Uhlinger 1992; Fritzenwanker et al. 2007; Stefanik, Friedman, and Finnerty 2013). Juveniles are reared at 22°C and feeding starts from week two. Juveniles are fed once a week with smashed *Artemia*, until week 8. Until adulthood, animals are then fed with hatched brine shrimps.

Animal bisection and regeneration experiment

Regeneration experiments were all performed on six weeks old juveniles that were starved for two weeks. Prior cutting, animals are relaxed for 5 min in 5ml of 1/3ASW on a light table then 1ml of 7.13% of MgCl2 in ASW is added to anesthetize the animals. Sub-pharyngeal bisection is done using a microsurgery scalpel n°15 (Swann-Morton, Sheffield, UK). After dissection, animals are washed three times with 1/3 ASW and incubated at 22°C in darkness for regeneration. The JNK inhibitor, SP600125 was purchased from Sigma (ref: S5567-5MG) and resuspended in DMSO for a stock solution of 10mM. For each treatment, the culture medium and animals were incubated in darkness.

Screening protocol

Approximately 1,000 juveniles were cut per 24-well plate (Falcon® 24-well multiwall plate with low evaporation lid) and 40 juveniles were distributed in each well. To analyze the effects on whole body regeneration of the entire kinase inhibitor library approximately 4,000 juveniles were used. One well served as a regeneration control with only 1/3 ASW and another one was reserved for the DMSO control that contained 1/3ASW + 0.5% Dmso. The library was purchased from Enzo life science (BML-2831 SCREEN-WELL® Kinase Inhibitor library). All compounds were stored in DMSO as a stock solution at 10mM. Based on available functional information on the effects of kinase inhibitors in *Nematostella* (Rentzsch et al. 2008; Trevino et al. 2011; Röttinger, Dahlin, and Martindale 2012; Marlow et al. 2012; DuBuc, Traylor-Knowles, and Martindale 2014), we performed the screen using a fixed concentration of 10µM for each compound. Thus, each compound was diluted freshly to 10µM in 1ml of 1/3 ASW and mixed for 1 min before adding it to the well. Inhibitors were renewed every 48hpa during which regenerating animals were checked for survival under a binocular. After 144hpa of treatment animals where relaxed and imaged alive directly within the wells. For each compound the percentage of regeneration was calculated according to a scoring system described in (Amiel et al. 2015). The threshold was set at 50%, meaning that every treatment that blocked regeneration in more than 50% of the analyzed animals were considered regeneration inhibiting compound (Figure 1b).

Fixation and animal staining

Prior to fixation, juveniles are relaxed for 5 to 10 min on light before adding 7.13% MgCl2 for another 5 to 10 min. Then animals are gently transferred to 1,5ml Eppendorf tubes, coated with PBw 0.1% (1X PBS + 0.1% Tween-20). Fixation is carried out by incubating the animals with 4% paraformaldehyde (Electron Microscopy Sciences #15714, Hatfield, PA, USA) in 1/3 ASW for one hour at room temperature or overnight at 4°C. Thereafter the samples are washed five times with PBw 0.1%. To analyze the general morphology, Hoechst staining (Invitrogen #33342, Carlsbad, CA, USA) at 1/5000 was used to label the nucleus, and BODIPY® FL PhallAcidin 488 (Molecular Probes #B607, Eugene, OR, USA) staining was used at 1/200 to label actin microfilaments (cell membranes and muscle fibers). Additionally, cell proliferation analysis was carried out using the Click-it EdU kit (Invitrogen #C10337 or #C10339, Carlsbad, CA, USA) following the protocol from (Passamaneck and Martindale 2012).

Protein extraction and Western blot

Proteins were extracted from 15 adults per condition. Animals where placed in 1.5 ml eppendorf tubes and spun using a bench centrifuge to pellet the animals and remove as much 1/3 ASW as possible. Immediately after, 300µl of lysis buffer (HEPES 50mM, NaCl 150mM, NaF 100mM, EDTA 10mM, NA4P207 10mM) was added followed by five rounds of 10sec sonication. Between each round, samples were incubated on ice for 1min. Thereafter, 200µl of lysis buffer with 1% Triton X-100 and an protease inhibitor cocktail (Apoprotine 20µg/ml, Vanadate 1mM, AEBSF 250µg/ml, Leupeptine 5µg/ml) is mixed to the sonicated samples. Finally the

samples are centrifuged at 12,000 rpm for 20 min at 4°C to pellet the remaining tissue and transfer the supernatant into a new tube that will be store at -80°C. The protein concentration of the samples was assessed using the BC assay protein quantification kit (Interchim Upima, 40840A) and each sample was subsequently aliquoted by mixing 75µl of protein extract with 25µl of Laemmli buffer 4x (Bio-Rad #1610747) and stored at -20°C. Before loading the aliquoted samples onto the 7.5% SDS polyacrylamide gel, they were denaturated with an incubation at 85°C for 5 min.

Electrophoresis was performed with 30µg of protein in migration buffer (Tris 3g/L, Glycine 14.2g/L, SDS 1%), following the protocol described in (Gilmore, Wolenski, and Finnerty 2012). The transfer was performed in transfer buffer (Tris 3g/L, Glycine 14,4g/L, 20% Ethanol). Afterwards the nitrocellulose membrane was saturated with saline buffer (Tris 0,24g/L, NaCl 1,63g/L, 5% BSA, 0.5% Tween-20) and the membrane incubated for 1 hour at room temperature with the primary antibody anti-pJNK (Cat.#9251; Cell Signaling Technology) diluted 1/1000 in the saline buffer. For positive controls of the antibody, proteins were extracted from uncut adults treated with 1µg/ml of Anisomicyne (Sigma A9789-5MG) for 30 min at 22°C. Revelation was carried out by chimioluminescence (EMD Millipore™ Substrats de chimioluminescence HRP Western Luminata™) on a chemioluminescence Imaging – Fusion SL (Vilber).

Imaging

Scoring of phenotypes and counting EdU+ cells was performed on either a Zeiss Axio Imager A2 microscope or a Zeiss LSM710 for confocal imaging running the LSM ZEN software (Carl Zeiss). Fluorescent images were false-colored, the fluorescent

channels merged using ImageJ (http://rsbweb.nih.gov/ij/) and cropped to final size in Photoshop Cs6 (Adobe Inc.). Analysis of the screening plates was done using a Zeiss Stereo discovery V8 mounted with a Canon 6D digital camera, triggering two external Canon Speedlite 430 EX II Flashes and controlled by the Canon Digital Photo Professional software (Canon Inc., Tokyo, Japan).

Acknowledgements

The authors also acknowledge Aldine Amiel for the discussion, Jacob Warner for the bioinformatics guidance, Valérie Carlin for animal care and the IRCAN's, the trainee. The Van Obberghen lab and in particular Gaia Fabris and Nadine Gautier for the western blot reagent and apparatus. Molecular and Cellular Core Imaging (PICMI) Facility. PICMI was supported financially by Cancéropole PACA, Région Provence Alpes-Côte d′ Azur, Conseil Départemental 06 and INSERM.

Competing interests

The authors declare no competing or financial interests

Author contributions

HJ and ER – Conceived, designed and performed experiments. HJ– generated, collected and analyzed data. ER, - Contributed reagents/materials/analysis tools, CG, - contributed BML-2831 SCREEN-WELL® Kinase Inhibitor library. HJ, ER - Drafted the manuscript. All authors read and approved the final manuscript

Funding

This work was supported by the ATIP-Avenir program (Institut National de la Santé et de la Recherche Médicale and Centre National de la Recherche Scientifique) funded by the Plan Cancer (Institut National Du Cancer, C13992AS), Seventh Framework Programme (631665), Association pour la Recherche sur le Cancer (PJA 2014120186) to ER, the Ministère de l'Enseignement Supérieur et de la Recherche as well as the Fondation pour la recherche médicale (FDT 20170437124) to HJ.

References

Agata, Kiyokazu, Junichi Tasaki, Elizabeth Nakajima, and Yoshihiko Umesono. 2014. "Recent Identification of an ERK Signal Gradient Governing Planarian Regeneration.." *Zoology (Jena, Germany)* 117 (3): 161–62. doi:10.1016/j.zool.2014.04.001.

Almuedo-Castillo, María, Xenia Crespo, Florian Seebeck, Kerstin Bartscherer, Emili Salò, and Teresa Adell. 2014. "JNK Controls the Onset of Mitosis in Planarian Stem Cells and Triggers Apoptotic Cell Death Required for Regeneration and Remodeling.." *PLoS Genetics* 10 (6): e1004400. doi:10.1371/journal.pgen.1004400.

Amiel, Aldine, Hereroa Johnston, Karine Nedoncelle, Jacob Warner, Solène Ferreira, and Eric Röttinger. 2015. "Characterization of Morphological and Cellular Events Underlying Oral Regeneration in the Sea Anemone, Nematostella Vectensis." *International Journal of Molecular Sciences* 16 (12): 28449–71. doi:10.3390/ijms161226100.

Bely, Alexandra E, and Kevin G Nyberg. 2010. "Evolution of Animal Regeneration: Re-Emergence of a Field.." *Trends in Ecology & Evolution* 25 (3): 161–70. doi:10.1016/j.tree.2009.08.005.

Bennett, B L, D T Sasaki, B W Murray, E C O'Leary, S T Sakata, W Xu, J C Leisten, et al. 2001. "SP600125, an Anthrapyrazolone Inhibitor of Jun N-Terminal Kinase.." *Proceedings of the National Academy of Sciences* 98 (24). National Acad Sciences: 13681–86. doi:10.1073/pnas.251194298.

Bosch, Thomas C G. 2007. "Why Polyps Regenerate and We Don't: Towards a Cellular and Molecular Framework for Hydra Regeneration.." *Developmental Biology* 303 (2): 421–33. doi:10.1016/j.ydbio.2006.12.012.

Burton, Patrick M, and John R Finnerty. 2009. "Conserved and Novel Gene Expression Between Regeneration and Asexual Fission in Nematostella Vectensis.." *Development Genes and Evolution* 219 (2): 79–87. doi:10.1007/s00427-009-0271-2.

Cheng, Zhenchao, Lijuan Duan, Xiaoxia Hao, Zhanpeng Li, Gaiping Wang, and Cunshuan Xu. 2012. "Ten Paths of PKA Signaling Pathway Regulate Hepatocyte Proliferation in Rat Liver Regeneration." *Genes & Genomics* 34 (4): 391–99. doi:10.1007/s13258-011-0195-x.

Courtial, Lucile, Vincent Picco, Renaud Grover, Yann Cormerais, Cécile Rottier, Antoine Labbe, Gilles Pagès, and Christine Ferrier-Pagès. 2017. "The C-Jun N-Terminal Kinase Prevents Oxidative Stress Induced by UV and Thermal Stresses in Corals and Human Cells.." *Scientific Reports* 7 (April). Nature Publishing Group: 45713. doi:10.1038/srep45713.

D'Aniello, S, M Irimia, I Maeso, J Pascual-Anaya, S Jimenez-Delgado, S Bertrand, and J Garcia-Fernandez. 2008. "Gene Expansion and Retention Leads to a Diverse Tyrosine Kinase Superfamily in Amphioxus." *Molecular Biology and Evolution* 25 (9): 1841–54. doi:10.1093/molbev/msn132.

Darling, John A, Adam R Reitzel, Patrick M Burton, Maureen E Mazza, Joseph F Ryan, James C Sullivan, and John R Finnerty. 2005. "Rising Starlet: the Starlet Sea Anemone, Nematostella Vectensis.." *BioEssays : News and Reviews in Molecular, Cellular and Developmental Biology* 27 (2): 211–21. doi:10.1002/bies.20181.

697 Davies, S P, H Reddy, M Caivano, and P Cohen. 2000. “Specificity and Mechanism of
698 Action of Some Commonly Used Protein Kinase Inhibitors..” *The Biochemical*
699 *Journal* 351 (Pt 1): 95–105.
700 Davis, R J. 2000. “Signal Transduction by the JNK Group of MAP Kinases..” *Cell* 103
701 (2): 239–52.
702 DuBuc, Timothy Q, Nikki Traylor-Knowles, and Mark Q Martindale. 2014. “Initiating a
703 Regenerative Response; Cellular and Molecular Features of Wound Healing in
704 the Cnidarian Nematostella Vectensis..” *BMC Biology* 12 (1). BioMed Central Ltd:
705 24. doi:10.1186/1741-7007-12-24.
706 Elliott, Sarah A, and Alejandro Sánchez Alvarado. 2013. “The History and Enduring
707 Contributions of Planarians to the Study of Animal Regeneration..” *Wiley*
708 *Interdisciplinary Reviews. Developmental Biology* 2 (3): 301–26.
709 doi:10.1002/wdev.82.
710 Farkas, Johanna E, Polina D Freitas, Donald M Bryant, Jessica L Whited, and James R
711 Monaghan. 2016. “Neuregulin-1 Signaling Is Essential for Nerve-Dependent
712 Axolotl Limb Regeneration..” *Development* 143 (15). Oxford University Press for
713 The Company of Biologists Limited: 2724–31. doi:10.1242/dev.133363.
714 Fouraschen, Suomi Mg, Petra E de Ruiter, Jaap Kwekkeboom, Ron Wf de Bruin, Geert
715 Kazemier, Herold J Metselaar, Hugo W Tilanus, Luc Jw van der Laan, and Jeroen
716 de Jonge. 2013. “mTOR Signaling in Liver Regeneration: Rapamycin Combined
717 with Growth Factor Treatment..” *World Journal of Transplantation* 3 (3): 36–47.
718 doi:10.5500/wjt.v3.i3.36.
719 Fritzenwanker, Jens H, Grigory Genikhovich, Yulia Kraus, and Ulrich Technau. 2007.
720 “Early Development and Axis Specification in the Sea Anemone Nematostella
721 Vectensis..” *Developmental Biology* 310 (2): 264–79.
722 doi:10.1016/j.ydbio.2007.07.029.
723 Gauron, Carole, Christine Rampon, Mohamed Bouzaffour, Eliane Ipendey, Jérémie
724 Teillon, Michel Volovitch, and Sophie Vriz. 2013. “Sustained Production of ROS
725 Triggers Compensatory Proliferation and Is Required for Regeneration to
726 Proceed..” *Scientific Reports* 3. Nature Publishing Group: 2084.
727 doi:10.1038/srep02084.
728 Gemberling, Matthew, Ravi Karra, Amy L Dickson, and Kenneth D Poss. 2015. “Nrg1
729 Is an Injury-Induced Cardiomyocyte Mitogen for the Endogenous Heart
730 Regeneration Program in Zebrafish.” *eLife* 4: 2139. doi:10.7554/elife.05871.
731 Gilmore, Thomas, Francis Wolenski, and John Finnerty. 2012. “Preparation of
732 Antiserum and Detection of Proteins by Western Blotting Using the Starlet Sea
733 Anemone, Nematostella Vectensis.” *Protocol Exchange*, December.
734 doi:10.1038/protex.2012.057.
735 González-Estévez, Cristina, Daniel A Felix, Matthew D Smith, Jordi Paps, Simon J
736 Morley, Victoria James, Tyson V Sharp, and A Aziz Aboobaker. 2012. “SMG-1 and
737 mTORC1 Act Antagonistically to Regulate Response to Injury and Growth in
738 Planarians..” *PLoS Genetics* 8 (3): e1002619. doi:10.1371/journal.pgen.1002619.
739 Hand, C, and K R Uhlinger. 1992. “The Culture, Sexual and Asexual Reproduction, and
740 Growth of the Sea Anemone Nematostella Vectensis..” *The Biological Bulletin*
741 182 (2): 169–76. doi:10.2307/1542110.
742 Ishida, Takashi, Teruhiro Nakajima, Akira Kudo, and Atsushi Kawakami. 2010.
743 “Phosphorylation of Junb Family Proteins by the Jun N-Terminal Kinase Supports

744 Tissue Regeneration in Zebrafish..” *Developmental Biology* 340 (2): 468–79.
745 doi:10.1016/j.ydbio.2010.01.036.
746 Jopling, Chris, Guillermo Suñe, Cristina Morera, and Juan Carlos Izpisua Belmonte.
747 2012. “P38α MAPK Regulates Myocardial Regeneration in Zebrafish..” *Cell Cycle*
748 *(Georgetown, Tex.)* 11 (6). Taylor & Francis: 1195–1201.
749 doi:10.4161/cc.11.6.19637.
750 Layden, Michael J, Hereroa Johnston, Aldine R Amiel, Jamie Havrilak, Bailey
751 Steinworth, Taylor Chock, Eric Röttinger, and Mark Q Martindale. 2016. “MAPK
752 Signaling Is Necessary for Neurogenesis in Nematostella Vectensis.” *BMC*
753 *Biology*, July. BMC Biology, 1–19. doi:10.1186/s12915-016-0282-1.
754 Lee, Kyoung Eun, Michelle Spata, Richard Maduka, Robert H Vonderheide, and M
755 Celeste Simon. 2018. “Hif1Α Deletion Limits Tissue Regeneration via
756 Aberrant B Cell Accumulation in Experimental Pancreatitis.” *CellReports* 23 (12).
757 ElsevierCompany.: 3457–64. doi:10.1016/j.celrep.2018.05.071.
758 Liu, Peiyun, and Tao P Zhong. 2017. “MAPK/ERK Signalling Is Required for Zebrafish
759 Cardiac Regeneration..” *Biotechnology Letters*, March. Springer Netherlands, 1–
760 9. doi:10.1007/s10529-017-2327-0.
761 Liu, Zhen, Haiping Zhao, Datao Wang, Chris McMahon, and Chunyi Li. 2018.
762 “Differential Effects of the PI3K/AKT Pathway on Antler Stem Cells for
763 Generation and Regeneration of Antlers in Vitro..” *Frontiers in Bioscience*
764 *(Landmark Edition)* 23 (June): 1848–63.
765 Makanae, Aki, Ayako Hirata, Yasuko Honjo, Kazumasa Mitogawa, and Akira Satoh.
766 2013. “Nerve Independent Limb Induction in Axolotls..” *Developmental Biology*
767 381 (1): 213–26. doi:10.1016/j.ydbio.2013.05.010.
768 Manuel, Gema C, Rosalia Reynoso, Lydia Gee, Luis M Salgado, and Hans R Bode.
769 2006. “PI3K and ERK 1-2 Regulate Early Stages During Head Regeneration in
770 Hydra..” *Development, Growth & Differentiation* 48 (2). Blackwell Publishing
771 Asia: 129–38. doi:10.1111/j.1440-169X.2006.00847.x.
772 Marlow, Heather, Eric Roettinger, Michiel Boekhout, and Mark Q Martindale. 2012.
773 “Functional Roles of Notch Signaling in the Cnidarian Nematostella Vectensis..”
774 *Developmental Biology* 362 (2): 295–308. doi:10.1016/j.ydbio.2011.11.012.
775 McCusker, Catherine, Susan V Bryant, and David M Gardiner. 2015. “The Axolotl
776 Limb Blastema: Cellular and Molecular Mechanisms Driving Blastema Formation
777 and Limb Regeneration in Tetrapods..” *Regeneration (Oxford, England)* 2 (2): 54–
778 71. doi:10.1002/reg2.32.
779 Michalopoulos, G K. 1997. “Liver Regeneration.” *Science* 276 (5309): 60–66.
780 doi:10.1126/science.276.5309.60.
781 Passamaneck, Yale J, and Mark Q Martindale. 2012. “Cell Proliferation Is Necessary
782 for the Regeneration of Oral Structures in the Anthozoan Cnidarian Nematostella
783 Vectensis..” *BMC Developmental Biology* 12 (1). BioMed Central Ltd: 34.
784 doi:10.1186/1471-213X-12-34.
785 Petersen, Hendrik O, Stefanie K Höger, Mario Looso, Tobias Lengfeld, Anne Kuhn,
786 Uwe Warnken, Chiemi Nishimiya-Fujisawa, et al. 2015. “A Comprehensive
787 Transcriptomic and Proteomic Analysis of Hydra Head Regeneration..” *Molecular*
788 *Biology and Evolution* 32 (8): 1928–47. doi:10.1093/molbev/msv079.
789 Philipp, Isabelle, Thomas W Holstein, and Bert Hobmayer. 2005. “HvJNK, a Hydra
790 Member of the C-Jun NH2-Terminal Kinase Gene Family, Is Expressed During

Nematocyte Differentiation..” *Gene Expression Patterns : GEP* 5 (3): 397–402. doi:10.1016/j.modgep.2004.09.007.
Putnam, Nicolas H. 2007. “Sea Anemone Genome Reveals Ancestral Eumetaozoan Gene Repertoire and Genomic Organization.” *Science* 317 (5834): 83–86. doi:10.1126/science.1143254.
Rentzsch, Fabian, Jens H Fritzenwanker, Corinna B Scholz, and Ulrich Technau. 2008. “FGF Signalling Controls Formation of the Apical Sensory Organ in the Cnidarian Nematostella Vectensis..” *Development* 135 (10). The Company of Biologists Ltd: 1761–69. doi:10.1242/dev.020784.
Rojas-Muñoz, Agustin, Shibani Rajadhyksha, Darren Gilmour, Frauke van Bebber, Christopher Antos, Concepción Rodríguez-Esteban, Christiane Nüsslein-Volhard, and Juan Carlos Izpisua Belmonte. 2009. “ErbB2 and ErbB3 Regulate Amputation-Induced Proliferation and Migration During Vertebrate Regeneration..” *Developmental Biology* 327 (1): 177–90. doi:10.1016/j.ydbio.2008.12.012.
Rosser, Edward M, Simon Morton, Kate S Ashton, Philip Cohen, and Alison N Hulme. 2004. “Synthetic Anisomycin Analogues Activating the JNK/SAPK1 and P38/SAPK2 Pathways..” *Organic & Biomolecular Chemistry* 2 (1). The Royal Society of Chemistry: 142–49. doi:10.1039/b311242j.
Röttinger, Eric, Paul Dahlin, and Mark Q Martindale. 2012. “A Framework for the Establishment of a Cnidarian Gene Regulatory Network for ‘Endomesoderm’ Specification: the Inputs of SS-Catenin/TCF Signaling..” Edited by Mary C Mullins. *PLoS Genetics* 8 (12). Public Library of Science: e1003164. doi:10.1371/journal.pgen.1003164.
Sadler, Kirsten C, Katherine N Krahn, Naseem A Gaur, and Chinweike Ukomadu. 2007. “Liver Growth in the Embryo and During Liver Regeneration in Zebrafish Requires the Cell Cycle Regulator, Uhrf1..” *Proceedings of the National Academy of Sciences* 104 (5). National Academy of Sciences: 1570–75. doi:10.1073/pnas.0610774104.
Schaffer, Amos A, Michael Bazarsky, Karine Levy, Vered Chalifa-Caspi, and Uri Gat. 2016. “A Transcriptional Time-Course Analysis of Oral vs. Aboral Whole-Body Regeneration in the Sea Anemone Nematostella Vectensis..” *BMC Genomics* 17 (September): 718. doi:10.1186/s12864-016-3027-1.
Seger, R, and E G Krebs. 1995. “The MAPK Signaling Cascade..” *FASEB Journal : Official Publication of the Federation of American Societies for Experimental Biology* 9 (9): 726–35.
Stefanik, Derek J, Lauren E Friedman, and John R Finnerty. 2013. “Collecting, Rearing, Spawning and Inducing Regeneration of the Starlet Sea Anemone, Nematostella Vectensis..” *Nature Protocols* 8 (5): 916–23. doi:10.1038/nprot.2013.044.
Tanaka, Elly M, and Peter W Reddien. 2011. “The Cellular Basis for Animal Regeneration..” *Developmental Cell* 21 (1): 172–85. doi:10.1016/j.devcel.2011.06.016.
Tasaki, Junichi, Norito Shibata, Osamu Nishimura, Kazu Itomi, Yoshimichi Tabata, Fuyan Son, Nobuko Suzuki, et al. 2011. “ERK Signaling Controls Blastema Cell Differentiation During Planarian Regeneration..” *Development* 138 (12). Oxford University Press for The Company of Biologists Limited: 2417–27. doi:10.1242/dev.060764.

838 Tasaki, Junichi, Norito Shibata, Toshihide Sakurai, Kiyokazu Agata, and Yoshihiko
839 Umesono. 2011. “Role of C-Jun N-Terminal Kinase Activation in Blastema
840 Formation During Planarian Regeneration..” *Development, Growth &*
841 *Differentiation* 53 (3): 389–400. doi:10.1111/j.1440-169X.2011.01254.x.
842 Tejada-Romero, Belen, Jean-Michel Carter, Yuliana Mihaylova, Bjoern Neumann, and
843 A Aziz Aboobaker. 2015. “JNK Signalling Is Necessary for a Wnt- and Stem Cell-
844 Dependent Regeneration Programme..” *Development* 142 (14). Oxford
845 University Press for The Company of Biologists Limited: 2413–24.
846 doi:10.1242/dev.115139.
847 Trevino, Michael, Derek J Stefanik, Richard Rodriguez, Shane Harmon, and Patrick M
848 Burton. 2011. “Induction of Canonical Wnt Signaling by Alsterpaullone Is
849 Sufficient for Oral Tissue Fate During Regeneration and Embryogenesis in
850 Nematostella Vectensis.” *Developmental Dynamics : an Official Publication of the*
851 *American Association of Anatomists* 240 (12): 2673–79. doi:10.1002/dvdy.22774.
852 Varga, M, M Sass, D Papp, K Takács-Vellai, J Kobolak, A Dinnyés, D J Klionsky, and T
853 Vellai. 2014. “Autophagy Is Required for Zebrafish Caudal Fin Regeneration..”
854 *Cell Death and Differentiation* 21 (4): 547–56. doi:10.1038/cdd.2013.175.
855 Warner, Jacob F, Vincent Guerlais, Aldine R Amiel, Hereroa Johnston, Karine
856 Nedoncelle, and Eric Röttinger. 2018. “NvERTx: a Gene Expression Database to
857 Compare Embryogenesis and Regeneration in the Sea Anemone Nematostella
858 Vectensis..” *Development* 145 (10). Oxford University Press for The Company of
859 Biologists Limited: dev162867. doi:10.1242/dev.162867.
860 Wikramanayake, Athula H, Melanie Hong, Patricia N Lee, Kevin Pang, Christine A
861 Byrum, Joanna M Bince, Ronghui Xu, and Mark Q Martindale. 2003. “An Ancient
862 Role for Nuclear Beta-Catenin in the Evolution of Axial Polarity and Germ Layer
863 Segregation..” *Nature* 426 (6965): 446–50. doi:10.1038/nature02113.
864 Yoo, Sa Kan, Christina M Freisinger, Danny C LeBert, and Anna Huttenlocher. 2012.
865 “Early Redox, Src Family Kinase, and Calcium Signaling Integrate Wound
866 Responses and Tissue Regeneration in Zebrafish..” *The Journal of Cell Biology*
867 199 (2). Rockefeller Univ Press: 225–34. doi:10.1083/jcb.201203154.
868

Discussion & Future directions

During my PhD I have strongly contributed to the development of an emerging whole body regeneration model and set up the bases for molecularly comparing embryogenesis and regeneration in the same organisms. In particular, I have studied the MEK/ERK/Erg dependent gene regulatory network underlying embryonic development in *Nematostella vectensis* (Articles 1 and 2), contributed to developing a detailed morphological and basic cellular characterization of regeneration (Article 3) as well as transcriptomic resources to bio-informatically compare embryogenesis and regeneration (Article 4 and 5). I then focused on functionally dissecting the role of MEK/ERK during regeneration, establish its gene regulatory network module and compare it to the one described from embryonic development (Article 6). Finally, I performed a kinase inhibitor screen that highlighted the potential role of 14 kinases families in the *Nematostella* regeneration process and have identified that one of them, JNK, is crucial for controlling regeneration-specific proliferation (Article 7).

In the following sections I will discuss how the work from my PhD has contributed to the development of the novel whole body regeneration model *Nematostella*, how I addressed the century old hypothesis concerning the reuse of the embryonic program during regeneration and finish with an opening on the similarities and differences of the GRN architecture between regeneration and embryogenesis.

1 Regeneration of Nematostella vectensis

The first description of Nematostella regeneration after fission dates back to a publication from 1995 (hand1995). Since then and until the beginning of my PhD studies on Nematostella regeneration remained sparse and heterogeneous in regard to, the bisection site, the animals “age”, their metabolic state and the temperature condictions ((Reitzel et al. 2007; Burton and Finnerty 2009; Renfer et al. 2010; Trevino et al. 2011; Tucker, Shibata, and Blankenship 2011)). Therefore the goal of the first project I participated in when I started my PhD, was to carefully characterize regeneration of Nematostella at the morphological and cellular level, and this under defined conditions(Amiel et al. 2017). This work laid down a common groundwork for future studies within the lab, but also in order to facilitate comparisons across laboratories working on this model of regeneration.

This work has also consolidated the data concerning the importance of cell proliferation during regeneration (Passamaneck and Martindale 2012). In fact, we were able to determine a proliferation-independent phase (wound-healing, transition from step 0 – step 1) as well as a proliferation dependent phase (step 2 to step 4) (Amiel et al. 2015) . This observation naturally raises additional questions such as i) the nature of the signal initiating proliferation, ii) the cells that are proliferatin and iii) if it is a homogeneous population of cells that are proliferating? While these question are at first instance aspects of cellular behavior, these questions also point out the lack of molecular information (e.g. signaling pathway and molecular markers) concerning the control of the various steps of oral regeneration after sub-pharyngeal bisection. This lack of molecular resolution is discussed further down in this chapter.

At the end of this study, the only additional molecular data I provided was a global transcriptional dynamics concerning the neo-synthesis of all types of RNA

(e.g. rRNA, tRNA and mRNA, (Amiel et al. 2015)). The visualization of neo-transcription by incorporating EU (Ethynyl Uridine) into nascent RNA, revealed an increasing transcriptional activity at the amputation site starting from 1.5hpa until 144hpa. These results suggest an early deployment of the genetic/signaling program underlying regeneration, that is supported by transcriptomic data (see Article 4 – Transcriptome database) in which genes are already upregulated between 0 and 2hpa. Interestingly, a recent review has suggested that activation of hypertranscription (i.e. what we called neo-transcription) is utilized in adult stem /progenitor cells to support organ renewal by contributing to fueling the biosynthetic demand imposed by regeneration(Percharde, Bulut-Karslioglu, and Ramalho-Santos 2017). It would thus be interesting to assess whether the cells that are in a state of hypertranscription/neotranscription are associated to the activation of stem or progenitor cells during regeneration in *Nematostella*.

1.1 Kinases implicated during regeneration

The approach chosen to gain insight into potential signaling pathways involved in regeneration in *Nematostella* was to perform a screening of kinase inhibitors, rather than a candidate approach. The choice of targeting this class of enzyme was based on two facts, i) it is a widespread family of enzymes (Hanks 2003) and ii) they play a pivotal role in many signaling pathways (Petersen et al. 2015). By analyzing the effects of 78 kinase inhibitors, I have been able to identify 14 kinases that affect reformation of the lost body parts; EGFR, VEGFR, PDGFR, Btk, JNK, Src, CamkII, PKA, PKC, PKG, MLCK, CDK, mTOR and MEK. Given the obtained results, this approach has been proven to be fruitful. Interestingly, according to the literature these 14 candidate kinases have been associated to seven different pathways involved in various contexts of regeneration: For example

MAPK (ERK and JNK) signaling is crucial for early steps of planarian regeneration(Tasaki, Shibata, Nishimura, et al. 2011; Agata et al. 2014), PI-3k/akt antler regeneration (Z. Liu et al. 2018), PI3-K/BTK, pancreas regeneration (K. E. Lee et al. 2018), PI3K/ERK for Hydra regeneration(Manuel et al. 2006), the cAMP/PKA for rat liver regeneration (Cheng et al. 2012), Src signaling for zebrafish fin regeneration (Yoo et al. 2012), and mTOR pathway in mice liver regeneration planarian (Fouraschen et al. 2013; González-Estévez et al. 2012).

For the sake of the experiment, a fix concentration of 10µM was used for all the treatments, based on the range of pharmacological drug treatments usually used in *Nematostella* (Rentzsch et al. 2008; Röttinger, Dahlin, and Martindale 2012; Marlow et al. 2012; DuBuc, Traylor-Knowles, and Martindale 2014). One of the drawbacks of such approach is the false-negative result generated by the use of a unique concentration, since some drugs might be more effective at higher concentrations. Interestingly, the library of kinase inhibitors I used, contained many redundant drugs targeting the same kinase. Among the 14 candidate kinases identified to be important for regeneration, some had multiple compounds affecting regeneration, thus providing an additional evidence for an involvement of a given kinase in this process. For instance, EGFR (8 out 13), Btk (2 out 2), Src (2 out 2) were blocked by redundant inhibitors. While Mek (1 out 2), PDGFR (1 out 3), CamkII (1 out 2) and CDK (1 out 3) had at least one inhibitor blocking regeneration. The other compounds targeting theses kinases were either not affecting regeneration or toxic at 10µM. But still their could be verified with through optimization of the concentration, which can be use to validate their effect on regeneration.

When using a unique drug concentration, the inverse, i.e. getting false positive results caused by off-target effects is also true. Therefore additional rounds

of screening, by i) increasing the concentration of the drugs not affecting regeneration and ii) decreasing the concentration of the drugs that are toxic at 10µM, would have been necessary to identify more precisely the kinases involved in regeneration in *Nematostella*.

This preliminary screening was performed based on macro-morphological phenotypes *e.i* the presence of a clear pharynx and tentacles. This approach has the advantage to provide a fast way of assessing the affects of the various treatments on regeneration. However, this approach lacks the resolution to identify subtle effects, such as an inhibition of regeneration at late stages such as step 3, i.e. no mouth opening. The molecular data that I and other members of my team obtained during my PhD, may provide useful information to create transgenic lines to molecularly define the regeneration steps and increase the *in vivo* resolution of our approach.

Nevertheless, this screening was set up as a preliminary approach to provide a list of candidate kinases that has successfully allowed me to identify a large pool of kinases that are involved in *Nematostella* regeneration. In fact, almost 50% (14/32) of the kinases targeted by the library I used appear to prevent proper regeneration when blocked. As mentioned in the discussion of article 7, in order to validate the implication of these candidate kinases in the regeneration process, a more thorough experimentation, i.e. gene specific approach, is still required given the potential non-specific effects of the drug treatment. Thus, it is crucial to identify the presence of the targeted candidate gene in the genome by a basic alignment and/or an advanced phylogenetic analysis if there is no clear homology. This was performed in regard to the RTK complement in *Nematostella*, which has revealed the absence of EGFR orthologs in this sea anemone (Article 6), suggesting non-specific effects of these compounds on the PDVEGFR family of GFRs. Thus, the uses of antibodies directed

against its activate form is crucial to validate the effect of the inhibitor on a specific kinase (Bain et al. 2007). Alternatively, one could also take advantage of the amenability of *Nematostella* for gene editing *via* CRISPR/cas and develop a inducible KD/KO transgenic line (Ikmi et al. 2014; Servetnick et al. 2017; He et al. 2018).

1.2 MAPK kinases orchestrating the regeneration events of *Nematostella vectensis*

The first study on regeneration from our lab has established a chronological map of tissular and cellular events underlying the reformation of lost body parts. Briefly, this time line can be separate in three phases, i) wound healing (DuBuc, Traylor-Knowles, and Martindale 2014; Amiel et al. 2015), ii) the initiation of regeneration correlating with the initiation of proliferation at the amputation site at 12hpa amie(Passamaneck and Martindale 2012; Amiel et al. 2015) and the transition from step 1 to step 2 (Amiel et al. 2015) and iii) the actual reformation of the head structures (step 3 and step 4) supported by a high mitotic activity (Passamaneck and Martindale 2012; Amiel et al. 2015). These various events are suggesting multiple signaling inputs for coordinating the regenerative process (Fig 20). My first choice was to investigate the input of MAPKs, given their implication in many regeneration contexts (see section 2 table 1). And the results obtained during the kinase inhibitor screen are in line with this idea, in particular the roles of ERK and JNK in the early phases of the regeneration process (see Article 6 and Article 7).

1.2.1 The MAPK ERK

The MAPK ERK has already been proposed to be involved in wound healing in *Nematostella* were it is activated soon after injury (DuBuc, Traylor-Knowles, and Martindale 2014). While my work has mostly focused on regeneration rather than wound-healing, loss of ERK function has revealed that this signaling pathway is not required for wound healing but delays this process for several hours (Article 6). We further described the activation pattern of this MAPK in the tissues at the amputation site and implicated in the regrowth of the head. Furthermore, we where able to demonstrate the importance of this signaling pathway for the initiation of regeneration and the transition to step 1, as well as for maintaining cell proliferation during later phases of regeneration (Article 6) (Fig 20)

Interestingly the various roles of ERK described during *Nematostella* regeneration display conserved traits compared to other cnidarian and bilaterian regeneration models. For instance, in *Hydra*, planarian, zebrafish and urodele, the response to injury is also associated with a swift activation of ERK (Manuel et al. 2006; Varga et al. 2014; Makanae et al. 2013; Owlarn et al. 2017). Beside its activation after injury, the MAPK ERK is also associated with the control of the mitotic activity in a context specific manner. It controls apoptosis-dependent proliferation during *Hydra* regeneration (Kaloulis et al. 2004; Chera et al. 2011), the mitosis exit of neoblasts during planarian regeneration (Tasaki, Shibata, Nishimura, et al. 2011; Umesono et al. 2013; Agata et al. 2014) and it activates proliferation of the cardiomyocytes during zebrafish heart regeneration (P. Han et al. 2014; P. Liu and Zhong 2017).

Overall, the role of ERK signaling seems to be conserved as a response mechanism to injury and its involvement in the regulation of mitotic events.

1.2.2 The MAPK JNK

The other MAPK I have been studying during my PhD is the stress-associated kinase JNK (see Article 7). Inhibition of JNK using the drug SP600125, for which the target site in *Nematostella* JNK is conserved (data not shown), dramatically blocked head reformation. Characterization of JNK expression and activation revealed that transcript levels and the level of phosphorylation of the protein is only slightly increased upon injury. However, this study is still lacking spatial data on its domain of activation or even the expression domain of the genes, which could point out a potential domain of activation. By treating the amputated polyps at different time points, I have been able to highlight an essential role of JNK for transitioning from step 1 to step 2. Since this transition is cell proliferation-dependent (Article 3), I investigated the link between JNK and the regeneration-associated mitotic activity. The treatment with SP600125 in uncut polyps didn't affect significantly the proliferation in both the body column and the mesenteries. However, during regeneration, when animals were treated between 24-48hpa, proliferating cells decreased in both the mesenteries and the body wall epithelia, with a most dramatic effect in the latter. Inhibition at later time windows of treatment (36-60hpa, 48-72hpa) interestingly affected significantly only the population of proliferating cells from the body wall epithelium. Overall these results suggest that the regeneration phenotype in step 2 is linked to the inhibition of a sub-population of proliferating cells present mainly in the body wall epithelia.

When compared to other regeneration models, we observe a striking conservation of JNK signaling in controlling the mitotic activity necessary for blastema formation in planarian (Tasaki, Shibata, Sakurai, et al. 2011) and zebrafish regeneration (Ishida et al. 2010). Interestingly, blastema associated proliferation in both models is linked to the pool of stem cells and in flies JNK is also regulating intestinal stem cell proliferation (Cordero et al. 2012; Biteau, Hochmuth, and Jasper 2008). Thus, is it plausible that in Nematostella JNK controls proliferation of stem/progenitors cells that are located within the injured body wall epithelia. .

Altogether the data gathered on the MAPKs ERK and JNK during *Nematostella* regeneration suggest no overlap between their respective roles (Fig 20). While ERK is crucial to reach step one and to maintain cellular proliferation after step 2, JNK is required for launching the regeneration specific proliferation and for reaching step 2. However, additional experiments are required to; i) finalize the study on JNK is required to better understand the precise role of this pathway and ii) gain insight into the relationship between ERK and JNK during *Nematostella* regeneration.

Figure 20:

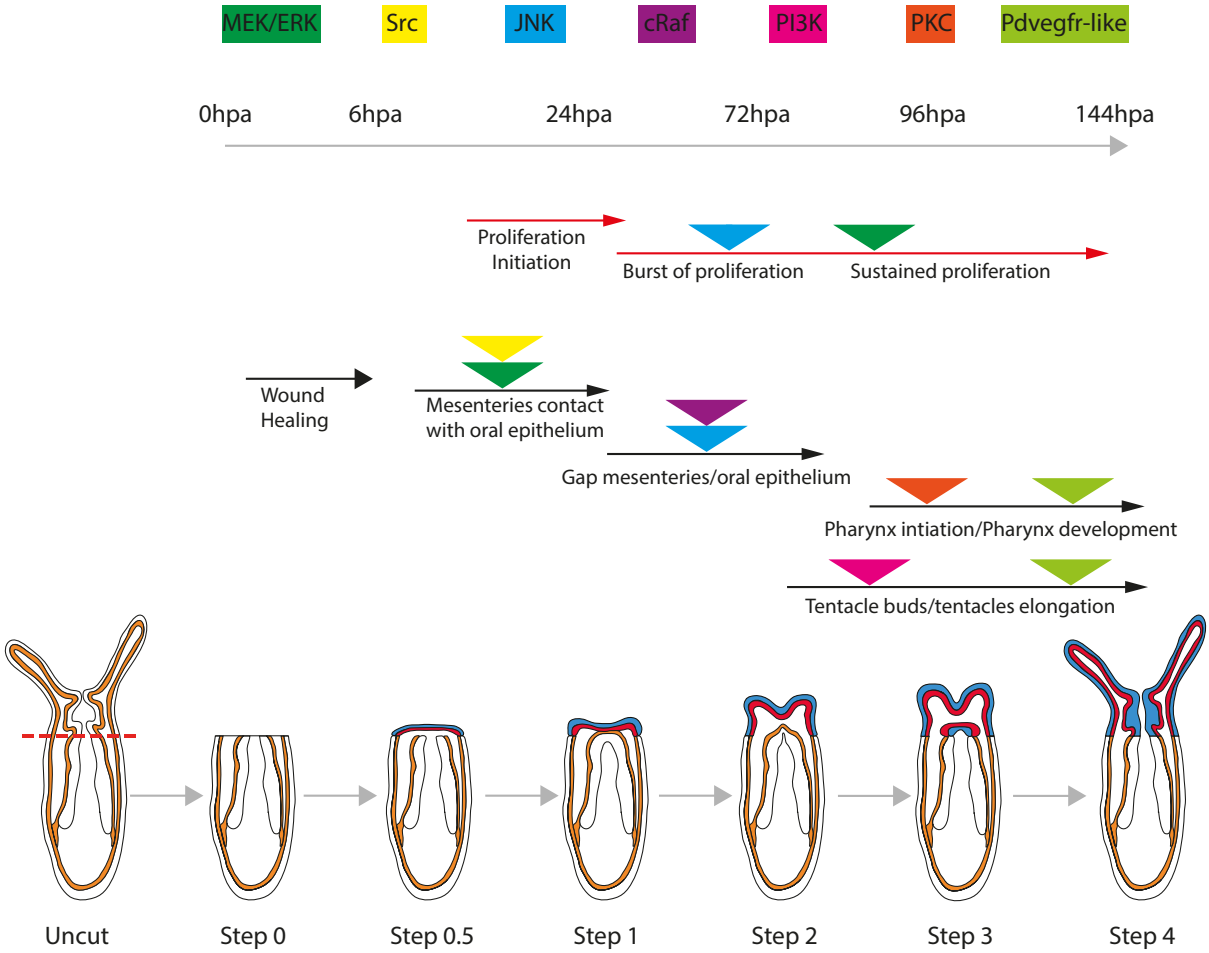

Regeneration time line and kinase input. Morphology of the steps occurring during oral regeneration in Nematostella. The black arrow represents the tissuelar events of head regeneration and the red arrow represents the proliferation supporting head reformation. Each the candidate kinase are listed with a color code associated to their input during regeneration represented by the colored triangles.

1.3 Other Kinases

During my PhD I also initiated the investigation of several other kinase during *Nematostella* regeneration (Article 7: Additional data), such as growth factor receptors of the Pdvegfr-like family, PI3K, PKC, Raf and Src. Although the obtained results are still preliminary, an interesting panel of phenotypes has been characterized, spanning the whole process of regeneration (Article 7: Additional data). For instance if all the results were to be confirmed, Src would be implicated

like MEK/ERK in the transition to step 1, Raf in the transition to step 2 like JNK (Article 7: Fig. 2a), PKC would be a key player in the formation of the pharyngeal lip, therefore in the transition to step 3 and the Pdvegfr-like family in the transition to step 4 while PI3K would be regulating the formation of tentacles (Fig 19). The detailed investigation of these various kinases would open the path to decipher the molecular program underlying each of these regeneration events in *Nematostella* by associating this kinase mapping along the regeneration timeline with the transcriptomic resource NvERTx (http://nvertx.kahikai.org, Article 4, (Warner et al. 2018)). This would create important opportunities to predict signaling/gene interactions that once functionally verified would give rise to a global regeneration GRN spanning all major phases of this process.

1.4 Investigating the genetic program downstream of the candidate kinases

The primary goal of the kinase inhibitor screening was to gain novel molecular insight into the regeneration program of *Nematostella*, and to link it to the morphological and cellular staging system (Article 3, (Amiel et al. 2015)). Besides identifying candidate kinases involved in this process, the long-term goal is to gain insight into the genetic program underlying the morphogenetic and cellular events of regeneration in *Nematostella.*

The database NvERTx contains the regeneration transcriptomes of *Nematostella* and is a valuable resource to begin investigating the genetic program supporting this developmental process (Article 4, (Warner et al. 2018)). This database regroups the expression profile of all the transcripts expressed in uncut juveniles and in dissected polyps from 0 to 144hpa for a total of 16 time points. In order to gain a more comprehensive view of the transcriptional dynamics, all

transcripts have been clustered using the fuzzy c-means clustering method ((L. Kumar and E Futschik 2007) in nine co-expression groups (Article 4, (Warner et al. 2018)). This approach has the advantages of identifing genes that are potentially i) regulated by the same inputs (similar regulatory module) and ii) involved in the same biological functions.

The obtained regeneration cluster (Article 5, (Warner et al. 2018)) can be categorize according to their expression dynamics, indicating the increase or decrease of the transcripts during regeneration. For instance the clusters R1 and R2 are increasing early between 0 and 8hpa, the clusters R2, R3 and R5 increase later between 16-60hpa, while other clusters (e.g. R6 and R7) have two distinct phases of up-regulation both increasing first between 0-4hpa and later between 8-16hpa or 12-36hpa. Other clusters however, indicate a steady decrease of transcript levels during regeneration such as cluster R4 that decreases between 20-144hpa or R9 that decreases right after injury, between 0-24hpa.

Altogether these co-expression groups provide a global view of the activation or repression period of each cluster that could be mapped together with the morphological and cellular hallmarks of regeneration (Article 3, (Amiel et al. 2015)). In addition, one can include the potential kinase inputs within the same diagram and predict the potentially associated genetic program, i.e. downstream targets. To refine this large pool of potential downstream targets, the first approach would be to select signaling molecules and transcription factors, which are the main component of a gene regulatory network (GRN). Secondly, and given the fact that Fuzzy c-mean clustering is not strict and can regroup somewhat related profiles (L. Kumar and E Futschik 2007) , a refinement of the selected clusters is required to gain a better resolution and build a hierarchy between the set of genes. Thus, in addition to an

often-used candidate approach (discussed in section 2.3), the presented alternative strategy corresponds to an unbiased way to create testable hypotheses that can subsequently be validated/invalidated functionally.

2 The relationship between embryogenesis and regeneration in *Nematostella vectensis*

Previous studies using a variety of regeneration models have proposed that gene expressed during embryonic development are re-activated during regeneration ((Gardiner and Bryant 1996; Carlson et al. 2001; “Distal Expression of Sprouty (Spry) Genes During Xenopus Laevis Limb Development and Regeneration.” 2014)). However, these studies have mainly analyzed expression patterns of individual or a small set of gene in both developmental contexts. Using a similar approach other studies have highlighted “embryonic-specific” or “regeneration-specific” gene expressions or expression patterns (Gardiner et al. 1995; Brzóska et al. 2009). Overall, these studies indicated an overall resemblance between embryogenesis and regeneration when looking at specific genes in a given context and that such comparison could highlight the existence of regeneration-specific genes.

Thus, the overall goal of my PhD was to provide a novel unbiased, large-scale and functional insight into the relationship between embryonic development and regeneration aiming and potentially highlighting a regeneration specific regulatory logic. I did this using the uniquely suited whole body regeneration model *Nematostella vectensis*.

2.1 Partial reuse of the embryonic program during regeneration

To overcome any bias based on timing and/or tissue we performed a large-scale comparative transcriptomics analysis spanning 35 embryonic and 16 regeneration time points extracted from entire embryos or regenerating juveniles (Article 4 and 5). The first results gathered from this global comparison was the striking difference in the number of dynamically expressed transcripts between the two datasets. In fact, we observed a ten-fold difference between embryogenesis (~14 000 genes) and regeneration (~1 250 genes), Interestingly, 90% of the regeneration transcripts are shared with embryogenesis, indicating that about 10% (126 genes) have a regeneration specific transcriptional dynamics (Article 5). To dig deeper in the potential network logic, we analyzed to what extend genes that belong to a given regeneration cluster are conserved in any of the embryonic co-expression clusters. This analysis revealed that clusters associated to cell proliferation or differentiation process appear conserved, while one cluster in particular (R6) contained genes encoding members of developmental signaling pathways, morphogenesis or apoptosis has no embryonic pendent (Article 5). Taken together, these results strongly suggest not only that regeneration is a partial reuse of the embryonic program but also that it rewired to include regeneration specific elements (Article 5). Latter hypothesis is what I functionally tested/validated by analyzing the role of MEK/ERK signaling and by comparing the resulting regeneration GRN (Article 6) with the one deployed during embryonic development (Articles 1 and 6).

Part of the reason the relationship between embryonic development and whole body regeneration has never been addressed before as we did, is that the historical and powerful regeneration models *Hydra* and planarians are poor models to study embryonic development. Molecular embryonic data from Hydra

((Genikhovich et al. 2006; Fröbius et al. 2003) are sparse and transcriptomic data to date are existing. Recently the first detailed description of planarian embryonic development and its associated transcriptomes have been published (Davies et al. 2017). In this study the authors have focused on the embryonic origin of the neoblasts (adult piwi-positive stem cells) and observed that i) embryonic and adult piwi positive cells have a different molecular signature and that ii) the adult neoblast signature appears during organogenesis (Davies et al. 2017). By taking advantage of this novel resource, combined with the existing regeneration datasets from this species (Sandmann et al. 2011; Kao, Felix, and Aboobaker 2013), it would be interesting to repeat the type of study we did to see to what extend our conclusions are also valid in a different phylum and if there are evolutionarily conserved 'regeneration-specific" genes. This should and could also be extended by including other cnidarian or lophotrochozoan regeneration models in which one can study embryogenesis and regeneration such as Hydractina (Kraus et al. 2014; Gahan et al. 2016), Macrostomum(Ladurner et al. 2004; Egger et al. 2006) or Platynereis (Gazave et al. 2013; Chou et al. 2016) to further validate any evolutionary conservation. One could push this even further and include data from Zebrafish that is extremely well suited for such intra-specific approaches. In fact, a wealth of transcriptomics data describing embryogenesis and organogenesis (Howe et al. 2013) as well as organ regeneration such as the heart(Cao et al. 2017) in this system. But unfortunately such study hasn’t been performed yet.

2.2 Analogous role of MAPK in *Nematostella* embryogenesis and regeneration

The study in which the authors compared piwi-positive cells during embryonic development and regeneration in planarians (Davies et al. 2017), illustrates nicely the general concern about what is comparable between these two developmental trajectories. In fact, this observation suggests that for this specific question (i.e. appearance of adult neoblasts), comparing regeneration to late embryonic program is the most relevant.

To address this concern, I took advantage of the characterized role of MEK/ERK during embryogenesis (Article 1 and Article 2) and discovered a potentially analogous role of this MAPK during regeneration (Article 6). Indeed in both developmental trajectories, this kinase is involved in the initiation of the morphogenetic movements underlying gastrulation and the tissue rearrangements of the mesenteries towards the epithelia of the amputation site (step 1).

According to this potential analogy I have investigated the genetic program activated by MEK/ERK during the initiation of regeneration. To do so I have combined an unbiased differential gene expression approach to identify all the genes up-regulated at 20hpa (Article 6) and a candidate approach based on the genes described in the embryonic GRN of gastrulation (Article 2) and the "regeneration-specific" genes identified in the comparative transcriptomics analysis (Article 5). This strategy allowed me to build the very first framework of the GRN underlying regeneration initiation and functionally show that regeneration is a partial and rewired redeployment of the embryonic GRN that is connected to regeneration-specific elements (Article 6) (discussed in more detail in the next section). In addition, this approach has provided additional evidence for a potential analogous role of

MEK/ERK during embryogenesis and regeneration. In fact, during embryogenesis this MAPK signaling is responsible for the specification of the endomesoderm domain and its loss is indirectly responsible for a failed gastrulation phenotype (Article 2). During regeneration the inhibition of the same pathway also causes the loss of specifying specific domains at the amputation site domain (Article 6). Thus, in both contexts it is plausible to suggest that the MEK/ERK-dependent specification of gene expression domains is indirectly responsible for initiating the morphogenetic movements leading either to gastrulation or to the regeneration step 1

In addition, the candidate approach applied at 20hpa revealed that only 19 out of the 90 embryonic MEK/ERK downstream targets are highly upregulated significantly upregulated between 0-20hpa and all being still downstream of MEK/ERK at 20hpa. Interestingly, the same gene candidate approach carried out at 48hpa revealed that 23 embryonic MEK/ERK downstream targets are up regulated (0-48hpa). In contrast following the inhibition of MEK/ERK between 24-48hpa, only 10 downstream targets of MEK/ERK are conserved with embryogenesis, supporting the idea that MEK/ERK has analogous roles at the onset of these to morphogenetic movements initiating gastrulation and regeneration. Overall this comparison between the initiation of embryogenesis and regeneration suggest that not only the re-/formation or differentiation of structures are comparable between the two developmental trajectories, but that there are evidences that indicate the presence of a core embryonic program that is redeployed but regeneration-specifically rewired during the initiation of regeneration.

In the future it would be interesting to applied the described strategy to the process of tentacle morphogenesis and regeneration. The molecular program underlying tentacle formation during embryogenesis has been investigated (Fritz et

al. 2013) and morphologically, the genesis and reformation of tentacles are undoubtedly analogous. Fritz and colleagues have observed that Notch signaling and its down stream targets are required for the formation of the tentacles after metamorphosis. They thus set a solid groundwork for comparing this process to the one involved in tentacle regeneration in *Nematostella*. While it is not clear in what step regeneration is blocked, interestingly, Notch inhibition prevents the reformation of lost body parts in *Nematstella*, including the reformation of tentacles (DuBuc, Traylor-Knowles, and Martindale 2014). Thus, this presents a solid groundwork and a great opportunity to perform an additional comparative study of embryogenesis and regeneration in *Nematostella* by focusing on the Notch GRN underlying tentacle formation and regeneration.

2.3 Rewiring the embryonic program during regeneration

While the global transcriptomic comparison between embryogenesis and regeneration has revealed that regeneration is transcriptionally modest compared to embryogenesis, this analysis has also revealed that among the genes activated during regeneration a large proportion (90%) are re-deployed embryonic genes (Article 5). This of course raises the question to what extend the architecture of the genetic program is re-deployed in a conserved or in a rewired manner. The comparative cluster analysis performed in the same study hypothesized that embryonic developmental regulatory modules are reused in a rewired manner during regeneration (Article 5).

The first evidence supporting this hypothesis is the observation that in addition to embryonic MEK/ERK targets, several embryonic cWnt downstream targets are under the control of MEK/ERK signaling during regeneration (Article 6). Interestingly, during embryogenesis, cWnt signaling is active prior to MEK/ERK

signaling (Röttinger, Dahlin, and Martindale 2012; Leclère et al. 2016; Layden et al. 2016; Amiel et al. 2017) and these two pathways have distinct and non shared downstream targets (Röttinger, Dahlin, and Martindale 2012; Layden et al. 2016; Amiel et al. 2017). Thus, the observation of co-opted downstream targets clearly highlights a re-wiring of the embryonic network during regeneration. In this regard a thorough analysis of the role of cWnt signaling during regeneration would be crucial. In particular to investigate if the cWnt network is still upstream of the MEK/ERK network or if the hierarchy has been inverted during regeneration.

The second evidence of a regeneration specific re-wiring, is the implementation of "regeneration-specific" genes (Article 5) in the MEK/ERK GRN (Article 6). In fact, I have identified 15 regeneration specific genes that are downstream of MEK/ERK signaling during regeneration (Article 6). This clearly highlights the different composition of the MEK/ERK downstream networks between embryogenesis and regeneration. The regeneration-specific inputs of the regeneration GRN are further discussed in a section below.

In addition to these two strong evidences, I made additional observations that underline my point but certainly require complementary experiments to be considered evidences for a deployment of a deconstructed/rewired embryonic GRN during regeneration. These observations concern the neurogenic role of MEK/ERK during embryonic development. In fact, putative neuronal markers are expressed prior to gastrulation in a salt and pepper pattern, where 18 of them have been described to be downstream of MEK/ERK at 24hpf (Article 1). Curiously, out of the 18 embryonic neurogenic MEK/ERK downstream target genes only *Nvhes1/3* is upregulated at 20hpa and downstream after MEK/ERK inhibition (Article 6: Fig. 5). At 48hpa three additional salt and pepper genes are upregulated (*Nvsox2*, *NvpaxA*,

Nvath-like), however, *Nvhes1/3*, appears still to be the only downstream of MEK/ERK (Article 6: Fig. S3, Table S3). At 60hpa, only the genes *Nvcoup-like1*, *Nvhes1/3*, *Nvath-like*, *NvpaxA* and *Nvsox2* appear to be upregulated (data not shown). However, I have not tested if they are controlled by MEK/ERK at this later phase of regeneration.

It is noteworthy to mention that aside the potential neuronal genes mentioned above, all other embryonic salt and pepper genes are not significantly upregulated during the entire time course of the regeneration. Which doesn't exclude their activation during regeneration. Accordingly, they are distributed among the clusters R6, R5, R3 and R2 (Article 6: Table S3), displaying a general upregulations starting at 8hpa, 16hpa, 24hpa or 36hpa (Article 4, nvertx.kahikai.org,). This distribution is suggesting that the initial network regrouping these salt and pepper genes during embryogenesis at 24hpf is not conserved during regeneration. It further suggests that during regeneration the onset of the neurogenic program is stretched out between 8hpa and 36hpa. Altogether, these data strongly suggest that neural regeneration happens in a different way during regeneration compared to embryonic neurogenesis

The difference between the neurogenic program during embryogenesis and regeneration could be explained by the presence of an existing neuronal network in the body column of regenerating polyps. This network could be supporting the re-establishment of the neuronal network in the reforming head without the need to re-launch an embryonic program. To confirm this hypothesis it will be essential to define exactly when the neuronal network is re-established in the reforming head and perform functional assays.

2.4 Nematostella vectensis regeneration GRN

The investigation of MEK/ERK signaling during regeneration, specifically during the transition to step 1 has enabled me to establish the first GRN framework during regeneration in *Nematostella* (Article 6: Fig. 8). This framework is composed of three expression domains at the amputation site *i.e* amputation ectoderm (AE), amputation site gastroderm (AG), amputation site mesenteries tip (AMT), in addition to the entire mesenteries (M) and the physa (P) at the opposite side. The current version of the regeneration GRN framework contains only genes that have been validated by qPCR and in situ hybridization after MEK/ERK inhibition. In total, 23 embryonic genes (12 MEK/ERK and 11 Wnt) and one regeneration-specific gene (*Nvwls*), representing the identified and confirmed regulatory state at 20hpa. In order to establish the link between all these genes, the next step would be to define accurately their activation prior to 20hpa by using the NvERTx database (NvERTx.kahikai.org, Article 4). This will help to get a better understanding of the potential hierarchy among the genes and have an approximation of their mutual inputs. Besides establishing this hierarchy, it will be crucial to identify the effectors of MEK/ERK and Wnt signaling. This can be achieved by using a candidate approach based on the embryonic data, since we have shown that the transcription factor NvErg is one of the MEK/ERK effectors during embryogenesis (Amiel et al. 2017) and the transcription factor NvTcf the main effector of the cWnt pathway.(Röttinger, Dahlin, and Martindale 2012) Interestingly, the temporal expression profiles indicate that high *Nverg* transcript (NvERTx.4.84016) levels after injury progressively reduces, while *Nvtcf* (NvERTx.4.100051) is strongly upregulated at 20hpa (data not shown). This observation fuels the idea of an inverted chronological input of these

signaling pathways during the process of regeneration compared to the one during embryogenesis.

Finally, to establish the links between the putative effectors and the genes composing the GRN framework at 20hpa, functional studies of NvErg and NvTcf are required. During embryogenesis this was performed by morpholino or dominant-negative-based knock-down approaches via micro-injections into fertilized eggs (Röttinger, Dahlin, and Martindale 2012) (Article 2, (Amiel et al. 2017). Other studies on *Nematostella* embryonic development, were by performing constitutive F0 knock-outs of the genes of interest using the CRISPR/cas9 technology (Servetnick et al. 2017; Wijesena, Simmons, and Martindale 2017; Nakanishi and Martindale 2018; He et al. 2018).

Unfortunately, these approaches currently cannot be used to investigate the role of the putative MEK/ERK and cWnt effectors during regeneration. The reason being that the phenotypes obtained after knock-down of NvErg and NvTcf are to severe (lack of gastrulation or pharynx, respectively) for proper metamorphosis and subsequent growth. Unfortunately, this is a common limitation when studying regeneration. In order to overcome this issue, the establishment of inducible transgenic line would offer the best solution to induce genetic perturbation in post-embryonic development that would otherwise be lethal. Although the CRISPR/Cas9 and or meganuclease technology is amenable to create transgenic lines in *Nematostella* (Renfer et al. 2010; Ikmi et al. 2014), until this day no inducible system has been reported.

However, one opportunity that resulted from the comparison of transcriptoms from embryogenesis and regeneration approach (Article 5), is the regeneration specific pool of genes, and in particular the one upregulaetd at 20hpa and

downstream of MEK/ERK (Article 6: Fig. 5h). Since these genes are potentially not required for embryonic development, they offer the possibility to perform constitutive knock-out approaches that may specifically affect regeneration.

While the *Nematostella* regeneration GRN framework I established during my PhD lays down the foundations, an important amount of work is still required to complete it. Although, this era of high-end high-throughput technology can participate to accelerate the process of building the GRN. For instance, by using single-cell RNA sequencing (sc-RNA seq) it is possible to reach a cellular resolution for the GRN. For instance, performing a sc-RNA seq at 20hpa, we could question inquire the 20hpa GRN in distinct population of cells e.g cells exhibiting a progenitor state (Sebé-Pedrós et al. 2018), and define in which cells this GRN is deployed.s

Furthermore, in the same sc-RNA seq study, the authors have also used the ATAC seq technology, allowing to sequence the accessible genomic region (Buenrostro et al. 2015), therefore highlighting potential active promoter regions. The ATAC seq, thus allowed the authors to screen for enriched sequence motives in neural cells (Sebé-Pedrós et al. 2018). This, if applied during regeneration could facilitate the identification of downstream target according to motif enrichment corresponding to a candidate transcription factor. While this high-throughput workflow would accelerate considerably the building of the GRN, it nevertheless would necessitate experimental validation.

3 Concluding remarks on the relationship between embryogenesis and regeneration

In the last two sections of my discussion, I will be proposing a model on the relationship between embryo and regeneration. A time line of regeneration has been proposed to be subdivided into three major phases; 1) wound healing, 2) the activation/recruitment of stem/progenitor cells and 3) morphogenesis/differentiation (Tiozzo and Copley 2015). This time line can also be transposed to *Nematostella* regeneration, to which I implemented additional information according to the data we gathered in-house (Fig 21A). In *Nematostella*, the injury-induced stress response is translated into wound healing by re-arrangements of the remaining tissue (Amiel2015). This step is followed by the activation/recruitment phase of stem cell/progenitor cells (Amiel et al, in revision) and finally leading to morphogenesis and differentiation to reform the missing head. It is based on that model that I will expose the comparison between embryogenesis and regeneration in *Nematostella*. I will be starting from the potentially most conserved features and finish with the regeneration specific elements.

3.1 Similarities between embryogenesis and regeneration

Regeneration is proposed to be comparable to embryogenesis in terms of reformation of the missing structures (Tiozzo and Copley 2015). Indeed it is supported by several evidences, such as the resemblance of tissue patterning between developing and regeneration limbs (Muneoka and Bryant 1982). Additionally, embryonic genes are reactivated and have been reported to exhibit similar patterning during the regeneration process (Imokawa and Yoshisato 1997; Carlson et al. 2001; Gardiner and Bryant 1996; Gardiner et al. 1995). These

observations raise the question to what extend the embryonic-like patterning GRN is conserved within the regeneration GRN.

On the other hand, the identity of cells supporting regeneration is different from the embryonic stem cell and appears to have various origins according to the level of regeneration (Introduction – 1.3 Regeneration levels and cellular process). This has been shown in adult planarian neoblasts (Davies et al. 2017). Besides invertebrate stem cells, vertebrates also display major differences in the cell types involved in development and regeneration. For example, satellites cells, involved in adult muscle regeneration appear to have a different embryonic origin than the myoblast that are involved in muscle development (Daughters, Chen, and Slack 2011; De Angelis et al. 1999; Gussoni et al. 1999; Seale and Rudnicki 2000). Therefore, raising the question of the activation/recruitment program during regeneration and the identity of the cells re-expressing the embryonic program.

In *Nematostella* embryogenesis and regeneration display some similarities in late phase of development and reformation, which is supported by transcriptomic data. Indeed co-expression cluster comparisons between these developmental trajectories, have highlighted the strong conservation of the regeneration cluster R-2 with the embryonic clusters E-6 and E-8. All three display a late activation during regeneration and embryogenesis respectively, suggesting their involvement in terminal differentiation (Article 5 – Warner et al, in submission).

In terms of stem cells/progenitors recruitment during *Nematostella* regeneration, a few proliferating cells are witnessed after Step 0.5 (12-18hpa) at the amputation site (Amiel et al. 2015), while the bulk of proliferation supporting regeneration is activated after Step 1 (Passamaneck and Martindale 2012).

Concerning the recruitment process, unpublished data from the laboratory report, in addition to the proliferation of resident cells, a migration of proliferating cell when the regeneration process transitions to Step 2 (Amiel et al, in revision). My data on MEK/ERK during regeneration have shown no effect on the initial proliferation event (Article 6 – Fig. 3), suggesting that the embryonic-like role of MEK/ERK may not influence the activation of these early proliferating cells, but rather potentially the recruitment of those cells, which could involve a more specific regeneration program.

Regarding, the specification events, I have previously highlighted that a rewired embryonic program is connected to regeneration-specific genes during the initiation of *Nematostella* regeneration. In the case of the signaling pathway I studied in detail, there are evidences that MEK/ERK is involved in re-patterning and re-specifying the amputation site. For instance, *NvfoxB* and *Nvrunt* are expressed in the entire body column in uncut polyps, and *Nvaxin-like*, *Nvsprouty* and *Nvtwist* are expressed at the most oral side of the pharynx (Article 6: Fig. 7). Upon, sub-pharyngeal amputation, the expression domains of these MEK/ERK downstream genes are all relocated to the amputation site at 20hpa, thus demonstrating a re-patterning. If one considers that MEK/ERK may have partially analogous roles during embryogenesis and regeneration, it is important to note that during embryonic development MEK/ERK is involved in specifying and patterning the presumptive endomesoderm, where its downstream targets *Nvrunt* and *Nsprouty* are expressed in stacked embryonic domain at the oral pole (Article 2 – Fig. 7) together with the cWnt downstream targets *NvfoxB*, *Nvtwist*, *Nvaxin-like* (Röttinger, Dahlin, and Martindale 2012). These results therefore re-enforce the idea, that the embryonic and regeneration specification role of MEK/ERK is maintained during regeneration, but to which a re-wired embryonic GRN is associated.

As a concluding remark, in *Nematostella,* I believe that not only morphogenesis shares comparable features between embryogenesis and regeneration but also earlier events appear to reuse embryonic-like programs that are embedded in the regeneration GRN. In particular, I am convinced that the program involved in regulating tissue specification during regeneration might display a certain similarity with the one initially set up for specifying germ layers in the embryo. Nevertheless the link with stem cell/progenitor activation recruitment has to be clarified and investigate if this embryonic-like program could be part of the stem cell/progenitor program to re-pattern the reforming head.

Figure 21:

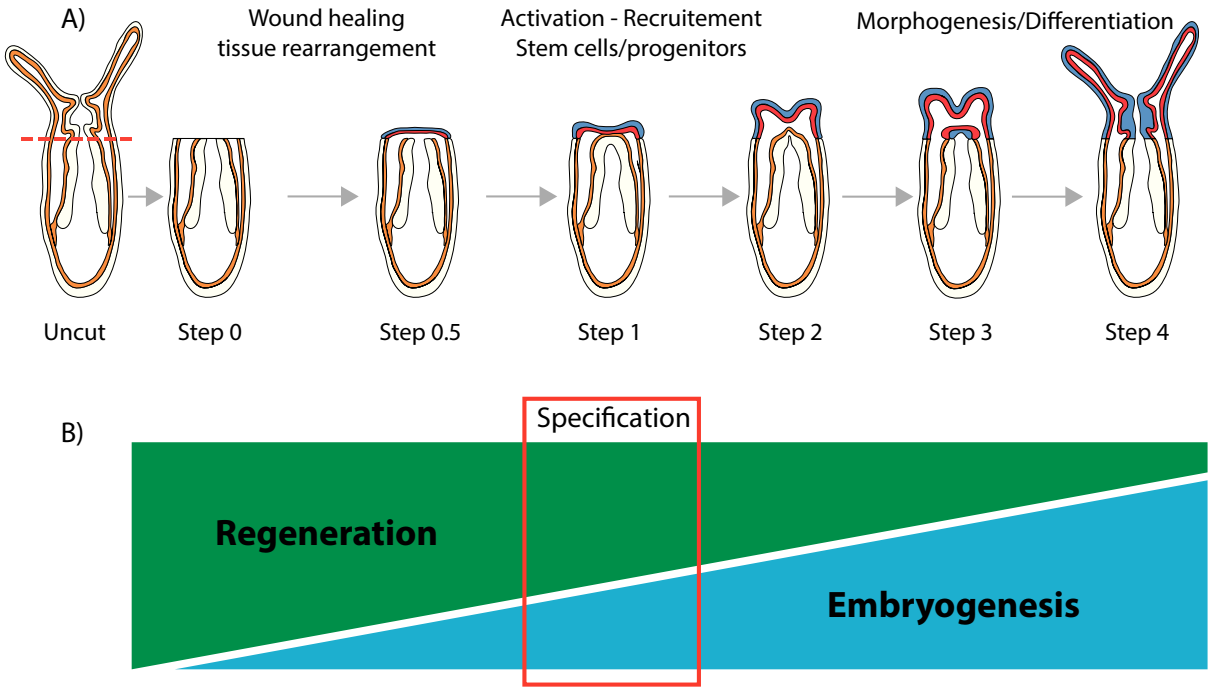

Model representing the relationship between embryogenesis and regeneration in Nematostella. A) The chronology of regeneration events associated with the regeneration step of *Nematostella*. B) Representation of the hypothetical proportions regeneration (green) and embryonic (blue) program inputs.

3.2 Regeneration specific program

In the previous sections, I have discussed the relationship between embryogenesis and regeneration and what might be comparable in those two developmental trajectories. In this section I will be discussing the specificity of regeneration in regard to embryogenesis. Before initiating regeneration, the wound has to be properly closed, which implies a proper re-epithelialization (Bibb and Campbell 1973; Sánchez Alvarado and Newmark 1998; Tanner et al. 2009; Bryant, Endo, and Gardiner 2002; Brockes and Kumar 2008), which doesn't occur normally during embryogenesis.

In *Nematostella*, the transcriptomic comparison between embryonic and regeneration has led to the identification of a regeneration-specific cluster (R-6) that displays little conservation with any of the embryonic clusters (Article 5 – Fig. 3). Strikingly, this cluster is enriched in apoptosis-related GO terms, and inhibition of caspase-dependent apoptosis during embryonic development and regeneration has revealed that it is indeed a regeneration-specific feature of *Nematostella*. Ultimately its inhibition blocks regeneration in which a disorganized epithelium at the amputation site is witness (Article 5 – Fig. 4). Suggesting, that tissue re-arrangement mechanisms during the wound healing process that relying on apoptosis, are specific to regeneration in *Nematostella*.

As mentioned, wound healing is most likely a regeneration specific event in the injury-response program. Interestingly, in Nematostella there are already valuable resources available that could be used to build a GRN underlying wound-healing: a microarray of the downstream targets of MEK/ERK during wound healing (DuBuc, Traylor-Knowles, and Martindale 2014) and a comparative transcriptomic analysis between oral and aboral regeneration of Nematostella (Schaffer et al.

2016). In latter study the authors have characterized, among others, the phase following wound healing at 8hpa. Doing so they demonstrate that approximately 70% of genes differentially expressed during wound healing are common between oral and aboral regeneration (Schaffer et al. 2016). Characterizing in detail this gene set and cross-referencing it with the data obtained from (DuBuc, Traylor-Knowles, and Martindale 2014), offers therefore a solid groundwork to establish the generic GRN underlying the wound-healing phase of *Nematostella*. The establishment of this GRN will be beneficial for future study on identifying the genetic program supporting the recruitment of progenitor cells to complete the GRN associated to the initiation of regeneration. Additionally, a comparison with the embryonic GRN can participate to identify a strict regeneration GRN.

The approach of identifying a specific regeneration GRN will ultimately be also beneficial for the comparison with non-regenerative contexts to potentially identify the barriers that need to be lifted to re-activate a regenerative potential. For instance, wound closure is vital for both regenerative and non-regenerative context but the major difference relies in a successful wound healing. In fact, a disorganized epithelial structure is a hindrance for the reformation of lost structure (Mescher and Neff 2005b; Farkas et al. 2016; P. Liu and Zhong 2017). While in a permissive regeneration context, the wound is closed by a proper re-epithelialization (Bibb and Campbell 1973; Sánchez Alvarado and Newmark 1998; Tanner et al. 2009; Bryant, Endo, and Gardiner 2002; Brockes and Kumar 2008). Another important aspect differentiating a permissive regenerative context to non-regenerating context is the recruitment of competent cells, including the stem cells in invertebrates (Lai and Aboobaker 2018) or the progenitor cells during appendage regeneration (Morrison et al. 2006; Sánchez Alvarado and Tsonis 2006).

Overall, according to the chronological events of regeneration, there are many evidences supporting that wound healing and the activation and recruitment of progenitors are crucial factors to allow regeneration to proceed. Importantly, I believe that these processes are controlled by “regeneration-specific” GRNs. In accordance to my PhD, a potential hypothesis on the loss of regenerative ability could be link to a default of wound healing affecting the recruitment of competent cells for regeneration, in which an embryonic-like program is re-deployed to support patterning and morphogenesis.

References

Adams, Dany S, Alessio Masi, and Michael Levin. 2007. “H+ Pump-Dependent Changes in Membrane Voltage Are an Early Mechanism Necessary and Sufficient to Induce Xenopus Tail Regeneration..” *Development* 134 (7). The Company of Biologists Ltd: 1323–35. doi:10.1242/dev.02812.

Adams, T E, V C Epa, T P Garrett, and C W Ward. 2000. “Structure and Function of the Type 1 Insulin-Like Growth Factor Receptor..” *Cellular and Molecular Life Sciences : CMLS* 57 (7): 1050–93. doi:10.1007/PL00000744.

Affolter, Markus, Rolf Zeller, and Emmanuel Caussinus. 2009. “Tissue Remodelling Through Branching Morphogenesis..” *Nature Reviews. Molecular Cell Biology* 10 (12): 831–42. doi:10.1038/nrm2797.

Agata, K, and Y Umesono. 2008. “Brain Regeneration From Pluripotent Stem Cells in Planarian.” *Philosophical Transactions of the Royal Society B: Biological Sciences* 363 (1500): 2071–78. doi:10.1098/rstb.2008.2260.

Agata, Kiyokazu, Junichi Tasaki, Elizabeth Nakajima, and Yoshihiko Umesono. 2014. “Recent Identification of an ERK Signal Gradient Governing Planarian Regeneration..” *Zoology (Jena, Germany)* 117 (3): 161–62. doi:10.1016/j.zool.2014.04.001.

Almuedo-Castillo, María, Xenia Crespo, Florian Seebeck, Kerstin Bartscherer, Emili Salò, and Teresa Adell. 2014. “JNK Controls the Onset of Mitosis in Planarian Stem Cells and Triggers Apoptotic Cell Death Required for Regeneration and Remodeling..” *PLoS Genetics* 10 (6): e1004400. doi:10.1371/journal.pgen.1004400.

Amiel, Aldine R, Hereroa Johnston, Taylor Chock, Paul Dahlin, Marta Iglesias, Michael Layden, Eric Röttinger, and Mark Q Martindale. 2017. “A Bipolar Role of the Transcription Factor ERG for Cnidarian Germ Layer Formation and Apical Domain Patterning..” *Developmental Biology*, August. doi:10.1016/j.ydbio.2017.08.015.

Amiel, Aldine, Hereroa Johnston, Karine Nedoncelle, Jacob Warner, Solène Ferreira, and Eric Röttinger. 2015. “Characterization of Morphological and Cellular Events Underlying Oral Regeneration in the Sea Anemone, Nematostella Vectensis.” *International Journal of Molecular Sciences* 16 (12): 28449–71. doi:10.3390/ijms161226100.

Arendt, Detlev, Maria Antonietta Tosches, and Heather Marlow. 2016. “From Nerve Net to Nerve Ring, Nerve Cord and Brain--Evolution of the Nervous System..” *Nature Reviews. Neuroscience* 17 (1): 61–72. doi:10.1038/nrn.2015.15.

Arvizu, Fernando, Asdrubal Aguilera, and Luis M Salgado. 2006. “Activities of the Protein Kinases STK, PI3K, MEK, and ERK Are Required for the Development of the Head Organizer in Hydra Magnipapillata..” *Differentiation; Research in Biological Diversity* 74 (6): 305–12. doi:10.1111/j.1432-0436.2006.00078.x.

Bain, Jenny, Lorna Plater, Matt Elliott, Natalia Shpiro, C James Hastie, Hilary McLauchlan, Iva Klevernic, J Simon C Arthur, Dario R Alessi, and Philip Cohen. 2007. “The Selectivity of Protein Kinase Inhibitors: a Further Update..” *The Biochemical Journal* 408 (3). Portland Press Limited: 297–315. doi:10.1042/BJ20070797.

Barberán, Sara, José M Martín-Durán, and Francesc Cebrià. 2016. “Evolution of the EGFR Pathway in Metazoa and Its Diversification in the Planarian Schmidtea

Mediterranea..” *Scientific Reports* 6 (1). Nature Publishing Group: 28071. doi:10.1038/srep28071.
Bardwell, Lee, and Kandarp Shah. 2006. “Analysis of Mitogen-Activated Protein Kinase Activation and Interactions with Regulators and Substrates..” *Methods (San Diego, Calif.)* 40 (3): 213–23. doi:10.1016/j.ymeth.2006.06.008.
Bassnett, Steven, Yanrong Shi, and Gijs F J M Vrensen. 2011. “Biological Glass: Structural Determinants of Eye Lens Transparency..” *Philosophical Transactions of the Royal Society of London. Series B, Biological Sciences* 366 (1568). The Royal Society: 1250–64. doi:10.1098/rstb.2010.0302.
Bayliss, Peter E, Kimberly L Bellavance, Geoffrey G Whitehead, Joshua M Abrams, Sandrine Aegerter, Heather S Robbins, Douglas B Cowan, et al. 2006. “Chemical Modulation of Receptor Signaling Inhibits Regenerative Angiogenesis in Adult Zebrafish..” *Nature Chemical Biology* 2 (5). Nature Publishing Group: 265–73. doi:10.1038/nchembio778.
Becker, T, M F Wullimann, C G Becker, R R Bernhardt, and M Schachner. 1997. “Axonal Regrowth After Spinal Cord Transection in Adult Zebrafish..” *The Journal of Comparative Neurology* 377 (4): 577–95.
Bely, Alexandra E, and Kevin G Nyberg. 2010. “Evolution of Animal Regeneration: Re-Emergence of a Field..” *Trends in Ecology & Evolution* 25 (3): 161–70. doi:10.1016/j.tree.2009.08.005.
Bertrand, Stéphanie, Thomas Iwema, and Hector Escriva. 2014. “FGF Signaling Emerged Concomitantly with the Origin of Eumetazoans..” *Molecular Biology and Evolution* 31 (2). Oxford University Press: 310–18. doi:10.1093/molbev/mst222.
Bibb, C, and R D Campbell. 1973. “Cell Affinity Determining Heterospecific Graft Intolerance in Hydra..” *Tissue & Cell* 5 (2): 199–208.
Binari, L A, G M Lewis, and S Kucenas. 2013. “Perineurial Glia Require Notch Signaling During Motor Nerve Development but Not Regeneration.” *Journal of Neuroscience* 33 (10): 4241–52. doi:10.1523/JNEUROSCI.4893-12.2013.
Biteau, Benoît, Christine E Hochmuth, and Heinrich Jasper. 2008. “JNK Activity in Somatic Stem Cells Causes Loss of Tissue Homeostasis in the Aging Drosophila Gut.” *Cell Stem Cell* 3 (4): 442–55. doi:10.1016/j.stem.2008.07.024.
Boehm, Anna-Marei, Konstantin Khalturin, Friederike Anton-Erxleben, Georg Hemmrich, Ulrich C Klostermeier, Javier A Lopez-Quintero, Hans-Heinrich Oberg, et al. 2012. “FoxO Is a Critical Regulator of Stem Cell Maintenance in Immortal Hydra..” *Proceedings of the National Academy of Sciences of the United States of America* 109 (48). National Academy of Sciences: 19697–702. doi:10.1073/pnas.1209714109.
Bosch, Thomas C G. 2007. “Why Polyps Regenerate and We Don't: Towards a Cellular and Molecular Framework for Hydra Regeneration..” *Developmental Biology* 303 (2): 421–33. doi:10.1016/j.ydbio.2006.12.012.
Bosch, Thomas C G, and Charles N David. 1987. “Stem Cells of Hydra Magnipapillata Can Differentiate Into Somatic Cells and Germ Line Cells.” *Developmental Biology* 121 (1): 182–91. doi:10.1016/0012-1606(87)90151-5.
Bossert, Patricia E, Matthew P Dunn, and Gerald H Thomsen. 2013. “A Staging System for the Regeneration of a Polyp From the Aboral Physa of the Anthozoan Cnidarian Nematostella Vectensis.” *Developmental Dynamics : an Official Publication of the American Association of Anatomists* 242 (11): 1320–31. doi:10.1002/dvdy.24021.
Boucher, Jeremie, Yu-Hua Tseng, and C Ronald Kahn. 2010. “Insulin and Insulin-Like Growth Factor-1 Receptors Act as Ligand-Specific Amplitude Modulators of

a Common Pathway Regulating Gene Transcription..” *Journal of Biological Chemistry* 285 (22). American Society for Biochemistry and Molecular Biology: 17235–45. doi:10.1074/jbc.M110.118620.
Brockes, Jeremy P, and Anoop Kumar. 2008. “Comparative Aspects of Animal Regeneration..” *Annual Review of Cell and Developmental Biology* 24: 525–49. doi:10.1146/annurev.cellbio.24.110707.175336.
Bryant, Susan V, Tetsuya Endo, and David M Gardiner. 2002. “Vertebrate Limb Regeneration and the Origin of Limb Stem Cells..” *The International Journal of Developmental Biology* 46 (7): 887–96.
Brzóska, Edyta, Marta Przewoźniak, Iwona Grabowska, Katarzyna Jańczyk-Ilach, and Jerzy Moraczewski. 2009. “Pax3 and Pax7 Expression During Myoblast Differentiation in Vitro and Fast and Slow Muscle Regeneration in Vivo..” *Cell Biology International* 33 (4): 483–92. doi:10.1016/j.cellbi.2008.11.015.
Buenrostro, Jason D, Beijing Wu, Howard Y Chang, and William J Greenleaf. 2015. “ATAC-Seq: a Method for Assaying Chromatin Accessibility Genome-Wide..” *Current Protocols in Molecular Biology* 109 (January): 21.29.1–.29.9. doi:10.1002/0471142727.mb2129s109.
Burton, Patrick M, and John R Finnerty. 2009. “Conserved and Novel Gene Expression Between Regeneration and Asexual Fission in Nematostella Vectensis..” *Development Genes and Evolution* 219 (2): 79–87. doi:10.1007/s00427-009-0271-2.
Butler, Elmer G, and Margery B Ward. 1967. “Reconstitution of the Spinal Cord After Ablation in Adult Triturus.” *Developmental Biology* 15 (5): 464–86. doi:10.1016/0012-1606(67)90038-3.
Campos, A, M P Cummings, J L Reyes, and J P Laclette. 1998. “Phylogenetic Relationships of Platyhelminthes Based on 18S Ribosomal Gene Sequences..” *Molecular Phylogenetics and Evolution* 10 (1): 1–10. doi:10.1006/mpev.1997.0483.
Cano-Martínez, Agustina, Alvaro Vargas-González, Verónica Guarner-Lans, Esteban Prado-Zayago, Martha León-Oleda, and Betzabé Nieto-Lima. 2010. “Functional and Structural Regeneration in the Axolotl Heart (Ambystoma Mexicanum) After Partial Ventricular Amputation..” *Archivos De Cardiologia De Mexico* 80 (2): 79–86.
Cao, Junyue, Jonathan S Packer, Vijay Ramani, Darren A Cusanovich, Chau Huynh, Riza Daza, Xiaojie Qiu, et al. 2017. “Comprehensive Single-Cell Transcriptional Profiling of a Multicellular Organism..” *Science* 357 (6352): 661–67. doi:10.1126/science.aam8940.
Carlson, M R, Y Komine, S V Bryant, and D M Gardiner. 2001. “Expression of Hoxb13 and Hoxc10 in Developing and Regenerating Axolotl Limbs and Tails..” *Developmental Biology* 229 (2): 396–406. doi:10.1006/dbio.2000.0104.
Cebrià, Francesc, Chiyoko Kobayashi, Yoshihiko Umesono, Masumi Nakazawa, Katsuhiko Mineta, Kazuho Ikeo, Takashi Gojobori, et al. 2002. “FGFR-Related Gene Nou-Darake Restricts Brain Tissues to the Head Region of Planarians..” *Nature* 419 (6907): 620–24. doi:10.1038/nature01042.
Chablais, Fabian, and Anna Jaźwińska. 2010. “IGF Signaling Between Blastema and Wound Epidermis Is Required for Fin Regeneration..” *Development* 137 (6). Oxford University Press for The Company of Biologists Limited: 871–79. doi:10.1242/dev.043885.
Chablais, Fabian, Julia Veit, Gregor Rainer, and Anna Jaźwińska. 2011. “The Zebrafish Heart Regenerates After Cryoinjury-Induced Myocardial Infarction..”

BMC Developmental Biology 11 (April): 21. doi:10.1186/1471-213X-11-21.
Cheng, Zhenchao, Lijuan Duan, Xiaoxia Hao, Zhanpeng Li, Gaiping Wang, and Cunshuan Xu. 2012. “Ten Paths of PKA Signaling Pathway Regulate Hepatocyte Proliferation in Rat Liver Regeneration.” *Genes & Genomics* 34 (4): 391–99. doi:10.1007/s13258-011-0195-x.
Chera, Simona, Luiza Ghila, Yvan Wenger, and Brigitte Galliot. 2011. “Injury-Induced Activation of the MAPK/CREB Pathway Triggers Apoptosis-Induced Compensatory Proliferation in Hydra Head Regeneration..” *Development, Growth & Differentiation* 53 (2). Blackwell Publishing Ltd: 186–201. doi:10.1111/j.1440-169X.2011.01250.x.
Chernoff, Ellen A G, Kazuna Sato, Angela Corn, and Rachel E Karcavich. 2002. “Spinal Cord Regeneration: Intrinsic Properties and Emerging Mechanisms.” *Cell Developmental Biology* 13 (September): 361–68. doi:10.1016/S1084–9521(02)00092-7.
Chou, Hsien-Chao, Margaret M Pruitt, Benjamin R Bastin, and Stephan Q Schneider. 2016. “A Transcriptional Blueprint for a Spiral-Cleaving Embryo.” *BMC Genomics*, August. BMC Genomics, 1–25. doi:10.1186/s12864-016-2860-6.
Christensen, R N, M Weinstein, and R A Tassava. 2001. “Fibroblast Growth Factors in Regenerating Limbs of Ambystoma: Cloning and Semi-Quantitative RT-PCR Expression Studies..” *The Journal of Experimental Zoology* 290 (5): 529–40.
Christensen, Randolph N, michael Weinstein, and Roy A Tassava. 2002. “Expression of Fibroblast Growth Factors 4, 8, and 10 in Limbs, Flanks, and Blastemas of Ambystoma..” *Developmental Dynamics : an Official Publication of the American Association of Anatomists* 223 (2). Wiley Subscription Services, Inc., A Wiley Company: 193–203. doi:10.1002/dvdy.10049.
Clauss, M. 2000. “Molecular Biology of the VEGF and the VEGF Receptor Family..” *Seminars in Thrombosis and Hemostasis* 26 (5). Copyright © 2000 by Thieme Medical Publishers, Inc., 333 Seventh Avenue, New York, NY 10001, USA. Tel.: +1(212) 584-4662: 561–69. doi:10.1055/s-2000-13213.
Cordero, Julia B, Rhoda K Stefanatos, Alessandro Scopelliti, Marcos Vidal, and Owen J Sansom. 2012. “Inducible Progenitor-Derived Wingless Regulates Adult Midgut Regeneration in Drosophila.” *The EMBO Journal* 31 (19). Nature Publishing Group: 3901–17. doi:10.1038/emboj.2012.248.
Currie, Joshua D, Akane Kawaguchi, Ricardo Moreno Traspas, Maritta Schuez, Osvaldo Chara, and Elly M Tanaka. 2016. “Live Imaging of Axolotl Digit Regeneration Reveals Spatiotemporal Choreography of Diverse Connective Tissue Progenitor Pools..” *Developmental Cell* 39 (4): 411–23. doi:10.1016/j.devcel.2016.10.013.
Custodio, M R, I Prokic, R Steffen, C Koziol, R Borojevic, F Brümmer, M Nickel, and W E Müller. 1998. “Primmorphs Generated From Dissociated Cells of the Sponge Suberites Domuncula: a Model System for Studies of Cell Proliferation and Cell Death..” *Mechanisms of Ageing and Development* 105 (1-2): 45–59.
D'Aniello, S, M Irimia, I Maeso, J Pascual-Anaya, S Jimenez-Delgado, S Bertrand, and J Garcia-Fernandez. 2008. “Gene Expansion and Retention Leads to a Diverse Tyrosine Kinase Superfamily in Amphioxus.” *Molecular Biology and Evolution* 25 (9): 1841–54. doi:10.1093/molbev/msn132.
Darling, John A, Adam R Reitzel, Patrick M Burton, Maureen E Mazza, Joseph F Ryan, James C Sullivan, and John R Finnerty. 2005. “Rising Starlet: the Starlet Sea Anemone, Nematostella Vectensis..” *BioEssays : News and Reviews in*

Molecular, Cellular and Developmental Biology 27 (2): 211–21. doi:10.1002/bies.20181.
Daughters, Randall S, Ying Chen, and Jonathan M W Slack. 2011. “Origin of Muscle Satellite Cells in the Xenopus Embryo..” *Development* 138 (5): 821–30. doi:10.1242/dev.056481.
David, Charles N, and Ida Plotnick. 1980. “Distribution of Interstitial Stem Cells in Hydra.”
DAVIDSON, E. 2006. *Gene Regulatory Networks for DevelopmentWhat They Are, How They Work, and What They Mean*. *The Regulatory Genome*. Elsevier. doi:10.1016/b978-012088563-3/50022-5.
Davidson, Eric H. 2011. “Evolutionary Bioscience as Regulatory Systems Biology..” *Developmental Biology* 357 (1): 35–40. doi:10.1016/j.ydbio.2011.02.004.
Davies, Erin L, Kai Lei, Christopher W Seidel, Amanda E Kroesen, Sean A McKinney, Longhua Guo, Sofia Mc Robb, Eric J Ross, Kirsten Gotting, and Alejandro Sánchez Alvarado. 2017. “Embryonic Origin of Adult Stem Cells Required for Tissue Homeostasis and Regeneration..” *eLife* 6 (January). doi:10.7554/eLife.21052.
De Angelis, L, L Berghella, M Coletta, L Lattanzi, M Zanchi, M G Cusella-De Angelis, C Ponzetto, and G Cossu. 1999. “Skeletal Myogenic Progenitors Originating From Embryonic Dorsal Aorta Coexpress Endothelial and Myogenic Markers and Contribute to Postnatal Muscle Growth and Regeneration..” *The Journal of Cell Biology* 147 (4): 869–78.
de Preux Charles, Anne-Sophie, Thomas Bise, Felix Baier, Jan Marro, and Anna Jaźwińska. 2016. “Distinct Effects of Inflammation on Preconditioning and Regeneration of the Adult Zebrafish Heart..” *Open Biology* 6 (7). Royal Society Journals: 160102. doi:10.1098/rsob.160102.
Doudna, Jennifer A, and Emmanuelle Charpentier. 2014. “Genome Editing. the New Frontier of Genome Engineering with CRISPR-Cas9..” *Science* 346 (6213): 1258096–96. doi:10.1126/science.1258096.
Draper, B W, P A Morcos, and C B Kimmel. 2001. “Inhibition of Zebrafish Fgf8 Pre-mRNA Splicing with Morpholino Oligos: a Quantifiable Method for Gene Knockdown..” *Genesis (New York, N.Y. : 2000)* 30 (3): 154–56.
DuBuc, Timothy Q, Nikki Traylor-Knowles, and Mark Q Martindale. 2014. “Initiating a Regenerative Response; Cellular and Molecular Features of Wound Healing in the Cnidarian Nematostella Vectensis..” *BMC Biology* 12 (1). BioMed Central Ltd: 24. doi:10.1186/1741-7007-12-24.
Earp, H Shelton, Benjamin F Calvo, and Carolyn I Sartor. 2003. “The EGF Receptor Family--Multiple Roles in Proliferation, Differentiation, and Neoplasia with an Emphasis on HER4..” *Transactions of the American Clinical and Climatological Association* 114: 315–33–discussion333–4.
Egger, B, P Ladurner, K Nimeth, R Gschwentner, and R Rieger. 2006. “The Regeneration Capacity of the Flatworm Macrostomum Lignano—on Repeated Regeneration, Rejuvenation, and the Minimal Size Needed for Regeneration.” *Development Genes and Evolution* 216 (10): 565–77. doi:10.1007/s00427-006-0069-4.
Elliott, Sarah A, and Alejandro Sánchez Alvarado. 2013. “The History and Enduring Contributions of Planarians to the Study of Animal Regeneration..” *Wiley Interdisciplinary Reviews. Developmental Biology* 2 (3): 301–26. doi:10.1002/wdev.82.
Endo, Tetsuya, Jun Yoshino, Koji Kado, and Shin Tochinai. 2007. “Brain

Regeneration in Anuran Amphibians." *Development, Growth & Differentiation* 49 (2): 121–29. doi:10.1111/j.1440-169X.2007.00914.x.
Engel, Felix B, Michael Schebesta, Mychelle T Duong, Gang Lu, Shuxun Ren, Jeffery B Madwed, Huiping Jiang, Yibin Wang, and Mark T Keating. 2005. "P38 MAP Kinase Inhibition Enables Proliferation of Adult Mammalian Cardiomyocytes.." *Genes & Development* 19 (10). Cold Spring Harbor Lab: 1175–87. doi:10.1101/gad.1306705.
Extavour, Cassandra G, Kevin Pang, David Q Matus, and Mark Q Martindale. 2005. "Vasa and Nanos Expression Patterns in a Sea Anemone and the Evolution of Bilaterian Germ Cell Specification Mechanisms.." *Evolution & Development* 7 (3). Blackwell Science Inc: 201–15. doi:10.1111/j.1525-142X.2005.05023.x.
Fahmy, Gehan H, and Marie Z Moftah. 2010. "Fgf-2 in Astroglial Cells During Vertebrate Spinal Cord Recovery.." *Frontiers in Cellular Neuroscience* 4. Frontiers: 129. doi:10.3389/fncel.2010.00129.
Farkas, Johanna E, Polina D Freitas, Donald M Bryant, Jessica L Whited, and James R Monaghan. 2016. "Neuregulin-1 Signaling Is Essential for Nerve-Dependent Axolotl Limb Regeneration.." *Development* 143 (15). Oxford University Press for The Company of Biologists Limited: 2724–31. doi:10.1242/dev.133363.
Finnerty, John R, Kevin Pang, Pat Burton, Dave Paulson, and Mark Q Martindale. 2004. "Origins of Bilateral Symmetry: Hox and Dpp Expression in a Sea Anemone.." *Science* 304 (5675): 1335–37. doi:10.1126/science.1091946.
Fouraschen, Suomi Mg, Petra E de Ruiter, Jaap Kwekkeboom, Ron Wf de Bruin, Geert Kazemier, Herold J Metselaar, Hugo W Tilanus, Luc Jw van der Laan, and Jeroen de Jonge. 2013. "mTOR Signaling in Liver Regeneration: Rapamycin Combined with Growth Factor Treatment.." *World Journal of Transplantation* 3 (3): 36–47. doi:10.5500/wjt.v3.i3.36.
Fraguas, Susanna, Sara Barberán, and Francesc Cebrià. 2011. "EGFR Signaling Regulates Cell Proliferation, Differentiation and Morphogenesis During Planarian Regeneration and Homeostasis.." *Developmental Biology* 354 (1): 87–101. doi:10.1016/j.ydbio.2011.03.023.
Fraguas, Susanna, Yoshihiko Umesono, Kiyokazu Agata, and Francesc Cebrià. 2017. "Analyzing pERK Activation During Planarian Regeneration.." *Methods in Molecular Biology (Clifton, N.J.)* 1487 (Chapter 23). New York, NY: Springer New York: 303–15. doi:10.1007/978-1-4939-6424-6_23.
Fredriksson, Linda, Hong Li, and Ulf Eriksson. 2004. "The PDGF Family: Four Gene Products Form Five Dimeric Isoforms.." *Cytokine & Growth Factor Reviews* 15 (4): 197–204. doi:10.1016/j.cytogfr.2004.03.007.
Fritz, Ashleigh E, Aissam Ikmi, Christopher Seidel, Ariel Paulson, and Matthew C Gibson. 2013. "Mechanisms of Tentacle Morphogenesis in the Sea Anemone Nematostella Vectensis.." *Development* 140 (10). Oxford University Press for The Company of Biologists Limited: 2212–23. doi:10.1242/dev.088260.
Fritzenwanker, Jens H, Grigory Genikhovich, Yulia Kraus, and Ulrich Technau. 2007. "Early Development and Axis Specification in the Sea Anemone Nematostella Vectensis.." *Developmental Biology* 310 (2): 264–79. doi:10.1016/j.ydbio.2007.07.029.
Fröbius, Andreas C, Gregory Genikhovich, Ulrich Kürn, Friederike Anton-Erxleben, and Thomas C G Bosch. 2003. "Expression of Developmental Genes During Early Embryogenesis of Hydra.." *Development Genes and Evolution* 213 (9): 445–55. doi:10.1007/s00427-003-0344-6.

Gahan, James M, Brian Bradshaw, Hakima Flici, and Uri Frank. 2016. “ScienceDirectThe Interstitial Stem Cells in Hydractinia and Their Role in Regeneration.” *Current Opinion in Genetics & Development* 40 (October). Elsevier Ltd: 65–73. doi:10.1016/j.gde.2016.06.006.
Galliot, Brigitte, and Volker Schmid. 2002. “Cnidarians as a Model System for Understanding Evolution and Regeneration..” *The International Journal of Developmental Biology* 46 (1): 39–48.
Gardiner, D M, and S V Bryant. 1996. “Molecular Mechanisms in the Control of Limb Regeneration: the Role of Homeobox Genes..” *The International Journal of Developmental Biology* 40 (4): 797–805.
Gardiner, D M, B Blumberg, Y Komine, and S V Bryant. 1995. “Regulation of HoxA Expression in Developing and Regenerating Axolotl Limbs..” *Development* 121 (6): 1731–41.
Gauron, Carole, Christine Rampon, Mohamed Bouzaffour, Eliane Ipendey, Jérémie Teillon, Michel Volovitch, and Sophie Vriz. 2013. “Sustained Production of ROS Triggers Compensatory Proliferation and Is Required for Regeneration to Proceed..” *Scientific Reports* 3. Nature Publishing Group: 2084. doi:10.1038/srep02084.
Gazave, Eve, Julien Béhague, Lucie Laplane, Aurélien Guillou, Laetitia Préau, Adrien Demilly, Guillaume Balavoine, and Michel Vervoort. 2013. “Posterior Elongation in the Annelid Platynereis Dumerilii Involves Stem Cells Molecularly Related to Primordial Germ Cells.” *Developmental Biology* 382 (1). Elsevier: 246–67. doi:10.1016/j.ydbio.2013.07.013.
Gemberling, Matthew, Ravi Karra, Amy L Dickson, and Kenneth D Poss. 2015. “Nrg1 Is an Injury-Induced Cardiomyocyte Mitogen for the Endogenous Heart Regeneration Program in Zebrafish.” *eLife* 4: 2139. doi:10.7554/elife.05871.
Gemberling, Matthew, Travis J Bailey, David R Hyde, and Kenneth D Poss. 2013. “The Zebrafish as a Model for Complex Tissue Regeneration..” *Trends in Genetics : TIG* 29 (11): 611–20. doi:10.1016/j.tig.2013.07.003.
Genikhovich, Grigory, and Ulrich Technau. 2009. “In Situ Hybridization of Starlet Sea Anemone (Nematostella Vectensis) Embryos, Larvae, and Polyps..” *Cold Spring Harbor Protocols* 2009 (9). Cold Spring Harbor Laboratory Press: pdb.prot5282. doi:10.1101/pdb.prot5282.
Genikhovich, Grigory, Patrick Fried, M Mandela Prünster, Johannes B Schinko, Anna F Gilles, David Fredman, Karin Meier, Dagmar Iber, and Ulrich Technau. 2015. “Axis Patterning by BMPs: Cnidarian Network Reveals Evolutionary Constraints.” *CellReports* 10 (10). The Authors: 1646–54. doi:10.1016/j.celrep.2015.02.035.
Genikhovich, Grigory, Ulrich Kürn, Georg Hemmrich, and Thomas C G Bosch. 2006. “Discovery of Genes Expressed in Hydra Embryogenesis..” *Developmental Biology* 289 (2): 466–81. doi:10.1016/j.ydbio.2005.10.028.
Gentile, Luca, Francesc Cebrià, and Kerstin Bartscherer. 2011. “The Planarian Flatworm: an in Vivo Model for Stem Cell Biology and Nervous System Regeneration..” *Disease Models & Mechanisms* 4 (1). The Company of Biologists Ltd: 12–19. doi:10.1242/dmm.006692.
Glaze, K A, and J E Turner. 1978. “Regenerative Repair in the Severed Optic Nerve of the Newt (Triturus Viridescens): Effect of Nerve Growth Factor Antiserum..” *Experimental Neurology* 58 (3): 500–510.
Godwin, J W, R Debuque, E Salimova, and N A Rosenthal. 2017. “Heart Regeneration in the Salamander Relies on Macrophage-Mediated Control of

Fibroblast Activation and the Extracellular Landscape..” *NPJ Regenerative Medicine* 2. doi:10.1038/s41536-017-0027-y.
Godwin, James W, Alexander R Pinto, and Nadia A Rosenthal. 2013. “Macrophages Are Required for Adult Salamander Limb Regeneration..” *Proceedings of the National Academy of Sciences of the United States of America* 110 (23). National Academy of Sciences: 9415–20. doi:10.1073/pnas.1300290110.
Goldshmit, Yona, Tamar E Sztal, Patricia R Jusuf, Thomas E Hall, Mai Nguyen-Chi, and Peter D Currie. 2012. “Fgf-Dependent Glial Cell Bridges Facilitate Spinal Cord Regeneration in Zebrafish..” *The Journal of Neuroscience : the Official Journal of the Society for Neuroscience* 32 (22). Society for Neuroscience: 7477–92. doi:10.1523/JNEUROSCI.0758-12.2012.
González-Estévez, Cristina, Daniel A Felix, Matthew D Smith, Jordi Paps, Simon J Morley, Victoria James, Tyson V Sharp, and A Aziz Aboobaker. 2012. “SMG-1 and mTORC1 Act Antagonistically to Regulate Response to Injury and Growth in Planarians..” *PLoS Genetics* 8 (3): e1002619. doi:10.1371/journal.pgen.1002619.
González-Rosa, Juan Manuel, Caroline E Burns, and C Geoffrey Burns. 2017. “Zebrafish Heart Regeneration: 15 Years of Discoveries..” *Regeneration (Oxford, England)* 4 (3): 105–23. doi:10.1002/reg2.83.
González-Rosa, Juan Manuel, Víctor Martín, Marina Peralta, Miguel Torres, and Nadia Mercader. 2011. “Extensive Scar Formation and Regression During Heart Regeneration After Cryoinjury in Zebrafish..” *Development* 138 (9). Oxford University Press for The Company of Biologists Limited: 1663–74. doi:10.1242/dev.060897.
Goodman, Reba, Avary Lin-Ye, Matthew S Geddis, Priya J Wickramaratne, Susan E Hodge, Spiro P Pantazatos, Martin Blank, and Richard T Ambron. 2009. “Extremely Low Frequency Electromagnetic Fields Activate the ERK Cascade, Increase Hsp70 Protein Levels and Promote Regeneration in Planaria..” *International Journal of Radiation Biology* 85 (10): 851–59. doi:10.1080/09553000903072488.
Goss, R J. 1992. “The Evolution of Regeneration: Adaptive or Inherent?.” *Journal of Theoretical Biology* 159 (2): 241–60.
Gussoni, E, Y Soneoka, C D Strickland, E A Buzney, M K Khan, A F Flint, L M Kunkel, and R C Mulligan. 1999. “Dystrophin Expression in the Mdx Mouse Restored by Stem Cell Transplantation..” *Nature* 401 (6751): 390–94. doi:10.1038/43919.
Gustin, M C, J Albertyn, M Alexander, and K Davenport. 1998. “MAP Kinase Pathways in the Yeast Saccharomyces Cerevisiae..” *Microbiology and Molecular Biology Reviews : MMBR* 62 (4): 1264–1300.
Hammond, Scott M. 2005. “Dicing and Slicing: the Core Machinery of the RNA Interference Pathway..” *FEBS Letters* 579 (26): 5822–29. doi:10.1016/j.febslet.2005.08.079.
Han, M J, J Y An, and W S Kim. 2001. “Expression Patterns of Fgf-8 During Development and Limb Regeneration of the Axolotl..” *Developmental Dynamics : an Official Publication of the American Association of Anatomists* 220 (1). John Wiley & Sons, Inc.: 40–48. doi:10.1002/1097-0177(2000)9999:9999<::AID-DVDY1085>3.0.CO;2-8.
Han, Peidong, Xiao-Hai Zhou, Nannan Chang, Cheng-Lu Xiao, Shouyu Yan, He Ren, Xin-Zhuang Yang, et al. 2014. “Hydrogen Peroxide Primes Heart Regeneration with a Derepression Mechanism..” *Cell Research* 24 (9): 1091–1107. doi:10.1038/cr.2014.108.

Hand, C, and K R Uhlinger. 1992. “The Culture, Sexual and Asexual Reproduction, and Growth of the Sea Anemone Nematostella Vectensis..” *The Biological Bulletin* 182 (2): 169–76. doi:10.2307/1542110.
Hanks, S K, and T Hunter. 1995. “Protein Kinases 6. the Eukaryotic Protein Kinase Superfamily: Kinase (Catalytic) Domain Structure and Classification..” *FASEB Journal : Official Publication of the Federation of American Societies for Experimental Biology* 9 (8): 576–96.
Hanks, Steven K. 2003. “Genomic Analysis of the Eukaryotic Protein Kinase Superfamily: a Perspective..” *Genome Biology* 4 (5): 111.
Harris, Raymond C, Eunkyung Chung, and Robert J Coffey. 2003. “EGF Receptor Ligands..” *Experimental Cell Research* 284 (1): 2–13.
He, Shuonan, Florencia Del Viso, Cheng-Yi Chen, Aissam Ikmi, Amanda E Kroesen, and Matthew C Gibson. 2018. “An Axial Hox Code Controls Tissue Segmentation and Body Patterning in Nematostella Vectensis..” *Science* 361 (6409): 1377–80. doi:10.1126/science.aar8384.
Helm, Rebecca Rae, Stefan Siebert, Sarah Tulin, Joel Smith, and Casey William Dunn. 2013. “Characterization of Differential Transcript Abundance Through Time During Nematostella Vectensis Development..” *BMC Genomics* 14 (1): 266. doi:10.1186/1471-2164-14-266.
Henry, Jonathan J, Alvin G Thomas, Paul W Hamilton, Lisa Moore, and Kimberly J Perry. 2013. “Cell Signaling Pathways in Vertebrate Lens Regeneration..” *Current Topics in Microbiology and Immunology* 367 (Chapter 289). Berlin, Heidelberg: Springer Berlin Heidelberg: 75–98. doi:10.1007/82_2012_289.
Henry, Jonathan J, and Panagiotis A Tsonis. 2010. “Molecular and Cellular Aspects of Amphibian Lens Regeneration..” *Progress in Retinal and Eye Research* 29 (6): 543–55. doi:10.1016/j.preteyeres.2010.07.002.
Hernández-Sánchez, Catalina, Alicia Mansilla, Flora de Pablo, and Rafael Zardoya. 2008. “Evolution of the Insulin Receptor Family and Receptor Isoform Expression in Vertebrates..” *Molecular Biology and Evolution* 25 (6): 1043–53. doi:10.1093/molbev/msn036.
Herskowitz, I. 1987. “Functional Inactivation of Genes by Dominant Negative Mutations..” *Nature* 329 (6136): 219–22. doi:10.1038/329219a0.
Hinman, Veronica F, Albert Nguyen, and Eric H Davidson. 2007. “Caught in the Evolutionary Act: Precise Cis-Regulatory Basis of Difference in the Organization of Gene Networks of Sea Stars and Sea Urchins..” *Developmental Biology* 312 (2): 584–95. doi:10.1016/j.ydbio.2007.09.006.
Hinman, Veronica F, and Alys M Cheatle Jarvela. 2014. “Developmental Gene Regulatory Network Evolution: Insights From Comparative Studies in Echinoderms.” Edited by David McClay and Charles Ettensohn. *Genesis (New York, N.Y. : 2000)* 52 (3): 193–207. doi:10.1002/dvg.22757.
Holtzer, Howard. 1951. “Reconstitution of the Urodele Spinal Cord Following Unilateral Ablation. Part I. Chronology of Neuron Regulation.” *Journal of Experimental Zoology* 117 (3): 523–57. doi:10.1002/jez.1401170308.
Holtzer, Howard. 1952. “Reconstitution of the Urodele Spinal Cord Following Unilateral Ablation. II. Regeneration of the Longitudinal Tracts and Ectopic Synaptic Unions of the Mauthner's Fibers.” *Journal of Experimental Zoology* 119 (2): 263–301. doi:10.1002/jez.1401190205.
Howe, Douglas G, Yvonne M Bradford, Tom Conlin, Anne E Eagle, David Fashena, Ken Frazer, Jonathan Knight, et al. 2013. “ZFIN, the Zebrafish Model Organism Database: Increased Support for Mutants and Transgenics..” *Nucleic Acids*

Research 41 (Database issue): D854–60. doi:10.1093/nar/gks938.
Huang, Ying, Michael R Harrison, Arthela Osorio, Jieun Kim, Aaron Baugh, Cunming Duan, Henry M Sucov, and Ching-Ling Lien. 2013. “Igf Signaling Is Required for Cardiomyocyte Proliferation During Zebrafish Heart Development and Regeneration..” *PloS One* 8 (6): e67266. doi:10.1371/journal.pone.0067266.
Hubbard, S R. 1999. “Structural Analysis of Receptor Tyrosine Kinases..” *Progress in Biophysics and Molecular Biology* 71 (3-4): 343–58.
Huebner, Eric A, and Stephen M Strittmatter. 2009. “Axon Regeneration in the Peripheral and Central Nervous Systems..” *Results and Problems in Cell Differentiation* 48: 339–51. doi:10.1007/400_2009_19.
Ikmi, Aissam, Sean A McKinney, Kym M Delventhal, and Matthew C Gibson. 2014. “TALEN and CRISPR/Cas9-Mediated Genome Editing in the Early-Branching Metazoan Nematostella Vectensis..” *Nature Communications* 5 (November). Nature Publishing Group: 5486. doi:10.1038/ncomms6486.
Imokawa, Yutaka, and Jeremy P Brockes. 2003. “Selective Activation of Thrombin Is a Critical Determinant for Vertebrate Lens Regeneration..” *Current Biology : CB* 13 (10): 877–81.
Imokawa, Yutaka, András Simon, and Jeremy P Brockes. 2004. “A Critical Role for Thrombin in Vertebrate Lens Regeneration..” *Philosophical Transactions of the Royal Society of London. Series B, Biological Sciences* 359 (1445). The Royal Society: 765–76. doi:10.1098/rstb.2004.1467.
Ishida, Takashi, Teruhiro Nakajima, Akira Kudo, and Atsushi Kawakami. 2010. “Phosphorylation of Junb Family Proteins by the Jun N-Terminal Kinase Supports Tissue Regeneration in Zebrafish..” *Developmental Biology* 340 (2): 468–79. doi:10.1016/j.ydbio.2010.01.036.
Itou, Junji, Isao Oishi, Hiroko Kawakami, Tiffany J Glass, Jenna Richter, Austin Johnson, Troy C Lund, and Yasuhiko Kawakami. 2012. “Migration of Cardiomyocytes Is Essential for Heart Regeneration in Zebrafish..” *Development* 139 (22). Oxford University Press for The Company of Biologists Limited: 4133–42. doi:10.1242/dev.079756.
Jahnel, Stefan M, Manfred Walzl, and Ulrich Technau. 2014. “Development and Epithelial Organisation of Muscle Cells in the Sea Anemone Nematostella Vectensis..” *Frontiers in Zoology* 11: 44. doi:10.1186/1742-9994-11-44.
Jensen, Jan Nygaard, Erin Cameron, Maria Veronica R Garay, Thomas W Starkey, Roberto Gianani, and Jan Jensen. 2005. “Recapitulation of Elements of Embryonic Development in Adult Mouse Pancreatic Regeneration..” *Gastroenterology* 128 (3): 728–41.
Jopling, Chris, Eduard Sleep, Marina Raya, Mercè Martí, Angel Raya, and Juan Carlos Izpisua Belmonte. 2010. “Zebrafish Heart Regeneration Occurs by Cardiomyocyte Dedifferentiation and Proliferation..” *Nature* 464 (7288): 606–9. doi:10.1038/nature08899.
Jopling, Chris, Guillermo Suñe, Cristina Morera, and Juan Carlos Izpisua Belmonte. 2012. “P38α MAPK Regulates Myocardial Regeneration in Zebrafish..” *Cell Cycle (Georgetown, Tex.)* 11 (6). Taylor & Francis: 1195–1201. doi:10.4161/cc.11.6.19637.
Joven, Alberto, and András Simon. 2018. “Homeostatic and Regenerative Neurogenesis in Salamanders..” *Progress in Neurobiology*, April. doi:10.1016/j.pneurobio.2018.04.006.
Kadam, Snehalata, Amy McMahon, Phoebe Tzou, and Angelike Stathopoulos. 2009. “FGF Ligands in Drosophila Have Distinct Activities Required to Support Cell

Migration and Differentiation..” *Development* 136 (5). The Company of Biologists Ltd: 739–47. doi:10.1242/dev.027904.
Kaloulis, Kostas, Simona Chera, Monika Hassel, Dominique Gauchat, and Brigitte Galliot. 2004. “Reactivation of Developmental Programs: the cAMP-Response Element-Binding Protein Pathway Is Involved in Hydra Head Regeneration..” *Proceedings of the National Academy of Sciences* 101 (8): 2363–68.
Kao, Damian, Daniel Felix, and Aziz Aboobaker. 2013. “The Planarian Regeneration Transcriptome Reveals a Shared but Temporally Shifted Regulatory Program Between Opposing Head and Tail Scenarios..” *BMC Genomics* 14 (November): 797. doi:10.1186/1471-2164-14-797.
Khatib, Abdel-Majid, Rachid Lahlil, Nathalie Scamuffa, Marie-Andrée Akimenko, Sylvain Ernest, Abdderahim Lomri, Claude Lalou, et al. 2010. “Zebrafish ProVEGF-C Expression, Proteolytic Processing and Inhibitory Effect of Unprocessed ProVEGF-C During Fin Regeneration..” Edited by Ferenc Mueller. *PloS One* 5 (7). Public Library of Science: e11438. doi:10.1371/journal.pone.0011438.
Kikuchi, Kazu, Jennifer E Holdway, Andreas A Werdich, Ryan M Anderson, Yi Fang, Gregory F Egnaczyk, Todd Evans, Calum A Macrae, Didier Y R Stainier, and Kenneth D Poss. 2010. “Primary Contribution to Zebrafish Heart Regeneration by Gata4(+) Cardiomyocytes..” *Nature* 464 (7288): 601–5. doi:10.1038/nature08804.
Kikuchi, Kazu, Jennifer E Holdway, Robert J Major, Nicola Blum, Randall D Dahn, Gerrit Begemann, and Kenneth D Poss. 2011. “Retinoic Acid Production by Endocardium and Epicardium Is an Injury Response Essential for Zebrafish Heart Regeneration..” *Developmental Cell* 20 (3): 397–404. doi:10.1016/j.devcel.2011.01.010.
Kim, Jieun, Qiong Wu, Yolanda Zhang, Katie M Wiens, Ying Huang, Nicole Rubin, Hiroyuki Shimada, et al. 2010. “PDGF Signaling Is Required for Epicardial Function and Blood Vessel Formation in Regenerating Zebrafish Hearts..” *Proceedings of the National Academy of Sciences of the United States of America* 107 (40). National Acad Sciences: 17206–10. doi:10.1073/pnas.0915016107.
Kim, Woong-Hee, Da-Woon Jung, Jinmi Kim, Sin-Hyeog Im, Seung Yong Hwang, and Darren R Williams. 2012. “Small Molecules That Recapitulate the Early Steps of Urodele Amphibian Limb Regeneration and Confer Multipotency..” *ACS Chemical Biology* 7 (4): 732–43. doi:10.1021/cb200532v.
Kirsche, Walter. 1983. *The Significance of Matrix Zones for Brain Regeneration and Brain Transplantation with Special Consideration of Lower Vertebrates*. *Proceedings in Life Sciences*. Proceedings in Life Sciences. New York, NY: Springer New York. doi:10.1007/978-1-4612-5539-0_2.
Kizil, Caghan, Jan Kaslin, Volker Kroehne, and Michael Brand. 2012. “Adult Neurogenesis and Brain Regeneration in Zebrafish..” *Developmental Neurobiology* 72 (3): 429–61. doi:10.1002/dneu.20918.
Klingseisen, A, I B N Clark, T Gryzik, and H A J Muller. 2009. “Differential and Overlapping Functions of Two Closely Related Drosophila FGF8-Like Growth Factors in Mesoderm Development.” *Development* 136 (14): 2393–2402. doi:10.1242/dev.035451.
Knopf, Franziska, Christina Hammond, Avinash Chekuru, Thomas Kurth, Stefan Hans, Christopher W Weber, Gina Mahatma, et al. 2011. “Bone Regenerates via Dedifferentiation of Osteoblasts in the Zebrafish Fin..” *Developmental Cell* 20 (5):

713–24. doi:10.1016/j.devcel.2011.04.014.
Kopec, Anna K, Nikita Joshi, Holly Cline-Fedewa, Anna V Wojcicki, Jessica L Ray, Bradley P Sullivan, John E Froehlich, Brendan F Johnson, Matthew J Flick, and James P Luyendyk. 2017. “Fibrin(Ogen) Drives Repair After Acetaminophen-Induced Liver Injury via Leukocyte αMβ2 Integrin-Dependent Upregulation of Mmp12..” *Journal of Hepatology* 66 (4): 787–97. doi:10.1016/j.jhep.2016.12.004.
Kraus, Yulia, Hakima Flici, Katrin Hensel, Günter Plickert, Thomas Leitz, and Uri Frank. 2014. “The Embryonic Development of the Cnidarian Hydractinia Echinata.” *Evolution & Development* 16 (6): 323–38. doi:10.1111/ede.12100.
Krishnapati, Lakshmi-Surekha, and Surendra Ghaskadbi. 2013. “Identification and Characterization of VEGF and FGF From Hydra.” *The International Journal of Developmental Biology* 57 (11-12): 897–906. doi:10.1387/ijdb.130077sg.
Kroehne, Volker, Dorian Freudenreich, Stefan Hans, Jan Kaslin, and Michael Brand. 2011. “Regeneration of the Adult Zebrafish Brain From Neurogenic Radial Glia-Type Progenitors..” *Development* 138 (22). Oxford University Press for The Company of Biologists Limited: 4831–41. doi:10.1242/dev.072587.
Kumar, Lokesh, and Matthias E Futschik. 2007. “Mfuzz: a Software Package for Soft Clustering of Microarray Data..” *Bioinformation* 2 (1): 5–7.
Kusserow, Arne, Kevin Pang, Carsten Sturm, Martina Hrouda, Jan Lentfer, Heiko A Schmidt, Ulrich Technau, et al. 2005. “Unexpected Complexity of the Wnt Gene Family in a Sea Anemone..” *Nature* 433 (7022): 156–60. doi:10.1038/nature03158.
Kyritsis, N, C Kizil, S Zocher, V Kroehne, J Kaslin, D Freudenreich, A Iltzsche, and M Brand. 2012. “Acute Inflammation Initiates the Regenerative Response in the Adult Zebrafish Brain.” *Science* 338 (6112): 1353–56. doi:10.1126/science.1228773.
Ladurner, Peter, Bernhard Egger, Reinhard Rieger, Volker Hartenstein, Joshua Morris, and Ramachandra Nallur. 2004. “The Embryonic Development of the Flatworm Macrostomum Sp..” *Development Genes and Evolution* 214 (5): 220–39. doi:10.1007/s00427-004-0406-4.
Lai, Alvina G, and A Aziz Aboobaker. 2018. “EvoRegen in Animals: Time to Uncover Deep Conservation or Convergence of Adult Stem Cell Evolution and Regenerative Processes..” *Developmental Biology* 433 (2): 118–31. doi:10.1016/j.ydbio.2017.10.010.
Laisney, Juliette A G C, Ingo Braasch, Ronald B Walter, Svenja Meierjohann, and Manfred Schartl. 2010. “Lineage-Specific Co-Evolution of the Egf Receptor/Ligand Signaling System..” *BMC Evolutionary Biology* 10 (January): 27. doi:10.1186/1471-2148-10-27.
Lam, Nicholas T, Peter D Currie, Graham J Lieschke, Nadia A Rosenthal, and David M Kaye. 2012. “Nerve Growth Factor Stimulates Cardiac Regeneration via Cardiomyocyte Proliferation in Experimental Heart Failure..” *PloS One* 7 (12): e53210. doi:10.1371/journal.pone.0053210.
Lange, Ellen, Stéphanie Bertrand, Oliver Holz, Nicole Rebscher, and Monika Hassel. 2014. “Dynamic Expression of a Hydra FGF at Boundaries and Termini.” *Development Genes and Evolution* 224 (4-6): 235–44. doi:10.1007/s00427-014-0480-1.
Lawrence, Christian, Isaac Adatto, Jason Best, Althea James, and Kara Maloney. 2012. “Generation Time of Zebrafish (Danio Rerio) and Medakas (Oryzias Latipes) Housed in the Same Aquaculture Facility..” *Lab Animal* 41 (6): 158–65. doi:10.1038/laban0612-158.

Layden, Michael J, and Mark Q Martindale. 2014. “Non-Canonical Notch Signaling Represents an Ancestral Mechanism to Regulate Neural Differentiation” 5 (1): 1–14. doi:10.1186/2041-9139-5-30.
Layden, Michael J, Eric Röttinger, Francis S Wolenski, Thomas D Gilmore, and Mark Q Martindale. 2013. “Microinjection of mRNA or Morpholinos for Reverse Genetic Analysis in the Starlet Sea Anemone, Nematostella Vectensis.” *Nature Protocols* 8 (5): 924–34. doi:10.1038/nprot.2013.009.
Layden, Michael J, Hereroa Johnston, Aldine R Amiel, Jamie Havrilak, Bailey Steinworth, Taylor Chock, Eric Röttinger, and Mark Q Martindale. 2016. “MAPK Signaling Is Necessary for Neurogenesis in Nematostella Vectensis.” *BMC Biology*, July. BMC Biology, 1–19. doi:10.1186/s12915-016-0282-1.
Layden, Michael J, Michiel Boekhout, and Mark Q Martindale. 2012. “Nematostella Vectensis Achaete-Scute Homolog NvashA Regulates Embryonic Ectodermal Neurogenesis and Represents an Ancient Component of the Metazoan Neural Specification Pathway..” *Development* 139 (5). Oxford University Press for The Company of Biologists Limited: 1013–22. doi:10.1242/dev.073221.
Leclère, Lucas, and Eric Röttinger. 2016. “Diversity of Cnidarian Muscles: Function, Anatomy, Development and Regeneration..” *Frontiers in Cell and Developmental Biology* 4. Frontiers: 157. doi:10.3389/fcell.2016.00157.
Leclère, Lucas, Markus Bause, Chiara Sinigaglia, Julia Steger, and Fabian Rentzsch. 2016. “Development of the Aboral Domain in Nematostella Requires B-Catenin and the Opposing Activities of Six3/6 and Frizzled5/8..” *Development* 143 (10). Oxford University Press for The Company of Biologists Limited: 1766–77. doi:10.1242/dev.120931.
Lee, Kyoung Eun, Michelle Spata, Richard Maduka, Robert H Vonderheide, and M Celeste Simon. 2018. “Hif1Α Deletion Limits Tissue Regeneration via Aberrant B Cell Accumulation in Experimental Pancreatitis.” *CellReports* 23 (12). ElsevierCompany.: 3457–64. doi:10.1016/j.celrep.2018.05.071.
Lee, Patricia N, Kevin Pang, David Q Matus, and Mark Q Martindale. 2006. “A WNT of Things to Come: Evolution of Wnt Signaling and Polarity in Cnidarians..” *Seminars in Cell & Developmental Biology* 17 (2): 157–67. doi:10.1016/j.semcdb.2006.05.002.
Lee, Patricia N, Shalika Kumburegama, Heather Q Marlow, Mark Q Martindale, and Athula H Wikramanayake. 2007. “Asymmetric Developmental Potential Along the Animal-Vegetal Axis in the Anthozoan Cnidarian, Nematostella Vectensis, Is Mediated by Dishevelled..” *Developmental Biology* 310 (1): 169–86. doi:10.1016/j.ydbio.2007.05.040.
Lee, Yoonsung, Sara Grill, Angela Sanchez, Maureen Murphy-Ryan, and Kenneth D Poss. 2005. “Fgf Signaling Instructs Position-Dependent Growth Rate During Zebrafish Fin Regeneration..” *Development* 132 (23). The Company of Biologists Ltd: 5173–83. doi:10.1242/dev.02101.
Lei, Kai, Hanh Thi-Kim Vu, Ryan D Mohan, Sean A McKinney, Chris W Seidel, Richard Alexander, Kirsten Gotting, Jerry L Workman, and Alejandro Sánchez Alvarado. 2016. “Egf Signaling Directs Neoblast Repopulation by Regulating Asymmetric Cell Division in Planarians..” *Developmental Cell* 38 (4): 413–29. doi:10.1016/j.devcel.2016.07.012.
Lemmon, Mark A, and Joseph Schlessinger. 2010. “Cell Signaling by Receptor Tyrosine Kinases..” *Cell* 141 (7): 1117–34. doi:10.1016/j.cell.2010.06.011.
Lepilina, Alexandra, Ashley N Coon, Kazu Kikuchi, Jennifer E Holdway, Richard W Roberts, C Geoffrey Burns, and Kenneth D Poss. 2006. “A Dynamic Epicardial

Injury Response Supports Progenitor Cell Activity During Zebrafish Heart Regeneration..” *Cell* 127 (3): 607–19. doi:10.1016/j.cell.2006.08.052.
LeRoith, D, V M Kavsan, A P Koval, and C T Roberts. 1993. “Phylogeny of the Insulin-Like Growth Factors (IGFs) and Receptors: a Molecular Approach..” *Molecular Reproduction and Development* 35 (4): 332–6–discussion337–8. doi:10.1002/mrd.1080350403.
Lesurtel, Mickael, Rolf Graf, Boris Aleil, Diego J Walther, Yinghua Tian, Wolfram Jochum, Christian Gachet, Michael Bader, and Pierre-Alain Clavien. 2006. “Platelet-Derived Serotonin Mediates Liver Regeneration..” *Science* 312 (5770): 104–7. doi:10.1126/science.1123842.
Levin, Michael. 2007. “Large-Scale Biophysics: Ion Flows and Regeneration..” *Trends in Cell Biology* 17 (6): 261–70. doi:10.1016/j.tcb.2007.04.007.
Levin, Michael. 2009. “Bioelectric Mechanisms in Regeneration: Unique Aspects and Future Perspectives..” *Seminars in Cell & Developmental Biology* 20 (5): 543–56. doi:10.1016/j.semcdb.2009.04.013.
Li, Meng, Jun Liu, and Chiyu Zhang. 2011. “Evolutionary History of the Vertebrate Mitogen Activated Protein Kinases Family..” *PloS One* 6 (10): e26999. doi:10.1371/journal.pone.0026999.
Lien, Ching-Ling, Michael Schebesta, Shinji Makino, Gerhard J Weber, and Mark T Keating. 2006. “Gene Expression Analysis of Zebrafish Heart Regeneration..” Edited by Derek Stemple. *PLoS Biology* 4 (8). Public Library of Science: e260. doi:10.1371/journal.pbio.0040260.
Liu, Peiyun, and Tao P Zhong. 2017. “MAPK/ERK Signalling Is Required for Zebrafish Cardiac Regeneration..” *Biotechnology Letters*, March. Springer Netherlands, 1–9. doi:10.1007/s10529-017-2327-0.
Liu, Zhen, Haiping Zhao, Datao Wang, Chris McMahon, and Chunyi Li. 2018. “Differential Effects of the PI3K/AKT Pathway on Antler Stem Cells for Generation and Regeneration of Antlers in Vitro..” *Frontiers in Bioscience (Landmark Edition)* 23 (June): 1848–63.
Magie, Craig R, Kevin Pang, and Mark Q Martindale. 2005. “Genomic Inventory and Expression of Sox and Fox Genes in the Cnidarian Nematostella Vectensis.” *Development Genes and Evolution* 215 (12): 618–30. doi:10.1007/s00427-005-0022-y.
Makanae, Aki, Ayako Hirata, Yasuko Honjo, Kazumasa Mitogawa, and Akira Satoh. 2013. “Nerve Independent Limb Induction in Axolotls..” *Developmental Biology* 381 (1): 213–26. doi:10.1016/j.ydbio.2013.05.010.
Makanae, Aki, Kazumasa Mitogawa, and Akira Satoh. 2014. “Co-Operative Bmp- and Fgf-Signaling Inputs Convert Skin Wound Healing to Limb Formation in Urodele Amphibians..” *Developmental Biology* 396 (1): 57–66. doi:10.1016/j.ydbio.2014.09.021.
Makanae, Aki, Kazumasa Mitogawa, and Akira Satoh. 2016. “Cooperative Inputs of Bmp and Fgf Signaling Induce Tail Regeneration in Urodele Amphibians..” *Developmental Biology* 410 (1): 45–55. doi:10.1016/j.ydbio.2015.12.012.
Malloch, Erica L, Kimberly J Perry, Lisa Fukui, Verity R Johnson, Jason Wever, Caroline W Beck, Michael W King, and Jonathan J Henry. 2009. “Gene Expression Profiles of Lens Regeneration and Development in Xenopus Laevis..” *Developmental Dynamics : an Official Publication of the American Association of Anatomists* 238 (9): 2340–56. doi:10.1002/dvdy.21998.
Manuel, Gema C, Rosalia Reynoso, Lydia Gee, Luis M Salgado, and Hans R Bode. 2006. “PI3K and ERK 1-2 Regulate Early Stages During Head Regeneration in

Hydra..” *Development, Growth & Differentiation* 48 (2). Blackwell Publishing Asia: 129–38. doi:10.1111/j.1440-169X.2006.00847.x.
Marín-Juez, Rubén, Michele Marass, Sebastien Gauvrit, Andrea Rossi, Shih-Lei Lai, Stefan C Materna, Brian L Black, and Didier Y R Stainier. 2016. “Fast Revascularization of the Injured Area Is Essential to Support Zebrafish Heart Regeneration..” *Proceedings of the National Academy of Sciences of the United States of America* 113 (40). National Acad Sciences: 11237–42. doi:10.1073/pnas.1605431113.
Marlow, Heather Q, Mansi Srivastava, David Q Matus, Daniel Rokhsar, and Mark Q Martindale. 2009. “Anatomy and Development of the Nervous System of Nematostella Vectensis, an Anthozoan Cnidarian..” *Developmental Neurobiology* 69 (4): 235–54. doi:10.1002/dneu.20698.
Marlow, Heather, Eric Roettinger, Michiel Boekhout, and Mark Q Martindale. 2012. “Functional Roles of Notch Signaling in the Cnidarian Nematostella Vectensis..” *Developmental Biology* 362 (2): 295–308. doi:10.1016/j.ydbio.2011.11.012.
Marshall, C J. 1995. “Specificity of Receptor Tyrosine Kinase Signaling: Transient Versus Sustained Extracellular Signal-Regulated Kinase Activation..” *Cell* 80 (2): 179–85.
Martin, V J, C L Littlefield, W E Archer, and H R Bode. 1997. “Embryogenesis in Hydra..” *The Biological Bulletin* 192 (3): 345–63. doi:10.2307/1542745.
Martindale, Mark Q, Kevin Pang, and John R Finnerty. 2004. “Investigating the Origins of Triploblasty: ‘Mesodermal’ Gene Expression in a Diploblastic Animal, the Sea Anemone Nematostella Vectensis (Phylum, Cnidaria; Class, Anthozoa)..” *Development* 131 (10). The Company of Biologists Ltd: 2463–74. doi:10.1242/dev.01119.
Mazza, Maureen E, Kevin Pang, Mark Q Martindale, and John R Finnerty. 2007. “Genomic Organization, Gene Structure, and Developmental Expression of Three Clustered Otx Genes in the Sea Anemone Nematostella Vectensis..” *Journal of Experimental Zoology. Part B, Molecular and Developmental Evolution* 308 (4): 494–506. doi:10.1002/jez.b.21158.
McCusker, Catherine, Susan V Bryant, and David M Gardiner. 2015. “The Axolotl Limb Blastema: Cellular and Molecular Mechanisms Driving Blastema Formation and Limb Regeneration in Tetrapods..” *Regeneration (Oxford, England)* 2 (2): 54–71. doi:10.1002/reg2.32.
Meakin, S O, and E M Shooter. 1992. “The Nerve Growth Factor Family of Receptors..” *Trends in Neurosciences* 15 (9): 323–31.
Mescher, Anthony L, and Anton W Neff. 2005a. “Regenerative Capacity and the Developing Immune System.” In *Regenerative Medicine I*, 93:39–66. Advances in Biochemical Engineering/Biotechnology. Berlin, Heidelberg: Springer Berlin Heidelberg. doi:10.1007/b99966.
Mescher, Anthony L, and Anton W Neff. 2005b. “Regenerative Capacity and the Developing Immune System.” In *Regenerative Medicine I*, 93:39–66. Advances in Biochemical Engineering/Biotechnology. Berlin, Heidelberg: Springer Berlin Heidelberg. doi:10.1007/b99966.
Mescher, Anthony L, and Denis Gospodarowicz. 1979. “Mitogenic Effect of a Growth Factor Derived From Myelin on Denervated Regenerates of Newt Forelimbs.” *Journal of Experimental Zoology* 207 (3): 497–504. doi:10.1002/jez.1402070318.
Millimaki, Bonny B, Elly M Sweet, and Bruce B Riley. 2010. “Sox2 Is Required for Maintenance and Regeneration, but Not Initial Development, of Hair Cells in the Zebrafish Inner Ear..” *Developmental Biology* 338 (2): 262–69.

doi:10.1016/j.ydbio.2009.12.011.
Momose, Tsuyoshi, and Evelyn Houliston. 2007. “Two Oppositely Localised Frizzled RNAs as Axis Determinants in a Cnidarian Embryo..” *PLoS Biology* 5 (4): e70. doi:10.1371/journal.pbio.0050070.
Momose, Tsuyoshi, Romain Derelle, and Evelyn Houliston. 2008. “A Maternally Localised Wnt Ligand Required for Axial Patterning in the Cnidarian Clytia Hemisphaerica..” *Development* 135 (12). The Company of Biologists Ltd: 2105–13. doi:10.1242/dev.021543.
Morgan, Thomas Hunt. 1901. “Regeneration,” July, 1–341.
Mori, Tatsuro, Xiaoying Wang, Jae-Chang Jung, Toshihisa Sumii, Aneesh B Singhal, M Elizabeth Fini, C Edward Dixon, Alessandro Alessandrini, and Eng H Lo. 2002. “Mitogen-Activated Protein Kinase Inhibition in Traumatic Brain Injury: in Vitro and in Vivo Effects..” *Journal of Cerebral Blood Flow and Metabolism : Official Journal of the International Society of Cerebral Blood Flow and Metabolism* 22 (4): 444–52. doi:10.1097/00004647-200204000-00008.
Morrison, Jamie I, Sara Lööf, Pingping He, and András Simon. 2006. “Salamander Limb Regeneration Involves the Activation of a Multipotent Skeletal Muscle Satellite Cell Population..” *The Journal of Cell Biology* 172 (3). Rockefeller University Press: 433–40. doi:10.1083/jcb.200509011.
Mullen, L M, S V Bryant, M A Torok, B Blumberg, and D M Gardiner. 1996. “Nerve Dependency of Regeneration: the Role of Distal-Less and FGF Signaling in Amphibian Limb Regeneration..” *Development* 122 (11): 3487–97.
Muneoka, K, and S V Bryant. 1982. “Evidence That Patterning Mechanisms in Developing and Regenerating Limbs Are the Same..” *Nature* 298 (5872): 369–71.
Muneoka, K, and S V Bryant. 1984. “Cellular Contribution to Supernumerary Limbs Resulting From the Interaction Between Developing and Regenerating Tissues in the Axolotl..” *Developmental Biology* 105 (1): 179–87.
Nacu, Eugeniu, Elena Gromberg, Catarina R Oliveira, David Drechsel, and Elly M Tanaka. 2016. “FGF8 and SHH Substitute for Anterior-Posterior Tissue Interactions to Induce Limb Regeneration..” *Nature* 533 (7603). Nature Research: 407–10. doi:10.1038/nature17972.
Nakanishi, Nagayasu, and Mark Q Martindale. 2018. “CRISPR Knockouts Reveal an Endogenous Role for Ancient Neuropeptides in Regulating Developmental Timing in a Sea Anemone..” *eLife* 7 (September). doi:10.7554/eLife.39742.
Nakanishi, Nagayasu, Eduard Renfer, Ulrich Technau, and Fabian Rentzsch. 2012. “Nervous Systems of the Sea Anemone Nematostella Vectensis Are Generated by Ectoderm and Endoderm and Shaped by Distinct Mechanisms..” *Development* 139 (2). Oxford University Press for The Company of Biologists Limited: 347–57. doi:10.1242/dev.071902.
Nandety, Raja Sekhar, Yen-Wen Kuo, Shahideh Nouri, and Bryce W Falk. 2015. “Emerging Strategies for RNA Interference (RNAi) Applications in Insects..” *Bioengineered* 6 (1): 8–19. doi:10.4161/21655979.2014.979701.
Newmark, Philip A, and Alejandro Sánchez Alvarado. 2002. “Not Your Father's Planarian: a Classic Model Enters the Era of Functional Genomics..” *Nature Reviews. Genetics* 3 (3): 210–19. doi:10.1038/nrg759.
Niethammer, Philipp. 2016. “The Early Wound Signals..” *Current Opinion in Genetics & Development* 40 (October): 17–22. doi:10.1016/j.gde.2016.05.001.
Obata, T, G E Brown, and M B Yaffe. 2000. “MAP Kinase Pathways Activated by Stress: the P38 MAPK Pathway..” *Critical Care Medicine* 28 (4 Suppl): N67–N77.

Oberpriller, J. 1971. “Mitosis in Adult Newt Ventricle.” *The Journal of Cell Biology* 49 (2): 560–63. doi:10.1083/jcb.49.2.560.
Oberpriller, J O, and J C Oberpriller. 1974. “Response of the Adult Newt Ventricle to Injury..” *The Journal of Experimental Zoology* 187 (2): 249–53. doi:10.1002/jez.1401870208.
Ogawa, Kazuya, Chiyoko Kobayashi, Tetsutaro Hayashi, Hidefumi Orii, Kenji Watanabe, and Kiyokazu Agata. 2002. “Planarian Fibroblast Growth Factor Receptor Homologs Expressed in Stem Cells and Cephalic Ganglions..” *Development, Growth & Differentiation* 44 (3): 191–204.
Ohnmacht, Jochen, Yujie Yang, Gianna W Maurer, Antón Barreiro-Iglesias, Themistoklis M Tsarouchas, Daniel Wehner, Dirk Sieger, Catherina G Becker, and Thomas Becker. 2016. “Spinal Motor Neurons Are Regenerated After Mechanical Lesion and Genetic Ablation in Larval Zebrafish..” *Development* 143 (9). Oxford University Press for The Company of Biologists Limited: 1464–74. doi:10.1242/dev.129155.
Owlarn, Suthira, Felix Klenner, David Schmidt, Franziska Rabert, Antonio Tomasso, Hanna Reuter, Medhanie A Mulaw, et al. 2017. “Generic Wound Signals Initiate Regeneration in Missing-Tissue Contexts..” *Nature Communications* 8 (1). Nature Publishing Group: 2282. doi:10.1038/s41467-017-02338-x.
Parish, Clare L, Anna Beljajeva, Ernest Arenas, and András Simon. 2007. “Midbrain Dopaminergic Neurogenesis and Behavioural Recovery in a Salamander Lesion-Induced Regeneration Model..” *Development* 134 (15). The Company of Biologists Ltd: 2881–87. doi:10.1242/dev.002329.
Park, Peter J. 2009. “ChIP-Seq: Advantages and Challenges of a Maturing Technology..” *Nature Reviews. Genetics* 10 (10): 669–80. doi:10.1038/nrg2641.
Passamaneck, Yale J, and Mark Q Martindale. 2012. “Cell Proliferation Is Necessary for the Regeneration of Oral Structures in the Anthozoan Cnidarian Nematostella Vectensis..” *BMC Developmental Biology* 12 (1). BioMed Central Ltd: 34. doi:10.1186/1471-213X-12-34.
Pearson, G, F Robinson, T Beers Gibson, B E Xu, M Karandikar, K Berman, and M H Cobb. 2001. “Mitogen-Activated Protein (MAP) Kinase Pathways: Regulation and Physiological Functions..” *Endocrine Reviews* 22 (2): 153–83. doi:10.1210/edrv.22.2.0428.
Percharde, Michelle, Aydan Bulut-Karslioglu, and Miguel Ramalho-Santos. 2017. “Hypertranscription in Development, Stem Cells, and Regeneration.” *Developmental Cell* 40 (1). Elsevier Inc.: 9–21. doi:10.1016/j.devcel.2016.11.010.
Peter, Isabelle S. 2017. “Regulatory States in the Developmental Control of Gene Expression..” *Briefings in Functional Genomics* 16 (5): 281–87. doi:10.1093/bfgp/elx009.
Petersen, Hendrik O, Stefanie K Höger, Mario Looso, Tobias Lengfeld, Anne Kuhn, Uwe Warnken, Chiemi Nishimiya-Fujisawa, et al. 2015. “A Comprehensive Transcriptomic and Proteomic Analysis of Hydra Head Regeneration..” *Molecular Biology and Evolution* 32 (8): 1928–47. doi:10.1093/molbev/msv079.
Pfefferli, Catherine, and Anna Jaźwińska. 2015. “The Art of Fin Regeneration in Zebrafish..” *Regeneration (Oxford, England)* 2 (2): 72–83. doi:10.1002/reg2.33.
Philipp, Isabelle, Roland Aufschnaiter, Suat Özbek, Stefanie Pontasch, Marcell Jenewein, Hiroshi Watanabe, Fabian Rentzsch, Thomas W Holstein, and Bert Hobmayer. 2009. “Wnt/Beta-Catenin and Noncanonical Wnt Signaling Interact in Tissue Evagination in the Simple Eumetazoan Hydra..” *Proceedings of the National Academy of Sciences of the United States of America* 106 (11). National

Academy of Sciences: 4290–95. doi:10.1073/pnas.0812847106.
Philipp, Isabelle, Thomas W Holstein, and Bert Hobmayer. 2005. “HvJNK, a Hydra Member of the C-Jun NH2-Terminal Kinase Gene Family, Is Expressed During Nematocyte Differentiation..” *Gene Expression Patterns : GEP* 5 (3): 397–402. doi:10.1016/j.modgep.2004.09.007.
Piatt, Jean. 1955. “Regeneration of the Spinal Cord in the Salamander.” *Journal of Experimental Zoology* 129 (1): 177–207. doi:10.1002/jez.1401290109.
Poleo, G, C W Brown, L Laforest, and M A Akimenko. 2001. “Cell Proliferation and Movement During Early Fin Regeneration in Zebrafish..” *Developmental Dynamics : an Official Publication of the American Association of Anatomists* 221 (4): 380–90. doi:10.1002/dvdy.1152.
Poss, K D, J Shen, A Nechiporuk, G McMahon, B Thisse, C Thisse, and M T Keating. 2000. “Roles for Fgf Signaling During Zebrafish Fin Regeneration..” *Developmental Biology* 222 (2). Academic Press: 347–58. doi:10.1006/dbio.2000.9722.
Poss, Kenneth D. 2007. “Getting to the Heart of Regeneration in Zebrafish..” *Seminars in Cell & Developmental Biology* 18 (1): 36–45. doi:10.1016/j.semcdb.2006.11.009.
Putnam, Nicolas H. 2007. “Sea Anemone Genome Reveals Ancestral Eumetaozoan Gene Repertoire and Genomic Organization.” *Science* 317 (5834): 83–86. doi:10.1126/science.1143254.
Rao, Donald D, John S Vorhies, Neil Senzer, and John Nemunaitis. 2009. “siRNA vs. shRNA: Similarities and Differences..” *Advanced Drug Delivery Reviews* 61 (9): 746–59. doi:10.1016/j.addr.2009.04.004.
Raya, Angel, Christopher M Koth, Dirk Büscher, Yasuhiko Kawakami, Tohru Itoh, R Marina Raya, Gabriel Sternik, Huai-Jen Tsai, Concepción Rodríguez-Esteban, and Juan Carlos Izpisua Belmonte. 2003. “Activation of Notch Signaling Pathway Precedes Heart Regeneration in Zebrafish..” *Proceedings of the National Academy of Sciences* 100 Suppl 1 (Supplement 1). National Academy of Sciences: 11889–95. doi:10.1073/pnas.1834204100.
Rebscher, Nicole, Christina Deichmann, Stefanie Sudhop, Jens Holger Fritzenwanker, Stephen Green, and Monika Hassel. 2009. “Conserved Intron Positions in FGFR Genes Reflect the Modular Structure of FGFR and Reveal Stepwise Addition of Domains to an Already Complex Ancestral FGFR.” *Development Genes and Evolution* 219 (9-10): 455–68. doi:10.1007/s00427-009-0309-5.
Reddien, Peter W, and Alejandro Sánchez Alvarado. 2004. “Fundamentals of Planarian Regeneration..” *Annual Review of Cell and Developmental Biology* 20: 725–57. doi:10.1146/annurev.cellbio.20.010403.095114.
Reddy, P C, Salil S Bidaye, and Surendra Ghaskadbi. 2011. “Genome-Wide Screening Reveals the Emergence and Divergence of RTK Homologues in Basal Metazoan Hydra Magnipapillata.” *Journal of Biosciences* 36 (2): 289–96. doi:10.1007/s12038-011-9065-6.
Reimer, Michell M, Inga Sörensen, Veronika Kuscha, Rebecca E Frank, Chong Liu, Catherina G Becker, and Thomas Becker. 2008. “Motor Neuron Regeneration in Adult Zebrafish..” *The Journal of Neuroscience : the Official Journal of the Society for Neuroscience* 28 (34). Society for Neuroscience: 8510–16. doi:10.1523/JNEUROSCI.1189-08.2008.
Reitzel, Adam M, Patrick M Burton, Cassandra Krone, and John R Finnerty. 2007. “Comparison of Developmental Trajectories in the Starlet Sea Anemone

Nematostella Vectensis: Embryogenesis, Regeneration, and Two Forms of Asexual Fission." *Invertebrate Biology* 126 (2): 99–112. doi:10.1111/j.1744-7410.2007.00081.x.
Renfer, E, A Amon-Hassenzahl, P R H Steinmetz, and U Technau. 2010. "A Muscle-Specific Transgenic Reporter Line of the Sea Anemone, Nematostella Vectensis." *Proceedings of the National Academy of Sciences* 107 (1): 104–8. doi:10.1073/pnas.0909148107.
Rentzsch, Fabian, Jens H Fritzenwanker, Corinna B Scholz, and Ulrich Technau. 2008. "FGF Signalling Controls Formation of the Apical Sensory Organ in the Cnidarian Nematostella Vectensis.." *Development* 135 (10). The Company of Biologists Ltd: 1761–69. doi:10.1242/dev.020784.
Repesh, L A, and J C Oberpriller. 1980. "Ultrastructural Studies on Migrating Epidermal Cells During the Wound Healing Stage of Regeneration in the Adult Newt, Notophthalmus Viridescens.." *The American Journal of Anatomy* 159 (2): 187–208. doi:10.1002/aja.1001590207.
Richards, Gemma Sian, and Fabian Rentzsch. 2014. "Transgenic Analysis of a SoxB Gene Reveals Neural Progenitor Cells in the Cnidarian Nematostella Vectensis.." *Development* 141 (24). Oxford University Press for The Company of Biologists Limited: 4681–89. doi:10.1242/dev.112029.
Richards, Gemma Sian, and Fabian Rentzsch. 2015. "Regulation of Nematostella Neural Progenitors by SoxB, Notch and bHLH Genes.." *Development* 142 (19). Oxford University Press for The Company of Biologists Limited: 3332–42. doi:10.1242/dev.123745.
Rink, Jochen C. 2013. "Stem Cell Systems and Regeneration in Planaria.." *Development Genes and Evolution* 223 (1-2): 67–84. doi:10.1007/s00427-012-0426-4.
Ritenour, Angela M, and Renee Dickie. 2017. "Inhibition of Vascular Endothelial Growth Factor Receptor Decreases Regenerative Angiogenesis in Axolotls.." *Anatomical Record (Hoboken, N.J. : 2007)* 300 (12): 2273–80. doi:10.1002/ar.23689.
Roberts, P J, and C J Der. 2007. "Targeting the Raf-MEK-ERK Mitogen-Activated Protein Kinase Cascade for the Treatment of Cancer." *Oncogene* 26 (22): 3291–3310. doi:10.1038/sj.onc.1210422.
Rojas-Muñoz, Agustin, Shibani Rajadhyksha, Darren Gilmour, Frauke van Bebber, Christopher Antos, Concepción Rodríguez-Esteban, Christiane Nüsslein-Volhard, and Juan Carlos Izpisua Belmonte. 2009. "ErbB2 and ErbB3 Regulate Amputation-Induced Proliferation and Migration During Vertebrate Regeneration.." *Developmental Biology* 327 (1): 177–90. doi:10.1016/j.ydbio.2008.12.012.
Röttinger, Eric, Paul Dahlin, and Mark Q Martindale. 2012. "A Framework for the Establishment of a Cnidarian Gene Regulatory Network for 'Endomesoderm' Specification: the Inputs of SS-Catenin/TCF Signaling.." Edited by Mary C Mullins. *PLoS Genetics* 8 (12). Public Library of Science: e1003164. doi:10.1371/journal.pgen.1003164.
Sadler, Kirsten C, Katherine N Krahn, Naseem A Gaur, and Chinweike Ukomadu. 2007. "Liver Growth in the Embryo and During Liver Regeneration in Zebrafish Requires the Cell Cycle Regulator, Uhrf1.." *Proceedings of the National Academy of Sciences* 104 (5). National Academy of Sciences: 1570–75. doi:10.1073/pnas.0610774104.
Salo, E, and J Baguna. 1989. "Regeneration and Pattern Formation in Planarians. II.

and Role of Cell Movements in Blastema Formation." *Development* 107 (1). The Company of Biologists Ltd: 69–76.
Sandmann, Thomas, Matthias C Vogg, Suthira Owlarn, Michael Boutros, and Kerstin Bartscherer. 2011. "The Head-Regeneration Transcriptome of the Planarian Schmidtea Mediterranea." *Genome Biology* 12 (8): R76. doi:10.1186/gb-2011-12-8-r76.
Satoh, A, G M C Graham, S V Bryant, and D M Gardiner. 2008. "Neurotrophic Regulation of Epidermal Dedifferentiation During Wound Healing and Limb Regeneration in the Axolotl (Ambystoma Mexicanum).." *Developmental Biology* 319 (2): 321–35. doi:10.1016/j.ydbio.2008.04.030.
Sánchez Alvarado, A, and P A Newmark. 1998. "The Use of Planarians to Dissect the Molecular Basis of Metazoan Regeneration.." *Wound Repair and Regeneration : Official Publication of the Wound Healing Society [and] the European Tissue Repair Society* 6 (4): 413–20.
Sánchez Alvarado, Alejandro, and Panagiotis A Tsonis. 2006. "Bridging the Regeneration Gap: Genetic Insights From Diverse Animal Models.." *Nature Reviews. Genetics* 7 (11): 873–84. doi:10.1038/nrg1923.
Schaeffer, H J, and M J Weber. 1999. "Mitogen-Activated Protein Kinases: Specific Messages From Ubiquitous Messengers.." *Molecular and Cellular Biology* 19 (4): 2435–44.
Schaffer, Amos A, Michael Bazarsky, Karine Levy, Vered Chalifa-Caspi, and Uri Gat. 2016. "A Transcriptional Time-Course Analysis of Oral vs. Aboral Whole-Body Regeneration in the Sea Anemone Nematostella Vectensis.." *BMC Genomics* 17 (September): 718. doi:10.1186/s12864-016-3027-1.
Schmidt, Rebecca, Tanja Beil, Uwe Strähle, and Sepand Rastegar. 2014. "Stab Wound Injury of the Zebrafish Adult Telencephalon: a Method to Investigate Vertebrate Brain Neurogenesis and Regeneration.." *Journal of Visualized Experiments : JoVE*, no. 90 (August): e51753–53. doi:10.3791/51753.
Schwaiger, M, A Schonauer, A F Rendeiro, C Pribitzer, A Schauer, A F Gilles, J B Schinko, E Renfer, D Fredman, and U Technau. 2014. "Evolutionary Conservation of the Eumetazoan Gene Regulatory Landscape." *Genome Research* 24 (4): 639–50. doi:10.1101/gr.162529.113.
Scimone, M Lucila, Kellie M Kravarik, Sylvain W Lapan, and Peter W Reddien. 2014. "Neoblast Specialization in Regeneration of the Planarian Schmidtea Mediterranea.." *Stem Cell Reports* 3 (2): 339–52. doi:10.1016/j.stemcr.2014.06.001.
Seale, Patrick, and Michael A Rudnicki. 2000. "A New Look at the Origin, Function, and 'Stem-Cell' Status of Muscle Satellite Cells." *Developmental Biology* 218 (2): 115–24. doi:10.1006/dbio.1999.9565.
Sebé-Pedrós, Arnau, Baptiste Saudemont, Elad Chomsky, Flora Plessier, Marie-Pierre Mailhé, Justine Renno, Yann Loe-Mie, et al. 2018. "Cnidarian Cell Type Diversity and Regulation Revealed by Whole-Organism Single-Cell RNA-Seq.." *Cell* 173 (6): 1520–20. doi:10.1016/j.cell.2018.05.019.
Seifert, Ashley W, James R Monaghan, S Randal Voss, and Malcolm Maden. 2012. "Skin Regeneration in Adult Axolotls: a Blueprint for Scar-Free Healing in Vertebrates.." *PloS One* 7 (4): e32875. doi:10.1371/journal.pone.0032875.
Seipel, Katka, Michael Eberhardt, Peter Müller, Elena Pescia, Nathalie Yanze, and Volker Schmid. 2004. "Homologs of Vascular Endothelial Growth Factor and Receptor, VEGF and VEGFR, in the Jellyfish Podocoryne Carnea.." *Developmental Dynamics : an Official Publication of the American Association of*

Anatomists 231 (2). Wiley Subscription Services, Inc., A Wiley Company: 303–12. doi:10.1002/dvdy.20139.
Servetnick, Marc D, Bailey Steinworth, Leslie S Babonis, David Simmons, Miguel Salinas-Saavedra, and Mark Q Martindale. 2017. “Cas9-Mediated Excision of Nematostella Brachyury Disrupts Endoderm Development, Pharynx Formation and Oral-Aboral Patterning..” *Development* 144 (16). Oxford University Press for The Company of Biologists Limited: 2951–60. doi:10.1242/dev.145839.
Simões, Mariana G, Anabela Bensimon-Brito, Mariana Fonseca, Ana Farinho, Fábio Valério, Sara Sousa, Nuno Afonso, Anoop Kumar, and Antonio Jacinto. 2014. “Denervation Impairs Regeneration of Amputated Zebrafish Fins..” *BMC Developmental Biology* 14 (1). BioMed Central: 49. doi:10.1186/s12861-014-0049-2.
Sinigaglia, Chiara, Henriette Busengdal, Lucas Leclère, Ulrich Technau, and Fabian Rentzsch. 2013. “The Bilaterian Head Patterning Gene Six3/6 Controls Aboral Domain Development in a Cnidarian..” *PLoS Biology* 11 (2). Public Library of Science: e1001488. doi:10.1371/journal.pbio.1001488.
Smid, Iris, and Pierre Tardent. 1986. “The Potentialities of Endoderm Interstitial Cells in Hydra Attenuata Pall.” *Developmental Biology* 117 (2): 672–75. doi:10.1016/0012-1606(86)90336-2.
Smith, Joel. 2008. “A Protocol Describing the Principles of Cis-Regulatory Analysis in the Sea Urchin..” *Nature Protocols* 3 (4): 710–18. doi:10.1038/nprot.2008.39.
Stefanik, Derek J, Lauren E Friedman, and John R Finnerty. 2013. “Collecting, Rearing, Spawning and Inducing Regeneration of the Starlet Sea Anemone, Nematostella Vectensis..” *Nature Protocols* 8 (5): 916–23. doi:10.1038/nprot.2013.044.
Steinmetz, Patrick R H, Andy Aman, Johanna E M Kraus, and Ulrich Technau. 2017. “Gut-Like Ectodermal Tissue in a Sea Anemone Challenges Germ Layer Homology..” *Nature Ecology & Evolution* 1 (10): 1535–42. doi:10.1038/s41559-017-0285-5.
Stewart, Zachary K, Ana Pavasovic, Daniella H Hock, and Peter J Prentis. 2017. “Transcriptomic Investigation of Wound Healing and Regeneration in the Cnidarian Calliactis Polypus..” *Scientific Reports* 7 (February): 41458. doi:10.1038/srep41458.
Stocum, David L. 2011. “The Role of Peripheral Nerves in Urodele Limb Regeneration..” *The European Journal of Neuroscience* 34 (6). Blackwell Publishing Ltd: 908–16. doi:10.1111/j.1460-9568.2011.07827.x.
Streisinger, G, F Singer, C Walker, D Knauber, and N Dower. 1986. “Segregation Analyses and Gene-Centromere Distances in Zebrafish..” *Genetics* 112 (2): 311–19.
Sudhop, S. 2004. “Signalling by the FGFR-Like Tyrosine Kinase, Kringelchen, Is Essential for Bud Detachment in Hydra Vulgaris.” *Development* 131 (16): 4001–11. doi:10.1242/dev.01267.
Takaku, Yasuharu, Takahiko Hariyama, and Toshitaka Fujisawa. 2005. “Motility of Endodermal Epithelial Cells Plays a Major Role in Reorganizing the Two Epithelial Layers in Hydra..” *Mechanisms of Development* 122 (1): 109–22. doi:10.1016/j.mod.2004.08.004.
Takeo, Makoto, Wendy Lee, and Mayumi Ito. 2015. “Wound Healing and Skin Regeneration..” *Cold Spring Harbor Perspectives in Medicine* 5 (1). Cold Spring Harbor Laboratory Press: a023267. doi:10.1101/cshperspect.a023267.
Tanaka, Elly M, and Peter W Reddien. 2011. “The Cellular Basis for Animal

Regeneration..” *Developmental Cell* 21 (1): 172–85. doi:10.1016/j.devcel.2011.06.016.
Tanner, Kandice, Donald R Ferris, Luca Lanzano, Berhan Mandefro, William W Mantulin, David M Gardiner, Elizabeth L Rugg, and Enrico Gratton. 2009. “Coherent Movement of Cell Layers During Wound Healing by Image Correlation Spectroscopy..” *Biophysical Journal* 97 (7): 2098–2106. doi:10.1016/j.bpj.2009.06.052.
Tasaki, Junichi, Norito Shibata, Osamu Nishimura, Kazu Itomi, Yoshimichi Tabata, Fuyan Son, Nobuko Suzuki, et al. 2011. “ERK Signaling Controls Blastema Cell Differentiation During Planarian Regeneration..” *Development* 138 (12). Oxford University Press for The Company of Biologists Limited: 2417–27. doi:10.1242/dev.060764.
Tasaki, Junichi, Norito Shibata, Toshihide Sakurai, Kiyokazu Agata, and Yoshihiko Umesono. 2011. “Role of C-Jun N-Terminal Kinase Activation in Blastema Formation During Planarian Regeneration..” *Development, Growth & Differentiation* 53 (3): 389–400. doi:10.1111/j.1440-169X.2011.01254.x.
Technau, U, C Cramer von Laue, F Rentzsch, S Luft, B Hobmayer, H R Bode, and T W Holstein. 2000. “Parameters of Self-Organization in Hydra Aggregates..” *Proceedings of the National Academy of Sciences* 97 (22). National Academy of Sciences: 12127–31. doi:10.1073/pnas.97.22.12127.
Technau, Ulrich, and Robert E Steele. 2011. “Evolutionary Crossroads in Developmental Biology: Cnidaria..” *Development* 138 (8). Oxford University Press for The Company of Biologists Limited: 1447–58. doi:10.1242/dev.048959.
Tejada-Romero, Belen, Jean-Michel Carter, Yuliana Mihaylova, Bjoern Neumann, and A Aziz Aboobaker. 2015. “JNK Signalling Is Necessary for a Wnt- and Stem Cell-Dependent Regeneration Programme..” *Development* 142 (14). Oxford University Press for The Company of Biologists Limited: 2413–24. doi:10.1242/dev.115139.
Tiozzo, Stefano, and Richard R Copley. 2015. “Reconsidering Regeneration in Metazoans: an Evo-Devo Approach.” *Frontiers in Ecology and Evolution* 3 (June). doi:10.3389/fevo.2015.00067.
Tiozzo, Stefano, Ayelet Voskoboynik, Federico D Brown, and Anthony W De Tomaso. 2008. “A Conserved Role of the VEGF Pathway in Angiogenesis of an Ectodermally-Derived Vasculature..” *Developmental Biology* 315 (1): 243–55. doi:10.1016/j.ydbio.2007.12.035.
Trevino, Michael, Derek J Stefanik, Richard Rodriguez, Shane Harmon, and Patrick M Burton. 2011. “Induction of Canonical Wnt Signaling by Alsterpaullone Is Sufficient for Oral Tissue Fate During Regeneration and Embryogenesis in Nematostella Vectensis..” *Developmental Dynamics : an Official Publication of the American Association of Anatomists* 240 (12). Wiley-Liss, Inc.: 2673–79. doi:10.1002/dvdy.22774.
Tseng, Wen-Fang, Te-Hsuan Jang, Chang-Ben Huang, and Chiou-Hwa Yuh. 2011. “An Evolutionarily Conserved Kernel of Gata5, Gata6, Otx2 and Prdm1a Operates in the Formation of Endoderm in Zebrafish..” *Developmental Biology* 357 (2): 541–57. doi:10.1016/j.ydbio.2011.06.040.
Tu, Shu, and Stephen L Johnson. 2011. “Fate Restriction in the Growing and Regenerating Zebrafish Fin..” *Developmental Cell* 20 (5): 725–32. doi:10.1016/j.devcel.2011.04.013.
Tucker, Richard P, Bradley Shibata, and Thomas N Blankenship. 2011. “Ultrastructure of the Mesoglea of the Sea Anemone Nematostella Vectensis

(Edwardsiidae).” *Invertebrate Biology* 130 (1): 11–24. doi:10.1111/j.1744-7410.2010.00219.x.
Tulin, Sarah, Derek Aguiar, Sorin Istrail, and Joel Smith. 2013. “A Quantitative Reference Transcriptome for Nematostella Vectensis Early Embryonic Development: a Pipeline for De Novo Assembly in Emerging Model Systems..” *EvoDevo* 4 (1): 16. doi:10.1186/2041-9139-4-16.
Turner, J E, and K A Glaze. 1977. “Regenerative Repair in the Severed Optic Nerve of the Newt (Triturus Viridescens): Effect of Nerve Growth Factor..” *Experimental Neurology* 57 (3): 687–97.
Umesono, Yoshihiko, Junichi Tasaki, Yui Nishimura, Martina Hrouda, Eri Kawaguchi, Shigenobu Yazawa, Osamu Nishimura, Kazutaka Hosoda, Takeshi Inoue, and Kiyokazu Agata. 2013. “The Molecular Logic for Planarian Regeneration Along the Anterior-Posterior Axis..” *Nature* 500 (7460): 73–76. doi:10.1038/nature12359.
van der Geer, P, T Hunter, and R A Lindberg. 1994. “Receptor Protein-Tyrosine Kinases and Their Signal Transduction Pathways..” *Annual Review of Cell Biology* 10 (1): 251–337. doi:10.1146/annurev.cb.10.110194.001343.
van Kesteren, R E, M Fainzilber, G Hauser, J van Minnen, E Vreugdenhil, A B Smit, C F Ibáñez, W P Geraerts, and A G Bulloch. 1998. “Early Evolutionary Origin of the Neurotrophin Receptor Family..” *The EMBO Journal* 17 (9). EMBO Press: 2534–42. doi:10.1093/emboj/17.9.2534.
Varga, M, M Sass, D Papp, K Takács-Vellai, J Kobolak, A Dinnyés, D J Klionsky, and T Vellai. 2014. “Autophagy Is Required for Zebrafish Caudal Fin Regeneration..” *Cell Death and Differentiation* 21 (4): 547–56. doi:10.1038/cdd.2013.175.
Vargas, R, I Th Jóhannesdóttir, B Sigurgeirsson, H Thorsteinsson, and K A E Karlsson. 2011. “The Zebrafish Brain in Research and Teaching: a Simple in Vivo and in Vitro Model for the Study of Spontaneous Neural Activity..” *Advances in Physiology Education* 35 (2): 188–96. doi:10.1152/advan.00099.2010.
Vinarsky, Vladimir, Donald L Atkinson, Tamara J Stevenson, Mark T Keating, and Shannon J Odelberg. 2005. “Normal Newt Limb Regeneration Requires Matrix Metalloproteinase Function..” *Developmental Biology* 279 (1): 86–98. doi:10.1016/j.ydbio.2004.12.003.
Wagner, Daniel E, Irving E Wang, and Peter W Reddien. 2011. “Clonogenic Neoblasts Are Pluripotent Adult Stem Cells That Underlie Planarian Regeneration..” *Science* 332 (6031): 811–16. doi:10.1126/science.1203983.
Wan, Jin, Rajesh Ramachandran, and Daniel Goldman. 2012. “HB-EGF Is Necessary and Sufficient for Müller Glia Dedifferentiation and Retina Regeneration..” *Developmental Cell* 22 (2): 334–47. doi:10.1016/j.devcel.2011.11.020.
Wang, Jinhu, Daniela Panáková, Kazu Kikuchi, Jennifer E Holdway, Matthew Gemberling, James S Burris, Sumeet Pal Singh, et al. 2011. “The Regenerative Capacity of Zebrafish Reverses Cardiac Failure Caused by Genetic Cardiomyocyte Depletion..” *Development* 138 (16). Oxford University Press for The Company of Biologists Limited: 3421–30. doi:10.1242/dev.068601.
Warner, Jacob F, Vincent Guerlais, Aldine R Amiel, Hereroa Johnston, Karine Nedoncelle, and Eric Röttinger. 2018. “NvERTx: a Gene Expression Database to Compare Embryogenesis and Regeneration in the Sea Anemone Nematostella Vectensis..” *Development* 145 (10). Oxford University Press for The Company of Biologists Limited: dev162867. doi:10.1242/dev.162867.

Wenemoser, Danielle, and Peter W Reddien. 2010. “Planarian Regeneration Involves Distinct Stem Cell Responses to Wounds and Tissue Absence..” *Developmental Biology* 344 (2): 979–91. doi:10.1016/j.ydbio.2010.06.017.
Whitehead, Geoffrey G, Shinji Makino, Ching-Ling Lien, and Mark T Keating. 2005. “Fgf20 Is Essential for Initiating Zebrafish Fin Regeneration..” *Science* 310 (5756): 1957–60. doi:10.1126/science.1117637.
Wiesmann, C, M H Ultsch, S H Bass, and A M de Vos. 1999. “Crystal Structure of Nerve Growth Factor in Complex with the Ligand-Binding Domain of the TrkA Receptor..” *Nature* 401 (6749): 184–88. doi:10.1038/43705.
Wijesena, Naveen, David K Simmons, and Mark Q Martindale. 2017. “Antagonistic BMP-cWNT Signaling in the Cnidarian Nematostella Vectensis Reveals Insight Into the Evolution of Mesoderm..” *Proceedings of the National Academy of Sciences of the United States of America* 114 (28). National Academy of Sciences: E5608–15. doi:10.1073/pnas.1701607114.
Wikramanayake, Athula H, Melanie Hong, Patricia N Lee, Kevin Pang, Christine A Byrum, Joanna M Bince, Ronghui Xu, and Mark Q Martindale. 2003. “An Ancient Role for Nuclear Beta-Catenin in the Evolution of Axial Polarity and Germ Layer Segregation..” *Nature* 426 (6965): 446–50. doi:10.1038/nature02113.
Wittlieb, Jörg, Konstantin Khalturin, Jan U Lohmann, Friederike Anton-Erxleben, and Thomas C G Bosch. 2006. “Transgenic Hydra Allow in Vivo Tracking of Individual Stem Cells During Morphogenesis..” *Proceedings of the National Academy of Sciences* 103 (16). National Academy of Sciences: 6208–11. doi:10.1073/pnas.0510163103.
Wolberg, Alisa S, and Robert A Campbell. 2008. “Thrombin Generation, Fibrin Clot Formation and Hemostasis..” *Transfusion and Apheresis Science : Official Journal of the World Apheresis Association : Official Journal of the European Society for Haemapheresis* 38 (1): 15–23. doi:10.1016/j.transci.2007.12.005.
Wynn, T A. 2008. “Cellular and Molecular Mechanisms of Fibrosis..” *The Journal of Pathology* 214 (2): 199–210. doi:10.1002/path.2277.
Xu, Zhiliang, Oleg Kim, Malgorzata Kamocka, Elliot D Rosen, and Mark Alber. 2012. “Multiscale Models of Thrombogenesis..” *Wiley Interdisciplinary Reviews. Systems Biology and Medicine* 4 (3): 237–46. doi:10.1002/wsbm.1160.
Yokoyama, Hitoshi, Tamae Maruoka, Akio Aruga, Takanori Amano, Shiro Ohgo, Toshihiko Shiroishi, and Koji Tamura. 2011. “Prx-1 Expression in Xenopus Laevis Scarless Skin-Wound Healing and Its Resemblance to Epimorphic Regeneration..” *The Journal of Investigative Dermatology* 131 (12): 2477–85. doi:10.1038/jid.2011.223.
Yoo, Sa Kan, Christina M Freisinger, Danny C LeBert, and Anna Huttenlocher. 2012. “Early Redox, Src Family Kinase, and Calcium Signaling Integrate Wound Responses and Tissue Regeneration in Zebrafish..” *The Journal of Cell Biology* 199 (2). Rockefeller Univ Press: 225–34. doi:10.1083/jcb.201203154.
Zhang, F, J D Clarke, and P Ferretti. 2000. “FGF-2 Up-Regulation and Proliferation of Neural Progenitors in the Regenerating Amphibian Spinal Cord in Vivo..” *Developmental Biology* 225 (2): 381–91. doi:10.1006/dbio.2000.9843.
Zhang, F, J D W Clarke, L Santos-Ruiz, and P Ferretti. 2002. “Differential Regulation of Fibroblast Growth Factor Receptors in the Regenerating Amphibian Spinal Cord in Vivo..” *Neuroscience* 114 (4): 837–48.
Zhao, Long, Asya L Borikova, Raz Ben-Yair, Burcu Guner-Ataman, Calum A Macrae, Richard T Lee, C Geoffrey Burns, and Caroline E Burns. 2014. “Notch Signaling Regulates Cardiomyocyte Proliferation During Zebrafish Heart

Regeneration..” *Proceedings of the National Academy of Sciences of the United States of America* 111 (4). National Academy of Sciences: 1403–8. doi:10.1073/pnas.1311705111.
1997. “Expression of Sonic Hedgehog Gene in Regenerating Newt Limb Blastemas Recapitulates That in Developing Limb Buds” 94 (17). National Academy of Sciences: 9159–64. doi:10.1073/pnas.94.17.9159.
2012. “Regeneration of the Elbow Joint in the Developing Chick Embryo Recapitulates Development.” 372 (2): 229–38. doi:10.1016/j.ydbio.2012.09.020.
2014. “Distal Expression of Sprouty (Spry) Genes During Xenopus Laevis Limb Development and Regeneration.” 15 (1): 61–66. doi:10.1016/j.gep.2014.04.004.